Fundamental Theories of Physics 178

Xavier Calmet *Editor*

Quantum Aspects of Black Holes

Springer

Fundamental Theories of Physics

Volume 178

More information about this series at http://www.springer.com/series/6001

Xavier Calmet
Editor

Quantum Aspects of Black Holes

Springer

Editor
Xavier Calmet
Department of Physics and Astronomy
University of Sussex
Brighton
UK

ISBN 978-3-319-10851-3 ISBN 978-3-319-10852-0 (eBook)
DOI 10.1007/978-3-319-10852-0

Library of Congress Control Number: 2014951685

Springer Cham Heidelberg New York Dordrecht London

Printed on acid-free paper

Springer is part of Springer Science+Business Media (www.springer.com)

Preface

The decision to write this book arose in discussions among members of the Working Group 1 (WG1) of the European Cooperation in Science and Technology (COST) action MP0905 "Black Holes in a Violent Universe," which started in 2010 and ended in May 2014.

The four years of the action have been absolutely fantastic for the research themes represented by WG1. The discovery of the Higgs boson which completes the standard model of particle physics was crowned by the 2013 Nobel prize. This discovery has important implications for the unification of the standard model with general relativity which is important for Planck size black holes. Understanding at what energy scale these forces merge into a unified theory, will tell us what is the lightest possible mass for a black hole. In other words, the Large Hadron Collider (LHC) at CERN data allows us to set bounds on the Planck scale. We now know that the Planck scale is above 5 TeV. Thus, Planckian black holes are heavier than 5 TeV. The fact that no dark matter has been discovered at the LHC in the form of a new particle strengthens the assumption that primordial black holes could play that role.

The data from the Planck satellite reinforce the need for inflation. Planckian black holes can make an important contribution at the earliest moment of our universe, namely during inflation if the scale at which inflation took place is close enough to the Planck scale. There have been several interesting proposals relating the Higgs boson of the standard model of particle physics with inflation. Indeed, the LHC data imply that the Higgs boson could be the inflation if the Higgs boson is non-minimally coupled to space-time curvature.

In relation to the black hole information paradox, there has been much excitement about firewalls or what happens when an observer falls through the horizon of a black hole. However, firewalls rely on a theorem by Banks, Susskind and Peskin [Nucl. Phys. B244 (1984) 125] for which there are known counter examples as shown in 1995 by Wald and Unruh [Phys. Rev. D52 (1995) 2176–2182]. It will be interesting to see how the situation evolves in the next few years.

These then are the reasons for writing this book, which reflects on the progress made in recent years in a field which is still developing rapidly. As well as some of the members of our working group, several other international experts have kindly agreed to contribute to the book. The result is a collection of 10 chapters dealing with different aspects of quantum effects in black holes. By quantum effects we mean both quantum mechanical effects such as Hawking radiation and quantum gravitational effects such as Planck size quantum black hole.

Chapter 1 is meant to provide a broad introduction to the field of quantum effects in black holes before focusing on Planckian quantum black holes. Chapter 2 covers the thermodynamics of black holes while Chap. 3 deals with the famous information paradox. Chapter 4 discusses another type of object, so-called monsters, which have more entropy than black holes of equal mass. Primordial black holes are discussed in Chaps. 5 and 6 reviews self-gravitating Bose-Einstein condensates which open up the exciting possibility that black holes are Bose-Einstein condensates. The formation of black holes in supersymmetric theories is investigated in Chap. 7. Chapter 8 covers Hawking radiation in higher dimensional black holes. Chapter 9 presents the latest bounds on the mass of small black holes which could have been produced at the LHC. Last but not least, Chap. 10 covers non-minimal length effects in black holes. All chapters have been through a strict reviewing process.

This book would not have been possible without the COST action MP0905. In particular we would like to thank Silke Britzen, the chair of our action, the members of the core group (Antxon Alberdi, Andreas Eckart, Robert Ferdman, Karl-Heinz Mack, Iossif Papadakis, Eduardo Ros, Anthony Rushton, Merja Tornikoski and Ulrike Wyputta in addition to myself) and all the members of this action for fascinating meetings and conferences. We are very grateful to Dr. Angela Lahee, our contact at Springer, for her constant support during the completion of this book.

Brighton, August 2014 Xavier Calmet

Contents

Chapter 1
Fundamental Physics with Black Holes

Xavier Calmet

Abstract In this chapter we discuss how quantum gravitational and quantum mechanical effects can affect black holes. In particular, we discuss how Planckian quantum black holes enable us to probe quantum gravitational physics either directly if the Planck scale is low enough or indirectly if we integrate out quantum black holes from our low energy effective action. We discuss how quantum black holes can resolve the information paradox of black holes and explain that quantum black holes lead to one of the few hard facts we have so far about quantum gravity, namely the existence of a minimal length in nature.

Keywords Black holes · Quantum black holes · Tests of the Planck scale · General relativity · Effective field theory of quantum gravity · Planck length

1.1 Introduction

Black holes are among the most fascinating objects in our universe. Their existence is now indisputable. Astrophysicists have observed very massive objects, which do not emit light. Obviously, these objects cannot be seen directly, but their gravitational effects on visible matter have clearly been established. The only reasonable explanation for these observations is that black holes do truly exist as predicted by Einstein's theory of general relativity. From an astrophysicist point of view, black holes are regions of space-time where gravity is so strong that nothing, not even light, can escape from that region of space-time. Astrophysical black holes can have an accretion disk and sometimes a jet. A real black hole system is thus a rather complicated environment.

In contrast, from a mathematical point of view, stationary black holes are very simple objects. They are vacuum solutions to Einsteins equations. The simplicity of black holes is reflected in the no-hair theorem [1] which states that black holes are uniquely defined in terms of just three parameters their mass, their electric charge and

X. Calmet (✉)
Physics and Astronomy, University of Sussex, Falmer, Brighton, BN1 9QH, UK
e-mail: x.calmet@sussex.ac.uk

X. Calmet (ed.), *Quantum Aspects of Black Holes*,
Fundamental Theories of Physics 178, DOI 10.1007/978-3-319-10852-0_1

their angular momentum. How comes such simple objects can be so interesting? The answer lies in the fact that their physics merges three different branches of physics: general relativity, quantum mechanics and statistical physics.

The first black hole solution was found by Schwarzschild only a couple of years after the publication of Einstein's theory of general relativity [2]. The Schwarzschild metric is given by:

$$ds^2 = -\left(1-\frac{2MG}{c^2 r}\right)c^2 dt^2 + \left(1-\frac{2MG}{c^2 r}\right)^{-1} dr^2 + r^2\left(d\theta^2 + \sin^2\theta\, d\varphi^2\right), \quad (1.1)$$

where G is Newton's constant, M is the mass of the black hole and c is the speed of light in vacuum and (r, θ, φ) are the usual spherical polar coordinates. The Kerr solution [3], which is relevant to astrophysical black holes was found much later in 1963. The Kerr solution represents a black hole which is rotating. The metric takes the following form, in spheroidal polar coordinates (r, θ, φ):

$$ds^2 = -\frac{\Delta}{\Sigma}\left[c dt - a\sin^2\theta\, d\varphi\right]^2 + \frac{\Sigma}{\Delta}dr^2 + \Sigma\, d\theta^2 + \frac{\sin^2\theta}{\Sigma}\left[\left(r^2+a^2\right)d\varphi - a\, c dt\right]^2, \quad (1.2)$$

where

$$\Delta = r^2 - 2MGr/c^2 + a^2, \qquad \Sigma = r^2 + a^2\cos^2\theta. \quad (1.3)$$

This solution describes a rotating black hole with an angular momentum $J = acM$, where $a > 0$ is a constant. The Kerr-Newman solution for a rotating black hole carrying an electric charge Q is obtained by replacing Δ in the Kerr solution by

$$\Delta_Q = r^2 - 2MGr/c^2 + a^2 + \frac{GQ^2}{4\pi\varepsilon_0 c^4} \quad (1.4)$$

where ε_0 is permittivity of free space. It is worth noting that objects whose gravitational fields are too strong for light to escape were first considered in the 18th century by John Michell [4] and Pierre-Simon Laplace [5], i.e. before the discovery of general relativity.

Black hole solutions are known to have a real singularity at the origin ($r = 0$ where r is the radial coordinate of the solution). While the apparent singularity at the horizon (i.e. for a neutral and non-rotating black hole at the Schwarzschild radius $r_S = 2GM/c^2$, is not a real one (one can do a variable transformation to show that there is no real singularity at the horizon), the singularity at the center of a black hole is a real one. The gravitational potential becomes arbitrarily strong and the laws of physics as we know them must breakdown. However, this singularity is hidden from us by the horizon. The cosmic censorship principle prevents us from observing regions of space-time with naked singularities. While black holes are very simple objects at the classical physics level, their physics at the quantum level is much more complicated and to a certain extend much more interesting. The existence of the

singularity mentioned above forces us to consider quantum effects in black holes since close to the singularity quantum gravity effects must become relevant. While in general relativity, singularities are unavoidable, quantum effects may smear space-time or prevent measurements of distances shorter than the Planck scale and make it impossible to resolve singularities. In some alternatives to general relativity, black hole singularities may not appear at all [6]. However, since it is impossible to observe inside a black hole for an outside observer, we may never be in a situation that allows us to differentiate between general relativity and its alternatives without singularities.

While quantum gravitational effects are relevant at, or very close to, the singularity of black holes, there is another type of quantum effect, which might be observable at the horizon of black holes. This is not a quantum gravitational effect, but simply a quantum mechanical effect. Hawking has discovered that black holes are not truly black, but that they emit a radiation which is almost that of a black body (see e.g. [7] and references therein). This has several fascinating consequences. Hawking radiations are plain quantum mechanical effects and do not require a knowledge of quantum gravity. The Hawking effect is thus calculable with our current theoretical tools using quantum field theory in curved space-time. Hawking's work implies that black holes have a temperature and thus an entropy. This is a beautiful result. It implies a deep relation between thermodynamics, quantum mechanics and general relativity [8]. Black holes are not the only interesting objects in general relativity. Indeed, there are certain configurations in general relativity called monsters [9] that can have more entropy than a black hole of equal mass. This can be challenging for certain interpretations of black hole entropy and the AdS/CFT duality.

Hawking's radiation is also the origin for the information paradox of black holes [10]. As emphasized already Hawking radiation is a quantum mechanical effects in general relativity. In quantum mechanics, one assumes that the evolution of the wave function is governed by a unitary operator. Unitarity implies that information is conserved in the quantum sense. One could imagine the following thought experiment, if one sends the quantum information (for example an entangled state) into a black hole, it will come out as Hawking radiation which is thermal and thus does not carry any information. What has happened to quantum information? Is the assumption that the evolution of the wave function is governed by a unitary operator compatible with black hole physics? There are several directions to resolve this problem, see for example [10] for a review.

Another important application of Hawking radiation is in the field of primordial black holes which could be a sizable fraction of the missing matter in our universe (see e.g. [11]). Indeed, Hawking radiation determines the lifetime of primordial black holes which could have been created in an early phase transition of our universe, for example, during inflation. If they are sufficiently long-lived, they could still be around today. If they are stable Planck mass objects they could constitute all of dark matter [12].

We should emphasize that Hawking's work assumes that black holes are essentially classical objects. It has been suggested that Bose-Einstein condensate could play an important role in astrophysics. Indeed, dark matter halos could be gigantic quantum objects made of Bose-Einstein condensates [13]. It has been speculated

that black holes could themselves be Bose-Einstein condensates [14], in which case they would be purely quantum objects which would not have Hawking radiation. If correct, this fascinating development implies that Bose-Einstein black holes do not suffer from the information paradox.

Black holes come in a wide range of masses from supermassive black holes at the center of galaxies to Planck-size quantum black holes. While astrophysical black holes have been observed, quantum black holes are much more speculative but as mentioned before also much more interesting since a proper description of their physical properties requires an understanding of general relativity in the quantum regime.

In this chapter we will be dealing with quantum black holes. We shall first describe the production cross section for quantum black holes. We will then describe how quantum black holes can be used to probe the scale of quantum gravity physics, first at colliders by direct production and then via effective field theories techniques. We shall then describe how stable quantum black holes, called remnants could resolve the information paradox of black holes and finally describe how quantum black holes lead to a thought experiment which demonstrates that a unification of quantum mechanics and general relativity implies the existence of a minimal length in nature. Finally we describe how quantum black holes could lead to small departure from locality and causality at energies of the order of the Planck scale.

1.2 Quantum Black Holes

As discussed above, the no-hair theorem [1] implies that a stationary black hole is a very simple object which can be fully described by only three quantities namely its mass, its angular momentum and its electric charge. Because black holes are characterised by a few quantum numbers, it is tempting to treat them as elementary particles and thus to include them in the Hilbert space, at least for the lightest of these objects.

The mass of a black hole is linked to its temperature. If the mass of the black hole is much larger than the Planck scale M_P, it is a classical object and it has a well defined temperature. The semi-classical region starts between 5 and 20 times the Planck scale [15]. Semi-classical black holes are also thermal objects. On the other hand, black holes with masses of the order of the Planck scale are non-thermal objects [16]. We shall call these Planckian objects quantum black holes. A thermal black hole will decay via Hawking radiation and thus couples effectively to many degrees of freedom. The decay of a non-thermal black hole is not well described by Hawking radiation. Rather than decaying to many degrees of freedom, one expects that it will only decay to a few particles only, typically two because this object is non-thermal.

The production of black holes in the high energy collision of elementary particles can be modeled by the collision of shockwaves. In the limit of the center of mass E_{CM} going to infinity, Penrose [17] and independently Eardley and Giddings [18]

have shown that even when the impact parameter is non zero a classical black hole ($M_{BH} \sim E_{CM} \gg M_P$) will form. They were able to prove the formation of a closed trapped surface. Their result justifies using the geometrical cross section to describe the production of black holes in the high energy collisions of two particles. It is given by

$$\sigma = \pi r_S^2 \theta(s - M_{BH}^2) \sim \frac{s}{M_P^4} \theta(s - M_{BH}^2), \tag{1.5}$$

where $s = E_{CM}^2$ is the center of mass squared, r_S the Schwarzschild radius and θ is the Heaviside step function. The step function implies a threshold for black hole formation. The work of Eardley and Giddings can be extrapolated into the semi-classical regime using path integral methods [19]. A final leap of faith leads to an extrapolation into the full quantum regime. It is usually assumed that the geometrical cross section holds for Planck size black holes as well. This has interesting consequences as we shall see shortly. Note that similar constructions can be developed in supersymmetric theories in which case quantum gravitational effects are easier to handle (see e.g. [20]).

1.3 Low Scale Quantum Gravity and Black Holes at Colliders

One of the most exciting developments in theoretical physics in the last 20 years has been the realization that the scale of quantum gravity could be in the TeV region instead of the usually assumed 10^{19} GeV. Indeed, the strength of gravity can be affected by the size of potential extra-dimensions [21–24] or the quantum fluctuations of a large hidden sector of particles [25].

Models with large extra dimensions assume that standard model excitations are confined to a $3+1$ sub-geometry, and employ the following trick. The higher dimensional action is of the form

$$S = \int d^4x \, d^{d-4}x' \, \sqrt{-g} \left(M_{fund}^{d-2} \mathscr{R} + \cdots \right) \tag{1.6}$$

and the effective $3+1$ gravitational energy scale (Planck scale) is given by

$$M_p^2 = M_{fund}^{d-2} V_{d-4} \tag{1.7}$$

where V_{d-4} is the volume of the extra dimensions. By taking V_{d-4} large, M_p can be made of order 10^{19} GeV while the fundamental scale $M_{fund} \sim$ TeV, at the cost of some strong dynamical assumptions about the geometry of space-time. There are different realizations of this idea. In the ADD, which stands for Arkani-Hamed et al. [21, 22] brane world model, the particles of the standard model are assumed to be confined to a three dimensional surface, called a brane, whereas gravity can propagate everywhere

i.e. on the brane and in the extra-dimensional volume called the bulk. The number of extra-dimensions is not determined from first principles. In the version proposed by Randall and Sundrum (RS) [24], a five-dimensional space-time is considered with two branes. In the simplest version of the RS model, the standard model particles are confined to the so-called IR brane while gravity propagates in the bulk as well. One of the main difficulties of models with large extra-dimensions is that of proton decay. In the case of RS, it was later on proposed to allow the leptons and quarks to propagate in the bulk to suppress proton decay operators [26].

While models with large extra-dimensions have been extensively studied, it is also possible to lower the Planck scale in four-dimensional models. The idea consists in playing with the renormalization of the Planck scale.

Let us consider matter fields of spin 0, 1/2 and 1 coupled to gravity:

$$S[g,\phi,\psi,A_\mu] = -\int d^4x\sqrt{-\det(g)}\ \left(\frac{1}{16\pi G_N}R + \frac{1}{2}g^{\mu\nu}\partial_\mu\phi\partial_\nu\phi + \xi R\phi^2 + e\bar{\psi}i\gamma^\mu D_\mu\psi + \frac{1}{4}F_{\mu\nu}F^{\mu\nu}\right) \tag{1.8}$$

where e is the tetrad, $D_\mu = \partial_\mu + w_\mu^{ab}\sigma_{ab}/2$ and w_μ^{ab} is the spin connection which can be expressed in terms of the tetrad, finally ξ is the non-minimal coupling.

We first study the contribution of the real scalar field with a non-minimal coupling $\xi = 0$ to the renormalization of the Planck mass. Consider the gravitational potential between two heavy, non-relativistic sources, which arises through graviton exchange (Fig. 1.1). The leading term in the gravitational Lagrangian is $G_N^{-1}R \sim G_N^{-1}h\Box h$ with $g_{\mu\nu} = \eta_{\mu\nu} + h_{\mu\nu}$. By not absorbing G_N into the definition of the small fluctuations h we can interpret quantum corrections to the graviton propagator from the loop in Fig. 1.1 as a renormalization of G_N. Neglecting the index structure, the graviton propagator with one-loop correction is

$$D_h(q) \sim \frac{iG_N}{q^2} + \frac{iG_N}{q^2}\Sigma\frac{iG_N}{q^2} + \cdots, \tag{1.9}$$

where q is the momentum carried by the graviton. The term in Σ proportional to q^2 can be interpreted as a renormalization of G_N, and is easily estimated from the Feynman diagram:

$$\Sigma \sim -iq^2\int^\Lambda d^4p\, D(p)^2p^2 + \cdots, \tag{1.10}$$

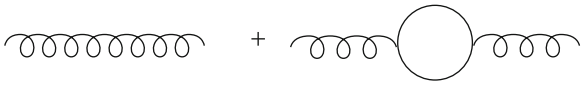

Fig. 1.1 Contributions to the running of Newton's constant

where $D(p)$ is the propagator of the particle in the loop. In the case of a scalar field the loop integral is quadratically divergent, and by absorbing this piece into a redefinition of G_N in the usual way one obtains an equation of the form

$$\frac{1}{G_{N,\text{ren}}} = \frac{1}{G_{N,\text{bare}}} + c\Lambda^2 , \tag{1.11}$$

where Λ is the ultraviolet cutoff of the loop and $c \sim 1/16\pi^2$. $G_{N,\text{ren}}$ is the renormalized Newton constant measured in low energy experiments. This result can be derived rigorously using the heat kernel method (see e.g. [27]).

The running of the reduced Planck mass due to non-minimally coupled real scalar fields, Weyl fermions and vector bosons can be deduced from the running of Newton's constant [25] see also [28–30]:

$$\bar{M}(\mu)^2 = \bar{M}(0)^2 - \frac{1}{16\pi^2}\left(\frac{1}{6}N_l + 2\xi N_\xi\right)\mu^2 \tag{1.12}$$

where μ is the renormalization scale and $N_l = N_S + N_F - 4N_V$ where N_S, N_F and N_V are respectively the numbers of real, minimally coupled, scalar fields, Weyl fermions and vector bosons in the model and N_ξ is the number of real scalar fields in the model with a non-minimal coupling to gravity. Note that the conformal value of ξ in our convention is $1/12$. The renormalization group equation at one loop for the reduced Planck mass is obtained using the heat kernel method which preserves the symmetries of the problem.

The scale at which quantum gravitational effects become strong, $\mu_\star$, follows from the requirement that the reduced Planck mass at this scale $\mu_\star$ be comparable to the inverse of the size of the fluctuations of the geometry, in other words, $\bar{M}(\mu_\star) \sim \mu_\star$. One finds:

$$\mu_\star = \frac{\bar{M}(0)}{\sqrt{1 + \frac{1}{16\pi^2}\left(\frac{1}{6}N_l + 2\xi N_\xi\right)}}. \tag{1.13}$$

Clearly the energy scale at which quantum gravitational effects become relevant depends on the number of fields present in the theory and on the non-minimal coupling ξ. While minimally coupled spin 0 and spin $1/2$ fields lower $\mu_\star$, spin 1 fields increase the effective reduced Planck mass and non-minimally coupled scalar fields can increase or lower $\mu_\star$ depending on the algebraic sign of ξ. The contribution of the graviton is a $1/N_l$ effect and very small if N_l is reasonably large.

There are different ways to obtain $\mu_\star = 1$ TeV. The first one is to introduce a large hidden sector of scalars and/or Weyl fermions with some 10^{33} particles. The other one is to consider a real scalar field that is non-minimally coupled with $\xi \sim 10^{32}$.

There are thus different models which can lead to an effective Planck scale which is very different from the naively assumed $\sim 10^{19}$ GeV. A dramatic signal of quantum gravity in the TeV region would be the production of small black holes in high energy collisions of particles at colliders. The possibility of creating small black holes at

colliders has led to some wonderful theoretical works on the formation of black holes in the collisions of particles.

Let us now discuss the production cross section for small black holes at colliders. Earlier estimate of the production cross section had been done using the hoop conjecture [31] which is a dynamical condition for gravitational collapse. It states that if an amount of energy E is confined at any instant to a ball of size R, where $R < E$, then that region will eventually evolve into a black hole. Here we use natural units where $\hbar$, c and Newton's constant (or the Planck length l_P) are unity. We have also neglected numerical factors of order one. Although the hoop conjecture is, as its name says, a conjecture, it rests on firm footing. The least favorable case, i.e. as asymmetric as possible, is the one of two particles colliding head on. For that reason, some did not trust the hoop conjecture, thinking that in the collision of particles the situation was too asymmetrical to trust this conjecture. As explained above, the paper of Eardley and Giddings [18] settled the issue. Proving the formation of a closed trapped surface is enough to establish gravitational collapse and hence the formation of a black hole. As mentioned already, this work has been extended into the semi-classical region using path integral methods [19] . One can thus claim with confidence that black holes with masses 5 to 20 times the Planck scale, depending on the model of quantum gravity, could form in the collision of particles at the CERN LHC if the Planck scale was low enough. Early phenomenological studies can be found in [32–38]. The cross section for semi-classical black holes is taken to be:

$$\sigma^{pp}(s, x_{\rm min}, n, M_D) = \int_0^1 2zdz \int_{\frac{(x_{min}M_D)^2}{y(z)^2 s}}^1 du \int_u^1 \frac{dv}{v} \times F(n)\pi r_s^2(us, n, M_D) \sum_{i,j} f_i(v, Q) f_j(u/v, Q) \tag{1.14}$$

where $x_{\rm min} = M_{BH,\rm min}/M_D$, M_D is the reduced Planck scale, Q is the momentum transfer variable, n is the number of extra-dimensions, $F(n)$ and $y(z)$ are the factors introduced by Eardley and Giddings and by Yoshino and Nambu [39, 40]. The factors $F(n)$ describe the deviation from head-on collision while the inelasticity factors $y(z)$ describe the energy lost in terms of gravitational radiation. The n dimensional Schwarzschild radius is given by:

$$r_s(us, n, M_D) = k(n) M_D^{-1} [\sqrt{us}/M_D]^{1/(1+n)} \tag{1.15}$$

where

$$k(n) = \left[2^n \sqrt{\pi}^{n-3} \frac{\Gamma((3+n)/2)}{2+n} \right]^{1/(1+n)}, \tag{1.16}$$

and M_D is the reduced Planck mass. $M_{BH,min}$ is defined as the minimal value of black hole mass for which the semi-classical extrapolation can be trusted.

The decomposition of semi-classical black holes is well described by Hawking radiation, however this classical work has to be extend to extra-dimensional space-times (see e.g. [7]).

However, it is obvious that even if the Planck scale was precisely at 1 TeV not many semi-classical black holes could be produced at the LHC since the center of mass energy of the collisions between the protons was at most of 8 TeV so far [15]. Even with the 14 TeV LHC, not many if any semi-classical black holes will be produced since the semi-classical regime starts at 5–20 times the Planck scale.

We thus focussed on quantum black holes, which are black holes with masses of the order of the Planck mass which could be produced copiously at the LHC or in cosmic ray experiments [16, 27, 41–48]. As explained before, we assume that the cross section for quantum black holes can be extrapolated from that of semi-classical black holes. Searches are based on the well justified assumption that quantum black holes preserve gauged quantum numbers such as $SU(3)_c$ or $U(1)_{em}$. One can thus classify the quantum black holes which would be produced in the high energy collisions of partons at the LHC according to the quantum numbers of these partons. Generically speaking, quantum black holes form representations of $SU(3)_c$ and carry a QED charge. The process of two partons p_i, p_j forming a quantum black hole in the c representation of $SU(3)_c$ and charge q as: $p_i + p_j \rightarrow \mathrm{QBH}_c^q$ is considered in [16]. The following different transitions are possible at a proton collider:

(i) $\mathbf{3} \times \bar{\mathbf{3}} = \mathbf{8} + \mathbf{1}$

(ii) $\mathbf{3} \times \mathbf{3} = \mathbf{6} + \bar{\mathbf{3}}$

(iii) $\mathbf{3} \times \mathbf{8} = \mathbf{3} + \bar{\mathbf{6}} + \mathbf{15}$

(iv) $\mathbf{8} \times \mathbf{8} = \mathbf{1}_S + \mathbf{8}_S + \mathbf{8}_A + \mathbf{10} + \overline{\mathbf{10}}_A + \mathbf{27}_S$

Most of the time the black holes which are created in the collision of partons will carry a $SU(3)_c$ charge as well as QED charge. This allows to predict how they will decay since these charges have to be carried by the final state particles.

It is interesting to note that quantum black holes can be represented by quantum fields [46]. As a matter of simplicity, let us focus on the production of spinless quantum black holes in the collisions of two fermions (quarks for example with the appropriate color factor). We start with the Lagrangian

$$L_{fermion+fermion} = \frac{c}{\bar{M}_p^2} \partial_\mu \partial^\mu \phi \bar{\psi}_1 \psi_2 + h.c. \tag{1.17}$$

where c is a (non-local) parameter we will use to match the semiclassical cross section, $\bar{M}_p$ is the reduced Planck mass, ϕ is a scalar field representing the quantum black hole, and ψ_i is a fermion field. The cross section for ϕ production is:

$$\sigma(2\psi \rightarrow \phi) = \frac{\pi}{s} |A|^2 \delta(s - M_{BH}^2) \tag{1.18}$$

where M_{BH} is the mass of the black hole, $s = (p_1 + p_2)^2$ and p_1, p_2 are the four-momenta of ψ_1 ψ_2. We find [46]

$$|A|^2 = s^2 \frac{c^2}{\bar{M}_p^4} \left(s - (m_1 + m_2)^2\right) \tag{1.19}$$

where m_1 and m_2 are the masses of the fermions ψ_1 and ψ_2. We now compare this cross section with the geometrical cross section. If we use the representation for the delta-function:

$$\delta(s - M_{BH}^2) = \frac{\Gamma M_{BH}}{\pi \left((s - M_{BH}^2)^2 + \Gamma^2 M_{BH}^2\right)} \tag{1.20}$$

where Γ is the decay width of ϕ we find:

$$c^2 = \frac{9}{4} \frac{4s^{\frac{3}{2}} - 8sM_{BH} + 4\sqrt{s}M_{BH}^2 + \sqrt{s}\Gamma^2}{\Gamma\pi \left(s - (m_1 + m_2)^2\right)} \tag{1.21}$$

Finally Γ can be calculated using the Lagrangian (1.17) as:

$$\Gamma = \frac{c^2}{8\pi} \frac{M_{BH}\sqrt{(M_{BH}^2 - (m_1 + m_2)^2)(M_{BH}^2 - (m_1 - m_2)^2)}}{\bar{M}_p^4} \tag{1.22}$$

We can thus find an expression for our non-local parameter c by inserting Γ into the expression for c (1.21). In the case $m_1 = m_2 = 0$, one has a remarkably simple expression:

$$c^2 = \frac{8\pi \bar{M}_p^4 (s - M_{BH}^2)}{M_{BH}^3 \sqrt{128\pi^2 \bar{M}_p^4 s - M_{BH}^6}} \tag{1.23}$$

Obviously our results could be generalized easily to the case of higher dimensional quantum black holes or to initial state particles with different spins and colors. Such representations can be useful in implementing quantum black holes into event generators based on a Lagrangian approach. Note that we have considered the case of a single quantum black hole with a definite (i.e. not continuous) mass here.

The current bound derived using LHC data on the first quantum black hole mass is of the order of 5.3 TeV [49–51]. Note that this bound is slightly model dependent. However, this is a clear sign that there are no quantum gravitational effects at 1 TeV.

1.4 An Effective Theory for Quantum Gravity

Instead of trying to probe the Planck scale directly by producing small black holes directly at colliders, it is useful to think of alternative ways to probe the scale of quantum gravity. Effective field theory techniques are very powerful when we know the symmetries of the low energy action which is the case for the standard model of particle physics coupled to general relativity. Integrating out all quantum gravitational effects, we are left with an effective action which we can use to probe the scale of quantum gravity at low energies. We thus consider:

$$S = \int d^4x \sqrt{-g} \left[\left(\frac{1}{2} M^2 + \xi H^\dagger H \right) R - \Lambda_C^4 + c_1 R^2 + c_2 R_{\mu\nu} R^{\mu\nu} + L_{SM} + O(M_\star^{-2}) \right] \tag{1.24}$$

The Higgs boson H has a non-zero vacuum expectation value, $v = 246$ GeV and thus contribute to the value of the reduced Planck scale:

$$(M^2 + \xi v^2) = \bar{M}_P^2. \tag{1.25}$$

The parameter ξ is the non-minimal coupling between the Higgs boson and space-time curvature. The three parameters c_1, c_2 and ξ are dimensionless free parameters. The Planck scale $\bar{M}_P$ is equal to 2.4335×10^{18} GeV and the cosmological constant Λ_C is of order of 10^{-3} eV. The scale of the expansion $M_\star$ is often identified with M_P but there is no necessity for that and experiments are very useful to set limits on higher dimensional operators suppressed by $M_\star$. Submillimeter pendulum tests of Newton's law [52] are used to set limits on c_1 and c_2. In the absence of accidental cancellations between the coefficients of the terms R^2 and $R_{\mu\nu}R^{\mu\nu}$, these coefficients are constrained to be less than 10^{61} [25]. It has been shown that astrophysical observations are unlikely to improve these bounds [53]. The LHC data can be used to set a limit on the value of the Higgs boson non-minimal coupling to space-time curvature: one finds that $|\xi| > 2.6 \times 10^{15}$ is excluded at the 95 % C.L. [54]. Very little is known about higher dimensional operators. The Kretschmann scalar $K = R^{\mu\nu\rho\sigma} R_{\mu\nu\rho\sigma}$ which can be coupled to the Higgs field via $KH^\dagger H$ has been studied in [55], but it seems that any observable effect requires an anomalously large Wilson coefficient for this operator. Clearly one will have to be very creative to find a way to measure the parameters of this effective action. This is important as these terms are in principle calculable in a theory of quantum gravity and this might be the only possibility to ever probe quantum gravity indirectly.

Finally we note that this effective theory approach can be useful to probe specific models. For example, Higgs inflation with a non-minimal coupling of the Higgs boson to curvature [56] requires $\xi = 10^4$, while Starobinsky inflation R^2 [57] requires $c_1 \sim 10^9$. Unfortunately, the bounds on the coefficient of the effective action are still too weak to probe this parameter range.

Planck suppressed operators can also have an important impact in grand unified theories. For example, the lowest order effective operators induced by a quantum

theory of gravity are of dimension five, such as [58–62]

$$\frac{c_5}{\bar{M}_P}\mathrm{Tr}\left(G_{\mu\nu}G^{\mu\nu}H\right), \tag{1.26}$$

where $G_{\mu\nu}$ is the grand unified theory field strength and H is a scalar multiplet. These operators can modify the unification condition of the gauge couplings of the standard model. It was pointed out in [58, 59], that supersymmetry is not needed to obtain the numerical unification of the gauge couplings of the standard model if these operators are present. Furthermore, Planckian effects can spoil the unification in supersymmetric theories [58]. It is thus impossible to claim, as done in e.g. [63], that a specific model of low energy physics leads to satisfactory unification at the grand unification scale without making strong assumptions about quantum gravitational effects. The same is true of the Yukawa sector [64–66], operators of the type

$$\frac{c_5}{\bar{M}_P}\bar{\Psi}\phi\Psi H + h.c. \tag{1.27}$$

where Ψ are fermion fields, ϕ and H some scalar bosons multiplets chosen in appropriate representations, give sizable contributions to the unification of the Yukawa couplings [64].

So far, in this section, we have considered the parametrization of quantum gravitational effects within the standard model of particle physics or grand unified theories. We now discuss how to parametrize quantum black hole effects in cosmology. There are strong reasons to believe that the universe went through a period of inflation in the very first moments of its existence. This most likely requires the introduction of a new scalar degree of freedom called the inflation. We consider the most generic effective theory for a scalar field ϕ coupled to gravity [67]:

$$S = \int d^4x\sqrt{-g}\left(\frac{\bar{M}_P^2}{2}R + f(\phi)F(R, R_{\mu\nu}) + g^{\mu\nu}\partial_\mu\phi\partial^\nu\phi + V_{ren}(\phi) + \sum_{n=5}^{\infty} c_n\frac{\phi^n}{\bar{M}_P^{n-4}}\right), \tag{1.28}$$

where here again $\bar{M}_P$ is the reduced Planck scale, and $V_{ren}(\phi)$ contains all renormalizable terms up to dimension-four, for example $V_{ren} \supset v^3\phi + m^2\phi^2 + \lambda_3\phi^3 + \lambda_4\phi^4$, and c_n are Wilson coefficients of the higher-dimensional operators. This effective action can be viewed as an effective action which results from integrating out quantum black holes from the path integral. It was shown in [68] that such operators could help to escape tensions arising when fitting CMB data coming from different observations. It should be emphasized that these higher dimensional operators are usually seen as a challenge for models of inflation since they can easily destabilize the scalar potential which needs to be sufficiently flat to produce enough inflation. Model builders often invoke a shift symmetry to try to prevent these terms as these operators can lead to large effects and destabilize the inflaton potential which, in large field models, needs to be very flat to produce enough inflation.

1.5 Quantum Black Holes in Loops

It is often argued that Planck size black holes may affect low energy measurements because of the large multiplicity of states. This is particularly true if one thinks of Planck size black holes as remnants which could resolve the information paradox of black holes, see e.g. for a review [69], by storing the information within the volume in their Schwarzschild radius.

Our first observation is that the on-shell production of the lightest possible black holes, i.e. Planckian quantum black holes, if we accept the geometrical cross section, would require doing collisions at the Planck scale which is conservatively taken to be of the order of 10^{19} GeV since there is a step function in energy which implies an energy threshold. We have never probed physics beyond the few TeV region directly at colliders and cosmic ray collisions have center of mass energies of a few 100 TeV. Unless we live in a world with large extra-dimensions [22, 24] or with large hidden sector of hidden particles [25], there is no reason to expect to produce on-shell Planckian quantum black holes in low energy experiments since the center of mass energy of such collisions is below the production threshold according to the geometrical cross section. Direct production thus cannot probe the existence of Planckian quantum black holes or remnants.

If one considers quantum field theoretical corrections to particle physics processes, the situation is different. Let us consider the contribution of quantum black holes in loops, i.e. virtual quantum black holes. For definiteness let us consider a single spin-0 black hole with mass M_{BH}. If we close a loop with a massive scalar field of mass M_{BH}, one expects contributions to loops of the type

$$I = \int_0^{\Lambda} d^4p \frac{1}{p^2 - M_{BH}^2 + i\varepsilon} \tag{1.29}$$

where Λ is some ultra-violet cutoff. Such integrals behave as Λ^4/M_{BH}^2 for momenta much smaller than M_{BH}. The cutoff Λ is much smaller than M_{BH} since we are looking at low energy experiments. Heavy particles decouple from the low energy effective theory as naively expected. When one calculates the anomalous magnetic moment of the muon, one need not worry about very high energy embeddings of the standard model such as grand unified theories. One probes, as we shall see shortly, at most the few TeV region if new physics respects chirality or the 10^7 GeV region if it does not. As long as a high energy theory does not violate symmetries of the low energy effective theory, one expects its particles to decouple from the low energy regime.

The situation for quantum black holes is different since the spectrum of quantum gravity contains potentially a large number of states. If we sum over the number N of scalar fields with masses $M_{BH,i}$ (where i stands for the *i-th* quantum black hole) these contributions can be very large and potentially impact in a sizable way low energy observables. In the case of a continuous mass spectrum however, the sum is replaced by an integral over the mass spectrum of the black holes. We have

$$I = \int_{M_{BH,l}}^{M_{BH,h}} \frac{\Lambda^4}{M^2} \rho(M) dM \tag{1.30}$$

where $\rho(M_{BH})$ is the black hole mass density, $M_{BH,l}$ is the lightest black hole mass, while $M_{BH,h}$ is the heaviest mass a black hole can have. For a single black hole, $\rho(M_{BH}) = \delta(M - M_{BH})$ while for a continuous mass spectrum, one has $\rho(M) = NM^{-1}$ where N is the number of black states which leads to

$$I_{continuous} = \int_{M_{BH,l}}^{M_{BH,h}} \frac{\Lambda^4}{M^2} \rho(M) dM \sim \frac{\Lambda^4 (M_{BH,h}^2 - M_{BH,l}^2)}{M_{BH,h}^2 M_{BH,l}^2} N. \tag{1.31}$$

Here N is the number of black holes states between $M_{BH,h}$ and $M_{BH,l}$, which is indeed infinite for a continuous mass distribution. Furthermore, in the case of remnants as a solution to the information paradox, it is argued that their might be large multiplicity factor $\mathscr{M}$ arising from a sum over all the possible quantum numbers of the black holes contributing in the loop. This is the standard argument against the resolution of the black hole information paradox based on remnants [70]. It would apply as well to quantum black holes predicted by models of low scale quantum gravity.

The aforementioned work on the production of black holes in the collisions of particles at very high energy can help us to identify reasonable values for $M_{BH,h}$ and $M_{BH,l}$. The lightest black hole produced cannot have a mass below M_P, we shall thus identify $M_{BH,l} \sim M_P$. On the other hand, we know that black holes with mass 5–20 times M_P are semi-classical objects. It does not make much sense to include these objects in the Hilbert space and we should thus identify $M_{BH,h}$ with 5–20 M_P. The contribution of quantum black holes to the loop integral discussed above is thus of the order of

$$I_{continuous} = \frac{\Lambda^4}{M_P^2} N \mathscr{M} \tag{1.32}$$

Since $\Lambda \ll M_P$ as we are interested in low energy experiments, the number of states N and the potential large multiplicity $\mathscr{M}$ are the source of potentially large contributions to low energy physics observables.

An obvious solution to the large (actually infinite) factor N is that the spectrum of quantum black holes with masses up to 5–20 M_P is quantized. This is perfectly reasonable as we have strong arguments in favor of a quantization of space-time in terms of the Planck scale [71, 72]. If we assume that the mass spectrum in quantized is terms of M_P then $N = 5$–20 and is not a large factor.

Let us now discuss how large $\mathscr{M}$ might be. Its value depends on whether quantum black holes have hair or not. If we naively extrapolate from classical objects, one would expect the no-hair theorem to hold. In the case of remnants one could argue that the information is contained inside the black hole horizon but that for an observer outside the black hole, the black hole is still described in terms of very few quantities, namely its mass, its angular momentum and its electric charge. In that case, the multiplicity factor $\mathscr{M}$ is small and the contribution of quantum black holes to low

energy observables is negligible. The following thought experiment shows that in all likelihood quantum black holes are slightly more complicated than their classical counterparts. If we think of the creation of a quantum black holes in the collision of two colored particles, we have to accept that either the black hole is not formed or that the quantum black hole will carry the color charges of the particles which created it. Quantum numbers corresponding to gauged quantities must be conserved. However, in that case we do not expect $\mathscr{M}$ to be large, it will merely be a group theoretical factor. Such factors are usually of order unity. While the no-hair theorem probably cannot be valid for quantum black holes if they exist, we do not expect that there will be a multitude of new quantum numbers carried by the black holes, merely the quantum numbers corresponding to the gauge groups of the standard model of particle physics. Even though two remnants may contain different information inside their Schwarzschild radius, if their quantum numbers observed by an outside observer are the same, they should be treated as only one state of the Hilbert space and there will not be a large multiplicity of states from the low energy effective theory point of view.

We now show that the number of quantum black hole states is not strongly constrained by low energy experiments. One of the most precise experiments done to date is that of the measurement of the anomalous magnetic moment of the muon. If gravity respects chiral symmetry as perturbative quantum gravity indicates, Quantum black holes will typically lead to dimension 6 operators of the type [46]

$$N\frac{e}{2}\frac{m_\mu}{16\pi^2\bar{M}_P^2}\bar{\psi}\sigma_{\mu\nu}\psi F^{\mu\nu} \tag{1.33}$$

where e is the electron charge, N is the number of quantum black holes propagating in the diagram depicted in Fig. 1.2, $\bar{M}_P$ is the reduced Planck mass, m_μ is the muon mass, ψ its wavefunction and $F^{\mu\nu}$ the electromagnetic field strength tensor. The generic bound on the scale of new physics Λ_{NP} which suppresses a dimension six operator $(e/2 \times m_\mu/\Lambda_{NP}^2)\bar{\psi}\sigma_{\mu\nu}\psi F^{\mu\nu}$ [73] is of the order of a few TeV. We can

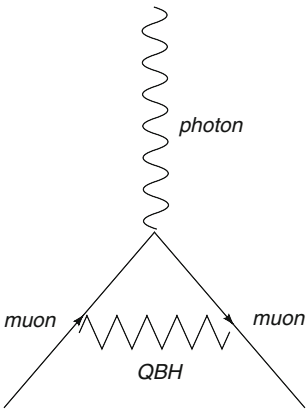

Fig. 1.2 Contribution of a quantum black hole (QBH) to the muon anomalous magnetic moment

thus use this result to set a bound on N which appears in Eq. (1.33). We find $N < 16\pi^2 M_P^2/\Lambda_{NP}^2 \sim 10^{32}$ which is a very weak bound. We thus see that unless there is truly an infinite number of quantum black holes states, they cannot impact low energy observables in a sizeable manner.

The bound is slightly tighter if chirality is violated by quantum gravity at the non-perturbative level, one expects low energy effective operators of the type

$$N\frac{e}{2}\frac{1}{\bar{M}_P}\bar{\psi}\sigma_{\mu\nu}\psi F^{\mu\nu}. \tag{1.34}$$

Note that perturbative effects cannot violate chirality, if such an effect happens it is at the non-perturbative level and we thus do not include the factor $16\pi^2$ in the denominator. The bound on the scale of new physics suppressing the operator $(e/2 \times 1/\Lambda_{NP})\bar{\psi}\sigma_{\mu\nu}\psi F^{\mu\nu}$ is of the order of 2.5×10^7 GeV [73]. We thus get a bound on N of the order of 10^{11}.

We see that the bounds on the number of quantum black holes (or remnants) interacting with low energy particles are rather weak unless some low energy symmetry is violated by quantum gravity. There is thus no reason, from a low energy effective theory point of view to rule out Planck size quantum black holes or remnants. Remnants are thus a perfectly acceptable solution to the black hole information paradox.

After discussing some physical implications of quantum black holes, we now focus our attention towards a thought experiment involving quantum black holes. This thought experiment reveals that a unification of general relativity and quantum mechanics implies a minimal length in nature. We note that there has been attempts to incorporate this minimal length into black hole physics (see e.g. [74]).

1.6 Quantum Black Holes and the Unification of General Relativity and Quantum Mechanics

Twentieth century Physics has been a quest for unification. The unification of quantum mechanics and special relativity required the introduction of quantum field theory. The unification of magnetism and electricity led to electrodynamics, which was unified with the weak interactions into the electroweak interactions. There are good reasons to believe that the electroweak interactions and the strong interactions originate from the same underlying gauge theory: the grand unified theory. If general relativity is to be unified with a gauge theory, one first needs to understand how to unify general relativity and quantum mechanics, just as it was first necessary to understand how to unify quantum mechanics and special relativity before three of the forces of nature could be unified. The aim of this section is much more modest–we want to understand some of the features of a quantum mechanical description of general relativity using some simple tools from quantum mechanics and general relativity. In particular, we shall show that if quantum mechanics and general relativity

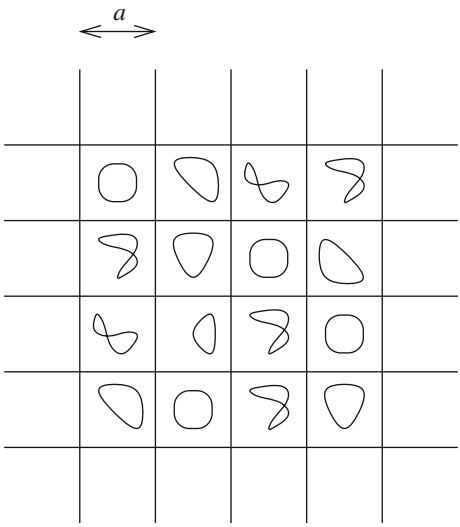

Fig. 1.3 We choose a spacetime lattice of spacing a of the order of the Planck length or smaller. This formulation does not depend on the details of quantum gravity

are valid theories of nature up to the Planck scale, they imply the existence of a minimal length in nature [75–78]. Black holes play a central role in this derivation.

We will review the results obtained in [71]. We show that quantum mechanics and classical general relativity considered simultaneously imply the existence of a minimal length in the following sense: no operational procedure exists that can measure a distance less than this fundamental length. The key ingredients used to reach this conclusion are the uncertainty principle from quantum mechanics and gravitational collapse from classical general relativity (i.e. black holes) in forms of the hoop conjecture we have encountered earlier on.[1]

From the hoop conjecture and the uncertainty principle, we immediately deduce the existence of a minimum ball of size l_P. Consider a particle of energy E which is not already a black hole. Its size r must satisfy

$$r \sim \mathbf{max}\left[\, 1/E\,,\; E\,\right], \tag{1.35}$$

where $\lambda_C \sim 1/E$ is its Compton wavelength and E arises from the hoop conjecture. Minimization with respect to E results in r of order unity in Planck units or $r \sim l_P$. If the particle *is* a black hole, then its radius grows with mass: $r \sim E \sim 1/\lambda_C$. This relationship suggests that an experiment designed (in the absence of gravity) to measure a short distance $l << l_P$ will (in the presence of gravity) only be sensitive to scales $1/l$.

[1] In this section, we set $\hbar = 1$, $c = 1$ and $G_N = 1$.

Let us give a concrete model of minimum length. Let the position operator $\hat{x}$ have discrete eigenvalues $\{x_i\}$, with the separation between eigenvalues either of order l_P or smaller. (For regularly distributed eigenvalues with a constant separation, this would be equivalent to a spatial lattice, as seen in Fig. 1.3). We do not mean to imply that in Nature a minimum length is realized in this particular fashion—most likely, the physical mechanism is more complicated and may involve, for example, spacetime foam or strings. However, our concrete formulation lends itself to detailed analysis. We show below that this formulation cannot be excluded by any gedanken experiment, which is strong evidence for the existence of a minimum length.

Quantization of position does not by itself imply quantization of momentum. Conversely, a continuous spectrum of momentum does not imply a continuous spectrum of position. In a formulation of quantum mechanics on a regular spatial lattice, with spacing a and size L, the momentum operator has eigenvalues which are spaced by $1/L$. In the infinite volume limit the momentum operator can have continuous eigenvalues even if the spatial lattice spacing is kept fixed. This means that the displacement operator

$$\hat{x}(t) - \hat{x}(0) = \hat{p}(0)\frac{t}{M} \tag{1.36}$$

(where t is the time of the measurement and M the mass of the system under consideration) does not necessarily have discrete eigenvalues (the right hand side of (1.36) assumes free evolution; we use the Heisenberg picture throughout). Since the time evolution operator is unitary, the eigenvalues of $\hat{x}(t)$ are the same as $\hat{x}(0)$. Importantly, though, the spectrum of $\hat{x}(0)$ (or $\hat{x}(t)$) is completely unrelated to the spectrum of the $\hat{p}(0)$, even though they are related by (1.36). A measurement of arbitrarily small displacement (1.36) does not exclude our model of minimum length. To exclude it, one would have to measure a position eigenvalue x *and* a nearby eigenvalue x', with $|x - x'| << l_P$.

Many minimum length arguments are obviated by the simple observation of the minimum ball. However, the existence of a minimum ball does not by itself preclude the localization of a macroscopic object to very high precision. Hence, one might attempt to measure the spectrum of $\hat{x}(0)$ through a time of flight experiment in which wavepackets of primitive probes are bounced off of well-localised macroscopic objects. Disregarding gravitational effects, the discrete spectrum of $\hat{x}(0)$ is in principle obtainable this way. But detecting the discreteness of $\hat{x}(0)$ requires wavelengths comparable to the eigenvalue spacing. For eigenvalue spacing comparable or smaller than l_P, gravitational effects cannot be ignored because the process produces minimal balls (black holes) of size l_P or larger. This suggests that a direct measurement of the position spectrum to accuracy better than l_P is not possible. The failure here is due to the use of probes with very short wavelength.

A different class of instrument, the interferometer, is capable of measuring distances much smaller than the size of any of its sub-components. Nevertheless, the uncertainty principle and gravitational collapse prevent an arbitrarily accurate measurement of eigenvalue spacing. First, the limit from quantum mechanics—consider

the Heisenberg operators for position $\hat{x}(t)$ and momentum $\hat{p}(t)$ and recall the standard inequality

$$(\Delta A)^2(\Delta B)^2 \geq \ -\frac{1}{4}(\langle[\hat{A},\hat{B}]\rangle)^2. \tag{1.37}$$

Suppose that the position of a *free* test mass is measured at time $t = 0$ and *again* at a later time. The position operator at a later time t is

$$\hat{x}(t) = \hat{x}(0) \ + \ \hat{p}(0)\frac{t}{M}. \tag{1.38}$$

We assume a free particle Hamiltonian here for simplicity, but the argument can be generalized [71]. The commutator between the position operators at $t = 0$ and t is

$$[\hat{x}(0), \hat{x}(t)] \ = \ i\frac{t}{M}, \tag{1.39}$$

so using (1.37) we have

$$|\Delta x(0)||\Delta x(t)| \geq \frac{t}{2M}. \tag{1.40}$$

We see that at least one of the uncertainties $\Delta x(0)$ or $\Delta x(t)$ must be larger than of order $\sqrt{t/M}$. As a measurement of the discreteness of $\hat{x}(0)$ requires *two* position measurements, it is limited by the greater of $\Delta x(0)$ or $\Delta x(t)$, that is, by $\sqrt{t/M}$,

$$\Delta x \equiv \ \mathbf{max}\,[\Delta x(0), \Delta x(t)] \geq \sqrt{\frac{t}{2M}}, \tag{1.41}$$

where t is the time over which the measurement occurs and M the mass of the object whose position is measured. In order to push Δx below l_P, we take M to be large. In order to avoid gravitational collapse, the size R of our measuring device must also grow such that $R > M$. By causality, however, R cannot exceed t. Any component of the device a distance greater than t away cannot affect the measurement, hence we should not consider it part of the device. These considerations can be summarized in the inequalities

$$t > R > M. \tag{1.42}$$

Combined with (1.41), they require $\Delta x > 1$ in Planck units, or

$$\Delta x > l_P. \tag{1.43}$$

Notice that the considerations leading to (1.41), (1.42) and (1.43) were in no way specific to an interferometer, and hence are *device independent*. We repeat: no device

subject to quantum mechanics, gravity and causality can exclude the quantization of position on distances less than the Planck length.

It is important to emphasize that we are deducing a minimum length which is parametrically of order l_P, but may be larger or smaller by a numerical factor. This point is relevant to the question of whether an experimenter might be able to transmit the result of the measurement before the formation of a closed trapped surface, which prevents the escape of any signal. If we decrease the minimum length by a numerical factor, the inequality (1.41) requires $M >> R$, so we force the experimenter to work from deep inside an apparatus which has far exceeded the criteria for gravitational collapse (i.e. it is much denser than a black hole of the same size R as the apparatus). For such an apparatus a horizon will already exist before the measurement begins. The radius of the horizon, which is of order M, is very large compared to R, so that no signal can escape.

An implication of our result is that there may only be a finite number of degrees of freedom per unit volume in our universe—no true continuum of space or time. Equivalently, there is only a finite amount of information or entropy in any finite region of our universe.

One of the main problems encountered in the quantization of gravity is a proliferation of divergences coming from short distance fluctuations of the metric (or graviton). However, these divergences might only be artifacts of perturbation theory: minimum length, which is itself a non-perturbative effect, might provide a cutoff which removes the infinities. This conjecture could be verified by lattice simulations of quantum gravity (for example, in the Euclidean path integral formulation), by checking to see if they yield finite results even in the continuum limit.

1.7 Quantum Black Holes, Causality and Locality

A minimal length could be a sign of non-local interactions at the Planck scale. In this section, we study another indication that a unification of quantum mechanics and general relativity must lead to non-local effects. Our main result is a calculation of the mass and width of the lightest black hole. These black holes lead to tiny acausal effects at energy scales comparable to the Planck scale. We show that the mass of the black hole precursors is dependent on the number of fields in the theory.

Recently, there has been a renewed interest in the gravitational scattering of fields and the question of whether perturbative unitarity could be violated below the Planck scale [79–87]. By studying the two to two elastic gravitational scattering of fields, it

Fig. 1.4 Resummation of the gravitaton propagator

has been argued that perturbative unitarity is violated at an energy scale $E \sim \bar{M}_P/\sqrt{N}$ [85], where N is loosely speaking the number of fields in the model and $\bar{M}_P$ the reduced Planck mass. However, it has been shown in [83] that perturbative unitarity is restored by resumming an infinite series of matter loops on a graviton line (see Fig. 1.4) in the large N limit, where N stands for the number of fields in the model, while keeping NG_N small. This large N resummation leads to resummed graviton propagator given by

$$iD^{\alpha\beta,\mu\nu}(q^2) = \frac{i\left(L^{\alpha\mu}L^{\beta\nu} + L^{\alpha\nu}L^{\beta\mu} - L^{\alpha\beta}L^{\mu\nu}\right)}{2q^2\left(1 - \frac{NG_Nq^2}{120\pi}\log\left(-\frac{q^2}{\mu^2}\right)\right)} \tag{1.44}$$

with $L^{\mu\nu}(q) = \eta^{\mu\nu} - q^\mu q^\nu/q^2$, $N = N_s + 3N_f + 12N_V$ where N_s, N_f and N_V are respectively the number of real scalar fields, fermions and spin 1 fields in the model. This mechanism was dubbed self-healing by the authors of [83]. While [83] emphasized the fact that perturbative unitarity is restored by the resummation, the authors of [85] who had studied the same phenomenon before had pointed out that the denominator of this resummed propagator has a pair of complex poles which lead to acausal effects (see also [88, 89] for earlier work in the same direction and where essentially the same conclusion was reached). These acausal effects should become appreciable at energies near $(G_N N)^{-1/2}$. Unitarity is restored but at the price of non-causality.

We propose to interpret these complex poles as Planck size black hole precursors or quantum black holes. This enables us to calculate the mass and the width of the lightest black hole. This pair of complex poles which appears at an energy of about $(G_N N)^{-1/2}$ is a sign of strong gravitational dynamics. It is thus natural to think that this is the energy scale at which black holes start to form. Note that our interpretation is not controversial, one expects black holes to have a lifetime of order their Schwarzschild radius and thus to be described by propagators of the type $(s - M_{BH}^2 + iM_P^2)^{-1}$ [90]. Let us now calculate the poles of the resummed propagator (1.44). We find

$$\begin{aligned} q_1^2 &= 0, \\ q_2^2 &= \frac{1}{G_N N}\frac{120\pi}{W\left(\frac{-120\pi M_P^2}{\mu^2 N}\right)}, \\ q_3^2 &= (q_2^2)^*, \end{aligned} \tag{1.45}$$

where $W(x)$ is the Lambert W-function. It is easy to see that for $\mu \sim M_P$, $q_{2/3} \sim (G_N N)^{-1/2}$ as mentioned previously. The resummed propagator has three poles, one at $q^2 = 0$ which corresponds to the usual massless graviton and a pair of complex poles $q_{2,3}^2$. In the standard model of particle physics, one has $N_s = 4$, $N_f = 45$, and $N_V = 12$. We thus find $N = 283$ and the pair of complex poles at $(7 - 3i) \times 10^{18}$ GeV and $(7 + 3i) \times 10^{18}$ GeV. The first of these pair of poles corresponds to an object with

mass 7×10^{18} GeV with a width Γ of 6×10^{18} GeV. In our interpretation, these are the mass and width of the lightest of black holes assuming that the standard model of particle physics is valid up to the Planck scale.[2] It is a quantum black hole with a mass just above the reduced Planck scale (2.435×10^{18} GeV) and a lifetime given by $1/\Gamma$. Obviously, these estimates depend on the renormalization scale. Since the only scale in the problem is the reduced Planck scale, here we have taken μ of the order of the reduced Planck scale. We have checked that our predictions are not numerically very sensitive to small changes of the renormalization scale. Note that we have used the definition for the mass and width introduced in [91], namely we identify the mass and width of the black hole precursor with the position of pole in the resummed propagator: $p_0^2 = (m - i\Gamma/2)^2$. The second complex pole at $(7 + 3i) \times 10^{18}$ GeV leads to the acausal effects.

Since black holes are extended objects with a radius $R_S = 2G_N M/c^2$, it is not surprising that they lead to non-local effects. It has been shown in [92] that the momentum space equivalent of the non-local term in the resummed propagator is of the type

$$S = \int d^4x \sqrt{g} \left[R \log \left(\frac{\Box}{\mu^2} \right) R \right]. \tag{1.46}$$

Furthermore, it has been argued by Wald in [93] that when the space-time metric is treated as a quantum field, there should be fluctuations in the local light cone structure which could be large at the Planck scale. These fluctuations imply that the causal relationships between events may not be well defined and that there is a nonzero probability for acausal propagation at energies around the Planck scale. The Planckian black hole we are studying here is the black hole for which quantum gravitational effects are the most important of all, it is thus not very surprising that it leads to acausal effect according to Wald's argument. Note that acausal effects of this type have been discussed in the framework of the Lee Wick formalism [94, 95] (see also [96] for more recent work in that direction).

With our interpretation in mind, a consistent and beautiful picture emerges. Self-healing in the case of gravitational interactions implies unitarization of quantum amplitudes via quantum black holes. As the center of mass energy increases so does the mass of the black hole and it becomes more and more classical. This is nothing but classicalization [97, 98]. Furthermore, one expects as well a modification of the uncertainty relation of the type:

$$\Delta x \Delta p > \hbar + \alpha f(\Delta p^2), \tag{1.47}$$

[2] Note that in [83], it was argued that one could identify the σ-meson as the pole of a resummed scattering amplitude in the large N limit of chiral perturbation theory. This resummed amplitude is an example of self-healing in chiral perturbation theory. In low energy QCD, the position of the pole does correspond to the correct value of the mass and width of the σ-meson.

where the parameter α is positive. As mentioned before, as we increase the center of mass energy, so does the mass of the black hole in the pole of the resummed propagator. The black hole becomes larger and the magnitude of the nonlocal effects increases. Thus, as in the case studied in [99–102], increasing the center of mass energy of the scattering experiment does not allow to resolve shorter distances as the Δx probed by the scattering experiment increases with the center of mass energy. Since we cannot trust our calculation in the trans-Planckian regime we cannot calculate the function $f(\Delta p^2)$ in contrast to what has been done in [99–102] using the eikonal approximation in string theory.

It is worth mentioning that a potential non-minimal coupling ξ of the scalar fields to the Ricci scalar plays no role in the resummed propagator (1.44). A non-minimal coupling of scalars to the Ricci scalar does not affect the mass of black hole precursors. This is consistent with the results obtained in [84] where it was shown that the large ξN limit leads to a resummed graviton propagator which does not have a pole. In other words, models such as Higgs inflation which rely on a non-minimal coupling of the Higgs boson to curvature are perfectly valid and there is no sign of strong dynamics below the Planck scale.

In this section, we have calculated the mass and width of the lightest of black holes. We have shown that the values of these parameters are dependent on the number of fields in the theory. In the case of the standard model, these results are consistent with expectations: we find that both the mass and the width of the lightest black hole is of the order of the reduced Planck scale. Interpreting the poles of the resummed graviton propagator in the large N limit leads to a beautiful insight into the unification of quantum mechanics and general relativity. Noncausality seems to be a feature of such a unification in the form of quantum black holes and it may be a sign that quantum gravity is made finite by a mechanism of the Lee Wick type. The self-healing mechanism and the classicalization mechanism appear to be necessary ingredients of quantum gravity and the generalized uncertainty principle a necessary consequence of these mechanisms.

1.8 Conclusions

In this chapter we have seen how quantum gravitational and quantum mechanical effects can impact black holes. In particular we have discussed how Planckian quantum black holes enable us to probe quantum gravitational physics either directly if the Planck scale is low enough or indirectly if we integrate out quantum black holes from our low energy effective action. We have discussed how quantum black holes can resolve the information paradox of black holes and explained that quantum black holes lead to one of the few hard facts we have about quantum gravity, namely the existence of a minimal length in nature. We then argued that quantum black holes are likely to involve acausal and non-local effects at the energies close to the Planck scale.

Acknowledgments This work is supported in part by the European Cooperation in Science and Technology (COST) action MP0905 "Black Holes in a Violent Universe" and by the Science and Technology Facilities Council (grant number ST/L000504/1).

References

1. Wald, R.M.: General Relativity, p. 491. University Press, Chicago (1984)
2. Schwarzschild, K.: Sitzungsber. Preuss. Akad. Wiss. Berlin (Math. Phys.) **1916**, 189–196 (1916)
3. Kerr, R.P.: Phys. Rev. Lett. **11**, 237–238 (1963)
4. Michell, J.: On the means of discovering the distance, magnitude, & c. of the fixed stars, in consequence of the diminution of the velocity of their light, in case such a diminution should be found to take place in any of them, and such other data should be procured from observations, as would be farther necessary for that purpose. By the Rev. John Michell, B. D. F. R. S. In a Letter to Henry Cavendish, Esq. F. R. S. and A. S., philosophical transactions of the royal society of London (the royal society) 74, 3557, 1784. ISSN 0080–4614
5. de Laplace, P.-S.: Exposition du système du Monde (English tran: Rev. H. Harte, Dublin 1830). Part 11, Paris (1796)
6. Klinkhamer, F.R.: Mod. Phys. Lett. A **28**, 1350136 (2013). arXiv:1304.2305 [gr-qc]
7. Kanti, P., Winstanley, E.: Hawking radiation from higher-dimensional black holes. In: Quantum Aspects of Black Holes, Chap. 8. Springer (2015)
8. Grumiller, D., McNees, R., Salzer, J.: Black holes and thermodynamics the first half century. In: Quantum Aspects of Black Holes, Chap. 2. Springer (2015)
9. Hsu, S.: Monsters, black holes and entropy. In: Quantum Aspects of Black Holes, Chap. 4. Springer (2015)
10. Mann, R.: Black holes: thermodynamics, information, and firewalls. In: Quantum Aspects of Black Holes, Chap. 3. Springer (2015)
11. Green, A.: Primordial black holes: sirens of the early universe. In: Quantum Aspects of Black Holes, Chap. 5. Springer (2015)
12. Barrow, J.D., Copeland, E.J., Liddle, A.R.: Phys. Rev. D **46**, 645 (1992)
13. Chavanis, P.-H.: Self-gravitating Bose-Einstein condensates. In: Quantum Aspects of Black Holes, Chap. 6. Springer (2015)
14. Dvali, G., Gomez, C.: Eur. Phys. J. C **74**, 2752 (2014). arXiv:1207.4059 [hep-th]
15. Meade, P., Randall, L.: JHEP **0805**, 003 (2008). arXiv:0708.3017 [hep-ph]
16. Calmet, X., Gong, W., Hsu, S.D.H.: Phys. Lett. B **668**, 20 (2008). arXiv:0806.4605 [hep-ph]
17. Penrose, R.: Unpublished in the 1970s, Private communication
18. Eardley, D.M., Giddings, S.B.: Phys. Rev. D **66**, 044011 (2002). gr-qc/0201034
19. Hsu, S.D.H.: Phys. Lett. B **555**, 92 (2003). hep-ph/0203154
20. D'Eath, P., Farley, A.N.S.J.: Quantum amplitudes in blackhole evaporation with local supersymmetry. In: Quantum Aspects of Black Holes, Chap. 7. Springer (2015)
21. Antoniadis, I., Arkani-Hamed, N., Dimopoulos, S., Dvali, G.R.: Phys. Lett. B **436**, 257 (1998). hep-ph/9804398
22. Arkani-Hamed, N., Dimopoulos, S., Dvali, G.R.: Phys. Lett. B **429**, 263 (1998). hep-ph/9803315
23. Gogberashvili, M.: Int. J. Mod. Phys. D **11**, 1635 (2002). hep-ph/9812296
24. Randall, L., Sundrum, R.: Phys. Rev. Lett. **83**, 3370 (1999). hep-ph/9905221
25. Calmet, X., Hsu, S.D.H., Reeb, D.: Phys. Rev. D **77**, 125015 (2008). arXiv:0803.1836 [hep-th]
26. Huber, S.J.: Nucl. Phys. B **666**, 269 (2003). hep-ph/0303183
27. Calmet, X.: Mod. Phys. Lett. A **25**, 1553 (2010). arXiv:1005.1805 [hep-ph]
28. Kabat, D.N.: Nucl. Phys. B **453**, 281 (1995). hep-th/9503016
29. Larsen, F., Wilczek, F.: Nucl. Phys. B **458**, 249 (1996). hep-th/9506066

30. Vassilevich, D.V.: Phys. Rev. D **52**, 999 (1995). gr-qc/9411036
31. Thorne, K.S.: Nonspherical gravitational collapse: a short review. In: Klauder J.R. (ed.) Magic Without Magic, pp. 231–258. San Francisco (1972)
32. Anchordoqui, L.A., Feng, J.L., Goldberg, H., Shapere, A.D.: Phys. Rev. D **65**, 124027 (2002). hep-ph/0112247
33. Anchordoqui, L.A., Feng, J.L., Goldberg, H., Shapere, A.D.: Phys. Rev. D **68**, 104025 (2003). hep-ph/0307228
34. Anchordoqui, L.A., Feng, J.L., Goldberg, H., Shapere, A.D.: Phys. Lett. B **594**, 363 (2004). hep-ph/0311365
35. Dimopoulos, S., Landsberg, G.L.: Phys. Rev. Lett. **87**, 161602 (2001). hep-ph/0106295
36. Feng, J.L., Shapere, A.D.: Phys. Rev. Lett. **88**, 021303 (2002). hep-ph/0109106
37. Giddings, S.B., Thomas, S.D.: Phys. Rev. D **65**, 056010 (2002). hep-ph/0106219
38. Hossenfelder, S., Hofmann, S., Bleicher, M., Stoecker, H.: Phys. Rev. D **66**, 101502 (2002). [hep-ph/0109085]
39. Yoshino, H., Rychkov, V.S.: Phys. Rev. D **71**, 104028 (2005) [Erratum-ibid. D 77, 089905 (2008)] hep-th/0503171
40. Yoshino, H., Nambu, Y.: Phys. Rev. D **67**, 024009 (2003). gr-qc/0209003
41. Alberghi, G.L., Bellagamba, L., Calmet, X., Casadio, R., Micu, O.: Eur. Phys. J. C **73**, 2448 (2013). [arXiv:1303.3150]
42. Arsene, N., Calmet, X., Caramete, L.I., Micu, O.: Astropart. Phys. **54**, 132 (2014) arXiv:1303.4603 [hep-ph]
43. Calmet, X., Fragkakis, D., Gausmann, N.: Non thermal small black holes. In: Bauer, A.J., Eiffel, D.G. (eds.) Black Holes: Evolution, Theory and Thermodynamics, Chap. 8. Nova Publishers, New York (2012). arXiv:1201.4463 [hep-ph]
44. Calmet, X., Landsberg, G.: Lower dimensional quantum black holes. In: Bauer, A.J., Eiffel, D.G. (eds.) Black Holes: Evolution, Theory and Thermodynamics, Chap. 7. Nova Publishers, New York (2012). arXiv:1008.3390 [hep-ph]
45. Calmet, X., Feliciangeli, M.: Phys. Rev. D **78**, 067702 (2008). arXiv:0806.4304 [hep-ph]
46. Calmet, X., Fragkakis, D., Gausmann, N.: Eur. Phys. J. C **71**, 1781 (2011). arXiv:1105.1779 [hep-ph]
47. Calmet, X., Caramete, L.I., Micu, O.: JHEP **1211**, 104 (2012). arXiv:1204.2520 [hep-ph]
48. Calmet, X., Gausmann, N.: Non-thermal quantum black holes with quantized masses. Int. J. Mod. Phys. A **28**, 1350045 (2013). arXiv:1209.4618 [hep-ph]
49. Aad, G., et al.: ATLAS collaboration. arXiv:1311.2006 [hep-ex]
50. Landsberg, G.. In: Quantum Aspects of Black Holes, Chap. 9. Springer (2015)
51. Savina, M.V.: CMS collaboration. Phys. Atom. Nucl. **76**, 1090 (2013) [Yad. Fiz. 76, no. 9, 11501159 (2013)]
52. Hoyle, C.D., Kapner, D.J., Heckel, B.R., Adelberger, E.G., Gundlach, J.H., Schmidt, U., Swanson, H.E.: Phys. Rev. D **70**, 042004 (2004). [hep-ph/0405262]
53. Calmet, X.: Int. J. Mod. Phys. D **22**, 1342014 (2013) arXiv:1308.6155 [gr-qc]
54. Atkins, M., Calmet, X.: Phys. Rev. Lett. **110**(5), 051301 (2013). arXiv:1211.0281 [hep-ph]
55. Onofrio, R.: Eur. Phys. J. C **72**, 2006 (2012). arXiv:1303.5695 [gr-qc]
56. Bezrukov, F.L., Shaposhnikov, M.: Phys. Lett. B **659**, 703 (2008). arXiv:0710.3755 [hep-th]
57. Starobinsky, A.A.: Phys. Lett. B **91**, 99 (1980)
58. Calmet, X., Hsu, S.D.H., Reeb, D.: Phys. Rev. Lett. **101**, 171802 (2008). arXiv:0805.0145 [hep-ph]
59. Calmet, X., Hsu, S.D.H., Reeb, D.: Phys. Rev. D **81**, 035007 (2010). arXiv:0911.0415 [hep-ph]
60. Hall, L.J., Sarid, U.: Phys. Rev. Lett. **70**, 2673 (1993). hep-ph/9210240
61. Hill, C.T.: Phys. Lett. B **135**, 47 (1984)
62. Shafi, Q., Wetterich, C.: Phys. Rev. Lett. **52**, 875 (1984)
63. Amaldi, U., de Boer, W., Furstenau, H.: Phys. Lett. B **260**, 447 (1991)
64. Calmet, X., Yang, T.-C.: Phys. Rev. D **84**, 037701 (2011). arXiv:1105.0424 [hep-ph]
65. Ellis, J.R., Gaillard, M.K.: Phys. Lett. B **88**, 315 (1979)
66. Panagiotakopoulos, C., Shafi, Q.: Phys. Rev. Lett. **52**, 2336 (1984)

67. Enqvist, K., Maalampi, J.: Phys. Lett. B **180**, 14 (1986)
68. Calmet, X., Sanz, V.: Phys. Lett. B **737**,12 (2014) arXiv:1403.5100 [hep-ph]
69. Strominger, A.: Les Houches lectures on black holes. arXiv:9501071 [hep-th]
70. Giddings, S.B.: Phys. Rev. D **46**, 1347 (1992). ([hep-th/9203059]; Phys. Rev. D 49, 947 (1994)[hep-th/9304027])
71. Calmet, X., Graesser, M., Hsu, S.D.H.: Phys. Rev. Lett. **93**, 211101 (2004). ([hep-th/0405033]; Int. J. Mod. Phys. D 14, 2195 (2005) [hep-th/0505144]; X. Calmet, Eur. Phys. J. C 54, 501 (2008) [Subnucl. Ser. 44, 625 (2008)] [hep-th/0701073])
72. Dvali, G., Gomez, C., Mukhanov, S.: Black Hole masses are quantized. arXiv:1106.5894 [hep-ph]
73. Calmet, X., Fritzsch, H., Holtmannspotter, D.: Phys. Rev. D **64**, 037701 (2001). ([hep-ph/0103012])
74. Casadio, R., Micu, O., Nicolini, P.: Minimum length effects in black hole physics. In: Quantum Aspects of Black Holes, Chap. 10. Springer (2015)
75. Garay, L.J.: Int. J. Mod. Phys. A **10**, 145 (1995). arXiv:gr-qc/9403008
76. Mead, C.A.: Phys. Rev. **135**, B849 (1964)
77. Padmanabhan, T.: Class. Quant. Grav. **4**, L107 (1987)
78. Salecker, H., Wigner, E.P.: Phys. Rev. **109**, 571 (1958)
79. Antoniadis, I., Atkins, M., Calmet, X.: JHEP **1111**, 039 (2011). arXiv:1109.1160 [hep-ph]
80. Atkins, M., Calmet, X.: Eur. Phys. J. C **70**, 381 (2010). arXiv:1005.1075 [hep-ph]
81. Atkins, M., Calmet, X.: Phys. Lett. B **695**, 298 (2011). arXiv:1002.0003 [hep-th]
82. Atkins, M., Calmet, X.: Phys. Lett. B **697**, 37 (2011). arXiv:1011.4179 [hep-ph]
83. Aydemir, U., Anber, M.M., Donoghue, J.F.: Phys. Rev. D **86**, 014025 (2012). arXiv:1203.5153 [hep-ph]
84. Calmet, X., Casadio, R.: Phys. Lett. B **734**,17 (2014) arXiv:1310.7410 [hep-ph]
85. Han, T., Willenbrock, S.: Phys. Lett. B **616**, 215 (2005). ([hep-ph/0404182])
86. Ren, J., Xianyu, Z.-Z., He, H.-J.: JCAP **1406**, 032 (2014). arXiv:1404.4627 [gr-qc]
87. Xianyu, Z.-Z., Ren, J., He, H.-J.: Phys. Rev. D **88**(9), 096013 (2013). arXiv:1305.0251 [hep-ph]
88. Tomboulis, E.: Phys. Lett. B **70**, 361 (1977)
89. Tomboulis, E.: Phys. Lett. B **97**, 77 (1980)
90. Amati, D., Ciafaloni, M., Veneziano, G.: JHEP **0802**, 049 (2008). arXiv:0712.1209 [hep-th]
91. Bhattacharya, T., Willenbrock, S.: Phys. Rev. D **47**, 4022 (1993)
92. Donoghue, J.F., El-Menoufi, B.K.: Phys. Rev. D **89**, 104062 (2014). arXiv:1402.3252 [gr-qc]
93. Wald, R.M.: Quantum Field Theory in Curved Space-Time and Black Hole Thermodynamics. Univ. Pr, Chicago (1994)
94. Lee, T.D., Wick, G.C.: Nucl. Phys. B **9**, 209 (1969)
95. Lee, T.D., Wick, G.C.: Phys. Rev. D **2**, 1033 (1970)
96. Grinstein, B., O'Connell, D., Wise, M.B.: Phys. Rev. D **79**, 105019 (2009). arXiv:0805.2156 [hep-th]
97. Calmet, X.: Int. J. Mod. Phys. A **26**, 2855 (2011). arXiv:1012.5529 [hep-ph]
98. Dvali, G., Giudice, G.F., Gomez, C., Kehagias, A.: JHEP **1108**, 108 (2011). arXiv:1010.1415 [hep-ph]
99. Amati, D., Ciafaloni, M., Veneziano, G.: Phys. Lett. B **216**, 41 (1989)
100. Amati, D., Ciafaloni, M., Veneziano, G.: Phys. Lett. B **289**, 87 (1992)
101. Amati, D., Ciafaloni, M., Veneziano, G.: Nucl. Phys. B **403**, 707 (1993)
102. Hossenfelder, S.: Living Rev. Rel. **16**, 2 (2013). arXiv:1203.6191 [gr-qc]

Chapter 2
Black Holes and Thermodynamics: The First Half Century

Daniel Grumiller, Robert McNees and Jakob Salzer

Abstract Black hole thermodynamics emerged from the classical general relativistic laws of black hole mechanics, summarized by Bardeen–Carter–Hawking, together with the physical insights by Bekenstein about black hole entropy and the semi-classical derivation by Hawking of black hole evaporation. The black hole entropy law inspired the formulation of the holographic principle by 't Hooft and Susskind, which is famously realized in the gauge/gravity correspondence by Maldacena, Gubser–Klebanov–Polaykov and Witten within string theory. Moreover, the microscopic derivation of black hole entropy, pioneered by Strominger–Vafa within string theory, often serves as a consistency check for putative theories of quantum gravity. In this book chapter we review these developments over five decades, starting in the 1960s.

Keywords Black hole thermodynamics · History of black holes · Hawking radiation · Information loss · Holographic principle · Quantum gravity

2.1 Introduction and Prehistory

Introductory remarks. The history of black hole thermodynamics is intertwined with the history of quantum gravity. In the absence of experimental data capable of probing Planck scale physics the best we can do is to subject putative theories of quantum gravity to stringent consistency checks. Black hole thermodynamics provides a number of highly non-trivial consistency checks. Perhaps most famously, any theory of quantum gravity that fails to reproduce the Bekenstein–Hawking relation

D. Grumiller (✉) · J. Salzer
Institute for Theoretical Physics, Vienna University of Technology,
Wiedner Hauptstrasse 8-10, 1040 Vienna, Austria
e-mail: grumil@hep.itp.tuwien.ac.at

J. Salzer
e-mail: salzer@hep.itp.tuwien.ac.at

R. McNees
Department of Physics, Loyola University Chicago, Chicago, IL 60660, USA
e-mail: rmcnees@luc.edu

X. Calmet (ed.), *Quantum Aspects of Black Holes*,
Fundamental Theories of Physics 178, DOI 10.1007/978-3-319-10852-0_2

$$S_{\text{BH}} = \frac{k_B\, c^3 A_h}{4\hbar G} \tag{2.1}$$

between the black hole entropy S_{BH}, the area of the event horizon A_h, and Newton's constant G would be regarded with a great amount of skepticism (see e.g [1]).

In addition to providing a template for the falsification of speculative models of quantum gravity, black hole thermodynamics has also sparked essential developments in the field of quantum gravity and remains a vital source of insight and new ideas. Discussions about information loss, the holographic principle, the microscopic origin of black hole entropy, gravity as an emergent phenomenon, and the more recent firewall paradox all have roots in black hole thermodynamics. Furthermore, it is an interesting subject in its own right, with unusual behavior of specific heat, a rich phenomenology, and remarkable phase transitions between different spacetimes.

In this review we summarize the development of black hole thermodynamics chronologically, except when the narrative demands deviations from a strictly historical account. While we have tried to be comprehensive, our coverage is limited by a number of factors, not the least of which is our own knowledge of the literature on the subject. Each of the following five sections describes a decade, beginning with the discovery of the Kerr solution in 1963 [2]. In our concluding section we look forward to future developments. But before starting we comment on some early insights that had the potential to impact the way we view the result (2.1).

Prehistory. If the history of black hole thermodynamics begins with the papers of Bekenstein [3] and Bardeen et al. [4], then the prehistory of the subject stretches back nearly forty additional years to the work of Tolman, Oppenheimer, and Volkoff in the 1930s [5–7]. These authors considered the conditions for a 'star'—a spherically symmetric, self-gravitating object composed of a perfect fluid with a linear equation of state—to be in hydrostatic equilibrium. Later, in the 1960s, Zel'dovich showed that linear equations of state besides the familiar $p = 0$ (dust) and $p = \rho/3$ (radiation) are consistent with relativity [8]. He established the bound $p \leq \rho$, with $p = \rho$ representing a causal limit where the fluid's speed of sound is equal to the speed of light. A few years after that, Bondi considered massive spheres composed of such fluids and included the case $p = \rho$ in his analysis [9].

The self-gravitating, spherically symmetric perfect fluids considered by these and other authors possess interesting thermodynamic properties. In particular, the entropy of such objects (which are always outside their Schwarzschild radius) is not extensive in the usual sense. For example, a configuration composed of radiation has an entropy that scales with the size of the system as $S(R) \sim R^{3/2}$, and a configuration with the ultra-relativistic equation of state $p = \rho$ has an entropy $S(R) \sim R^2$ that scales like the area. But these results do not appear in the early literature (at least, not prominently) because there was no compelling reason to scrutinize the relationship between the entropy and size of a gravitating system before the 1970s. It was not until the 1980s, well after the initial work of Bekenstein and Hawking, that Wald, Sorkin, and Zhang studied the entropy of self-gravitating perfect fluids with $p = \rho/3$ [10]. They showed that the conditions for hydrostatic equilibrium—the same conditions

set out by Tolman, Oppenheimer, and Volkoff—give at least local extrema of the entropy. With reasonable physical assumptions these objects quite easily satisfy the Bekenstein bound, $S \leq 2\pi k_B RE/(\hbar c)$, where R and E are the object's size and energy, respectively.

The area law (2.1) is often presented as a surprising deviation from the volume scaling of the entropy in a non-gravitating system. But the early work described above suggests, without invoking anything as extreme as a black hole, that this is something we should expect from General Relativity. Even a somewhat mundane system like a sufficiently massive ball of radiation has an entropy that is not proportional to its volume. The surprising thing about the area law is not that the entropy of the system grows much more slowly than a volume. Rather, it is that the entropy of a black hole seems to saturate, at least parametrically, an *upper* bound on the growth of entropy with the size of a gravitating system. Such a bound, which follows from causality, could have been conjectured several years before the work of Bekenstein and Hawking.

2.2 1963–1973

Black hole solutions and the uniqueness theorem. After the first black hole solutions were found in immediate consequence to the publication of Einstein's equations, it took almost 50 years for the next exact black hole solution to be discovered. The Kerr solution [2] describes a rotating black hole of mass M and angular momentum $J = aM$

$$\begin{aligned} \mathrm{d}s^2 = &-\left(1-\frac{2Mr}{\rho^2}\right)\mathrm{d}t^2 - \frac{4Mra\sin^2\theta}{\rho^2}\,\mathrm{d}t\,\mathrm{d}\phi + \left(r^2+a^2+\frac{2Mra^2\sin^2\theta}{\rho^2}\right)\sin^2\theta\,\mathrm{d}\phi^2 \\ &+\frac{\rho^2}{r^2-2Mr+a^2}\,\mathrm{d}r^2 + \rho^2\,\mathrm{d}\theta^2 \qquad \text{with } \rho^2 := r^2 + a^2\cos^2\theta\,. \end{aligned} \tag{2.2}$$

Only 2 years later this solution was extended to include charged rotating black holes [11]. These black hole solutions exhibit the remarkable property that they are parameterized in terms of only three quantities as measured from infinity: mass, angular momentum, charge. It was therefore natural to ask whether this was the case for all black hole solutions.

Building on earlier work concerning the persistence of the horizon under asymmetric perturbations [12, 13], Israel proved that—assuming some regularity conditions—the Schwarzschild solution is the only static, asymptotically flat vacuum spacetime that exhibits a regular horizon [14]. Later, this proof was generalized to static asymptotically flat electrovac spacetimes, now with the Reissner–Nordström black hole as the only admissible spacetime [15]. In the case of axisymmetric stationary black holes Carter was later able to show that these spacetimes fall into discrete sets of continuous families, each of them depending on one or two independent parameters, with the Kerr solutions as the unique family to allow vanishing angular momentum [16]. The key point of Carter's proof is the observation that Einstein's equations for

an axisymmetric spacetime can be reduced to a two-dimensional boundary value problem. Building on this, Robinson showed that in fact only the Kerr family exists, thus establishing the uniqueness of the Kerr black hole [17]. Similar results concerning the classification and uniqueness of charged axisymmetric stationary black holes were worked out independently by Mazur [18], Bunting [19] and more recently by Chrusciel and Costa [20]. However, due to different initial hypotheses in the statement of the theorem and some technical gaps, the uniqueness theorem is still extensively studied (cf. [21] for a review).

Referring to these results, John Wheeler coined the expression "black holes have no hair" [22], i.e. black holes can be described entirely by a small amount of quantities measured from infinity. The no-hair conjecture thus suggests a resemblance of black holes to systems in thermodynamic equilibrium, whose macroscopic state is parameterized by a small number of macroscopic variables.

Penrose process and superradiant scattering. Another similarity between black holes and thermodynamical systems was revealed with Penrose's suggestion that energy can be extracted from a rotating black hole [23]. The Penrose process relies on the presence of an ergosphere in Kerr spacetime. In this region the Killing field ξ^a that asymptotically corresponds to time translation is spacelike. Consequently, the energy $E = -p_a\xi^a$ of a particle of 4-momentum p^a need not be positive. In the Penrose process a particle with positive energy E_0 is released from infinity. In the ergosphere the particle breaks up in such a way that one fragment has negative energy E_1 whereas the other has positive energy $E_2 = E_0 - E_1 > E_0$. If the latter returns back to infinity on a geodesic one has effectively gained the energy $|E_1|$. The negative energy particle falls into the black hole and therefore reduces its mass. Thus, energy is indeed extracted from the black hole. Angular momentum j_2^a and energy of the particle falling into the black hole have to obey the inequality $j^a \leq E_2/\Omega_H$, where Ω_H is the angular velocity of the black hole. Therefore, the change in the black hole's mass and angular momentum δM and δJ, respectively, are related by $\delta M \geq \Omega_H \delta J$. This equation can be rewritten in a form that bears a clear resemblance to the second law of thermodynamics [24]

$$\delta M_{irr} \geq 0, \tag{2.3}$$

where $M_{irr}^2 = \frac{1}{2}\left(M^2 + \sqrt{M^4 - J^2}\right)$ is the irreducible mass. Expressed in terms of irreducible mass and angular momentum, the mass of the black hole reads

$$M^2 = M_{irr}^2 + \frac{J^2}{4M_{irr}^2} \geq M_{irr}^2. \tag{2.4}$$

The maximum amount of energy that can be extracted from a black hole with initial mass M_0 and angular momentum J_0 is therefore $\Delta M = M_0 - M_{irr}(M_0, J_0)$, which is maximized for an extremal black hole, i.e. $J_0 = M_0^2$, with an efficiency of 0.29. A generalization to charged rotating black holes yields the Christodoulou–Ruffini mass formula

$$M^2 = \left(M_{irr} + \frac{Q^2}{4M_{irr}}\right)^2 + \frac{J^2}{4M_{irr}^2}, \tag{2.5}$$

which pushes the efficiency of the Penrose process up to 0.5 [25].

The fact that a Penrose process cannot reduce the irreducible mass of a black hole is a particular consequence of Hawking's area theorem, discussed below.

The Penrose process has a corresponding phenomenon in wave scattering on a stationary axisymmetric black hole background known as superradiant scattering [26–28]. Similar effects were already studied in [29, 30] where scalar waves incident on a rotating cylinder were examined. For a qualitative understanding of superradiant scattering consider the scalar wave equation $\nabla^a \nabla_a \Phi = 0$ on a Kerr background. It was shown in [31] by studying the Hamilton–Jacobi equation for a test particle that this equation is separable, therefore Φ can be written as: $\Phi = \mathrm{e}^{\mathrm{i}(m\phi - \omega t)} R(r) P(\theta)$ where $P(\theta)$ is a spheroidal harmonic. The solutions for $R(r)$ were studied in detail in [32]. Suitable boundary conditions for Φ read

$$\Phi(r) = \begin{cases} \mathrm{e}^{-\mathrm{i}(\omega - m\Omega)r_*} & r \to r_+ \\ A_{out}(\omega)\mathrm{e}^{\mathrm{i}\omega r_*} + A_{in}(\omega)\mathrm{e}^{-\mathrm{i}\omega r_*} & r \to \infty \end{cases} \tag{2.6}$$

where r_* denotes the tortoise coordinate for the Kerr spacetime. The choice of boundary condition at the horizon $r \to r_+$ is motivated by the requirement that physical observers at the horizon should see exclusively ingoing waves. The Wronskian determinant for this solution and its complex conjugate evaluated in both limits leads to

$$|R|^2 = 1 - \left(1 - \frac{m\Omega_H}{\omega}\right)|T|^2. \tag{2.7}$$

Therefore, superradiance is observed for $\omega < m\Omega_H$. Interestingly, the amplification of the incoming amplitude depends on the spin of the incident wave [33, 34]: 0.003 for a scalar wave, 0.044 for an electromagnetic field and 1.38 for gravitational waves. Half-integer fields do not appear, as fermions show no superradiant scattering behavior. This can be understood from the exclusion principle which allows only one particle in each outgoing mode and thus prevents an enhancement of the scattered wave [35, 36].

The occurrence of superradiant scattering in quantum mechanics is well known from the Klein paradox [37–39]. The Klein paradox describes the quantum effect that a wave incident on a step potential is reflected with a coefficient $|R| > 1$ for a particular relation between potential height and energy of the incident wave. This effect is attributed to pair creation in the strong electric field near the potential step. Therefore, the presence of superradiant scattering in a black hole background suggests the occurrence of particle creation as was already noted in [28–30, 33] and later famously shown by Hawking [40] (cf. next section).

The area theorem. The above mechanisms of energy extraction are closely related to the important area theorem. The area theorem and the four laws of black hole

mechanics rely on a couple of earlier theorems, which are described in the following with no intention of mathematical rigor (cf. the standard reference [41] for details).

The rigidity theorem shows under suitable assumptions that the event horizon of a stationary black hole is a Killing horizon. This result can be proven in two independent ways. Carter showed that the horizon of a static black hole is normal to the static Killing vector ξ^a, and the horizon of a stationary black hole is normal to the linear combination $\chi^a = \xi^a + \Omega_H \phi^a$ under the assumption of $t - \phi$ orthogonality [42]. Here Ω_H denotes the angular velocity of the horizon and ϕ^a is the Killing vector generating the axial symmetry. In the second proof, Einstein's equations are assumed in order to show that the event horizon of every stationary black hole in vacuum or electrovacuum is a Killing horizon [41].

The Penrose theorem proven in [43] states that the null geodesics generating the horizon may have past end points but no end points in the future. In particular, no caustics of the generators can occur when extended into the future. A consequence of this theorem is that black holes cannot bifurcate or vanish [41].

The focusing theorem follows from the Raychaudhuri equation for lightlike congruences. It states that, given a positive convergence at any point of the congruence, the cross-section of the beam vanishes in a finite distance provided the weak energy condition and Einstein's equations hold.

The area theorem follows from the two latter statements: If the lightlike generators of the horizon had a positive convergence at any point, a caustic would occur in finite distance which is forbidden by Penrose's theorem. Therefore, the area of the horizon cannot decrease [44, 45]. The only possibility to evade this conclusion is the presence of a naked singularity, i.e. a singularity not shielded by a horizon. Thus, the presence of such singularities must be excluded by adopting the cosmic censorship conjecture [23]. In summary, the prerequisites of the area theorem put strong restrictions on both causal structure (cosmic censorship conjecture) and matter (weak energy condition) in spacetime. In particular, the latter is in general not met when quantum theory is taken into account [46].

The area theorem provides an explanation for the bound on the Penrose process (2.3), since M_{irr} is proportional to the area of the Kerr black hole [44, 45]. Similarly, the need for superradiant scattering of waves as described above and the existence of a spin-spin interaction between a Kerr black hole and a spinning particle can both be seen just from the area law [46, 47]. The argument for superradiant scattering from the area theorem breaks down for fermions since the respective energy-momentum tensor does not obey the weak energy condition [35, 36].

The four laws of black hole mechanics. The work of this decade culminated in the famous four laws of black hole mechanics by Bardeen et al. [4]. These laws, which show a remarkable similarity to the laws of thermodynamics, are stated in the following.

- The zeroth law of black hole mechanics states that the surface gravity κ is constant on the horizon of a black hole. The proof of this result as given in [4] requires the dominant energy condition to hold and the use of Einstein's equations. Similar results were already obtained in [16, 45]. Another proof was given in [42] by using

the assumption of $t - \phi$ orthogonality [42]. The zeroth law suggests a similarity between κ and the temperature of a body in thermal equilibrium.

- The first law establishes a relation between changes in the mass M, horizon area A, angular momentum J_H, and charge Q_H if the black hole is perturbed.

$$\delta M = \frac{\kappa}{8\pi}\delta A + \Omega_H \delta J_H + \Phi_H \delta Q \tag{2.8}$$

  In [4] the first law was derived from a generalized version of the Smarr mass formula [48]. The first law bears a clear resemblance to the first law of thermodynamics with κ as temperature, the horizon area A taking the place of entropy, and the mass M taking the role of energy. As pointed out in [49], in fact two different versions of the first law exist: an equilibrium version, wherein one compares the parameters of neighboring equilibrium solutions, and a physical process version in which the parameters of the black hole are changed, e.g. by dropping in matter, and analyzing the change in the parameters after the black hole has settled down. These two independent versions yield the same result.
- The second law of black hole mechanics is Hawking's area theorem:

$$\delta A \geq 0. \tag{2.9}$$

  Here, the analogy between horizon area A and entropy becomes evident.
- The third law states that the surface gravity of a black hole cannot be reduced to zero in a finite number of processes. This formulation is an analogue of the Nernst unattainability principle [50]. The Planck formulation of the third law of thermodynamics does not hold in black hole mechanics, as the horizon area of an extremal black hole is finite despite vanishing surface gravity. It follows from the third law that non-extremal black holes cannot be made extremal in a finite number of steps. A proof for the third law was presented later in [51].

The close mathematical and physical analogy between the four laws of black hole mechanics and the laws of thermodynamics is remarkable. Nonetheless, it appears to be a mere analogy in classical general relativity. Classical black holes do not have temperature since they cannot radiate, and entropy is a dimensionless quantity in contrast to the horizon area that has a dimension of length squared. It is only when quantum theory is taken into account that the analogy becomes an identity.

2.3 1973–1983

Bekenstein–Hawking entropy. In 1971, when Wheeler proposed the now famous gedankenexperiment of pouring a hot cup of tea into a black hole, he was questioning whether black holes violate the second law of thermodynamics. Another possible violation of the second law of thermodynamics by classical black holes was put forward by Geroch: A box of matter with mass m is lowered close to the horizon

of a black hole from infinity where its energy (as measured from infinity) is nearly zero, thus providing an amount m of work. At the horizon the box radiates away an amount δm of its mass and is hauled back to infinity, requiring an amount $m - \delta m$ of work. In this process an amount δm of heat is transformed entirely into work thereby violating the second law of thermodynamics.

These evident violations of the second law of thermodynamics and Hawking's area theorem led Bekenstein to propose an entropy for black holes that is proportional to horizon area measured in units of Planck area with a coefficient η of order one [3, 52]:

$$S_{BH} = \eta \frac{k_B c^3 A}{\hbar G}. \tag{2.10}$$

The second law of thermodynamics is then replaced by a generalized second law of thermodynamics which states that the change in the sum of matter entropy and black hole entropy is strictly nonnegative. Bekenstein showed that this generalized second law resolves the problems associated with the Geroch process [52]. Furthermore, he tested the law for the cases of a harmonic oscillator enclosed in a spherical box and infalling radiation.

Hawking radiation. The relation between black hole entropy and horizon area together with the first law of black hole mechanics indicates that black holes do have a temperature that should be proportional to κ. If the black hole is immersed in black body radiation of lower temperature then the generalized second law is violated, unless the black hole also emits radiation. Therefore, spontaneous particle creation is needed to prevent a violation of the generalized second law. Eventually, Hawking showed that black holes spontaneously emit radiation characteristic of a black body at temperature

$$T_H = \frac{\hbar \kappa}{2\pi c k_B}, \tag{2.11}$$

thus establishing also further evidence for the validity of the generalized second law [36, 40]. The coefficient η in (2.10) is fixed to $\eta = \frac{1}{4}$ as can be seen from the first law of black hole mechanics (2.8). Consequently, black holes can be treated as thermodynamic systems, and the four laws of black hole mechanics cease to be mere analogies, but describe black holes as thermodynamic systems.

In the original derivation of Hawking radiation a massless scalar field is studied in the background metric of gravitational collapse. The scalar field yields a decomposition in terms of a complete set of solutions both on lightlike past infinite, $\mathscr{I}^-$, and on the union of the horizon and lightlike future infinity, $\mathscr{I}^+$. Both sets of solutions contain positive frequency modes with respect to the appropriate affine parameters on $\mathscr{I}^+$ and $\mathscr{I}^-$. The different decompositions of the field induce a Bogoliubov transformation on the two sets of creation and annihilation operators on $\mathscr{I}^+$ and $\mathscr{I}^-$. Therefore, the vacuum state with respect to the operators for the ingoing particles

yields a nonzero expectation value for the number operator for an observer in $\mathscr{I}^+$.[1] This is the Hawking radiation. The particle number measured at $\mathscr{I}^+$ of a particular mode is given by [36]

$$\langle n_J \rangle = \frac{\Gamma_J}{\exp\left[(2\pi\bar{\omega}_J)/\kappa\right] \pm 1}, \tag{2.12}$$

where the index J denotes collectively frequency ω, angular momentum l, azimuthal quantum number m, sign of the charge, and spin. The upper sign is for fermions and the lower sign for bosons. Here the quantity $\bar{\omega}$ is defined as $\bar{\omega_J} = \omega_J - m_j\Omega_H - q\Phi_H$, and Γ_J denotes the fraction of the incident radiation that enters the collapsing body, i.e. $\Gamma_J = 1 - |R_J|^2$. Expression (2.12) is precisely the result expected for a black body with temperature $\kappa/(2\pi)$ and greybody factor Γ_J. In fact, Hawking radiation is completely identical to black body radiation, since the density matrices for Hawking radiation and black body radiation coincide [54–56]. Furthermore, it was shown that black holes behave like black bodies even in the presence of incoming radiation. Expressions for the probability of emission of k particles when m particles have arrived, $P(k|m)$, and the Einstein coefficients for induced emission, spontaneous emission and absorptions were obtained in [57, 58]. The derivation of Hawking was repeated subsequently in various approaches and generalizations (cf. [59–63]).

The Hawking effect is often described heuristically as Schwinger pair creation in the gravitational field of a black hole, where the negative energy particle drops into the black hole and the other particle escapes to infinity [36]. A derivation of the Hawking effect that closely resembles this picture of a tunneling process was presented in [64].

Hawking radiation from anomalies. Particularly striking is the connection between Hawking radiation and anomalies of the stress-energy tensor. If restricted to the s-wave sector, Hawking radiation can be studied in an effectively two dimensional spacetime. In this geometry, Hawking radiation can be shown to arise from the trace anomaly of the energy-momentum tensor for a massless field, by requiring finiteness of $T_{\mu\nu}$ at the horizon for a geodesic observer [65] (cf. e.g. [66] for a general discussion, and [67]).

More recently, it was shown that Hawking radiation is necessary for the cancellation of gravitational anomalies [68]—i.e. non-conservation of $T_{\mu\nu}$—in Schwarzschild spacetimes of any dimension. A gravitational anomaly occurs if one assumes that modes propagating along the horizon can be integrated out, so that $T_{\mu\nu}$ is regular on the horizon. Thus, the resulting theory is effectively chiral near the horizon and acquires a gravitational anomaly, which is removed by Hawking radiation. This method can be generalized to charged and rotating black holes [69, 70].

Euclidean path integral. Due to its intimate connection with the partition function, the Euclidean path integral formalism of quantum gravity is widely used when studying black hole thermodynamics.

---

[1] In quantum information language the vacuum quantum state in a black hole space-time for each mode is a two-mode squeezed vacuum, similar to what happens for primordial density fluctuations in cosmology [53].

The singularities encountered in black hole spacetimes can be avoided by a Wick rotation into the Euclidean sector. This requires a periodic Euclidean time with periodicity of inverse temperature. In general, the Euclidean path integral does not converge due to the presence of the conformal mode [71]. However, in the semi-classical approximation to the partition function, i.e. expanding the path integral around solutions of the classical equations of motion, the above results for entropy and temperature of black holes are recovered [72, 73].

In the case of flat spacetime at non-zero temperature studied in [74], a sum over the Schwarzschild instanton in the path integral leads to a non-zero probability for the decay of flat space into a black hole. Gravitational instantons and their thermodynamic properties were studied and classified in [75–77].

Modes of black hole decay. It is seen from (2.12) that the emission of particles with charge of the same sign as the charge of the black hole is enhanced. Thus, the charge of the black hole is radiated away [78–82]. The resulting current is proportional to the particle number (2.12) times the charge of the emitted particle. An estimation of the discharge rate yields that the timescale over which the discharge occurs is in general much shorter than the relevant timescale for formation of the black hole [79], provided that $Q/M \geq Mm_e^2/e$. Thus, only very large black holes show a significant charge Q. All other black holes show only random charge fluctuations of order $(\hbar c)^{1/2}$ after sufficiently long time [81, 82].

For fixed angular momentum l the emission of particles with positive azimuthal quantum number m is enhanced, and the black hole loses angular momentum. When radiation of massless particles only is considered, the black hole loses angular momentum considerably faster than mass [83]. Curiously, the emission of neutrinos shows parity violation: antineutrinos are emitted preferentially parallel to angular momentum whereas more neutrinos are emitted in the opposite direction [84–86].

Radiation of the black hole mass occurs over a timescale $\tau \propto G^2 M_0^3/(\hbar c^4)$, which exceeds the age of the present universe unless the black hole is sufficiently light, $M_0 \leq 5 \times 10^{11}$ kg. The species of the emitted particles changes with the mass of the black hole: black holes emit massless particles only as long as $M \geq 10^{14}$ kg at which point electron-positron emission starts; the onset for emission of heavier particles lies at $M \approx 10^{11}$ kg [81–83]. Consequences of black hole evaporation for unitarity are discussed below.

Unruh effect. The Unruh effect describes the detection of vacuum fluctuations of the Minkowski vacuum as thermal radiation by a constantly accelerated observer, i.e. an observer in Rindler spacetime [61, 87–89]. The Minkowski vacuum—the vacuum for an observer measuring time along the Killing vector ∂_t—can be represented as the sum

$$|0\rangle = \sum_n \exp\left(-2\pi a^{-1}\omega_n\right)|n\rangle_L \times |n\rangle_R. \tag{2.13}$$

where $|n\rangle_L (|n\rangle_R)$ are states with energy ω_n measured by an observer moving with acceleration a along the respective Killing vectors in the left (right) wedge of Rindler

spacetime [89, 90].[2] The Minkowski vacuum thus contains correlations between states in different wedges of Rindler spacetime and is regarded as a thermal bath of temperature

$$T_{\mathrm{U}} = \frac{\hbar a}{2\pi c k_B} \tag{2.14}$$

by the accelerating observer. Although the original derivation was given for free fields, the validity of the Unruh effect for interacting fields is a consequence of general results obtained in axiomatic quantum field theory [91, 92], as first recognized in [93]. The Unruh effect indicates that already in flat spacetime the notion of particles is observer dependent. Other seemingly paradoxical aspects of the Unruh effect are covered in [94]. Recent developments and issues regarding experimental detection are reviewed in [95].

The Unruh effect is also invoked to prevent a violation of the generalized second law in the following form: A box with given energy and entropy is released from infinity and its content dropped into the black hole. The energy gain of the black hole can be made arbitrarily small by dropping the box from a point close to the horizon. The horizon area might not increase enough to compensate the loss of entropy, thus violating the generalized second law. In [96], a universal upper bound on the ratio entropy to energy was proposed, which would prevent such violations of the generalized second law. On the other hand, it was argued that the box would feel an effective buoyancy force near the black hole originating from the acceleration radiation. This buoyancy force guarantees a lower bound on the energy gain of the black hole, thus saving the generalized second law without the need for an entropy bound [97, 98].

The similarities between Hawking and Unruh effect are due to the similar horizon structure: any non-extremal Killing horizon looks like a Rindler horizon in the near-horizon approximation. Depending on the choice of boundary conditions different vacua exist, which are suitable for different physical applications. The Unruh vacuum fixes boundary conditions on the past horizon H^- and $\mathscr{I}^-$ [88]. This state is analogous to the original treatment of black hole evaporation by Hawking. For the Hartle–Hawking vacuum one defines boundary conditions on both future and past horizon H^+ and H^- [99, 100], which describes a black hole in equilibrium with incoming radiation, and is therefore the relevant state for the curved spacetime generalization of the Unruh effect. This state does not exist for Kerr black holes [101]. The Boulware vacuum sets boundary condition on $\mathscr{I}^+$ and $\mathscr{I}^-$ and describes a state with no radiation [59], but is singular on past and future horizon and therefore of little physical significance.

The transplanckian problem and black hole analogue systems. Since the direct experimental verification of black hole thermodynamics effects is (and most likely will remain) out of reach, analog systems have been proposed in which the Hawking effect could be studied. One of the first proposed systems concerns sound waves

[2] The sum should be regarded as formal since the quantum theory constructions of the two observers are unitarily inequivalent [49].

in a convergent fluid flow [102]. The linearized equations of motion correspond to the equations for a massless scalar field in a background metric that can be brought in a Schwarzschild-like form, thus producing a sonic black hole with the speed of light replaced by the speed of sound. Quantization of the scalar field in this background leads to the emission of sound waves in a thermal spectrum at the sonic horizon, the temperature of which is given by a quantity analogous to the Hawking temperature. Albeit very small, this quantity should be measurable in principle. The field of analogue gravity has grown rapidly in the last decades; the interested reader is referred to [103, 104] and references therein.

Black hole analogue systems play an important role in the study of the transplanckian puzzle. A Hawking mode of frequency ω measured at infinity that was emitted a time t after formation of the black hole stems from a fluctuation of frequency $\omega \exp(\kappa t)$. This means that modes emitted a sufficiently long time after the formation of the black hole originated from modes beyond the Planck energy, where the theory can no longer be trusted. This raises the question if the Hawking effect depends on the details of a transplanckian theory. Certainly, Lorentz invariance would guarantee the validity of the derivation, but it is a logical possibility (though one that is highly-constrained by observations from the Fermi Large Area Telescope [105]) that Lorentz invariance is broken at arbitrarily high energies, see [106] for a discussion. A viable option, at least for analogue systems, is the study of Hawking radiation with a modified dispersion relation at high frequencies. Since this situation is similar to the study of black hole analog systems in fluid mechanics, where the theory breaks down at wavelengths comparable to the atomic scale, these systems are used in the study of the transplanckian problem. A particular example was presented in [107], where it was shown that Hawking radiation occurs despite a change in the dispersion relation at high frequencies.

The transplanckian problem was far from being settled in that decade, but it seems that Hawking radiation is robust enough to persist, even if the theory is modified at ultrahigh energies like in analogue systems [108–113].

Black hole evaporation and information loss. As pointed out above, black holes evaporate due to Hawking radiation on a timescale $\tau \propto G^2 M_0^3/(\hbar c^4)$, which is of order 10^{70}s for a solar mass black hole. Although this amount of time is enormous already for solar mass black holes, the very fact that black holes evaporate reveals the deep conceptual problem of information loss, first raised in [56]. At the classical level, the no-hair theorem implies that the large amount of data needed to describe the precollapse geometry is reduced to a small number of quantities that describe the black hole. The remaining information of the precollapse geometry is not accessible to the outside observer, but in principle can be thought of as residing in the black hole. The real paradox rears its head when Hawking radiation is taken into account. Consider an initial pure state that describes an object falling into the black hole. The Hawking radiation emitted by the black hole is in a mixed state due to correlations between states outside the horizon and states inside the black hole, but after some time the black hole has evaporated completely, and one is left only with the mixed state of Hawking radiation. The evolution from the initial pure state to perfectly thermal

Hawking radiation is therefore not unitary and information appears to be lost in the process. This is in contrast to ordinary physical systems like a star or a burning lump of coal, where the emissions contain correlations that would in principle allow one to reconstruct the initial state. It was not clear at the time if this might also be a viable explanation for an evaporating black hole, mostly due to the lack of a sufficiently detailed theory of quantum gravity.

2.4 1983–1993

The results of the previous decade revealed several problems—the information paradox, the universality of the area law, and the nature of the states underlying the Bekenstein-Hawking entropy—that became the focus of research during the period 1983–1993. Many researchers turned their attention towards lower-dimensional models, where theories are more tractable but still suffer from conceptual issues such as the information paradox. At the same time, investigations into a diverse array of gravitational theories revealed certain universal features of black hole thermodynamics and led to the first early successes in a state-counting approach to explaining black hole entropy. Before delving into lower-dimensional gravity we state some of the main conclusions that were reached from its study.

What to do with information loss? The information loss problem is of conceptual rather than technical nature. Like other conceptual issues in classical and quantum gravity, it arises independently from the spacetime dimension. Therefore, a useful strategy is to consider lower-dimensional models of gravity where the technical problems become more manageable, conceptual issues can be addressed and, ideally, resolved. See [114] for a textbook on lower-dimensional gravity from 1988. Particularly the CGHS model of string-inspired 2-dimensional dilaton gravity with matter [115] (see below) inspired numerous investigations of evaporating black holes in two dimensions, such as the one by Russo et al. [116]. Exact solubility (even in the presence of quantum effects) is a key feature of the RST model, which allows to address the endpoint of Hawking evaporation. Depending on the energy flux of the infalling matter either no horizon forms or an apparent horizon does form and eventually evaporates to a naked singularity, which requires the imposition of suitable boundary conditions, for which a natural choice exists in this model. Most importantly, the whole process is described in a unitary way, so that all information is recovered in this case.

Black hole complementarity. Based on studies of 2-dimensional dilaton gravity models, Susskind, Thorlacius and Uglum advocated the "black hole complementarity" principle [117] (which was formulated independently in [118]). The essence of this principle is captured by four postulates (three of which were spelled out explicitly in [117], which we quote verbatim): 1. The process of formation and evaporation of a black hole, as viewed by a distant observer, can be described entirely within the

context of standard quantum theory. In particular, there exists a unitary S-matrix which describes the evolution from infalling matter to outgoing Hawking-like radiation. 2. Outside the stretched horizon[3] of a massive black hole, physics can be described to good approximation by a set of semi-classical field equations. 3. To a distant observer, a black hole appears to be a quantum system with discrete energy levels. The dimension of the subspace of states describing a black hole of mass M is the exponential of the Bekenstein entropy (2.1). 4. A freely falling observer experiences nothing extraordinary when entering the black hole.

The attribute "complementarity" refers to the fact that the outside observer detects a membrane-like structure near the black hole horizon where information is stored, while the infalling observer sees no membrane at the horizon. The reason why these mutually exclusive viewpoints do not necessarily generate a contradiction is because there should not exist any "super-observer" that simultaneously has access to both viewpoints.

Lower-dimensional gravity. The lowest spacetime dimension that makes sense to consider is $1+1$, since this is the lowest dimension where the notions of black holes, causal structure and curvature exist. If additionally the existence of graviton excitations (at least off-shell) is required then the lowest dimension one can consider is $2+1$, since this is the lowest dimension where linearized perturbations of the metric $h_{\mu\nu}$ have a transverse-traceless part, $h_{\mu\nu} = h^{\rm TT}_{\mu\nu} + \nabla_{(\mu}\xi_{\nu)} + \frac{1}{3}\, h\, g_{\mu\nu}$. Moreover, $2+1$ is the lowest dimension where the notion of the area of the event horizon is meaningful (in $1+1$ dimensions this 'area' is just a point). For these reasons, the main focus in lower-dimensional gravity is on $1+1$ and $2+1$ dimensional models, depending on the scope of the model.

Dilaton gravity in two dimensions. In two dimensions there are various ways to motivate which kind of gravity model one should consider. The theory *not* to consider is Einstein gravity, since there are no meaningful Einstein equations in two dimensions (the 2-dimensional Einstein tensor vanishes trivially for any metric). Instead, there are (at least) five different ways to end up with the same class of models, namely 2-dimensional dilaton gravity. Its bulk action

$$I = \frac{1}{16\pi G} \int \mathrm{d}^2x \sqrt{-g} \left(XR - U(X)(\partial X)^2 - 2V(X) \right) \tag{2.15}$$

depends on two free functions, $U(X)$ and $V(X)$, of the dilaton field X. We summarize briefly five different ways to end up with an action of type (2.15).

1. **Gravity as gauge theory**. Jackiw [120] and Teitelboim [121] considered a 2-dimensional gravity model with constant curvature, which can be formulated as a non-abelian BF-theory with gauge group $SO(2,1)$ [122, 123]. The generators P_a and J are interpreted as translation and boost generators, respectively. They obey the algebra $[P_a,\ P_b] = \Lambda \varepsilon_{ab}\, J$ and $[P_a,\ J] = \varepsilon_a{}^b P_b$, where Λ is a

[3] The stretched horizon (or the earlier "brick wall" [119]) is also discussed in these papers and captures the membrane description of a black hole suitable for a distant observer.

parameter that sets the scale of curvature (one could call it 'cosmological constant'). The $so(2,1)$ connection $A = e^a P_a + \omega J$ decomposes into zweibein e^a and (dualized) connection $\omega = \frac{1}{2}\,\omega^{ab}\varepsilon_{ab}$. Its non-abelian field strength F is then coupled linearly to co-adjoint scalars in the BF-action, which reads explicitly

$$I \sim \int \left(X_a(\mathrm{d}e^a + \varepsilon^a{}_b \omega e^b) + X\,\mathrm{d}\omega + \varepsilon_{ab}\, e^a \wedge e^b\, \Lambda X\right). \tag{2.16}$$

Integrating out the auxiliary field X_a establishes the constraint of vanishing torsion, which allows to eliminate also the spin-connection ω and to convert the first order action (2.16) into the second order action (2.15) with $U(X) = 0$ and $V(X) = \Lambda X$. A similar BF-type of construction was provided by Cangemi and Jackiw [124] for a string inspired model discussed below. The gauge theoretic formulation for arbitrary dilaton gravity theories was provided by Ikeda and Izawa [125, 126] and by Schaller and Strobl [127], dubbed "Poisson-σ model".

2. **Dimensional reduction**. Assuming spherical symmetry in D spacetime dimensions leads to a line-element in adapted coordinates that depends on a 2-dimensional metric and a scalar field, $\mathrm{d}s^2 = g_{\alpha\beta}\,\mathrm{d}x^\alpha\,\mathrm{d}x^\beta + X^{1/(D-2)}\,\mathrm{d}\Omega^2_{S^{D-2}}$, where $\mathrm{d}\Omega^2_{S^{D-2}}$ denotes the line-element of the round $(D-2)$-sphere [128–132]. Inserting this ansatz into the D-dimensional Einstein–Hilbert action permits to integrate out all angular coordinates and eventually establishes an effective 2-dimensional model whose bulk action is precisely (2.15), with $U(X) = -(D-3)/[(D-2)X]$ and $V(X) \propto X^{(D-4)/(D-2)}$. Curiously, in the limit $D \to \infty$ the model derived from bosonic string theory is recovered (with 2-dimensional target space, see below) [67, 133, 134].
3. **Limiting case of Einstein–Hilbert in $2+\varepsilon$ dimensions**. Weinberg's idea of asymptotic safety in gravity emerged from his consideration of gravity in $2+\varepsilon$ dimensions, in the limit of small ε [135]. As we mentioned above, taking $\varepsilon \to 0$ leads to trivial equations of motion. However, if simultaneously Newton's constant scales to zero appropriately, then the limiting action can be non-trivial. In fact, Mann and Ross argued that the action obtained in this way is a 2-dimensional dilaton gravity action (2.15) with $U(X) =$ const. and $V(X) = 0$ [136]. A more recent analysis confirms the result for $U(X)$, but finds $V(X) \propto e^{-2X}$ [137].[4] Such an action describes Liouville gravity, see [138, 139] for reviews.
4. **Higher power curvature theories**. Models that are non-linear in curvature and/or torsion are viable in two dimensions. In particular, the Katanaev–Volovich model describes 2-dimensional Poincaré gauge theory, i.e., a model with Lagrange density $R^2 + T^2$, where R is curvature and T torsion [140]. The Katanaev–Volovich model is classically equivalent to dilaton gravity (2.16) with $U(X) =$ const. and $V(X) \propto X^2$, see [126, 141, 142]. Similarly, generic theories with non-linear Lagrangians in curvature and torsion are equivalent to generic dilaton gravity, provided the potentials $U(X)$ and $V(X)$ are chosen appropriately [143].

[4] The derivation in [137] exploits a spherically symmetric ansatz in $2+\varepsilon$ dimensions, dualizes to a different action for which the limit $\varepsilon \to 0$ is well-defined and dualizes back after taking the limit.

5. **Strings in two dimensions**. Conformal invariance of the sigma model action for the closed bosonic string,

$$I^{(\sigma)} = \frac{1}{4\pi\alpha'} \int \mathrm{d}^2 z \sqrt{-h} \left(g_{\mu\nu} h^{ij} \partial_i X^\mu \partial_j X^\nu + \alpha' \Phi \mathscr{R} \right) \tag{2.17}$$

requires that the trace of the world-sheet energy-momentum tensor vanishes

$$T_i^i \propto \beta^\Phi \mathscr{R} + \beta^g_{\mu\nu} h^{ij} \partial_i X^\mu \partial_j X^\nu = 0 \,. \tag{2.18}$$

The parameter α' is the string tension, h_{ij} is the world-sheet metric, $\mathscr{R}$ its Ricci scalar, X^μ are the target space coordinates, and Φ is the dilaton field. Thus, for consistency the β-functions appearing in (2.18) have to vanish [144].

$$\beta^\Phi = -\frac{\alpha'}{4\pi^2} \left(\tfrac{26-D}{12\alpha'} + (\partial\Phi)^2 - 4\nabla^\mu \partial_\mu \Phi - \tfrac{1}{4} R \right) = 0 \tag{2.19}$$

$$\beta^g_{\mu\nu} = R_{\mu\nu} + 2\nabla_\mu \partial_\nu \Phi = 0 \tag{2.20}$$

Here D is the dimension of the target space, $R_{\mu\nu}$ its Ricci tensor and ∇_μ the associated covariant derivative. The conditions of conformal invariance, $\beta^\Phi = \beta^g_{\mu\nu} = 0$, follow as equations of motion from a target space action, which for $D = 2$ turns out to be equivalent to dilaton gravity (2.15) with $U(X) = -1/X$ and $V(X) = 2\lambda^2 X$, upon identifying $X = e^{-2\Phi}$. See [145–148] for some early literature on black holes in 2-dimensional string theory and [138, 149] for some reviews. The model by Callan, Giddings, Harvey and Strominger (CGHS) uses the same target space action as derived from string theory and adds matter fields to describe evaporating black holes [115]; the CGHS model engendered a lot of further research in 2-dimensional dilaton gravity with and without matter, see [67, 150, 151] for reviews.

Thermodynamics of 2-dimensional dilaton gravity models (2.15) was discussed assuming $U(X) = 0$ by Gegenberg et al. [152]. A comprehensive discussion of quasi-local thermodynamics for generic models (2.15) was provided using the Euclidean path integral approach more than a decade later [153].

Taken together, the body of results that these diverse two-dimensional models have in common suggests that certain features of black hole thermodynamics are universal. This is an important observation in its own right, independent of insights into the information paradox and other problems. In particular, with appropriate normalizations the 'classical' contribution to the entropy always takes the form

$$S = 2\pi X_h \tag{2.21}$$

where X_h is the value of the dilaton at the horizon. This result encapsulates inherently two-dimensional models, as well as the s-wave reduction down to two dimensions of the area law for higher dimensional theories. The robust nature of black hole

entropy was made apparent in the work of Wald, who gave a succinct geometric characterization of the entropy for any diffeomorphism-invariant theory of gravity [154, 155].

Quasi-local thermodynamics and Hawking–Page phase transition. A simple calculation shows that the Schwarzschild black hole has a negative specific heat, and therefore cannot be treated as an equilibrium thermodynamic system. York addressed the issue of negative specific heat by putting the black hole inside a cavity of some finite radius that provides a heat bath of fixed temperature [156]. For a sufficiently small cavity the specific heat is positive, leading to a well-defined canonical ensemble. It was shown later that some spacetimes, in particular asymptotically AdS spacetimes, naturally provide a covariant version of such a cavity. In all these examples the existence of a well-defined canonical ensemble means that interesting phase structures can be unraveled. Probably the most famous example is the Hawking-Page phase transition between "hot AdS"—anti-de Sitter space with periodic euclidean time $\tau \sim \tau + T^{-1}$—and an asymptotically AdS black hole [157]. For sufficiently small temperatures the minimum of the free energy is hot AdS, while at high temperatures the ensemble is dominated by the black hole.

Gravity in three dimensions and a connection with conformal field theory. During the same period there was a great deal of pioneering work in 3-dimensional gravity. Deser, Jackiw and Templeton constructed topologically massive gauge theories by adding a Chern–Simons term to the action [158–160]. In the case of gravity this leads to topologically massive gravity, a 3-dimensional theory of gravity that has a local (massive) gravitational degree of freedom. Its bulk action reads

$$16\pi G I^{\text{TMG}} = \int \mathrm{d}^3x\sqrt{-g}\,(R - 2\Lambda) + \frac{1}{2\mu}\int \mathrm{d}^3x\,\varepsilon^{\mu\nu\lambda}\,\Gamma^{\alpha}{}_{\mu\beta}\left(\partial_\nu\Gamma^{\beta}{}_{\lambda\alpha} + \tfrac{2}{3}\,\Gamma^{\beta}{}_{\nu\gamma}\Gamma^{\gamma}{}_{\lambda\alpha}\right) \tag{2.22}$$

Without the gravitational Chern–Simons term, $\mu \to \infty$, Einstein gravity becomes locally trivial [161], but globally it can be non-trivial. In particular, in a seminal paper Brown and Henneaux found that the Hilbert space of any 3-dimensional theory of quantum gravity with AdS boundary conditions falls into representations of two copies of the Virasoro algebra, with central charges for Einstein gravity given by [162]

$$c = \bar{c} = \frac{3\ell}{2G} \qquad \text{where } \Lambda = -\frac{1}{\ell^2}\,. \tag{2.23}$$

This unexpected set of symmetries suggested that such theories might be amenable to an analysis using conformal field theory (CFT) techniques. The Brown–Henneaux results were an important precursor of the AdS/CFT correspondence found a decade later.

Black holes in three dimensions. Another crucial development was the discovery, by Bañados, Teitelboim and Zanelli (BTZ), of black hole solutions of 3-dimensional Einstein gravity with negative cosmological constant [163]. As discussed in [164], the BTZ black holes are locally AdS, but globally differ from AdS. In fact, they are certain orbifolds of AdS such that the ensuing solutions are locally AdS and remain

regular on and outside the event horizon. The line-element in 'Boyer–Lindquist' type coordinates ($\varphi \sim \varphi + 2\pi$),

$$\mathrm{d}s^2_{\mathrm{BTZ}} = -\frac{(r^2-r_+^2)(r^2-r_-^2)}{r^2\ell^2}\,\mathrm{d}t^2 + \frac{r^2\ell^2}{(r^2-r_+^2)(r^2-r_-^2)}\,\mathrm{d}r^2 + r^2\left(\mathrm{d}\varphi + \frac{r_+r_-}{\ell r^2}\,\mathrm{d}t\right)^2 \tag{2.24}$$

makes the similarity to rotating black holes in higher dimensions manifest: there is an ergosphere at $r = (r_+^2 + r_-^2)^{1/2}$, an outer horizon (with rotation) at $r = r_+$, an inner horizon at $r = r_-$, and a singularity behind the inner horizon. Moreover, there is a conserved mass, $M = (r_+^2 + r_-^2)/(8G\ell^2)$, and angular momentum, $J = r_+r_-/(4G\ell)$. The presence of rotating black holes makes 3-dimensional AdS gravity a particularly interesting toy model to address classical and quantum aspects of black holes and their thermodynamical properties. In particular, the entropy is given by the Bekenstein–Hawking result (2.1)

$$S_{\mathrm{BTZ}} = \frac{2\pi r_+}{4G}. \tag{2.25}$$

Cardy formula. The existence of the BTZ solution and the results of Brown and Henneaux led to the first attempt to explain black hole entropy by counting microscopic states. Since the Hilbert space of the theory is organized according to the symmetries of a two-dimensional CFT, one can carry out the state counting by exploiting a result of Cardy [165, 166]. Namely, given some assumptions there is a universal formula for the asymptotic density of states in a CFT_2. The log of the density of states leads to the Cardy formula for entropy

$$S_{\mathrm{Cardy}} = 2\pi\sqrt{\frac{ch}{6}} + 2\pi\sqrt{\frac{\bar{c}\bar{h}}{6}}\,, \tag{2.26}$$

where c, $\bar{c}$ are the central charges and $h, \bar{h}$ are the Virasoro zero-mode charges. Evaluating the Cardy formula (2.26) for the Brown–Henneaux central charges (2.23) and the zero-mode charges $h = (\ell M + J)/2, \bar{h} = (\ell M - J)/2$ of the BTZ black hole (2.24) gives precisely the Bekenstein–Hawking entropy (2.25). This observation was the basis for the near horizon microstate counting pioneered by Strominger and Vafa a decade later [167, 168].

The explanation of (2.25) via microscopic state counting was a significant insight into the nature of black hole entropy. But it also left many important questions unanswered. In particular, the Cardy formula provides information about the asymptotic density of states but it gives no insight into the states themselves. An explanation of black hole entropy that proceeds from the *identification* of microscopic states would not be achieved until the following decade.

Towards holography. Counting black hole microstates through a CFT calculation is a remarkable manifestation of an idea that began to emerge at the end of the third

decade. In an essay dedicated to Abdus Salam, 't Hooft postulated that there is no information loss, i.e., the evolution describing collapse and quantum evaporation of a black hole should only incorporate processes that are not at odds with unitarity [169]. From this postulate and the observation that the Bekenstein–Hawking entropy (2.1) scales like the area, 't Hooft then argued that there could be an equivalent description of the system in terms of an ordinary quantum field theory in one dimension lower.[5] A year later Susskind first coined the expression "holographic principle" and pointed out that string theory could be a candidate for a theory of quantum gravity realizing the holographic principle. But this part of the story already belongs to the next decade.

2.5 1993–2003

As described in the previous section, Cardy's formula relates the Bekenstein-Hawking entropy of the BTZ black hole to the central charge of a two-dimensional CFT. This result foreshadows three major developments during the period 1993–2003: a complete accounting in string theory of microscopic states responsible for the entropy of certain black holes, the emergence of 't Hooft and Susskind's holographic principle, and the development of the AdS/CFT correspondence as a fully-fledged example of holography.

Counting black hole microstates in string theory. String theory is a consistent theory of quantum gravity and is therefore a natural framework for investigating the microscopic origin of black hole entropy. As early as 1993, it was suggested that the density of states in perturbative string theory might be sufficient to explain the Bekenstein-Hawking entropy [170–172]. The main development during this period (and arguably one of the most significant accomplishments of string theory in any period) was Strominger and Vafa's calculation of the density of states for certain supersymmetric black holes [173].

String theory contains both bosonic and fermionic degrees of freedom, with the bosonic sector including multiple p-form gauge fields under which black holes may be charged. In the case of supersymmetric black holes these charges completely characterize the horizon, which has an area that is independent of moduli like the string coupling or compactification volumes. The simplest such black holes involve either one or two charges, but such configurations possess either singular horizons or horizons with zero area. The Bekenstein-Hawking entropy is relevant for non-singular horizons with macroscopic area, which requires at least three charges. Strominger and Vafa considered these sorts of black holes in string theory compactified on the five dimensional product spaces $S^1 \times T^4$ and $S^1 \times K3$. Their construction involves q_1 D1-branes wrapping the circle, q_5 D5-branes wrapping all five compact dimensions, and massless strings stretched between the branes carrying n units of momentum

[5] 't Hooft also provided as an example a realization of the holographic principle in terms of some cellular automaton model.

around the S^1. At weak coupling this system is described by a supersymmetric field theory on the worldvolume of the branes, and it is possible to enumerate the states with given charges. The resulting density of states is approximately

$$\rho \approx \exp\left(2\pi\sqrt{q_1\, q_5\, n}\right). \tag{2.27}$$

As the gravitational (string) coupling is increased the picture changes, and at strong coupling the appropriate description of the system is a black hole. The horizon of this black hole has area

$$A_H = 8\pi G\sqrt{q_1\, q_5\, n}\,, \tag{2.28}$$

where each of the charges must be large to suppress various types of corrections. Although the descriptions at weak and strong coupling are radically different, the state counting is protected by supersymmetry. So even though the density of states (2.27) was derived at weak coupling, it still applies in the limit where the system is described by the black hole. To leading order the log of the density of states exactly reproduces the area law

$$S = \log\rho = 2\pi\sqrt{q_1\, q_5\, n} = \frac{A_H}{4G}\,. \tag{2.29}$$

Thus, this result of Strominger and Vafa provides the first derivation of the Bekenstein–Hawking entropy that identifies and counts a specific set of microscopic states associated with the parameters describing the macroscopic black hole. Similar calculations have been carried out for supersymmetric black holes in four dimensions [174], near-extremal black holes [175, 176], and even certain extremal black holes with broken supersymmetry [177]. Comprehensive reviews can be found in [178, 179].

Despite the success of this program, there is still no explicit construction of the microstates of non-supersymmetric, non-extremal black holes like the Schwarzschild or Kerr solutions (though, in the latter case progress has been made for the extremal solution [180]). It is also important to point out that while the counting of states is protected by supersymmetry, the states in the strong coupling regime bear no resemblance to the states at weak coupling. In this sense, it is not clear what constitutes the "states of the black hole". Indeed, given a generic state in the weakly coupled regime it is not clear what happens as the coupling is increased. It is possible (and with hindsight also plausible) that the states in the strongly coupled regime are free of horizons. This idea has motivated a tremendous amount of work—the so-called *microstate* and *fuzzball* programs—which will be discussed in the next section.

Holographic principle. Around the same time that a stringy origin for the black hole density of states was first being considered, 't Hooft put forth a radical suggestion: that gravitational physics in $3+1$ dimensions must effectively become $2+1$ dimensional at Planckian scales [169]. Susskind, building off his own work on the role of string theory in explaining the Bekenstein–Hawking entropy, explored the consequences of this idea and dubbed it the "holographic principle" [181]. This principle

is often regarded as synonymous with the Bekenstein–Hawking area law for black hole entropy, but it is in fact a much deeper statement about locality, unitarity, and the nature of quantum gravitational physics.

In its earliest form, the holographic principle was interpreted as a bound on the number of degrees of freedom needed to describe physics in a spatial region. Quantum field theory suggests that any such region contains an infinite number of degrees of freedom associated with the infinite number of harmonic oscillator states possible at each of the infinite number of points in the region. Including gravity changes this counting, since exciting too many of these states would provide enough energy to form a black hole. A better estimate would 'coarse grain' space on lengths of order the Planck scale and, at the very least, place an upper limit on the energy contained in any Planck volume to avoid creating a black hole. With these restrictions the number of degrees of freedom scales like the volume V of the region. But this must be a gross over-counting, since black holes could still form on larger scales even if the energy bound on each Planck volume was not saturated. And since the largest black hole that 'fits' in the region has an entropy given by $A/4$, it must be that the number of accessible degrees of freedom in a region scales like the area bounding the region rather than its volume.

The conclusion described above forces a choice between locality and unitarity. If all the degrees of freedom predicted by local physics were available in a region of volume V, then it would not be possible to accommodate all possible states of the system with the dramatically reduced number of states after gravitational collapse. To preserve unitarity, it must be that physics in any region bounded by a surface of area A is described by no more than $A/4$ degrees of freedom, even in the absence of a black hole.

This early form of the holographic principle depends crucially on the idea that the entropy in a spatial region V is limited by the area of the surface $B = \partial V$ bounding the region

$$S[V] \leq \frac{c^3}{4\,G\,\hbar}\,A(B)\,. \tag{2.30}$$

But it was soon realized that this spacelike form of the entropy bound can fail [182, 183], leading researchers to attempt a reformulation of the bound in terms of light cones. This program culminated with Bousso's Covariant Entropy Conjecture [184], a covariant generalization of the original bound which replaces the spacelike region V with a null hypersurface. Specifically, given some surface B with area $A(B)$ the light sheet $L(B)$ is the null hypersurface generated by following light rays from B until they begin to expand. The entropy on any light sheet of a surface is then bounded according to

$$S[L(B)] \leq \frac{c^3}{4\,G\,\hbar}\,A(B)\,. \tag{2.31}$$

A comprehensive review of the Covariant Entropy Conjecture and the holographic principle in general is given in [185].

Like other entropy bounds, there is no formal derivation of (2.31). Rather, it is a conjecture for which there is strong circumstantial evidence and a lack of counterexamples. Since any derivation of this result would require a complete theory of quantum gravity, it is hoped that the holographic principle will instead provide some guidance as to what such a theory might be. It is tempting, given the form of the bounds (2.30) and (2.31), to assume that the physics interior to a region is somehow encoded on its boundary. The holographic principle offers little direct insight as to whether this is the case, or how it might be accomplished[6]. Nevertheless, this assumption, combined with calculations inspired by the work of Strominger and Vafa, leads to a fully realized form of the holographic principle in Maldacena's AdS/CFT correspondence.

AdS/CFT correspondence. The work of Strominger–Vafa showed how the entropy of certain supersymmetric black holes may be understood via a calculation in a field theory on the world volume of a D-brane bound state. The entropy is not the only quantity that can be explained this way. For instance, absorption cross sections calculated using both the gravity and field theory descriptions are found to agree. This observation inspired similar comparisons for a stack of D3-branes in type IIB string theory [186–188]. The agreement between the gravity and field theory calculations for the D3-brane system gives the first pieces of evidence for the AdS/CFT correspondence.

Given a stack of N parallel D3-branes, low energy excitations on the worldvolume are described by a four-dimensional $U(N)$ gauge theory with $\mathcal{N} = 4$ supersymmetry [189] and a coupling constant related to the string coupling by $g_{YM}^2 \sim g_s$. For N large and $g_{YM}^2 N \ll 1$ the theory is well-described by perturbation theory with non-planar diagrams suppressed by factors of $1/N$. On the other hand, the near-horizon geometry of the stack of branes looks like a product space of the form $\mathrm{AdS}_5 \times \mathrm{S}^5$, with both factors having a radius of curvature ℓ that satisfies

$$\ell^4 = 4\pi g_s N (\alpha')^2 \,. \tag{2.32}$$

The description of the system in terms of gravitational physics requires curvatures to be much smaller than the string scale, $\ell \gg \sqrt{\alpha'}$, which implies $g_s N \gg 1$. In other words, the gravitational description can be trusted precisely when the worldvolume field theory is strongly coupled. Maldacena conjectured that these descriptions are in fact *the same*; two sides of a strong-weak coupling duality [190]. In this picture the conformal symmetries of the field theory are realized by the $SO(4, 2)$ isometries of AdS_5, while the R-symmetries are encoded in the $SO(6)$ symmetries of the S^5.

The strongest form of Maldacena's conjecture asserts that type IIB string theory with $\mathrm{AdS}_5 \times \mathrm{S}^5$ boundary conditions is completely equivalent to four-dimensional Super Yang-Mills for all values of the parameters g_s and N. This is the most tantalizing and least tested form of the correspondence. When $N \to \infty$ at fixed $g_{YM}^2 N$ the duality relates classical string theory to Super Yang-Mills with finite coupling, and

[6] Such an encoding results in an entropy that scales like the area, which suggests a local and non-gravitational description on the boundary.

many consequences of this form of the conjecture have been tested using unexpected integrability properties of the planar sector of SYM [191]. The weakest and most thoroughly examined form of the conjecture follows from letting $g_{YM}^2 N \to \infty$. In that case the gravitational side of the duality reduces simply to type IIB supergravity on $AdS_5 \times S^5$, which is equivalent to the strong-coupling limit of SYM. All forms of the duality are manifestly holographic, in the sense that the gravitational physics of a $d+1$ dimensional asymptotically AdS spacetime is encoded in a local field theory on the spacetime's d dimensional conformal boundary.

Maldacena's original conjecture, which includes a number of other brane configurations with low-energy descriptions in terms of various supergravities, has been extended, deformed, and modified in various ways. It has primarily been used to extract useful statements about strongly coupled gauge theories. For instance, correlation functions of operators in the gauge theory can be calculated from the string theory partition function, which in the standard (weak) form of the correspondence is dominated by contributions from saddle points of the supergravity action. The on-shell action can be expressed as a functional of 'boundary data' ϕ_0 for the fields ϕ that play the role of sources J for operators $\mathcal{O}$ in the dual field theory

$$Z_{\text{sugra}}\big[\phi_0 = \phi|_{\partial \text{AdS}}\big] = Z_{\text{CFT}}\big[\phi_0 = J\big] \sim \langle \exp\big(\int \mathcal{O}\phi_0\big)\rangle_{\text{CFT}} \,. \tag{2.33}$$

The full impact of AdS/CFT on the study of strongly coupled gauge theories is beyond both the purpose and scope of this review. But the duality does offer several useful insights into black hole thermodynamics, which we will focus on for the rest of this section.

Not long after the AdS/CFT correspondence was first proposed, Witten showed how the thermodynamics of an AdS black hole can be understood in terms of the (large N) thermodynamics of the dual gauge theory [192]. In particular, the usual Hawking–Page transition from AdS-Schwarzschild to "hot AdS" corresponds to a confining/deconfining phase transition in the dual field theory [7]. This can be seen from the free energy of the two bulk configurations, which when expressed in terms of field theory quantities scales as $F \sim O(1)$ and $F \sim O(N^2)$, respectively, in the confined and deconfined phases.

The AdS/CFT correspondence also illuminates calculations of the entropy of the BTZ black hole, raising Brown and Henneaux's result [162] from an analogy to an actual counting of states in a dual CFT [167, 193]. This is especially important for a number of black holes that arise in string theory, which typically have near-horizon geometries of the form $\text{BTZ} \times Y$ for some space (or product of spaces) Y. The entropy of these black holes can then be explained via a similar state counting without having to work out the full details in the worldvolume theory. For a review, see [178, 179].

Perhaps the most important consequence of AdS/CFT for black hole thermodynamics is the idea that a gravitational theory, which presumably includes black

[7] The dual field theory at finite temperature is defined on $S^3 \times S^1$ and therefore has compact volume. Nevertheless, a phase transition is possible because the theory is considered in the large N limit.

holes, is equivalent to a theory that is unitary. There are many ways to interpret such a statement in the context of the information paradox. Since the duality applies to the dynamics of both theories it is tempting to 'resolve' the paradox by pointing out that any process on the gravity side—including the formation and eventual evaporation of a black hole—is encoded in unitary physics on the field theory side. But this is far from a complete argument. In particular, the unitary evaporation of a AdS-Schwarzschild black hole still forces one to either abandon local Hamiltonian evolution (in the bulk) in a setting where it is expected to be a good description, accept the formation of some sort of macroscopic remnant that remains entangled with the Hawking radiation, or else revisit assumptions about the formation of black holes in string theory [194]. One possible resolution is that the weakly coupled D-brane states that are counted in, for example, the Strominger–Vafa calculation do not form horizons as the gravitational coupling is increased. Instead, such states possess significant structure on horizon scales, and the traditional black hole is viewed as a coarse-grained description of the actual states. This possibility, which was mentioned earlier, is the basis for the *microstate* and *fuzzball* programs described in the next section.

The AdS/CFT correspondence is, at present, the most fully realized implementation of the holographic principle. It therefore owes its existence, at least in part, to the comparatively humble idea that the entropy of a black hole scales like the horizon area (2.1). In turn, AdS/CFT has inspired a number of generalizations, extensions, and applications which may be considered descendants of black hole thermodynamics. Some early examples during the period 1993–2003 include duals of confining field theories with $\mathcal{N} = 1$ supersymmetry [195], the dS/CFT correspondence relating quantum gravity on de Sitter space to a Euclidean CFT [196, 197], proposed duals of $O(N)$ vector models in terms of higher spin gauge theories [198], and even applications of gauge/gravity duality techniques to calculations in inflationary cosmology [199–201].

The topics discussed in this section represent major achievements during the period 1993–2003, but they were certainly not the only interesting developments during that time. For instance, in 1995 Jacobson was able to extract, under certain assumptions, the Einstein equations from horizon thermodynamics [202]. This result inspired a fair amount of subsequent work, especially in recent years [203, 204].

2.6 2003–2013

The previous decade saw great progress in microscopic state counting, and the emergence of holography as an important and perhaps fundamental property of quantum gravity. In recent years there has been a focus on applications and generalizations of AdS/CFT, efforts to identify the gravitational states associated with a black hole, and attempts to comprehensively resolve the information paradox. Some new problems have arisen, but developments that touch on two or more of these issues suggest

a convergence towards a deeper understanding of quantum gravity and black hole thermodynamics.

Tests and applications of AdS/CFT? Early tests of AdS/CFT spawned a number of further checks that probed different regimes of the correspondence. For instance, methods known from integrable systems, such as the thermodynamic Bethe Ansatz, allowed to check aspects of AdS/CFT beyond perturbation theory (in particular, for arbitrary values of the 't Hooft coupling constant λ); see [191] for a review. As the correspondence matured a number of new applications were uncovered. An emblematic example is the prediction of the ratio of shear viscosity η to entropy density s in the infinite coupling limit [205, 206].

$$\frac{\eta}{s} = \frac{\hbar}{4\pi k_B} \tag{2.34}$$

In relativistic heavy ion collisions the same order of magnitude was observed for η/s (see [207]), which inspired both phenomenologists and theoreticians to apply AdS/CFT methods to the description of relativistic plasmas, see e.g. [208–211] for reviews. The key feature of the η/s story is that a complicated calculation on the field theory side—determining the shear viscosity for a strongly coupled plasma—is mapped to a problem on the gravity side that is suitable for a bright PhD student. Indeed, Damour provided a comparable calculation in his PhD thesis already in 1979 [212].

Gauge/gravity correspondences. The past decade has seen numerous further attempts to phenomenologically apply ideas from the AdS/CFT correspondence to more general settings. These 'gauge/gravity' correspondences began with deformations of AdS/CFT, but were soon extended to conjectured dualities between theories that bear little resemblance to asymptotically AdS gravity or $\mathcal{N} = 4$ Super-Yang–Mills. As above, the idea is to map complicated (strong coupling) problems on the gauge theory side to fairly simple problems on the gravity side. Examples include condensed matter applications such as cold atoms [213–215], Lifshitz fixed points with non-relativistic scaling symmetries [216], superfluids/superconductors [217–219], non-Fermi liquids/strange metals [220–223] and the gravity/fluid correspondence [224–228] (based on the membrane paradigm [229]). Some applications of proposed gauge/gravity dualities to condensed matter systems are reviewed in [230–235].

Limits of holography. We discuss now in a bit more detail some extensions of the AdS/CFT correspondence that are more in line with the main topic of our review. An interesting theoretically motivated question to ask is, how general is holography? Originally, the holographic principle was motivated by avoidance of information loss and preservation of unitarity, but the way the AdS/CFT correspondence works makes it plausible that it could also apply to systems that are non-unitary. Moreover, if the holographic principle is a true statement about Nature then it should be realized in settings other than AdS, such as asymptotically flat or accelerating Friedmann–Lemaitre–Robertson–Walker spacetimes.

Finally, it is interesting to ask whether there are theories apart from string theory that permit a holographic description. A conclusive answer to this question would be an important achievement. If affirmative, then such theories might provide novel playgrounds for theoretical considerations about holography as well as new applications along the lines of AdS/CFT. If negative, we would have established a direct link between holography and string theory, i.e., holography would necessarily imply string theory.

Non-unitary holography. Partly for simplicity and partly because there were many developments in the past decade, we restrict ourselves mostly to 3-dimensional theories of gravity in order to address the issues raised in the previous paragraph. Let us start with the question to what extent holography could apply to non-unitary theories. This question is somewhat delicate, because non-unitarity is often associated with some sickness of the theory. However, there are also systems that exhibit non-unitarity in a 'controlled' way. This includes, for instance, open quantum systems and systems with quenched disorder. In a story with several interesting twists, it appears that TMG (2.22) at the critical point $\mu\ell = 1$ corresponds to a log CFT, as suggested first in [236]. Log CFTs are specific non-unitary CFTs where two or more operators have degenerate scaling dimensions and the Hamiltonian acquires a Jordan block structure [237–239]. They are used, for example, in the description of systems with quenched disorder. A key element on the gravity side is the emergence of log modes [236]

$$\psi^{\log}_{\alpha\beta} = \lim_{\varepsilon\to 0} \frac{\psi^M_{\alpha\beta} - \psi^L_{\alpha\beta}}{\varepsilon} = -2(it + \ln\cosh\rho)\,\psi^L_{\alpha\beta} \tag{2.35}$$

as linearized perturbation on the AdS background. The middle equation indicates the degeneration of the massive graviton modes ψ^M with the 'left-moving boundary graviton' modes ψ^L (specific Einstein-gravity modes at linearized level). The latter are eigenstates of the Hamiltonian, $H\psi^L = i\partial_t\psi^L = h\psi^L$, while the former are not: $H\psi^{\log} = i\partial_t\psi^{\log} = h\psi^{\log} + 2\psi^L$. These two equations make manifest the Jordan block structure of the Hamiltonian H when acting on the pair $\psi^{\log}$, ψ^L. See [240] for a full account of various checks, generalizations and possible applications of the AdS/log CFT correspondence. Thus, it seems that it is possible to extend the holographic principle to theories that exhibit non-unitarity in a controlled way.

Flat space holography. There was some progress on extracting features of the flat space S-matrix from AdS/CFT correlators, see e.g. [241–245], but it is still fair to say that efforts at flat-space holography have not met with a great deal of success in dimension four and above. In three dimensions one can essentially repeat the Brown–Henneaux construction, which was done by Barnich and Compere [246]. The asymptotic symmetry algebra was found to be the Bondi–van der Burg–Metzner–Sachs (BMS) algebra [247, 248] in three dimensions, which arises also as the ultra-relativistic contraction (or large AdS radius limit) of the two-dimensional conformal algebra. These algebras are also known as Galilean conformal algebras [249, 250], which led to the notion of a 'BMS/GCA correspondence' [251]. A specific proposal

for a flat space/CFT correspondence is flat space chiral gravity (TMG (2.22) in the limit $\ell \to \infty$ and $G \to \infty$, with μG kept finite), which is conjectured to be dual to a chiral half of a CFT [252]. In particular, for central charge $c = 24$ the conjectured CFT is a chiral half of the monster CFT (proposed originally by Witten in the context of Einstein gravity [253]), exactly like in the chiral gravity proposal by Li et al. [254]. Its partition function is given by the J-function [253, 255] and due to chirality depends solely on the 'left-moving' modular parameter q.

$$Z(q) = J(q) = \frac{1}{q} + 196884\, q + \mathcal{O}(q^2) \tag{2.36}$$

The number 196884 is interpreted as one Virasoro descendant of the vacuum plus 196883 primary fields corresponding to flat space cosmology horizon microstates (see below). The flat space chiral gravity quantum entropy $S = \ln 196883 \approx 12.2$ differs only by about 3 % from the semi-classical Bekenstein–Hawking result $S_{\text{BH}} = 4\pi \approx 12.6$ (in suitable units). For quantum gravity applications the (flat space) chiral gravity situation seems optimal: there are quantum corrections that are not completely negligible (of the order of a few percent), but the theory is not "ultra-quantum" so that geometric notions associated with the semi-classical limit, like black hole horizons, can still be discussed meaningfully. Flat space cosmologies [256, 257] are the flat space analog of BTZ black holes (2.24) and permit a microstate counting similar to AdS (2.26), see [258, 259]. They are subject to a Hawking–Page like phase transition [260] so that at least in three dimensions cosmic evolution can be generated by heating (and gently stirring) flat space. For further aspects of flat space holography see e.g. [261–269].

Higher spin holography. Remarkably, AdS spacetimes permit interacting massless particles with spin greater than two [270–273]. These 'higher spin' theories could be relevant for the holographic description of certain sectors of large N gauge theories. In particular, Klebanov and Polyakov proposed that a particular Vasiliev-type higher spin theory on AdS_4 might be exactly dual to the $O(N)$ vector model (at large N) in three dimensions. This conjecture triggered an intensive study of the subject with impressive achievements [274–277]. An interesting technical aspect of higher spin holography is that it provides a weak/weak duality and therefore allows to test holography with high precision (the other side of the coin is that higher spin holography is of less practical use than AdS/CFT, since strong/weak dualities can map hard calculations to simple ones). Coming back to three bulk dimensions, Henneaux and Rey (and independently Campoleoni, Fredenhagen, Pfenninger and Theisen) generalized the Brown–Henneaux analysis to higher spin theories with AdS boundary conditions [281, 282], and a few months later Gaberdiel and Gopakumar proposed a correspondence between Vasiliev-type higher spin gravity and minimal model CFTs [278–280]. Some selected papers and reviews are [283–292]. Recently, the topics of flat space and higher spin holography were combined [293, 294], in the spirit of non-AdS holography for three dimensional higher spin gravity [295]. The main observation is that unlike the spin-2 case, higher spin theories allow for many different

backgrounds, including Lobachevsky, Lifshitz, Schrödinger and warped AdS besides more common backgrounds such as AdS or flat space, without the addition of matter fields.

Holographic entanglement entropy. Entanglement entropy is an entanglement measure for bipartite pure states $|\Psi\rangle$ and is defined as the von Neumann entropy

$$S_A = -\mathrm{tr}\rho_A \ln \rho_A = -\lim_{n\to 1} \frac{\mathrm{d}}{\mathrm{d}n} \mathrm{tr}\rho_A^n \tag{2.37}$$

associated with the reduced density matrix $\rho_A = \mathrm{tr}_B|\Psi\rangle\langle\Psi|$ of a subsystem A, where the total system is divided into two subsystems A and B, see e.g. [296]. For the present context one can think of $A(B)$ as the exterior (interior) of a black hole. Then S_A can be thought of as the entropy for an observer who has access only to the black hole exterior. The fact that entanglement entropy obeys an area law led to the suggestion [297–299] that Bekenstein–Hawking entropy could be interpreted as entanglement entropy (see [300] for a review).

Entanglement entropy has found many applications in quantum systems, see e.g. [301–304], but is not easy to calculate in interacting quantum field theories in dimension greater than two [sometimes the so-called replica trick can be used, which exploits the second equality in (2.37)]. The holographic entanglement entropy proposal by Ryu and Takayanagi [305, 306] applies holographic ideas to map the difficult calculation of entanglement entropy on the field theory side to an elementary calculation of minimal surfaces on the gravity side. This proposal has passed several tests by successfully reproducing the entanglement entropy in well-understood cases, see [307] for a review. Taking the proposal for granted it can then be applied to situations in which no other method exists (currently) to determine entanglement entropy. Thus, holographic entanglement entropy, which provides a link between black hole thermodynamics and quantum information,[8] is another example of the utility of weak/strong dualities like AdS/CFT.

Geometry of black hole thermodynamics and cosmological constant as state parameter. Over the last decade most of the work inspired by black hole thermodynamics focused on holography, AdS/CFT, and related issues. But there were also some interesting purely thermodynamical developments. For example, the geometry of black hole thermodynamics was investigated in numerous papers, see for instance [310–316]. The basic idea goes back to Ruppeiner [317–319], namely to associate the Hessian of the entropy (with respect to some state space variables x^i) with a metric, $g_{ij} = -\partial_i\partial_j S(x^k)$, whose geometric properties are related to the thermodynamics of the system.

Another example is the recent revival of the idea to treat the cosmological constant as a state parameter. This concept goes back to the germinal work of [320, 321]. In order to treat the cosmological constant as a state variable, Λ is introduced as a

[8] We mention in the conclusions that this link is likely to grow stronger in the future. Besides the numerous recent papers on holographic entanglement entropy, some selected papers that also provide such links are [308, 309] and references therein.

constant of integration by coupling a four form field strength to gravity. The value of the cosmological constant can change by spontaneous nucleation of membranes that act as sources for the four form [322–324], or by thermal decay together with the creation of a black hole [325]. These results motivate the study of black hole thermodynamics in AdS, in a phase space extended by Λ and its conjugate variable Θ, the negative of which turns out to be a suitable "thermodynamic" definition for the volume of a black hole [326–333]. See [334] for a review.

Kerr/CFT. The counting of black hole microstates pioneered by Strominger and Vafa in the previous decade initially was restricted to simple but astrophysically irrelevant black holes. In the decade discussed in this section a similar counting was applied to Kerr black holes, which established the 'Kerr/CFT' correspondence, see e.g. [335–345]. Particularly the early papers were based on the near horizon extremal Kerr (NHEK) metric constructed by Bardeen and Horowitz [346].

$$\mathrm{d}s^2_{\mathrm{NHEK}} = M^2(1+\cos^2\theta)\left(\frac{-\mathrm{d}\hat{t}^2+\mathrm{d}\hat{r}^2}{\hat{r}^2}+\frac{4\sin^2\theta}{(1+\cos^2\theta)^2}\left(\mathrm{d}\hat{\phi}+\frac{\mathrm{d}\hat{t}}{\hat{r}}\right)^2+\mathrm{d}\theta^2\right) \tag{2.38}$$

The line-element (2.38) is obtained from the Kerr geometry (2.2) by rescaling $\hat{t} = \frac{\lambda t}{2M}$, $\hat{r} = \frac{\lambda M}{r-M}$, $\hat{\phi} = \phi - \frac{t}{2M}$ and taking the limit $\lambda \to 0$ while keeping $\hat{t}, \hat{r}, \hat{\phi}, \theta$ fixed. The entropy counted by CFT methods then matches the Bekenstein–Hawking result (2.1).

$$S_{\mathrm{CFT}} = \frac{2\pi J}{\hbar} = \frac{A_h}{4G} = S_{\mathrm{BH}} \tag{2.39}$$

While astrophysical black holes are never exactly extremal (the Thorne bound on the dimensionless Kerr parameter is $a < 0.998$ [347]), some of them come very close to this bound. A possible example is GRS1915+105 whose dimensionless Kerr parameter appears to exceed $a \gtrsim 0.98$ [348, 349] (however, see [350]).

Fuzzballs. The various successes of counting black hole microstates all failed to answer an important question: what do the corresponding microstate geometries look like? The fuzzball proposal [351] addresses this question in the context of string theory, stating that there should be $\mathcal{O}(e^S)$ horizonless and regular solutions that asymptote to the geometry of a given black hole, but differ from this geometry at the scale of the horizon, see also [352, 353], and [354–357] for reviews. The fuzzball proposal is motivated by the AdS/CFT correspondence as follows: for every state in the CFT counted by the Cardy formula there is a corresponding regular asymptotically AdS geometry. Each of these geometries encodes the vacuum expectation values of gauge invariant operators in that state through the standard AdS/CFT dictionary. These solutions can be stringy in the interior, though large classes of solutions have been identified that are well-described by the supergravity approximation.

One of the main achievements claimed by proponents of the fuzzball program is a resolution of the information paradox. This can be traced back to a key property of the proposal, which is that quantum gravity effects in string theory can take place on scales much larger than the Planck scale due to 'fractionation' [194]. This results in

significant modifications of Hawking radiation at wavelengths of order GM, allowing information to escape the 'hole' and be recovered (in principle) by external observers. On the other hand, if the system is probed with some object of sufficiently high energy, $E \gg T$ (where T is the Hawking temperature), then collective modes of the fuzzball are excited, which is well-approximated by a description in terms of an ensemble average over all fuzzballs. The latter reproduces the black hole geometry, so that the dynamics of sufficiently energetic objects over short timescales (like an astronaut falling into a black hole) are essentially the same as one would expect in a classical black hole geometry.

Firewalls. The information loss problem has resurfaced in the past few years through an ingenious gedankenexperiment set up by Almheiri, Marolf, Polchinski and Sully (AMPS) that highlighted their difficulty of reconciling black hole complementarity with the equivalence principle [358]. AMPS and several other authors argued that a possible resolution of this incompatibility results in an infalling observer encountering a 'firewall' close to the horizon, see [359, 360] and references therein. The AMPS gedankenexperiment has engendered a lot of discussion and is an excellent demonstration that, at least collectively, the days of confusion regarding black hole thermodynamics and information loss are not over yet. There is of course a simple resolution of the apparent firewall paradox, but the margin is too small to include it here.

2.7 Conclusions and Future

Log corrections to entropy. We started our journey through the past 50 years of black hole thermodynamics with the Bekenstein–Hawking relation (2.1) and the statement that black hole thermodynamics provides non-trivial consistency checks for quantum gravity. We will end our review on a similar note, by going one step further than Bekenstein and Hawking. Namely, in the semi-classical approximation the area law obtains quantum corrections, which can be organized in an expansion in terms of $1/S_{\text{BH}}$ (the same kind of correction is obtained from subleading contributions to the Cardy formula [361]).

$$S = S_{\text{BH}} + \gamma_1 \ln S_{\text{BH}} + \gamma_2 + \mathcal{O}(1/S_{\text{BH}}) \tag{2.40}$$

While the subleading terms and the $\mathcal{O}(1)$ term depend on the specific quantum gravity theory, the leading and first subleading term depend only on the classical limit of that theory and the validity of the semi-classical approximation. In other words, any theory of quantum gravity that is supposed to be equivalent to Einstein gravity in its semi-classical limit must not only reproduce the Bekenstein–Hawking law (2.1), but also the same result for the numerical coefficient γ_1 in front of the logarithmic correction term as obtained from perturbative (1-loop) quantization of Einstein gravity (with a given set of matter degrees of freedom—the precise coef-

ficient depends on the specific matter content). A recent summary of logarithmic corrections to Schwarzschild and other non-extremal black holes was provided by Sen [362]. He found that string theory calculations, whenever available, agree precisely with the semi-classical result. Interestingly, the simplest of all black holes, the Schwarzschild black hole, still presents a challenge: currently, string theory does not provide a prediction for γ_1 of the Schwarzschild black hole.[9]

Future developments. Predictions of future developments often serve as a source of amusement for future generations [365], but we will venture one as our closing statement. While a lot of our current understanding of black hole thermodynamics and quantum gravity was achieved through consistently applying Feynman's dictum "everything is particle"—most prominently epitomized by the Hawking effect—we predict that most of our future understanding will be achieved through consistently applying Wheeler's dictum "everything is information" [366], like in the recent slogan "ER = EPR" [367] that emerged from the firewall discussions.

Acknowledgments DG and RM thank their respective collaborators for numerous discussions on black hole thermodynamics in the past 15 years. DG and JS were supported by the START project Y 435-N16 of the Austrian Science Fund (FWF) and the FWF projects I 952-N16 and I 1030-N27.

References

1. Carlip, S.: Quantum gravity: a progress report. Rept. Prog. Phys. **64**, 885 (2001). arXiv:gr-qc/0108040
2. Kerr, R.P.: Gravitational field of a spinning mass as an example of algebraically special metrics. Phys. Rev. Lett. **11**, 237–238 (1963)
3. Bekenstein, J.: Black holes and the second law. Lett. Nuovo Cim. **4**, 737–740 (1972)
4. Bardeen, J.M., Carter, B., Hawking, S.: The four laws of black hole mechanics. Commun. Math. Phys. **31**, 161–170 (1973)
5. Tolman, R.: Relativity, Thermodynamics, and Cosmology. Dover Books on Physics Series. Dover Publications, New York (1987)
6. Oppenheimer, J., Volkoff, G.: On massive neutron cores. Phys. Rev. **55**, 374–381 (1939)
7. Tolman, R.C.: Static solutions of einstein's field equations for spheres of fluid, Phys. Rev. **55**, 364–373 (1939)
8. Zel'dovich Y.B.: Zh. Eksp. Teoret. Fiz.**41**, 1609 (1961)
9. Bondi, H.: Massive spheres in general relativity. Proc. Roy. Soc. Lond. **A281**, 303–317 (1964)
10. Sorkin, R.D., Wald, R.M., Zhang, Z.J.: Entropy of selfgravitating radiation. Gen. Rel. Grav. **13**, 1127–1146 (1981)
11. Newman, E.T., Couch, R., Chinnapared, K., Exton, A., Prakash, A., et al.: Metric of a rotating, charged mass. J. Math. Phys. **6**, 918–919 (1965)
12. Ginzburg, V., Ozernoi, L.: Sov. Phys. JETP **20**, 689 (1965)
13. Doroshkevich, A., Zel'dovich, Y., Novikov I.: Gravitational collapse of nonsymmetric and rotating masses, JETP **49** (1965)
14. Israel, W.: Event horizons in static vacuum space-times. Phys. Rev. **164**, 1776–1779 (1967)
15. Israel, W.: Event horizons in static electrovac space-times. Commun. Math. Phys. **8**, 245–260 (1968)

[9] Loop quantum gravity does provide such a prediction [363, 364], and it disagrees with the semi-classical result.

16. Carter, B.: Axisymmetric black hole has only two degrees of freedom. Phys. Rev. Lett. **26**, 331–333 (1971)
17. Robinson, D.: Uniqueness of the kerr black hole. Phys. Rev. Lett. **34**, 905–906 (1975)
18. Mazur, P.: Proof of uniqueness of the kerr-newman black hole solution. J. Phys. **A15**, 3173–3180 (1982)
19. Bunting, G.: Proof of the uniqueness conjecture for Black Holes. Ph.D. thesis, University. New England, Armadale (1983)
20. Chrusciel, P.T., Costa J.L.: On uniqueness of stationary vacuum black holes, Asterisque **321**, 195–265 (2008). arXiv:0806.0016
21. Chrusciel, P.T., Costa, J.L., Heusler, M.: Stationary black holes: uniqueness and beyond, Living Rev. Rel. **15**, 7 (2012). arXiv:1205.6112
22. Misner, C.W., Thorne, K., Wheeler, J.: Gravitation. W.H Freeman, Londan (1973)
23. Penrose, R.: Gravitational collapse: the role of general relativity. Riv. Nuovo Cim. **1**, 252–276 (1969)
24. Christodoulou, D.: Reversible and irreversible transformations in black hole physics. Phys. Rev. Lett. **25**, 1596–1597 (1970)
25. Christodoulou, D., Ruffini, R.: Reversible transformations of a charged black hole. Phys. Rev. **D4**, 3552–3555 (1971)
26. Misner, C.W.: Interpretation of gravitational-wave observations. Phys. Rev. Lett. **28**, 994–997 (1972)
27. Press, W.H., Teukolsky, S.A.: Floating orbits, superradiant scattering and the black-hole bomb. Nature **238**, 211–212 (1972)
28. Starobinsky, A.: Amplification of waves during reflection from a rotating black hole. JETP **64**(1), 28 (1972)
29. Zel'dovich, Y.B.: Amplification of cylindrical electromagnetic waves reflected from a rotating body. JETP **35**(6), 1085 (1971)
30. Zel'dovich, Y.B.: Generation of waves by a rotating body. Sov. Phys. JETP Lett. **14**, 180 (1971)
31. Carter, B.: Global structure of the kerr family of gravitational fields. Phys. Rev. **174**, 1559–1571 (1968)
32. Teukolsky, S.A.: Perturbations of a rotating black hole. 1. Fundamental equations for gravitational electromagnetic and neutrino field perturbations. Astrophys. J. **185**, 635–647 (1973)
33. Teukolsky, S., Press, W.: Perturbations of a rotating black hole. III-interaction of the hole with gravitational and electromagnet ic radiation. Astrophys. J. **193**, 443–461 (1974)
34. Starobinsky, A., Churilov, S.: Amplification of electromagnetic and gravitational waves scattered by a rotating black hole. JETP **38**1, 1 (1974)
35. Unruh, W.: Separability of the neutrino equations in a kerr background. Phys. Rev. Lett. **31**, 1265–1267 (1973)
36. Hawking, S.: Particle creation by black holes. Commun. Math. Phys. **43**, 199–220 (1975)
37. Klein, O.: Die reflexion von elektronen an einem potential sprung nach der relativistischen dynamik von dirac. Z. Phys. **53**, 157 (1929)
38. Dombey, N., Calogeracos, A.: Seventy years of the klein paradox. Phys. Rept. **315**, 41–58 (1999)
39. Wald, R.M.: General Relativity. The University of Chicago Press, Chicago (1984)
40. Hawking, S.W.: Black hole explosions. Nature **248**, 30–31 (1974)
41. Hawking, S., Ellis, G.: The large scale structure of space-time. Cambridge University Press, Cambridge (1973)
42. Carter, B.: Black hole equilibrium states, In Black Holes—Les astres occlus. Gordon and Breach Science Publishers, (1973)
43. Penrose, R.: Structure of space-time. In: DeWitt, J.W.C.M. (ed.) Battelle Rencontres, 1967 Lectures in Mathematics and Physics. Benjamin, New York (1968)
44. Hawking, S.W.: Gravitational radiation from colliding black holes. Phys. Rev. Lett. **26**, 1344–1346 (1971)
45. Hawking, S.: Black holes in general relativity. Commun. Math. Phys. **25**, 152–166 (1972)

46. Bekenstein, J.: Extraction of energy and charge from a black hole. Phys. Rev. **D7**, 949–953 (1973)
47. Wald, R.M.: Gravitational spin interaction. Phys. Rev. **D6**, 406–413 (1972)
48. Smarr, L.: Mass formula for kerr black holes. Phys. Rev. Lett. **30**, 71–73 (1973)
49. Wald, R.M.: Quantum Field Theory in Curved Spacetime and Black Hole Thermodynamics. University of Chicago Press, Chicago (1994)
50. Nernst, W.: Thermodynamik und spezifische wärme. Preuss. Akad. Wiss. Sitzungsberichte **1**, 134140 (1912)
51. Israel, W.: Third law of black-hole dynamics: a formulation and proof, Phys. Rev. Lett. **57**, 397–399 (1986)
52. Bekenstein, J.D.: Black holes and entropy. Phys. Rev. **D7**, 2333–2346 (1973)
53. Grishchuk, L., Sidorov, Y.: Squeezed quantum states of relic gravitons and primordial density fluctuations. Phys. Rev. **D42**, 3413–3421 (1990)
54. Wald, R.M.: On particle creation by black holes. Commun. Math. Phys. **45**, 9–34 (1975)
55. Parker, L.: Probability distribution of particles created by a black hole. Phys. Rev. **D12**, 1519–1525 (1975)
56. Hawking, S.W.: Breakdown of predictability in gravitational collapse. Phys. Rev. **D14**, 2460–2473 (1976)
57. Bekenstein, J., Meisels, A.: Einstein a and b coefficients for a black hole. Phys. Rev. **D15**, 2775–2781 (1977)
58. Panangaden, P., Wald, R.M.: Probability distribution for radiation from a black hole in the presence of incoming radiation. Phys. Rev. **D16**, 929–932 (1977)
59. Boulware, D.G.: Quantum field theory in schwarzschild and rindler spaces. Phys. Rev. **D11**, 1404 (1975)
60. Gibbons, G., Perry, M.: Black holes and thermal green's functions. Proc. Roy. Soc. Lond. **A358**, 467–494 (1978)
61. Davies, P.: Scalar particle production in schwarzschild and rindler metrics. J. Phys. **A8**, 609–616 (1975)
62. DeWitt, B.S.: Quantum field theory in curved space-time. Phys. Rept. **19**, 295–357 (1975)
63. Gerlach, U.: The mechanism of black body radiation from an incipient black hole. Phys. Rev. **D14**, 1479–1508 (1976)
64. Parikh, M.K., Wilczek, F.: Hawking radiation as tunneling, Phys. Rev. Lett. **85**, 5042–5045 (2000). arXiv:hep-th/9907001
65. Christensen, S.M., Fulling, S.A.: Trace anomalies and the hawking effect. Phys. Rev. **D15**, 2088–2104 (1977)
66. Strominger, A.: Les Houches lectures on black holes. arXiv:hep-th/9501071
67. Grumiller, D., Kummer, W., Vassilevich, D.V.: Dilaton gravity in two dimensions, Phys. Rept. **369**, 327–429 (2002). arXiv:hep-th/0204253
68. Robinson, S.P., Wilczek, F.: A relationship between hawking radiation and gravitational anomalies, Phys. Rev. Lett. **95**, 011303 (2005). arXiv:gr-qc/0502074
69. Iso, S., Umetsu, H., Wilczek, F.: Anomalies, hawking radiations and regularity in rotating black holes, Phys. Rev. D **74**, 044017 (2006). arXiv:hep-th/0606018
70. Iso, S., Umetsu, H., Wilczek, F.: Hawking radiation from charged black holes via gauge and gravitational anomalies, Phys. Rev. Lett. **96**, 151302 (2006). arXiv:hep-th/0602146
71. Gibbons, G., Hawking, S., Perry, M.: Path integrals and the indefiniteness of the gravitational action. Nucl. Phys. **B138**, 141 (1978)
72. Gibbons, G.W., Hawking, S.W.: Action integrals and partition functions in quantum gravity. Phys. Rev. **D15**, 2752–2756 (1977)
73. Hawking, S.: Quantum gravity and path integrals. Phys. Rev. **D18**, 1747–1753 (1978)
74. Gross, D.J., Perry, M.J., Yaffe, L.G.: Instability of flat space at finite temperature. Phys. Rev. **D25**, 330–355 (1982)
75. Gibbons, G.W., Hawking, S.W.: Classification of gravitational instanton symmetries. Commun. Math. Phys. **66**, 291–310 (1979)

76. Gibbons, G., Perry, M.J.: New gravitational instantons and their interactions. Phys. Rev. **D22**, 313 (1980)
77. Gibbons, G., Perry, M.: Quantizing gravitational instantons. Nucl. Phys. **B146**, 90 (1978)
78. Zaumen, W.: Upper bound on the electric charge of a black hole. Nature **247**, 530 (1974)
79. Carter, B.: Charge and particle conservation in black hole decay. Phys. Rev. Lett. **33**, 558–561 (1974)
80. Gibbons, G.: Vacuum polarization and the spontaneous loss of charge by black holes. Commun. Math. Phys. **44**, 245–264 (1975)
81. Page, D.N.: Particle emission rates from a black hole: massless particles from an uncharged, nonrotating hole. Phys. Rev. **D13**, 198–206 (1976)
82. Page, D.N.: Particle emission rates from a black hole. 3. Charged leptons from a nonrotating hole. Phys. Rev. **D16**, 2402–2411 (1977)
83. Page, D.N.: Particle emission rates from a black hole. 2. Massless particles from a rotating hole. Phys. Rev. **D14**, 3260–3273 (1976)
84. Unruh, W.: Second quantization in the kerr metric. Phys. Rev. **D10**, 3194–3205 (1974)
85. Vilenkin, A.: Macroscopic parity violating effects: neutrino fluxes from rotating black holes and in rotating thermal radiation. Phys. Rev. **D20**, 1807–1812 (1979)
86. Leahy, D., Unruh, W.: Angular dependence of neutrino emission from rotating black holes. Phys. Rev. **D19**, 3509–3515 (1979)
87. Fulling, S.A.: Nonuniqueness of canonical field quantization in riemannian space-time. Phys. Rev. **D7**, 2850–2862 (1973)
88. Unruh, W.G.: Notes on black hole evaporation. Phys. Rev. **D14**, 870 (1976)
89. Unruh, W.G., Weiss, N.: Acceleration radiation in interacting field theories. Phys. Rev. **D29**, 1656 (1984)
90. Fulling, S., Ruijsenaars, S.: Temperature, periodicity and horizons. Phys. Rep. **152**(3), 135–176 (1987)
91. Bisognano, J., Wichmann, E.: On the duality condition for a hermitian scalar field. J. Math. Phys. **16**, 985–1007 (1975)
92. Bisognano, J., Wichmann, E.: On the duality condition for quantum fields. J. Math. Phys. **17**, 303–321 (1976)
93. Sewell, G.L.: Quantum fields on manifolds: PCT and gravitationally induced thermal states. Annals Phys. **141**, 201–224 (1982)
94. Unruh, W.G., Wald, R.M.: What happens when an accelerating observer detects a rindler particle. Phys. Rev. **D29**, 1047–1056 (1984)
95. Crispino, L.C., Higuchi, A., Matsas, G.E.: The Unruh effect and its applications, Rev. Mod. Phys. **80**, 787–838 (2008). arXiv:0710.5373
96. Bekenstein, J.D.: A universal upper bound on the entropy to energy ratio for bounded systems. Phys. Rev. **D23**, 287 (1981)
97. Unruh, W., Wald, R.M.: Acceleration radiation and generalized second law of thermodynamics. Phys. Rev. **D25**, 942–958 (1982)
98. Unruh, W., Wald, R.M.: Entropy bounds, acceleration radiation, and the generalized second law. Phys. Rev. **D27**, 2271–2276 (1983)
99. Hartle, J.B., Hawking, S.W.: Path integral derivation of black hole radiance. Phys. Rev. **D13**, 2188–2203 (1976)
100. Israel, W.: Thermo field dynamics of black holes. Phys. Lett. **A57**, 107–110 (1976)
101. Kay, B.S., Wald, R.M.: Theorems on the uniqueness and thermal properties of stationary, nonsingular, quasifree states on space-times with a bifurcate killing horizon. Phys. Rept. **207**, 49–136 (1991)
102. Unruh, W.G.: Experimental black-hole evaporation? Phys. Rev. Lett. **46**, 1351–1353 (1981)
103. Novello, M., Visser, M., Volovik, G. (eds.): Artificial Black Holes. World Scientific, River Edge, USA (2002)
104. Barcelo, C., Liberati, S., Visser, M.: Analogue gravity. Living Rev. Rel. **8**, 12 (2005). arXiv:gr-qc/0505065

105. Ackermann, M et al., Fermi GBM/LAT Collaborations Collaboration A limit on the variation of the speed of light arising from quantum gravity effects, Nature **462**, 331–334 (2009) .arXiv:0908.1832
106. Jacobson, T.: Black hole evaporation and ultrashort distances. Phys. Rev. **D44**, 1731–1739 (1991)
107. Unruh, W.: Sonic analog of black holes and the effects of high frequencies on black hole evaporation. Phys. Rev. **D51**, 2827–2838 (1995)
108. Corley, S., Jacobson, T.: Hawking spectrum and high frequency dispersion, Phys. Rev. D **54**, 1568–1586 (1996). arXiv:hep-th/9601073
109. Jacobson T.: Black hole radiation in the presence of a short distance cutoff, Phys. Rev. D **48**, 728–741 (1993). arXiv:hep-th/9303103
110. Brout, R, Massar S, Parentani, R., Spindel, P.: Hawking radiation without transPlanckian frequencies, Phys. Rev. D**52**, 4559–4568 (1995). arXiv:hep-th/9506121
111. Visser, M.: Hawking radiation without black hole entropy, Phys. Rev. Lett. **80**, 3436–3439 (1998). arXiv:gr-qc/9712016
112. Jacobson, T.: On the origin of the outgoing black hole modes, Phys. Rev. D**53**, 7082–7088 (1996). arXiv:hep-th/9601064
113. Visser, M.: Acoustic black holes: horizons, ergospheres, and hawking radiation, Class. Quant. Grav. **15**, 1767–1791 (1998), http://www.arXiv.org/abs/gr-qc/9712010
114. Brown, J.: Lower dimensional gravity. World Scientific, Singapore (1988)
115. Callan, C.G., Giddings, Jr S.B., Harvey, J.A., Strominger, A.: Evanescent black holes, Phys. Rev. D **45**, 1005–1009 (1992). arXiv:hep-th/9111056
116. Russo, J.G., Susskind, L., Thorlacius, L.: The endpoint of hawking radiation. Phys. Rev. D **46**, 3444–3449 (1992). arXiv:hep-th/9206070
117. Susskind, L., Thorlacius, L., Uglum, J.: The Stretched horizon and black hole complementarity. Phys. Rev. D **48** 3743–3761 (1993). arXiv:hep-th/9306069
118. Stephens, C.R., 't Hooft, G., Whiting, B.F.: Black hole evaporation without information loss. Class. Quant. Grav. **11**, 621–648 (1994). arXiv:gr-qc/9310006
119. 't Hooft, G.: On the quantum structure of a black hole, Nucl. Phys. B **256**, 727 (1985)
120. Jackiw, R.: Liouville field theory: a two-dimensional model for gravity? In: Christensen, S. (ed.) Quantum Theory Of Gravity, pp. 403–420. Adam Hilger, Bristol (1984)
121. Teitelboim, C.: The hamiltonian structure of two-dimensional space-time and its relation with the conformal anomaly. In: Christensen, S. (ed.) Quantum Theory Of Gravity, pp. 327–344. Adam Hilger, Bristol (1984)
122. Isler, K., Trugenberger, C.A.: A gauge theory of two-dimensional quantum gravity. Phys. Rev. Lett. **63**, 834 (1989)
123. Chamseddine, A.H., Wyler, D.: Gauge theory of topological gravity in (1+1)-dimensions. Phys. Lett. **B228**, 75 (1989)
124. Cangemi, D., Jackiw, R.: Gauge invariant formulations of lineal gravity. Phys. Rev. Lett. **69**, 233–236 (1992). arXiv:hep-th/9203056
125. Ikeda, N., Izawa, K.I.: General form of dilaton gravity and nonlinear gauge theory. Prog. Theor. Phys. **90**, 237–246 (1993). arXiv:hep-th/9304012
126. Ikeda, N.: Two-dimensional gravity and nonlinear gauge theory. Ann. Phys. **235**, 435–464 (1994). arXiv:hep-th/9312059
127. Schaller, P., Strobl, T.: Poisson structure induced (topological) field theories. Mod. Phys. Lett. A **9**, 3129–3136 (1994), arXiv:hep-th/9405110
128. Berger, B.K., Chitre, D.M., Moncrief, V.E., Nutku, Y.: Hamiltonian formulation of spherically symmetric gravitational fields. Phys. Rev. **D5**, 2467–2470 (1972)
129. Benguria, R., Cordero, P., Teitelboim, C.: Aspects of the hamiltonian dynamics of interacting gravitational gauge and higgs fields with applications to spherical symmetry. Nucl. Phys. **B122**, 61 (1977)
130. Thomi, P., Isaak, B., Hájíček, P.: Spherically symmetric systems of fields and black holes. 1. definition and properties of apparent horizon. Phys. Rev. **D30**, 1168 (1984)

131. Hájíček, P.: Spherically symmetric systems of fields and black holes. 2. Apparent horizon in canonical formalism. Phys. Rev. **D30**, 1178 (1984)
132. Kuchař, K.V.: Geometrodynamics of schwarzschild black holes. Phys. Rev. D **50**, 3961–3981 (1994). arXiv:gr-qc/9403003
133. Soda, J.: Hierarchical dimensional reduction and gluing geometries. Prog. Theor. Phys. **89**, 1303–1310 (1993)
134. Emparan, R., Grumiller, D., Tanabe, K.: Large D gravity and low D strings, Phys. Rev. Lett. **110**, 251102 (2013). arXiv:1303.1995
135. Weinberg, S.: In General Relativity, In: Hawking, S., Israel, W. (eds.) An Einstein Centenary Survey. Cambridge University Press, Cambridge (1979)
136. Mann, R.B. Ross, S.F.: The D $\rightarrow$ 2 limit of general relativity. Class. Quant. Grav. **10**, 345–351 (1993). arXiv:gr-qc/9208004
137. Grumiller, D., Jackiw, R.: Liouville Gravity from Einstein Gravity, In: Recent Developments in Theoretical Physics, Gosh, S., Kar, G. (eds.) World Scientific, Singapore pp. 331–343, 2010. arXiv:0712.3775
138. Ginsparg, P., Moore, G.W.: Lectures on 2-d gravity and 2-d string theory, arXiv:hep-th/9304011
139. Nakayama, Y.: Liouville field theory: a decade after the revolution. Int. J. Mod. Phys. A **19**, 2771–2930 (2004). arXiv:hep-th/0402009
140. Katanaev, M.O., Volovich, I.V.: String model with dynamical geometry and torsion. Phys. Lett. **B175**, 413–416 (1986)
141. Kummer, W., Schwarz, D.J.: General analytic solution of r**2 gravity with dynamical torsion in two-dimensions. Phys. Rev. **D45**, 3628–3635 (1992)
142. Schaller, P., Strobl, T.: Canonical quantization of nonEinsteinian gravity and the problem of time. Class. Quant. Grav. **11**, 331–346 (1994). arXiv:hep-th/9211054
143. Katanaev, M.O., Kummer, W,. Liebl, H.: Geometric interpretation and classification of global solutions in generalized dilaton gravity. Phys. Rev. D**53**, 5609–5618 (1996). arXiv:gr-qc/9511009
144. Callan Jr, C.G., Martinec, E.J., Perry, M.J., Friedan, D.: Strings in background fields. Nucl. Phys. **B262**, 593 (1985)
145. Mandal, G., Sengupta, A.M., Wadia, S.R.: Classical solutions of two-dimensional string theory. Mod. Phys. Lett. **A6**, 1685–1692 (1991)
146. Elitzur, S., Forge, A., Rabinovici, E.: Some global aspects of string compactifications. Nucl. Phys. **B359**, 581–610 (1991)
147. Witten, E.: On string theory and black holes. Phys. Rev. **D44**, 314–324 (1991)
148. Dijkgraaf, R., Verlinde, H., Verlinde, E.: String propagation in a black hole geometry. Nucl. Phys. **B371**, 269–314 (1992)
149. Klebanov, I.R.: String theory in two-dimensions, arXiv:hep-th/9108019
150. Strominger, A.: Les Houches lectures on black holes, Talk given at NATO Advanced Study Institute arXiv:hep-th/9501071
151. Grumiller, D., Meyer, R.: Ramifications of lineland. Turk. J. Phys. **30**, 349–378 (2006). arXiv:hep-th/0604049
152. Gegenberg, J., Kunstatter, G., Louis-Martinez, D.: Observables for two-dimensional black holes. Phys. Rev. D **51**, 1781–1786 (1995). arXiv:gr-qc/9408015
153. Grumiller D., McNees, R.: Thermodynamics of black holes in two (and higher) dimensions. JHEP **04**, 074 (2007). arXiv:hep-th/0703230
154. Wald, R.M.: Black hole entropy is the Noether charge. Phys. Rev. D **48**, 3427–3431 (1993) arXiv:gr-qc/9307038
155. Iyer V., Wald, R.M.: Some properties of Noether charge and a proposal for dynamical black hole entropy. Phys. Rev. D**50**, 846–864 (1994). arXiv:gr-qc/9403028
156. York Jr, J.W.: Black hole thermodynamics and the euclidean einstein action. Phys. Rev. **D33**, 2092–2099 (1986)
157. Hawking, S.W., Page, D.N.: Thermodynamics of black holes in anti-de sitter space. Commun. Math. Phys. **87**, 577 (1983)

158. Deser, S., Jackiw, R., Templeton, S.: Three-dimensional massive gauge theories. Phys. Rev. Lett. **48**, 975–978 (1982)
159. Deser, S., Jackiw, R., Templeton, S.: Topologically massive gauge theories. Ann. Phys. **140**, 372–411 (1982)
160. Deser, S., Jackiw, R., Templeton, S.: Topologically massive gauge theories. Erratum-ibid. **185**, 406 (1988)
161. Deser S., Jackiw R., 't Hooft G.: Three-dimensional Einstein Gravity: dynamics of flat space. Ann. Phys. **152**, 220 (1984)
162. Brown, J.D., Henneaux, M.: Central charges in the canonical realization of asymptotic symmetries: an example from three-dimensional gravity. Commun. Math. Phys. **104**, 207–226 (1986)
163. Bañados, M., Teitelboim, C., Zanelli, J.: The black hole in three-dimensional space-time. Phys. Rev. Lett. **69**, 1849–1851 (1992). arXiv:hep-th/9204099
164. Bañados, M., Henneaux, M., Teitelboim, C., Zanelli, J.: Geometry of the (2+1) black hole. Phys. Rev. D **48**, 1506–1525 (1993). arXiv:gr-qc/9302012
165. Cardy, J.L.: Operator content of two-dimensional conformally invariant theories. Nucl. Phys. **B270**, 186–204 (1986)
166. Bloete, H.W.J., Cardy, J.L., Nightingale, M.P.: Conformal invariance, the central charge, and universal finite size amplitudes at criticality. Phys. Rev. Lett. **56**, 742–745 (1986)
167. Strominger, A.: Black hole entropy from near-horizon microstates. JHEP **02**, 009 (1998). arXiv:hep-th/9712251
168. Carlip, S.: Black hole entropy from conformal field theory in any dimension. Phys. Rev. Lett. **82**, 2828–2831 (1999). arXiv:hep-th/9812013
169. 't Hooft, G.: Dimensional reduction in quantum gravity. Salamfest **0284-296** (1993). arXiv:gr-qc/9310026
170. Susskind, L.: Some speculations about black hole entropy in string theory. In Teitelboim, C. (ed.) The Black Hole, pp. 118–131. arXiv:hep-th/9309145
171. Susskind, L., Uglum, J.: Black hole entropy in canonical quantum gravity and superstring theory. Phys. Rev. D**50**, 2700–2711 (1994). arXiv:hep-th/9401070
172. Sen, A.: Extremal black holes and elementary string states. Mod. Phys. Lett. A**10**, 2081–2094 (1995). arXiv:hep-th/9504147
173. Strominger., Vafa, C.: Microscopic origin of the bekenstein-hawking entropy. Phys. Lett. B**379**, 99–104 (1996). arXiv:hep-th/9601029
174. Maldacena, J.M., Strominger, A.: Statistical entropy of four-dimensional extremal black holes. Phys. Rev. Lett. **77**, 428–429 (1996). arXiv:hep-th/9603060
175. Callan C.G., Maldacena, J.M.: D-brane approach to black hole quantum mechanics. Nucl. Phys. B**472**, 591–610 (1996). arXiv:hep-th/9602043
176. Horowitz, G.T., Strominger, A.: Counting states of near extremal black holes. Phys. Rev. Lett. **77**, 2368–2371 (1996). arXiv:hep-th/9602051
177. Emparan, R., Horowitz, G.T.: Microstates of a neutral black hole in M Theory. Phys. Rev. Lett. **97**, 141601 (2006). arXiv:hep-th/0607023
178. Skenderis, K.: Black holes and branes in string theory. Lect. Notes Phys. **541**, 325–364 (2000). arXiv:hep-th/9901050
179. Peet, A.W.: TASI lectures on black holes in string theory. arXiv:hep-th/0008241
180. Horowitz, G.T., Roberts, M.M.: Counting the microstates of a Kerr Black Hole. Phys. Rev. Lett. **99**, 221601 (2007). arXiv:0708.1346
181. Susskind, L.: The World as a hologram. J. Math. Phys. **36**, 6377–6396 (1995). arXiv:hep-th/9409089
182. Fischler, W., Susskind, L.: Holography and cosmology. arXiv:hep-th/9806039
183. Easther, R., Lowe, D.A.: Holography, cosmology and the second law of thermodynamics. Phys. Rev. Lett. **82**, 4967–4970 (1999). arXiv:hep-th/9902088
184. Bousso, R.: A covariant entropy conjecture. JHEP **9907**, 004, (1999). arXiv:hep-th/9905177
185. Bousso, R.: The holographic principle. Rev. Mod. Phys. 74, 825–874 (2002). arXiv:hep-th/0203101

186. Klebanov, I.R. : World volume approach to absorption by nondilatonic branes, Nucl. Phys. B **496**, 231–242 (1997). arXiv:hep-th/9702076
187. Gubser, S.S., Klebanov, I.R., Tseytlin, A.A.: String theory and classical absorption by three-branes. Nucl. Phys. B**499**, 217–240 (1997). arXiv:hep-th/9703040
188. Gubser, S.S., Klebanov, I.R.: Absorption by branes and Schwinger terms in the world volume theory. Phys. Lett. B**413**, 41–48 (1997). arXiv:hep-th/9708005
189. Witten, E.: Bound states of strings and p-branes. Nucl. Phys. B **460**, 335–350 (1996). arXiv:hep-th/9510135
190. Maldacena, J.M.: The large N limit of superconformal field theories and supergravity. Adv. Theor. Math. Phys. **2**, 231–252 (1998). arXiv:hep-th/9711200
191. Beisert, N., Ahn, L., Alday, C., Bajnok, Z., Drummond, J.M. et al.: Review of AdS/CFT Integrability: An Overview. Lett. Math. Phys. **99**, 3–32 (2012). arXiv:1012.3982
192. Witten, E.: Anti-de sitter space, thermal phase transition, and confinement in gauge theories. Adv. Theor. Math. Phys. **2**, 505–532 (1998). arXiv:hep-th/9803131
193. Birmingham, D., Sachs, I., Sen, S.: Entropy of three-dimensional black holes in string theory. Phys. Lett. B **424**, 275–280 (1998). arXiv:hep-th/9801019
194. Mathur, S.D.: The Information paradox: a pedagogical introduction. Class. Quant. Grav. **26**, 224001, (2009). arXiv:0909.1038
195. Polchinski, J,. Strassler, M.J.: The String dual of a confining four-dimensional gauge theory. arXiv:hep-th/0003136
196. Strominger, A.: The dS/CFT correspondence. JHEP 0110 **034** (2001). arXiv:hep-th/0106113
197. Strominger, A.: Inflation and the dS/CFT correspondence. JHEP 0111 **049** (2001). arXiv:hep-th/0110087
198. Klebanov I., Polyakov, A.: AdS dual of the critical O(N) vector model. Phys. Lett. B **550**, 213–219 (2002). arXiv:hep-th/0210114
199. Maldacena, J.M.: Non-Gaussian features of primordial fluctuations in single field inflationary models. JHEP **0305**, 013 (2003). arXiv:astro-ph/0210603
200. Larsen, F.: van der Schaar, J.P., Leigh, R.G.: De sitter holography and the cosmic microwave background. JHEP **0204**, 047 (2002). http://www.arXiv.org/abs/hep-th/0202127
201. Larsen, F., McNees, R.: Inflation and de sitter holography. JHEP **0307**, 051 (2003). hep-th/0307026
202. Jacobson, T.: Thermodynamics of space-time: the Einstein equation of state, Phys. Rev. Lett. **75**, 1260–1263 (1995). gr-qc/9504004
203. Padmanabhan, T.: Thermodynamical aspects of gravity: new insights, Rept. Prog. Phys. **73**, 046901 (2010). 0911.5004
204. Verlinde, E.P.: On the origin of gravity and the laws of Newton. JHEP 1104 (2011) 029. arXiv:1001.0785
205. Policastro, G., Son, D., Starinets, A.: The shear viscosity of strongly coupled N=4 supersymmetric Yang-Mills plasma. Phys. Rev. Lett. **87**, 081601 (2001). hep-th/0104066
206. Kovtun, P., Son, D.T., Starinets, A.O.: Viscosity in strongly interacting quantum field theories from black hole physics. Phys. Rev. Lett. 94 (2005) 111601. arXiv:hep-th/0405231
207. Romatschke, P., Romatschke, U.: Viscosity information from relativistic nuclear collisions: how perfect is the fluid observed at RHIC? Phys. Rev. Lett. **99**, 172301 (2007). arXiv:0706.1522
208. Hwa, R.C., Wang, X.N.: Quark-gluon Plasma 4. World Scientific Publishing, Singapore (2010). arXiv:0905.2433
209. Casalderrey-Solana, J., Liu, H., Mateos, D., Rajagopal, K., Wiedemann, U.A.: Gauge/string duality, hot QCD and heavy ion collisions. Cambridge University Press, Cambridge (2014). http://books.google.com/books?id=WDeNAwAAQBAJ, arXiv:1101.0618
210. Shuryak, E.: Toward the AdS/CFT dual of the 'Little Bang'. J. Phys. G **39**, 054001 (2012). arXiv:1112.2573
211. DeWolfe, O., Gubser, S.S., Rosen, C., Teaney, D.: Heavy ions and string theory. Prog. Part. Nucl. Phys. **75**, 86–132 (2014). arXiv:1304.7794

212. T. Damour, Quelques propriétés, méchaniques, électromagnéiques, thermodynamiques et quantiques des trous noirs. Ph.D. thesis, Université Pierre et Marie Curie, Paris, 1979.
213. Son, D.T.: Toward an AdS/cold atoms correspondence: a geometric realization of the schroedinger symmetry, Phys. Rev. **D78**, 046003 (2008). arXiv:0804.3972
214. Balasubramanian K., McGreevy, J.: Gravity duals for non-relativistic CFTs, Phys. Rev. Lett. **101**, 061601 (2008). arXiv:0804.4053
215. Adams, A., Balasubramanian, K., McGreevy, J.: Hot spacetimes for cold Atoms, JHEP **11**, 059 (2008). arXiv:0807.1111
216. Kachru, S., Liu, X., Mulligan, M.: Gravity duals of lifshitz-like fixed points, Phys. Rev. **D78**, 106005 (2008). arXiv:0808.1725
217. Gubser, S.S.: Breaking an abelian gauge symmetry near a black hole horizon, Phys. Rev. **D78**, 065034 (2008). arXiv:0801.2977
218. Hartnoll, S.A., Herzog, C.P., Horowitz, G.T.: Building a holographic superconductor, Phys. Rev. Lett. **101**, 031601 (2008). arXiv:0803.3295
219. Hartnoll, S.A., Herzog, C.P., Horowitz, G.T.: Holographic superconductors, JHEP **0812**, 015 (2008). arXiv:0810.1563
220. Hartnoll, S.A., Polchinski, J., Silverstein, E., Tong, D.: Towards strange metallic holography, JHEP **1004**, 120 (2010). arXiv:0912.1061
221. Liu, H., McGreevy, J., Vegh, D.: Non-Fermi liquids from holography, Phys. Rev. **D83**, 065029 (2011). arXiv:0903.2477
222. Faulkner, T., Iqbal, N., Liu, H., McGreevy, J., Vegh, D.: Strange metal transport realized by gauge/gravity duality. Science **329**, 1043–1047 (2010)
223. Faulkner, T., Iqbal, N., Liu, H., McGreevy, J., Vegh, D.: Holographic non-Fermi liquid fixed points. Philos. Trans. Roy. Soc. **A369**, 1640 (2011). arXiv:1101.0597
224. Iqbal, N., Liu, H.: Universality of the hydrodynamic limit in AdS/CFT and the membrane paradigm. Phys. Rev. **D79**, 025023 (2009). arXiv:0809.3808
225. Bredberg, I., Keeler, C., Lysov, V., Strominger, A.: Wilsonian approach to fluid/gravity duality. JHEP **1103**, 141 (2011). arXiv:1006.1902
226. Compere, G., McFadden, P., Skenderis, K., Taylor, M.: The holographic fluid dual to vacuum Einstein gravity. JHEP **1107**, 050 (2011). arXiv:1103.3022
227. Bredberg, I., Keeler, C., Lysov, V., Strominger, A.: From Navier-Stokes to Einstein. JHEP **1207**, 146 (2012). arXiv:1101.2451
228. Compere, G., McFadden, P., Skenderis, K., Taylor, M.: The relativistic fluid dual to vacuum Einstein gravity. JHEP **1203**, 076 (2012). arXiv:1201.2678
229. Thorne, K.S., Price, R., Macdonald, D.: Black holes: The Membrane Paradigm, p. 367. Yale University Press, USA (1986)
230. McGreevy, J.: Holographic duality with a view toward many-body physics. Adv. High Energy Phys. **2010**, 723105 (2010). arXiv:0909.0518
231. Sachdev, S.: Strange metals and the AdS/CFT correspondence, J. Stat. Mech. **1011**, P11022 (2010). arXiv:1010.0682
232. Horowitz, G.T.: Black Holes in Higher Dimensions. Cambridge University Press (2012). http://books.google.com/books?id=12eGVHojt2UC, arXiv:1106.4324
233. Sachdev, S.: What can gauge-gravity duality teach us about condensed matter physics? Ann. Rev. Condensed Matter Phys. **3**, 9–33 (2012). arXiv:1108.1197
234. Iqbal, N., Liu, H., Mezei, M.: TASI 2010 From meV to the Planck Scale. World Scientific (2012). arXiv:1110.3814
235. Son, D.T.: Holography for strongly coupled media. Lect. Notes Phys. **851**, 147–163 (2012)
236. Grumiller, D., Johansson,N.: Instability in cosmological topologically massive gravity at the chiral point, JHEP **07**, 134 (2008). arXiv:0805.2610
237. Flohr, M.: Bits and pieces in logarithmic conformal field theory, Int. J. Mod. Phys. **A18**, 4497–4592 (2003). arXiv:hep-th/0111228
238. Gaberdiel, M.R.: An algebraic approach to logarithmic conformal field theory, Int. J. Mod. Phys. **A18**, 4593–4638 (2003). arXiv:hep-th/0111260

239. Cardy, J,. et al..: Logarithmic conformal field theories, J. Phys. **A46**, special issue (2013). Gainutdinov, A., Ridout D., Runkel, I. (eds.) Logarithmic conformal field theories
240. Grumiller, D., Riedler, W., Rosseel, J., Zojer, T.: Holographic applications of logarithmic conformal field theories, J. Phys. A: Math. Theor. **46**, 494002 (2013). arXiv:1302.0280
241. Burgess, C.P., Myers, Robert C.: General relativity and relativistic astrophysics. In Burgess, C.P. (ed.) Proceedings: 8th Canadian Conference, Montreal, Canada, 10–12 June 1999. http://www.arXiv.org/abs/hep-th/9901079
242. Polchinski, J.: S matrices from AdS space-time. arXiv:hep-th/9901076
243. Giddings, S.B.: Flat space scattering and bulk locality in the AdS/CFT correspondence, Phys. Rev. **D61**, 106008 (2000). arXiv:hep-th/9907129
244. Gary, M., Giddings, S.B., Penedones, J.: Local bulk S-matrix elements and CFT singularities, Phys. Rev. **D80**, 085005 (2009). arXiv:0903.4437
245. Gary, M., Giddings, S.B.: The flat space S-matrix from the AdS/CFT correspondence? Phys. Rev. **D80**, 046008 (2009). arXiv:0904.3544
246. Barnich, G., Compere, G.: Classical central extension for asymptotic symmetries at null infinity in three spacetime dimensions, Class. Quant. Grav. **24**, F15–F23 (2007). arXiv:gr-qc/0610130
247. Bondi, H., van der Burg, M., Metzner, A.: Gravitational waves in general relativity vii. waves from axi-symmetric isolated systems. Proc. R. Soc. London **A269**, 21–51 (1962)
248. Sachs, R.: Asymptotic symmetries in gravitational theory. Phys. Rev. **128**, 2851–2864 (1962)
249. Bagchi, A., Gopakumar, R.: Galilean conformal algebras and AdS/CFT, JHEP **0907**, 037 (2009). arXiv:0902.1385
250. Bagchi, A., Gopakumar, R., Mandal, I., Miwa, A.: GCA in 2d, JHEP **1008**, 004 (2010). arXiv:0912.1090
251. Bagchi, A.: Correspondence between asymptotically flat spacetimes and nonrelativistic conformal field theories. Phys. Rev. Lett. **105**, 171601 (2010)
252. Bagchi, A., Detournay, S., Grumiller, D.: Flat-space chiral gravity, Phys. Rev. Lett. **109**, 151301 (2012). arXiv:1208.1658
253. Witten, E.: Three-Dimensional Gravity Revisited. arXiv:0706.3359
254. Li, W., Song, W., Strominger, A.: Chiral gravity in three dimensions, JHEP **04**, 082 (2008). arXiv:0801.4566
255. Maloney, A., Song, W., Strominger, A.: Chiral gravity, log gravity and extremal CFT, Phys. Rev. **D81**, 064007 (2010). arXiv:0903.4573
256. Cornalba, L., Costa, M.S.: A New cosmological scenario in string theory, Phys. Rev. **D66**, 066001 (2002). arXiv:hep-th/0203031
257. Cornalba, L., Costa, M.S.: Time dependent orbifolds and string cosmology, Fortsch. Phys. **52**, 145–199 (2004). arXiv:hep-th/0310099
258. Barnich, G.: Entropy of three-dimensional asymptotically flat cosmological solutions, JHEP **1210**, 095 (2012). arXiv:1208.4371
259. Bagchi, A., Detournay, S., Fareghbal, R., Simon, J.: Holography of 3d flat cosmological horizons, Phys. Rev. Lett. **110**, 141302 (2013). arXiv:1208.4372
260. Bagchi, A., Detournay, S., Grumiller, D., Simon, J.: Cosmic evolution from phase transition of 3-dimensional flat space, Phys. Rev. Lett. **111**, 181301 (2013). arXiv:1305.2919
261. Barnich, G., Troessaert, C.: Aspects of the BMS/CFT correspondence, JHEP **1005**, 062 (2010). arXiv:1001.1541
262. Barnich, G., Troessaert, C.: BMS charge algebra, JHEP **1112**, 105 (2011). arXiv:1106.0213
263. Barnich, G., Gomberoff, A., Gonzalez, H.A.: The Flat limit of three dimensional asymptotically anti-de sitter spacetimes, Phys. Rev. **D86**, 024020 (2012). arXiv:1204.3288
264. Barnich, G., Gomberoff, A., Gonzalez, H.A.: BMS_3 invariant two dimensional field theories as flat limit of liouville, Phys. Rev. **D87**, 124032 (2013). arXiv.:1210.0731
265. Bagchi, A., Fareghbal, R.: BMS/GCA redux: towards flatspace holography from nonrelativistic symmetries, JHEP **1210**, 092 (2012). arXiv:203.5795
266. Barnich, G., Gonzalez, H.A.: Dual dynamics of three dimensional asymptotically flat Einstein gravity at null infinity, JHEP **1305**, 016 (2013). arXiv:1303.1075

267. Barnich, G., Troessaert, C.: Comments on holographic current algebras and asymptotically flat four dimensional spacetimes at null infinity, JHEP **1311**, 003 (2013). arXiv:1309.0794
268. Bagchi, A., Basu, R.: 3D flat holography: entropy and logarithmic corrections. (2013). arXiv:1312.5748
269. Costa, R.N.C.: Aspects of the zero Λ limit in the AdS/CFT correspondence. arXiv:1311.7339
270. Fradkin, E., Vasiliev, M.A.: Cubic interaction in extended theories of massless higher spin fields. Nucl. Phys. **B291**, 141 (1987)
271. Fradkin, E., Vasiliev, M.A.: On the gravitational interaction of massless higher spin fields. Phys. Lett. **B189**, 89–95 (1987)
272. Vasiliev, M.A.: Consistent equation for interacting gauge fields of all spins in (3+1)-dimensions. Phys. Lett. **B243**, 378–382 (1990)
273. Vasiliev, M.: Nonlinear equations for symmetric massless higher spin fields in (A)dS(d), Phys. Lett. **B567**, 139–151 (2003). arXiv:hep-th/0304049
274. Giombi, S., Yin, X.: Higher spin gauge theory and holography: the three-point functions, JHEP **1009**, 115 (2010). arXiv:0912.3462
275. Giombi, S., Yin, X.: Higher spins in AdS and twistorial holography, JHEP **1104**, 086 (2011). arXiv:1004.3736
276. Koch, R.d.M., Jevicki, A., Jin, K., Rodrigues, J.P.: AdS_4/CFT_3 construction from collective fields, Phys. Rev. **D83**, 025006 (2011). arXiv:1008.0633
277. Giombi, S., Yin, X.: On higher spin gauge theory and the critical O(N) model, Phys. Rev. **D85**, 086005 (2012). arXiv.org/abs/1105.4011
278. Gaberdiel, M.R., Gopakumar, R.: An AdS_3 dual for minimal model CFTs, Phys. Rev. **D83**, 066007 (2011). arXiv:1011.2986
279. Gaberdiel, M.R., Gopakumar, R., Hartman, T., Raju, S.: Partition functions of holographic minimal models", JHEP **1108**, 077 (2011). arXiv:1106.1897
280. Gaberdiel, M.R., Gopakumar, R.: Minimal model holography, J. Phys. **A46**, 214002 (2013). arXiv:1207.6697
281. Henneaux, M., Rey, S.-J.: Nonlinear $W_{infinity}$ as asymptotic symmetry of three-dimensional higher spin anti-de sitter gravity, JHEP **1012**, 007 (2010). arXiv:1008.4579
282. Campoleoni, A., Fredenhagen, S., Pfenninger, S., Theisen, S.: Asymptotic symmetries of three-dimensional gravity coupled to higher-spin fields, JHEP **1011**, 007 (2010). arXiv:1008.4744
283. Fotopoulos, A., Tsulaia, M.: Gauge invariant lagrangians for free and interacting higher spin fields. a review of the brst formulation, Int. J. Mod. Phys. **A24**, 1–60 (2009). arXiv:0805.1346
284. Sagnotti, A., Taronna, M.: String lessons for higher-spin interactions, Nucl. Phys. **B842**, 299–361 (2011). arXiv:1006.5242
285. Bekaert, X., Boulanger, N., Sundell, P.: How higher-spin gravity surpasses the spin two barrier: no-go theorems versus yes-go examples, Rev. Mod. Phys. **84**, 987–1009 (2012). arXiv:1007.0435
286. Campoleoni, A., Fredenhagen, S., Pfenninger, S.: Asymptotic W-symmetries in three-dimensional higher-spin gauge theories, JHEP **1109**, 113 (2011). arXiv:1107.0290
287. Ammon, M., Gutperle, M., Kraus, P., Perlmutter, E.: Spacetime geometry in higher spin gravity. J. High Energy Phys. **2011**(10) (2011). doi:10.1007/JHEP10(2011)053, arXiv:1106.4788
288. Anninos, D., Hartman, T., Strominger, A.: Higher spin realization of the dS/CFT correspondence. arXiv:1108.5735
289. Maldacena, J., Zhiboedov, A.: Constraining conformal field theories with a higher spin symmetry. J. Phys. **A46**, 214011 (2013). arXiv:1112.1016
290. Ammon, M., Gutperle, M., Kraus, P., Perlmutter, E.: Black holes in three dimensional higher spin gravity: A review, J. Phys. **A46**, 214001 (2013). arXiv:1208.5182
291. Vasiliev, M.A.: Holography, unfolding and higher-spin theory, J. Phys. **A46**, 214013 (2013). arXiv:1203.5554
292. Maldacena, J., Zhiboedov, A.: Constraining conformal field theories with a slightly broken higher spin symmetry, Class. Quant. Grav. **30**, 104003 (2013). arXiv:1204.3882

293. Afshar, H., Bagchi, A., Fareghbal, R., Grumiller, D., Rosseel, J.; Higher spin theory in 3-dimensional flat space, Phys. Rev. Lett. **111**, 121603 (2013). arXiv:1307.4768
294. Gonzalez, H.A., Matulich, J., Pino, M., Troncoso, R.: Asymptotically flat spacetimes in three-dimensional higher spin gravity, JHEP **1309** 016, (2013). arXiv:1307.5651
295. Gary, M., Grumiller, D., Rashkov, R.: Towards non-AdS holography in 3-dimensional higher spin gravity, JHEP **1203**, 022 (2012). arXiv:1201.0013
296. Nielsen, N., Chuang, I.L.: Quantum Computation and Quantum Information. Cambridge University Press, Cambridge (2000)
297. Sorkin, R.D.: On the entropy of the vacuum outside a horizon. arXiv:1402.3589
298. Bombelli, L., Koul, R.K., Lee, J., Sorkin, R.D.: A quantum source of entropy for black holes. Phys. Rev. **D34**, 373–383 (1986)
299. Srednicki, M.: Entropy and area. Phys. Rev. Lett. **71**, 666–669 (1993). arXiv:hep-th/9303048
300. Solodukhin, S.N.: Entanglement entropy of black holes. Living Rev. Rel. **14**, 8 (2011). arXiv:1104.3712
301. Vidal, G., Latorre, J., Rico, E., Kitaev, A.: Entanglement in quantum critical phenomena, Phys. Rev. Lett. **90**, 227902 (2003). arXiv:quant-ph/0211074
302. Calabrese, P., Cardy, J.L.: Entanglement entropy and quantum field theory, J. Stat. Mech. 0406, P06002 (2004). arXiv:hep-th/0405152
303. Kitaev, A., Preskill, J.: Topological entanglement entropy. Phys. Rev. Lett. **96**, 110404, (2006). arXiv:hep-th/0510092
304. Levin, M., Wen, X.-G.: Detecting topological order in a ground state wave function. Phys. Rev. Lett. **96**, 110405 (2006)
305. Ryu, S., Takayanagi, T.: Holographic derivation of entanglement entropy from AdS/CFT, Phys. Rev. Lett. **96**, 181602 (2006). arXiv:hep-th/0603001
306. Ryu, S., Takayanagi, T.: Aspects of holographic entanglement entropy, JHEP **0608**, 045, (2006). arXiv:hep-th/0605073
307. Nishioka, T., Ryu, S., Takayanagi, T.: Holographic entanglement entropy: an overview, J. Phys. **A42**, 504008 (2009). arXiv:0905.0932
308. Hayden, P., Preskill, J.: Black holes as mirrors: quantum information in random subsystems. JHEP **0709**, 120 (2007). arXiv:0708.4025
309. Harlow, D., Hayden, P.: Quantum vomputation versus firewalls. JHEP **1306** 085, (2013). arXiv:1301.4504
310. Aman, J.E., Bengtsson, I., Pidokrajt, N.: Geometry of black hole thermodynamics, Gen. Rel. Grav. **35**, 1733 (2003). arXiv:gr-qc/0304015
311. Arcioni, G., Lozano-Tellechea, E.: Stability and critical phenomena of black holes and black rings, Phys. Rev. **D72**, 104021 (2005). arXiv:hep-th/0412118
312. Aman, J.E., Pidokrajt, N.: Geometry of higher-dimensional black hole thermodynamics, Phys. Rev. **D73**, 024017 (2006). arXiv:hep-th/0510139
313. Shen, J.-Y., Cai, R.-G., Wang, B., Su, R.-K.: Thermodynamic geometry and critical behavior of black holes, Int. J. Mod. Phys. **A22**, 11–27, (2007). arXiv:gr-qc/0512035
314. Sarkar, T., Sengupta, G., Tiwari, B.N: On the thermodynamic geometry of BTZ black holes, JHEP **0611**, 015 (2006). arXiv:hep-th/0606084
315. Alvarez, J.L., Quevedo, H., Sanchez, A.: Unified geometric description of black hole thermodynamics, Phys. Rev. **D77**, 084004 (2008). arXiv:0801.2279
316. Ruppeiner, G.: Thermodynamic curvature and phase transitions in Kerr-Newman black holes, Phys. Rev. **D78**, 024016 (2008). arXiv:0802.1326
317. Ruppeiner, G.: Thermodynamics: a riemannian geometric model. Phys. Rev. **A20**, 1608 (1979)
318. Ruppeiner, G.: Riemannian geometry in thermodynamic fluctuation theory, Rev. Mod. Phys. **67**, 605–659 (1995)
319. Ruppeiner, G.: Erratum: riemannian geometry in thermodynamic fluctuation theory, Rev. Mod. Phys. **68**,313 (1996)
320. Henneaux, M., Teitelboim, C.: The cosmological constant as a canonical variable. Phys. Lett. **B143**, 415–420 (1984)

321. Henneaux, M., Teitelboim, C.: Asymptotically anti-de sitter spaces. Commun. Math. Phys. **98**, 391–424 (1985)
322. Brown, J.D., Teitelboim, C.: Dynamical neutralization of the cosmological constant. Phys. Lett. **B195**, 177–182 (1987)
323. Brown, J.D., Teitelboim, C.: Neutralization of the cosmological constant by membrane creation. Nucl. Phys. **B297**, 787–836 (1988)
324. Bousso, R., Polchinski, J.: Quantization of four form fluxes and dynamical neutralization of the cosmological constant, JHEP **0006**, 006 (2000). arXiv:hep-th/0004134
325. Gomberoff, A., Henneaux, M., Teitelboim, C., Wilczek, F.: Thermal decay of the cosmological constant into black holes, Phys. Rev. **D69**, 083520 (2004). arXiv:hep-th/0311011
326. Caldarelli, M.M., Cognola, G., Klemm, D.: Thermodynamics of Kerr-Newman-AdS black holes and conformal field theories, Class. Quant. Grav. **17**, 399–420 (2000). arXiv:hep-th/9908022
327. Kastor, D., Ray, S., Traschen, J.: Enthalpy and the mechanics of AdS black holes, Class. Quant. Grav. **26**, 195011 (2009). arXiv:0904.2765
328. Cvetic, M., Gibbons, G., Kubiznak, D., Pope, C.: Black hole enthalpy and an entropy inequality for the thermodynamic volume, Phys. Rev. **D84**, 024037 (2011). arXiv:1012.2888
329. Dolan, B.P.: The cosmological constant and black hole thermodynamic potentials, Class. Quant. Grav. **28**, 125020 (2011). arXiv:1008.5023
330. Dolan, B.P.: Pressure and volume in the first law of black hole thermodynamics, Class. Quant. Grav. **28**, 235017 (2011). arXiv:1106.6260
331. Kubiznak, D., Mann, R.B.: P-V criticality of charged AdS black holes, JHEP **1207**, 033 (2012). arXiv:1205.0559
332. Dolan, B.P.: The compressibility of rotating black holes in D-dimensions, Class. Quant. Grav. **31**, 035022 (2014). arXiv:1308.5403
333. Dolan, B.P., Kastor, D., Kubiznak, D., Mann, R.B., Traschen, J.: Thermodynamic volumes and Isoperimetric Inequalities for de Sitter Black Holes, Phys. Rev. **D87**, 104017, (2013). arXiv:1301.5926
334. Altamirano, N., Kubiznak, D., Mann, R.B., Sherkatghanad, Z.: Thermodynamics of rotating black holes and black rings: phase transitions and thermodynamic volume. Galaxies. **2**(4), 89–159 (2014). http://www.mdpi.com/2075-4434/2/1/89, arXiv:1401.2586
335. Guica, M., Hartman, T., Song, W., Strominger, A.: The Kerr/CFT Correspondence, Phys. Rev. **D80**, 124008, (2009). arXiv:0809.4266
336. Lu, H., Mei, J., Pope, C.: Kerr/CFT correspondence in diverse dimensions, JHEP **0904**, 054 (2009). arXiv:0811.2225
337. Azeyanagi, T., Ogawa, N., Terashima, S.: The Kerr/CFT correspondence and string theory, Phys. Rev. **D79**, 106009 (2009). arXiv:0812.4883
338. Bredberg, I., Hartman, T., Song, W., Strominger, A.: Black hole superradiance from Kerr/CFT", JHEP **1004**, 019 (2010). arXiv:0907.3477
339. Cvetic, M., Larsen, F.: Greybody factors and charges in Kerr/CFT, JHEP **0909**, 088 (2009). arXiv:0908.1136
340. Castro, A., Larsen, F.: Near extremal kerr entropy from AdS(2) quantum gravity, JHEP **0912**, 037 (2009). arXiv:0908.1121
341. Dias, O.J., Reall, H.S., Santos, J.E.: Kerr-CFT and gravitational perturbations, JHEP **0908**, 101 (2009). arXiv:0906.2380
342. Amsel, A.J., Horowitz, G.T., Marolf, D., Roberts, M.M.: No dynamics in the extremal Kerr Throat. (2009). arXiv:0906.2376
343. Castro, A., Maloney, A., Strominger, A.: Hidden conformal symmetry of the Kerr Black Hole, Phys. Rev. **D82**, 024008 (2010). arXiv:1004.0996
344. Guica, M., Strominger, A.: Microscopic realization of the Kerr/CFT correspondence, JHEP **1102**, 010 (2011). arXiv:1009.5039
345. Compere, G.: The Kerr/CFT correspondence and its extensions: a comprehensive review, Living Rev. Rel. **15** 11 (2012). arXiv:1203.3561

346. Bardeen, J.M., Horowitz, G.T.: The extreme Kerr throat geometry: a vacuum analog of AdS(2) × S(2), Phys. Rev. **D60**, 104030 (1999) Xiv:hep-th/9905099
347. Thorne, K.S.: Disk accretion onto a black hole. 2. Evolution of the hole. Astrophys. J. **191**, 507 (1974)
348. McClintock, J.E., Shafee, R., Narayan, R., Remillard, R.A., Davis, S.W. et al.: The spin of the near-extreme kerr black hole GRS 1915+105, Astrophys. J. **652**, 518–539 (2006). arXiv:astro-ph/0606076
349. McClintock, J.E., Remillard, R.A.: Measuring the spins of stellar-mass black holes. In: Astro2010: The Astronomy and Astrophysics Decadal Survey, vol. 2010, p. 197 (2009). http://adsabs.harvard.edu/abs/2009astro2010S.197M, arXiv:0902.3488
350. Fender, R., Gallo, E., Russell, D.: No evidence for black hole spin powering of jets in X-ray binaries, Mon. Not. R. Astron. Soc. **406**, 1425–1434 (2010). arXiv:1003.5516
351. Lunin, O., Mathur, S.D.: AdS / CFT duality and the black hole information paradox, Nucl. Phys. **B623**, 342–394 (2002). arXiv:hep-th/0109154
352. Lin, H., Lunin, O., Maldacena, J.M.: Bubbling AdS space and 1/2 BPS geometries, JHEP **10**, 025 (2004) arxiv:hep-th/0409174
353. Grant, L., Maoz, L., Marsano, J., Papadodimas, K., Rychkov, V.S.: Minisuperspace quantization of 'bubbling AdS' and free fermion droplets,JHEP **08**, 025, (2005). arxiv:hep-th/0505079
354. Mathur, S.D.: The fuzzball proposal for black holes: an Elementary review, Fortsch. Phys. **53**, 793–827, (2005). arXiv:hep-th/0502050
355. Bena, I., Warner, N.P.: Black holes, black rings and their microstates, Lect. Notes Phys. **755**, 1–92, (2008). arXiv:hep-th/0701216
356. Skenderis, K., Taylor, M.: The fuzzball proposal for black holes, Phys. Rept. **467**, 117–171 (2008). arXiv:0804.0552
357. Mathur, S.D.: Fuzzballs and the information paradox: a summary and conjectures. arXiv:0810.4525
358. Almheiri, A., Marolf, D., Polchinski, J,. Sully, J.: Black holes: complementarity or firewalls?". JHEP 1302 (2013) 062. arXiv:1207.3123; cf. Braunstein, S. L..: Black hole entropy as entropy of entanglement, or it's curtains for the equivalence principle. arXiv:0907.1190 published as Braunstein, S.L., Pirandola, S., Zyczkowski, K..: Better late than never: information retrieval from black holes. Phys. Rev. Lett. 110 (2013) 101301 for a similar prediction from different assumptions
359. Almheiri, A., Marolf, D., Polchinski, J., Stanford, D., Sully, J.: An apologia for firewalls. JHEP **1309**, 018 (2013). arXiv:1304.6483
360. Marolf D., Polchinski, J.: Gauge/gravity duality and the black hole Interior, Phys. Rev. Lett. **111**, 171301 (2013). arXiv:1307.4706
361. Carlip, S.: Logarithmic corrections to black hole entropy from the Cardy formula, Class. Quant. Grav. **17**, 4175–4186 (2000). arXiv:gr-qc/0005017
362. Sen, A.: Logarithmic corrections to Schwarzschild and other non-extremal black hole entropy in different dimensions, JHEP **1304**, 156, (2013). arXiv:1205.0971
363. Kaul, R.K., Majumdar, P.: Quantum black hole entropy, Phys. Lett. **B439**, 267–270 (1998). arXiv:gr-qc/9801080
364. Kaul, R.K., Majumdar, P., Logarithmic correction to the bekenstein-hawking entropy, Phys. Rev. Lett. **84**, 5255–5257, (2000). arXiv:gr-qc/0002040
365. Watson, T.: I think there is a world market for maybe five computers. (president of IBM), (1943)
366. Wheeler, J.: Everything is information or "It from bit" was a slogan that replaced Wheeler's earlier belief everything is geometry. Indeed, taking geometry too seriously can be misleading in the context of quantum gravity. (1990)
367. Maldacena, J., Susskind, L., Cool horizons for entangled black holes, Fortsch. Phys. **61**, 781–811 (2013). arXiv:1306.0533

Chapter 3
The Firewall Phenomenon

R.B. Mann

Abstract Black holes have presented us with some of the most baffling paradoxes in physics. From their original conception as dark stars, they have come to be understood as physical systems with their own thermodynamic behaviour. This same behaviour leads to paradoxical conflicts between some of the basic principles of physics whose resolution is not straightforward and that suggest a new structure—known as a firewall—may be present. This chapter provides an overview of the firewall problem, as it emerges from our understanding of black hole thermodynamics.

Keywords Information paradox · Black hole thermodynamics · Firewall

3.1 Introduction

Black Holes have presented us with paradoxical situations ever since their conceptualization in 1783 by the Reverend Michell [1]. Originally seeking a means for determining stellar masses by measuring the reduction in the speed of corpuscular light due to a given star's gravitational pull, Michell reasoned that the maximal effect measurable would be limited by the escape velocity from the star. This would have to be the speed of light, most recently measured by Bradley to be 301,000 km/s [2]. Any star more massive than this upper bound (500 times the mass of the sun assuming the same average density) would not permit light to escape from its surface. While no theoretical constraints for objects having speeds greater than c were known at the time, there were no empirical measurements indicating such objects existed either. Paradoxically, such stars would be *dark stars*, invisible to an outside observer, though they could be indirectly inferred from their gravitational influence on nearby luminous objects. The relationship between their mass and radius is given by the same relativistic value $R = \sqrt{2GM/c^2}$ for Schwarzschild black holes. Ironically, Michell's proposal for measuring the mass of a star by measuring its speed of light

R.B. Mann (✉)
Department of Physics and Astronomy, University of Waterloo, Waterloo, Canada
e-mail: rbmann@uwaterloo.ca

X. Calmet (ed.), *Quantum Aspects of Black Holes*,
Fundamental Theories of Physics 178, DOI 10.1007/978-3-319-10852-0_3

fails because light moves through space at constant speed regardless of the local strength of gravity.

It would take nearly two centuries before the paradoxes associated with dark stars—now referred to as black holes—would dawn upon the physics community at large. Their inexorable gravitational chokehold on matter turns from puzzle to paradox once the quantum information content of the matter is taken into account. At this point in time there is no consistent understanding of how quantum physics allows information to either be retained in or escape from a black hole.

Over the past two years this conundrum has received a new degree of scrutiny. It appears that a profound conflict between three core principles of physics—unitary, locality, and the equivalence principle—indicates that black holes may erect around themselves a new structure called a *firewall* [3]. The basic notion of a firewall is that of a chaotically violent surface of highly energetic quantum states. Whereas standard expectations from local gravitational physics would indicate that any detector (or observer) falling into a black hole would encounter nothing out of the ordinary, the reasoning behind the firewall argument implies that this encounter would be very damaging to pretty much any detection device.

The purpose of this chapter is to present the firewall argument in the context of its roots in black hole thermodynamics and the previously-understood paradoxes associated with this phenomenon. After a review of the notion of a black hole in Sect. 3.2, I will briefly describe the relationship between the laws of black hole mechanics and the laws of thermodynamics (Sect. 3.3). These laws in turn depend upon our understanding of quantum field theory in curved space-time and of pair creation, yielding in turn our basic understanding of black hole radiation (Sect. 3.4). This confluence of ideas led to what became known as the information paradox: the puzzle of how a thermally radiating black hole can be consistent with the unitary evolution quantum physics requires, discussed in Sect. 3.5. It was generally thought for a time that recent conjectures about duality between gravitational physics and gauge theories straightforwardly resolve the problem (at least in principle). However more detailed study of the information paradox indicates that the resolution of this problem is not at all straightforward [4], and that a new structure—known as a firewall—may be present. This strange phenomenon is discussed in Sect. 3.6, along with responses to this new perspective on black holes. A brief summary appears in Sect. 3.7.

3.2 Black Holes

The physical notion of a black hole is essentially the same as that contemplated by Michell: a region of space where the gravity is so strong that nothing can escape from it. If the region is spherical, then a particle will be trapped there if its kinetic energy is less than its gravitational potential energy

$$\frac{1}{2}mv^2 - \frac{GMm}{r} < \frac{1}{2}mc^2 - \frac{GMm}{r} < 0 \quad \Longrightarrow r < \frac{2GM}{c^2} \equiv r_+ \tag{3.1}$$

and so if the mass M is concentrated within a region smaller than r_+ it will trap all particles moving at subliminal speed—the object will be a black hole.

Relativistic considerations imply that this is a firm limit: the invariance of the speed of light for all observers indicates that all matter travels at subliminal speed. Hence (without taking quantum effects into account) a black hole will absorb all matter and emit nothing. It is a perfect absorber, whose physical temperature is zero.

The earliest and best known example of a black hole is the Schwarzschild solution

$$ds^2 = -c^2\left(1 - \frac{r_+}{r}\right)dt^2 + \frac{dr^2}{1 - \frac{r_+}{r}} + r^2 d\Omega_2^2 \tag{3.2}$$

where $d\Omega_2^2 = d\theta^2 + (\sin\theta d\phi)^2$ is the standard line element on the sphere S^2. Curiously, the quantity r_+ plays the same limiting role as in Newtonian theory.

The metric appears to be singular at both $r = r_+$ and $r = 0$, but the former singularity is due simply to a coordinate choice. Writing

$$t = t_* \qquad r = r_+\left[W\left(\exp\left(\frac{r_*}{r_+} - 1\right)\right) + 1\right] \tag{3.3}$$

yields from (3.2)

$$ds^2 = -\frac{W\left(\exp\left(\frac{u-v}{2r_+} - 1\right)\right)}{W\left(\exp\left(\frac{u-v}{2r_+} - 1\right)\right) + 1} du dv + r_+^2\left[W\left(\exp\left(\frac{u-v}{2r_+} - 1\right)\right) + 1\right]^2 d\Omega_2^2 \tag{3.4}$$

where $(u, v) = ct_* \pm r_*$ and W is the Lambert-W function, defined via $W(y)\exp(W(y)) = y$. The horizon $r = r_+$ is at $r_* = -\infty$. The space-time smoothly continues through $r = r_+$.

A particle moving on a radial trajectory will have $d\theta/ds = d\phi/ds = 0$; if the particle moves at the speed of light (e.g. a photon) then $ds^2 = 0$. Hence from (3.4) it is easy to see that ingoing (outgoing) radial light rays follow lines $du/ds = 0$ ($dv/ds = 0$) or u = constant (v = constant). The metric (3.2) can be extended across $r = r_+$ along either of these null lines. Writing $(u', v') = (\exp(u/2r_+), -\exp(-v/2r_+)) = \sqrt{r/r_+ - 1}(\exp((r + ct)/2r_+), -\exp((r - ct)/2r_+))$ transforms (3.2) to

$$ds^2 = -\frac{4r_+^2 e^{-\left[W\left(-\left(\frac{u'v'}{e}\right)\right)+1\right]}}{W\left(-\left(\frac{u'v'}{e}\right)\right) + 1} du' dv' + r_+^2\left[W\left(-\left(\frac{u'v'}{e}\right)\right) + 1\right]^2 d\Omega_2^2 \tag{3.5}$$

which are referred to as Kruskal coordinates. A plot of the function $W(-x/e)$ indicates that it monotonically increases with increasing negative x and diverges at $x = 1$. Hence the metric is finite at $u'v' = 0$ (corresponding to $r = r_+$) but diverges at $u'v' = -1$ or $r = 0$. The Kretschmann scalar $R_{abcd}R^{abcd}$ diverges at this point and so this is a genuine curvature singularity. All geodesics either meet this singularity

or else extend to infinite affine parameter—in this sense Kruskal coordinates are maximal.

The causal structure is more easily shown in a Penrose diagram, which maps the entire space-time to a finite region. For flat Minkowski space-time the metric becomes

$$\begin{aligned} ds^2 &= -c^2dt^2 + dr^2 + r^2 d\Omega_2^2 \\ &= (\sec^2 X_+ \sec^2 X_-)\left[dX_- dX_+ + \left(\frac{\tan X_+ - \tan X_-}{2\sec X_+ \sec X_-}\right)^2 d\Omega_2^2\right] \\ &= (\sec^2 X_+ \sec^2 X_-) d\tilde{s}^2 \end{aligned} \tag{3.6}$$

upon setting $\tan X_\pm = ct \pm r$. Since light rays obey $ds^2 = 0 = d\tilde{s}^2$ the causal relations between various regions are preserved in going from ds^2 to $d\tilde{s}^2$. The range of $X_\pm$ is between $\pm\frac{\pi}{2}$, and the entire space-time is mapped into a finite region, as shown at the top of Fig. 3.1.

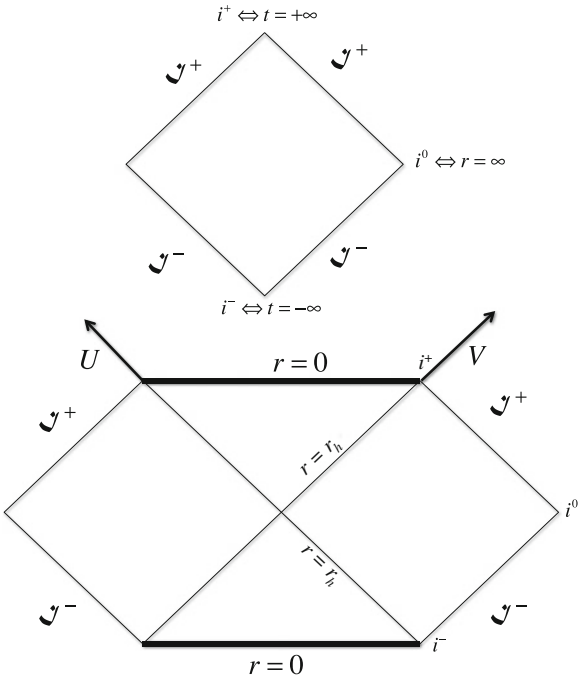

Fig. 3.1 Penrose Diagram The causal structure of Minkowski space-time (*top*) and Schwarzschild space-time (*bottom*). The coordinates U and V are depicted as well

More generally one maps a given spacetime manifold $\mathbb{M}$ with metric g_{ab} into a subset of a manifold $\tilde{\mathbb{M}}$ with metric $\tilde{g}_{ab}$. The conformal relation between the metrics is $\tilde{g}_{ab} = \Omega^2 g_{ab}$. The boundary of the image of $\mathbb{M}$ in $\tilde{\mathbb{M}}$ represents the 'points at infinity' in the original spacetime. Returning to the Schwarzschild metric and writing

$$\tan U = u' \qquad \tan V = v' \tag{3.7}$$

yields a metric conformal to (3.4), with the coordinates (U, V) playing the respective roles of $X_{\pm}$.

We see from the bottom part of Fig. 3.1 that whereas in Minkowski space-time all future-directed light rays can reach infinity $\mathcal{I}^+$ ('scri-plus'), in Schwarzschild space-time any future-directed light rays that cross $r = r_+$ will encounter the singularity, and hence so will all future-directed timeline curves. This is the idea of the trapped region a black hole induces. To make this notion more precise, we need to define a region to which particles are able to escape. From Fig. 3.1 this region should be the portion 'near infinity', i.e. at $\mathcal{I}^+$. So a black hole region $\mathbb{B}$, in mathematical terms, is defined as

$$\mathcal{B} = \mathbb{M} - \mathbb{I}^-(\mathcal{I}^+) \tag{3.8}$$

where $\mathbb{I}^-(A)$ denotes the chronological past of a region A. Hence a black hole is that part of space-time not in the past of the escape-region of light rays (not in the past of $\mathcal{I}^+$ or future null infinity).

The event horizon $\mathbb{H}$ of the black hole is the boundary of $\mathbb{B}$. It is a null hypersurface (generally assumed to be at least once-differentiable) composed of future null geodesics without caustics that cannot be extended. In other words the expansion of the null geodesics comprising the horizon cannot become negatively infinite.

3.2.1 Gravitational Collapse

The Schwarzschild black hole (3.4) is very instructive for understanding the properties of black holes, but is physically unrealistic. Due to time-reversal symmetry, the singularity at $r = 0$ in the future has a counterpart in the past, yielding a 'white hole' structure at the bottom of the Penrose diagram in Fig. 3.1. The white hole $\mathbb{W}$ is defined as $\mathbb{W} = \mathbb{M} - \mathbb{I}^+(\mathcal{I}^-)$: it is the part of the manifold not in the future of the distant past of a time-reversed escape region. Just as a black hole is a total absorber, a white hole is a total emitter: nothing can enter it but anything can leave.

A more physically realistic solution to Einstein's equations matches a collapsing ball of dust (a form of stress-energy with density but no pressure) onto the metric (3.2), yielding a space-time that modelled the collapse of a star into a black hole. Known as the Oppenheimer-Snyder solution [5], it has since been generalized to many other cases. The general form of the Penrose diagrams for such spacetimes is given in Fig. 3.2. The left and bottom parts of the original space-time are no longer present, but the future event horizon remains. There is a point in time at which the

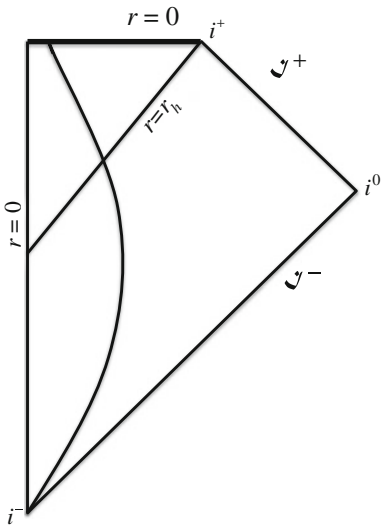

Fig. 3.2 Fluid Collapse The Penrose diagram of the collapse of a ball of dust. The boundary of the dust is given by the *curved line*

fluid collapses beyond which nothing can escape, even though the singularity has yet to form. This is given by the intersection of the diagonal line from i^+ with the vertical line in Fig. 3.2. This is the kind of black hole relevant to astrophysics. A depiction of the process in more familiar coordinates is given in Fig. 3.3.

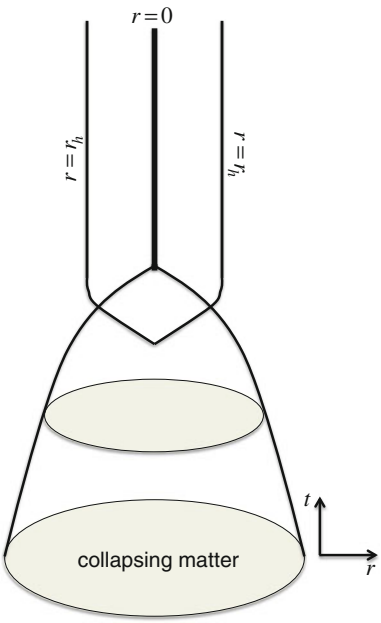

Fig. 3.3 Gravitational Collapse Gravitational collapse of matter in more familiar coordinates

It is also relevant to considerations of black hole thermodynamics. The vacuum solution (3.2) is applicable everywhere outside of the fluid. Since it has an event horizon, the general properties of black hole radiation—and the conundrums they introduce—that are deduced from (3.2) will also be present for the collapse solution shown in Fig. 3.3.

3.2.2 Anti de Sitter Black Holes

An important class of solutions of particular relevance to string theory are solutions in which the space-time is asymptotic to a space-time of constant negative curvature. This latter space-time is known as anti de Sitter (AdS) spacetime, and is a solution to the Einstein equations

$$R_{ab} - \frac{1}{2} g_{ab} R - \Lambda g_{ab} = T_{ab} \tag{3.9}$$

with matter stress-energy tensor $T_{ab} = 0$ and cosmological constant $\Lambda = -(d-1)(d-2)/2\ell^2 < 0$ in d-dimensions. The most general vacuum metric in the static spherically symmetric case is

$$ds^2 = -c^2 \left(\frac{r^2}{\ell^2} + k - \left(\frac{r_0}{r} \right)^{d-3} \right) dt^2 + \frac{dr^2}{\frac{r^2}{\ell^2} + k - \left(\frac{r_0}{r} \right)^{d-3}} + r^2 d\Omega_k^2 \tag{3.10}$$

where $d\Omega_k^2$ is the metric on a compact space Σ_k of constant curvature with sign k, $k = 1$ being the $(d-2)$-sphere, $k = 0$ being a torus, and $k = -1$ being a compact hyperbolic space (obtained via well-known identifications [6]. The metric (3.10) describes what is called a Schwarzschild-AdS black hole, with the constant of integration r_0 given by

$$r_0^{d-3} = \frac{16\pi G M}{(d-2)\mathcal{V}(\Sigma_k)} \tag{3.11}$$

where M is the mass of the black hole and $\mathcal{V}(\Sigma_k)$ is the volume of Σ_k (4π for a two-dimensional sphere). When $M = 0$ then $r_0 = 0$ and the metric (3.10) is that of anti de Sitter space-time.

Light cone (u, v) and Kruskal (u', v') coordinates are defined by

$$u, v = t \pm r_* = t \pm \int \frac{dr}{\frac{r^2}{\ell^2} + k - \left(\frac{r_0}{r} \right)^{d-3}} \qquad u' = e^{\kappa u} \quad v' = -e^{-\kappa v} \tag{3.12}$$

and repeating the procedure for the Schwarzschild case yields Fig. 3.4. There is no choice of conformal factor that allows both the asymptotic boundaries $\mathcal{I}$ and the singularity at $r = 0$ to be represented as straight lines [7], though it is common in the literature to do so.

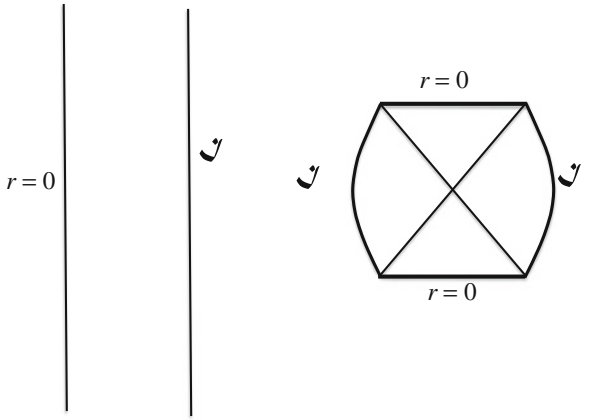

Fig. 3.4 Penrose Diagram for Schwarzschild-AdS Penrose diagrams for AdS (*left*) and the $k = 1$ Schwarzschild-AdS (*right*) space times

Note that asymptotic infinity is timelike in the Schwarzschild-AdS case. Any massive object projected away from the black hole will inevitably return to its starting point; the cosmological constant induces a confining potential for any massive particle, as an analysis of the geodesic equation shows. Light rays, however, can reach $r = \infty$ in finite time. It is common to put reflecting boundary conditions at $r = \infty$ so that light rays are 'confined' like massive objects. The negative cosmological constant thus prevents radiation emitted by the black hole from escaping to infinity, allowing the black hole to reach equilibrium with its Hawking radiation, provided it is large enough. In this sense the eternal black hole (3.10) depicted at the right of Fig. 3.4 is more physically relevant than its asymptotically flat counterpart in Fig. 3.1.

3.3 Black Hole Thermodynamics

The first hints of a fundamental relationship between gravitation, thermodynamics, and quantum theory came from studying black holes. While this subject is covered elsewhere in this volume, it is worth recapitulating the four laws of black hole mechanics [8]:

0th Law Surface gravity κ_+ is constant over the event horizon.

1st Law Differences in mass between nearby solutions are equal to differences in area times the surface gravity plus additional work-type terms

2nd Law The area $\mathcal{A}_+$ of the event horizon never decreases in any physical process provided the energy of matter is positive and space-time is regular

3rd Law No procedure can reduce the surface gravity to zero by a finite number of steps.

Henceforth setting for simplicity the constants G, c, and $\hbar$ to unity, if $\Lambda \neq 0$ then geometric arguments [9–12] indicate that the first law is

$$\delta \mathcal{M} = \kappa_+ \frac{\delta \mathcal{A}_+}{8\pi} + \sum_i (\Omega^i_+ - \Omega^i_\infty)\delta \mathcal{J}^i + V\delta P + \sum_j \Phi^j_+ \delta Q^j \tag{3.13}$$

where $\mathcal{M}$, $\mathcal{J}^i$ are respectively the mass and angular momenta of the D-dimensional black hole. The surface gravity κ_+ is obtained from

$$\kappa^2 = -\frac{1}{2}\nabla^a \xi^b \nabla_a \xi_b|_{r=r_+}$$

where ξ^a is a timelike Killing vector, always present for static black holes. For simplicity κ will be used to denote κ_+ henceforth. For each independent rotational plane, there is one $\mathcal{J}^i$, each with its corresponding conjugate angular velocity Ω_i; the quantities Ω^i_∞ allow for the possibility of a rotating frame at infinity [13]. The Φ^i_h are the potentials for the electric (and magnetic) $U(1)$ charges evaluated at the black hole horizon.

The inclusion of the $V\delta P$ term in (3.13) is a new addition, of considerable recent interest in black hole thermodynamics. Since a negative cosmological constant Λ induces a vacuum pressure, it seems reasonable to consider it as a thermodynamic variable [14] analogous to pressure in the first law [9, 10, 15]. The mass M is then understood as a gravitational version of chemical enthalpy. This is the total energy of a system including both its internal energy E and the energy PV required to "make room for it" by displacing its (vacuum energy) environment: $M = E + PV$. In other words, M is the total energy required to "create a black hole and place it in a cosmological environment". A new perspective on black hole thermodynamics thus emerges, leading to a different understanding of known processes and to the discovery of new phenomena. The thermodynamic correspondence with black hole mechanics is completed to include the familiar pressure/volume terms:

Thermodynamics		Black hole mechanics	
Enthalpy	H	Mass	M
Temperature	T	Surface gravity	$\frac{\kappa}{2\pi}$
Entropy	S	Horizon area	$\frac{A}{4}$
Pressure	P	Cosmological constant	$-\frac{\Lambda}{8\pi}$
First law	$dH = TdS + VdP + \cdots$	First law	$dM = \frac{\kappa}{8\pi}dA + VdP + \cdots$

(3.14)

where the black hole work terms are $\sum_i \Omega_i dJ_i + \Phi dQ$ for multiply rotating and charged black holes.

A number of interesting implications have been recently worked out, including the discovery that charged black holes behave as Van der Waals fluids [16, 17], the realization well-known first-order phase transition between radiation and large AdS black holes [18] can be understood as a "solid/liquid" phase transition, and the discoveries of *reentrant phase transitions* [12] and *triple points* [19] for Kerr-AdS

black holes. The former refers to a situation in which a system can undergo a transition from one phase to another and then back to the first by continuously changing one thermodynamic variable, and the latter is a coalescence of small, medium, and large sized black holes into a single kind at a particular critical value of the pressure and temperature, analogous to the triple point of water. A recent review appears in [12].

3.4 Black Hole Radiation

The striking parallel between black hole mechanics and black hole thermodynamics raises the question as to the origin of this correspondence. Pivotal to this relationship is the derivation of black hole temperature, which necessarily relies on the incorporation of quantum physics into curved space-time settings [20]. There is not the space to review this vast subject here, so I shall sketch the situation to provide the necessary context for the information paradox and firewall argument.

3.4.1 Quantum Field Theory in Curved Spacetime

A scalar field D spacetime dimensions obeys the equation

$$\nabla^2\varphi - m^2\varphi = 0 \tag{3.15}$$

and can be decomposed into a *mode expansion*

$$\varphi(x) = \int d^3\,\boldsymbol{k}\left[\phi_{\boldsymbol{k}}(x)\hat{a}_{\boldsymbol{k}} + \phi^*_{\boldsymbol{k}}(x)\hat{a}^\dagger_{\boldsymbol{k}}\right]. \tag{3.16}$$

where the functions $\phi_{\boldsymbol{k}}(x)$ are called *mode functions*. They are each solutions to (3.15) and together form an orthonormal basis for the space of solutions in the sense that

$$\langle\langle\phi_{\boldsymbol{k}}(x), \phi_{\boldsymbol{k}'}(x)\rangle\rangle = -\langle\langle\phi_{\boldsymbol{k}}(x)^*, \phi_{\boldsymbol{k}'}(x)^*\rangle\rangle = \delta^3(\boldsymbol{k} - \boldsymbol{k}'), \quad \langle\langle\phi_{\boldsymbol{k}}(x), \phi_{\boldsymbol{k}'}(x)^*\rangle\rangle = 0, \tag{3.17}$$

with the inner product between fields defined as

$$\langle\langle\chi, \phi\rangle\rangle \equiv \int_\Sigma d\Sigma_a\, j^a(\chi, \phi) \tag{3.18}$$

where Σ_a is the volume element on Σ with unit normal n^a and the current

$$j^a(\chi, \phi) = -i\sqrt{g}g^{ab}(\chi^*\nabla_b\phi - (\nabla_b\chi^*)\phi) \tag{3.19}$$

is conserved ($\nabla_a j^a = 0$) provided both χ and ϕ) are solutions to (3.15). The conservation of j^a ensures that the inner product is independent of the choice of slice Σ. The operators $\hat{a}_{\boldsymbol{k}}$ are called *mode operators*, which obey the relations

$$[\hat{a}_{\boldsymbol{k}}, \hat{a}^{\dagger}_{\boldsymbol{k}'}] = \delta^3(\boldsymbol{k} - \boldsymbol{k}') \tag{3.20}$$

Particle creation is understood to be

$$\prod_{n=1}^{N} \left(\hat{a}^{\dagger}_{k_i}\right)^{n_{k_i}} |0\rangle = \left|n_{\boldsymbol{k}_1}, n_{\boldsymbol{k}_2}, \ldots\right\rangle \tag{3.21}$$

where the notation $n_{\boldsymbol{k}}$ refers to n quanta in the k-th frequency mode of the field. For example if the scalar field is replaced with an electromagnetic field, this would be n photons of wave vector k.

The state $|0\rangle$ is the lowest-energy state—the vacuum, having no particles—with the property

$$\hat{a}_{k_i}|0\rangle = 0 \quad \forall \chi \in \mathcal{Q}_+ \tag{3.22}$$

with $\mathcal{Q}_+$ the space of states of positive energy. In spacetimes that possess time translation symmetry (with timelike Killing vector ξ) it is defined to be the space of solutions such that

$$\xi^a \partial_a \phi_{\boldsymbol{k}}(x) = -i\omega_{\boldsymbol{k}} \phi_{\boldsymbol{k}}(x), \quad \xi^a \partial_a \phi^*_{\boldsymbol{k}}(x) = i\omega_{\boldsymbol{k}} \phi^*_{\boldsymbol{k}}(x), \tag{3.23}$$

where $\omega_{\boldsymbol{k}} > 0$. The *positive/negative frequency* modes have eigenvalues $\mp i\omega_{\boldsymbol{k}}$ respectively.

In a general curved spacetime there are many ways of carrying out the above construction, with no particular subspace singled out as a natural choice for the positive frequency space [21]. Different notions of positive frequency will yield different Fock space constructions that are unitarily inequivalent [22], and the vacuum state $|0\rangle$ with respect to one choice of $\mathcal{Q}_+$ will not necessarily be in the Fock space constructed from the vacuum $|\tilde{0}\rangle$ with respect to another choice $\tilde{\mathcal{Q}}_+$.

However there is a linear relation between different choices. For another choice $\tilde{\mathcal{Q}}_+$ any $\tilde{\phi} \in \tilde{\mathcal{Q}}_+$ is a linear combination $\tilde{\phi} = \phi + \chi^*$ for some $(\chi, \phi) \in \mathcal{Q}_+$. Consequently two complete sets of modes $\{\phi_{\boldsymbol{k}}, \phi^*_{\boldsymbol{k}}\}$ and $\{\chi_{\boldsymbol{k}}, \chi^*_{\boldsymbol{k}}\}$ with associated mode operators $\hat{a}_{\boldsymbol{k}}$ and $\hat{\mathrm{a}}_{\boldsymbol{k}}$ are, by completeness and orthonormality, related by

$$\chi_{\boldsymbol{k}}(x) = \int d^3\boldsymbol{k}' \left[\overline{\alpha}_{\boldsymbol{k}\boldsymbol{k}'} \phi_{\boldsymbol{k}'}(x) + \overline{\beta}_{\boldsymbol{k}\boldsymbol{k}'} \phi^*_{\boldsymbol{k}'}(x)\right],$$

where $\overline{\alpha}_{\boldsymbol{k}\boldsymbol{k}'} = \langle\langle \chi_{\boldsymbol{k}}(x), \phi_{\boldsymbol{k}'}(x)\rangle\rangle$ and $\overline{\beta}_{\boldsymbol{k}\boldsymbol{k}'} = -\langle\langle \chi_{\boldsymbol{k}}(x), \phi^*_{\boldsymbol{k}'}(x)\rangle\rangle$. This is called a *Bogoliubov transformation* [20] and the complex numbers $\overline{\alpha}_{\boldsymbol{k}\boldsymbol{k}'}$ and $\overline{\beta}_{\boldsymbol{k}\boldsymbol{k}'}$ are called *Bogoliubov coefficients*. Inverting this transformation yields

$$\phi_{\boldsymbol{k}} = \int d^3\,\boldsymbol{k}'\,\left[\overline{\alpha}^*_{\boldsymbol{k}'\,\boldsymbol{k}}\chi_{\boldsymbol{k}'}(x) - \overline{\beta}_{\boldsymbol{k}'\,\boldsymbol{k}}\chi^*_{\boldsymbol{k}'}(x)\right]$$

inducing in turn the following transformations

$$\hat{a}_{\boldsymbol{k}} = \int d^3\,\boldsymbol{k}'\,\left[\overline{\alpha}_{\boldsymbol{k}'\,\boldsymbol{k}}\hat{\mathrm{a}}_{\boldsymbol{k}'} + \overline{\beta}^*_{\boldsymbol{k}'\,\boldsymbol{k}}\hat{\mathrm{a}}^\dagger_{\boldsymbol{k}'}\right] \qquad \hat{\mathrm{a}}_{\boldsymbol{k}} = \int d^3\,\boldsymbol{k}'\,\left[\overline{\alpha}^*_{\boldsymbol{k}\,\boldsymbol{k}'}\hat{a}_{\boldsymbol{k}'} - \overline{\beta}^*_{\boldsymbol{k}\,\boldsymbol{k}'}\hat{a}^\dagger_{\boldsymbol{k}'}\right] \tag{3.24}$$

on the mode operators.

The commutation relations (3.20) of the mode operators imply

$$\begin{pmatrix} \overline{\alpha} & \overline{\beta} \\ \overline{\beta}^* & \overline{\alpha}^* \end{pmatrix}\begin{pmatrix} \overline{\alpha}^\dagger & -\overline{\beta}^{\mathrm{T}} \\ -\overline{\beta}^\dagger & \overline{\alpha}^{\mathrm{T}} \end{pmatrix} = \begin{pmatrix} 1 & 0 \\ 0 & 1 \end{pmatrix},$$

where the individual entries are to be interpreted as block matrices. From (3.24) we see that the Fock bases associated with these two mode expansions differ, leading to two different particle interpretations of the field excitations. Whenever any of the $\overline{\beta}$-coefficients are nonzero, positive frequency states get transformed into a combination of positive and negative frequency states, leading to particle production. Specifically, according to the particle interpretation based on the $\phi_{\boldsymbol{k}}(x)$ modes, particles are present in the vacuum of the $\chi_{\boldsymbol{k}}(x)$ mode expansion $|0\rangle_\chi$. The average number of particles present in mode $\boldsymbol{k}$ is given by

$${}_\chi\langle 0|N_k|0\rangle_\chi = {}_\chi\langle 0|\hat{a}^\dagger_{\boldsymbol{k}}\hat{a}_{\boldsymbol{k}}|0\rangle_\chi = \int d^3\,\boldsymbol{k}'\,|\overline{\beta}_{\boldsymbol{k}\,\boldsymbol{k}'}|^2.$$

In this sense, there is no invariant notion of particles in quantum field theory: as with simultaneity, particle interpretations are observer-dependent.

To cope with this, several key assumptions must be made.

1. All quantum states are defined on a spacelike slice Σ of 4-dimensional space-time, whose intrinsic curvature $R^{(3)}_{abcd}$ and extrinsic curvature K_{ab} are both everywhere small compared to the Planck length: $|R^{(3)}_{abcd}| \ll 1/l_p^2$, $|K_{ab}| \ll 1/l_p^2$.
2. There is some neighbourhood of Σ where the full space-time curvature R_{abcd} is also small: $|R_{abcd}| \ll 1/l_p^2$.
3. The wavelength λ of any quanta on Σ is much longer than the Planck length $\lambda \gg l_p$.
4. The stress-energy of all matter obeys positive energy conditions and the energy and momentum densities of the matter are small compared to the Planck density $(\tilde{1}/l_p^4)$.
5. For a least a certain interval of proper time τ, Σ evolves sufficiently smoothly (so that $dN/d\tau \ll 1/l_p$ and $dN^a/d\tau \ll 1/l_p$) into future slices that respect the preceding four properties.

The preceding conditions are sometimes referred to as the 'niceness' conditions [4], and are regarded as ensuring that semiclassical physics is valid (Fig. 3.5).

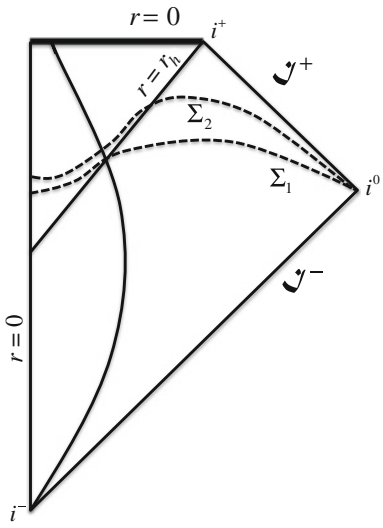

Fig. 3.5 Nice Slices Two different slices for the collapse diagram that satisfy the niceness conditions

3.4.2 Pair Creation

Generally black hole radiation can be understood as a phenomenon of pair-creation of particles due to the distortion of spacetime near the horizon. An intuitive argument illustrating how this can take place was recently given by Mathur [4]. Consider a choice of spacelike slices in which one spatial region evolves further in time than another, as shown in Fig. 3.6. This situation is permitted in generally covariant theories of gravity such as general relativity. Both slices satisfy the semiclassical (niceness) conditions. No particle creation occurs classically, but if a quantum field

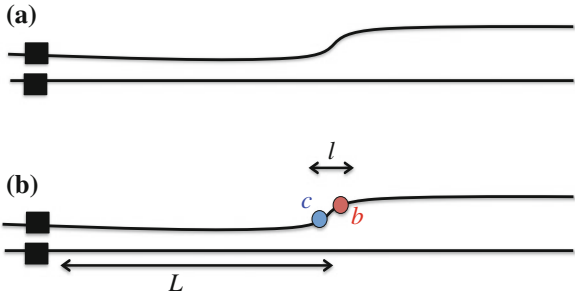

Fig. 3.6 Particle Creation due to Spacetime distortion The intrinsic geometry of the initial spatial slice (*horizontal line*) evolves forward in time differently on the *left* than on the *right*, with a concentration of (classical) matter symbolized by the box at the *left*. In **a** the evolution is fully classical and no pairs are created. In **b** the quantum field on the initial slice is in the vacuum, with the space-time distortion on the next slice creating a pair of quanta

is in the vacuum state (in Fig. 3.6b) then the created-pair state will be in the state

$$|\psi\rangle = (\alpha|0\rangle_c|0\rangle_b + \beta|1\rangle_c|1\rangle_b) + \cdots \tag{3.25}$$

where $|\alpha|^2 + |\beta|^2 = 1$; the ellipsis refers to multi-pair creation, neglected in the above. In Hawking radiation the created pair is maximally entangled, with $|\alpha| = |\beta| = 1/\sqrt{2}$, but we can understand what is going on for arbitrary entanglement. The quantum state of the entire system is

$$|\Psi\rangle \approx |\Phi\rangle_M \otimes \Big(\alpha|0\rangle_c|0\rangle_b + \beta|1\rangle_c|1\rangle_b\Big) \tag{3.26}$$

where $|\Phi\rangle_M$ is the quantum state of the matter, symbolized by the box at the left of Fig. 3.6. If $l \ll L$ then the influence of the matter on the created pair can be neglected (though in principle there is always some influence), and the full state is well approximated by the tensor product (3.26).

The locality assumption ensures that the state Ψ is a tensor product. Small departures from whatever physics yielding the (α, β) coefficients are permitted

$$|\Psi\rangle \approx \Big(\tilde{\alpha}|\Phi_0\rangle_M + \tilde{\beta}|\Phi_1\rangle_M\Big) \otimes \Big((\alpha+\epsilon)|0\rangle_c|0\rangle_b + (\beta-\epsilon)|1\rangle_c|1\rangle_b\Big) \tag{3.27}$$

but not states of the form

$$|\Psi\rangle \approx \Big((\tilde{\alpha}+\epsilon)|\Phi_0\rangle_M|0\rangle_c + (\tilde{\beta}-\epsilon)|\Phi_1\rangle_M|1\rangle_c\Big) \otimes \Big(\alpha|0\rangle_b + \beta|1\rangle_b\Big) \tag{3.28}$$

where for simplicity the matter is assumed to be a single qubit in one of two possible states $|\Phi_0\rangle_M$ or $|\Phi_1\rangle_M$. For the former case (3.27) the entanglement entropy is, upon tracing over the matter and state c,

$$\begin{aligned} S_{\text{ent}} &= -\,\text{tr}_{c,M}[\rho \ln \rho] \\ &= -\Big(|\alpha|^2 \ln|\alpha| + |\beta|^2 \ln|\beta|\Big) \\ &\quad + 2\epsilon\Big(|\beta| \ln(2|\beta|^2) - |\alpha| \ln(2|\alpha|^2)\Big) \\ &\quad - \epsilon^2\Big(6 + 2\ln(|\alpha||\beta|)\Big) \end{aligned} \tag{3.29}$$

which has the value $S_{\text{ent}} = \ln 2 - \epsilon^2(6 - 2\ln 2) \approx \ln 2$ for maximal entanglement. However for the latter case (3.28) the entanglement entropy is

$$S_{\text{ent}} = -\text{tr}_{c,M}[\rho \ln \rho] = 0 \tag{3.30}$$

since the state b is a direct product with the remaining states. So for $l_p \ll l \ll L$, the entanglement entropy is

$$\left|\frac{S_{\text{ent}}}{\ln 2} - 1\right| \ll 1 \tag{3.31}$$

from pair creation due to space-time distortion when the semiclassal assumptions are valid.

The key distinction between radiation emitted from a black hole and that emitted from a hot material object (such as a lump of coal) is in how the emitted quanta are generated. A lump of coal emits radiation because the atoms near its surface are excited, and emit quanta as they fall to states of lower energy. A black hole, however, emits quanta that arise due to entangled pair creation from the distortion of space-time, with one partner in the pair remaining inside the black hole and thus inaccessible to observers outside. Put another way, hot material bodies emit radiation from their constituents whereas black holes pull entangled pairs of quanta out of the vacuum as the result of 'stretching' a region of a space-like slice. The situation is illustrated in Fig. 3.7.

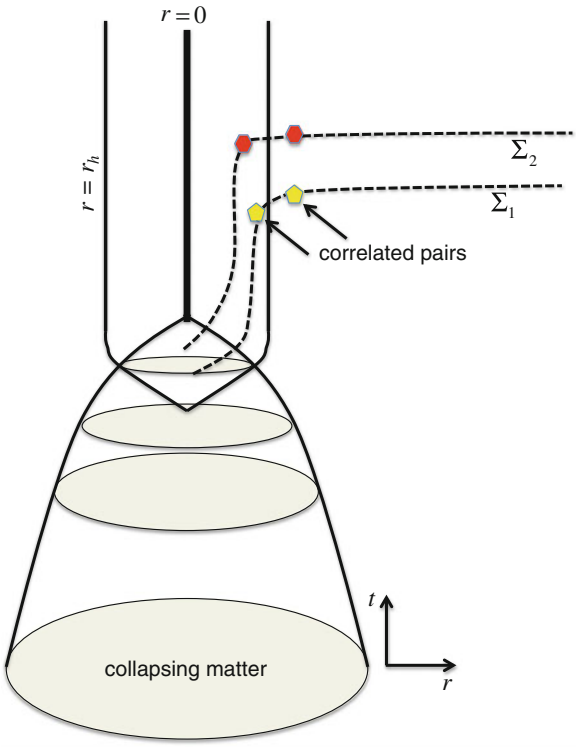

Fig. 3.7 Creation of Correlated Pairs outside a Black Hole Pairs of quanta (*symbolized* by the *shapes*) are created near the event horizon. The collapsing matter on the same corresponding spatial slices is very far from these pairs

The laws of black hole mechanics imply that the temperature T of a black hole is given by its surface gravity, $T = \kappa/2\pi$. The metric of any static black hole can be written as

$$ds^2 = -f(r)dt^2 + \frac{dr^2}{g(r)} + r^2 d\Omega_2^2 \tag{3.32}$$

and

$$\kappa^2 = -\frac{1}{2}\nabla^a \xi^b \nabla_a \xi_b|_{r=r_+} = \frac{g(r)(f'(r))^2}{4f(r)}\Big|_{r=r_+} = \frac{g'_+ f'_+}{4} \tag{3.33}$$

yields the surface gravity at the horizon. Hawking's original calculation [23] was for a free scalar field propagating in a classical background spacetime describing gravitational collapse of matter to a Schwarzschild black hole. Prior to collapse the scalar is initially in its vacuum state. At late times, long after the black hole has formed, the positive frequency mode function corresponding to a particle state is traced backwards in time to determine its positive and negative frequency parts in the asymptotic past. The expected number of particles at infinity corresponds to emission from a perfect black body (of finite size) at the temperature $T = \kappa/2\pi$. Note that, other than in justifying use of the background space-time, nowhere are any gravitational field equations employed in this calculation. A collapse situation is well approximated by the eternal black hole (3.2) but with boundary conditions that are regular (Hadamard) only on the future horizon. This is called the Unruh state.

Despite this, there are a number of caveats and assumptions underlying the calculations of black hole temperature [4, 24].

A1 Invariant Hadamard states do not exist for all stationary black holes. The Kerr solution, describing a rotating black hole, is one such example, and as a consequence has a super-radiant instability [25–27].

A2 Asymptotically flat black holes will lose mass as they radiate, invalidating the late-time stationarity assumption. However the outgoing radiation will only carry an appreciable fraction of the mass over timescales $t \sim (M/M_P)^3$ [28].

A3 One of the most crucial assumptions is that the quantum state of the field is regular (Hadamard) at the horizon: its local behaviour at the horizon is the same as it would be in the Minkowski vacuum. This is an application of the equivalence principle, that locally (on sufficiently short time and distance scales) gravity and acceleration are indistinguishable. Freely-falling observers near the horizon should not see any unusual behaviour in high-energy processes. This is sometimes call the "no drama" assumption.

The no-drama assumption is somewhat paradoxical. An observer distant from a black hole formed from collapse who detects a mode at any finite frequency ω_f will realize that it has been redshifted. This must mean that it had a very large frequency in the past when it was propagating near the event horizon, of order $\omega = e^{\kappa t}\omega_f$ where t is the time it takes for the mode to reach the distant observer: the mode is

blueshifted in the past. There is no past horizon (or other obvious physical effect) to provide a compensating effect for a mode propagating through the collapsing matter from the asymptotic past. Within a time scale of order $1/\kappa$ of the black hole's formation, the intermediate steps of the derivation implicitly involve propagation of trans-Planckian modes, modes that are much higher that the Planck frequency $\omega_P = \sqrt{c^5/\hbar G} \sim 10^{43}\ \mathrm{s}^{-1}$. This suggests lots of drama, since it is difficult to believe in the reliability of free-field theory (or any other known physical theory) at such high frequencies/energies [29].

Extensive study of this trans-Planckian problem [30–38] suggests that, despite the above, Hawking radiation is actually a low-energy phenomenon. Studies of quantized sound waves in a fluid undergoing supersonic flow indicate that a sonic analogue of the Hawking effect is present here as well. There is also a past-blueshift effect that renders invalid the continuum fluid equations that described the situation in the first place. However modifying these equations to yield a dispersion relation that is altered at ultra-high frequencies to alleviate this problem still yields sonic Hawking radiation. A variety of alternative models that significantly modify the continuum fluid equations at high energies have verified this, and a recent experiment with water waves [39] is in accord with the basic theoretical predictions.

The low-energy character of Hawking radiation appears to emerge from the behaviour of the field in the WKB regime [40]. Moving backward in time, the past-blueshift effect will bring the field into the WKB regime before it enters the trans-Planckian regime. The WKB approximation remains valid throughout the evolution provided the Hawking temperature is much smaller than the trans-Planckian scale (the scale at which the modified dispersion relation is relevant). The outgoing radiation does not come about because of any interaction with other degrees of freedom but rather is a consequence of the tidal disruption (or space-time distortion) of free-field evolution by stretching the wavelengths. The major ingredient of Hawking radiation appears to be a "tearing apart" of the waves into an outgoing (positive norm) component and its infalling (negative norm) partner (Fig. 3.8).

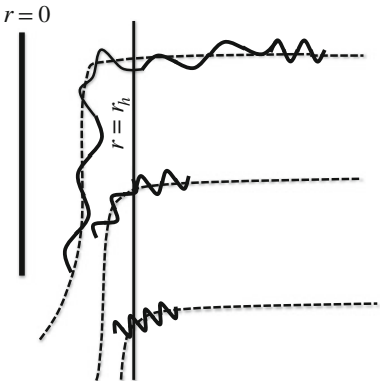

Fig. 3.8 Mode Stretching A Fourier mode created on some slice (represented by the *dashed line*) is stretched as it evolves to later slices. This eventually leads to a distorted waveform, resulting in particle creation

3.5 The Information Paradox

The no-drama assumption is tantamount to assuming the horizon of the black hole is 'information-free': that field modes with wavelengths $l_p \ll \lambda \lesssim M$ are described by curved space-time quantum field theory on the black hole background. We have seen that the notion of a particle is contingent on what the vacuum, or 'empty space' is taken to be. Modes with wavelengths λ smaller than the curvature scale R will yield differing definitions of particle quanta, but the difference between definitions will consist of about 1 quanta for wavelengths as large as the curvature scale, $\lambda \sim R$. For black holes $R \sim M$ and so different particle-definitions will differ by about 1 quanta for wavelength $\lambda \sim M$, but by a negligible number of quanta for wavelengths $\lambda < \tilde{k}M$, where $\tilde{k} \sim 10^{-1}$. Hence a robust notion of vacuum, or empty space, is well defined for such wavelengths: no modes are present for $l_p \ll \lambda < \tilde{k}M$.

In illustrating the information paradox, the assumptions A1–A3 will be assumed to hold, and so it will be sufficient to employ the metric (3.2). At late times this can describe a collapsing black hole, formed perhaps by a shell of matter or a ball of dust. Since this metric has a singularity at $r = 0$, spacelike slices must avoid this singularity or else the niceness conditions will not hold, undermining the calculations yielding black hole radiation.

The slicing choice will be taken to obey the following criteria [4]

Outside Σ_O	Slices are at $t =$ constant for $r > 4M$; this portion is outside the black hole.
Inside Σ_I	Slices are at $r =$ constant for $M/2 < r < 3M/2$; this portion is inside the black hole. This segment will be smoothly extended to $r = 0$ at early times before the singularity has formed.
Connect Σ_C	The preceding two segments are joined by a smooth connecting segment $\mathcal{C}$; this portion crosses the event horizon. The spatio-temporal dimensions of this segment are both of size $\sim M$.

thereby respecting the niceness conditions. Nowhere does the slice $\Sigma(t, r, \mathcal{C}) = \Sigma_O \cup \Sigma_I \cup \Sigma_C$ go near the singularity, and the appropriate connecting segment can always be appropriately chosen.

Each slice is contingent on the choice of time, and it is essential that the slices smoothly evolve into each other (not merging or crossing). If $\Sigma_0 = \Sigma(t_0, r_0, \mathcal{C}_0)$ describes an initial slice, then a subsequent slice is $\Sigma_1 = \Sigma(t_1, r_1, \mathcal{C}_1) = \Sigma(t_0 + \delta t, r_0 + \delta r, \mathcal{C}_0 + \delta\mathcal{C})$. Increasing t_0 and r_0 respectively correspond forward evolution outside and inside the black hole. The geometry of the connecting segments can be taken to be the same for all slices provided $\delta r \ll M$ is sufficiently small. This has the consequence that the constant-r segments of the slices become increasingly longer since the constant-t parts outside the horizon are further in the future. The dashed lines in Fig. 3.7 are illustrative of this choice of slicing.

Foliating the space-time with these slices $\Sigma(t, r, \mathcal{C})$ along a unit timelike normal u^a (with zero shift vector) indicates that only the connecting segment $\mathcal{C}$ becomes stretched. The segment Σ_O advances forward in time with lapse function $N = \sqrt{1 - 2M/r}$, and the segment Σ_I will remain unchanged in its intrinsic geometry

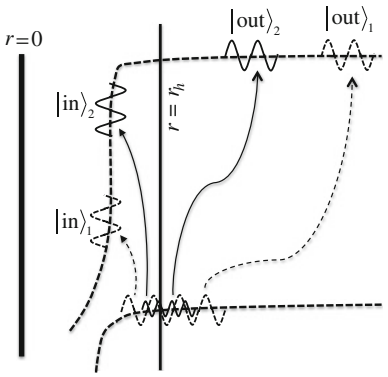

Fig. 3.9 Mode Evolution Long wavelength modes (*dashed*) and short wavelength modes (*solid*) created on the same slice generate created pairs differently. The long wavelength modes get distorted earlier, creating an entangled pair first ($|\text{outside}\rangle_1$, $|\text{inside}\rangle_1$). The short wavelength modes take longer to distort, and so the pairs they create ($|\text{outside}\rangle_2$, $|\text{inside}\rangle_2$) emerge later

provided δr is sufficiently small, though its length increases. The connecting segment Σ_C must therefore stretch since it has to evolve to cover the additional part of Σ_I and the connecting segment of the next slice.

The slicing is therefore time-dependent since it must cover both the outside and inside of the black hole; it therefore depends on the temporal coordinate r on the inside of the hole. The Kretschmann scalar and all other measures of curvature are small for all slices in this evolution. It is the time-dependent stretching of Σ_C, and not large-curvature effects, that yields particle production. This choice of slicing (and its resultant stretching) is a necessary consequence of the existence of the black hole. It is not an option in flat space-time: any such choice will necessarily force the slices to eventually become null and then timelike at some point in the evolution. Since spatial and temporal directions interchange roles for a black hole, the slices always remain spacelike. The stretching of the slices is localized to a region in the vicinity of the horizon: a field mode in this region will become increasingly stretched to longer wavelengths, generating particles for as long as the assumptions concerning the use of (3.2) are valid (Fig. 3.9).

The particle creation scenario proceeds along the following lines. The quantum state on the initial slice Σ_0 is that of the matter field $|\Phi(t, r)\rangle$ that will later form the black hole. This can be taken to be a sharply-peaked wavepacket that in the classical limit describes a shell of collapsing matter. Prior to formation of the black hole no particles are created since the entire slice is outside of the black hole. Upon formation of the black hole the quantum state is $|\Phi\rangle$. On some subsequent slice there will be sufficient stretching of region Σ_C to create a pair of quanta of sufficiently short wavelength $\lambda = 2\pi/k$. The matter state $|\Phi\rangle$ will be localized in Σ_I and so will be negligibly affected by this process. Consider for simplicity a single mode. The quantum state on this slice will therefore be

$$|\Psi\rangle_1 \approx \frac{1}{\sqrt{2}}|\Phi\rangle_{\mathrm{I}_1} \otimes \left(|0_k\rangle^+_{\mathrm{I}_1}|0_{-k}\rangle^-_{\mathrm{O}_1} + |1_k\rangle^+_{\mathrm{I}_1}|1_{-k}\rangle^-_{\mathrm{O}_1}\right) \tag{3.34}$$

where the subscripts I/O refer to inside/outside the horizon. An outside observer has no access to the states inside, and so must employ the reduced density matrix

$$\rho_{\mathrm{O}_1} = \mathrm{tr}_{\mathrm{I}}\Big[|\Psi\rangle\langle\Psi|\Big] = \begin{pmatrix} \frac{1}{2} & 0 \\ 0 & \frac{1}{2} \end{pmatrix} \tag{3.35}$$

in describing the physics of the outside state. The entanglement entropy of the outside state with the state inside the black hole is

$$S_{\mathrm{ent}} = -\mathrm{tr}\left[\rho_{\mathrm{O}_1} \ln \rho_{\mathrm{O}_1}\right] = 2 \times \frac{1}{2} \ln 2 = 2 \ln 2 \tag{3.36}$$

On the next slice the process repeats. The inside state $|\psi\rangle_{\mathrm{I}}$ moves into region Σ_I and the matter state $|\Phi\rangle_{\mathrm{I}_1}$ moves deeper into this region, becoming the state $|\Phi\rangle_{\mathrm{I}_2}$. The outside state $|\psi\rangle_{\mathrm{O}}$ moves into region Σ_O. The additional stretching of region Σ_C creates a new pair, yielding the state

$$|\Psi\rangle_2 \approx \frac{1}{\sqrt{2}}|\Phi\rangle_{\mathrm{I}_2} \otimes \left(|0_k\rangle^+_{\mathrm{I}_1}|0_{-k}\rangle^-_{\mathrm{O}_1} + |1_k\rangle^+_{\mathrm{I}_1}|1_{-k}\rangle^-_{\mathrm{O}_1}\right) \otimes \left(|0_k\rangle^+_{\mathrm{I}_2}|0_{-k}\rangle^-_{\mathrm{O}_2} + |1_k\rangle^+_{\mathrm{I}_2}|1_{-k}\rangle^-_{\mathrm{O}_2}\right) \tag{3.37}$$

assuming the stretching region has negligible influence on the first pair of states. The reduced density matrix is now

$$\rho_{\mathrm{O}_2} = \mathrm{tr}_{\mathrm{I}}\Big[|\Psi\rangle\langle\Psi|\Big] = \begin{pmatrix} \frac{1}{4} & 0 & 0 & 0 \\ 0 & \frac{1}{4} & 0 & 0 \\ 0 & 0 & \frac{1}{4} & 0 \\ 0 & 0 & 0 & \frac{1}{4} \end{pmatrix} \tag{3.38}$$

and

$$S_{\mathrm{ent}} = -\mathrm{tr}\left[\rho_{\mathrm{O}_2} \ln \rho_{\mathrm{O}_2}\right] = 4 \times \frac{1}{4} \ln 4 = 2 \ln 2 \tag{3.39}$$

is entanglement entropy of the outside state on this next slice.

After n steps the quantum state is

$$|\Psi\rangle_n \approx \frac{1}{\sqrt{2}}|\Phi\rangle_{\mathrm{I}_n} \prod_{m=1}^{n} \left[\otimes\left(|0_k\rangle^+_{\mathrm{I}_m}|0_{-k}\rangle^-_{\mathrm{O}_m} + |1_k\rangle^+_{\mathrm{I}_m}|1_{-k}\rangle^-_{\mathrm{O}_m}\right)\right] \tag{3.40}$$

and the reduced density matrix is $\rho_{\mathrm{O}_n} = \mathrm{diag}(2^{-n}, 2^{-n}, \ldots, 2^{-n})$, yielding

$$S_{\text{ent}} = -\text{tr}\left[\rho_{O_n} \ln \rho_{O_n}\right] = -n \times \frac{1}{2^n} \ln 2^{-n} = n \ln 2 \tag{3.41}$$

for the entanglement entropy.

The quantity n is an enormously large number, as can be seen from energy conservation. Suppose each quanta contains the same amount of energy in units of the Planck mass. For a mass M black hole, the energy per quanta is $E_Q = \sigma(M_p/M)M_p \ll M$ where σ is a parameter of order unity. The total mass of the black hole is $nE_Q = M$ implying $n = (M/M_P)^2/\sigma$. For a solar mass black hole $n \sim (2 \times 10^{30}/(2 \times 10^{-8}))^2 = 10^{76}$. There is no upper bound on n since in principle the mass of the black hole can be arbitrarily large, though one might argue that the largest black hole possible is constrained by the mass of the universe, $M_U = 10^{52}$ kg, giving $n \leq 10^{120}$.

Expression (3.41) contains the nub of the information paradox: the entanglement entropy of the radiation state $|\psi\rangle_{\text{O}}$ grows without bound as more pairs are created. Eventually it must terminate, of course, as the radiation cannot contain more energy than was in the initial quantum state $|\Phi\rangle$ (or the mass M of the black hole). Indeed the niceness conditions will (at least) fail to hold once $M \sim M_p$, since the Kretschmann scalar (for example) $K = 48M^2/r^6 \to M_p^2/l_p^6 = l_p^4$ becomes too large for semi-classicality to hold. Of course the assumptions leading to (3.41) do not hold in full generality. The mass of the black hole is not constant, the created pairs might interact with each other, and the state $|\Phi\rangle$ could have some interaction with the created pairs. Gravitational instantons, for example, yield tiny corrections proportional to $\exp\{-(M/M_P)^2\}$. Could such small corrections from these effects invalidate the argument in some way?

Unfortunately this proves not to be the case [4]. Suppose at the j-th step of the process, the full quantum state is not of the form (3.40) but is rather

$$|\tilde{\Psi}\rangle_j = |\tilde{\Psi}\rangle_{j-1}^{(+)} |\Xi\rangle_j^{(+)} + |\tilde{\Psi}\rangle_{j-1}^{(-)} |\Xi\rangle_j^{(-)} \tag{3.42}$$

where

$$|\Xi\rangle_j^{(\pm)} = \frac{1}{\sqrt{2}} \left(|0_k\rangle_{\text{I}_j}^+ |0_{-k}\rangle_{\text{O}_j}^- \pm |1_k\rangle_{\text{I}_j}^+ |1_{-k}\rangle_{\text{O}_j}^- \right) \tag{3.43}$$

and the state $|\tilde{\Psi}\rangle_{j-1}^{(+)}$ can be expressed as

$$|\tilde{\Psi}\rangle_{j-1}^{(\pm)} = \sum_{l,m} \alpha_{l,m} |\tilde{\tilde{\psi}}_l^{\pm}(\Phi, \text{I})\rangle |\chi_m(\text{O})\rangle = \sum_m \gamma_m |\tilde{\psi}_m^{\pm}(\Phi, \text{I})\rangle |\chi_m(\text{O})\rangle \tag{3.44}$$

where $|\tilde{\psi}_m^{\pm}(\Phi, \text{I})\rangle$ and $|\chi_m(\text{O})\rangle$ are orthonormal bases for the respective inside and outside states, and a unitary transformation has been applied to obtain the second equality. The newly created state is spanned by $\Xi_j^{(\pm)}$. Assuming locality, the outside

states $\left|\psi\right\rangle_{\mathrm{O}_j}^{-}$ generated in earlier stages of the evolution are not affected by the proposed step (3.42); hence the basis $|\chi_m(\mathrm{O})\rangle$ remains unchanged.

The proposed correction (3.42) to the Hawking process is a deformation of the original process (3.40), in which $|\tilde{\Psi}\rangle_{j-1}^{(-)} = 0$. Unitarity implies that

$$\left|\,{}_{j-1}^{(+)}\langle\tilde{\Psi}|\tilde{\Psi}\rangle_{j-1}^{(+)}\,\right|^2 + \left|\,{}_{j-1}^{(-)}\langle\tilde{\Psi}|\tilde{\Psi}\rangle_{j-1}^{(-)}\,\right|^2 = 1 \tag{3.45}$$

since the $\Xi_j^{(\pm)}$ are orthonormal. If the corrections to (3.40) due to (3.42) are small, then

$$\left|\,{}_{j-1}^{(-)}\langle\tilde{\Psi}|\tilde{\Psi}\rangle_{j-1}^{(-)}\,\right| < \epsilon \tag{3.46}$$

where $\epsilon \ll 1$. To say that corrections to the Hawking radiation process are small is to say that one obtains the state $\Xi_j^{(+)}$ with high probability when the pair is created, and that the orthogonal state $\Xi_j^{(-)}$ is observed with low probability.

There are thus three subsystems at stage-j of the evolution: (i) the outside state $\{\mathrm{O}_{j-1}\}$ of all previously emitted outside quanta, (ii) the inside state $|\tilde{\psi}(\Phi,\mathrm{I})\rangle_{j-1}$ consisting of the original matter state and previously-created inside partner quanta, modified perhaps by previous interactions, and (iii) the newly created pair described by the state $|\Xi\rangle_j$, spanned by the basis $|\Xi\rangle_j^{(\pm)}$. The reduced density matrix for this newly created pair is

$$\begin{aligned}\rho_{\Xi_j} &= \mathrm{tr}_{|\tilde{\psi}(\Phi,\mathrm{I})\rangle_{j-1},\mathrm{O}_{j-1}}\left[|\tilde{\Psi}\rangle_j\,{}_j\langle\tilde{\Psi}|\right] \\ &= \begin{pmatrix} {}_{j-1}^{(+)}\langle\tilde{\Psi}|\tilde{\Psi}\rangle_{j-1}^{(+)} & {}_{j-1}^{(+)}\langle\tilde{\Psi}|\tilde{\Psi}\rangle_{j-1}^{(-)} \\ {}_{j-1}^{(-)}\langle\tilde{\Psi}|\tilde{\Psi}\rangle_{j-1}^{(+)} & {}_{j-1}^{(-)}\langle\tilde{\Psi}|\tilde{\Psi}\rangle_{j-1}^{(-)} \end{pmatrix} \\ &= \begin{pmatrix} 1-\epsilon_-^2 & \epsilon_{+-} \\ \epsilon_{+-}^* & \epsilon_-^2 \end{pmatrix}\end{aligned} \tag{3.47}$$

where by (3.46), $|\epsilon_{+-}| < \epsilon$ and $|\epsilon_-| < \epsilon$. The eigenvalues of this matrix are $\frac{1}{2}(1 \pm \sqrt{1+4(|\epsilon_{+-}|^2 - \epsilon_-^2)}$ to this order, yielding

$$S(\Xi_j)_{\mathrm{ent}} = \left(|\epsilon_{+-}|^2 - \epsilon_-^2\right)\ln\left(\frac{e}{|\epsilon_{+-}|^2 - \epsilon_-^2}\right) + \cdots < \epsilon^2 \ln\epsilon < \epsilon \tag{3.48}$$

for the entanglement entropy of the newly created pair. The entropy of the joint subsystem $\{\mathrm{O}_{j-1}, \Xi_j\}$ is therefore

$$S(\{\mathrm{O}_{j-1}, \Xi_j\}) \geq |S(\{\mathrm{O}_{j-1}\}) - S(\Xi_j)| = S(\{\mathrm{O}_{j-1}\}) - \epsilon \tag{3.49}$$

using the strong subadditivity property of entropy.

Next, tracing over everything except the inside state I_j yields

$$\begin{aligned}\rho_{\mathrm{I}_j} &= \mathrm{tr}_{|\tilde{\psi}(\Phi,\mathrm{I})\rangle_{j-1},\mathrm{O}_j}\left[|\tilde{\Psi}\rangle_{j\ j}\langle\tilde{\Psi}|\right] \\ &= \frac{1}{2}\begin{pmatrix} \left({}^{(+)}_{j-1}\langle\tilde{\Psi}| + {}^{(-)}_{j-1}\langle\tilde{\Psi}|\right)\left(|\tilde{\Psi}\rangle^{(+)}_{j-1} + |\tilde{\Psi}\rangle^{(-)}_{j-1}\right) & 0 \\ 0 & \left({}^{(+)}_{j-1}\langle\tilde{\Psi}| - {}^{(-)}_{j-1}\langle\tilde{\Psi}|\right)\left(|\tilde{\Psi}\rangle^{(+)}_{j-1} - |\tilde{\Psi}\rangle^{(-)}_{j-1}\right) \end{pmatrix} \\ &= \frac{1}{2}\begin{pmatrix} 1+\Re(\epsilon_{+-}) & 0 \\ 0 & 1-\Re(\epsilon_{+-}) \end{pmatrix} \end{aligned} \tag{3.50}$$

and so

$$S(\mathrm{I}_j)_{\mathrm{ent}} = \ln 2 - 2[\Re(\epsilon_{+-})]^2 > \ln 2 - 2\epsilon^2 > \ln 2 - \epsilon \tag{3.51}$$

for the entanglement entropy of the inside partner of the newly created pair. Applying strong subadditivity to the system $\{\{\mathrm{O}_{j-1}\}, \mathrm{O}_j, \mathrm{I}_j\}$ gives

$$S(\{\mathrm{O}_j\})_{\mathrm{ent}} + S(\Xi_j)_{\mathrm{ent}} = S(\{\mathrm{O}_{j-1}\}, \mathrm{O}_j)_{\mathrm{ent}} + S(\mathrm{O}_j, \mathrm{I}_j)_{\mathrm{ent}} > S(\{\mathrm{O}_{j-1}\}) + S(\mathrm{I}_j)_{\mathrm{ent}} \tag{3.52}$$

or

$$S(\{\mathrm{O}_j\})_{\mathrm{ent}} > S(\{\mathrm{O}_{j-1}\}) + S(\mathrm{I}_j)_{\mathrm{ent}} - S(\Xi_j)_{\mathrm{ent}} > S(\{\mathrm{O}_{j-1}\}) + \ln 2 - 2\epsilon \tag{3.53}$$

using (3.48), (3.51).

The relation (3.53) is very important for the information paradox. It demonstrates that the entanglement entropy of the outgoing radiation always increases by at least $\ln 2 - 2\epsilon$ as each new pair is created. In other words, the increase of entanglement entropy is stable, and small corrections cannot accumulate to invalidate the result (3.41) [4].

This is unlike the situation for radiation emitted from normal matter, in which the matter/radiation interaction necessarily increases the dimensionality of the space of entangled states to leading order in the interaction. Each emission of radiation can be entangled with the emitting atom(s) in the matter in any one of a number of orthogonal states. The data of the state of the hot matter is shared amongst many quanta of radiation, making its original state difficult to extract; the actual correlations themselves change radically from emission to emission. In contrast to this, the stretching of space-time requires that the outgoing radiation is always entangled in the same way to leading order regardless of the state of the black hole. The actual correlations themselves do not change radically from emission to emission, but at best receive only small corrections, assuming semiclassical physics is valid at and near the horizon.

3.5.1 Implications of the Information Paradox

To summarize: if (a) the niceness conditions admit local Hamiltonian evolution and (b) the event horizon of the black hole is information-free (or alternatively freely-falling observers do not see any unusual behaviour in high-energy processes) then the end state of evaporation of the black hole is that of a remnant or a mixed state. These two conditions imply that any outgoing mode $|\vartheta\rangle$ whose wavelength λ is within the range $l_p \ll \lambda \lesssim M$ will predominantly be a vacuum state when expanded in a Fock basis near the horizon

$$|\vartheta\rangle = \alpha_0|0\rangle + \alpha_1|1\rangle + \alpha_2|2\rangle + \cdots \tag{3.54}$$

with $\sum_{j>0} |\alpha_j|^2 = \varepsilon \ll 1$, since otherwise the state at the horizon would not be a vacuum state. The evolution of $|\vartheta\rangle$ must therefore agree with the standard vacuum evolution to leading order such that any corrections are constrained by (3.46). The entanglement entropy S_{ent} therefore increases by $\ln 2 - 2\epsilon$ (with $\epsilon \sim \varepsilon$) during each step of the evolution. After n steps $S_{\rm ent} > n/2 \ln 2$ since $\epsilon \ll 1$. This process will continue until $n \sim (M/M_P)^2$, when the size of the black hole is about a Planck length L_p. At this point either the process stops, leaving behind a highly-degenerate remnant or the hole fully evaporates, leaving the outgoing radiation in a mixed state (it is entangled with nothing) violating unitarity.

What might resolve the information problem? Clearly what is needed is that the outgoing radiation at least contain the information of the matter state that forms the black hole. To see what this means in a simple example, consider the matter to be a shell collapsing to a black hole that is initially in the state $|\Phi\rangle = \alpha|\Phi_0\rangle + \beta|\Phi_1\rangle$ where $\{|\Phi_0\rangle, |\Phi_1\rangle\}$ are two possible orthogonal states of the shell. The information would escape the black hole if the pairs were created such that the evolution of the state were

$$|\Phi\rangle = \alpha|\Phi_0\rangle + \beta|\Phi_1\rangle \to \frac{1}{\sqrt{2}}\left(|\Phi_0\rangle|1_k\rangle^+_{\rm I_1} + |\Phi_1\rangle|0_k\rangle^+_{\rm I_1}\right) \otimes \left(\alpha|0_{-k}\rangle^-_{\rm O_1} + \beta|1_{-k}\rangle^-_{\rm O_1}\right) \tag{3.55}$$

since tracing over the inside will yield the density matrix of the pure state $\alpha|0_{-k}\rangle^-_{\rm O_1} + \beta|1_{-k}\rangle^-_{\rm O_1}$, which has all the information of the infalling matter. A resolution of the information paradox must implement this kind of evolution. However there are significant obstacles to overcome.

First, the proposed evolution (3.55) is a radical departure from that in (3.34) or even (3.42). It is *not* a small correction to the standard pair-creation process at the horizon, and so its implementation is not obvious. It would represent a radical departure from our understanding of the behaviour of quantum field theory in curved space-time as described in preceding sections, at least near the event horizon.

Second, there can be no other pair-creation processes accompanying (3.55). To see why, suppose that there are further steps to the evolution (prior and/or afterward) such that for the k-th mode

$$|\Phi\rangle = \alpha|\Phi_0\rangle + \beta|\Phi_1\rangle \to \frac{1}{\sqrt{2}}\left(|\Phi_0\rangle|1_k\rangle^+_{\mathrm{I}_1} + |\Phi_0\rangle|0_k\rangle^+_{\mathrm{I}_1}\right) \otimes \left(\alpha|0_{-k}\rangle^-_{\mathrm{O}_1} + \beta|1_{-k}\rangle^-_{\mathrm{O}_1}\right) \left[\otimes\left(|0_k\rangle^+_{\mathrm{I}_1}|0_{-k}\rangle^-_{\mathrm{O}_1} + |1_k\rangle^+_{\mathrm{I}_1}|1_{-k}\rangle^-_{\mathrm{O}_1}\right)\right]^n \tag{3.56}$$

after n steps. Even though the information forming the black hole comes out, the end point of the evolution is still either a mixed state or a remnant due to all of the other created pairs. It is not sufficient to modify the evolution so that the information comes out. It must be modified to prevent the growth in entanglement entropy from the extra created pairs. The number of quanta emitted from the black hole is somewhat larger than the number needed to retain the information of the infalling matter (the entropy of the emitted radiation is about 30 % larger than the horizon entropy $A/4$ [41]), and it is just as important that these additional quanta do not yield remnants or mixed states.

Third, purity of the outside state is not sufficient. An evolution of the form

$$|\Phi\rangle = \alpha|\Phi_0\rangle + \beta|\Phi_1\rangle \to \frac{1}{\sqrt{2}}\left(\alpha|\Phi_0\rangle|1_k\rangle^+_{\mathrm{I}_1} + \beta|\Phi_0\rangle|0_k\rangle^+_{\mathrm{I}_1}\right) \otimes \left(|0_{-k}\rangle^-_{\mathrm{O}_1} + |1_{-k}\rangle^-_{\mathrm{O}_1}\right) \tag{3.57}$$

yields a pure outside state, but this state retains no information about the (α, β) coefficients of the infalling matter. The challenge of resolving the information paradox is to construct an evolution in which the final state of the outside radiation is both pure and information-retaining. Pair-creation at the horizon does neither.

3.5.2 Complementarity

One idea that emerged as a means of reconciling black hole radiation with known quantum physics was complementarity [42, 43]. The idea here is that one cannot ask a physical theory to yield descriptions of observers that cannot exist—specifically observers that can make measurements both inside and outside of the black hole.

Consider a choice of spacelike slices describing an evaporating black hole. The original slice Σ contains matter that will go into forming the black hole, and the slices that go through the event horizon obey the niceness conditions. This breaks down at the point P (contained in the slice Σ_P) where the black hole finally evaporates (no remnant assumed), but one might expect that a proper understanding of quantum gravity will ameliorate this, leading to a well-defined physical description of the end point of evaporation. After evaporation, the slices Σ' obey the niceness conditions.

The problem presented by black hole evaporation is that the quantum state on Σ' must be described by unitary evolution from the quantum state on Σ. However the only way this can happen is if the quantum state on the part of the slice inside the black hole has no dependence on the initial state. This is effectively a 'bleaching' of the information: all distinctions between the initial states of infalling matter must

be expunged before the state crosses the global event horizon. In other words, the evolution of the quantum state must proceed as follows

$$\begin{aligned} &\big|\Psi(\Sigma)\big\rangle \to \big|\Psi(\Sigma_P)\big\rangle = \big|\Xi(\Sigma_{\rm IN})\big\rangle \otimes \big|\Upsilon(\Sigma_{\rm OUT})\big\rangle \to \big|\Psi(\Sigma')\big\rangle \\ &\text{where } \big|\Psi(\Sigma')\big\rangle = U_2\big|\Upsilon(\Sigma_{\rm OUT})\big\rangle = U_1\big|\Psi(\Sigma)\big\rangle \end{aligned} \tag{3.58}$$

with U_1 and U_2 unitary operators and with the Hilbert space of states on Σ_P likewise decomposing into a tensor product $\mathcal{H}_P = \mathcal{H}_{\rm IN} \otimes \mathcal{H}_{\rm OUT}$ with $\Xi(\Sigma_{\rm IN}) \subset \mathcal{H}_{\rm BH}$ and $\Upsilon(\Sigma_{\rm OUT}) \subset \mathcal{H}_{\rm OUT}$. The evolution between $\big|\Psi(\Sigma')\big\rangle$ and $\big|\Psi(\Sigma)\big\rangle$ is fully unitary and reversible, uninfluenced by $\big|\Xi(\Sigma_{\rm IN})\big\rangle$.

Complementarity posits that the flaw in the above argument is in the assumption of the existence of $\big|\Psi(\Sigma_P)\big\rangle$. This is a quantum state that simultaneously describes both the interior and the exterior of a black hole. The claim is that any state of this nature has no operational meaning, since no "super-observers" exist that compare measurements both inside and outside the black hole. Rather any observer must choose a basis in which to work: either one describes particles beyond the horizon or the particles in the Hawking radiation, but not both. Indeed, the trans-Planckian problem suggests that large non-vanishing commutators exist between operators describing ingoing material and those describing outgoing Hawking radiation, and so correlations between inside and outside the hole lose any operational meaning.

The advent of the Anti de Sitter/Conformal Field Theory correspondence [44] provided further confidence for this perspective, suggesting that all information is indeed carried away by the Hawking radiation. The idea here is that the quantum states (and their evolution) of any gravity theory whose solutions are asymptotic to anti de Sitter (AdS) space-time are in 1–1 correspondence with those of a Conformal Field Theory (CFT). This conjecture has more recently has broadened to a proposed duality between gravitational and gauge theories (gauge/gravity duality) under more general asymptotic conditions and symmetries. The CFT (or dual gauge theory) is unitary and so cannot admit any information loss, and its duality with gravity indicates that the same must be true there as well. There is strong circumstantial evidence in favour of this kind of duality, and hence of the purity of radiation emitted by a black hole.

Of course gauge/gravity duality does not prove that information loss cannot occur. Rather it provides a new paradigm by which one might seek to understand the process of black hole formation and evaporation. If indeed a dual gauge theory can describe this process, then the onus is on this theory to explain either (a) which conditions are modified so that mixedness is avoided, (b) the formation of remnants, or (c) new physics in the gravity theory that either prevents black hole formation or modifies the state near the horizon. So far such a description has yet to be given.

So complementarity asserts that there is no logical contradiction in assuming that a distant outside observer sees all infalling information returned in Hawking-like radiation, and that the infalling observer experiences nothing unusual before or during horizon crossing. The thermality of Hawking radiation will be affected by interactions very near the horizon, and these presumably ensure that the net emission

process is pure as seen by the outside observer. The physical model an outside observer employs will therefore postulate a boundary condition for all fields a few Planck distances away from the horizon. These include the brick wall model [45, 46], bounce models, and stretched horizon models [42]. A full quantum theory of gravity is expected to set this distance, but it can be input into the theory for the purpose of doing phenomenological calculations. This membrane/wall distance is dependent on the matter content of the theory (the number of fields, for example), and so constraining this distance to be consistent with observation will constrain the matter content of the theory, providing (in principle) an additional degree of falsifiability. From the perspective of the outside observer the membrane/wall absorbs infalling matter and then thermalizes it, unitarily re-radiating it as Hawking radiation via a process similar to the manner in which a normal body radiates. Complementarity implies that an observer falling into the black hole will see no such membrane or brick wall, in contrast to the outside observer for whom this virtual structure is quite real [42].

The postulates of black hole complementarity are as follows:

1. **Unitarity** The process of formation and evaporation of a black hole, as viewed by a distant observer, can be described entirely within the context of standard quantum theory. In particular, there exists a unitary S-matrix which describes the evolution from infalling matter to outgoing Hawking-like radiation.
2. **Semi-Classicality** Outside the stretched horizon of a massive black hole, physics can be described to good approximation by a set of semi-classical field equations. The semi-classical field equations are those of a low energy effective field theory with local Lorentz invariance.
3. **Placidity** A freely falling observer experiences nothing out of the ordinary when crossing the horizon, as expected from the equivalence principle—gravity is locally indistinguishable from acceleration. This is basically the 'information-free' condition mentioned earlier: it is exponentially unlikely for infalling observer to measure a quantum of energy $E \gg 1/r_+$.
4. **Thermality** To a distant observer, a black hole appears to be a quantum system with discrete energy levels. The dimension of the subspace of states describing a black hole of mass M, angular momentum J, and charge Q is is the exponential of the Bekenstein entropy $S(M, J, Q)$, so that the standard black hole thermodynamic relations are obeyed.

These postulates have been slightly modified from their original form, but contain the essential aspects of what black hole complementarity is based on. Black hole no-hair theorems implied that the membrane/wall must be virtual, as noted above; no known physics at the time complementarity was proposed could generate such a structure, though new ideas have been put forward recently [47]. But even though the degrees of freedom of the membrane/wall are virtual, they must be generated by some nonlocal effect. The reason is that if normal semiclassical physics is valid for small curvatures, then pair creation takes place via the Hawking process described above and not reflection/generation from a wall or membrane. This is a consequence

of the niceness conditions, namely the assumption that one can always choose a set of slices through the black hole where curvatures are everywhere small and the vacuum is well-defined. If complementarity is valid then some new, nonlocal, physics must dominate—over scales of the horizon size—since semiclassical physics yielding pair creation is valid along the slices [48].

3.6 Firewalls

The Firewall argument asserts that the postulates of black hole complementarity are not self-consistent [3, 49]. Specifically one of the first three postulates must be incorrect, since assuming all three together yields a contradiction.

3.6.1 The Firewall Argument

This rather surprising claim follows from a fairly straightforward argument, put forward by Almheiri, Marolf, Polchinski and Sully (known as AMPS) [3]. The unitarity postulate #1 implies that radiation emitted from the black hole must not be in a mixed state, and so some process must convert the state (3.40) to

$$|\Psi\rangle_n \approx \frac{1}{\sqrt{2}}|\Phi\rangle_{\mathrm{I}_n}\prod_{m=1}^{n}\left[\otimes\left(|0_k\rangle^+_{\mathrm{I}_m}|0_{-k}\rangle^-_{\mathrm{O}_m}+|1_k\rangle^+_{\mathrm{I}_m}|1_{-k}\rangle^-_{\mathrm{O}_m}\right)\right]\to|\tilde{\Phi}\rangle_{\mathrm{I}_n}|\tilde{\Xi}\rangle_{\mathrm{O}_n} \tag{3.59}$$

after some large number n of steps, where the outside radiation state $|\tilde{\Xi}\rangle_{\mathrm{O}_n}$ is pure. At some point in time (called the Page time [28]) the entanglement entropy of the emitted radiation must reach a maximum, after which point there is more entropy in the radiation than there is in the black hole. The black hole continues to shrink in size and entropy, emitting successively fewer quanta. Consequently the number of states N_L accessible after the Page time [50] (the 'late' subspace) will be much smaller than the number N_E in the space of states prior to this (the 'early' subspace): $N_L \ll N_E$. Expanding the full outside radiation state $|\tilde{\Xi}\rangle_{\mathrm{O}_n}$ in an orthonormal basis $\{|\mathsf{j}\rangle_L\}$ of the late subspace yields

$$|\tilde{\Xi}\rangle_{\mathrm{O}_n} = \sum_{\mathsf{k}}^{N_L}|\psi_{\mathsf{k}}\rangle_E\otimes|\mathsf{k}\rangle_L \tag{3.60}$$

where $\{|\psi_1\rangle_E, |\psi_2\rangle_E, \ldots, |\psi_{N_E}\rangle_E\}$ span the early subspace. Consider the norm of the state $\mathcal{P}^{\mathsf{j}}|\tilde{\Xi}\rangle_{\mathrm{O}_n}$, where the operator $\mathcal{P}^{\mathsf{j}} \equiv P^{\mathsf{j}} - \hat{P}^{\mathsf{j}} = |\mathsf{j}\rangle_L\,{}_L\langle\mathsf{j}| - N_L|\psi_{\mathsf{j}}\rangle_E\,{}_E\langle\psi_{\mathsf{j}}|$. Expanding this out yields

$$\begin{aligned}
\left|\left|\mathcal{P}^{\mathsf{j}}|\tilde{\Xi}\rangle_{\mathrm{O}_n}\right|\right|^2 &= \left|\left| |\mathsf{j}\rangle_L \, {}_L\langle \mathsf{j}|\tilde{\Xi}\rangle_{\mathrm{O}_n} - N_L|\psi_{\mathsf{j}}\rangle_E \, {}_E\langle\psi_{\mathsf{j}}|\tilde{\Xi}\rangle_{\mathrm{O}_n}\right|\right|^2 \\
&= \left|\left| |\mathsf{j}\rangle_L \, |\psi_{\mathsf{j}}\rangle_E - N_L|\psi_{\mathsf{j}}\rangle_E \sum_{\mathsf{k}}^{N_L} {}_E\langle\psi_{\mathsf{j}}|\psi_{\mathsf{k}}\rangle_E \otimes |\mathsf{k}\rangle_L\right|\right|^2 \\
&= |||\psi_{\mathsf{j}}\rangle_E||^2 \left|\left| |\mathsf{j}\rangle_L - N_L \sum_{\mathsf{k}}^{N_L} {}_E\langle\psi_{\mathsf{j}}|\psi_{\mathsf{k}}\rangle_E \otimes |\mathsf{k}\rangle_L\right|\right|^2 \\
&= |||\psi_{\mathsf{j}}\rangle_E||^2 \left[\left(1 - N_L \, {}_E\langle\psi_{\mathsf{j}}|\psi_{\mathsf{j}}\rangle_E\right)^2 + N_L^2 \sum_{\mathsf{k}\neq\mathsf{j}}^{N_L} |{}_E\langle\psi_{\mathsf{j}}|\psi_{\mathsf{k}}\rangle_E|^2 \right] \qquad (3.61)
\end{aligned}$$

Expanding the state $|\psi_{\mathsf{k}}\rangle_E = \sum_{\mathsf{k}=1}^{N_E} c_{\mathsf{k}\mathsf{a}}|\mathrm{a}\rangle$ in an orthonormal basis $|\mathrm{a}\rangle$ of the early states yields

$$\overline{c_{\mathsf{j}\mathrm{a}} c^*_{\mathsf{k}\mathrm{b}}} = \frac{1}{N_L N_E}\delta_{\mathsf{j}\mathsf{k}}\delta_{\mathrm{a}\mathrm{b}} \qquad \overline{c_{\mathsf{j}\mathrm{a}} c^*_{\mathsf{k}\mathrm{b}} c_{\mathsf{i}\mathrm{c}} c^*_{\mathsf{l}\mathrm{d}}} = \frac{1}{N_L^2 N_E^2}\left(\delta_{\mathsf{j}\mathsf{k}}\delta_{\mathrm{a}\mathrm{b}}\delta_{\mathsf{i}\mathsf{l}}\delta_{\mathrm{c}\mathrm{d}} + \delta_{\mathsf{j}\mathsf{l}}\delta_{\mathrm{a}\mathrm{d}}\delta_{\mathsf{i}\mathsf{k}}\delta_{\mathrm{b}\mathrm{c}}\right) \quad (3.62)$$

upon averaging over $|\tilde{\Xi}\rangle_{\mathrm{O}_n}$, assuming a uniform measure for the outside state. Consequently $\overline{{}_E\langle\psi_{\mathsf{j}}|\psi_{\mathsf{k}}\rangle_E} = \delta_{\mathsf{j}\mathsf{k}}/N_L$ and $\overline{{}_E\langle\psi_{\mathsf{j}}|\psi_{\mathsf{k}}\rangle_E \, {}_E\langle\psi_{\mathsf{i}}|\psi_{\mathsf{l}}\rangle_E} = \delta_{\mathsf{j}\mathsf{k}}\delta_{\mathsf{i}\mathsf{l}}/N_L^2 + \delta_{\mathsf{j}\mathsf{l}}\delta_{\mathsf{i}\mathsf{k}}/(N_L^2 N_E)$, yielding

$$\begin{aligned}
\overline{\mathcal{E}} &= \frac{\overline{\left|\left|\mathcal{P}^{\mathsf{j}}|\tilde{\Xi}\rangle_{\mathrm{O}_n}\right|\right|^2}}{|||\psi_{\mathsf{j}}\rangle_E||^2} = 1 - 2N_L \, \overline{{}_E\langle\psi_{\mathsf{j}}|\psi_{\mathsf{j}}\rangle_E} + N_L^2 \sum_{\mathsf{k}}^{N_L} \overline{{}_E\langle\psi_{\mathsf{j}}|\psi_{\mathsf{k}}\rangle_E \, {}_E\langle\psi_{\mathsf{j}}|\psi_{\mathsf{k}}\rangle_E^*} \\
&= 1 - 2N_L\frac{\delta_{\mathsf{j}\mathsf{j}}}{N_L} + \frac{N_L^2}{N_L^2 N_E^2}\left(N_E^2\delta_{\mathsf{j}\mathsf{j}} + N_E\sum_k \delta_{\mathsf{k}\mathsf{k}}\right) = \frac{N_L}{N_E} \qquad (3.63)
\end{aligned}$$

in the limit $N_E \gg N_L \gg 1$. Hence

$$P^{\mathsf{j}}|\tilde{\Xi}\rangle_{\mathrm{O}_n} \approx \hat{P}^{\mathsf{j}}|\tilde{\Xi}\rangle_{\mathrm{O}_n} = |\psi_{\mathsf{j}}\rangle_E \otimes |\mathsf{j}\rangle_L \qquad (3.64)$$

and so it is possible to project onto any given subspace of the late radiation, up to a relative error of order N_L/N_E. The argument is essentially the same if grey-body factors are taken into account.

So for a distant observer after n steps the radiation $|\tilde{\Xi}\rangle_{\mathrm{O}_n}$ is near infinity and can be decomposed into a set of modes $\{|\mathsf{j}\rangle\}$. In particular, it is possible to project onto eigenspaces of the number operator in an observer-independent way, according to the semi-classicality assumption. These modes can be evolved backward in time toward the horizon—they will be of much higher frequency at these earlier times, but can be kept to the sub-Planckian regime if one does not evolve too far back. However the placidity assumption #3 implies that an infalling observer sees the vacuum near the horizon, and so the number operator of the radiation $|\tilde{\Xi}\rangle_{\mathrm{O}_n}$ must be zero, in contradiction to what the observer at infinity measures. This contradiction can be

avoided if the infalling observer does not see a vacuum, but instead encounters a large number of high-energy modes: in other words, a firewall.

A regular horizon implies increasing entanglement, as shown in (3.53). Conversely, if entanglement is to decrease, then the state at the horizon cannot be the vacuum. This is the firewall argument in a nutshell.

An alternative version of the argument employs the strong subadditivity condition [47]. The radiation after n steps is $|\tilde{\Xi}\rangle_{O_n}$, with the next mode $|n{+}1\rangle_O$ emitted near the horizon. The former can be evolved backward in time near the horizon. Semiclassicality implies that

$$|\tilde{\Xi}\rangle'_{O_n} = |\tilde{\Xi}\rangle_{O_n} \qquad |n{+}1\rangle'_O = |n{+}1\rangle_O \tag{3.65}$$

where the primes refer to the states measured by the infalling observer. Since this observer sees a vacuum at the horizon, the state $|n{+}1\rangle'_O$ must be entangled with some state $|n{+}1\rangle'_I$ inside the horizon. Strong subadditivity then implies that (3.53) holds

$$S'(n{+}1)_{\rm ent} > S'(n)_{\rm ent} + \ln 2 - 2\epsilon \tag{3.66}$$

and the equivalence (3.65) implies

$$S(n{+}1)_{\rm ent} > S(n)_{\rm ent} + \ln 2 - 2\epsilon \tag{3.67}$$

which means the entanglement between the black hole and the radiation cannot decrease, in contradiction with the unitarity postulate, which implies that it must decrease after the halfway point.

So complementarity is incompatible with the local evolution that creates the pairs of Hawking quanta. Even though complementarity invoked non-locality to argue that the slices permitted by the niceness conditions are not valid, it requires that local semiclassical physics applies outside the membrane or stretched horizon. Non-local physics is therefore constrained to be inside the horizon. The firewall argument rules out this kind of complementarity and hence this kind of sharply-limited non-locality.

3.6.2 Responses to the Firewall Argument

The response of the physics community to the firewall argument was rapid, intense, and diverse, ranging from skepticism to ambivalence to endorsement.

Those endorsing the firewall argument have emphasized that standard arguments from quantum field theory in curved spacetime and quantum information should lead one to expect this result [51–63]. Standard semi-classical methods analyzing causal patches [59], string-creation [63], and freely-falling observers [60] have each been used to buttress the argument. Indeed numerical analysis of a particular class of models suggests a breakdown of effective field theory, in turn implying the existence of firewalls on black hole horizons [61]. It has even been suggested that alternatives

to firewalls may suffer contradictions similar to those associated with time travel [52]. Rindler horizons have been argued to be immune (or at least not necessarily susceptible) to the firewall argument [64].

Nevertheless initial skepticism [65] was soon followed by a number of challenging responses to the firewall argument. A number were rebutted by Almheiri and collaborators [66]. Here I shall summarize some of the main responses.

3.6.2.1 Absorbing the Interior Hilbert Space

Since the outside modes must be entangled with both the early outside modes and with their inside pair-created partners (violating quantum limits on entanglement) then perhaps the interior Hilbert space of an old black hole is embedded in the larger Hilbert space of the early radiation. The claim is that the firewall phenomenon can occur only for an exponentially fine-tuned (and intrinsically quantum mechanical) initial state, analogous to an entropy decreasing process in a system with large degrees of freedom [67–72]. Alternatively, quantum computations required to do carry out the thought experiments undergirding the firewall argument take so long (a time exponential in the entropy of the black hole) that this prevents the experiments from being done [73, 74]. In other words, excitations exist at the horizon only if such quantum computations have been performed.

Both considerations run afoul of standard quantum mechanics. Assuming unitarity, an observer outside the black hole (Charlie) can extract a bit of information that will be entangled with a later outside pair-created bit. Another spacelike separated observer (Alice, say) can jump into the black hole later and extract information about both the inside and outside later-created pair, whilst Charlie can send the quantum state of the early bit to Alice. Alice will then possess information concerning three quantum bits, two of which are are maximally entangled with the third, which violates quantum mechanics.

More generally, operators associated with the early radiation will generically not commute with operators associated with the Hilbert space of an infalling observer if the the interior Hilbert space is embedded in the early radiation Hilbert space [66]. Consider the parity operator $(-1)^{N_e}$ of an early outside bit $e \subset E$

$$(-1)^{N_e} = \sigma^z \otimes I \tag{3.68}$$

written above in a basis factorized into the measured parity and everything else. Since the interior Hilbert space is a subset of the outside early radiation space, we can expand the parity operator of an inside bit $i \subset I$

$$(-1)^{N_i} = I \otimes S^0 + \sigma^x \otimes S^x + \sigma^y \otimes S^y + \sigma^z \otimes S^z \tag{3.69}$$

where the matrices S^λ are constrained by the requirement $(-1)^{N_i}(-1)^{N_i} = 1$. Suppose the parity of an early state $|\psi\rangle$ is positive, so that $(-1)^{N_e}|\psi\rangle = +|\psi\rangle$.

Then the expectation value of $(-1)^{N_e}$ for the state $(-1)^{N_i}|\psi\rangle$ is

$$\begin{aligned}
&\langle\psi|(-1)^{N_i}(-1)^{N_e}(-1)^{N_i}|\psi\rangle \\
&\quad = \langle\psi|\sigma^z \otimes (S^0)^2 + \sigma^x\sigma^z\sigma^x \otimes (S^x)^2 + \sigma^y\sigma^z\sigma^y \otimes (S^y)^2 \\
&\qquad + (\sigma^z)^3 \otimes (S^z)^2|\psi\rangle + \text{cross terms} \\
&\quad = \langle\psi|\sigma^z \otimes \left((S^0)^2 - (S^x)^2 - (S^y)^2 + (S^z)^2\right)|\psi\rangle + \text{cross terms}
\end{aligned}$$

Upon averaging over all all possible operators S^λ (requiring $(-1)^{N_i}(-1)^{N_i} = 1$) the cross-terms will average to zero since independent sign flips in parity are allowed. Each $(S^\lambda)^2$ term will average to the same value since these operators are generic and so their eigenvalues will be comparable in size. Hence $\langle\psi|(-1)^{N_i}(-1)^{N_e}(-1)^{N_i}|\psi\rangle$ averages to zero.

So if we start with an eigenstate of $(-1)^{N_e}$ and measure the parity $(-1)^{N_i}$, the expectation value flips from 1 to 0. Hence the eigenvalue changes with near-unit probability, implying the commutator of $(-1)^{N_i}$ and $(-1)^{N_e}$ is of order unity, and hence the commutator of early and interior operators is also of order unity. Hence if an infalling observer sees a vacuum (so that $\mathtt{a}|\psi\rangle = 0$ where $\mathtt{a}$ is an annihilation operator in the Hilbert space of the infalling observer), then since the interior operators can be expanded in terms of the infalling operators, the early creation/annihilation operators will not commute with any of the operators $\mathtt{a}$, strongly perturbing the infalling vacuum and creating a firewall. This abolishes (or at least renders highly problematic) the notion that infalling observers see no firewall because the deviation from thermality is too small to detect [75].

3.6.2.2 Broadening Complementarity

One recent proposal posits that each observer has their own Hilbert space, with suitable overlap conditions [76–86]. This broadens the notion of complementarity insofar as there is no global Hilbert space. The idea is that space-time physics is described in terms of an infinite number of quantum systems, each of which encodes the physics as seen along a particular time-like trajectory, in a proper time dependent Hamiltonian [76]. Extending these ideas to a matrix theory model of black holes suggests that there are no high energy particles available that could constitute the firewall [79]. The vacuum entanglement that is a crucial feature of Hawking radiation is claimed not to be a feature of the physics described by matrix theory. Whether or not this proposal can be fully consistently implemented remains to be seen.

3.6.2.3 Non-locality

Prior to the advent of the Firewall argument, the idea that non-locality can and should play a role in resolving the information paradox was already being actively explored [87, 88]. Although generic nonlocality leads to causality paradoxes, perhaps there

are regions (near a black hole, for example) where locality is not exact but only approximate. The idea here is to weaken the assumptions of the semi-classicality postulate #2 and introduce some form of mild (or non-violent) non-local physics [89–94].

Since if locality is exact outside the horizon any information transfer from the black hole to the radiation produces singular behaviour at the horizon [4, 49], it is necessary to weaken locality outside of the black hole. Each black hole would therefore have a "nonlocal zone" (about the size of the black hole itself) within which information transfer from the black hole to the outgoing radiation takes place. This information transfer is a transfer of the entanglement between the early radiation and black hole interior to entanglement between the early and late radiation. It requires an additional energy flux beyond that of the Hawking radiation [91, 92], and modulates the Hawking radiation in a sufficiently fine-grained manner so as to preserve the average properties of the Hawking flux. Leading order calculations in a model in which nonlocal metric perturbations couple to the stress tensor suggest in a two-dimensional model this might be possible [93].

The challenge such proposals face is that any scheme that physically separates transfer of energy from transfer of information runs into conflict with the Bekenstein-Hawking density of states $\exp[S]$ of the black hole. Consider a process in which quanta behind the horizon are transported to become outgoing quanta. Suppose a pair is created outside the black hole as in Eq. (3.34)

$$\begin{aligned}&\frac{1}{\sqrt{2}}|\Phi\rangle_{\rm I}\otimes\left(|0_k\rangle_{\rm I}^{+}|0_{-k}\rangle_{\rm O}^{-}+|1_k\rangle_{\rm I}^{+}|1_{-k}\rangle_{\rm O}^{-}\right)\\&\quad=\frac{1}{\sqrt{2}}\left(|\Phi_0\rangle+|\Phi_1\rangle\right)\otimes\left(|0_k\rangle_{\rm I}^{+}|0_{-k}\rangle_{\rm O}^{-}+|1_k\rangle_{\rm I}^{+}|1_{-k}\rangle_{\rm O}^{-}\right)\end{aligned}\tag{3.70}$$

where the Hilbert space has been separated into orthogonal states as in Eq. (3.55). As the outgoing mode moves through the nonlocal zone, some process will cause it to exchange information with a state in the interior so that

$$\begin{aligned}&\frac{1}{\sqrt{2}}|\Phi\rangle_{\rm I}\otimes\left(|0_k\rangle_{\rm I}^{+}|0_{-k}\rangle_{\rm O}^{-}+|1_k\rangle_{\rm I}^{+}|1_{-k}\rangle_{\rm O}^{-}\right)\\&\qquad\to\frac{1}{\sqrt{2}}\left(|\Phi_0\rangle|1_k\rangle_{\rm I_1}^{+}+|\Phi_0\rangle|0_k\rangle_{\rm I_1}^{+}\right)\\&\qquad\otimes\left(\alpha|0_{-k}\rangle_{\rm O_1}^{-}+\beta|1_{-k}\rangle_{\rm O_1}^{-}\right)\end{aligned}\tag{3.71}$$

This would avoid the firewall problem just as it resolved the information paradox problem. However this approach will also entail the same difficulties noted in the previous section, and will allow the number of internal states of the black hole to exceed the entropy $S = A/4$ discussed in Sect. 3.2. The reason is that it is possible

to interact with the outgoing bit as it moves through the nonlocal zone, say by introducing a phase

$$\begin{aligned}\frac{1}{\sqrt{2}}|\Phi\rangle_{\mathrm{I}} \otimes \left(|0_k\rangle_{\mathrm{I}}^{+}|0_{-k}\rangle_{\mathrm{O}}^{-} + |1_k\rangle_{\mathrm{I}}^{+}|1_{-k}\rangle_{\mathrm{O}}^{-}\right) \\ \rightarrow \frac{1}{\sqrt{2}}\left(|\Phi_0\rangle|1_k\rangle_{\mathrm{I}_1}^{+} - |\Phi_0\rangle|0_k\rangle_{\mathrm{I}_1}^{+}\right) \\ \otimes \left(\alpha|0_{-k}\rangle_{\mathrm{O}_1}^{-} + \beta|1_{-k}\rangle_{\mathrm{O}_1}^{-}\right) \end{aligned} \tag{3.72}$$

and so a larger set of interior states, beyond that given by $\exp[S]$ has been accessed by this process.

Another recent proposal involves using wormholes to transfer information beyond the horizon [95–99]. The idea is that the part of space-time connecting the right side of Fig. 3.1 ("our universe") and its left side (known as an Einstein Rosen bridge) is created by quantum correlations between the microstates of the black holes on each side. The conjecture is that any entangled pair of quantum states is connected a similar sort of space-time bridge or wormhole. These wormholes non-locally connect quantum states inside and outside of the horizon, allowing for information from the black hole to escape.

3.6.2.4 Exotic Objects

Of course if an event horizon never forms then a firewall can be avoided [100–102]. Could this be the resolution to the firewall problem?

One noteworthy attempt along these lines is the fuzzball proposal [103]. This approach grew out of several results that emerged from string theory that suggest the end-state of gravitationally collapsing matter is not a traditional black hole because the degrees of freedom of the hole distribute themselves throughout a horizon sized object referred to as a fuzzball. Particular examples of this kind of structure were obtained by considering various extremal black brane solutions to the low-energy string equations with multiple charges [104–117]. The basic idea is that as matter undergoes gravitational collapse, its (presumed) fundamentally stringy degrees of freedom distribute their momenta in such a way that the final solution has neither a horizon nor a singularity [108–110]. Instead of a black hole, matter undergoing gravitational collapse will quantum tunnel to a fuzzball: a complicated "hairy" structure that contains all of the degrees of freedom of the black hole. Hawking radiation would be due to emission from an ergoregion near the fuzzball. This radiation can carry information about the original state of matter because it is not entangled with any states inside a horizon because no such horizon exists [103].

The problem with the fuzzball proposal at the moment is its lack of generality. Notwithstanding the fact that first-order corrections suggest that perhaps fuzzballs can form from generic collapse [118, 119], the proposal only appears to work for particular brane configurations. However to resolve the firewall problem

(and information paradox) *all* possible matter configurations must form a fuzzball structure.

Other recent speculative ideas along these lines include Grireballs [120], leaky horizons [121], and aether-like fluids whose atmosphere mimics Hawking radiation [122, 123]. All of these ideas must universally replace the generic collapse of matter into a black hole if they are to be viable candidates for eliminating the firewall. Of course if a remnant forms, this could also avoid a firewall; an explicit example in two dimensions was recently given [124].

3.6.2.5 Additional Degrees of Freedom

Some responses to the firewall argument have suggested it is lacking because additional degrees of freedom are present in quantum gravity that are otherwise unaccounted for [125–127] or not properly treated.

One such approach involves distinguishing virtual qubits (the entangled created pairs) from real qubits (that store the information inside the black hole) [128, 129]. The idea is that black hole information is stored both inside and outside the stretched horizon, yielding twice the usual black hole entropy and therefore extra room to arrange the quantum degrees of freedom so that paradoxical results are avoided. The apparent firewall obstruction can be removed, via a universal entanglement swap operation that transports all free quantum information from the interior of the black hole to its exterior. This swap can be created locally and in the near horizon region; however this firewall-removing operation cannot be use to transfer information from an infalling state into the outgoing radiation [130, 131].

3.6.2.6 Loopholes

A number of papers have been written contending that the existence of firewalls depends on a chain of reasoning that is incomplete, and that one or more loopholes exist that allow one to escape the conclusions of the argument.

It has been suggested that the space of physical quantum gravity states does not factorize into a tensor product of localized degrees of freedom, invalidating one of the assumptions of the firewall argument [132]. The idea here is that in any diffeomorphism invariant ultra-violet complete theory with an asymptotic region in which an algebra of observables can be defined (which presumably is a feature of quantum gravity), the Hamiltonian is a surface integral in this asymptotic region (or boundary). The boundary encodes all degrees of freedom, including those inside the horizon, and the algebra of boundary observables evolves into itself unitarily over time. Hence no boundary information can ever be lost, not even temporarily. This is argued to invalidate a key assumption of the firewall argument, which is that the early time Hawking radiation is in a mixed quantum state and gets purified later by the late time Hawking radiation to preserve unitarity. Rather there must be continuous purity, with the Hawking quanta always entangled with exterior degrees of freedom

and never with interior ones. The Hilbert space does not factorize into exterior and interior state spaces, and so the 'partner behind the horizon' does not actually exist in a full quantum theory of gravity. Of course for this picture to be accepted, the details of the physical states and how they are encoded into the boundary needs to be made explicit.

Some effort has been put into seeing what happens if the horizon geometry undergoes quantum fluctuations [133]. The claim is that both the blackhole information paradox and firewalls originate from treating the geometry as strictly classical, and that it is an ill-posed problem to employ quantum fields in a classical curved space with a horizon. Instead, one should first integrate out fluctuations of the background geometry and then evaluate matter observables. Some models of shell collapse indicate that a firewall may or may not form depending on the ratio of the black hole entropy to the square of the number of coherently emitted particles [134, 135].

Additional evasive tactics have been proposed. Some have proposed that the firewall issue is purely quantum information theoretic and so should have an answer once we know exactly what computation we need to do [136]. Another argument posits that the firewall paradox is likely to be an artifact of using an effective theory beyond its domain of validity [137]. It has been suggested that a distillation-like process for extracting information needs to be clarified before one can conclude that black hole complementarity is not valid [138]; indeed this distillation process may back-react on the black hole, breaking cross-horizon entanglement and removing the firewall [139].

Another suggestion is that a firewall will not emerge if the energy cost of measurement on the early states (yielding information about the late states) is much smaller than the ultraviolet cutoff scale [140]. Perhaps it is necessary to modify the expected entanglement of states near a horizon [141] or to take macroscopic superpositions of black holes [142–144], or to introduce new causality requirements into physics [145].

The final state-proposal in which a generalization of quantum mechanics allows postselection on a final state at the black hole singularity, has been suggested as a resolution for the black hole information paradox [146] and for firewalls [147]. The idea here is that quantum information can escape from the black hole interior via postselected quantum teleportation [148]. The information moves forward in time to the singularity, backward in time from the singularity to the horizon, then forward in time from the horizon to future infinity. If suitable dynamical constraints are satisfied, this is equivalent to a causally ordered flow of information moving unitarily forward in time. However these constraints appear to be rigorously fulfilled only by fine tuning [147]. Furthermore, the final state projection postulate has been shown to be inadequate for abolishing firewalls [149].

Some have contented that the firewall follows from making assumptions about physics inside the stretched horizon that do not follow from the semiclassicality postulate #2. One claim [150, 151] is that firewalls are avoided if the degrees of freedom of the stretched horizon retain information for a sufficiently long time known as the scrambling time (the minimum time required for the information about the

initial state to be lost without measuring a large fraction of all the degrees of freedom). Alternatively, if the semiclassicality postulate holds, firewalls are avoided, but at the price of introducing remnants [152].

Finally it was recently shown that Einstein's field equations do not admit a solution in which a Planck-density, Planck-scale firewall is just outside the event horizon [153]. Any shell located at the horizon of an astrophysical black hole must necessarily have a density many orders of magnitude lower than the Planck density. A recent analysis of the behaviour of photons from the cosmic microwave background falling into a black hole indicates that they form a "classical firewall" in the frame of a static observer near the horizon, but that this firewall has negligible effects on both freely infalling observers and the evolution of the black hole [154].

3.7 Summary

Black holes retain a powerful grip on both the physical universe and the human imagination. At a classical level they absorb all matter and energy they encounter, growing ever larger in the process. Our best understanding of quantum physics indicates that they thermally radiate like black bodies, undergoing phase transitions into other forms and eventually evaporating away.

But away to what? We have no self-consistent description of this process. Our present understanding suggests that either a radiating black hole eventually either cools down into an information-rich nugget or erects a firewall around itself. Neither scenario appears to be compatible with our understanding of physics. The problem is not so much with particular models of black hole radiation but rather with a clash of the basic principles of relativity and quantum physics.

It appears we must either give up the predictive power of quantum mechanics (unitarity), or the notion that gravity is locally indistinguishable from acceleration (the equivalence principle), or the view that a physical phenomenon is influenced directly only by its immediate surroundings (locality). Each of these principles is supported—directly and indirectly—by a wealth of experimentation. The physics community at the moment is quite divided on the resolution to this problem, and may be for some time to come.

Acknowledgments I am grateful for discussions with Niayesh Afshordi, Mirjam Cvetic, Brian Dolan, David Kastor, David Kubiznak, Samir Mathur, Jonas Mureika, Don Page, Mehdi Saravani, Jennie Traschen, and Rafael Sorkin on various aspects of this work, which was supported in part by the Natural Sciences and Engineering Research Council of Canada.

References

1. Michell, J.: On the means of discovering the distance, magnitude, etc. of the fixed stars . . . . Phil. Trans. R. Soc. London **74**, 35 (1783)
2. Bradley, J.: Account of a new discoved motion of the Fix'd Stars. Phil. Trans. R. Soc. London **35**, 637 (1783).
3. A. Almheiri, D. Marolf, J. Polchinski, and J. Sully, Black Holes: Complementarity or firewalls? JHEP **1302**, 062 (2013). arXiv:1207.3123
4. Mathur, S.D.: The information paradox: a pedagogical introduction. Class. Quant. Grav. **26**, 224001 (2009). arXiv:0909.1038
5. Oppenheimer, J., Snyder, H.: On continued gravitational contraction. Phys. Rev. **56**, 455–459 (1939)
6. Mann, R.B.: Topological black holes: outside looking. In: Burko, L., Ori, A. (eds.) Internal structure of black holes and spacetime singularities, pp. 311–342. Technion Press (1998). gr-qc/9709039
7. Fidkowski, L., Hubeny, V., Kleban, M., Shenker, S.: The black hole singularity in AdS/CFT. JHEP **0402**, 014 (2004). hep-th/0306170
8. Bardeen, J.M., Carter, B., Hawking, S.: The four laws of black hole mechanics. Commun. Math. Phys. **31**, 161–170 (1973)
9. Kastor, D., Ray, S., Traschen, J.: Enthalpy and the mechanics of AdS black holes. Class. Quant. Grav. **26**, 195011 (2009). arXiv:0904.2765
10. Caldarelli, M.M., Cognola, G., Klemm, D.: Thermodynamics of Kerr-Newman-AdS black holes and conformal field theories. Class. Quant. Grav. **17**, 399–420 (2000). hep-th/9908022
11. Dolan, B., Kastor, D., Kubiznak, D., Mann, R., Traschen, J.: Thermodynamic volumes and isoperimetric inequalities for de sitter black holes. Phys. Rev. D. (2013). arXiv:1301.5926
12. Altamirano, N., Kubiznak, D., Mann, R.B., Sherkatghanad, Z.: Thermodynamics of rotating black holes and black rings: phase transitions and thermodynamic volume. Galaxies **2**, 89–159 (2014). arXiv:1401.2586
13. Gibbons, G., Perry, M., Pope, C.: The first law of thermodynamics for Kerr-anti-de Sitter black holes. Class. Quant. Grav. **22**, 1503–1526 (2005). hep-th/0408217
14. Creighton, J., Mann, R.B.: Quasilocal thermodynamics of dilaton gravity coupled to gauge fields. Phys. Rev. **D52**, 4569–4587 (1995). gr-qc/9505007
15. Dolan, B.: The cosmological constant and the black hole equation of state. Class. Quant. Grav. **28**, 125020 (2011). arXiv:1008.5023
16. Kubiznak, D., Mann, R.B.: P-V criticality of charged AdS black holes. JHEP **1207**, 033 (2012). arXiv:1205.0559
17. Gunasekaran, S., Kubiznak, D., Mann, R.: Extended phase space thermodynamics for charged and rotating black holes and Born-Infeld vacuum polarization. JHEP **1211**, 110 (2012). arXiv:1208.6251
18. Hawking, S., Page, D.N.: Thermodynamics of black holes in anti-de sitter space. Commun. Math. Phys. **87**, 577 (1983)
19. Altamirano, N., Kubiznak, D., Mann, R.B., Sherkatghanad, Z.: Kerr-AdS analogue of triple point and solid/liquid/gas phase transition. Class. Quant. Grav. **31**, 042001 (2014). arXiv:1308.2672
20. Birrell, N.D., Davies, P.C.W.: Quantum Fields in Curved Space. Cambridge University Press, Cambridge (1982)
21. Fulling, S.A.: Nonuniqueness of canonical field quantization in Riemannian space-time. Phys. Rev. **D7**, 2850–2862 (1973)
22. Wald, R.M.: Quantum Field Theory in Curved Spacetime and Black Hole Thermodynamics. The University of Chicago Press, Chicago (1994)
23. Hawking, S.: Particle creation by black holes. Commun. Math. Phys. **43**, 199–220 (1975)
24. Ross, S.F.: Black hole thermodynamics. hep-th/0502195
25. Starobinsky, A.A.: Amplification of waves during reflection from a rotating black hole. Sov. Phys. JETP **37**, 28–32 (1973)

26. Unruh, W.: Second quantization in the Kerr metric. Phys. Rev. **D10**, 3194–3205 (1974)
27. Chandrasekhar, S.: The mathematical theory of black holes (1983)
28. Page, D.N.: Average entropy of a subsystem. Phys. Rev. Lett. **71**, 1291–1294 (1993). gr-qc/9305007
29. Barcelo, C., Liberati, S., Visser, M.: Analogue gravity. Living Rev. Rel. **8**, 12 (2005). gr-qc/0505065
30. Unruh, W.: Experimental black hole evaporation. Phys. Rev. Lett. **46**, 1351–1353 (1981)
31. Unruh, W.: Sonic analog of black holes and the effects of high frequencies on black hole evaporation. Phys. Rev. **D51**, 2827–2838 (1995)
32. Brout, R., Massar, S., Parentani, R., Spindel, P.: Hawking radiation without transPlanckian frequencies. Phys. Rev. **D52**, 4559–4568 (1995). hep-th/9506121
33. Corley, S., Jacobson, T.: Hawking spectrum and high frequency dispersion. Phys. Rev. **D54**, 1568–1586 (1996). hep-th/9601073
34. Barrabes, C., Frolov, V.P., Parentani, R.: Metric fluctuation corrections to Hawking radiation. Phys. Rev. **D59**, 124010 (1999). gr-qc/9812076
35. Parentani, R.: Quantum metric fluctuations and Hawking radiation. Phys. Rev. **D63**, 041503 (2001). gr-qc/0009011
36. Barrabes, C., Frolov, V.P., Parentani, R.: Stochastically fluctuating black hole geometry, Hawking radiation and the transPlanckian problem. Phys. Rev. **D62**, 044020 (2000). gr-qc/0001102
37. Unruh, W.G., Schutzhold, R.: On the universality of the Hawking effect. Phys. Rev. **D71**, 024028 (2005). gr-qc/0408009
38. Liberati, S., Sindoni, L., Sonego, S.: Linking the trans-Planckian and the information loss problems in black hole physics. Gen. Rel. Grav. **42**, 1139–1152 (2010). arXiv:0904.0815
39. Weinfurtner , S., Tedford, E.W., Penrice, M.C.J., Unruh, W.G., Lawrence, G.A.: Measurement of stimulated Hawking emission in an analogue system. Phys. Rev. Lett. **106**, 021302 (2011). arXiv:1008.1911/gr-qc
40. Schtzhold, R., Unruh, W.: Hawking radiation with dispersion versus breakdown of the WKB approximation. Phys. Rev. **D88**(12), 124009 (2013). arXiv:1308.2159
41. Zurek, W.: Entropy evaporated by a black hole. Phys. Rev. Lett. **49**, 1683–1686 (1982)
42. Susskind, L., Thorlacius, L., Uglum, J.: The Stretched horizon and black hole complementarity. Phys. Rev. **D48**, 3743–3761 (1993). hep-th/9306069
43. Stephens, C.R., 't Hooft, G., Whiting, B.F.: Black hole evaporation without information loss. Class. Quant. Grav. **11**, 621–648 (1994). gr-qc/9310006
44. Maldacena, J.M.: The large N limit of superconformal field theories and supergravity. Adv. Theor. Math. Phys. **2**, 231–252 (1998). hep-th/9711200
45. Hooft, G.: On the quantum structure of a black hole. Nucl. Phys. **B256**, 727 (1985)
46. Mann, R.B., Tarasov, L., Zelnikov, A.: Brick walls for black holes. Class. Quant. Grav. **9**, 1487–1494 (1992)
47. Mathur, S.D., Turton, D.: The flaw in the firewall argument. Nucl. Phys. (2014). arXiv:1306.5488
48. Mathur, S.D.: Black holes and beyond. Ann. Phys. **327**, 2760–2793 (2012). arXiv:1205.0776
49. Braunstein, S.L., Pirandola, S., Zyczkowski, K.: Better late than never: information retrieval from black holes. Phys. Rev. Lett. **110**(10), 101301 (2013). arXiv:0907.1190
50. Page, D.N.: Time dependence of Hawking radiation entropy. J. Cosmol. Astropart. Phys. **1309**, 028 (2013). arXiv:1301.4995
51. Bousso, R.: Complementarity is not enough. Phys. Rev. **D87**(12), 124023 (2013). arXiv:1207.5192
52. Susskind, L.: The transfer of entanglement: the case for firewalls (2012). arXiv:1210.2098
53. Giveon, A., Itzhaki, N.: String theory versus black hole complementarity. JHEP **1212**, 094 (2012). arXiv:1208.3930
54. Giveon, A., Itzhaki, N.: String theory at the tip of the cigar. JHEP **1309**, 079 (2013). arXiv:1305.4799
55. Avery, S.G., Chowdhury, B.D.: Firewalls in AdS/CFT (2013). arXiv:1302.5428

56. Smerlak, M.: The two faces of Hawking radiation. Int. J. Mod. Phys. **D22**, 1342019 (2013). arXiv:1307.2227
57. Marolf, D., Polchinski, J.: Gauge/gravity duality and the black hole interior. Phys. Rev. Lett. **111**, 171301 (2013). arXiv:1307.4706
58. Chowdhury, B.D.: Cool horizons lead to information loss. JHEP **1310**, 034 (2013). arXiv:1307.5915
59. Bousso, R.: Firewalls from double purity. Phys. Rev. **D88**, 084035 (2013). arXiv:1308.2665
60. Kim, W., Son, E.J.: Freely falling observer and black hole radiation. Mod. Phys. Lett. **A29**, 1450052 (2014). arXiv:1310.1458
61. Berenstein, D., Dzienkowski, E.: Numerical evidence for firewalls (2013). arXiv:1311.1168
62. Park, I.: Indication for unsmooth horizon induced by quantum gravity interaction (2014). arXiv:1401.1492
63. Silverstein, E.: Backdraft: string creation in an old Schwarzschild black hole (2014). arXiv:1402.1486
64. Gary, M.: Still no Rindler firewalls (2013). arXiv:1307.4972
65. Susskind, L.: Singularities, firewalls, and complementarity (2012). arXiv:1208.3445
66. Almheiri, A., Marolf, D., Polchinski, J., Stanford, D., Sully, J.: An apologia for firewalls. JHEP **1309**, 018 (2013). arXiv:1304.6483
67. Nomura, Y., Varela, J., Weinberg, S.J.: Complementarity endures: no firewall for an infalling observer. JHEP **1303**, 059 (2013). arXiv:1207.6626
68. Nomura, Y., Varela, J., Weinberg, S.J.: Black holes, information, and Hilbert space for quantum gravity. Phys. Rev. **D87**(8), 084050 (2013). arXiv:1210.6348
69. Nomura, Y., Varela, J.: A note on (no) firewalls: the entropy argument. JHEP **1307**, 124 (2013). arXiv:1211.7033
70. Nomura, Y., Varela, J., Weinberg, S.J.: Low energy description of quantum gravity and complementarity (2014). arXiv:1304.0448
71. Nomura, Y., Varela, J., Weinberg, S.J.: Black holes or firewalls: a theory of horizons. Phys. Rev. **D88**, 084052 (2013). arXiv:1308.4121
72. Nomura, Y., Weinberg, S.J.: The entropy of a vacuum: what does the covariant entropy count? (2013). arXiv:1310.7564
73. Harlow, D., Hayden, P.: Quantum computation vs. firewalls. JHEP **1306**, 085 (2013). arXiv:1301.4504
74. Susskind, L.: Black hole complementarity and the Harlow-Hayden conjecture (2013). arXiv:1301.4505
75. Lowe, D.A., Thorlacius, L.: Pure states and black hole complementarity. Phys. Rev. **D88**, 044012 (2013). arXiv:1305.7459
76. Banks, T., Fischler, W.: Holographic space-time does not predict firewalls (2012). arXiv:1208.4757
77. Papadodimas, K., Raju, S.: An infalling observer in AdS/CFT. JHEP **1310**, 212 (2013). arXiv:1211.6767
78. Neiman, Y.: On-shell actions with lightlike boundary data (2012). arXiv:1212.2922
79. Banks, T., Fischler, W.: No firewalls in holographic space-time or matrix theory (2013). arXiv:1305.3923
80. Iizuka, N., Terashima, S.: Brick walls for black holes in AdS/CFT (2013). arXiv:1307.5933
81. Germani, C.: On the many saddle points description of quantum black holes. Phys. Lett. **B733**, 93–99 (2014). arXiv:1307.6238
82. Papadodimas, K., Raju, S.: The black hole interior in AdS/CFT and the information paradox. Phys. Rev. Lett. **112**, 051301 (2014). arXiv:1310.6334
83. Papadodimas, K., Raju, S.: State-dependent bulk-boundary maps and black hole complementarity. Phys. Rev. **D89**, 086010 (2014). arXiv:1310.6335
84. Verlinde, E., Verlinde, H.: Behind the horizon in AdS/CFT (2013). arXiv:1311.1137
85. Banks, T., Fischler, W., Kundu, S., Pedraza, J.F.: Holographic space-time and black holes: mirages as alternate reality (2014). arXiv:1401.3341

86. Sasaki, M., Yeom, D.-H.: Thin-shell bubbles and information loss problem in anti de Sitter background (2014). arXiv:1404.1565
87. Giddings, S.B.: Models for unitary black hole disintegration. Phys. Rev. **D85**, 044038 (2012). arXiv:1108.2015
88. Giddings, S.B.: Black holes, quantum information, and unitary evolution. Phys. Rev. **D85**, 124063 (2012). arXiv:1201.1037
89. Giddings, S.B.: Nonviolent nonlocality. Phys. Rev. **D88**, 064023 (2013). arXiv:1211.7070
90. Giddings, S.B.: Nonviolent information transfer from black holes: a field theory parametrization. Phys. Rev. **D88**(2), 024018 (2013). arXiv:1302.2613
91. Giddings, S.B.: Statistical physics of black holes as quantum-mechanical systems. Phys. Rev. **D88**, 104013 (2013). arXiv:1308.3488
92. Giddings, S.B., Shi, Y.: Effective field theory models for nonviolent information transfer from black holes (2013). arXiv:1310.5700
93. Giddings, S.B.: Modulated Hawking radiation and a nonviolent channel for information release (2014). arXiv:1404.7052
94. Berenstein, D.: Sketches of emergent geometry in the gauge/gravity duality (2014). arXiv:1401.5804
95. Maldacena, J., Susskind, L.: Cool horizons for entangled black holes. Fortsch. Phys. **61**, 781–811 (2013). arXiv:1306.0533
96. Susskind, L.: New concepts for old black holes (2013). arXiv:1311.3335
97. Susskind, L.: Butterflies on the stretched horizon (2013). arXiv:1311.7379
98. Susskind, L.: Computational complexity and black hole horizons (2014). arXiv:1402.5674
99. Susskind, L.: Addendum to computational complexity and black hole horizons (2014). arXiv:1403.5695
100. Hawking, S.: Information preservation and weather forecasting for black holes (2014). arXiv:1401.5761
101. Hewitt, M.: Thermal duality and gravitational collapse in heterotic string theories (2013). arXiv:1309.7578
102. Moffat, J.: Stochastic quantum gravity, gravitational collapse and grey holes (2014). arXiv:1402.0906
103. Mathur, S.D.: The fuzzball proposal for black holes: an elementary review. Fortsch. Phys. **53**, 793–827 (2005). hep-th/0502050
104. Cvetic, M., Youm, D.: General rotating five-dimensional black holes of toroidally compactified heterotic string. Nucl. Phys. **B476**, 118–132 (1996). hep-th/9603100
105. Balasubramanian, V., de Boer, J., Keski-Vakkuri, E., Ross, S.F.: Supersymmetric conical defects: towards a string theoretic description of black hole formation. Phys. Rev. **D64**, 064011 (2001). hep-th/0011217
106. Maldacena, J.M., Maoz, L.: Desingularization by rotation. JHEP **0212**, 055 (2002). hep-th/0012025
107. Lunin, O., Mathur, S.D.: Metric of the multiply wound rotating string. Nucl. Phys. **B610**, 49–76 (2001). hep-th/0105136
108. Lunin, O., Mathur, S.D.: AdS/CFT duality and the black hole information paradox. Nucl. Phys. **B623**, 342–394 (2002). hep-th/0109154
109. Lunin, O., Maldacena, J.M., Maoz, L.: Gravity solutions for the D1–D5 system with angular momentum (2002). hep-th/0212210
110. Kanitscheider, I., Skenderis, K., Taylor, M.: Fuzzballs with internal excitations. J. High Energy Phys. **0706**, 056 (2007). arXiv:0704.0690
111. Mathur, S.D., Saxena, A., Srivastava, Y.K.: Constructing 'hair' for the three charge hole. Nucl. Phys. **B680**, 415–449 (2004). hep-th/0311092
112. Giusto, S., Mathur, S.D., Saxena, A.: Dual geometries for a set of 3-charge microstates. Nucl. Phys. **B701**, 357–379 (2004). hep-th/0405017
113. Giusto, S., Mathur, S.D., Saxena, A.: 3-charge geometries and their CFT duals. Nucl. Phys. **B710**, 425–463 (2005). hep-th/0406103
114. Lunin, O.: Adding momentum to D-1 - D-5 system. JHEP **0404**, 054 (2004). hep-th/0404006

115. Giusto, S., Mathur, S.D.: Geometry of D1-D5-P bound states. Nucl. Phys. **B729**, 203–220 (2005). hep-th/0409067
116. Bena, I., Warner, N.P.: Black holes, black rings and their microstates. Lect. Notes Phys. **755**, 1–92 (2008). hep-th/0701216
117. Balasubramanian, V., Gimon, E.G., Levi, T.S.: Four dimensional black hole microstates: from D-branes to spacetime foam. JHEP **0801**, 056 (2008). hep-th/0606118
118. Giusto, S., Mathur, S.D.: Fuzzball geometries and higher derivative corrections for extremal holes. Nucl. Phys. **B738**, 48–75 (2006). hep-th/0412133
119. Mathur, S.D.: Black hole size and phase space volumes (2007). arXiv:0706.3884
120. Page, D.N.: Hyper-entropic gravitational fireballs (grireballs) with firewalls. J. Cosmol. Astropart. Phys. **1304**, 037 (2013). arXiv:1211.6734
121. Braunstein, S.L., Pirandola, S.: Evaporating black holes have leaky horizons or exotic atmospheres (2013). arXiv:1311.1326
122. Saravani, M., Afshordi, N., Mann, R.B.: Empty black holes, firewalls, and the origin of Bekenstein-Hawking entropy (2012). arXiv:1212.4176
123. Saravani, M., Afshordi, N., Mann, R.B.: Dynamical emergence of universal horizons during the formation of black holes. Phys. Rev. **D89**, 084029 (2014). arXiv:1310.4143
124. Almheiri, A., Sully, J.: An uneventful horizon in two dimensions. JHEP **1402**, 108 (2014). arXiv:1307.8149
125. Gambini, R., Pullin, J.: Loop quantization of the Schwarzschild black hole. Phys. Rev. Lett. **110**(21), 211301 (2013). arXiv:1302.5265
126. Golovnev, A.: Smooth horizons and quantum ripples (2014). arXiv:1401.2810
127. Freivogel, B.: Energy and information near black hole horizons (2014). arXiv:1401.5340
128. Verlinde, E., Verlinde, H.: Passing through the firewall (2013). arXiv:1306.0515
129. Verlinde, E., Verlinde, H.: Black hole information as topological qubits (2013). arXiv:1306.0516
130. Hossenfelder, S.: Comment on the black hole firewall (2012). arXiv:1210.5317
131. Hossenfelder, S.: Disentangling the black hole vacuum (2014). arXiv:1401.0288
132. Jacobson, T.: Boundary unitarity and the black hole information paradox. Int. J. Mod. Phys. **D22**, 1342002 (2013). arXiv:1212.6944
133. Brustein, R.: Origin of the blackhole information paradox. Fortsch. Phys. **62**, 255–265 (2014). arXiv:1209.2686
134. Brustein, R., Medved, A.: Semiclassical black holes expose forbidden charges and censor divergent densities. J. High Energy Phys. **1309**, 108 (2013). arXiv:1302.6086
135. Brustein, R., Medved, A.: Firewalls, smoke and mirrors (2014). arXiv:1401.1401
136. Varela, J.: Semi-classical field theory as decoherence free subspaces (2014). arXiv:1404.3498
137. Torrieri, G.: Some considerations on multi-particle correlations, many particle systems, and entropy in effective field theories (2013). arXiv:1306.5719
138. Ilgin, I., Yang, I.-S.: Causal patch complementarity: the inside story for old black holes. Phys. Rev. **D89**, 044007 (2014). arXiv:1311.1219
139. Hui, L., Yang, I.-S.: Complementarity + back-reaction is enough. Phys. Rev. **D89**, 084011 (2014). arXiv:1308.6268
140. Hotta, M., Matsumoto, J., Funo, K.: Black hole firewalls require huge energy of measurement (2013). arXiv:1306.5057
141. Hutchinson, J., Stojkovic, D.: Icezones instead of firewalls: extended entanglement beyond the event horizon and unitary evaporation of a black hole (2013). arXiv:1307.5861
142. Hsu, S.D.: Macroscopic superpositions and black hole unitarity (2013). arXiv:1302.0451
143. Hsu, S.D.H.: Factorization of unitarity and black hole firewalls (2013). arXiv:1308.5686
144. Hollowood, T.J.: Schrodinger's cat and the firewall (2014). arXiv:1403.5947
145. Akhoury, R.: Unitary S matrices with long-range correlations and the quantum black hole (2013). arXiv:1311.5613
146. Horowitz, G.T., Maldacena, J.M.: The black hole final state. JHEP **0402**, 008 (2004). hep-th/0310281

147. Lloyd, S., Preskill, J.: Unitarity of black hole evaporation in final-state projection models (2013). arXiv:1308.4209
148. Ahn, D., Moon, Y., Mann, R.B., Fuentes-Schuller, I.: The black hole final state for the dirac fields in Schwarzschild spacetime. JHEP **0806**, 062 (2008). arXiv:0801.0471
149. Bousso, R., Stanford, D.: Measurements without probabilities in the final state proposal. Phys. Rev. **D89**, 044038 (2014). arXiv:1310.7457
150. Larjo, K., Lowe, D.A., Thorlacius, L.: Black holes without firewalls. Phys. Rev. **D87**(10), 104018 (2013). arXiv:1211.4620
151. Lowe, D.A., Thorlacius, L.: Black hole complementarity: the inside view (2014). arXiv:1402.4545
152. Ori, A.: Firewall or smooth horizon? (2012). arXiv:1208.6480
153. Abramowicz, M., Kluzniak, W., Lasota, J.P.: Mass of a black hole firewall. Phys. Rev. Lett. **112**, 091301 (2014). arXiv:1311.0239
154. Wielgus, M., Abramowicz, M.A., Ellis, G.F.R., Vincent, F.H.: Cosmic background radiation in the vicinity of a Schwarzschild black hole: no classic firewall (2014). arXiv:1406.6551

Chapter 4
Monsters, Black Holes and Entropy

Stephen D.H. Hsu

Abstract Classical general relativity allows for compact objects—"monsters"—with more entropy than black holes of equal mass. We construct examples of such configurations and describe their general properties. Monsters are problematic for certain versions of the AdS/CFT duality, and possibly even for the application of statistical mechanics to quantum gravity. It is possible that they are somehow excluded from the Hilbert space of quantum gravity, although this would be in contrast to the usual case in which coarse-grained, semiclassical configurations have (many) quantum counterparts.

Keywords Black holes · Entropy · General relativity · Entropy bounds

4.1 Introduction

In this review we describe the construction of *monsters* in classical general relativity. Monsters have finite ADM mass and surface area, but potentially unbounded entropy. From the curved space perspective they are objects with large proper volume that can be glued on to an asymptotically flat space. At no point is the curvature or energy density required to be large in Planck units, and quantum gravitational effects are, in the conventional effective field theory framework, small everywhere. Since they can have more entropy than a black hole of equal mass, monsters are problematic for certain interpretations of black hole entropy and the AdS/CFT duality. For related discussion, see [1, 2].

In the second part we describe recent developments in the foundations of statistical mechanics which make use of properties of high-dimensional (Hilbert) spaces. These results primarily depend on *kinematics*—essentially, the geometry of Hilbert space—and are relatively insensitive to dynamics. We discuss how this approach might be

S.D.H. Hsu (✉)
Department of Physics and Astronomy, Michigan State University,
East Lansing, MI 48824, USA
e-mail: hsu@msu.edu

X. Calmet (ed.), *Quantum Aspects of Black Holes*,
Fundamental Theories of Physics 178, DOI 10.1007/978-3-319-10852-0_4

adopted as a basis for the statistical mechanics of gravity. Interestingly, monsters and other highly entropic configurations play an important role.

4.2 What is Entropy?

Statistical (microcanonical) entropy S is the logarithm of the number of distinct microstates ψ of a system consistent with some imposed macroscopic properties, such as a restriction on the total energy. Thus, the entropy S is proportional to the logarithm of the dimensionality of the Hilbert space of allowed ψ's and measures the amount of information that is encoded in a particular microstate ψ. Unitarity forbids any change in the size of this Hilbert space during time evolution of the system, but entropy may increase if the macroscopic description changes so that more microstates become consistent with it.

Without a theory of quantum gravity, we do not know, so cannot count, the microstates of black holes (for results in string theory, see Refs. [3, 4]). But it has been established [5] semiclassically that a large black hole of mass M emits thermal radiation of temperature $T \sim M^{-1}$, so the entropy in this Hawking radiation is of order the area of the hole: $S = \int dQ/T \sim \int dM\, M \sim A$ (we use Planck units $\hbar = c = G = 1$ throughout). Strictly speaking, the Hawking process applies only to the semiclassical part of the evaporation, but the final quantum part releases at most of order the Planck energy, which can be made negligible compared to the initial mass of the hole and is thus unlikely to change the scaling with M of the total amount of radiation entropy. A total black hole entropy of $S_{BH} = A/4$, corresponding to an entropy density $\sim 10^{69}\,\mathrm{bit/m^2}$ on the horizon, is consistent with other evidence ranging from black hole thermodynamics [5, 6] to string theory [3, 4], although there are other interpretations of this area entropy as well [7].

A black hole has much more entropy than ordinary matter configurations of the same size[1] and energy. For ordinary matter in flat space, the following bound [8] applies: $S < A^{3/4}$. This result can be derived as follows. Given a thermal region of radius R and temperature T, we have $S \sim T^3 R^3$ and $E \sim T^4 R^3$. Requiring $E < R$ (using the hoop conjecture—a criterion for gravitational collapse [9–11]) then implies $T < R^{-1/2}$ and $S < R^{3/2} \sim A^{3/4}$. The use of a temperature T in this derivation is justified because the entropy of a system of fixed size and total energy is maximized in thermal equilibrium.

In Planck units, and for macroscopic objects, the gap between A and $A^{3/4}$ scaling is prodigious. Part of the motivation for the work described here was to understand whether this gap in scaling could be closed by considering curved, rather than flat, space. Another related question, also addressed below, is whether black holes are the most entropically dense objects in the universe. The answers to these questions

[1] Note, we need to restrict the size of the object as well as its total energy. An object with fixed total energy $E = T^4 R^3$, but no restriction on R, can have infinite entropy: we can take $R \to \infty$ and $T \to 0$ with E fixed, so that $S = T^3 R^3 = E/T \to \infty$.

are (at least in classical general relativity): Yes, non-black hole configurations can be found which have more than $A^{3/4}$ entropy, although such configurations are very non-Euclidean, and No, black holes are not the most entropic objects of fixed surface area and mass, unless some further principle (presumably of quantum nature) is introduced into the theory to remove even higher entropy configurations.

The highly entropic objects we have found all collapse into black holes, which is problematic if black hole evaporation is unitary, since unitary evolution cannot map a larger Hilbert space into a smaller one. (Of course, it is also possible that black hole evaporation violates unitarity [12, 13]). We discuss this further below.

4.3 Constructing Monsters

We present two examples of classes of such highly entropic configurations Σ_0 (matter + gravity). In both examples, the curvature of space on Σ_0 makes the ADM mass (i.e., the energy a distant external observer sees and that determines the black hole area after collapse and hence the eventual Hawking radiation entropy) and the surface area of the configuration much smaller than would be suspected from the proper internal volume, to which the initial entropy S_{Σ_0} is proportional. In the case of "*monsters*" (Sect. 4.3.1), this effect can be ascribed to large negative binding energy [14] which almost cancels the proper mass to yield a relatively small ADM mass. In Sect. 4.3.2, the Kruskal–FRW example, the reason is the non-monotonic behavior of the radius r of 2-spheres across the outer Einstein-Rosen bridge.

Unlike ordinary configurations such as stars, galaxies, or even black holes, monster-like configurations have unbounded entropy at fixed ADM mass and surface area: Even if we force the spacetime to be asymptotically flat and fix its ADM mass at M and if, moreover, we require all excited matter degrees of freedom to be contained within a 3-sphere of fixed surface area A (this definition is unambiguous in the case of spherical symmetry, which our examples will obey), there are still an infinite number of matter + gravity configurations inside this surface which conform to these restrictions. In fact, imagine that, additionally, the 3-geometry (at some instant in time, e.g. at a moment of time symmetry) inside the sphere is fixed and that one only looks for matter configurations which generate this given geometry (via the Einstein constraint equations of classical general relativity); then the entropy S characterizing these matter configurations *alone* is already unbounded as one varies the 3-geometry inside the surface A (Fig. 4.1). The stationary points of S as a function of the 3-geometry correspond [15] to solutions of the Tolman-Oppenheimer-Volkoff equation (i.e., they are stationary stars, etc.), but for some interior 3-geometries the entropy S can be much bigger and be even larger than A or M^2 (typically, the configuration will not be stationary in this case). Sections 4.3.1 and 4.3.2 describe examples of such configurations. Clearly, then, if the 3-geometry inside the surface is *not* specified at all, one has to ascribe an infinite entropy to the system.

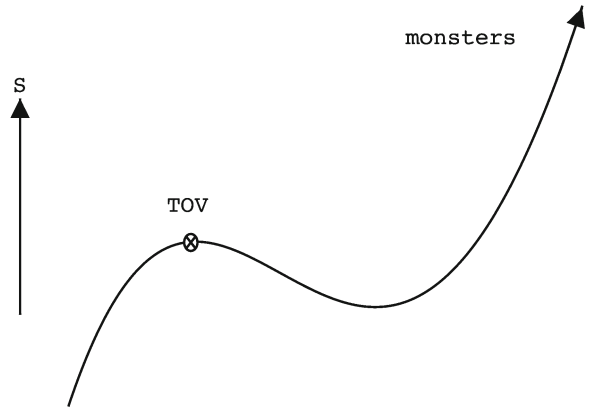

Fig. 4.1 As the 3-geometry inside a given 3-sphere A is varied, it can accommodate different numbers e^S of matter configurations. Stationary gravity-matter configurations (solutions to the Tolman-Oppenheimer-Volkoff equation) are local extrema of the entropy S, but, as one varies the internal 3-geometry, monster configurations can have unbounded entropy at fixed ADM mass M and surface area A

4.3.1 Monsters

Our first example is a ball of material which is on the verge of collapsing to form a black hole. Its energy density profile is arranged to produce a curved internal space with large proper volume (see Fig. 4.2a). The configuration is spherically symmetric, defined by initial data on a Cauchy slice Σ_0 at a moment of time symmetry (i.e., configuration initially "at rest") without (marginally) trapped surfaces, so that Σ_0 has geometry

$$ds^2\big|_{\Sigma_0} = \epsilon(r)^{-1}dr^2 + r^2 d\Omega^2 \ , \quad K_{ab}\big|_{\Sigma_0} = 0, \tag{4.1}$$

with $\epsilon(r) > 0$. For given initial matter distribution $\rho(r)$, Einstein's (constraint) equations determine

$$\epsilon(r) = 1 - \frac{2M(r)}{r}, \tag{4.2}$$

where

$$M(r) = 4\pi \int_0^r dr' \, r'^2 \rho(r'). \tag{4.3}$$

If a configuration has radius R, i.e. $\rho(r > R) = 0$, its ADM energy is $M = M(R)$. This quantity is constant during time evolution of the configuration (Birkhoff's theorem), and, if it collapses to a black hole, equals its mass.

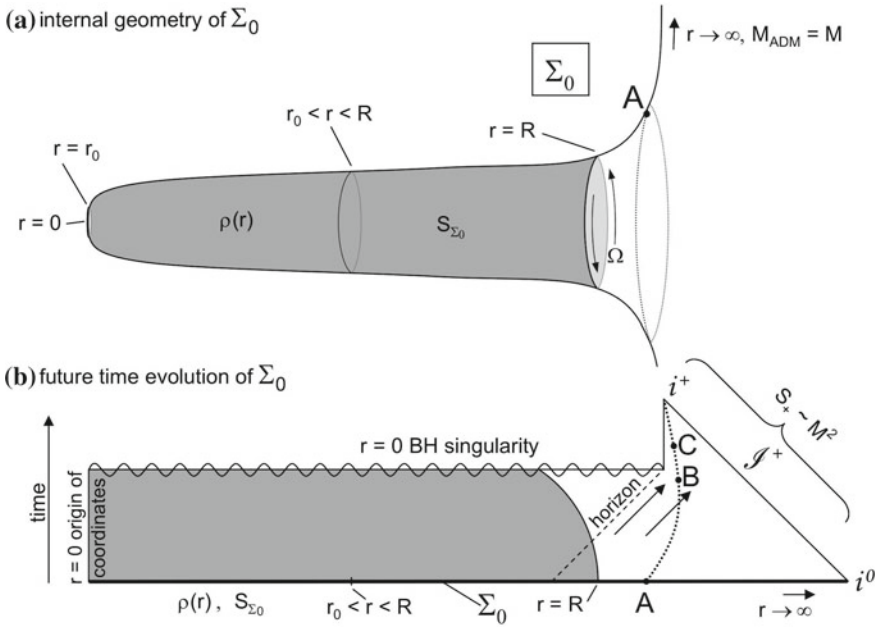

Fig. 4.2 **a** Embedding of the monster configuration Σ_0 into flat space with one angular dimension suppressed. The "neck" has proper length much bigger than $(R - r_0)$, due to the huge factor $\epsilon(r)^{-1/2}$, and contains all of the initial entropy S_{Σ_0}. For $r > R$ the geometry is just that of a Schwarzschild slice with mass $M = M_{ADM}$. **b** The monster's future time evolution is similar to ordinary gravitational collapse: (almost) all matter and entropy, if it was not already initially, will fall behind a horizon (infall of outer layers soon creates trapped surfaces) and form a black hole which then evaporates, radiating away entropy $S_+ \sim M^2 < S_{\Sigma_0}$ past the external observer to future infinity $\mathscr{I}^+ \cup i^+$

Now, consider a semiclassical configuration ("monster" [15, 16], Fig. 4.2a) with radius $R \gg 1$ that yields

$$\epsilon(r) = \left(\frac{r_0}{r}\right)^\gamma , \qquad r_0 < r < R, \tag{4.4}$$

with some $\gamma > 0$ and $r_0 \ll R$ (to avoid poles), so that the configuration comes increasingly closer to forming trapped surfaces as $r \nearrow R$ (long "neck" in Fig. 4.2a). It has ADM mass

$$M = \frac{R}{2}\,(1 - \epsilon(R)) \approx \frac{R}{2} \sim R \tag{4.5}$$

and energy density

$$\rho(r) = \frac{M'(r)}{4\pi r^2} \approx \frac{1}{8\pi r^2} \sim \frac{1}{r^2} , \qquad r_0 < r < R. \tag{4.6}$$

Finally, with a relation $s = \alpha\rho^\beta \sim \rho^\beta$ between energy and entropy density of the matter ($\alpha = \mathcal{O}(1)$), the initial entropy is

$$S_{\Sigma_0} = 4\pi \int_0^R dr\, r^2 \epsilon(r)^{-1/2} s(r) \sim \frac{R^{3-2\beta+\gamma/2}}{r_0^{\gamma/2}} \sim A^{3/2-\beta+\gamma/4}, \tag{4.7}$$

with the area $A \sim M^2$ of the black hole formed in collapse of this monster.

It is now evident that, if β is constant, one can always find configuration parameters γ such that the entropy of the monster exceeds area scaling (hence, the name). This is the case, e.g., if we model the matter (initially) as a perfect fluid with equation-of-state parameter w. Then $\beta = 1/(1+w)$, and we would just have to choose $\gamma > 1$ for a photon gas ($w = 1/3$) or $\gamma > 2$ for dust ($w = 0$; we assume the dust particles carry some kind of label or have spin).

Figure 4.2b depicts the time evolution of a monster, which resembles ordinary gravitational collapse. The main difference is that, due to our construction, the entropy S_{Σ_0} on the initial Cauchy slice can be much bigger than the entropy $S_+ = A/4$ on future infinity, assuming that black hole evaporation is unitary and the standard assumptions about Hawking radiation hold. In order to preserve unitarity (or the AdS/CFT duality [17]) one would somehow have to excise monsters with $S > A$ from the Hilbert space. Monsters with sufficiently high entropy are therefore semiclassical configurations with *no* corresponding microstates in a quantum theory of gravity.

Note, if r_0 is chosen a few orders of magnitude above the Planck length, all involved densities $\rho(r)$ and $s(r)$ are sub-Planckian, so that our semiclassical analysis naively applies. Furthermore, Bousso's covariant entropy bound [18] holds in the semiclassical monster spacetime since it falls under the general class of spacetimes for which a general theorem [19] applies (this assumes no large entropy gradients due to, e.g., shockwaves during evolution, which seems plausible, but has not been proven).

4.3.2 Kruskal–FRW Gluing

The second example [20] consists of slices of closed FRW universes which are glued together across Einstein-Rosen bridges, eventually connecting to a large asymptotically flat universe (Fig. 4.3a). Again, a larger proper volume can be accommodated at fixed ADM mass. The configuration is specified, as before, by initial data on a spherically symmetric and time symmetric ($K_{ab}|_{\Sigma_0} = 0$) Cauchy slice Σ_0: we take the part of a constant-time slice of the Kruskal spacetime with mass M_1 (e.g., part of the $U + V = 0$ slice, in usual Kruskal coordinates) that contains one asymptotic region with outside observer A, the Einstein-Rosen bridge at its maximal extent $r = 2M_1$ and the piece $r_{11} > r > 2M_1$ of the other asymptotic region (right

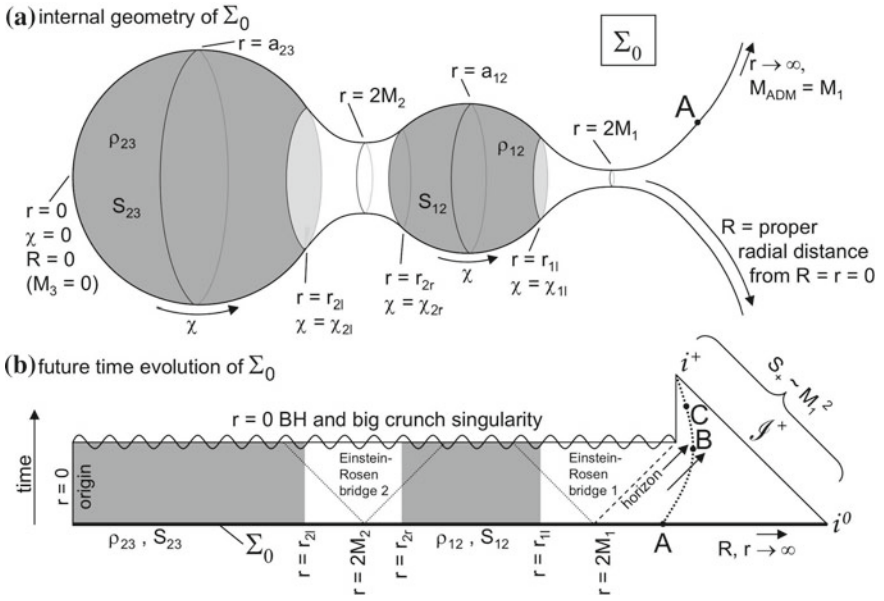

Fig. 4.3 **a** Embedding of a glued Kruskal-FRW initial slice Σ_0 into flat space with one angular dimension suppressed. R is the proper radial distance from the innermost point and $r = r(R)$ gives the radius of the 2-sphere labeled R. Additional or larger closed FRW pieces could be adjoined, and there could also be a second asymptotic Kruskal piece (even with mass parameter different from M_1) if the far left were not closed off with a 3-sphere. **b** By considering the rightmost Einstein-Rosen bridge, standard energy conditions suffice to show that a singularity will form and that the external observer will see a black hole of mass M_1 whose Hawking radiation then contains potentially much less entropy $S_+ \sim M_1^2$ than was present on Σ_0. In the case of pressureless dust, the time evolved spacetime can be given analytically as Kruskal spacetimes and FRW universes appropriately sewn together (Oppenheimer-Snyder collapse)

part in Fig. 4.3a). This is then glued onto the part $\chi < \chi_{1l}$ of the hypersurface $ds^2 = a_{12}^2 \left(d\chi^2 + \sin^2 \chi \, d\Omega^2\right)$ representing a closed FRW universe at the instant of its maximal expansion a_{12}. By cutting this 3-sphere off at $\chi = \chi_{2r}$, a second piece of Kruskal containing an Einstein-Rosen bridge can be joined, etc. In our notation the integer subscript n denotes the n-th Einstein-Rosen bridge, and l (r) denote left (right), see Fig. 4.3.

Matching the geometry across the common boundary requires the transverse metric to be continuous and continuously differentiable (i.e. the extrinsic curvature $K_{ab}^{(3)}$ has to be the same on either side); its second derivative can be discontinuous, as is the energy density ρ, consistent with Einstein's equation $G_{ab} = 8\pi T_{ab}$. At the rightmost joining surface in Fig. 4.3a, continuity of the transverse metric means equality of the areas of the spherical sections $\chi = \chi_{1l}$ and $r = r_{1l}$, i.e.

$$a_{12} \sin \chi_{1l} = r_{1l}. \tag{4.8}$$

And equality of extrinsic curvatures is, in the case of spherical symmetry, equivalent to continuous differentiability of the area $A(R)$ of 2-spheres with respect to proper radial distance R:

$$\frac{d}{a_{12}\, d\chi}\left(4\pi a_{12}^2 \sin^2\chi\right)\Big|_{\chi=\chi_{11}} = \frac{d}{-\left(1-2M_1/r\right)^{-1/2}\, dr}\left(4\pi r^2\right)\Big|_{r=r_{11}}, \tag{4.9}$$

which forces $\chi_{11} \in [\pi/2, \pi)$ and, with (4.8),

$$2M_1 = a_{12}\sin^3\chi_{11}. \tag{4.10}$$

Equations like (4.8) and (4.10) hold at every joining surface, with a modified constraint $\chi_r \in [0, \pi/2]$ if joining just *right* of an Einstein-Rosen bridge. From these formulae, a configuration like Fig. 4.3a can be constructed, e.g., in the following way: first pick masses $M_1,\ M_2, \ldots$ describing the Kruskal pieces ($M = 0$ forces the construction to an end), then sizes $a_{12},\ a_{23} \ldots$ of the FRW pieces subject to constraints $a_{12} \geq 2M_1,\ 2M_2$, etc. Σ_0 is then uniquely determined.

Invoking Friedmann's equation with vanishing instantaneous expansion, the FRW pieces have energy density $\rho_{12} = 3/8\pi a_{12}^2$. With $s \sim \rho^\beta$, the entropy of one piece becomes

$$S_{12} = 4\pi a_{12}^3 s \int_{\chi_{2r}}^{\chi_{11}} d\chi\, \sin^2\chi \sim a_{12}^{3-2\beta}\left[\chi_{11} - \chi_{2r} - \frac{1}{2}\sin 2\chi_{11} + \frac{1}{2}\sin 2\chi_{2r}\right]. \tag{4.11}$$

The bracket in (4.11) approaches $\pi = \mathcal{O}(1)$ as a_{12} becomes a few times bigger than $2M_1$ and $2M_2$. In that case, the total entropy on Σ_0 is

$$S_{\Sigma_0} = S_{12} + S_{23} + \cdots \sim a_{12}^{3-2\beta} + a_{23}^{3-2\beta} + \cdots, \tag{4.12}$$

and so can be made arbitrarily big (for any $\beta = 1/(1+w) < 3/2$) by either taking the size of the FRW pieces or their number to be large.

Evolved forward in time (Fig. 4.3b), the entropy in the Hawking radiation that passes the external observer and reaches future infinity is $S_+ \sim M_1^2$, so again is potentially much less than the entropy on the initial slice (4.12). As in the case of monsters, the Kruskal-FRW configurations are reasonable semiclassical initial data insofar as all involved densities are well sub-Planckian (if the FRW pieces are a few orders of magnitude bigger than the Planck length). The spacetimes do not violate the covariant entropy bound by the same arguments [19] as before (cf. also Ref. [18] for more specific discussion of entropy bounds in closed FRW universes).

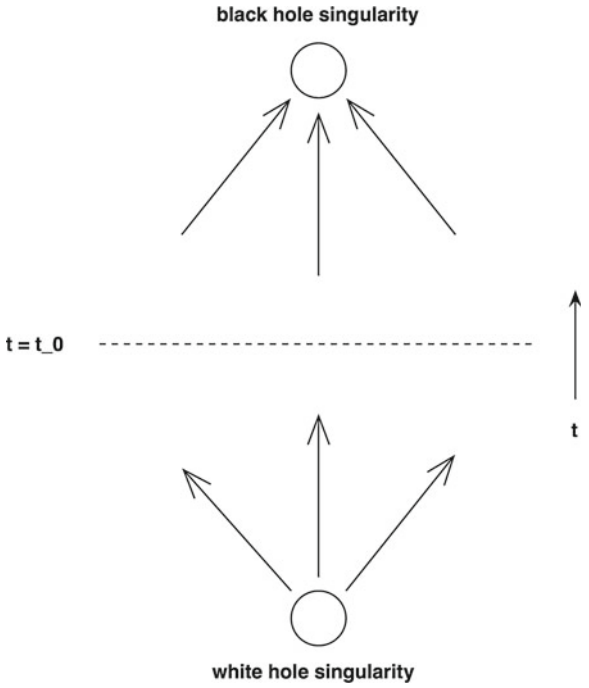

Fig. 4.4 An isolated monster (time-symmetric configuration at $t = t_0$) evolved forward in time becomes a *black hole* with a future singularity. The same monster therefore emerges from a past *white hole* singularity

4.4 Evolution and Singularities

Both types of configurations have the pathological property that, under isolated evolution, they must have emerged from a past singularity (white hole; see Fig. 4.4). This can be seen via backward evolution of the time-symmetric initial data, noting that forward evolution leads to a black hole and future singularity. The monster itself can be thought of as an object whose negative gravitational binding energy almost cancels the positive kinetic and rest mass energy of its constituents. In Fig. 4.4, the monster explodes out of an initial white hole singularity. Because of the large gravitational binding energy, the constituents are unable to separate to infinity, but rather reach a turning point at $t = t_0$ and subsequently collapse back into a black hole.

To avoid the white hole singularity, one can relax the assumption of isolation, and consider monster initial data at $t = t_0$, perhaps constructed "in the laboratory" by outside intervention. One can show that the configurations with $S > A$ cannot be constructed, even via intervention by an arbitrarily advanced civilization [15, 16]; that is, there seem to be fundamental physical limits on the construction of monsters. Despite their pathologies, these configurations represent valid semiclassical states of a matter-gravity system: they are all locally well behaved, in particular do not

require large energy or entropy densities, and—if present in the Hilbert space—could be accessible via tunneling starting from an ordinary matter configuration with the same quantum numbers (ADM energy, angular momentum, charge).

4.5 Quantum Foundations of Statistical Mechanics

Recently, the foundations of statistical mechanics have been established as a consequence of the geometry of high-dimensional Hilbert spaces [21, 22].

Consider a large system subject to a linear constraint R (e.g., that it be in a superposition of energy eigenstates with the energy eigenvalues all being below some $E_{\max}$), which reduces its Hilbert space from $\mathcal{H}$ to a subspace $\mathcal{H}_R$. Divide the system into a subsystem X, to be measured, and the remaining degrees of freedom which constitute an environment E, so $\mathcal{H} = \mathcal{H}_X \otimes \mathcal{H}_E$ and

$$\rho_X \equiv \rho_X(\psi) = \mathrm{Tr}_E |\psi\rangle\langle\psi| \tag{4.13}$$

is the density matrix which governs measurements on X for a given pure state ψ of the whole system. Note the assumption that these measurements are local to X, hence the trace over E.

It can be shown [21], using the concentration of measure on hyperspheres [23] (Levy's theorem), that for almost all $\psi \in \mathcal{H}_R$,

$$\rho_X(\psi) \approx \mathrm{Tr}_E\,(\rho_*) \equiv \Omega_X, \tag{4.14}$$

where $\rho_* = \mathbb{1}_R/d_R$ is the equiprobable maximally mixed state on the restricted Hilbert space $\mathcal{H}_R$ ($\mathbb{1}_R$ is the identity projection on $\mathcal{H}_R$ and d_R the dimensionality of $\mathcal{H}_R$). $\Omega_X = \mathrm{Tr}_E\,(\rho_*)$ is the corresponding canonical state of the subsystem X. The result holds as long as $d_E \gg d_X$, where $d_{E,X}$ are the dimensionalities of the $\mathcal{H}_E$ and $\mathcal{H}_X$ Hilbert spaces. (Recall that these dimensionalities grow exponentially with the number of degrees of freedom. The Hilbert space of an n qubit system is 2^n dimensional.) In the case of an energy constraint R, Ω_X describes a perfectly thermalized subsystem with temperature determined by the total energy of the system.

To state the theorem in Ref. [21] more precisely, the (measurement-theoretic) notion of the *trace-norm* is required, which can be used to characterize the distance between two mixed states ρ_X and Ω_X:

$$\|\rho_X - \Omega_X\|_1 \equiv \mathrm{Tr}\sqrt{(\rho_X - \Omega_X)^2}. \tag{4.15}$$

This sensibly quantifies how easily the two states can be distinguished by measurements, according to the identity

$$\|\rho_X - \Omega_X\|_1 = \sup_{\|O\|\leq 1} \mathrm{Tr}\,(\rho_X O - \Omega_X O)\,, \tag{4.16}$$

where the supremum runs over all observables O with operator norm $\|O\|$ smaller than 1 (projectors $P = O$ are in some sense the best observables, all other observables can be composed out of them, and they have $\|P\| = 1$). Note that the trace on the right-hand side of (4.16) is the difference of the observable averages $\langle O \rangle$ evaluated on the two states ρ_X and Ω_X, and therefore specifies the experimental accuracy necessary to distinguish these states in measurements of O. The theorem then states that the probability that

$$\|\rho_X(\psi) - \mathrm{Tr}_E(\rho_*)\|_1 \;\geq\; \epsilon + \sqrt{\frac{d_X^2}{d_R}} \tag{4.17}$$

is less than $2\exp(-\epsilon^2 d_R/18\pi^3)$. In words: let ψ be chosen randomly (according to the Haar measure on the Hilbert space) out of the space of allowed states $\mathcal{H}_R$; the probability that a measurement on the subsystem X *only*, with measurement accuracy given by the rhs of (4.17), will be able to tell the pure state ψ (of the entire system) apart from the maximally mixed state ρ_* is exponentially small in the dimension of the space $\mathcal{H}_R$ of allowed states. Conversely, for almost all pure states ψ any small subsystem X will be found to be extremely close to perfectly thermalized (assuming the constraint R on the whole system was an energy constraint).

As mentioned, the overwhelming dominance of "typical" states ψ is due to the geometry of high-dimensional Hilbert space and the resulting concentration of measure. It is a consequence of kinematics only—no assumptions have been made about the dynamics. Almost any dynamics—i.e., choice of Hamiltonian and resulting unitary evolution of ψ—leads to the system spending nearly all of its time in typical states for which the density matrix describing any small subsystem X is nearly thermal [24]. Typical states ψ are maximally entangled, and the approach to equilibrium can be thought of in terms of the spread of entanglement, as opposed to the more familiar non-equilibrium kinetic equations.

We can restate these results in terms of the entanglement entropy of the subsystem X, thereby making contact with the Second Law of Thermodynamics. The entanglement entropy is simply the von Neumann entropy of ρ_X:

$$S(X) = -\mathrm{Tr}\,\rho_X \log \rho_X. \tag{4.18}$$

Using the same results on the concentration of measure, it can be shown [25] that, for the overwhelming majority of pure states ψ, $S(X)$ is extremely close to its maximum value $\log d_X$:

$$\mathrm{Prob}\left[\; S(X) \;<\; \log d_X - \alpha - \beta \;\right] \leq \exp\left(-\frac{(d_X d_E - 1)C\alpha^2}{(\log d_X)^2}\right), \tag{4.19}$$

where $\beta = \frac{1}{\ln 2}\frac{d_X}{d_E}$ and $C = (8\pi^2 \ln 2)^{-1}$. This implies [24] that, for almost any choice of dynamics, a subsystem X is overwhelmingly likely to be found with nearly maximal entropy $S(X)$. The Second Law is seen to hold, in a probabilistic sense, even

though the underlying dynamics is time-reversal invariant: density matrices ρ_X with small entropy are highly improbable, and if X is found in a low-entropy state, the entropy is more likely to increase than decrease over any macroscopic time interval.

In our earlier discussion of monsters, the entropy we used was not the entanglement entropy $S(X)$ in (4.18). Instead, we defined the entropy of a monster or black hole to be the logarithm of the number of distinct quantum states consistent with the imposed macroscopic conditions (e.g., fixed ADM mass M, object of area A). This entropy is directly proportional to the logarithm of the dimensionality of the Hilbert space consistent with the macroscopic description, so in the current discussion it is simply $\log d_X$ if we consider only the subset of X configurations which are consistent with the description. Note that $\log d_X \geq S(X)$ and that, for typical pure states of the larger system, any subsystem X will have entanglement entropy $S(X)$ near its maximum value $\log d_X$. Thus, within the framework for statistical mechanics discussed in this section, the entropy we defined earlier can be used to characterize the most likely ("equilibrium") configurations to be found in X.

4.6 Statistical Mechanics of Gravity?

Can the quantum mechanical derivation of statistical mechanics given above be applied to gravity? For example, can we deduce the Second Law of Thermodynamics on semiclassical spacetimes (i.e., including, for example, large black holes)?

This might seem overly ambitious since we currently lack a theory of quantum gravity. However, the results described above are primarily a consequence of the high-dimensional character of Hilbert spaces. If the state space of quantum gravity continues to be described by something like a Hilbert space, then its dimensionality will almost certainly be large, even for systems of modest size. Further, it seems a less formidable task to characterize some aspects of the state space of quantum gravity than to fully understand its dynamics. Indeed, for our purposes here we only consider semiclassical spacetimes.

Early attempts at quantization, culminating in the Wheeler-DeWitt equation, were based on the classical Hamiltonian formulation of general relativity [26, 27]. These led to a configuration space ("superspace") of 3-geometries, modulo diffeomorphisms, and to the wavefunction, $\Psi[h_{ab}, \phi]$, of the universe as a functional over 3-metrics h_{ab} and matter fields ϕ. This description of the state space seems quite plausible, at least in a coarse grained sense, even if the fundamental objects of the underlying theory are something else (strings, loops, etc.). Let us assume that some form of short-distance regulator is in place (or, alternatively, that the dynamics itself generates such a regulator in the form of a minimum spacetime interval), so that we can neglect ultraviolet divergences.

Now consider the set of asymptotically flat, non-compact 3-geometries. Impose conditions on the asymptotic behavior so that the total ADM mass of the system is M, and further assume that all the energy density is confined to a region of surface area A. This results in a restricted state space $\mathcal{H}_R$. If the concentration of measure

results apply to $\mathcal{H}_R$, then the observed properties of any small subsystem X are likely to be the same as if the universe were in the equiprobable, maximally mixed state $\rho_* = \mathbb{1}_R/d_R$. In the flat space case this leads to the usual canonical (Boltzmann) distribution in X.

However, from our monster analysis we know that we are already in trouble. Despite the short distance regulator and the restrictions on total energy and surface area, the Hilbert space dimension d_R and entropy are infinite because of monsters and related configurations, see Fig. 4.1. (In a sense this is a trivial consequence of the fact that they can have infinite proper volume but nevertheless be glued into the region of interest with surface area A). Without a *further regularization* which limits the proper volumes and entropies of monster-like configurations, the maximally mixed state is ill-defined and we cannot recover the familiar thermodynamics of semiclassical spacetimes in the same way as in Sect. 4.5 for ordinary quantum systems. In effect, to obtain any reasonable results we have to eliminate the highest entropy configurations from the state space.[2]

For this approach to produce the familiar results from ordinary and black hole thermodynamics, it is therefore necessary to invoke some new principle which excises the $S > A/4$ monsters from the state space. (Indeed, as discussed earlier, such an excision was already suggested by the requirement that black hole evolution be unitary, although it is *not* required by the covariant entropy bound [18]). Once this is done, Schwarzschild black holes become the most highly entropic objects of mass M and $A = 16\pi M^2$. It then seems possible that the statistical mechanics of gravitational systems might result from typicality of the state $\Psi[h_{ab}, \phi]$. In particular, one might be able to deduce a modification of the Second Law into a Generalized Second Law that takes into account the entropy of black holes and of other curved space objects.

4.7 Conclusions

Classical general relativity allows configurations of fixed ADM mass and surface area, but unbounded entropy ("monsters"). These configurations can be constructed as initial data such that at no point are energy or entropy densities, or curvatures, large in Planck units. Thus, under the usual assumptions about gravity as an effective field theory, they are well described in the semiclassical approximation.

It is of course not known whether such configurations persist in the quantum theory of gravity. If they do, their existence seems problematic for unitary evaporation of black holes and for the AdS/CFT correspondence. If, to the contrary, they are to be excised from the theory, some new fundamental principle is required.

---

[2] Of course, it is also possible that the initial pure state is atypical and subsequent dynamics somehow keeps the state in a very atypical region of the Hilbert space over very long time scales, so that the highly entropic configurations are essentially never sampled. In that case one cannot deduce the thermodynamic properties of the system from the concentration of measure phenomenon (i.e., typicality) alone: the system does not actually reach ultimate equilibrium.

In the second part of this review we studied a fundamentally quantum approach to statistical mechanics. The high dimensionality of Hilbert space and consequent concentration of measure are used to show that almost any pure state will lead to approximate canonical behavior of the density matrix of small subsystems. This approach also provides a probabilistic justification of the Second Law of Thermodynamics. We investigated whether a similar framework can be applied to gravitational systems. The existence (or non-existence) of monster-like states plays a central role in the outcome: we conclude that this approach cannot work in the presence of gravity unless monster-like states are indeed excised from the theory.

Acknowledgments The author acknowledges support from the Office of the Vice-President for Research and Graduate Studies at Michigan State University.

References

1. Marolf, D.: Gen. Rel. Grav. **41**, 903 (2009). arXiv:0810.4886 [gr-qc]
2. Hossenfelder, S., Smolin, l.: Phys. Rev. D **81**, 064009 (2010). arXiv:0901.3156 [gr-qc]
3. Strominger, A., Vafa, C.: Phys. Lett. B **379**, 99 (1996)
4. Maldacena, J.M., Strominger, A., Witten, E.: JHEP **12**, 002 (1997)
5. Hawking, S.W.: Commun. Math. Phys. **43**, 199 (1975)
6. Bekenstein, J.D.: Phys. Rev. D **7**, 2333 (1973)
7. Jacobson, T. arXiv:gr-qc/9908031
8. Hooft, G.'t.: In:Ali et al. (eds.) Salamfestschrift. World Scientific (1994)
9. Thorne, K.S.: In: Klauder, J.R. (eds.) Magic Without Magic. Freeman (1973)
10. Eardley, D.M., Giddings, S.B.: Phys. Rev. D **66**, 044011 (2002)
11. Hsu, S.D.H.: Phys. Lett. B **555**, 92 (2003)
12. Hawking, S.W.: Phys. Rev. D **14**, 2460 (1976)
13. Hsu, S.D.H.: Phys. Lett. B **644**, 67 (2007)
14. Hsu, S.D.H. arXiv:gr-qc/9801106
15. Sorkin, R.D., Wald, R.M., Zhang, Z.J.: Gen. Rel. Grav. **13**, 1127 (1981)
16. Hsu, S.D.H., Reeb, D.: Phys. Lett. B **658**, 244 (2008)
17. Aharony, O., Gubser, S.S., Maldacena, J.M., Ooguri, H., Oz, Y.: Phys. Rept. **323**, 183 (2000)
18. Bousso, R.: JHEP **07**, 004 (1999)
19. Flanagan, E.E., Marolf, D., Wald, R.M.: Phys. Rev. D **62**, 084035 (2000)
20. Hsu, S.D.H., Reeb, D.: Class. Quant. Grav. **25**, 235007 (2008)
21. Popescu, S., Short, A.J., Winter, A.: Nat. Phys. **2**, 754 (2006). See also. arXiv:quant-ph/0511225
22. Gemmer, J., Michel, M., Mahler, G.: Quantum Thermodynamics: Emergence of Thermodynamic Behavior Within Composite Quantum Systems, Springer, Berlin (2004)
23. Ledoux, M.: The Concentration of Measure Phenomenon. American Mathematical Society, Providence (2001)
24. Linden, N., Popescu, S., Short, A.J., Winter, A. arXiv:0812.2385 [quant-ph]
25. Hayden, P., Leung, D.W., Winter, A.: Comm. Math. Phys. **265**, 95 (2006)
26. Misner, C.W., Thorne, K.S., Wheeler, J. A.: Gravitation. Freeman (1973)
27. Kiefer, C.: Quantum Gravity, 2nd edn. Oxford University Press, Oxford (2007)

Chapter 5
Primordial Black Holes: Sirens of the Early Universe

Anne M. Green

Abstract Primordial Black Holes (PBHs) are, typically light, black holes which can form in the early Universe. There are a number of formation mechanisms, including the collapse of large density perturbations, cosmic string loops and bubble collisions. The number of PBHs formed is tightly constrained by the consequences of their evaporation and their lensing and dynamical effects. Therefore PBHs are a powerful probe of the physics of the early Universe, in particular models of inflation. They are also a potential cold dark matter candidate.

5.1 Introduction

Primordial Black Holes (PBHs) are black holes which may form in the early Universe [55, 141]. There are various formation mechanisms: the collapse of large density fluctuations (Sect. 5.2.1), cosmic string loops [57] (Sect. 5.2.2) or bubble collisions [39, 58] (Sect. 5.2.3). In most cases the PBH mass, $M_{\rm PBH}$, is roughly equal to the horizon mass, $M_{\rm H}$, at the formation epoch (e.g. Ref. [30]):

$$M_{\rm PBH} \sim M_{\rm H} \sim \frac{c^3 t}{G} \sim 10^{15} \left(\frac{t}{10^{-23}\ {\rm s}} \right)\ {\rm g}. \tag{5.1}$$

For instance PBHs formed at the QCD phase transition at $t \sim 10^{-6}$ s would have mass of order a solar mass, $M_{\rm PBH} \sim M_\odot = 2 \times 10^{30}$ kg.

As famously realised by Hawking [56], PBHs radiate thermally and hence evaporate on a timescale, $\tau(M_{\rm PBH})$, (e.g. Ref. [30]):

$$\tau(M_{\rm PBH}) \sim \frac{\hbar c^4}{G^2 M_{\rm PBH}^3} \sim 10^{10} \left(\frac{M_{\rm PBH}}{10^{15}\ {\rm g}} \right)^3\ {\rm Gyr}. \tag{5.2}$$

A.M. Green (✉)
School of Physics and Astronomy, University of Nottingham, University Park, Nottingham NG7 2RD, UK
e-mail: anne.green@nottingham.ac.uk

X. Calmet (ed.), *Quantum Aspects of Black Holes*,
Fundamental Theories of Physics 178, DOI 10.1007/978-3-319-10852-0_5

PBHs with $M_{\rm PBH} \sim 10^{15}$ g will be evaporating today and their abundance is constrained by the flux of γ-rays [105] (Sect. 5.3.1.4). Lighter PBHs evaporated in the past and are constrained by the effects of their evaporation products on Big Bang Nucleosynthesis [130, 142] (Sect. 5.3.1.3) and the present day density of any stable relic particles [90] (Sect. 5.3.1.2). Heavier PBHs are stable and their abundance is limited by their lensing (Sect. 5.3.2) and dynamical [33] (Sect. 5.3.3) effects and also their effects on various other astrophysical processes and objects (Sect. 5.3.4). Since PBHs are matter, the fraction of the total energy density in the form of PBHs increases proportional to the scale factor, a, during radiation domination. Therefore the constraints on the fraction of the initial energy density in the form of PBHs, $\beta(M_{\rm PBH}) = \rho_{\rm PBH}/\rho_{\rm tot}$, are very tight, lying in the range $10^{-5} - 10^{-30}$.

Cosmological inflation, a period of accelerated expansion in the early Universe, may have generated the primordial fluctuations from which galaxies and large scale structure form (see e.g. Ref. [88]). The constraints on the initial fraction of the energy density in the form of PBHs can be translated into limits on the primordial power spectrum of density perturbations on small scales, and can therefore be used to constrain models of inflation [34] (Sect. 5.4).

Finally there is extensive astronomical and cosmological evidence that the majority of the matter in the universe is in the form of non-baryonic cold dark matter (CDM) (see e.g. Ref. [12]). Since PBHs form before nucleosynthesis they are non-baryonic and therefore a candidate for the CDM (Sect. 5.5).

5.2 PBH Formation Mechanisms

For a PBH to form a large over-density is required. In this section we discuss several ways of achieving this: large density fluctuations [31] (Sect. 5.2.1), cosmic string loops [57] (Sect. 5.2.2) and bubble collisions [39, 58].

5.2.1 Large Density Fluctuations

During radiation domination, if a density fluctuation is sufficiently large, then gravity overcomes pressure forces and the fluctuation collapses to form a PBH shortly after it enters the horizon [31]. We review the original calculations of this process in Sect. 5.2.1.1 and then discuss refinements in Sect. 5.2.1.2.

5.2.1.1 Original Calculations

The early pioneering calculations by Carr and Hawking [31] assumed that the over-dense region from which a PBH formed was spherically symmetric[1] and part

[1] PBHs from the rare large density fluctuations for which this assumption is justified [9, 41].

of a closed Friedmann universe. In this case, for gravity to overcome pressure at maximum expansion the region must be larger than the Jeans length, which is $\sqrt{w}$ times the horizon length (w is the equation of state parameter, $p = w\rho$, and $w = 1/3$ for radiation domination). This leads to a requirement that the density contrast, $\delta \equiv \delta\rho/\rho$, at horizon crossing must exceed a critical value $\delta_c \approx w$. It was thought at this time that if the fluctuation was larger than the horizon length, which corresponds to $\delta > 1$, then it would instead form a separate closed universe.

The PBHs formed would have mass of order the horizon mass, M_H, at the time they form: $M_{PBH} = w^{3/2} M_H$ [27]. If the fluctuations are scale invariant, so that PBHs form on all scales, then the PBHs will have an extended mass function [27]: $dn/dM_{PBH} \propto M_{PBH}^{-5/2}$. However, as we will see in Sect. 5.4.1, it is now known that for a scale-invariant power spectrum, normalised to observations on cosmological scales, the number of PBHs formed is completely negligible [32].

The criteria for PBH formation in a matter dominated universe with $w = 0$ are somewhat different. In this case, because the pressure is zero, it is possible for PBHs to form well within the horizon. However for this to happen the perturbation must be sufficiently spherically symmetric [74, 109].

5.2.1.2 Refinements

Early numerical simulations of PBH formation [99] roughly confirmed the earlier analytic calculations [27, 31]. More recently it has been realised that, as a consequence of near critical gravitational collapse [38], the PBH mass depends on the size of the fluctuation from which it formed [102, 103]:

$$M_{PBH} = \kappa M_H (\delta - \delta_c)^\gamma , \tag{5.3}$$

where γ and κ are constants of order unity which depend on the shape of the perturbation and the background equation of state [97, 102, 103]. This power law scaling of the PBH mass has been found to hold down to $(\delta - \delta_c) \sim 10^{-10}$ [96, 98]. Note, however, that the majority of the PBHs formed have masses within an order of magnitude or so of M_H [103]. For scale-dependent power spectra which produce an interesting PBH abundance it can be assumed that all PBHs form at a single epoch [50]. For a power spectrum which increases monotonically with decreasing scale, PBH formation occurs at the smallest scale, while if the power spectrum has a feature, PBH formation occurs on the scale on which the perturbations are largest. The spread in the mass function due to critical collapse can have an important effect on the constraints on the PBH abundance which are sensitive to the PBH mass function, for instance the constraint from the flux of gamma-rays [77, 139].

There has been a lot of interest in the exact value of the threshold for PBH formation, δ_c, since, as we will see in Sect. 5.4.1, the number of PBHs formed depends exponentially on δ_c. Reference [126] found that the peak value of the metric

perturbation was a good indicator of PBH formation, and Ref. [52] found, using peaks theory, that the threshold values from Ref. [126] were equivalent to density thresholds in the range $\delta_c \approx 0.3$–0.5. Reference [96], which used appropriate initial conditions (super-horizon perturbations which only contain a growing mode) for their simulations, found for radiation domination $\delta_c \approx 0.45$. This is in good agreement with recent analytic calculations, once gauge issues are taken into account [54].

Whether or not a fluctuation collapses to form a PBH depends on its shape as well as its amplitude [110, 111]. Reference [100] explored fluctuations with a range of shapes and found that the key parameters are the average value of the central overdensity and the width of the overdensity (for broad overdensities the threshold average density is reduced).

There has also been development regarding the fate of perturbations with $\delta \sim 1$. Reference [81] showed that they do not form a separate closed universe, and the upper limit was in fact a consequence of the gauge choice.

5.2.2 Cosmic String Loops

Cosmic string are one-dimensional topological defects which may form during phase transitions in the very early Universe (see e.g. Ref. [133]). As a cosmic string network evolves, long strings self-intersect and form cosmic string loops. There is a small probability that an oscillating cosmic string loop will be in a configuration where all of its dimensions are less than its Schwarzschild radius, and hence it will collapse to form a PBH with mass roughly equal to the horizon mass [22, 46, 57, 108, 135]. The number of PBHs formed depends on the mass per unit length of the strings, μ, which is related to the symmetry breaking scale. Cosmic string loops can collapse to form PBHs at any point during radiation domination, therefore the resulting PBHs have an extended mass function $\mathrm{d}n/\mathrm{d}M_{\rm PBH} \propto M_{\rm PBH}^{-5/2}$. The constraints on the number of PBHs formed (from the gamma-rays and cosmic-rays produced when they evaporate, see Sect. 5.3.1) place a limit on the cosmic string mass per unit length $G\mu/c^2 < 10^{-6}$ [135], comparable to the constraints from the effect of strings on the Cosmic Microwave Background radiation [2].

5.2.3 Bubble Collisions

First order phase transitions occur through the formation of bubbles of the new phase, which then expand and collide. PBHs, with mass of order the horizon mass, can form as a result of these bubble collisions [39, 58, 82]. However forming a cosmologically interesting abundance of PBHs requires fine tuning of the bubble formation rate, so that the bubbles collide but the phase transition doesn't occur instantaneously.

5.3 PBH Abundance Constraints

PBH abundance constraints are usually quoted in terms of the fraction of the energy density in the form of PBHs at the time they form

$$\beta(M_{\rm PBH}) \equiv \frac{\rho_{\rm PBH}}{\rho_{\rm tot}}. \tag{5.4}$$

The PBH density evolves as $\rho_{\rm PBH} \propto a^{-3}$, where a is the scale factor, while the radiation density varies as $\rho_{\rm rad} \propto a^{-4}$. Therefore during radiation domination the fraction of the total energy density which is in the form of PBHs grows proportional to a. So even if the fraction of the energy density of the Universe in PBHs is initially small it can grow to be significant at late times.

The lensing (Sect. 5.3.2) and dynamical (Sect. 5.3.3) constraints limit the fraction of the Milky Way (MW) halo in the form of compact objects, $f(M_{\rm CO})$. Assuming the density of other compact object is negligible and the MW's DM composition is the same as the Universe as a whole (which is a reasonable assumption) then $f(M_{\rm CO}) = \Omega_{\rm PBH}/\Omega_{\rm CDM}$, where $\Omega_{\rm PBH}$ and $\Omega_{\rm CDM}$ are the fraction of the critical density (for which the geometry of the Universe is flat) in the form of PBHs and CDM respectively. It is related to the initial PBH mass fraction, $\beta(M_{\rm PBH})$, via (see e.g. Ref. [35] for a more accurate expression)

$$f(M_{\rm CO}) \approx \left(\frac{\beta(M_{\rm PBH})}{10^{-8}}\right)\left(\frac{M_{\rm PBH}}{M_\odot}\right)^{-1/2}. \tag{5.5}$$

Most of the constraints that we discuss below effectively apply to the integral of the PBH mass function over the range of applicability. This range is usually significantly larger than the expected width of the PBH mass function (see Sect. 5.2.1), and therefore the constraints are not sensitive to the precise form of the mass function. However the constraints from cosmic-rays and gamma-rays produced by recently and currently evaporating PBHs are an exception to this (see e.g. Ref. [77, 139]).

For conciseness we only give order of magnitude values of the constraints and their range of validity, see Ref. [35] for the precise mass dependence of the constraints on the halo fraction in compact objects, $f(M_{\rm CO})$, and the initial mass fraction of PBHs, $\beta(M_{\rm PBH})$.

5.3.1 Evaporation

The current picture of PBH evaporation [91] is that they directly emit all particles which appear elementary at the energy scale of the PBH and have rest mass less than the black hole temperature. Therefore if the black hole temperature exceeds the QCD confinement scale, quark and gluon jets are emitted directly. The quark and gluon

jets then fragment and decay producing astrophysically stable particles: photons, neutrinos, electrons, protons and their anti-particles. It has been argued that QED or QCD interactions could lead to the formation of an optically thick photosphere [59, 60], however the emitted particles do not interact enough for this to occur [93].

There are also limits from photons distorting the spectrum of the Cosmic Microwave Background radiation [35, 142], the Super-Kamionkande limit on the flux of relic anti-neutrinos [35] and extragalactic anti-protons [35]. However these constraints are weaker than the nucleosynthesis and extragalactic gamma-ray background constraints [35], so we do not discuss them in detail here.

See Ref. [35] for detailed discussion of the evaporation constraints.

5.3.1.1 Entropy

The photons emitted by PBHs with $M_{\rm PBH} < 10^9$ g will thermalize and contribute to the baryon to photon ratio. The requirement that this ratio must not exceed the observed value of $\sim 10^9$ leads to a relatively weak constraint, $\beta(M_{\rm PBH}) < 10^{-5}(M_{\rm PBH}/10^9\ {\rm g})^{-1}$ for $10^6\ {\rm g} < M_{\rm PBH} < 10^9$ g [142].

5.3.1.2 Relic Particles

It has been argued that black hole evaporation could leave a stable Planck mass relic [90], in which case the present day density of relics must not exceed the upper limit on the present day CDM density. This leads to a constraint of order $\beta(M_{\rm PBH}) < (M_{\rm PBH}/10^{15}\ {\rm g})^{3/2}$ for $M_{\rm PBH} < 10^{15}$ g.

In many extensions of the standard model there are stable or long lived massive ($\mathcal{O}(100\ {\rm GeV/c^2})$) particles. PBHs with mass $M_{\rm PBH} < 10^{11}$ g can emit these particles and their abundance is consequently limited to be, roughly, $\beta(M_{\rm PBH}) < 10^{-18}(M_{\rm PBH}/10^{11}\ {\rm g})^{-1/2}$ by the present day abundance of stable massive particles [48] and the decay of long-lived particles [75, 85].

The limits from Planck mass relics and (quasi-) stable massive particles are weaker than those from nucleosynthesis, and also depend on the uncertain details of beyond the standard model physics. However they are the only potential constraints on PBHs with $M_{\rm PBH} < 10^6$ g and significantly tighter than the entropy constraints for $10^6\ {\rm g} < M_{\rm PBH} < 10^9$ g.

5.3.1.3 Nucleosynthesis

Extensive work on the effects of PBH evaporation on the products of Big Bang nucleosynthesis was carried out in the late 1970s [86, 95, 101, 130, 131, 142]. Carr et al. [35], using the results of Refs. [72, 79], have updated the resulting constraints on the abundance of PBHs, taking into account the latest observational data

on the abundances of the light elements and the neutron lifetime, and developments in the understanding of PBH evaporation [91].

PBHs with mass in the range 10^9 g $< M_{\rm PBH} < 10^{10}$ g have lifetime $\tau = 10^{-2}$–10^{-3} s and the mesons and anti-nucleons they emit would increase the neutron/proton ratio and hence the abundance of ^{4}He. This leads to a constraint which is very roughly $\beta < 10^{-20}(M_{\rm PBH}/10^{10}\ {\rm g})^{-2}$ [35]. For masses in the range 10^{10} g $< M_{\rm PBH} < 10^{12}$ g the lifetime is between 10^{-2} s and 10^2 s and the high-energy hadrons produced dissociate the light elements, reducing the abundance of ^{4}He and increasing the abundance of the other elements. The tightest constraints are from deuterium for 10^{10} g $< M_{\rm PBH} < 5 \times 10^{10}$ g and from non-thermally produced ^{6}Li for 5×10^{10} g $< M_{\rm PBH} < 10^{12}$ g. For both mass ranges the constraint is, roughly, $\beta(M_{\rm PBH}) < 10^{-23}$ [35]. Finally, for 10^{12} g $< M_{\rm PBH} < 10^{13}$ g the lifetime is $\tau = 10^7$–10^{12} s and photodissociation is instead important. The most stringent constraint, which is again of order $\beta(M_{\rm PBH}) < 10^{-23}$, comes from overproduction of ^{3}He or deuterium [35]. For further information, including the detailed mass dependence of the constraints see Ref. [35].

5.3.1.4 γ-rays

PBHs with masses in the range 10^{13} g $< M_{\rm PBH} < 10^{15}$ g will have evaporated between $z \sim 1000$ and the present day and can contribute to the diffuse extragalactic gamma-ray background [28, 92, 105]. Their abundance is limited by EGRET data to be roughly $\beta(M_{\rm PBH}) < 10^{-27}(M_{\rm PBH}/10^{15}\ {\rm g})^{-5/2}$ [35]. Slightly more massive PBHs, that have not evaporated completely by the present day, can also emit a significant flux of gamma-rays, and their abundance is limited to be roughly $\beta(M_{\rm PBH}) < 10^{-26}(M/10^{15}\ {\rm g})^{7/2}$ [35]. There is also a similar limit on PBHs with $M_{\rm PBH} \sim 10^{15}$ g that are evaporating today from Galactic gamma-rays [35].

The detailed values of these constraints, in particular those for $M_{\rm PBH} > 10^{15}$ g, depend on the exact shape of the PBH mass function [77, 139]. However the values stated are somewhat conservative as known astrophysical backgrounds have not been subtracted [35].

For PBHs with 10^{15} g $< M_{\rm PBH} < 10^{17}$ g the gamma-ray constraints constrain the fraction of the DM in the form of PBHs to be less than one. In other words, PBHs in this mass range can not make up all of the DM.

5.3.2 Lensing

If there is a cosmologically significant density of compact objects (COs) then there is a high probability that a distant point source is lensed [112]. For hundred solar mass and lighter lenses the image separation is too small for multiple images to be observed, however other observable effects can occur.

5.3.2.1 Gamma-ray Burst Femtolensing

For 10^{17} g $< M_{\rm CO} < 10^{20}$ g the image separation is of order femto arc-seconds. However the time delay between images, 10^{-17}–10^{-20} s, is approximately equal to the period of a gamma-ray. COs of this mass could therefore be detected by the interference pattern in the energy spectrum of a gamma-ray burst [47]. Analysis of data from the Gamma-ray Burst Monitor onboard the Fermi satellite finds that for 10^{17} g $< M_{\rm CO} < 10^{20}$ g, $f(M_{\rm CO}) < 1$ [10].

5.3.2.2 Galactic Microlensing

Microlensing occurs when a CO with mass in the range 10^{24} g $< M_{\rm CO} < 10^{34}$ g crosses the line of sight to a star. The image separation is too small (of order micro arc-seconds) for multiple images to be resolved, and the lensing leads to a temporary amplification of the star's flux [104]. The EROS and MACHO surveys of the Large and Small Magellanic Clouds found that for 10^{26} g $< M_{\rm CO} < 10^{34}$ g, $f(M_{\rm CO}) < 1$, with tighter limits within this mass range [7, 129]. Recently the lower limit of the excluded mass range has been lowered to 4×10^{24} g using Kepler data [53].

5.3.2.3 Quasar Microlensing

COs with 10^{30} g $< M_{\rm CO} < 10^{35}$ g can microlens quasars, amplifying the continuum emission, without affecting the line emission [23] and limits on the number of small equivalent width quasars place a constraint on COs in this mass range $f(M_{\rm CO}) < 1$ [40].

5.3.2.4 Radio Source Millilensing

Massive COs with 10^{39} g $< M_{\rm CO} < 10^{41}$ g can millilens radio sources, producing multiple images which can be resolved with Very Long Baseline Interferometry [70]. A null search limits COs in this mass range to make up less than 1% of the total energy density of the Universe [136].

5.3.3 Dynamical Effects

The abundance of massive COs in the MW halo is constrained by their dynamical effects on the constituents of the MW. These constraints have been studied in detail by Carr and Sakellariadou [33]. Here we briefly summarise the constraints which place the tightest limits on the halo fraction in COs. There is also a constraint from the tidal disruption of globular clusters (GCs) [33], however this depends sensitively

on the mass and radius of the GCs and is weaker than those from dynamical fiction and disk heating [35] so we do not discuss it in detail.

5.3.3.1 Disruption of Wide Binaries

Encounters with massive COs can disrupt [8] or change the orbital parameters [134] of wide binary stars. Observations of wide binaries [36, 114] constrain the halo mass fraction to be $f(M_{\rm CO}) < 0.4$ for 10^{36} g $< M_{\rm CO} < 10^{41}$ g [35, 114].

5.3.3.2 Dynamical Friction

COs will be dragged into the centre of the MW by the dynamical friction of spheroid stars and the population of COs themselves. Constraints on the central mass of the MW limit the halo fraction in COs with 10^{37} g $< M_{\rm CO} < 10^{45}$ g. The limit is tightest, $f(M_{\rm CO}) < 5 \times 10^{-5}$, at $M_{\rm CO} \sim 10^{41}$ g [33, 35].

5.3.3.3 Disk Heating

Massive COs traversing the Galactic disk will heat the disk, increasing the velocity dispersion of the disk stars [83]. This leads to a limit, from the observed stellar velocity dispersions, on the halo fraction in COs with 10^{40} g $< M_{\rm PBH} < 10^{45}$ g which is tightest, $f(M) < 10^{-3}$, at $M \sim 10^{43}$ g [33, 35].

5.3.4 Other Astrophysical Objects and Processes

There are also constraints on PBHs with $M_{\rm PBH} > 10^{15}$ g from their effects on various astrophysical objects and processes.

5.3.4.1 Stars

If a PBH is captured by a neutron star the star will be accreted and destroyed in a short time [25]. The existence of neutron stars in globular clusters (GCs) excludes PBHs with 10^{18} g $< M_{\rm PBH} < 10^{24}$ g comprising all of the DM, if the DM density in GCs is larger than $\sim$100 GeV cm^{-3} [25]. Similarly accretion of PBHs during star formation could exclude PBH DM in the range 10^{16} g $< M_{\rm PBH} < 10^{22}$ g [24]. Note, however, that a high DM density in GC is only expected if (a subset of) GCs are formed in DM mini halos rather than from baryonic processes and there is no direct observational evidence for a large DM density in GCs (see e.g. Ref. [17]). Recently Ref. [106] has argued that the existence of old neutron stars in the centres of the MW and Large Magellanic Cloud excludes PBHs in the range 10^{17} g $< M_{\rm PBH} < 10^{24}$ g comprising all of the DM, see however Ref. [26].

5.3.4.2 Gravitational Waves

For PBHs formed from the collapse of large density perturbations there is an indirect limit on their abundance from gravitational waves. Large density perturbations generate second order tensor perturbations and therefore limits on their amplitude constrain the amplitude of the density perturbations and hence the abundance of PBHs formed. Pulsar timing constraints place a tight limit on the present day density parameter of PBHs with 10^{35} g $< M_{\rm PBH} < 10^{37}$ g: $\Omega_{\rm PBH}h^2 \leq 10^{-5}$ (where $h \approx 0.7$ is the dimensionless Hubble constant) [118].

5.3.4.3 Cosmic Microwave Background Radiation

After decoupling massive PBHs can accrete material and the subsequent radiation can affect the thermal history of the Universe [29]. X-rays emitted by gas accreted onto PBHs modify the cosmic recombination history, producing measurable effects on the spectrum and anisotropies in the Cosmic Microwave Background radiation, which have been constrained using the FIRAS and WMAP data [117]. The precise limits depend on the accretion model, but are of order $f(M_{\rm PBH}) < 10^{-2}$ for 10^{34} g $< M_{\rm PBH} < 10^{36}$ g and $f(M_{\rm PBH}) < 10^{-5}$ for 10^{36} g $< M_{\rm PBH} < 10^{42}$ g, with weaker constraints outside these mass ranges [117].

5.3.4.4 Large Scale Structure

Massive PBHs would affect large scale structure formation due to the Poisson fluctuations in their number density which enhance the DM power spectrum [94]. Lyman-alpha forest observations constrain the fraction of the DM in PBHs with 10^{37} g $< M_{\rm PBH} < 10^{43}$ g [3, 35]. The limit is tightest, $f(M_{\rm PBH}) < 10^{-3}$, at $M \sim 10^{40}$ g [35].

5.4 Constraints on the Primordial Power Spectrum and Inflation

Cosmological inflation is a period of accelerated expansion proposed to have occurred in the very early Universe in order to solve various problems with the standard Hot Big Bang (namely the horizon, flatness and monopole problems). Accelerated expansion requires negative pressure, a requirement which is satisfied by a slowly-rolling scalar field. Inflation also provides a mechanism for the generation of the primordial fluctuations from which galaxies and large scale structure later form. During inflation the wavelengths of quantum fluctuations in the inflaton field become larger than the Hubble radius and a spectrum of super-Horizon curvature perturbations are

generated. After inflation the fluctuations re-enter the horizon and potentially provide the seeds for structure formation. For an overview see e.g. Ref. [88].

The amplitude and scale dependence of the primordial fluctuations depend on the inflaton potential. Therefore observational constraints on the power spectrum of the primordial curvature perturbation

$$\mathscr{P}_{\mathscr{R}}(k) \equiv \frac{k^3}{2\pi^2}\langle|\mathscr{R}_k|^2\rangle, \tag{5.6}$$

where $\mathscr{R}_k$ are the Fourier modes of the curvature perturbation and k is comoving wavenumber, constrain models of inflation. The power spectrum on cosmological scales, $k \sim 10^{-3}$–1 Mpc^{-1}, is accurately measured by Cosmic Microwave Background [1, 61] and large scale structure observations [13], and some inflation models are now ruled out [1].

Cosmological observations probe a fairly limited region of the inflaton potential. As we will see in this section, the PBH constraints on the power spectrum are fairly weak (many order of magnitude larger than the measurements on cosmological scales). However they apply over a very wide range of scales, $k \sim 10^{-2}$–10^{23} Mpc^{-1}, and therefore constrain a much broader region of the inflaton potential [32], and eliminate or constrain otherwise viable models [66, 107].

5.4.1 Translating Limits on the PBH Abundance into Constraints on the Primordial Power Spectrum

As we saw in Sect. 5.2.1 a fluctuation on a physical scale R will collapse to form a PBH, with mass $M_{\rm PBH}$ roughly equal to the horizon mass, if the smoothed density contrast at horizon entry, $\delta_{\rm hor}(R)$, exceeds a threshold value $\delta_{\rm c}$ which is slightly less than unity.[2] Assuming the initial perturbations have a Gaussian distribution then the probability distribution of the smoothed density contrast is given by (e.g. Ref. [88]):

$$P(\delta_{\rm hor}(R)) = \frac{1}{\sqrt{2\pi}\sigma_{\rm hor}(R)}\exp\left(-\frac{\delta^2_{\rm hor}(R)}{2\sigma^2_{\rm hor}(R)}\right), \tag{5.7}$$

where $\sigma_{\rm hor}(R)$ is the mass variance evaluated when the scale of interest enters the horizon. The mass variance is defined as

$$\sigma^2(R) = \int_0^\infty \tilde{W}^2(kR)\mathscr{P}_\delta(k,t)\frac{{\rm d}k}{k}, \tag{5.8}$$

[2] Reference [89] argues that PBHs can also form on sub-horizon scales which never exit the horizon.

while $\mathscr{P}_\delta(k,t)$ is the power spectrum of the (unsmoothed) density contrast

$$\mathscr{P}_\delta(k,t) \equiv \frac{k^3}{2\pi^2}\langle|\delta_k|^2\rangle, \tag{5.9}$$

and $\tilde{W}(kR)$ is the Fourier transform of the window function used to smooth the density contrast. See Appendix B of Ref. [16] for the detailed calculation of the relationship between the primordial power spectrum of the curvature perturbation and the mass variance at horizon crossing.

The initial PBH mass fraction is equal to the fraction of the energy density of the Universe contained in regions dense enough to form PBHs which is given, as in Press-Schechter theory [113], by

$$\beta(M_{\rm PBH}) = 2\int_{\delta_{\rm c}}^{\infty} P(\delta_{\rm hor}(R))\,{\rm d}\delta_{\rm hor}(R), \tag{5.10}$$

where the right hand side is usually multiplied by a factor of 2, so that all of the mass in the Universe is accounted for. The PBH initial mass fraction is then related to the mass variance by

$$\begin{aligned}\beta(M_{\rm PBH}) &= \frac{2}{\sqrt{2\pi}\sigma_{\rm hor}(R)}\int_{\delta_{\rm c}}^{\infty}\exp\left(-\frac{\delta_{\rm hor}^2(R)}{2\sigma_{\rm hor}^2(R)}\right){\rm d}\delta_{\rm hor}(R),\\ &= {\rm erfc}\left(\frac{\delta_{\rm c}}{\sqrt{2}\sigma_{\rm hor}(R)}\right).\end{aligned} \tag{5.11}$$

Note that if the power spectrum of the density perturbations were exactly scale invariant (so that $\sigma_{\rm hor}$ is independent of R) then the abundance of PBHs would be completely negligible, $\beta(M_{\rm PBH}) \sim \exp(-10^8)$, since on cosmological scales the mass variance is measured to be of order 10^{-5} [32].

The limits on the PBH abundance, $\beta(M_{\rm PBH})$, can be translated into constraints on the power spectrum of the primordial curvature perturbation by first inverting eq. (5.11) to find the limits on the mass variance at horizon crossing, $\sigma_{\rm hor}(R)$. Since the mass variance is given by an integral over the primordial power spectrum, it depends not just on the amplitude of the power spectrum on a single scale, but also its shape on neighbouring scales. In practice, however, if the power spectrum is featureless then it is a good approximation to parameterize it *locally* as a power-law and the constraints depend only weakly (at the per-cent level) on the slope of the power-law [16, 68]. The constraints on the initial abundance of PBHs, which lie in the range $\beta(M_{\rm PBH}) < 10^{-30}$–$10^{-5}$, translate into constraints on the amplitude of the power spectrum of the primordial curvature perturbation in the range $\mathscr{P}_{\mathscr{R}} < 10^{-2}$–$10^{-1}$ [18, 68]. See Fig. 2 of Ref. [68] for a plot of the detailed scale dependence of the constraints on the power spectrum.

The standard calculation as described above assumes that the probability distribution function (pdf) of the perturbations is gaussian. Since PBHs form from the

extremely rare large fluctuations in the tail of the distribution, non-gaussianity can have a significant effect on the abundance of PBHs formed [20, 62]. References [21, 140] jointly constrained the amplitude of the fluctuations and the local non-gaussianity parameters, ($f_{\rm nl}$, $g_{\rm nl}$, etc.) while Ref. [125] constrained the amplitude for two different physically motivated ansatzes for the scaling of the dimensionless moments of the density contrast. For some specific models (e.g. the curvaton where the primordial fluctuations arise from fluctuations of a second light scalar field which is subdominant during inflation [87]) the full non-gaussian pdf is known and can be taken into account directly (e.g. Refs. [19, 140]).

Gamma-ray emission from Ultra Compact Mini Halos [116, 122] (small dark matter halos which form at $z \sim 1000$ from smaller over-densities, with initial amplitude $\delta \sim 10^{-3}$) leads to tighter constraints on the primordial power spectrum than PBHs on scales $k \sim 1$–10^8 Mpc^{-1} [16, 67]. However these constraints rely on the assumption that the dark matter is in the form of self-annihilating Weakly Interacting Massive Particles.

5.4.2 Constraints on Inflation Models

The amplitude of the primordial power spectrum on cosmological scales is measured to be $\mathscr{P}_{\mathscr{R}}(k \approx 10^{-3}\ \text{Mpc}^{-1}) \approx 10^{-10}$ [1, 13, 61] while the PBH limits are of order $\mathscr{P}_{\mathscr{R}} < 10^{-2}$–$10^{-1}$ on scales $k \sim 10^{-2}$–10^{23} Mpc^{-1}. Therefore the PBH limits only constrain models in which the amplitude of the fluctuations is larger on small (physical) scales than on large scales (this is sometimes referred to as a 'blue' spectrum).

In the mid-1990s it was found that for a power-law power spectrum, $\mathscr{P}_{\mathscr{R}} \propto k^{n_{\rm s}-1}$, where $n_{\rm s}$ is the spectral index, PBHs placed a constraint on the spectral index $n_{\rm s} < 1.25$–1.30 [32, 49, 76]. This was tighter than the CMB constraints at that time, however the spectral index is now accurately measured to be $n_{\rm s} = 0.9603 \pm 0.0073$ on cosmological scales [1]. Therefore if the power spectrum were a pure power law on all scales, then the number of PBHs formed would be completely negligible. However only very specific inflation potentials produce a constant spectral index (e.g. Ref. [132]). Generically the power spectrum will deviate from a pure power law and, given the extremely wide range of scales probed by PBHs, it is possible for the amplitude of the perturbation to grow sufficiently with increasing wavenumber that PBHs could be produced in cosmologically interesting numbers.

References [66, 107] used the flow equations for the evolution of the Hubble slow-roll parameters [78] to generate a large ensemble of inflation models. They found that a significant fraction of the models generated (in which inflation is terminated by an auxiliary field) are compatible with all cosmological observations, but have perturbations on small scales which are sufficiently large to overproduce PBHs, and are hence excluded.

There are also specific inflation models that are constrained by PBH over-production. In the running-mass inflation model the false vacuum dominated potential

which arises in softly-broken global supersymmetry is flattened (so that slow-roll inflation, producing a close to scale-invariant power spectrum, can occur on cosmological scales) by quantum corrections [127, 128]. However this can only happen over a limited range of scales, and over a large part of the parameter space the power spectrum grows significantly with decreasing scale and PBHs are over-produced [42, 80, 84]. The power spectrum is also larger on small scales, potentially leading to PBH over-production [80], in hill top inflation models [15], where the potential flattens towards the end of inflation. In this case PBH constraints also exclude otherwise viable regions of parameter space [4, 43]. Modulations in the inflation potential can also enhance the power spectrum [43]. As we will discuss in Sect. 5.5, PBHs can also be produced in interesting numbers in double or multiple-field inflation models, where the primordial perturbation spectrum has a spike on a particular scale.

In many inflation models the reheating process at the end of inflation starts with a period of parametric resonance known as preheating (see e.g. Ref. [88] for an overview). During preheating the amplification of field fluctuations can lead to the generation of large curvature perturbations and avoiding the over-production of PBHs constrains the couplings of the inflaton field [11, 51].

5.5 PBHs as Dark Matter

Assuming general relativity is correct, there is extensive astronomical and cosmological evidence that the majority of the matter in the universe is in the form of non-baryonic cold dark matter (CDM). Since the CDM is non-baryonic, most candidates are new fundamental particles, for instance Weakly Interacting Massive Particles or axions. see e.g. Ref. [12]. As PBHs form before nucleosynthesis they are non-baryonic. Therefore PBHs with $M_{\rm PBH} > 10^{15}$ g, that have lifetime longer than the age of the Universe, are a potential CDM candidate. As we saw in Sect. 5.3 gamma-ray, lensing and dynamical constraints rule out PBHs with 10^{15} g $< M_{\rm PBH} < 10^{20}$ g or $M_{\rm PBH} > 10^{25}$ g making up all of the dark matter. However this leaves a mass window (10^{20} g $< M_{\rm PBH} < 10^{25}$ g) where PBHs can make up all of the CDM (see however Ref. [106]). Unlike other CDM candidates, PBH are not a new fundamental particle. However, as we saw in Sect. 5.2, producing the large over-densities required for PBHs to form does require particle physics beyond the standard model.

Interest in PBHs as a DM candidate peaked in the late 1990s and early 2000s, due to the results at that time of microlensing searches towards the Large Magellanic Cloud. In their first two years of data the MACHO collaboration found 8 events, significantly more than expected due to known stellar populations, and consistent with compact objects with $M_{\rm CO} \sim 0.5 M_\odot \approx 10^{33}$ g making up roughly half of the mass of the MW halo [5]. With subsequent analysis of 5.7 years of data the best fit halo fraction dropped to $\sim$20 % [6]. Limits from star counts [37] and chemical abundance constraints [44] rule-out baryonic objects, such as faint stars or white

dwarves, comprising such a large fraction of the halo, and hence PBHs were an attractive MACHO candidate.

PBHs with $M_{\rm PBH} \sim M_\odot$ would be formed at $t \sim 10^{-6}$ s, around the time of the QCD phase transition. If the QCD phase transition is first order the reduced pressure forces would lead to PBHs forming more easily at this epoch, however the amplitude of the primordial perturbations would still need to be significantly larger than on cosmological scales for an interesting number of PBHs to form [64, 65, 121]. In other words, a feature in the primordial power spectrum is required. Such a feature can be produced in various ways. Reference [63] used a plateau in the inflation potential, while Ref. [137] used multiple scalar fields to generate isocurvature perturbations and hence imprint a feature at a particular scale. In double inflation models, with either a single [138] or multiple scalar fields [45, 71, 115], there are two periods of inflation and the perturbations on small scales, which are produced during the second period of inflation, can be significantly larger than those on cosmological scales.

As discussed in Sect. 5.3.2.2, more recent microlensing results indicate that compact objects in the range 10^{25} g $< M_{\rm CO} < 10^{34}$ g can not make up all of the DM in the MW halo [53, 129]. Lens in the Magellanic clouds and variable stars are now thought to account for some of the events found by the MACHO collaboration [129]. Interest in solar mass PBHs as a CDM candidate has therefore waned, however many of the models constructed to produce solar mass PBHs could, with different parameter values, also produce PBHs in the remaining allowed mass window (e.g. Refs. [69, 120] for the case of double inflation). Another possibility for producing PBH DM is an inflaton potential with a step in its first derivative [14].

Ultimately the possibility of PBH CDM should be tested observationally. The constraints on PBHs with $M_{\rm PBH} \approx 10^{25-26}$ g come from a microlensing search using Kepler data [53]. Future data, from Kepler and WFIRST, will be sensitive to PBHs down to $M_{\rm PBH} \approx 10^{24}$ g [53]. Future space-based gravitational wave detectors will be able to indirectly constrain PBH DM produced from the collapse of large density perturbations in the mass range 10^{20} g $< M_{\rm PBH} < 10^{26}$ g (as discussed in Sect. 5.3.4.2) [119]. Future gravitational wave detectors could also detect PBHs with 10^{17} g $< M_{\rm PBH} < 10^{20}$ g directly as they passes through the Solar System [123], while PBHs with $M_{\rm PBH} \sim 10^{25}$ g could be detected via pulsar timing using the Square Kilometer Array [124]. Finally the oscillations produced when a PBH with $M_{\rm PBH} > 10^{21}$ g passes through a nearby star could be detected by the proposed Stellar Imager [73].

5.6 Summary

In Sect. 5.2 we reviewed the mechanisms via which PBHs can form, namely the collapse of large density fluctuations (Sect. 5.2.1), cosmic string loops (Sect. 5.2.2) or bubble collisions (Sect. 5.2.3). We concentrated mainly on the collapse of large density perturbations. After a review of the original pioneering calculations (Sect. 5.2.1.1) we described more recent developments (Sect. 5.2.1.2), including the

implications of critical collapse for the PBH mass function and determinations of the value of the threshold for PBH formation and its dependence on the shape of the density fluctuations.

We then looked at the observational constraints on the abundance of PBHs from the consequences of their evaporation products (Sect. 5.3.1), their lensing (Sect. 5.3.2) and dynamical effects (Sect. 5.3.3) and their effects on other astrophysical objects and processes (Sect. 5.3.4). The resulting limits on the fraction of the density of the Universe in the form of PBHs at the time they form, $\beta(M_{\rm PBH})$, depend on the PBH mass, $M_{\rm PBH}$, and lie in the range 10^{-5}–10^{-30}.

In Sect. 5.4.1 we explored how the PBH abundance constraints can be translated into limits on the primordial power spectrum, and how these limits can be used to constrain models of inflation (Sect. 5.4.2). Avoiding PBH over-production constrains the parameter space of otherwise viable inflation models.

Finally we discussed PBHs as a cold dark matter candidate (Sect. 5.5). PBHs with mass in the range 10^{20} g $< M_{\rm PBH} < 10^{25}$ g are a viable CDM candidate. To produce an interesting number of PBHs in this mass window requires a feature in the primordial power spectrum, and several inflation models have been constructed which achieve this. Various upcoming experiments/observations will be able to detect, or constrain, PBH DM.

Acknowledgments AMG is funded by the STFC.

References

1. Ade, P.A.R. et al.: Planck 2013 results. XXII. Constraints on inflation (2013). arXiv:1303.5082
2. Ade, P.A.R. et al.: Planck 2013 results. XXV. Searches for cosmic strings and other topological defects (2013). arXiv:1303.5085
3. Afshordi, N., McDonald, P., Spergel, D.N.: Primordial black holes as dark matter: the power spectrum and evaporation of early structures. Astrophys. J. **594**, 71–74 (2003)
4. Alabidi, L., Kohri, K.: Generating primordial black holes via hilltop-type inflation models. Phys. Rev. D **80**, 063511 (2009)
5. Alcock, C., et al.: The MACHO project LMC microlensing results from the first two years and the nature of the galactic dark halo. Astrophys. J. **486**, 697–726 (1997)
6. Alcock, C., et al.: The MACHO project: microlensing results from 5.7 years of LMC observations. Astrophys. J. **542**, 281–307 (2000)
7. Alcock, C., et al.: MACHO Project limits on black hole dark matter in the 1–30 Solar mass range. Astrophys. J. **550**, 169–172 (2001)
8. Bahcall, J.N., Hut, P., Tremaine, S.: Maximum mass of objects that constitute unseen disk material. Astrophys. J. **290**, 15–20 (1985)
9. Bardeen, J.M., Bond, J.R., Kaiser, N., Szalay, A.S.: The statistics of peaks of gaussian random fields. Astrophys. J. **304**, 15–61 (1986)
10. Barnacka, A., Glicenstein, J.F., Moderski, R.: New constraints on primordial black holes abundance from femtolensing of gamma-ray bursts. Phys. Rev. D **86**, 043001 (2012)
11. Bassett, B.A., Tsujikawa, S.: Inflationary preheating and primordial black holes. Phys. Rev. D **63**, 123503 (2001)
12. Bertone, G., Hooper, D., Silk, J.: Particle dark matter: evidence, candidates and constraints. Phys. Rept. **405**, 279–390 (2005)

13. Bird, S., Peiris, H.V., Viel, M.: Minimally parametric power spectrum reconstruction from the Lyman-alpha forest. Mon. Not. Roy. Astron. Soc. **413**, 1717–1728 (2011)
14. Blais, D., Kiefer, C., Polarski, D.: Can primordial black holes be a significant part of dark matter? Phys. Lett. B **535**, 11–16 (2002)
15. Boubeker, L., Lyth, D.H.: Hilltop inflation. JCAP **0507**, 010 (2005)
16. Bringmann, T., Scott, P., Akrami, Y.: Improved constraints on the primordial power spectrum at small scales from ultra compact minihalos. Phys. Rev. D **85**, 125027 (2012)
17. Brodie, J.P., Strader, J.: Extragalactic globular clusters and galaxy formation. Ann. Rev. Astron. Astrophys. **44**, 193–267 (2006)
18. Bugaev, E.V., Klimai, P.A.: Constraints on amplitudes of curvature perturbations from primordial black holes. Phys. Rev. D **79**, 103511 (2009)
19. Bugaev, E.V., Klimai, P.A.: Primordial black hole constraints for curvaton models with predicted large non-Gaussianity. Int. J. Mod. Phys. D **22**, 1350034 (2013)
20. Bullock, J.S., Primack, J.R.: Nongaussian fluctuations and primordial black holes from inflation. Phys. Rev. D **55**, 7423–7439 (1997)
21. Byrnes, C.T., Copeland, E.J., Green, A.M.: Primordial black holes as a tool for constraining non-gaussianity. Phys. Rev. D **86**, 043512 (2012)
22. Caldwell, R.R., Caspar, P.: Formation of black holes from collapsed cosmic string loops. Phys. Rev. D **53**, 3002–3010 (1996)
23. Canizares, C.R.: Manifestations of a cosmological density of compact objects in quasar light. Astrophys. J. **263**, 507–517 (1982)
24. Capela, F., Pshirkov, M., Tinyakov, P.: Constraints on primordial black holes as dark matter candidates from star formation. Phys. Rev. D **87**, 023507 (2013)
25. Cappela, F., Pshirkov, M., Tinyakov, P.: Constraints on primordial black holes as dark matter candidates from capture by neutron stars. Phys. Rev. D **87**, 12534 (2013)
26. Capela, F., Pshirkov, M., Tinyakov, P.: arXiv:1402.4671 [astro-ph.CO]
27. Carr, B.J.: The primordial black hole mass spectrum. Astrophys. J. **201**, 1–19 (1975)
28. Carr, B.J.: Some cosmological consequences of primordial black-hole evaporations. Astrophys. J. **206**, 8–25 (1976)
29. Carr, B.J.: Pregalactic black hole accretion and the thermal history of the universe. Mon. Not. Roy. Astron. Soc. **194**, 639–668 (1981)
30. Carr, B.J.: Primordial black holes-recent development. ECONF **C041213**, 0204 (2004)
31. Carr, B.J., Hawking, S.W.: Black holes in the early Universe. Mon. Not. Roy. Astron. Soc. **168**, 399–415 (1974)
32. Carr, B.J., Lidsey, J.E.: Primordial black holes and generalized constraints on chaotic inflation. Phys. Rev. D **48**, 543–553 (1993)
33. Carr, B.J., Sakellariadou, M.: Dynamical constraints on dark compact objects. Astrophys. J. **516**, 195–220 (1999)
34. Carr, B.J., Gilbert, J.H., Lidsey, J.E.: Black hole relics and inflation: limits on blue perturbation spectra. Phys. Rev. D **50**, 4853–4867 (1994)
35. Carr, B.J., Kohri, K., Yuuiti, S., Yokoyama, J.: New cosmological constraints on primordial black holes. Phys. Rev. D **81**, 104019 (2010)
36. Chaname, J., Gould, A.: Disk and halo wide binaries from the revised Luyten catalog: probes of star formation and MACHO dark matter. Astrophys. J. **601**, 289–310 (2004)
37. Charlot, S., Silk, J.: Signature of white dwarf galaxy halos. Astrophys. J. **445**, 124–132 (1995)
38. Choptuik, M.W.: Universality and scaling in gravitational collapse of a massless scalar field. Phys. Rev. Lett. **70**, 9–12 (1993)
39. Crawford, M., Schramm, D.N.: Spontaneous generation of density perturbations in the early universe. Nature **298**, 538–540 (1982)
40. Dalcanton, J.J., et al.: Observational limits on Omega in stars, brown dwarfs, and stellar remnants from gravitational microlensing. Astrophys. J **424**, 550–568 (1994)
41. Doroshkevich, A.G.: Spatial structure of perturbations and origin of galactic rotation in fluctuation theory. Astrophys. **6**, 320–330 (1970)

42. Drees, M., Erfani, E.: Running-mass inflation model and primordial black holes. JCAP **1104**, 005 (2011)
43. Erfani, E.: arXiv:1311.3090 [astro-ph.CO]
44. Fields, B.D., Freese, K., Graff, D.S.: Chemical abundance constraints on white dwarfs as halo dark matter. Astrophys. J. **534**, 265–276 (2000)
45. Garcia-Bellido, J., Linde, A.D., Wands, D.: Density perturbations and black hole formation in hybrid inflation. Phys. Rev. D **54**, 6040–6058 (1996)
46. Garriga, J., Sakellariadou, M.: Effects of friction on cosmic strings. Phys. Rev. D **48**, 2502–2525 (1993)
47. Gould, A.: Femtolensing of gamma-rays bursters. Astrophys. J. **386**, 5–7 (1992)
48. Green, A.M.: Supersymmetry and primordial black hole abundance constraints. Phys. Rev. D **60**, 063516 (1999)
49. Green, A.M., Liddle, A.R.: Constraints on the density perturbation spectrum from primordial black holes. Phys. Rev. D **56**, 6166–6174 (1997)
50. Green, A.M., Liddle, A.R.: Critical collapse and the primordial black hole initial mass function. Phys. Rev. D **60**, 063509 (1999)
51. Green, A.M., Malik, K.A.: Primordial black hole production due to preheating. Phys. Rev. D **64**, 021301 (2001)
52. Green, A.M., Liddle, A.R., Malik, K.A., Sasaki, M.: A new calculation of the mass fraction of primordial black holes. Phys. Rev. D **70**, 041502 (2004)
53. Griest, K., Cieplak, A.M., Lehner, M.J.: New limits on primordial black hole dark matter from an analysis of Kepler source microlensing. Phys Rev. Lett. **111**, 181302 (2013)
54. Harada, T., Yoo, C.-M., Kohri, K.: Threshold of primordial black hole formation. Phys. Rev. D **88**, 084051 (2013)
55. Hawking, S.H.: Gravitationally collapsed objects of very low mass. Mon. Not. Roy. Astron. Soc. **152**, 75–78 (1971)
56. Hawking, S.H.: Black hole explosions. Nature **248**, 30–31 (1974)
57. Hawking, S.H.: Black holes from cosmic strings. Phys. Lett. B **231**, 237–239 (1987)
58. Hawking, S.H., Moss, I.G., Stewart, J.M.: Bubble collisions in the very early universe. Phys. Rev. D. **26**, 2681–2693 (1982)
59. Heckler, A.F.: On the formation of a Hawking radiation photosphere around microscopic black holes. Phys. Rev. D **55**, 480–488 (1997)
60. Heckler, A.F.: Calculation of the emergent spectrum and observation of primordial black holes. Phys. Rev. Lett. **78**, 3430–3433 (1997)
61. Hlozek, R., et al.: The Atacama Cosmology Telescope: a measurement of the primordial power spectrum. Astrophys. J. **749**, 90–99 (2012)
62. Ivanov, P.: Nonlinear metric perturbations and production of primordial black holes. Phys. Rev. D **57**, 7145–7154 (1998)
63. Ivanov, P., Naselsky, P., Novikov, I.: Inflation and primordial black holes as dark matter. Phys. Rev. D **50**, 7173–7178 (1994)
64. Jedamzik, K.: Primordial black hole formation during the QCD epoch. Phys. Rev. D **55**, 5871–5875 (1997)
65. Jedamzik, K., Niemeyer, J.: Primordial black hole formation during first order phase transitions. Phys. Rev. D **59**, 124014 (1999)
66. Josan, A.S., Green, A.M.: Constraints from primordial black hole formation at the end of inflation. Phys. Rev. D **82**, 047303 (2010)
67. Josan, A.S., Green, A.M.: Gamma-rays from ultracompact minihalos: potential constrains on the primordial curvature perturbation. Phys. Rev. D **82**, 083527 (2010)
68. Josan, A.S., Green, A.M., Malik, K.A.: Generalised constraints on the curvature perturbation from primordial black holes. Phys. Rev. D **79**, 103520 (2009)
69. Kanazawa, T., Kawasaki, M., Yanagida, T.: Double inflation in supergravity and the primordial black hole formation. Phys. Lett. B **482**, 174–172 (2000)
70. Kassiola, A., Kovner, I., Blandford, R.D.: Bounds on intergalactic compact objects from observations of compact radio sources. Astrophys. J. **381**, 6–13 (1991)

71. Kawasaki, M., Sugiyama, N., Yanagida, T.: Primordial black hole formation in a double inflation model in supergravity. Phys. Rev. D **57**, 6050–6056 (1998)
72. Kawasaki, M., Kzunori, K., Moroi, T.: Hadronic decay of late-decaying particles and Big-Bang Nucleosynthesis. Phys. Lett. B **625**, 7–12 (2005)
73. Kesden, M., Hanasoge, S.: Transient solar oscillations driven by primordial black holes. Phys. Rev. Lett. **107**, 111101 (2011)
74. Khlopov, M.Y., Polnarev, A.G.: Primordial black holes as a cosmological test of grand unification. Phys. Lett. B **97**, 383–387 (1980)
75. Khlopov, M.Y., Barrau, A., Julien, G.: Gravitino production by primordial black hole evaporation and constraints on the inhomogeneity of the early universe. Class. Quant. Grav. **23**, 1875–1882 (2006)
76. Kim, H.I., Lee, C.H.: Constraints on the spectral index from primordial black holes. Phys. Rev. D **54**, 6001–6007 (1996)
77. Kim, H.I., Lee, C.H., MacGibbon, J.H.: Diffuse gamma-ray background and primordial black hole constraints on the spectral index of density fluctuations. Phys. Rev. D **59**, 064004 (1999)
78. Kinney, W.H.: Inflation: flow, fixed points and observables to arbitrary order in slow roll. Phys. Rev. D **66**, 083508 (2002)
79. Kohri, K., Yokoyama, J.: Primordial black holes and primordial nucleosynthesis. 1. Effects of hadron injection from low mass holes. Phys. Rev. D **61**, 023501 (2000)
80. Kohri, K., Lyth, D.H., Melchiorri, A.: Black hole formation and slow-roll inflation. JCAP **0804**, 038 (2008)
81. Kopp, M., Hofmann, S., Weller, J.: Separate universes do not constrain primordial black hole formation. Phys. Rev. D **83**, 124025 (2011)
82. La, D., Steinhardt, P.J.: Bubble percolation in extended inflationary models. Phys. Lett. B **220**, 375 (1989)
83. Lacey, C.G., Ostriker, J.P.: Massive black holes in galactic halos? Astrophys. J. **299**, 633–652 (1985)
84. Leach, S.M., Grivell, I.J., Liddle, A.R.: Black hole constraints on the running mass inflation model. Phys. Rev. D **62**, 043516 (2000)
85. Lemoine, M.: Moduli constraints on primordial black holes. Phys. Lett. B **481**, 333–338 (2000)
86. Lindley, D.: Primordial black holes and the deuterium abundance. Mon. Not. Roy. Astron. Soc. **193**, 593–601 (1980)
87. Lyth, D.H., Wands, D.: Generating the curvature perturbation without an inflation. Phys. Lett. B **254**, 5–14 (2002)
88. Lyth, D.H., Liddle, A.R.: The Primordial Density Perturbation: Cosmology, Inflation and the Origin of Structure. Cambridge University Press, Cambridge (2009)
89. Lyth, D.H., Malik, K.A., Sasaki, M., Zaballa, I.: Forming sub-horizon black holes at the end of inflation. JCAP **0601**, 011 (2006)
90. MacGibbon, J.H.: Can Planck-mass relics of evaporating black holes close the universe? Nature **329**, 308–309 (1987)
91. MacGibbon, J.H., Webber, B.R.: Quark and gluon jet emission from primordial black holes: The instantaneous spectra. Phys. Rev. D **41**, 3052–3079 (1990)
92. MacGibbon, J.H., Carr, B.J.: Cosmic rays from primordial black holes. Astrophys. J. **371**, 447–469 (1991)
93. MacGibbon, J.H., Carr, B.J., Page, D.N.: Do evaporating black holes form photospheres? Phys. Rev. D **78**, 064043 (2008)
94. Meszaros, P.: Primeval black holes and galaxy formation. Astron. Astrophys. **38**, 5–13 (1975)
95. Miyama, S., Sato, K.: The upper bound of the number density of primordial black holes from the Big Bang nucleosynthesis. Prog. Theor. Phys. **59**, 1012–1013 (1978)
96. Musco, I., Miller, J.C.: Primordial black hole formation in the early universe: critical behaviour and self-similarity. Class. Quant. Grav. **30**, 145009 (2013)
97. Musco, I., Miller, J.C., Rezzolla, L.: Computations of primordial black hole formation. Class. Quant Grav. **22**, 1405–1424 (2005)

98. Musco, I., Miller, J.C., Polnarev, A.: Primordial black hole formation in the radiative era: investigation of the critical nature of the collapse. Class. Quant. Grav. **26**, 235001 (2009)
99. Nadezhin, D.K., Novikov, I.D., Polnarev, A.G.: Hydrodynamics of primordial black hole formation. Sov. Astron. **22**, 129–138 (1978)
100. Nakama, T., Harada, T., Polnarev, A.G., Yokoyama, J.: Identifying the most crucial parameters of the initial curvature profile for primordial black hole formation (2013). arXiv:1310.3007
101. Naselskii, P.D.: Hydrogen recombination kinetics in the presence of low-mass primordial black holes. Sov. Astron. Lett. **4**, 209–211 (1978)
102. Niemeyer, J.C., Jedamzik, K.: Near-critical gravitational collapse and the initial mass function of primordial black holes. Phys. Rev. Lett. **80**, 5481–5484 (1998)
103. Niemeyer, J.C., Jedamzik, K.: Dynamics of primordial black hole formation. Phys. Rev. D **59**, 124013 (1999)
104. Paczynski, B.: Gravitational microlensing by the galactic halo. Astrophys. J. **304**, 1–5 (1986)
105. Page, D.N., Hawking, S.H.: Gamma rays from primordial black holes. Astrophys. J. **206**, 1–7 (1976)
106. Pani, P., Loeb, A.: Exclusion of the remaining mass window for primordial black holes as the dominant constituent of dark matter (2014). arXiv:1401.3025
107. Peiris, H.V., Easther, R.: Primordial black holes, eternal inflation and the inflationary parameter space after WMAP 5. JCAP **0807**, 024 (2008)
108. Polnarev, A.G., Zembowicz, R.: Formation of primordial black holes by cosmic strings. Phys. Rev. D **43**, 1106–1109 (1991)
109. Polnarev, A.G., Khlopov, M.Y.: Dustlike stages in the early universe and constraints on the primordial black hole spectrum. Sov. Astron. **26**, 391–395 (1992)
110. Polnarev, A.G., Musco, I.: Curvature profiles as initial conditions for primordial black hole formation. Class. Quant. Grav. **24**, 1405–1432 (2007)
111. Polnarev, A.G., Nakama, T., Yokoyama, J.: Self-consistent initial conditions for primordial black hole formation. JCAP **1209**, 027 (2012)
112. Press, W.H., Gunn, J.E.: Method for detecting a cosmological density of condensed objects. Astrophys. J. **185**, 397–412 (1973)
113. Press, W.H., Schechter, P.: Formation of galaxies and clusters of galaxies by self similar gravitational condensation. Astrophys. J. **187**, 425–438 (1974)
114. Quinn, D.P., et al.: On the reported death of the MACHO era. Mon. Not. Roy. Astron. Soc. **396**, 11–15 (2009)
115. Randall, L., Soljacic, M., Guth, A.H.: Supernatural inflation: inflation from supersymmetry with no (very) small parameters. Nucl. Phys. B **472**, 377–408 (1996)
116. Ricotti, M., Gould, A.: A new probe of dark matter and high-energy universe using microlensing. Astrophys. J. **707**, 979–987 (2009)
117. Ricotti, M., Ostriker, J.P., Mack, K.J.: Effect of primordial black holes on the cosmic microwave background and cosmological parameter estimates. Astrophys. J. **680**, 829 (2008)
118. Saito, R., Yokoyama, J.: Gravitational wave background as a probe of the primordial black hole abundance. Phys. Rev. Lett. **102**, 161101 (2009). (erratum-ibid 107 069901 (2011))
119. Saito, R., Yokoyama, J.: Gravitational-wave constraints on the abundance of primordial black holes. Prog. Theor. Phys. **123**, 867–886 (2010). (erratum-ibid 126 351–352 (2011))
120. Saito, R., Yokoyama, J., Nagata, R.: Single-field inflation, anomalous enhancement of superhorizon fluctuations, and non-Gaussianity in primordial black hole formation. JCAP **024**, 0806 (2008)
121. Schmid, C., Schwarz, D.J., Widerin, P.: Amplification of cosmological inhomogeneities from the QCD transition. Phys. Rev. D **59**, 043517 (1999)
122. Scott, P., Sivertsson, S.: Gamma-rays from ultra compact primordial dark matter mini halos. Phys. Rev. Lett. **103**, 211301 (2009)
123. Seto, N., Cooray, A.: Search for small-mass black hole dark matter with space-based gravitational wave detectors. Phys. Rev. D **70**, 063512 (2004)
124. Seto, N., Cooray, A.: Searching for primordial black hole dark matter with pulsar timing arrays. Astrophys. J. **659**, 33–36 (2007)

125. Shandera, S., Erickcek, A.L., Scott, P., Galarza, J.Y.: Number counts and non-gaussianity. Phys. Rev. D **88**, 103506 (2013)
126. Shibata, M., Sasaki, M.: Black hole formation in the Friedmann universe: Formulation and computation in numerical relativity. Phys. Rev. D **60**, 084002 (1999)
127. Stewart, E.D.: Flattening the inflaton's potential with quantum corrections. Phys. Lett. B **391**, 34–38 (1997)
128. Stewart, E.D.: Flattening the inflaton's potential with quantum corrections. 2. Phys. Rev. D **56**, 2019–2023 (1997)
129. Tisserand, P., et al.: Limits on the Macho content of the galactic halo from the EROS-2 survey of the Magellanic clouds. Astron. Astrophys. **469**, 387–404 (2007)
130. Vainer, B.N., Naselskii, P.D.: Observable consequences of the evaporation of low-mass primordial black holes. Sov. Astron. Lett. **3**, 76–78 (1977)
131. Vainer, B.N., Dryzhakova, O.V., Naselskii, P.D.: Primordial black holes and cosmological nucleosynthesis. Sov. Astron. Lett. **4**, 344–348 (1978)
132. Vallinotto, A., Copeland, E.J., Kolb, E.W., Liddle, A.R., Steer, D.A.: Inflationary potentials yielding constant scalar perturbation spectral indices. Phys. Rev. D **69**, 103519 (2004)
133. Vilenkin, A., Shellard, E.P.S.: Strings and Other Topological Defects. Cambridge University Press, Cambridge (1994)
134. Weinberg, M.D., Shapiro, S.L., Wasserman, I.: The dynamical fate of wide binaries in the solar neighborhood. Astrophys. J. **312**, 367–389 (1987)
135. Wichoski, U.F., MacGibbon, J.H., Brandenberger, R.H.: High-energy neutrinos, photons and cosmic ray fluxes from VHS cosmic strings. Phys. Rev. D **65**, 063005 (2002)
136. Wilkinson, P., et al.: Limits on the cosmological abundance of supermassive compact objects from a search for multiple imaging in compact radio sources. Phys. Rev. Lett. **86**, 584–587 (2001)
137. Yokoyama, J.: Formation of MACHO primordial black holes in inflationary cosmology. Astron. Astrophys. **318**, 673–679 (1997)
138. Yokoyama, J.: Chaotic new inflation and formation of primordial black holes. Phys. Rev. D **58**, 083510 (1998)
139. Yokoyama, J.: Cosmological constraints on primordial black holes produced in the near critical gravitational collapse. Phys. Rev. D **58**, 107502 (1998)
140. Young, S., Byrnes, C.T.: Primordial black holes in non-Gaussian regimes. JCAP **1208**, 052 (2013)
141. Zeldovich, Y.B., Novikov, I.D.: The hypothesis of cores retarded during expansion and the hot cosmological model. Sov. Astron. **10**, 602–603 (1967)
142. Zeldovich, Y.B., Starobinskii, A.A., Khlopov, M.Y., Chechetkin, V.M.: Primordial black holes and the deuterium problem. Sov. Astron. Lett. **3**, 110–112 (1977)

Chapter 6
Self-gravitating Bose-Einstein Condensates

Pierre-Henri Chavanis

Abstract Bose-Einstein condensates play a major role in condensed matter physics. Recently, it has been suggested that they could play an important role in astrophysics also. Indeed, dark matter halos could be gigantic quantum objects made of Bose-Einstein condensates. The pressure arising from the Heisenberg uncertainty principle or from the repulsive scattering of the bosons could stabilize dark matter halos against gravitational collapse and lead to smooth core densities instead of cuspy density profiles in agreement with observations. In order to reproduce the scales of dark matter halos, the mass of the bosons may range from $10^{-24}\,\mathrm{eV/c^2}$ to a few $\mathrm{eV/c^2}$ depending whether they interact or not. At the scale of galaxies, Newtonian gravity can be used so the evolution of the wave function is governed by the Gross-Pitaevskii-Poisson system. Self-gravitating Bose-Einstein condensates have also been proposed to describe boson stars. For these compact objects, one must use general relativity and couple the Klein-Gordon equation to the Einstein field equations. In that context, it has been proposed that neutron stars could be Bose-Einstein condensate stars due to their superfluid core. Indeed, the neutrons could form Cooper pairs and behave as bosons. In that case, the maximum mass of the neutron stars depends on the scattering length of the bosons and can be as large as $2M_\odot$. This could explain recent observations of neutron stars with a mass much larger than the Oppenheimer-Volkoff limit of $0.7M_\odot$ obtained by assuming that neutron stars are ideal fermion stars. Self-gravitating Bose-Einstein condensates may also find applications in the physics of black holes. For example, when the scattering length of the bosons is negative, a Newtonian self-gravitating Bose-Einstein condensate becomes unstable above a critical mass and undergoes a gravitational collapse leading ultimately to a singularity. On the other hand, stable boson stars with a positive scattering length could mimic supermassive black holes that reside at the center of galaxies. Finally, it has been proposed that microscopic quantum black holes could be Bose-Einstein condensates of gravitons. This contribution discusses fundamental aspects of the physics of self-gravitating Bose-Einstein condensates

P.-H. Chavanis (✉)
Laboratoire de Physique Théorique (IRSAMC), CNRS and UPS,
Université de Toulouse, Toulouse, France
e-mail: chavanis@irsamc.ups-tlse.fr

X. Calmet (ed.), *Quantum Aspects of Black Holes*,
Fundamental Theories of Physics 178, DOI 10.1007/978-3-319-10852-0_6

and considers recent applications in astrophysics, cosmology and black hole physics with promising perspectives.

Keywords Bose-Einstein condensates · Self-gravitating systems · Dark matter halos · Quantum black holes

6.1 Introduction

According to contemporary cosmology, the universe is made of about 70 % dark energy, 25 % dark matter, and 5 % baryonic (visible) matter [1]. Thus, the overwhelming preponderance of matter and energy in the universe is believed to be dark, i.e. unobservable by telescopes. The dark energy is responsible for the accelerated expansion of the universe. Its origin is mysterious and presumably related to the cosmological constant or to some form of exotic fluid with negative pressure such as the Chaplygin gas [2]. On the other hand, dark matter is necessary to account for the observed flat rotation curves of galaxies [3]. Its nature is one of the most important puzzles in particle physics and cosmology. Many candidates for dark matter have been proposed, the most popular ones being the axions and the weakly interacting massive particles (WIMPs) [4].

Dark matter is usually modeled as a cold classical collisionless gas with vanishing pressure. In the cold dark matter (ΛCDM) model, primordial density fluctuations are generated during the inflation and become the seeds of the bottom-up structure formation model. The ΛCDM model successfully describes the accelerated expansion of the universe, the temperature fluctuations of the cosmic microwave background (CMB), and the large-scale structures of the universe [5]. However, it seems to encounter many problems at the scale of galactic or sub-galactic structures. Indeed, ΛCDM simulations [6] lead to r^{-1} cuspy density profiles at galactic centers (in the scales of the order of 1 kpc and smaller) while most rotation curves indicate a smooth core density [7]. In addition, the predicted number of satellite galaxies around each galactic halo is far beyond what we see around the Milky Way [8].

These problems might be solved, without altering the virtues of the ΛCDM model, if the dark matter is composed of Bose-Einstein condensates (BECs) [9]. The wave properties of the dark matter may stabilize the system against gravitational collapse providing halo cores instead of cuspy profiles. The resulting coherent configuration may be understood as the ground state of some gigantic bosonic atom where the boson particles are condensed in a single macroscopic quantum state $\psi(\mathbf{r})$. In these models, the formation of dark matter structures at small scales is suppressed by quantum mechanics. This property could alleviate the problems of the ΛCDM model such as the cusp problem and the missing satellite problem.

At the scale of galaxies, the Newtonian approximation is very good so the evolution of the wave function $\psi(\mathbf{r}, t)$ is governed by the Gross-Pitaevskii-Poisson (GPP) system. Using the Madelung [10] transformation, the Gross-Pitaevskii (GP) equation

[11–14] turns out to be equivalent to hydrodynamic (Euler) equations involving an isotropic pressure due to short-range interactions (scattering) and an anisotropic quantum pressure arising from the Heisenberg uncertainty principle. At large scales, quantum effects are negligible and one recovers the classical hydrodynamic equations of the ΛCDM model which are remarkably successful in explaining the large-scale structure of the universe. At small scales, gravitational collapse is prevented by the repulsive scattering or by the uncertainty principle. Quantum mechanics may therefore be a way to solve the problems of the ΛCDM model.

The possibility that dark matter could be in the form of BECs has a long history (see a short review in [15, 16]). In some works [17–34], it is assumed that the bosons have no self-interaction. In that case, gravitational collapse is prevented by the Heisenberg uncertainty principle which is equivalent to a quantum pressure. This leads to a mass-radius relation $MR = 9.95\,\hbar^2/\mathrm{Gm}^2$. In order to account for the mass and size of dark matter halos, the mass of the bosons must be extremely small, of the order of $m \sim 10^{-24}\,\mathrm{eV}/c^2$. Ultralight scalar fields like axions may have such small masses (multidimensional string theories predict the existence of bosonic particles down to masses of the order of $m \sim 10^{-33}\,\mathrm{eV/c}^2$). This corresponds to "fuzzy cold dark matter" [23]. In other works [35–48], it is assumed that the bosons have a repulsive self-interaction measured by the scattering length $a > 0$. In that case, gravitational collapse is prevented by the pressure arising from the scattering. In the Thomas-Fermi (TF) approximation which amounts to neglecting the quantum pressure, the resulting structure is equivalent to a polytrope of index $n = 1$. Its radius is given by $R = \pi(a\hbar^2/Gm^3)^{1/2}$, independent on its mass M. For $a \sim 10^6$ fm, corresponding to the values of the scattering length observed in terrestrial BEC experiments [49], this gives a boson mass $m \sim 1\,\mathrm{eV/c}^2$ much larger than the mass $m \sim 10^{-24}\,\mathrm{eV}/c^2$ required in the absence of self-interaction. This may be more realistic from a particle physics point of view. The general mass-radius relation of self-gravitating BECs at $T = 0$ with arbitrary scattering length, connecting the non-interacting limit ($a = 0$) to the TF limit ($GM^2\,ma/\hbar^2 \gg 1$), has been determined analytically and numerically in [15, 16].

Since atoms like ^{7}Li have negative scattering lengths in terrestrial BEC experiments [49], it may be relevant to consider the possibility of self-gravitating BECs with attractive self-interaction ($a < 0$). In that case, there exist a maximum mass $M_{\max} = 1.01\hbar/\sqrt{|a|Gm} = 5.07M_P/\sqrt{|\lambda|}$, where $\lambda = 8\pi amc/\hbar$ is the self-interaction constant and $M_P = (\hbar c/G)^{1/2}$ is the Planck mass, above which the BEC collapses [15, 16]. In most applications, this mass is extremely small (when $|\lambda| \sim 1$ it is of the order of the Planck mass $M_P = 2.18 \times 10^{-8}$ kg!) so that the collapse of the BEC is very easily realized in the presence of attractive self-interactions. This may lead to the formation of supermassive black holes at the center of galaxies. On the other hand, when the BEC hypothesis is applied in a cosmological context, an attractive self-interaction can enhance the Jeans instability and accelerate the formation of structures in the universe [50].

Self-gravitating BECs have also been proposed to describe boson stars [51–73]. For these compact objects, we must use general relativity and couple the

Klein-Gordon equation to the Einstein field equations. Initially, the study of boson stars was motivated by the axion field, a pseudo-Nambu-Goldstone boson of the Peccei-Quinn phase transition that was proposed as a possible solution to the strong CP problem in QCD. In the early works of Kaup [51] and Ruffini and Bonazzola [52], it was assumed that the bosons have no self-interaction. This leads to a maximum mass of boson stars equal to $M_{Kaup}=0.633M_P^2/m$. Above that mass no equilibrium configuration exists. In that case, the system collapses to a black hole. This maximum mass is much smaller than the maximum mass $M_{OV}=0.376M_P^3/m^2$ of fermion stars determined by Oppenheimer and Volkoff [74] in general relativity. They differ by a factor $m/M_P\ll 1$. This is because boson stars are stopped from collapsing by Heisenberg's uncertainty principle while for fermion stars gravitational collapse is avoided by Pauli's exclusion principle. For $m\sim 1\,\mathrm{GeV}/c^2$, corresponding to the typical mass of the neutrons, the Kaup mass $M_{Kaup}\sim 10^{-19}M_\odot$ is very small while $M_{OV}\sim 1M_\odot$. This describes mini boson stars like axion black holes. The mass of these mini boson stars may be too small to be astrophysically relevant. They could play a role, however, if they exist in the universe in abundance [53] or if the axion mass is extraordinary small leading to macroscopic objects with a mass M_{Kaup} comparable to the mass of the sun (or even larger) [71]. For example, axionic boson stars could account for the mass of MACHOs (between 0.3 and $0.8M_\odot$) if the axions have a mass $m\sim 10^{-10}\,\mathrm{eV}/c^2$ [68]. It has also been proposed that stable boson stars with a boson mass $m\sim 10^{-17}\,\mathrm{eV}/c^2$ could mimic supermassive black holes ($M\sim 10^6M_\odot$, $R\sim 10^7\,\mathrm{km}$) that reside at the center of galaxies [69, 72]. On the other hand, Colpi et al. [56] assumed that the bosons have a repulsive self-interaction. In the TF approximation, this leads to a maximum mass $M_{\max}=0.0612\,\sqrt{\lambda}M_P^3/m^2$ which, for $\lambda\sim 1$, is of the order of the maximum mass of fermion stars $M_{OV}=0.376M_P^3/m^2$. The self-interaction has the same effect on the bosons as the exclusion principle on the fermions. It plays the role of an interparticle repulsion (for $\lambda>0$) that dominates over uncertainty pressure and prevents catastrophic gravitational collapse. Therefore, for $m\sim 1\,\mathrm{GeV}/c^2$ and $\lambda\sim 1$, this leads to a maximum mass of the order of the solar mass $M_\odot$, similar to the mass of neutron stars, which is much larger than the maximum mass $M_{Kaup}\sim 10^{-19}M_\odot$ obtained in the absence of self-interaction (an interpolation formula giving the maximum mass for any value of the self-interaction constant λ is given in [15]). Therefore, self-interaction can significantly change the physical dimensions of boson stars, making them much more astrophysically interesting. For example, stellar mass boson stars could constitute a part of dark matter [56, 68]. On the other hand, Chavanis and Harko [73] have proposed that, due to the superfluid properties of the core of neutron stars, the neutrons (fermions) could form Cooper pairs and behave as bosons of mass $2m_n$, where $m_n=0.940\,\mathrm{GeV/c^2}$ is the mass of the neutrons. Therefore, neutron stars could actually be BEC stars! Since the maximum mass of BEC stars $M_{\max}=0.0612\,\sqrt{\lambda}M_P^3/m^2=0.307\hbar c^2\sqrt{a}/(Gm)^{3/2}$ depends on the self-interaction constant λ (or scattering length a), this allows to overcome the (fixed) maximum mass of neutron stars $M_{OV}=0.376M_P^3/m^2=0.7M_\odot$ determined by Oppenheimer and Volkoff [74] by modeling a neutron star as an ideal gas of fermions of mass m_n. By taking a scattering length of the order of 10–20 fm, we obtain a maximum mass of the order of $2M_\odot$ [73]. This could account for the

recently observed neutron stars with masses in the range of 2–2.4$M_\odot$ much larger than the Oppenheimer-Volkoff limit. For $M > M_{\rm max}$, nothing prevents the gravitational collapse of the star which becomes a black hole. On the other hand, for a boson mass of the order of $m \sim 1\,{\rm MeV/c^2}$ and a self-interaction constant $\lambda \sim 1$ we get $M_{\rm max} \sim 10^6 M_\odot$ and $R_{\rm min} \sim 10^7$ km. These parameters are reminiscent of supermassive black holes in active galactic nuclei, so that stable self-interacting boson stars with $m \sim 1\,{\rm MeV/c^2}$ could be an alternative to black holes at the center of galaxies [67]. Finally, it has been proposed recently that microscopic quantum black holes could be BECs of gravitons stuck at a critical point [75, 76]. We will show that these results can be understood easily in terms of the Kaup mass and Kaup radius.

This contribution is organized as follows. In Sect. 6.2 we provide general results concerning the GPP system describing Newtonian self-gravitating BECs. We specifically consider the non-interacting limit and the TF limit. In Sect. 6.3, we obtain an analytical approximate expression of the mass-radius relation of Newtonian self-gravitating BECs with positive or negative scattering length by using a Gaussian ansatz for the wave function and developing a simple mechanical analogy. In Sect. 6.4, we consider astrophysical applications of Newtonian self-gravitating BECs to dark matter halos. Finally, in Sect. 6.5, we consider astrophysical applications of general relativistic BECs to neutron stars, dark matter stars, supermassive black holes, and microscopic quantum black holes.

6.2 Self-gravitating Bose-Einstein Condensates

6.2.1 The Gross-Pitaevskii-Poisson System

We consider a system of N bosons with mass m in interaction. At $T = 0$ all the bosons condense into the same quantum ground state and the system is described by one order parameter $\psi({\bf r}, t)$ called the condensate wave function.[1] In the mean-field approximation, this gas of interacting BECs is governed by the GP equation [11–14]:

$$i\hbar\frac{\partial\psi}{\partial t}({\bf r}, t) = -\frac{\hbar^2}{2m}\Delta\psi({\bf r}, t) + m\Phi_{tot}({\bf r}, t)\psi({\bf r}, t), \tag{6.1}$$

$$\Phi_{tot}({\bf r}, t) = \int \rho({\bf r}', t)u(|{\bf r} - {\bf r}'|)\, d{\bf r}', \tag{6.2}$$

$$\rho({\bf r}, t) = Nm|\psi({\bf r}, t)|^2, \quad \int |\psi({\bf r}, t)|^2\, d{\bf r} = 1. \tag{6.3}$$

[1] The condensation of the bosons takes place when their thermal (de Broglie) wavelength $\lambda_T = (2\pi\hbar^2/mk_BT)^{1/2}$ exceeds their mean separation $l = n^{-1/3}$ (n is the number density of the bosons). This leads to the inequality $n\lambda_T^3 > 1$ or $T < T_c$ where $T_c = 2\pi\hbar^2 n^{2/3}/mk_B$ is the critical condensation temperature (up to a numerical proportionality factor).

Equation (6.3) is the normalization condition, Eq. (6.3) gives the density of the BECs, Eq. (6.2) determines the associated potential, and Eq. (6.1) determines the evolution of the wave function. We assume that the potential of interaction can be written as $u = u_{LR} + u_{SR}$ where u_{LR} refers to long-range interactions and u_{SR} to short-range interactions. For self-gravitating BECs in the Newtonian approximation, the long-range potential of interaction is given by $u_{LR} = -G/|\mathbf{r} - \mathbf{r}'|$ where G is the constant of gravity. We assume that the short-range interaction corresponds to binary collisions that can be modeled by the effective potential $u_{SR} = g\delta(\mathbf{r} - \mathbf{r}')$ where the coupling constant (or pseudo-potential) g is related to the s-wave scattering length a through $g = 4\pi a\hbar^2/m^3$ [49]. For the sake of generality, we allow a to be positive or negative ($a > 0$ corresponds to a short-range repulsion and $a < 0$ corresponds to a short-range attraction). Under these conditions, the total potential can be written as $\Phi_{tot} = \Phi + h(\rho)$ where $\Phi(\mathbf{r}, t)$ is the gravitational potential that is the solution of the Poisson equation $\Delta\Phi = 4\pi G\rho$ and $h(\rho) = g\rho = gNm|\psi|^2$ is an effective potential modeling short-range interactions. Regrouping these results, we obtain the GPP system

$$i\hbar\frac{\partial\psi}{\partial t} = -\frac{\hbar^2}{2m}\Delta\psi + m\Phi\psi + N\frac{4\pi a\hbar^2}{m}|\psi|^2\psi, \tag{6.4}$$

$$\Delta\Phi = 4\pi GNm|\psi|^2. \tag{6.5}$$

6.2.2 Madelung Transformation

We use the Madelung [10] transformation to rewrite the GP equation (6.4) in the form of hydrodynamic equations. We write the wavefunction as

$$\psi(\mathbf{r}, t) = A(\mathbf{r}, t)e^{iS(\mathbf{r},t)/\hbar}, \tag{6.6}$$

where $A(\mathbf{r}, t)$ and $S(\mathbf{r}, t)$ are real functions. We clearly have $A = \sqrt{|\psi|^2}$ and $S = (\hbar/2i)\ln(\psi/\psi^*)$. Following Madelung, we introduce the density and the velocity fields

$$\rho = NmA^2 = Nm|\psi|^2, \quad \mathbf{u} = \frac{1}{m}\nabla S. \tag{6.7}$$

The flow is irrotational since $\nabla \times \mathbf{u} = \mathbf{0}$. Substituting Eq. (6.6) in Eq. (6.4) and separating real and imaginary parts, we obtain

$$\frac{\partial\rho}{\partial t} + \nabla\cdot(\rho\mathbf{u}) = 0, \tag{6.8}$$

$$\frac{\partial S}{\partial t} + \frac{1}{2m}(\nabla S)^2 + m\Phi + \frac{4\pi a\hbar^2}{m^2}\rho + Q = 0, \tag{6.9}$$

where

$$Q=-\frac{\hbar^2}{2m}\frac{\Delta\sqrt{\rho}}{\sqrt{\rho}}=-\frac{\hbar^2}{4m}\left[\frac{\Delta\rho}{\rho}-\frac{1}{2}\frac{(\nabla\rho)^2}{\rho^2}\right] \tag{6.10}$$

is the quantum potential. The first equation is similar to the equation of continuity in hydrodynamics. It accounts for the conservation of mass $M=\int\rho\,d\mathbf{r}$. The second equation has a form similar to the classical Hamilton-Jacobi equation with an additional quantum term. It can also be interpreted as a generalized Bernouilli equation for a potential flow. Taking the gradient of Eq. (6.9), and using the well-known identity $(\mathbf{u}\cdot\nabla)\mathbf{u}=\nabla(\mathbf{u}^2/2)-\mathbf{u}\times(\nabla\times\mathbf{u})$ which reduces to $(\mathbf{u}\cdot\nabla)\mathbf{u}=\nabla(\mathbf{u}^2/2)$ for an irrotational flow, we obtain an equation similar to the Euler equation

$$\frac{\partial\mathbf{u}}{\partial t}+(\mathbf{u}\cdot\nabla)\mathbf{u}=-\frac{1}{\rho}\nabla p-\nabla\Phi-\frac{1}{m}\nabla Q \tag{6.11}$$

with a quantum potential Q and a pressure

$$p=\frac{2\pi a\hbar^2}{m^3}\rho^2 \tag{6.12}$$

corresponding to a polytropic equation of state $p=K\rho^{1+1/n}$ with a polytropic constant $K=2\pi a\hbar^2/m^3$ and a polytropic index $n=1$ (i.e. $\gamma=1+1/n=2$). Using the equation of continuity (6.8), we can rewrite Eq. (6.11) as

$$\frac{\partial}{\partial t}(\rho\mathbf{u})+\nabla(\rho\mathbf{u}\otimes\mathbf{u})=-\nabla p-\rho\nabla\Phi-\frac{\rho}{m}\nabla Q. \tag{6.13}$$

In conclusion, the GPP system is equivalent to the hydrodynamic equations

$$\frac{\partial\rho}{\partial t}+\nabla\cdot(\rho\mathbf{u})=0, \tag{6.14}$$

$$\frac{\partial\mathbf{u}}{\partial t}+(\mathbf{u}\cdot\nabla)\mathbf{u}=-\frac{1}{\rho}\nabla p-\nabla\Phi-\frac{1}{m}\nabla Q, \tag{6.15}$$

$$\Delta\Phi=4\pi G\rho. \tag{6.16}$$

We shall refer to these equations as the quantum Euler-Poisson system. When the quantum potential can be neglected, we obtain the classical Euler-Poisson system. The quantum potential (6.10) first appeared in the work of Madelung [10] and was rediscovered by Bohm [77] (it is sometimes called "the Bohm potential"). We note the identity $-(1/m)\nabla Q\equiv-(1/\rho)\partial_j P_{ij}$ where P_{ij} is the quantum pressure tensor

$$P_{ij}=-\frac{\hbar^2}{4m^2}\rho\,\partial_i\partial_j\ln\rho\quad\text{or}\quad P_{ij}=\frac{\hbar^2}{4m^2}\left(\frac{1}{\rho}\partial_i\rho\partial_j\rho-\delta_{ij}\Delta\rho\right). \tag{6.17}$$

These identities show that the quantum potential Q is equivalent to an anisotropic pressure P_{ij}. By contrast, the potential of short-range interaction $h(\rho)$ is equivalent to an isotropic pressure $p(\rho)$. This pressure is different from a thermodynamic pressure. In particular, it is negative for an attractive self-interaction ($a < 0$).

6.2.3 Time-Independent GP Equation

If we consider a wavefunction of the form

$$\psi(\mathbf{r}, t) = A(\mathbf{r})e^{-iEt/\hbar}, \tag{6.18}$$

we obtain the time-independent GP equation

$$-\frac{\hbar^2}{2m}\Delta\phi(\mathbf{r}) + m\Phi(\mathbf{r})\phi(\mathbf{r}) + N\frac{4\pi a\hbar^2}{m}\phi(\mathbf{r})^3 = E\phi(\mathbf{r}), \tag{6.19}$$

where $\phi(\mathbf{r}) \equiv A(\mathbf{r})$ is real and $\rho(\mathbf{r}) = Nm\phi^2(\mathbf{r})$. Dividing Eq. (6.19) by $\phi(\mathbf{r})$, we get

$$m\Phi + \frac{4\pi a\hbar^2}{m^2}\rho - \frac{\hbar^2}{2m}\frac{\Delta\sqrt{\rho}}{\sqrt{\rho}} = E. \tag{6.20}$$

This relation can also be derived from the quantum Hamilton-Jacobi equation (6.9) by setting $S = -Et$. Combined with the Poisson equation (6.5) or (6.16), we obtain an eigenvalue equation for the wave function $\phi(\mathbf{r})$, or for the density $\rho(\mathbf{r})$, where the eigenvalue is the eigenenergy E. In the following, we shall be interested by the fundamental eigenmode corresponding to the smallest value of E. For this mode, the wave function $\phi(r)$ is spherically symmetric and has no node so that the density profile decreases monotonically with the distance. The "excited" modes (presenting nodes or oscillations) are unstable and decay to the ground state.

6.2.4 Hydrostatic Equilibrium

The time-independent solution (6.20) can also be obtained from the quantum Euler equation since it is equivalent to the GP equation. The steady state of the quantum Euler equation (6.15), obtained by setting $\partial_t = 0$ and $\mathbf{u} = \mathbf{0}$, satisfies

$$\nabla p + \rho\nabla\Phi - \frac{\hbar^2\rho}{2m^2}\nabla\left(\frac{\Delta\sqrt{\rho}}{\sqrt{\rho}}\right) = \mathbf{0}. \tag{6.21}$$

This generalizes the usual condition of hydrostatic equilibrium by incorporating the contribution of the quantum potential. Equation (6.21) describes the balance between the gravitational attraction, the repulsion due to the quantum potential, and the repulsion (for $a > 0$) or the attraction (for $a < 0$) due to the short-range interaction (scattering). This equation is equivalent to Eq. (6.20). Indeed, integrating Eq. (6.21) using Eq. (6.12), we obtain Eq. (6.20) where the eigenenergy E appears as a constant of integration. On the other hand, combining Eq. (6.21) with the Poisson equation (6.16), we obtain the fundamental equation of hydrostatic equilibrium for self-gravitating systems including the quantum potential

$$-\nabla\cdot\left(\frac{\nabla p}{\rho}\right)+\frac{\hbar^2}{2m^2}\Delta\left(\frac{\Delta\sqrt{\rho}}{\sqrt{\rho}}\right)=4\pi G\rho. \tag{6.22}$$

This equation is actually valid for an arbitrary equation of state $p(\rho)$ [15]. For the equation of state (6.12), it becomes

$$-\frac{4\pi a\hbar^2}{m^3}\Delta\rho+\frac{\hbar^2}{2m^2}\Delta\left(\frac{\Delta\sqrt{\rho}}{\sqrt{\rho}}\right)=4\pi G\rho. \tag{6.23}$$

Assuming spherical symmetry, this equation can be solved numerically [16] to yield the density profile $\rho(r)$ and the mass-radius relation for any value of the scattering length a. There are two important limits that we discuss in the following.

6.2.5 The Non-interacting Case

In the non-interacting case ($a = p = 0$), the condition of hydrostatic equilibrium (6.21) reduces to

$$\rho\nabla\Phi-\frac{\hbar^2\rho}{2m^2}\nabla\left(\frac{\Delta\sqrt{\rho}}{\sqrt{\rho}}\right)=\mathbf{0}. \tag{6.24}$$

This corresponds to the balance between the gravitational attraction and the repulsion due to the quantum pressure arising from the Heisenberg uncertainty principle. Combined with the Poisson equation (6.16), we obtain the differential equation

$$\frac{\hbar^2}{2m^2}\Delta\left(\frac{\Delta\sqrt{\rho}}{\sqrt{\rho}}\right)=4\pi G\rho. \tag{6.25}$$

This equation has been solved numerically in [16, 18, 52]. The density decays smoothly to infinity. The radius of the configuration containing 99 % of the mass is

$$R_{99} = 9.95\frac{\hbar^2}{GMm^2}. \tag{6.26}$$

We note that $R_{99} = 9.95a_B/N$ where $a_B = \hbar^2/Gm^3$ is the gravitational Bohr radius.

6.2.6 The Thomas-Fermi Approximation

The TF approximation amounts to neglecting the quantum potential in Eq. (6.21). In that case, Eq. (6.21) reduces to the usual condition of hydrostatic equilibrium

$$\nabla p + \rho\nabla\Phi = \mathbf{0}. \tag{6.27}$$

This corresponds to the balance between the gravitational attraction and the repulsion due to the short-range interaction (when $a > 0$). Combined with the Poisson equation (6.16), we obtain the fundamental equation of hydrostatic equilibrium for self-gravitating systems

$$-\nabla\cdot\left(\frac{\nabla p}{\rho}\right) = 4\pi G\rho. \tag{6.28}$$

For the equation of state (6.12), it can be rewritten as

$$\Delta\rho + \frac{Gm^3}{a\hbar^2}\rho = 0. \tag{6.29}$$

This equation, which is equivalent to the Lane-Emden equation for a polytrope of index $n = 1$, can be solved analytically [78]. The density profile is given by the formula

$$\rho(r) = \frac{\rho_0 R}{\pi r}\sin\left(\frac{\pi r}{R}\right), \tag{6.30}$$

where ρ_0 is the central density and

$$R = \pi\left(\frac{a\hbar^2}{Gm^3}\right)^{1/2} \tag{6.31}$$

is the radius of the configuration at which the density vanishes (the density has a compact support) [15, 35, 37, 39, 40]. The radius of a polytrope $n = 1$ is independent on its mass M [78]. The radius containing 99 % of the mass is given by $R_{99} = 0.954R$. The central density is determined by the mass according to $\rho_0 = \pi M/4R^3 = (M/4\pi^2)\left(Gm^3/a\hbar^2\right)^{3/2}$. Finally, it can be shown that polytropes with index $\gamma > 4/3$, including the polytrope $\gamma = 2$ ($n = 1$) corresponding to Eq. (6.12), are nonlinearly dynamically stable with respect to the classical Euler-Poisson system. Therefore, the density profile (6.30) valid in the TF limit is dynamically stable.

6.2.7 Validity of the Thomas-Fermi Approximation

In the absence of short-range interaction, the structure of the self-gravitating BEC results from the balance between the gravitational attraction and the quantum pressure arising from the Heisenberg uncertainty principle. Using dimensional analysis in Eq. (6.23), i.e. writing $\hbar^2/m^2R^4 \sim GM/R^3$, we obtain the length-scale

$$R_Q = \frac{\hbar^2}{GMm^2} \tag{6.32}$$

which gives the typical size of a self-gravitating BEC with mass M without short-range interaction ($a = 0$).

In the TF approximation, in which the quantum potential is negligible, the structure of the self-gravitating BEC results from the balance between the gravitational attraction and the short-range repulsion due to scattering (when $a > 0$). Using dimensional analysis in Eq. (6.23), i.e. writing $(a\hbar^2/m^3R^2)(M/R^3) \sim GM/R^3$, we obtain the length-scale

$$R_a = \left(\frac{a\hbar^2}{Gm^3}\right)^{1/2} = \left(\frac{\lambda\hbar^3}{8\pi Gm^4c}\right)^{1/2} = \sqrt{\frac{\lambda}{8\pi}}\frac{M_P}{m}\lambda_c \tag{6.33}$$

which gives the typical size of a self-gravitating BEC with scattering length $a > 0$ in the TF approximation (we have introduced the self-interaction constant λ and the Compton wavelength λ_c defined in Appendix 6.7).

Considering Eq. (6.23) again, the quantum pressure and the pressure arising from the short-range interaction become comparable when $(|a|\hbar^2/m^3R^2)(M/R^3) \sim \hbar^2/m^2R^4$, i.e. $N|a|/R \sim 1$. Estimating R by Eq. (6.32) or (6.33), this condition can be rewritten $\chi \sim 1$ where we have introduced the important dimensionless parameter

$$\chi \equiv \frac{GM^2m|a|}{\hbar^2} = \frac{|\lambda|}{8\pi}\frac{GM^2}{\hbar c} = \frac{|\lambda|}{8\pi}\frac{M^2}{M_P^2}. \tag{6.34}$$

When $\chi \gg 1$, we are in the TF limit in which the quantum potential is negligible. This corresponds to $R_a \gg R_Q$. In that case, the equilibrium state results from the balance between gravitational attraction and repulsive scattering (when $a > 0$). Alternatively, when $\chi \ll 1$, we are in the non-interacting limit in which scattering is negligible. This corresponds to $R_a \ll R_Q$. In that case, the equilibrium state results from the balance between gravitational attraction and quantum pressure. The transition between these two regimes occurs for $\chi \sim 1$. For a given value of the scattering length a, the TF approximation is valid when $M \gg M_a$ where

$$M_a = \frac{\hbar}{\sqrt{Gm|a|}} = \left(\frac{8\pi\hbar c}{G|\lambda|}\right)^{1/2} = \frac{M_P}{\sqrt{\frac{|\lambda|}{8\pi}}}, \tag{6.35}$$

and the non-interacting approximation is valid when $M \ll M_a$. For a given value of the mass M, the TF approximation is valid when

$$|a| \gg \frac{\hbar^2}{GM^2m}, \quad m \gg \frac{\hbar^2}{GM^2|a|}, \quad \frac{|\lambda|}{8\pi} \gg \frac{\hbar c}{GM^2} = \frac{M_P^2}{M^2}. \tag{6.36}$$

Remark With the mass M_a and the radius R_a we can form a density $\rho_a = M_a/R_a^3 = Gm^4/a^2\hbar^2$, an energy $E_a = GM_a^2/R_a = \hbar(Gm)^{1/2}/|a|^{3/2}$, and a time $t_a = 1/\sqrt{G\rho_a} = |a|\hbar/Gm^2$. In the figures we shall use dimensionless variables normalized by M_a, R_a, ρ_a, E_a, and t_a (for given a). This is equivalent to taking $\hbar = G = m = |a| = 1$ in the dimensional equations of the text.

6.2.8 The Total Energy

The total energy associated with the GPP system (6.4)–(6.5), or equivalently with the quantum Euler-Poisson system (6.14)–(6.16), can be written as

$$E_{tot} = \Theta_c + \Theta_Q + U + W. \tag{6.37}$$

The first two terms correspond to the total kinetic energy $\Theta = \frac{N\hbar^2}{2m}\int |\nabla\psi|^2\, d\mathbf{r}$. Using the Madelung transformation, it can be decomposed into the "classical" kinetic energy Θ_c and the "quantum" kinetic energy Θ_Q defined by

$$\Theta_c = \int \rho \frac{\mathbf{u}^2}{2}\, d\mathbf{r}, \quad \Theta_Q = \frac{1}{m}\int \rho Q\, d\mathbf{r}. \tag{6.38}$$

Substituting Eq. (6.10) in Eq. (6.38), the quantum kinetic energy can be rewritten as

$$\begin{aligned}\Theta_Q &= -\frac{\hbar^2}{2m^2}\int \sqrt{\rho}\Delta\sqrt{\rho}\, d\mathbf{r} \\ &= \frac{\hbar^2}{2m^2}\int (\nabla\sqrt{\rho})^2\, d\mathbf{r} = \frac{\hbar^2}{8m^2}\int \frac{(\nabla\rho)^2}{\rho}\, d\mathbf{r}.\end{aligned} \tag{6.39}$$

This functional was introduced by von Weizsäcker [79] and is related to the Fisher entropy $S_F = \int (\nabla\rho)^2/\rho\, d\mathbf{r}$ [80]. The third term in Eq. (6.37) is the internal energy

$$U = \frac{2\pi a\hbar^2}{m^3}\int \rho^2\, d\mathbf{r} = \frac{2\pi a\hbar^2}{m}N^2\int |\psi|^4\, d\mathbf{r} \tag{6.40}$$

which is quadratic in ρ and quartic in ψ. The fourth term is the gravitational potential energy of interaction

$$W = \frac{1}{2}\int \rho\Phi \, d\mathbf{r}. \tag{6.41}$$

It is shown in Appendix 6.8 that the total energy is conserved: $\dot{E}_{tot} = 0$. As a result, a minimum of the total energy functional $E_{tot}[\rho, \mathbf{u}]$ at fixed mass determines a steady state of the quantum Euler-Poisson system (6.14)–(6.16) that is formally nonlinearly dynamically stable [81]. Writing the variational principle in the form $\delta E_{tot} - \alpha\delta M = 0$ where α (chemical potential) is a Lagrange multiplier accounting for the mass constraint, and using the results of Appendix 6.8, we obtain $\mathbf{u} = \mathbf{0}$ and the steady state equation (6.20) with $E = m\alpha$. Therefore, the eigenenergy E/m may be interpreted as a chemical potential α.

Remark Since the stable steady states of the quantum Euler-Poisson system are minima of energy E_{tot} at fixed mass, they can be determined by a relaxation method. Indeed, they can be obtained by solving the quantum Smoluchowski-Poisson (SP) system (see Eqs. (120)–(121) of [82]) that decreases the energy E_{tot} at fixed mass (in this context, the quantum SP system is interpreted as a numerical algorithm).

6.2.9 The Virial Theorem

From the quantum Euler-Poisson system (6.14)–(6.16), we can derive the time-dependent Virial theorem (see Appendix 6.9):

$$\frac{1}{2}\ddot{I} = 2(\Theta_c + \Theta_Q) + 3U + W, \tag{6.42}$$

where $I = \int \rho r^2 \, d\mathbf{r}$ is the moment of inertia. At equilibrium ($\ddot{I} = \Theta_c = 0$), we obtain the time-independent Virial theorem

$$2\Theta_Q + 3U + W = 0. \tag{6.43}$$

On the other hand, the total energy reduces to $E_{tot} = \Theta_Q + U + W$. Finally, multiplying the steady state Eq. (6.20) by ρ and integrating over the configuration, we obtain the identity $\Theta_Q + 2U + 2W = NE$. These are exact results valid at equilibrium.

6.3 The Gaussian Ansatz

To obtain the density profile of a self-gravitating BEC and the mass-radius relation, we have to solve the differential Eq. (6.23) expressing the condition of hydrostatic equilibrium. This can be done numerically [16]. However, we can also obtain approximate analytical results by using a Gaussian ansatz [15].

6.3.1 The Total Energy

We shall calculate the energy functional (6.37) by making a Gaussian ansatz

$$\rho(\mathbf{r}) = \frac{M}{R^3}\frac{1}{\pi^{3/2}}e^{-\frac{r^2}{R^2}} \tag{6.44}$$

for the density profile. The central density is $\rho(0) = M/(\pi^{3/2}R^3)$. The radius containing 99 % of the total mass is $R_{99} = 2.38R$. Using Eq. (6.44), the moment of inertia, the quantum kinetic energy, the internal energy, and the gravitational energy are given by

$$I = \alpha MR^2, \quad \Theta_Q = \sigma\frac{\hbar^2 M}{m^2R^2}, \quad U = \zeta\frac{2\pi a\hbar^2M^2}{m^3R^3}, \quad W = -\nu\frac{GM^2}{R} \tag{6.45}$$

with the coefficients $\alpha = 3/2$, $\sigma = 3/4$, $\zeta = 1/(2\pi)^{3/2}$, and $\nu = 1/\sqrt{2\pi}$.

For a density profile of the form $\rho(\mathbf{r}, t) = (M/R(t)^3)f(\mathbf{r}/R(t))$ and for a velocity profile of the form $\mathbf{u}(\mathbf{r}, t) = H(t)\mathbf{r}$, the equation of continuity (6.14) implies that $H = \dot{R}/R$. We then find that the classical kinetic energy is given by $\Theta_c = \frac{1}{2}\alpha M\dot{R}^2$. Regrouping the foregoing expressions, the energy functional (6.37) can be rewritten as a function of R and $\dot{R}$ (for a fixed mass M) as

$$E_{tot} = \frac{1}{2}\alpha M\left(\frac{dR}{dt}\right)^2 + V(R) \tag{6.46}$$

with

$$V(R) = \sigma\frac{\hbar^2M}{m^2R^2} + \zeta\frac{2\pi a\hbar^2M^2}{m^3R^3} - \nu\frac{GM^2}{R}. \tag{6.47}$$

Equation (6.46) may be interpreted as the total energy of a fictive particle with mass αM and position R moving in a potential $V(R)$. The potential $V(R)$ is plotted in Fig. 6.1 in the different cases considered below.

6.3.2 The Mass-Radius Relation

A stable equilibrium state of the quantum Euler-Poisson system (6.14)–(6.16) is a minimum of the energy functional $E_{tot}[\rho, \mathbf{u}]$ given by Eq. (6.37) at fixed mass M. Within the Gaussian ansatz, we are led to determining the minimum of the function $E_{tot}(R, \dot{R})$ given by Eq. (6.46) at fixed mass M. Clearly, we must have $\dot{R} = 0$, implying that a minimum of energy at fixed mass is a steady state. Then, we must determine the minimum of the potential energy $V(R)$. Computing the first derivative of $V(R)$ and setting $V'(R) = 0$, we obtain the mass-radius relation

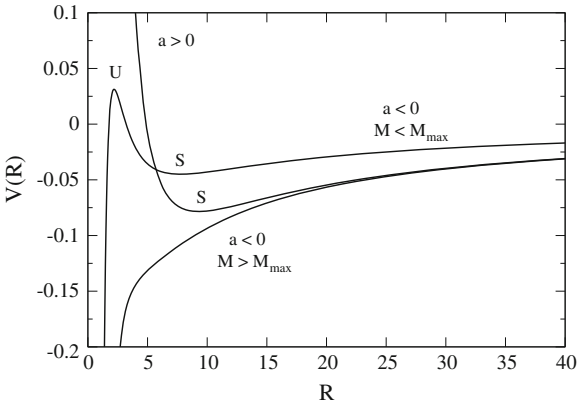

Fig. 6.1 The potential $V(R)$ of the effective mechanical problem

$$M = \frac{2\sigma}{\nu} \frac{\frac{\hbar^2}{Gm^2R}}{1 - \frac{6\pi\zeta a\hbar^2}{\nu Gm^3R^2}}. \tag{6.48}$$

This relation may also be obtained from the equilibrium Virial theorem (6.43) by making the Gaussian ansatz (see Sect. 6.3.3). On the other hand, a critical point of $V(R)$, satisfying $V'(R) = 0$, is an energy minimum if, and only if, $V''(R) > 0$. Computing the second derivative of $V(R)$ and using the mass-radius relation (6.48), we get

$$V''(R) = \frac{\nu GM^2}{R^3}\left(1 + \frac{6\pi\zeta a\hbar^2}{\nu Gm^3R^2}\right). \tag{6.49}$$

Let us consider asymptotic limits of the mass-radius relation:
(i) In the non-interacting case ($a = 0$), we obtain

$$R = \frac{2\sigma}{\nu}\frac{\hbar^2}{GMm^2}. \tag{6.50}$$

This relation results from the balance between the attractive effect of gravity and the repulsive effect of the quantum pressure (Heisenberg's uncertainty principle). This solution is stable because it is an energy minimum ($V''(R) > 0$). The radius R_{99} containing 99 % of the mass is $R_{99} = 8.96\,\hbar^2/GMm^2$. This can be compared with the exact result (6.26) giving $R_{99}^{exact} = 9.95\,\hbar^2/GMm^2$. The agreement is fairly good.
(ii) In the TF approximation when $a > 0$, we get

$$R = \left(\frac{6\pi\zeta}{\nu}\right)^{1/2}\left(\frac{a\hbar^2}{Gm^3}\right)^{1/2}. \tag{6.51}$$

This relation results from the balance between the attractive effect of gravity and the repulsive effect of the scattering (short-range interactions). This solution is stable because it is an energy minimum ($V''(R) > 0$). The radius is independent on the mass. The radius R_{99} containing 99 % of the mass is given by $R_{99} = 4.12(a\hbar^2/Gm^3)^{1/2}$. This can be compared with the exact result (6.31) giving $R_{99}^{exact} = 3.00(a\hbar^2/Gm^3)^{1/2}$. The agreement is less good than in the non-interacting case. The reason is related to the fact that the distribution (6.30) has a compact support so that it is quite different from a Gaussian.

(iii) In the non-gravitational limit when $a < 0$, we get

$$R = \frac{3\pi\zeta}{\sigma}\frac{M|a|}{m}. \tag{6.52}$$

This relation results from the balance between the attractive effect of the scattering and the repulsive effect of the quantum pressure. This solution is unstable because it is an energy maximum ($V''(R) < 0$). The radius R_{99} containing 99 % of the mass is given by $R_{99} = 1.90M|a|/m$.

We now come back to the general case:

(i) We first consider self-gravitating BECs with repulsive short-range interactions ($a > 0$). The mass-radius relation is represented in Fig. 6.2. There exist one, and only one, solution for each value of the mass and it is stable since, according to Eq. (6.49), it is an energy minimum ($V''(R) > 0$); see Fig. 6.1. The radius is a decreasing function of the mass. For $M \to +\infty$, the radius R tends to a minimum value $R_{\rm min}$ given by Eq. (6.51). For $M \to 0$, the radius $R \to +\infty$ with the scaling (6.50). The TF approximation is valid for $M \gg M_a$, i.e. $R \sim R_a \sim R_{\rm min}$ and the non-interacting approximation is valid for $M \ll M_a$, i.e. $R \gg R_a \sim R_{\rm min}$.

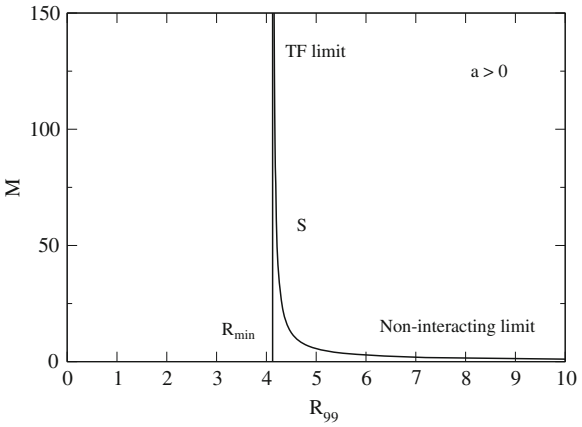

Fig. 6.2 Mass-radius relation of self-gravitating BECs with repulsive self-interaction ($a > 0$). There is a minimum radius $R_{\rm min}$ corresponding to $M \to +\infty$. All the configurations are stable

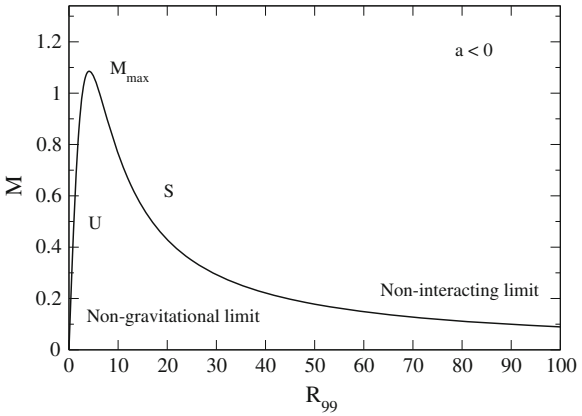

Fig. 6.3 Mass-radius relation of self-gravitating BECs with attractive self-interaction ($a < 0$). There is a maximum mass $M_{\max}$ corresponding to a critical radius R_*. The configurations with $R > R_*$ are stable and the configurations with $R < R_*$ are unstable

(ii) We now consider self-gravitating BECs with attractive short-range interactions ($a < 0$). The mass-radius relation is represented in Fig. 6.3. There exist a maximum mass and a corresponding critical radius

$$M_{\max} = \left(\frac{\sigma^2}{6\pi\zeta\nu}\right)^{1/2} \frac{\hbar}{\sqrt{Gm|a|}}, \quad R_* = \left(\frac{6\pi\zeta}{\nu}\right)^{1/2} \left(\frac{|a|\hbar^2}{Gm^3}\right)^{1/2}. \tag{6.53}$$

They are related to each other by $M_{\max} = (\sigma/\nu)\hbar^2/Gm^2R_*$. The approximate values $M_{\max} = 1.08\hbar/\sqrt{Gm|a|}$ and $R_{99}^* = 4.13(|a|\hbar^2/Gm^3)^{1/2}$ obtained with the Gaussian ansatz [15] are in fairly good agreement with the exact results $M_{\max}^{exact} = 1.01\hbar/\sqrt{Gm|a|}$ and $(R_{99}^*)^{exact} = 5.5(|a|\hbar^2/Gm^3)^{1/2}$ obtained numerically [16]. For $M > M_{\max}$, there is no equilibrium state (no critical point of energy) and the system undergoes gravitational collapse (see Fig. 6.4). Since quantum mechanics (Heisenberg's uncertainty principle) cannot arrest gravitational collapse, the self-gravitating BEC is expected to form a black hole. For $M < M_{\max}$, there exist two solutions with the same mass. However, according to Eq. (6.49), only the solution with the largest radius $R > R_*$ is stable (minimum of energy $V''(R) > 0$). The other solution is an unstable maximum of energy ($V''(R) < 0$); see Fig. 6.1. We can check that the change of stability ($V''(R) = 0$) occurs at the turning point of mass ($M'(R) = 0$) in agreement with the Poincaré theory of linear series of equilibria and with the theory of catastrophes (see [15] for more details). On the stable branch, the radius is a decreasing function of the mass. The non-interacting approximation is valid for $M \ll M_a \sim M_{\max}$ with $R \gg R_a \sim R_*$. For $M \to 0$, the radius $R \to +\infty$ with the scaling (6.50). For $M \to M_{\max}$, the radius R tends to the minimum stable value R_*. On the unstable branch, the radius is an increasing function of the mass. The non-gravitational approximation is valid for $M \ll M_a \sim M_{\max}$ with $R \ll R_a \sim R_*$.

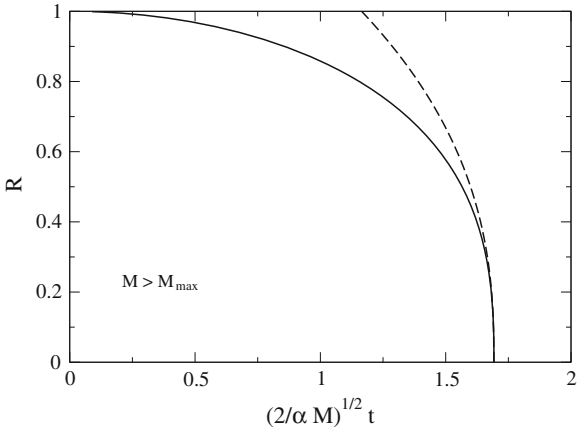

Fig. 6.4 Collapse of a self-gravitating BEC with attractive self-interaction ($a < 0$) when $M > M_{\rm max}$. We have represented the BEC radius $R(t)$ as a function of time by solving Eq. (6.54) starting from a configuration with a radius R_0 and without velocity ($\dot{R}_0 = 0$). The solution is $(2/\alpha M)^{1/2} t = \int_{R(t)}^{R_0} dR/\sqrt{V(R_0) - V(R)}$ (*solid line*). The collapse generates a finite time singularity, i.e. the radius vanishes in a finite time. The collapse time t_{coll} is obtained from the foregoing expression by setting $R(t_{coll}) = 0$ giving $(2/\alpha M)^{1/2} t_{coll} = \int_0^{R_0} dR/\sqrt{V(R_0) - V(R)}$. The solution can then be rewritten as $(2/\alpha M)^{1/2}(t_{coll} - t) = \int_0^{R(t)} dR/\sqrt{V(R_0) - V(R)}$. In the figure, we have taken $M = 1.2, R_0 = 1$, and $M_{\rm max} = 1.08$ yielding $(2/\alpha M)^{1/2} t_{coll} = 1.69$. For $t \to t_{coll}$, the collapse is only driven by the attractive self-interaction and the radius behaves as $R(t) \simeq (25\pi\zeta|a|\hbar^2 M/\alpha m^3)^{1/5}(t_{coll} - t)^{2/5}$ (*dashed line*). This scaling is different from the scaling $R(t) \propto (t_{coll} - t)^{1/2}$ obtained by directly solving the non-gravitational GP equation with an attractive self-interaction [83]. Therefore, the Gaussian ansatz is not qualitatively accurate to describe the collapse of a BEC

For $M \to 0$, the radius $R \to 0$ with the scaling (6.52). However, these configurations are inaccessible since they are dynamically unstable (energy maxima). If the system is initially placed on the unstable branch ($R_U < R_*$), it can either (i) undergo gravitational collapse ($R(t) \to 0$), (ii) evaporate ($R(t) \to +\infty$) if its energy E_{tot} is positive[2] or (iii) oscillate around the stable equilibrium state with a larger radius ($R_S > R_*$) if its energy E_{tot} is negative; see Fig. 6.1. It may also relax towards the stable equilibrium state with a larger radius ($R(t) \to R_S > R_*$) provided that it is able to dissipate energy, e.g. by radiation or due to some damping. On the other hand, since the stable states are only *metastable* (local minima of energy), due to classical or quantum fluctuations (tunneling effect), the system initially put in a metastable state may cross the barrier of potential played by the unstable state and ultimately collapse.

[2] Using Eq. (51) of [16] obtained with the Gaussian ansatz, we find that $E_{tot} > 0$ when $M < (\sqrt{3}/2)M_{\rm max}$ and $R < R_*/\sqrt{3}$.

6.3.3 The Virial Theorem

Using the Gaussian ansatz, the time-dependent Virial theorem (6.42) can be written after simplification as [15]:

$$\alpha M \frac{d^2R}{dt^2} = -\frac{dV}{dR}. \tag{6.54}$$

This equation describes the motion of a fictive particle with mass αM and position R in a potential $V(R)$. From Eq. (6.54), we find that the total energy $E_{tot} = \Theta_c + V$ defined by Eq. (6.46) is conserved: $\dot{E}_{tot} = 0$. The equilibrium Virial theorem ($d^2R/dt^2 = 0$) returns the mass-radius relation (6.48) obtained from the condition $dV/dR = 0$. In this mechanical analogy, a stable equilibrium state corresponds to a *minimum* of $V(R)$ as we have previously indicated.

6.3.4 The Pulsation Equation

To study the linear dynamical stability of a steady state of Eq. (6.54), we make a small perturbation about that state and write $R(t) = R + \varepsilon(t)$ where R is the equilibrium radius and $\varepsilon(t) \ll R$ is the perturbation. Using $V'(R) = 0$ and keeping only terms that are linear in ε, we obtain the equation

$$\frac{d^2\varepsilon}{dt^2} + \omega^2 \varepsilon = 0, \tag{6.55}$$

where ω is a complex pulsation given by

$$\omega^2 = \frac{1}{\alpha M} V''(R). \tag{6.56}$$

A steady state is linearly stable if, and only if, $\omega^2 > 0$; that is to say if, and only if, it is a (local) minimum of energy $V(R)$. In that case, the system oscillates about its equilibrium with a pulsation ω. Otherwise, the perturbation grows exponentially rapidly with a growth rate $\lambda_+ = \sqrt{-\omega^2} > 0$ (the other mode is damped at a rate $\lambda_- = -\sqrt{-\omega^2} < 0$). Computing $V''(R)$ from Eq. (6.47), and using Eq. (6.45), we find that

$$\omega^2 = \frac{6\Theta_Q + 12U + 2W}{I}. \tag{6.57}$$

In the non-interacting case ($U = 0$), using the Virial theorem (6.43), we get $\omega^2 = -W/I$. In the TF approximation ($\Theta_Q = 0$), using the Virial theorem (6.43), we obtain $\omega^2 = -2W/I$. This expression coincides with the Ledoux formula $\omega^2_{Ledoux} = (4 - 3\gamma)W/I$ [84] for a polytrope of index $\gamma = 2$. Using the Gaussian ansatz, we obtain $\omega = (\nu/\alpha)^{1/2} t_D^{-1} = 0.516\, t_D^{-1}$ in the non-interacting case and $\omega =$

$(2\nu/\alpha)^{1/2}t_D^{-1} = 0.729\, t_D^{-1}$ in the TF approximation, where $t_D = (R^3/GM)^{1/2}$ is the dynamical time.

From Eqs. (6.48), (6.49) and (6.56), we obtain the nice identity

$$\frac{dM}{dR} = -\frac{1}{2\sigma}\frac{m^2R^3}{\hbar^2}V''(R) = -\frac{\alpha}{2\sigma}\frac{m^2MR^3}{\hbar^2}\omega^2. \tag{6.58}$$

This identity relates the slope of the mass-radius relation $M(R)$ to the complex pulsation ω. It first shows that a change of stability ($\omega = 0$) occurs at a turning point of mass ($dM/dR = 0$). Furthermore, it shows that a branch with a negative slope ($dM/dR < 0$) is stable ($\omega^2 > 0$) whereas a branch with a positive slope ($dM/dR > 0$) is unstable. This is an illustration of the Poincaré turning point criterion.

6.4 Application of Newtonian Self-gravitating BECs to Dark Matter Halos

In this section, we apply the model of Newtonian self-gravitating BECs to dark matter halos. In the numerical applications, we consider a typical dark matter halo of mass $M = 3\times 10^{11}M_\odot$, radius $R = 10\,\mathrm{kpc} = 3.09\times 10^{20}\,\mathrm{m}$, density $\rho = M/R^3 = 2.02\times 10^{-23}\,\mathrm{g/cm^3}$, and dynamical time $t_D = 1/\sqrt{G\rho} = 27\,\mathrm{Myrs}$.

6.4.1 The Non-interacting Case

In the non-interacting case ($a = 0$), the typical radius of a self-gravitating BEC is given by Eq. (6.32). It may be rewritten as

$$\frac{R_Q}{1\,\mathrm{kpc}} = 8.54\times 10^{-37}\,\frac{M_\odot}{M}\left(\frac{1\,\mathrm{eV}/c^2}{m}\right)^2. \tag{6.59}$$

The exact radius of a self-gravitating BEC without self-interaction containing 99 % of the mass is $R_{99} = 9.95R_Q$. In order to reproduce the typical scales of dark matter halos, the mass of the bosons must be of the order of $m = 1.68\times 10^{-24}\,\mathrm{eV}/c^2$ [17]. Such an ultralight particle corresponds to "fuzzy cold dark matter" [23].

6.4.2 The Thomas-Fermi Approximation

In the TF approximation, the typical radius of a self-gravitating BEC with a repulsive self-interaction ($a > 0$) is given by Eq. (6.33). It may be rewritten as

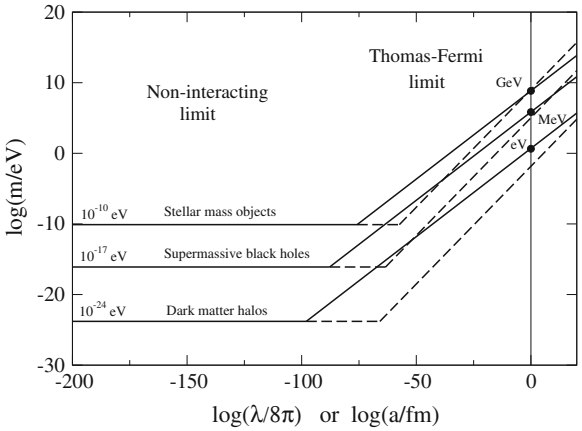

Fig. 6.5 Relation between the boson mass m and the self-interaction constant λ (*solid lines*) or the scattering length a (*dashed lines*) in order to reproduce the typical scales of dark matter halos, supermassive black holes, and stellar mass objects (neutron stars, Machos. . .). One can see that the TF approximation is valid even for very small values of a and λ, and that the self-interaction can considerably increase the required value of the boson mass as discussed in the text

$$\frac{R_a}{1\,\mathrm{kpc}} = 5.56\times 10^{-3}\left(\frac{a}{1\,\mathrm{fm}}\right)^{1/2}\left(\frac{1\,\mathrm{eV}/c^2}{m}\right)^{3/2}, \tag{6.60}$$

$$\frac{R_a}{1\,\mathrm{kpc}} = 78.1\sqrt{\frac{\lambda}{8\pi}}\left(\frac{1\,\mathrm{eV}/c^2}{m}\right)^{2}. \tag{6.61}$$

The exact radius of a self-gravitating BEC with a repulsive self-interaction in the TF approximation is $R = \pi R_a$. In order to reproduce the typical scales of dark matter halos, the mass of the bosons must be of the order of

$$\frac{m}{1\,\mathrm{eV}/c^2} = 1.45\times 10^{-2}\left(\frac{a}{1\,\mathrm{fm}}\right)^{1/3}, \quad \frac{m}{1\,\mathrm{eV}/c^2} = 4.95\left(\frac{\lambda}{8\pi}\right)^{1/4}. \tag{6.62}$$

For $a = 10^6\,\mathrm{fm}$, which corresponds to the typical value of the scattering length observed in laboratory BEC experiments [49], this gives a mass $m = 1.45\,\mathrm{eV/c^2}$ [40] much larger than in the non-interacting case (see Sect. 6.4.1). The corresponding value of the self-interaction constant is $\lambda/8\pi = 7.35\times 10^{-3}$. Therefore, a self-interaction $\lambda \sim 1$ can increase the required value of the boson mass from $m \sim 10^{-24}\,\mathrm{eV}/c^2$ to $m \sim 1\,\mathrm{eV}/c^2$ (see Fig. 6.5) which may be more realistic from a particle physics point of view.

It is important to realize that the radius R of a self-interacting BEC directly determines the ratio a/m^3 or λ/m^4. For a typical dark matter halo, we obtain $m^3/a = 3.05\times 10^{-6}\,(\mathrm{eV/c^2})^3/\mathrm{fm}$ and $m^4/\lambda = 23.9\,(\mathrm{eV}/c^2)^4$. Inversely, the specification of m and a (or λ) determines the radius of the halo.

6.4.3 Validity of the Thomas-Fermi Approximation

The TF approximation is valid when $M \gg M_a$ where M_a is the characteristic mass given by Eq. (6.35). It may be rewritten as

$$\frac{M_a}{M_\odot} = 1.54\times 10^{-34}\left(\frac{1\,\mathrm{fm}}{|a|}\right)^{1/2}\left(\frac{1\,\mathrm{eV}/c^2}{m}\right)^{1/2}, \quad \frac{M_a}{M_\odot} = 1.09\times 10^{-38}\sqrt{\frac{8\pi}{|\lambda|}}. \tag{6.63}$$

For a typical dark matter halo, the TF approximation is valid when [15, 16]:

$$\frac{m}{1\,\mathrm{eV}/c^2} \gg 2.63\times 10^{-91}\frac{1\,\mathrm{fm}}{|a|}, \quad \frac{|\lambda|}{8\pi} \gg 1.33\times 10^{-99}. \tag{6.64}$$

Therefore, the TF approximation is valid even for an extremely (!) small value of a or λ fulfilling the condition (6.64). According to Eq. (6.36), this is due to the smallness of $(M_P/M)^2$. For the values $a = 10^6$ fm, $m = 1.45\,\mathrm{eV/c^2}$, and $\lambda/8\pi = 7.35\times 10^{-3}$ considered in [40], the condition (6.64) is fulfilled by more than 90 orders of magnitude so that the TF approximation is perfect. In that case, the density profile (6.30) is steady and stable. Alternatively, for the values $m \sim 10^{-24}\,\mathrm{eV}/c^2$, $a \sim 10^{-67}$ fm, and $\lambda/8\pi \sim 10^{-99}$ considered in [44], the TF approximation is not valid. This is the reason why the authors of [48] find that the profile (6.30) is not steady in that case. Indeed, the TF condition on which this profile is based is not satisfied. Note that the general dark matter halo profile that is the solution of the full condition of hydrostatic equilibrium (6.21) has been calculated numerically in [16] for different values of a and m. This calculation does not make any approximation.

6.4.4 The Case of Attractive Self-interactions

For a self-gravitating BEC with an attractive self-interaction ($a < 0$), there exist a maximum mass $M_{\max} = 1.01M_a$. The corresponding radius containing 99 % of the mass is $R^*_{99} = 5.5R_a$. This can be rewritten as [15, 16]:

$$M_{\max} = 1.01\frac{M_P}{\sqrt{\frac{|\lambda|}{8\pi}}}, \quad R^*_{99} = 5.5\sqrt{\frac{|\lambda|}{8\pi}}\frac{M_P}{m}\lambda_c. \tag{6.65}$$

If $|\lambda| \sim 1$ the maximum mass is of the order of the Planck mass $M_P = 2.18\times 10^{-8}$ kg. Of course, this is ridiculously small at the scale of dark matter halos meaning that a self-gravitating BEC with an attractive self-interaction is extremely unstable. The maximum mass (6.65) becomes of the order of the typical mass of dark matter halos

for $|\lambda|/8\pi = 1.36 \times 10^{-99}$. The corresponding radius is of the order of the typical radius of dark matter halos provided that $m = 1.26 \times 10^{-24}\,\mathrm{eV/c^2}$. This corresponds to a scattering length $|a| = 2.13 \times 10^{-67}\,\mathrm{fm}$.

Let us consider a self-gravitating BEC without self-interaction ($\lambda = 0$) representing a typical dark matter halo of mass $M = 3 \times 10^{11} M_\odot$. This halo is stable. We now assume that the bosons have a small attractive self-interaction ($\lambda < 0$). The halo becomes unstable when $M > M_{\rm max}$. Using Eq. (6.65), we find that the dark matter halo becomes unstable as soon as

$$\frac{|a|}{1\,\mathrm{fm}} > 2.69 \times 10^{-91} \frac{1\,\mathrm{eV}/c^2}{m}, \quad \frac{|\lambda|}{8\pi} > 1.36 \times 10^{-99}. \tag{6.66}$$

Therefore, a very small attractive self-interaction can destabilize a dark matter halo. This shows that no self-interaction ($\lambda = 0$) is very different from a small self-interaction ($\lambda \to 0$). For $m = 1.68 \times 10^{-24}\,\mathrm{eV}/c^2$, we find that the halo becomes unstable when $|a| > 1.60 \times 10^{-67}\,\mathrm{fm}$. In that case, it forms a black hole.

In we assume $|\lambda| \sim 1$, we find that $M_{\rm max} \sim M_P$ and, consequently, $M \gg M_{\rm max}$ for dark matter halos. Therefore, we can make the TF approximation and neglect the effect of the quantum pressure. In that case, the BEC collapses due to the effect of self-gravity and attractive scattering (see Fig. 6.4). Since quantum mechanics (Heisenberg's uncertainty principle) cannot stabilize the BEC against gravitational collapse, this process can lead to a supermassive black hole (of course, close to the singularity, the Newtonian approximation is not relevant anymore and we must use general relativity). For the numerical application, we take $a = -10^6\,\mathrm{fm}$ which corresponds to the typical scattering length of ^{7}Li atoms in laboratory BEC experiments [49]. We also take a boson mass $m = 1.45\,\mathrm{eV/c^2}$ as in Sect. 6.4.2. This gives a self-interaction constant $\lambda/8\pi = -7.35 \times 10^{-3}$. The maximum mass is $M_{\rm max} = 1.29 \times 10^{-37} M_\odot$ much smaller than the mass $M = 3 \times 10^{11} M_\odot$ of dark matter halos. If we consider a configuration with an initial radius $R_0 = 10\,\mathrm{kpc}$, we find that the collapse time is of the order of $t_D \sim 1/(GM/R_0^3)^{1/2} \sim 27\,\mathrm{Myrs}$. To be specific, we have taken the parameters of Sect. 6.4.2 by just reverting the sign of a. Other numerical applications with a total mass $M \sim 10^6 M_\odot$ of the order of the mass of supermassive black holes, and a smaller initial radius R_0, could be more relevant.

6.5 Application of General Relativistic BECs to Neutron Stars, Dark Matter Stars, and Black Holes

The Newtonian approximation is valid when the radius R of a configuration with mass M is much larger than the Schwarzschild radius $R_S = 2GM/c^2$ or, equivalently, when $M \ll Rc^2/G$. This condition can be rewritten as $M/M_\odot \ll 0.677R/\mathrm{km}$. For a typical dark matter halo, the term in the left hand side is of order 10^{11} while the term in the right hand side is of order 10^{17}. Therefore, this condition is fulfilled by 6 orders of magnitude so that the Newtonian approximation is very good for dark matter halos.

By contrast, for compact objects similar to neutron stars for which $M \sim 1M_\odot$ and $R \sim 10\,\mathrm{km}$ (yielding a typical density $\rho \sim M/R^3 \sim 2\times 10^{15}\,\mathrm{g/cm^3}$ and a dynamical time $t_D \sim 1/\sqrt{G\rho} \sim 10^{-4}\,\mathrm{s}$), we must use general relativity.

6.5.1 Non-interacting Boson Stars

In the absence of short-range interaction, the mass-radius relation of a non-relativistic self-gravitating BEC is given by Eq. (6.26). This relation is valid as long as the radius is much larger than the Schwarzschild radius $R_S = 2GM/c^2$. Equating the two relationships, and introducing the Planck mass, we obtain the scaling of the maximum mass of a relativistic self-gravitating BEC without self-interaction

$$M_Q^r = \frac{\hbar c}{Gm} = \frac{M_P^2}{m}. \tag{6.67}$$

The exact value of the maximum mass of non-interacting boson stars was determined by Kaup [51] by solving the Klein-Gordon-Einstein equations. It is given by $M_{\rm max}^Q = 0.633M_Q^r$. The radius $R_Q^r = GM_Q^r/c^2$ corresponding to Eq. (6.67) is

$$R_Q^r = \frac{\hbar}{mc} = \lambda_c. \tag{6.68}$$

It scales as the Compton wavelength of the particles that compose the BEC. More precisely, the exact minimum radius of non-interacting boson stars containing 95 % of the mass is given by $R_{\rm min}^Q = 6.03R_Q^r$ [60]. The maximum mass and the minimum radius are related to each other by $R_{\rm min}^Q = 9.53GM_{\rm max}^Q/c^2$. The Newtonian approximation is valid when $M \ll M_{\rm max}^Q$ and $R \gg R_{\rm min}^Q$.

The typical mass and typical radius of non-interacting boson stars may be rewritten as

$$\frac{M_Q^r}{M_\odot} = 1.34\times 10^{-10}\,\frac{\mathrm{eV}/c^2}{m}, \quad \frac{R_Q^r}{\mathrm{km}} = 1.48\frac{M_Q^r}{M_\odot}. \tag{6.69}$$

For $m \sim 1\,\mathrm{GeV}/c^2$, corresponding to the typical mass of the neutrons, the Kaup mass $M_{\rm max}^Q \sim 10^{-19}M_\odot \sim 10^{11}\,\mathrm{kg}$ and the Kaup radius $R_{\rm min}^Q \sim 10^{-19}\,\mathrm{km}$ are very small. This describes mini boson stars. They have the characteristics of primordial black holes whose lifetime is of the order of the present age of the universe (∼3 billion years) [85]. These mini boson stars could play a role for dark matter if they exist in the universe in abundance.

The Kaup mass becomes of the order of the solar mass if the bosons have a mass $m \sim 10^{-10}\,\mathrm{eV}/c^2$ (leading to a Kaup radius of the order of the km). For example, axionic boson stars could account for the mass of MACHOs (between 0.3 and $0.8M_\odot$) if the axions have such a small mass [68].

For dark matter halos modeled as non-interacting BECs with a boson mass $m \sim 10^{-24}\,\mathrm{eV}/c^2$ (see Sect. 6.4.1), we find that $M^Q_{\max} \sim 10^{14} M_\odot$ much larger than the typical mass of dark matter halos $M \sim 10^{11} M_\odot$. Therefore, the Newtonian approximation can be used for dark matter halos since $M \ll M^Q_{\max}$.

6.5.2 The Thomas-Fermi Approximation for Boson Stars

In the TF approximation, the radius of a non-relativistic self-gravitating BEC with repulsive self-interaction ($a > 0$) is given by Eq. (6.31). It is independent on the mass M. The Newtonian approximation is valid as long as the radius (6.31) is much larger than the Schwarzschild radius $R_S = 2GM/c^2$. Equating these two relationships, and introducing the Planck mass, we obtain the scaling of the maximum mass of a relativistic self-gravitating BEC with repulsive self-interaction in the TF approximation

$$M^r_a = \frac{\hbar c^2 \sqrt{a}}{(Gm)^{3/2}} = \sqrt{\frac{\lambda}{8\pi}} \frac{1}{m^2} \left(\frac{\hbar c}{G}\right)^{3/2} = \sqrt{\frac{\lambda}{8\pi}} \frac{M_P^3}{m^2}. \tag{6.70}$$

The exact value of the maximum mass of a boson star in the TF approximation was determined by Colpi et al. [56] by solving the Klein-Gordon-Einstein equations and by Chavanis and Harko [73] by solving the Tolman-Oppenheimer-Volkoff (TOV) equation with an appropriate equation of state. It is given by $M^a_{\max} = 0.500 M^r_a$ if we use a non-relativistic equation of state and by $M^a_{\max} = 0.307 M^r_a$ if we use a relativistic equation of state [73]. For $\lambda \sim 1$, the maximum mass of self-interacting boson stars scales as the Oppenheimer-Volkoff maximum mass M_P^3/m^2 of neutron stars while the Kaup maximum mass of non-interacting boson stars scales as M_P^2/m. Therefore, in the presence of self-interaction, the maximum mass of a boson star is much larger than the Kaup mass by a factor $M_P/m \gg 1$, so that it becomes astrophysically relevant.

The radius $R^r_a = GM^r_a/c^2$ corresponding to Eq. (6.70) is given by

$$R^r_a = \left(\frac{a\hbar^2}{Gm^3}\right)^{1/2} = \left(\frac{\lambda \hbar^3}{8\pi G m^4 c}\right)^{1/2} = \sqrt{\frac{\lambda}{8\pi}} \frac{M_P}{m} \lambda_c \tag{6.71}$$

as in the Newtonian approximation. The exact minimum radius of a relativistic self-gravitating BEC with repulsive self-interactions in the TF approximation is given by $R^a_{\min} = 1.89 R^r_a$ for a non-relativistic equation of state and by $R^a_{\min} = 1.92 R^r_a$ for a relativistic equation of state [73]. For $\lambda \sim 1$, the radius of a self-interacting BEC is much larger than the Compton wavelength since $M_P/m \gg 1$. The maximum mass and the minimum radius are related to each other by $R^a_{\min} = 3.78 G M^a_{\max}/c^2$ for a non-relativistic equation of state and by $R^a_{\min} = 6.25\, G M^a_{\max}/c^2$ for a relativistic equation of state. The Newtonian approximation is valid when $M \ll M^a_{\max}$ and $R \gg R^a_{\min}$.

The previous equations may be rewritten as

$$\frac{M_a^r}{M_\odot} = 3.66 \left(\frac{a}{\mathrm{fm}}\right)^{1/2} \left(\frac{\mathrm{GeV}/c^2}{m}\right)^{3/2}, \tag{6.72}$$

$$\frac{M_a^r}{M_\odot} = 1.62 \sqrt{\frac{\lambda}{8\pi}} \left(\frac{\mathrm{GeV}/c^2}{m}\right)^{2}, \quad \frac{R_a^r}{\mathrm{km}} = 1.48 \frac{M_a^r}{M_\odot}. \tag{6.73}$$

For $m \sim 1\,\mathrm{GeV}/c^2$, corresponding to the typical mass of the neutrons, and $a \sim 1$ fm corresponding to $\lambda \sim 1$, the maximum mass M_{max}^a of self-interacting boson stars is of the order of the solar mass, and their corresponding radius R_{min}^a is of the order of the kilometer, as in the case of neutron stars. These parameters could describe boson stars with relevant masses.

We emphasize that the mass M or the radius R of a self-interacting boson star directly determines the ratio a/m^3 or λ/m^4. Taking $M = 1\,M_\odot$, we obtain $m^3/a = 3.35\,(\mathrm{GeV/c^2})^3/\mathrm{fm}$ and $m^4/\lambda = 2.61 \times 10^{-2}\,(\mathrm{GeV}/c^2)^4$ for a non-relativistic equation of state and $m^3/a = 1.26\,(\mathrm{GeV/c^2})^3/\mathrm{fm}$ and $m^4/\lambda = 9.84 \times 10^{-3}\,(\mathrm{GeV}/c^2)^4$ for a relativistic equation of state.

In order to reproduce the typical mass $M \sim 1\,M_\odot$ of neutron stars, the mass of the bosons must be of the order of

$$\frac{m}{1\,\mathrm{GeV}/c^2} = 1.50 \left(\frac{a}{1\,\mathrm{fm}}\right)^{1/3}, \quad \frac{m}{1\,\mathrm{GeV}/c^2} = 0.900 \left(\frac{\lambda}{8\pi}\right)^{1/4} \tag{6.74}$$

for a non-relativistic equation of state and

$$\frac{m}{1\,\mathrm{GeV}/c^2} = 1.08 \left(\frac{a}{1\,\mathrm{fm}}\right)^{1/3}, \quad \frac{m}{1\,\mathrm{GeV}/c^2} = 0.705 \left(\frac{\lambda}{8\pi}\right)^{1/4} \tag{6.75}$$

for a relativistic equation of state. For $a \sim 1$ fm, this gives a mass $m \sim 1\,\mathrm{GeV/c^2}$ much larger than in the non-interacting case (see Sect. 6.5.1). This corresponds to a self-interaction constant $\lambda \sim 1$. Therefore, a self-interaction $\lambda \sim 1$ can increase the required value of the boson mass from $m \sim 10^{-10}\,\mathrm{eV}/c^2$ to $m \sim 1\,\mathrm{GeV}/c^2$ (see Fig. 6.5).

For dark matter halos modeled as self-interacting BECs in the TF approximation with a boson mass $m \sim 1\,\mathrm{eV/c^2}$ and a scattering length $a \sim 10^6$ fm (see Sect. 6.4.2) we find that $M_{\mathrm{max}}^a \sim 10^{17} M_\odot$ much larger than the typical mass of dark matter halos $M \sim 10^{11} M_\odot$. Therefore, the Newtonian approximation can be used for dark matter halos since $M \ll M_{\mathrm{max}}^a$.

6.5.3 Validity of the Thomas-Fermi Approximation

The TF approximation is valid when $M_a^r \gg M_Q^r$ or $R_a^r \gg R_Q^r$. It is convenient to introduce the dimensionless parameter

$$\Lambda = \frac{|a|c^2}{Gm} = \frac{|\lambda|}{8\pi}\frac{\hbar c}{Gm^2} = \frac{|\lambda|}{8\pi}\frac{M_P^2}{m^2}. \tag{6.76}$$

The TF approximation is valid when $\Lambda \gg 1$ and the non-interacting approximation is valid when $\Lambda \ll 1$. For a given value of m, the TF approximation is valid when

$$|a| \gg \frac{Gm}{c^2}, \quad \frac{|\lambda|}{8\pi} \gg \frac{Gm^2}{c\hbar} = \frac{m^2}{M_P^2}. \tag{6.77}$$

For a given value of a or λ, the TF approximation is valid when

$$m \ll \frac{|a|c^2}{G}, \quad m \ll \left(\frac{|\lambda|c\hbar}{8\pi G}\right)^{1/2} = \sqrt{\frac{|\lambda|}{8\pi}}M_P. \tag{6.78}$$

These conditions may be rewritten as

$$\frac{|a|}{1\,\text{fm}}\frac{1\,\text{GeV}/c^2}{m} \gg 1.32\times 10^{-39}, \quad \frac{|\lambda|}{8\pi}\left(\frac{1\,\text{GeV}/c^2}{m}\right)^2 \gg 6.71\times 10^{-39}. \tag{6.79}$$

Therefore, the TF approximation is valid even for an extremely (!) small value of λ fulfilling the condition (6.79). According to Eq. (6.77), this is due to the smallness of m^2/M_P^2. For the values of a, m, and λ given in the previous section, the condition (6.79) is fulfilled by more than 30 orders of magnitude, so that the TF approximation is perfect.

6.5.4 An Interpolation Formula Between the Non-interacting Case and the TF Approximation

The mass-radius relation of a non-relativistic self-gravitating BEC with repulsive short-range interactions may be approximated by

$$M = 9.95\frac{\frac{\hbar^2}{Gm^2R}}{1-8.99\frac{a\hbar^2}{Gm^3R^2}}. \tag{6.80}$$

To obtain this expression, we have used Eq. (6.48) based on the Gaussian ansatz and we have adapted the numerical factors in order to recover the exact results in the

non-interacting case and in the TF limit (the radius R represents the radius containing 99 % of the mass). In the relativistic regime, equating the radius R with the Schwarzschild radius $R_S = 2GM/c^2$, we obtain the following approximate expressions for the maximum mass and the minimum radius of a relativistic self-gravitating BEC with repulsive short-range interactions

$$M_{\rm max} = 0.633\sqrt{1+c_1\Lambda}\frac{M_P^2}{m}, \quad R_{\rm min} = 6.03\sqrt{1+c_2\Lambda}\lambda_c, \tag{6.81}$$

where $(c_1, c_2) = (0.624, 0.0982)$ for a non-relativistic equation of state and $(c_1, c_2) = (0.235, 0.101)$ for a relativistic equation of state. Again, the numerical factors have been adapted in order to recover the exact results in the non-interacting case and in the TF limit (the radius R represents the radius containing 95 % of the mass).

When $M > M_{\rm max}$, there is no equilibrium state and the self-gravitating BEC is expected to collapse and form a black hole. When $M < M_{\rm max}$, there exist stable equilibrium states with $R > R_{\rm min}$ that correspond to boson stars for which gravitational collapse is prevented by quantum mechanics.

6.5.5 Application to Supermassive Black Holes

It has been proposed by certain authors [67, 69, 72] that stable boson stars could mimic supermassive black holes that reside at the center of galaxies. In the absence of self-interaction, the mass of the bosons must be of the order of $m = 3.25 \times 10^{-17}\,{\rm eV}/c^2$ in order to reproduce the mass $M = 2.61 \times 10^6 M_\odot$ of Sgr A* [69]. The corresponding boson star radius is $R = 3.68 \times 10^7$ km. These ultralight bosons could appear in very recent phase transitions and belong to the Goldstone sector. For self-interacting bosons with $\lambda \sim 1$ the required mass is raised from $m \sim 10^{-17}$ to $m \sim 1\,{\rm MeV/c^2}$ [67] (see Fig. 6.5). More generally, in order to reproduce the typical mass $M \sim 10^6 M_\odot$ of supermassive black holes, the mass of the bosons must be of the order of

$$\frac{m}{1\,{\rm MeV}/c^2} = 0.150\left(\frac{a}{1\,{\rm fm}}\right)^{1/3}, \quad \frac{m}{1\,{\rm MeV}/c^2} = 0.9\left(\frac{\lambda}{8\pi}\right)^{1/4} \tag{6.82}$$

for a non relativistic equation of state and

$$\frac{m}{1\,{\rm MeV}/c^2} = 0.108\left(\frac{a}{1\,{\rm fm}}\right)^{1/3}, \quad \frac{m}{1\,{\rm MeV}/c^2} = 0.705\left(\frac{\lambda}{8\pi}\right)^{1/4} \tag{6.83}$$

for a relativistic equation of state. These intermediate mass bosons could appear during cosmological evolution (e.g., soft inflationary events). Finally, if the boson mass is comparable to the Higgs mass ($\sim$125 GeV$/c^2$), then the center of the galaxy

could be a non-topological soliton star [86]. The Higgs particle could be a natural candidate as constituent of a boson condensation if the phase transition occurred in early epochs.

Furthermore, it has been shown that boson stars with $m = 1.2 \times 10^{-16}\,\mathrm{eV}/c^2$, $M = 2.8 \times 10^6 M_\odot$ and $\Lambda = 20$ can mimic the spectrum of an accretion disk produced by a Schwarzschild black hole with the same mass [72] (while boson stars with $\Lambda = 0$ show a hardening of the spectrum at high frequencies [87]). Therefore, it was suggested that boson stars with a small self-interaction can be black hole candidates [72].

6.5.6 Application to Neutron Stars and Dark Matter Stars

According to the study of Chavanis and Harko [73], the maximum mass and minimum radius of general relativistic BEC stars in the TF limit are

$$\frac{M^a_{\rm max}}{M_\odot} = 1.83\left(\frac{a}{\rm fm}\right)^{1/2}\left(\frac{\mathrm{GeV}/c^2}{m}\right)^{3/2}, \quad \frac{R^a_{\rm min}}{\rm km} = 5.59\,\frac{M^a_{\rm max}}{M_\odot} \tag{6.84}$$

for a non-relativistic equation of state and

$$\frac{M^a_{\rm max}}{M_\odot} = 1.12\left(\frac{a}{\rm fm}\right)^{1/2}\left(\frac{\mathrm{GeV}/c^2}{m}\right)^{3/2}, \quad \frac{R^a_{\rm min}}{\rm km} = 9.26\,\frac{M^a_{\rm max}}{M_\odot} \tag{6.85}$$

for a relativistic equation of state. The mass-radius relation is represented in Fig. 6.6. It is parameterized by the central density of the star. For a relativistic equation of state, it has a snail-like structure as in the case of neutron stars modeled by the ideal Fermi gas [74, 88, 89]. This is because the equation of state becomes linear ($p = \rho c^2/3$) in the ultra-relativistic regime (high central densities) [90]. In the non-relativistic regime (low central densities) we recover the Newtonian radius (6.31) that corresponds here to a maximum radius. Using the Poincaré theory, or the theory of catastrophes, one can show that the series of equilibria becomes unstable after the turning point of mass ($M'(R) = 0$) so that only configurations with $M < M^a_{\rm max}$ and $R^a_{\rm min} < R < R_{\rm max}$ are stable.

Chavanis and Harko [73] have proposed that, due to the superfluid properties of the core of neutron stars, the neutrons (fermions) could form Cooper pairs and behave as bosons of mass $2m_n$. They can then make a BEC through the BCS/BEC crossover mechanism. Therefore, neutron stars could actually be BEC stars. Since the maximum mass of BEC stars $M^a_{\rm max} = 0.0612\sqrt{\lambda}M_P^3/m^2 = 0.307\hbar c^2\sqrt{a}/(Gm)^{3/2}$ depends on the self-interaction constant λ (or scattering length a), it can be larger than the Oppenheimer-Volkoff limit $M_{OV} = 0.376M_P^3/m_n^2 = 0.7M_\odot$ obtained by assuming that neutron stars can be modeled as an ideal gas of fermions (the corresponding radius is $R = 9.36\,GM_{OV}/c^2 = 3.52(M_P/m_n)\lambda_c = 9.6\,\mathrm{km}$ and the corresponding

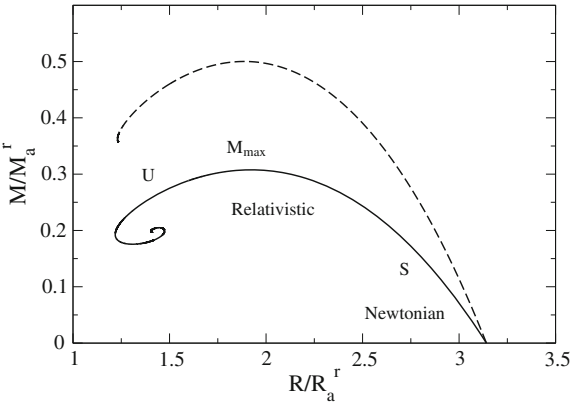

Fig. 6.6 Mass-radius relation of general relativistic BEC stars in the TF limit (*solid line* relativistic equation of state; *dashed line* non-relativistic equation of state). The series of equilibria is stable until the point of maximum mass

density is $\rho = 5 \times 10^{15}\,\mathrm{g\,cm^{-3}}$). By taking a scattering length of the order of 10–20 fm (hence $\lambda/8\pi \sim 95.2-190$), we obtain a maximum mass of the order of $2M_\odot$, a central density of the order of $1\text{–}3\times 10^{15}\,\mathrm{g\,cm^{-3}}$, and a radius in the range of 10–20 km [73]. This could account for the recently observed neutron stars with masses in the range of $2\text{–}2.4M_\odot$ larger than the Oppenheimer-Volkoff limit.

The general relativistic treatment of BEC stars by Chavanis and Harko [73] can also be applied straightforwardly to the description of condensate dark matter stars that may have formed in the primordial universe by Jeans instability. These compact objects should contain a significant fraction of condensate dark matter in their core and behave as BEC stars with the critical mass and radius given by Eqs. (6.84) and (6.85) above. When a condensate dark matter star is formed, it may accrete some material from space [91, 92]. The accretion process may increase the mass of the condensate star and, if the maximum mass is exceeded, cause the collapse of the condensate star. This collapse may form black holes from the dark matter star and have signature in the observations of high redshift long γ-ray bursts.

6.5.7 Are Microscopic Quantum Black Holes Bose-Einstein Condensates of Gravitons?

The Kaup mass (6.67), which is the maximum mass of a stable self-gravitating BEC resulting from the balance between quantum pressure (Heisenberg's uncertainty principle) and gravity in general relativity, scales as $M \sim M_P^2/m$. If N denotes the number of bosons in the BEC, so that $M = Nm$, we get $N \sim M_P^2/m^2$. On the other hand, the Kaup radius scales as $R \sim GM/c^2 \sim GM_P^2/mc^2 \sim \hbar/mc \sim \lambda_c \sim (M_P/m)l_P$ where $l_P = (\hbar G/c^3)^{1/2} = 1.62 \times 10^{-35}\,\mathrm{m}$ is the Planck length.

This corresponds to the "most packed" stable configuration. If we assume that the BEC remains stuck at the critical point, and if we take the number of bosons N as the sole characteristic of the BEC, the foregoing relations imply $m \sim M_P/\sqrt{N}$, $M \sim \sqrt{N}M_P$, and $R \sim \sqrt{N}l_P$. If we view microscopic quantum black holes as BECs of gravitons at a critical point, these scalings agree with those obtained by Dvali and Gomez [75] and Casadio and Orlandi [76] in a more phenomenological manner [the Gaussian profile obtained in [76] is also consistent with the Gaussian ansatz (6.44)]. In that interpretation, m is the effective mass of the gravitons and N is the occupation number of gravitons in the gravitational field, or the number of internal degrees of freedom of the black hole. For the gravitational interaction $-Gm^2/r$, the coupling constant scales as $\alpha \sim m^2/M_P^2 \sim l_P^2/\lambda_c^2 \sim 1/N$. We note that these scalings emerge naturally from the expression of the Kaup mass and Kaup radius, and N simply represents the number of bosons in the BEC. If we argue that the entropy of the "BEC black hole" scales as $S_{BH} \sim k_B N$ (originating from the exponentially growing with N number of quantum states [75]), we immediately recover the expression of the Bekenstein entropy $S_{BH} \sim k_B R^2/l_P^2$ stating that the entropy of a black hole scales as its area [93]. Finally, defining the temperature by the thermodynamical expression $d(Mc^2) = TdS_{BH}$, we obtain the scaling of the Hawking temperature $k_B T \sim mc^2 \sim M_P^2 c^2/M \sim \hbar c^3/GM \sim \hbar c/R \sim M_P c^2/\sqrt{N} \sim k_B T_P/\sqrt{N}$ where $T_P = (\hbar c^5/Gk_B^2)^{1/2} = 1.42 \times 10^{32}$ K is the Planck temperature. Inversely, if we define the temperature by $k_B T \sim mc^2$, we can derive from the first law of thermodynamics $d(Mc^2) = TdS_{BH}$ the black hole entropy $S_{BH} \sim N \sim k_B R^2/l_P^2$. In summary, we have the scalings

$$m \sim \frac{M_P}{\sqrt{N}}, \quad M \sim \sqrt{N}M_P, \quad R \sim \sqrt{N}l_P, \quad S \sim k_B N, \quad T \sim \frac{T_P}{\sqrt{N}}, \quad \alpha \sim \frac{1}{N}. \tag{6.86}$$

These scalings assume that the BEC remains stuck at the Kaup quantum critical point. As a result, the effective mass of the gravitons (that are massless) increases as N decreases (see below). We can also obtain the scalings (6.86) from the maximum mass (6.70) provided that the self-interaction constant scales as $\lambda \sim m^2/M_P^2 \sim 1/N$ (i.e. $a \sim \lambda\hbar/mc \sim Gm/c^2 \sim (m/M_P)l_P \sim l_P/\sqrt{N}$) which corresponds to the limit of validity of the TF approximation. We note that $a_S = 2Gm/c^2$ is the Schwarzschild radius of a particle of mass m.

As shown by Dvali and Gomez [75], the Hawking radiation[3] according to which black holes lose mass and energy, and the negative specific heat of the black holes[4] immediately result from the quantum depletion of the condensates by spontaneous

[3] In the semi-classical limit, the radiation of a black hole may be obtained from the Stefan-Boltzmann law $\dot{M}c^2 \sim -A\sigma T^4 \sim -\hbar c^6/G^2M^2$ where $\sigma \sim k_B^4/c^2\hbar^3$ is the black body constant and $A \sim R^2$ the black hole area. Using the scalings (6.86), this equation may be rewritten as $\dot{N} \sim -1/(t_P\sqrt{N})$ where $t_P = (\hbar G/c^5)^{1/2} = 5.39 \times 10^{-44}$ s is the Planck time. After integration, we obtain the scaling of the evaporation time of a black hole $\tau \sim M^3G^2/\hbar c^4 \sim N^{3/2}t_P$.

[4] Using $E \sim Mc^2 \sim \hbar c^5/Gk_B T$, we get $C = dE/dT \sim -\hbar c^5/Gk_B T^2 < 0$ so that the temperature increases as the black hole loses mass and energy.

particle emission. Actually, the arguments of Dvali and Gomez [75] generalize the semi-classical results of Hawking ($N \gg 1$) to the fully quantum regime (small N). We note that the mass $M \sim \sqrt{N}M_P$ and the area $A \sim R^2 \sim Nl_P^2$ of a black hole are *quantized* since N (occupation number) is an integer [94]. Each transition reduces the horizon area of a black hole by an integer number of Planck units. For $N = 1$ (ground state), we get $R \sim l_P$, $M = m \sim M_P$, and $T \sim T_P$ leading to Planck-size black holes (the Schwarzschild radius $a_S = 2Gm/c^2$ is of the order of the gravitational Bohr radius $a_B = \hbar^2/Gm^3$) [76] . These smallest black holes, instead of conventional Hawking evaporation [85, 95], are either stable (similarly to the $n = 1$ orbit of an electron around a proton whose stability is explained by quantum mechanics) or decay into the light fields in a single quantum jump. The classical limit is recovered for $N \gg 1$. Quantization of the horizons, and the notion of a minimal length in gravity, may eliminate physical singularities in cosmology (big bang and big crunch) [96]. Classical singularities may be replaced by a Planck black hole (with mass M_P and size l_P) and the scale factor $a(t)$ of the universe may become quantized as we approach the Planck scale. We note that in order to describe the inflationary era, the early universe viewed as a primordial black hole must gain energy and grow instead of radiating energy and decay. We therefore require a reversed flux of energy.

6.6 Conclusion

In this contribution, we have discussed some applications of self-gravitating BECs in astrophysics and their possible relation to black holes. We have exposed their elementary properties in Newtonian gravity and general relativity. There are many topics related to self-gravitating BECs that we have not discussed. They concern for example their formation by Jeans instability [15, 23, 28, 30, 33, 97, 98], their rotation leading to quantum vortex lattices [45, 99–103], their solitonic behavior [104–106], their gravitational cooling through emission of scalar field radiation [60, 65, 107], and their application to cosmology [50, 108–119]. Furthermore, we have exclusively considered BECs at $T = 0$ but the case of finite temperature BECs is also important [116, 120–126]. We refer to [64, 68, 127–136] for additional reviews on the subject.

An important potential application of self-gravitating BECs concerns the superfluid core of neutron stars and the notion of BEC stars [73]. For these compact objects, general relativity must be used and leads to the existence of a maximum mass $M_{\rm max} = 0.0612\sqrt{\lambda}M_P^3/m^2 = 0.307\hbar c^2\sqrt{a}/(Gm)^{3/2}$ above which no equilibrium is possible. For $M < M_{\rm max}$, stable BEC stars may describe neutron stars with a mass larger than the Oppenheimer-Volkoff limit [73]. For $M > M_{\rm max}$, the BECs should collapse and form stellar mass black holes. The formation of supermassive black holes is also possible if the BECs have negative scattering lengths corresponding to attractive short-range interactions. Again, there exist a maximum mass $M_{\rm max} = 1.012\hbar/\sqrt{|a|Gm} = 5.07M_P/\sqrt{|\lambda|}$ (usually very small) above which the BECs collapse [15]. On the other hand, stable BEC stars with a small (repulsive)

self-interaction may mimic supermassive black holes that reside at the center of galaxies [67, 69, 72]. Finally, the recent idea that black holes are BECs of gravitons stuck at a critical point [75] is fascinating.

Another application of self-gravitating BECs concerns dark matter halos. For these gigantic diluted objects, the Newtonian approximation can be used. In that context, the interest of the BEC model is to avoid the cusp problem and the missing satellite problem of the ΛCDM model. Indeed, gravitational collapse is prevented at small scales by the Heisenberg uncertainty principle or by repulsive short-range interactions. However, this scenario also encounters some problems. In the non-interacting case, the mass of the bosons must be extremely small, of the order of $m \sim 10^{-24}\,\mathrm{eV}/c^2$, in order to reproduce the properties of dark matter halos [17]. The existence of particles with such small masses is not established (but it is not ruled out neither). On the other hand, for self-interacting BECs in the TF approximation, the radius of the halo turns out to be independent on the total mass, and fixed by the properties of the bosons (their mass and scattering length) [40]. This is a major drawback of the BEC model because it implies that all the halos should have the same radius (unless the characteristics of the bosons change from halo to halo), which is clearly not the case. Going beyond the TF approximation does not help because it is found [15, 16] that the size of the self-gravitating BECs decreases with their mass while cosmological observations reveal that the size of the halos increases with the mass. It is possible that the BEC model at $T = 0$ describes only small halos (dwarf galaxies). In order to describe large halos, finite temperature effects should be taken into account. Finite temperature effects in the self-gravitating Bose gas have been studied in [120–122, 125]. In that case, the system has a core-halo structure with a small condensed core (equivalent to a BEC at $T = 0$) surrounded by an extended isothermal classical atmosphere of non-condensed bosons.

Another possible scenario is that dark matter is made of fermions (such as massive neutrinos) instead of bosons. This model also solves the cusp problem and the missing satellite problem. In that case, gravitational collapse is prevented at small scales by the Pauli exclusion principle. As for bosons, it may be necessary to consider the Fermi gas at finite temperature that displays interesting phase transitions between gaseous states and condensed states [137]. Originally, the self-gravitating Fermi gas at finite temperature with neutrino masses in the $\sim\ \mathrm{eV}/c^2$ range was proposed as a model for dark matter halos (e.g. $M = 10^{12}M_\odot$ and $R = 100\,\mathrm{kpc}$) and clusters of galaxies [138–140]. Then, it was suggested that degenerate superstars composed of weakly interacting fermions in the $\sim 10\,\mathrm{keV}/c^2$ range could be an alternative to the supermassive black holes that are reported to exist at the centers of galaxies (e.g. $M = 2.6 \times 10^6 M_\odot$ and $R = 18\,\mathrm{mpc}$ in our Galaxy) [141–143]. Finally, it was shown that a weakly interacting fermionic gas at finite temperature could provide a self-consistent model of dark matter that describes both the center and the halo of the galaxies [144]. Since the density of a self-gravitating isothermal sphere decreases as r^{-2} at large distances, this model is consistent with the flat rotation curves of the galaxies. On the other hand, since the core is degenerate in the sense of quantum

mechanics (Pauli exclusion principle), it leads to flat density profiles and avoids the cusp problem of cold dark matter models. In addition, the gravitational collapse of fermionic matter leads to a compact object (fermion ball) at the center of the galaxy that could be an alternative to a central black hole.

One difficulty with the finite temperature self-gravitating Bose and Fermi gases is to explain how the particles have thermalized and reached a statistical equilibrium state. Indeed, the relaxation time of self-gravitating systems is usually very large, exceeding the age of the universe by many orders of magnitude [1]. To solve this timescale problem, we have proposed [15] that dark matter should be considered as a collisionless system (made either of fermions or bosons) described by the Vlasov-Poisson system and undergoing a form of violent relaxation. This process, initially introduced by Lynden-Bell [145] in stellar dynamics, leads to a distribution function similar to the Fermi-Dirac distribution function. In that case, the origin of the "degeneracy" is due to dynamical constraints (Liouville's theorem) instead of quantum mechanics (Pauli's principle). This theory was initially developed to describe collisionless stellar systems such as elliptical galaxies. In that case, the non-degenerate limit may be the most relevant [145]. However, this approach (with dynamical degeneracy retained) could also apply to dark matter halos [146, 147]. In that case, gravitational collapse is prevented by Lynden-Bell's type of exclusion principle. Furthermore, this approach provides a much more efficient relaxation mechanism than the fermionic scenario. Indeed, the violent relaxation of collisionless systems (leading to the Lynden-Bell statistics) takes place on a few dynamical times while the collisional relaxation of fermions (leading to the Fermi-Dirac statistics) is very long and possibly unrealistic. Therefore, it is not clear how the fermions have thermalized and how they can possess sufficiently high temperatures. By contrast, the Lynden-Bell theory predicts a high effective temperature (even if $T = 0$ initially), a r^{-2} density profile at large distances consistent with the flat rotation curves of galaxies, and an effective exclusion principle at short distances that could avoid the cusp problem and lead to fermion balls mimicking black holes, just as in the fermionic scenario. These features are remarkably consistent with the observations of dark matter halos making this alternative scenario very attractive.

In the fermionic and bosonic models, the smooth core density of dark matter halos is justified by quantum mechanics. However, we would like to emphasize that a classical self-gravitating isothermal gas (possibly justified by the process of violent relaxation) also has a smooth core density due to finite temperature effects [148]. Therefore, classical isothermal, or almost isothermal, self-gravitating systems may be the most relevant description of large dark matter halos while quantum effects (for bosons or fermions) or Lynden-Bell's type of degeneracy (for collisionless systems) may be important only for small halos or in the very inner region of large halos. These promising ideas will be developed in future works.

Appendix

6.7 Self-interaction Constant

We define the self-interaction constant by [15]:

$$\frac{\lambda}{8\pi} \equiv \frac{a}{\lambda_c} = \frac{amc}{\hbar}, \tag{6.87}$$

where $\lambda_c = \hbar/mc$ is the Compton wavelength of the bosons. This is a dimensionless parameter measuring the strength of the short-range interactions. It can be written as

$$\frac{\lambda}{8\pi} = 5.07\, \frac{a}{1\,\text{fm}}\, \frac{m}{1\,\text{GeV}/c^2}. \tag{6.88}$$

Using this expression, we can express the results in terms of λ and m instead of a and m.

6.8 Conservation of Energy

The total energy associated with the quantum Euler-Poisson system (6.14)–(6.16) is given by Eq. (6.37). According to Eq. (6.38), we have

$$\delta\Theta_c = \int \frac{\mathbf{u}^2}{2}\delta\rho\, d\mathbf{r} + \int \rho\mathbf{u}\cdot\delta\mathbf{u}\, d\mathbf{r}. \tag{6.89}$$

On the other hand, using Eqs. (6.10) and (6.39), we find that

$$\begin{aligned}\delta\Theta_Q &= \frac{\hbar^2}{m^2}\int \nabla\sqrt{\rho}\cdot\delta\nabla\sqrt{\rho}\, d\mathbf{r} = \frac{\hbar^2}{m^2}\int \nabla\sqrt{\rho}\cdot\nabla\left(\frac{1}{2\sqrt{\rho}}\delta\rho\right) d\mathbf{r}\\ &= -\frac{\hbar^2}{2m^2}\int \frac{\Delta\sqrt{\rho}}{\sqrt{\rho}}\delta\rho\, d\mathbf{r} = \frac{1}{m}\int Q\delta\rho\, d\mathbf{r}.\end{aligned} \tag{6.90}$$

Finally, according to Eqs. (6.40) and (6.41), we have

$$\delta U = \frac{4\pi a\hbar^2}{m^3}\int \rho\delta\rho\, d\mathbf{r}, \quad \delta W = \int \Phi\delta\rho\, d\mathbf{r}. \tag{6.91}$$

Taking the time derivative of the total energy E_{tot} and using the previous relations, we get

$$\dot{E}_{tot} = \int\left(\frac{\mathbf{u}^2}{2} + \frac{Q}{m} + \frac{4\pi a\hbar^2}{m^3}\rho + \Phi\right)\frac{\partial\rho}{\partial t}\, d\mathbf{r} + \int \rho\mathbf{u}\cdot\frac{\partial\mathbf{u}}{\partial t}\, d\mathbf{r}. \tag{6.92}$$

Using the equation of continuity (6.14), integrating by parts, using the Euler equation (6.15) and the identity $(\mathbf{u}\cdot\nabla)\mathbf{u} = \nabla\left(\mathbf{u}^2/2\right) - \mathbf{u}\times(\nabla\times\mathbf{u})$, we obtain after simplification

$$\dot{E}_{tot} = \int \rho\mathbf{u}\cdot(\mathbf{u}\times(\nabla\times\mathbf{u}))\, d\mathbf{r}. \tag{6.93}$$

Since $\mathbf{u}$ is a potential flow, we have $\nabla\times\mathbf{u} = \mathbf{0}$ yielding $\dot{E}_{tot} = 0$. Actually, we note that this result remains valid even if $\mathbf{u}$ is not a potential flow since $\mathbf{u}\cdot(\mathbf{u}\times(\nabla\times\mathbf{u})) = 0$.

6.9 Virial Theorem

In this Appendix, we establish the time-dependent tensorial Virial theorem associated with the quantum Euler-Poisson system (6.14)–(6.16).

Taking the time derivative of the moment of inertia tensor $I_{ij} = \int \rho x_i x_j\, d\mathbf{r}$ and using the equation of continuity (6.14), we obtain after an integration by parts

$$\dot{I}_{ij} = \int \rho(x_i u_j + x_j u_i)\, d\mathbf{r}. \tag{6.94}$$

Taking the time derivative of Eq. (6.94), we get

$$\ddot{I}_{ij} = \int x_i \frac{\partial}{\partial t}(\rho u_j)\, d\mathbf{r} + (i\leftrightarrow j), \tag{6.95}$$

where $\partial_t(\rho u_j)$ is given by Eq. (6.13). We need to evaluate four terms. The first term is

$$-\int x_i \partial_k(\rho u_j u_k)\, d\mathbf{r} = \int \rho u_i u_j\, d\mathbf{r}. \tag{6.96}$$

The second term is

$$-\int x_i \frac{\partial p}{\partial x_j}\, d\mathbf{r} = \delta_{ij}\int p\, d\mathbf{r}. \tag{6.97}$$

The third term is

$$-\int \rho x_i \frac{\partial \Phi}{\partial x_j}\, d\mathbf{r} = W_{ij}, \tag{6.98}$$

where W_{ij} is the potential energy tensor. It is a simple matter to show that this tensor is symmetric: $W_{ij} = W_{ji}$ [1]. The fourth term is

$$-\int x_i \frac{\rho}{m}\frac{\partial Q}{\partial x_j}\, d\mathbf{r} = -\int x_i \partial_k P_{jk}\, d\mathbf{r} = \int P_{ij}\, d\mathbf{r}, \tag{6.99}$$

where P_{ij} is the quantum pressure tensor defined by Eq. (6.17). Substituting these results in Eq. (6.95), we obtain the tensorial Virial theorem

$$\frac{1}{2}\ddot{I}_{ij} = \int \rho u_i u_j \, d\mathbf{r} + \int P_{ij} \, d\mathbf{r} + \delta_{ij} \int p \, d\mathbf{r} + W_{ij}. \tag{6.100}$$

Contracting the indices and using the fact that $\int P_{ii} \, d\mathbf{r} = 2\Theta_Q$ [this can be obtained from Eqs. (6.17) and (6.39)] and $W_{ii} = -\int \rho \mathbf{r} \cdot \nabla \Phi \, d\mathbf{r} = W$ [the Virial of the gravitational force in $d = 3$ is equal to the potential energy [1]], we obtain

$$\frac{1}{2}\ddot{I} = 2(\Theta_c + \Theta_Q) + 3 \int p \, d\mathbf{r} + W, \tag{6.101}$$

where $I = \int \rho r^2 \, d\mathbf{r}$ is the moment of inertia. For a steady state ($\ddot{I}_{ij} = 0$ and $\mathbf{u} = \mathbf{0}$), we obtain the equilibrium tensorial Virial theorem

$$\int P_{ij} \, d\mathbf{r} + \delta_{ij} \int p \, d\mathbf{r} + W_{ij} = 0 \tag{6.102}$$

and the scalar Virial theorem

$$2\Theta_Q + 3 \int p \, d\mathbf{r} + W = 0. \tag{6.103}$$

These results are valid for an arbitrary equation of state $p(\rho)$. For the equation of state (6.12), using $\int p \, d\mathbf{r} = U$, Eqs. (6.101) and (6.103) reduce to Eqs. (6.42) and (6.43).

6.10 Stress Tensor

The equation of continuity (6.14) may be written as

$$\frac{\partial \rho}{\partial t} + \nabla \cdot \mathbf{j} = 0, \tag{6.104}$$

where $\mathbf{j} = \rho \mathbf{u}$ is the density current. Using Eqs. (6.6) and (6.7), the density current can be expressed in terms of the wave function as

$$\mathbf{j} = \frac{N\hbar}{2i} \left(\psi^* \nabla \psi - \psi \nabla \psi^* \right). \tag{6.105}$$

On the other hand, the quantum Euler equation (6.13) may be written as

$$\frac{\partial \mathbf{j}}{\partial t} = -\nabla(\rho \mathbf{u} \otimes \mathbf{u}) - \nabla p - \rho \nabla \Phi - \frac{\rho}{m} \nabla Q. \tag{6.106}$$

Introducing the quantum pressure tensor, we find that the equation for the density current is given by

$$\frac{\partial j_i}{\partial t} = -\partial_j T_{ij} - \rho \partial_i \Phi, \tag{6.107}$$

where

$$T_{ij} = \rho u_i u_j + p\delta_{ij} + P_{ij} \tag{6.108}$$

is the stress tensor. Using Eq. (6.17), we have

$$T_{ij} = \rho u_i u_j + p\delta_{ij} - \frac{\hbar^2}{4m^2}\rho \partial_i \partial_j \ln \rho \tag{6.109}$$

or, alternatively,

$$T_{ij} = \rho u_i u_j + \left(p - \frac{\hbar^2}{4m^2}\Delta\rho\right)\delta_{ij} + \frac{\hbar^2}{4m^2}\frac{1}{\rho}\partial_i\rho\partial_j\rho. \tag{6.110}$$

Using Eqs. (6.6) and (6.7), we find after straightforward algebra that

$$\frac{\hbar^2}{4m^2}\frac{1}{\rho}\partial_i\rho\partial_j\rho = \frac{N\hbar^2}{4m}\frac{1}{|\psi|^2}(\psi^*\partial_i\psi + \psi\partial_i\psi^*)(\psi^*\partial_j\psi + \psi\partial_j\psi^*) \tag{6.111}$$

and

$$\rho u_i u_j = -\frac{N\hbar^2}{4m}\frac{1}{|\psi|^2}(\psi^*\partial_i\psi - \psi\partial_i\psi^*)(\psi^*\partial_j\psi - \psi\partial_j\psi^*). \tag{6.112}$$

Therefore

$$\rho u_i u_j + \frac{\hbar^2}{4m^2}\frac{1}{\rho}\partial_i\rho\partial_j\rho = \frac{N\hbar^2}{m}\mathrm{Re}\left(\frac{\partial\psi}{\partial x_i}\frac{\partial\psi^*}{\partial x_j}\right). \tag{6.113}$$

Regrouping these results, the stress tensor can be expressed in terms of the wave function as

$$T_{ij} = \frac{N\hbar^2}{m}\mathrm{Re}\left(\frac{\partial\psi}{\partial x_i}\frac{\partial\psi^*}{\partial x_j}\right) + \left(\frac{2\pi a\hbar^2}{m}N^2|\psi|^4 - \frac{N\hbar^2}{4m}\Delta|\psi|^2\right)\delta_{ij}. \tag{6.114}$$

Finally, we introduce the density of energy

$$e = \frac{\mathbf{u}^2}{2} + \frac{Q}{m} + \frac{2\pi a\hbar^2}{m^3}\rho + \frac{\Phi}{2}. \tag{6.115}$$

Using the equation of continuity (6.14) and the quantum Euler equation (6.15), we obtain the energy equation

$$\frac{\partial}{\partial t}(\rho e) + \nabla \cdot (\rho e \mathbf{u}) = -\nabla \cdot (p\mathbf{u}) - \frac{1}{2}\rho \mathbf{u} \cdot \nabla \Phi + \frac{\rho}{m}\frac{\partial Q}{\partial t} + \frac{1}{2}\rho \frac{\partial \Phi}{\partial t}. \tag{6.116}$$

The conservation of energy directly results from this equation. Taking the time derivative of the total energy $E_{tot} = \int \rho e \, d\mathbf{r}$, and using Eq. (6.116), we get

$$\dot{E}_{tot} = -\frac{1}{2}\int \rho \mathbf{u} \cdot \nabla \Phi \, d\mathbf{r} + \int \frac{\rho}{m}\frac{\partial Q}{\partial t} \, d\mathbf{r} + \frac{1}{2}\int \rho \frac{\partial \Phi}{\partial t} \, d\mathbf{r}. \tag{6.117}$$

Using the Poisson equation (6.16) and the equation of continuity (6.14), and integrating by parts, we obtain

$$\begin{aligned} \frac{1}{2}\int \rho \frac{\partial \Phi}{\partial t} \, d\mathbf{r} &= \frac{1}{8\pi G}\int \Delta \Phi \frac{\partial \Phi}{\partial t} \, d\mathbf{r} = \frac{1}{2}\int \Phi \frac{\partial \rho}{\partial t} \, d\mathbf{r} \\ &= -\frac{1}{2}\int \Phi \nabla \cdot (\rho \mathbf{u}) \, d\mathbf{r} = \frac{1}{2}\int \rho \mathbf{u} \cdot \nabla \Phi \, d\mathbf{r}. \end{aligned} \tag{6.118}$$

On the other hand, using Eqs. (6.38) and (6.90), we find that

$$\int \rho \frac{\partial Q}{\partial t} \, d\mathbf{r} = m\frac{d\Theta_Q}{dt} - \int Q \frac{\partial \rho}{\partial t} \, d\mathbf{r} = \int Q \frac{\partial \rho}{\partial t} \, d\mathbf{r} - \int Q \frac{\partial \rho}{\partial t} \, d\mathbf{r} = 0. \tag{6.119}$$

Substituting these identities in Eq. (6.117), we obtain $\dot{E}_{tot} = 0$.

6.11 Lagrangian and Hamiltonian

In this Appendix, we discuss the Lagrangian and Hamiltonian structure of the GP equation and of the corresponding hydrodynamic equations.

The Lagrangian of the GP equation (6.4) is

$$L = \int \left\{ i\frac{\hbar}{2}N\left(\psi^* \frac{\partial \psi}{\partial t} - \psi \frac{\partial \psi^*}{\partial t}\right) - \frac{N\hbar^2}{2m}|\nabla \psi|^2 - \frac{1}{2}Nm|\psi|^2 \Phi - \frac{2\pi a \hbar^2}{m}N^2|\psi|^4 \right\} d\mathbf{r}. \tag{6.120}$$

We can view the Lagrangian (6.120) as a functional of ψ, $\dot{\psi}$, and $\nabla\psi$. The action is $S = \int L \, dt$. The least action principle $\delta S = 0$, which is equivalent to the Lagrange equations

$$\frac{\partial}{\partial t}\left(\frac{\delta L}{\delta \dot{\psi}}\right) + \nabla \cdot \left(\frac{\delta L}{\delta \nabla \psi}\right) - \frac{\delta L}{\delta \psi} = 0 \tag{6.121}$$

returns the GP equation (6.4). The Hamiltonian is obtained from the transformation

$$H=\int i\frac{\hbar}{2}N\left(\psi^*\frac{\partial\psi}{\partial t}-\psi\frac{\partial\psi^*}{\partial t}\right)d\mathbf{r}-L \tag{6.122}$$

leading to

$$H=\int\left\{\frac{N\hbar^2}{2m}|\nabla\psi|^2+\frac{1}{2}Nm|\psi|^2\Phi+\frac{2\pi a\hbar^2}{m}N^2|\psi|^4\right\}d\mathbf{r}. \tag{6.123}$$

Of course, this expression coincides with the total energy (6.37) in the wavefunction representation. Using the Lagrange equations, one can show that the Hamiltonian is conserved. On the other hand, the GP equation (6.4) can be written as

$$i\hbar\frac{\partial\psi}{\partial t}=\frac{1}{N}\frac{\delta H}{\delta\psi^*}. \tag{6.124}$$

A stable stationary solution of the GP equation is a minimum of energy under the normalization condition. Writing the variational principle as $\delta H-\alpha Nm\int|\psi|^2\,d\mathbf{r}=0$ where α is a Lagrange multiplier (chemical potential), we recover the time-independent GP equation (6.19) with $E=\alpha m$.

Using the Madelung transformation (see Sect. 6.2.2), we can rewrite the Lagrangian and the Hamiltonian in terms of hydrodynamic variables. According to Eqs. (6.6) and (6.7) we have

$$\frac{\partial S}{\partial t}=\frac{\hbar}{2i}\frac{1}{|\psi|^2}\left(\psi^*\frac{\partial\psi}{\partial t}-\psi\frac{\partial\psi^*}{\partial t}\right) \tag{6.125}$$

and

$$|\nabla\psi|^2=\frac{1}{Nm\hbar^2}\left[\rho(\nabla S)^2+\frac{\hbar^2}{4\rho}(\nabla\rho)^2\right]. \tag{6.126}$$

Substituting these identities in Eq. (6.120) we get

$$L=-\int\left\{\frac{\rho}{m}\frac{\partial S}{\partial t}+\frac{\rho}{2m^2}(\nabla S)^2+\frac{\hbar^2}{8m^2}\frac{(\nabla\rho)^2}{\rho}+\frac{1}{2}\rho\Phi+\frac{2\pi a\hbar^2}{m^3}\rho^2\right\}d\mathbf{r}. \tag{6.127}$$

We can view the Lagrangian (6.127) as a functional of S, $\dot{S}$, ∇S, ρ, $\dot{\rho}$, and $\nabla\rho$. The Lagrange equations for the phase

$$\frac{\partial}{\partial t}\left(\frac{\delta L}{\delta\dot{S}}\right)+\nabla\cdot\left(\frac{\delta L}{\delta\nabla S}\right)-\frac{\delta L}{\delta S}=0 \tag{6.128}$$

return the equation of continuity (6.8). The Lagrange equations for the density

$$\frac{\partial}{\partial t}\left(\frac{\delta L}{\delta \dot{\rho}}\right)+\nabla\cdot\left(\frac{\delta L}{\delta \nabla\rho}\right)-\frac{\delta L}{\delta\rho}=0 \tag{6.129}$$

return the quantum Hamilton-Jacobi (or Bernouilli) equation (6.9) leading to the quantum Euler equation (6.15). The Hamiltonian is obtained from the transformation

$$H=-\int\frac{\rho}{m}\frac{\partial S}{\partial t}\,d\mathbf{r}-L \tag{6.130}$$

leading to

$$H=\int\left\{\frac{1}{2}\rho\mathbf{u}^2+\frac{\hbar^2}{8m^2}\frac{(\nabla\rho)^2}{\rho}+\frac{1}{2}\rho\Phi+\frac{2\pi a\hbar^2}{m^3}\rho^2\right\}d\mathbf{r}. \tag{6.131}$$

Of course, this expression coincides with the total energy (6.37) in the hydrodynamical representation. Using the Lagrange equations, one can show that the Hamiltonian is conserved.

References

1. Binney, J., Tremaine, S.: Galactic Dynamics. Princeton University Press, Princeton (1987)
2. Copeland, E.J., Sami, M., Tsujikawa, S.: Int. J. Mod. Phys. D **15**, 1753 (2006)
3. Persic, M., Salucci, P., Stel, F.: Mon. Not. R. Astron. Soc. **281**, 27 (1996)
4. Overduin, J.M., Wesson, P.S.: Phys. Rep. **402**, 267 (2004)
5. Peebles, P.J.E., Ratra, B.: Rev. Mod. Phys. **75**, 559 (2003)
6. Navarro, J.F., Frenk, C.S., White, S.D.M.: Mon. Not. R. Astron. Soc. **462**, 563 (1996)
7. Burkert, A.: Astrophys. J. **447**, L25 (1995)
8. Kauffmann, G., White, S.D.M., Guiderdoni, B.: Mon. Not. R. Astron. Soc. **264**, 201 (1993)
9. Pethick, C.J., Smith, H.: Bose-Einstein Condensation in Dilute Gases. Cambridge University Press, Cambridge (2008)
10. Madelung, E.: Zeit. F. Phys. **40**, 322 (1927)
11. Gross, E.P.: Ann. Phys. **4**, 57 (1958)
12. Gross, E.P.: Nuovo Cimento **20**, 454 (1961)
13. Gross, E.P.: J. Math. Phys. **4**, 195 (1963)
14. Pitaevskii, L.P.: Sov. Phys. JETP **9**, 830 (1959); ibid 13, 451 (1961)
15. Chavanis, P.H.: Phys. Rev. D **84**, 043531 (2011)
16. Chavanis, P.H., Delfini, L.: Phys. Rev. D **84**, 043532 (2011)
17. Baldeschi, M.R., Gelmini, G.B., Ruffini, R.: Phys. Lett. B **122**, 221 (1983)
18. Membrado, M., Pacheco, A.F., Sanudo, J.: Phys. Rev. A **39**, 4207 (1989)
19. Sin, S.J.: Phys. Rev. D **50**, 3650 (1994)
20. Schunck, F.E.: astro-ph/9802258
21. Matos, T., Guzmán, F.S.: Astron. F. Nachr. **320**, 97 (1999)
22. Guzmán, F.S., Matos, T.: Class. Quantum Gravity **17**, L9 (2000)
23. Hu, W., Barkana, R., Gruzinov, A.: Phys. Rev. Lett. **85**, 1158 (2000)
24. Matos, T., Ureña-López, L.A.: Phys. Rev. D **63**, 063506 (2001)
25. Arbey, A., Lesgourgues, J., Salati, P.: Phys. Rev. D **64**, 123528 (2001)

26. Silverman, M.P., Mallett, R.L.: Class. Quantum Gravity **18**, L103 (2001)
27. Alcubierre, M., Guzmán, F.S., Matos, T., Núñez, D., Ureña-López, L.A., Wiederhold, P.: Class. Quantum. Gravity **19**, 5017 (2002)
28. Silverman, M.P., Mallett, R.L.: Gen. Relativ. Gravit. **34**, 633 (2002)
29. Bernal, A., Matos, T., Núñez, D.: Rev. Mex. Astron. Astrofis. **44**, 149 (2008)
30. Sikivie, P., Yang, Q.: Phys. Rev. Lett. **103**, 111301 (2009)
31. Matos, T., Vazquez-Gonzalez, A., Magana, J.: Mon. Not. R. Astron. Soc. **393**, 1359 (2009)
32. Lee, J.W.: Phys. Lett. B **681**, 118 (2009)
33. Lee, J.W., Lim, S.: J. Cosmol. Astropart. Phys. **01**, 007 (2010)
34. Manfredi, G., Hervieux, P.A., Haas, F.: Class. Quantum Gravity **30**, 075006 (2013)
35. Lee, J.W., Koh, I.: Phys. Rev. D **53**, 2236 (1996)
36. Peebles, P.J.E.: Astrophys. J. **534**, L127 (2000)
37. Goodman, J.: New Astron. **5**, 103 (2000)
38. Lesgourgues, J., Arbey, A., Salati, P.: New Astron. Rev. **46**, 791 (2002)
39. Arbey, A., Lesgourgues, J., Salati, P.: Phys. Rev. D **68**, 023511 (2003)
40. Böhmer, C.G., Harko, T.: J. Cosmol. Astropart. Phys. **06**, 025 (2007)
41. Briscese, F.: Phys. Lett. B **696**, 315 (2011)
42. Harko, T.: J. Cosmol. Astropart. Phys. **05**, 022 (2011)
43. Pires, M.O.C., de Souza, J.C.C.: J. Cosmol. Astropart. Phys. **11**, 024 (2012)
44. Robles, V.H., Matos, T.: Mon. Not. R. Astron. Soc. **422**, 282 (2012)
45. Rindler-Daller, T., Shapiro, P.R.: Mon. Not. R. Astron. Soc. **422**, 135 (2012)
46. Lora, V., Magaña, J., Bernal, A., Sánchez-Salcedo, F.J., Grebel, E.K.: J. Cosmol. Astropart. Phys. **02**, 011 (2012)
47. González-Morales, A.X., Diez-Tejedor, A., Ureña-López, L.A., Valenzuela, O.: Phys. Rev. D **87**, 021301(R) (2013)
48. Guzmán, F.S., Lora-Clavijo, F.D., González-Avilés, J.J., Rivera-Paleo, F.J.: J. Cosmol. Astropart. Phys. **09**, 034 (2013)
49. Dalfovo, F., Giorgini, S., Pitaevskii, L.P., Stringari, S.: Rev. Mod. Phys. **71**, 463 (1999)
50. Chavanis, P.H.: Astron. Astrophys. **537**, A127 (2012)
51. Kaup, D.J.: Phys. Rev. **172**, 1331 (1968)
52. Ruffini, R., Bonazzola, S.: Phys. Rev. **187**, 1767 (1969)
53. Thirring, W.: Phys. Lett. B **127**, 27 (1983)
54. Breit, J.D., Gupta, S., Zaks, A.: Phys. Lett. B **140**, 329 (1984)
55. Takasugi, E., Yoshimura, M.: Z. Phys. C **26**, 241 (1984)
56. Colpi, M., Shapiro, S.L., Wasserman, I.: Phys. Rev. Lett. **57**, 2485 (1986)
57. van der Bij, J.J., Gleiser, M.: Phys. Lett. B **194**, 482 (1987)
58. Gleiser, M.: Phys. Rev. D **38**, 2376 (1988)
59. Gleiser, M., Watkins, R.: Nucl. Phys. B **319**, 733 (1989)
60. Seidel, E., Suen, W.M.: Phys. Rev. D **42**, 384 (1990)
61. Kusmartsev, F.V., Mielke, E.W., Schunck, F.E.: Phys. Lett. A **157**, 465 (1991)
62. Kusmartsev, F.V., Mielke, E.W., Schunck, F.E.: Phys. Rev. D **43**, 3895 (1991)
63. Lee, T.D., Pang, Y.: Phys. Rep. **221**, 251 (1992)
64. Jetzer, P.: Phys. Rep. **220**, 163 (1992)
65. Seidel, E., Suen, W.M.: Phys. Rev. Lett. **72**, 2516 (1994)
66. Balakrishna, J., Seidel, E., Suen, W.M.: Phys. Rev. D **58**, 104004 (1998)
67. Schunck, F.E., Liddle, A.R.: Black holes: theory and observation. In: Hehl, F.W., Kiefer, C., Metzler, R.J.K. (eds.) Proceedings of the 179th W.E. Heraeus Seminar, p. 285. Springer (1998)
68. Mielke, E.W., Schunck, F.E.: Nucl. Phys. B **564**, 185 (2000)
69. Torres, D.F., Capozziello, S., Lambiase, G.: Phys. Rev. D **62**, 104012 (2000)
70. Wang, X.Z.: Phys. Rev. D **64**, 124009 (2001)
71. Schunck, F.E., Mielke, E.W.: Class. Quantum Gravity **20**, R301 (2003)
72. Guzmán, F.S.: Phys. Rev. D **73**, 021501 (2006)
73. Chavanis, P.H., Harko, T.: Phys. Rev. D **86**, 064011 (2012)

74. Oppenheimer, J.R., Volkoff, G.M.: Phys. Rev. **55**, 374 (1939)
75. Dvali, G., Gomez, C.: Fortschr. Phys. **61**, 742 (2013)
76. Casadio, R., Orlandi, A.: J. High Energy Phys. **8**, 25 (2013)
77. Bohm, D.: Phys. Rev. **85**, 166 (1952)
78. Chandrasekhar, S.: An Introduction to the Study of Stellar Structure. Dover, Mineola, New York (1958)
79. von Weizsäcker, C.F.: Z. Phys. **96**, 431 (1935)
80. Fisher, R.A.: Proc. Cambridge Philos. Soc. **22**, 700 (1925)
81. Holm, D., Marsden, J., Ratiu, T., Weinstein, A.: Phys. Rep. **123**, 1 (1985)
82. Chavanis, P.H.: Phys. Rev. E **84**, 031101 (2011)
83. Sulem, C., Sulem, P.L.: The Nonlinear Schrödinger Equation. Springer, Berlin (1999)
84. Ledoux, P., Pekeris, C.L.: Astrophys. J. **94**, 124 (1941)
85. Hawking, S.: Nature **248**, 30 (1974)
86. Lee, T.D.: Phys. Rev. D **35**, 3637 (1987)
87. Torres, D.F.: Nucl. Phys. B **26**, 377 (2002)
88. Misner, C.W., Zapolsky, H.S.: Phys. Rev. Lett. **12**, 635 (1964)
89. Harrison, B.K., Thorne, K.S., Wakano, M., Wheeler, J.A.: Gravitation Theory and Gravitational Collapse. University of Chicago Press, Chicago (1965)
90. Chavanis, P.H.: Astron. Astrophys. **381**, 709 (2002)
91. Li, X.Y., Harko, T., Cheng, K.S.: J. Cosmol. Astropart. Phys. **06**, 001 (2012)
92. Li, X.Y., Wang, F.Y., Cheng, K.S.: J. Cosmol. Astropart. Phys. **10**, 031 (2012)
93. Bekenstein, J.D.: Phys. Rev. D **7**, 2333 (1973)
94. Dvali, G., Gomez, C., Mukhanov, S.: arXiv:1106.5894
95. Hawking, S.: Commun. Math. Phys. **43**, 199 (1975)
96. Dvali, G., Gomez, C., Mukhanov, S.: J. High Energy Phys. **2**, 12 (2011)
97. Khlopov, M.Y., Malomed, B.A., Zeldovich, Y.B.: Mon. Not. R. Astron. Soc. **215**, 575 (1985)
98. Bianchi, M., Grasso, D., Ruffini, R.: Astron. Astrophys. **231**, 301 (1990)
99. Kobayashi, Y., Kasai, M., Futamase, T.: Phys. Rev. D **50**, 7721 (1994)
100. Yoshida, S., Eriguchi, Y.: Phys. Rev. D **56**, 762 (1997)
101. Schunck, F.E., Mielke, E.W.: Phys. Lett. A **249**, 389 (1998)
102. Kain, B., Ling, H.Y.: Phys. Rev. D **82**, 064042 (2010)
103. Guzmán, F.S., Lora-Clavijo, F.D., González-Avilés, J.J., Rivera-Paleo, F.J.: arXiv:1310.3909
104. Bernal, A., Guzmán, F.S.: Phys. Rev. D **74**, 103002 (2006)
105. Lee, J.W., Lim, S., Choi, D.: arXiv:0805.3827
106. González, J.A., Guzmán, F.S.: Phys. Rev. D **83**, 103513 (2011)
107. Guzmán, F.S., Ureña-López, L.A.: Phys. Rev. D **645**, 814 (2006)
108. Fukuyama, T., Morikawa, M., Tatekawa, T.: J. Cosmol. Astropart. Phys. **06**, 033 (2008)
109. Fukuyama, T., Morikawa, M.: Phys. Rev. D **80**, 063520 (2009)
110. Harko, T.: Mon. Not. R. Astron. Soc. **413**, 3095 (2011)
111. Chavanis, P.H.: Phys. Rev. D **84**, 063518 (2011)
112. Harko, T.: Phys. Rev. D **83**, 123515 (2011)
113. Bettoni, D., Liberati, S., Sindoni, L.: J. Cosmol. Astropart. Phys. **11**, 007 (2011)
114. Magaña, J., Matos, T., Suárez, A., Sánchez-Salcedo, F.J.: J. Cosmol. Astropart. Phys. **10**, 003 (2012)
115. Park, C.G., Hwang, J.C., Noh, H.: Phys. Rev. D **86**, 083535 (2012)
116. Harko, T., Mocanu, G.: Phys. Rev. D **85**, 084012 (2012)
117. Velten, H., Wamba, E.: Phys. Lett. B **709**, 1 (2012)
118. Kain, B., Ling, H.Y.: Phys. Rev. D **85**, 023527 (2012)
119. Li, B., Rindler-Daller, T., Shapiro, P.R.: arXiv:1310.6061
120. Ingrosso, G., Ruffini, R.: Nuovo Cimento **101**, 369 (1988)
121. Ingrosso, G., Merafina, M., Ruffini, R.: Nuovo Cimento **105**, 977 (1990)
122. Bilic, N., Nikolic, H.: Nucl. Phys. B **590**, 575 (2000)
123. Matos, T., Suárez, A.: Europhys. Lett. **96**, 56005 (2011)
124. Harko, T., Madarassy, E.: J. Cosmol. Astropart. Phys. **01**, 020 (2012)

125. Slepian, Z., Goodman, J.: Mon. Not. R. Astron. Soc. **427**, 839 (2012)
126. Robles, V.H., Matos, T.: Astrophys. J. **763**, 19 (2013)
127. Liddle, A.R., Madsen, M.S.: Int. J. Mod. Phys. D **1**, 101 (1992)
128. Guzmán, F.S.: J. Phys.: Conf. Series **91**, 012003 (2007)
129. Lee, J.W.: Korean Phys. Soc. **54**, 2622 (2009)
130. Liebling, S.L., Palenzuela, C.: Living Rev. Relativ. **15**, 6 (2012)
131. Magaña, J., Matos, T.: J. Phys.: Conf. Series **378**, 012012 (2012)
132. Magaña, J., Matos, T., Robles, V., Suárez, A.: arXiv:1201.6107
133. Rindler-Daller, T., Shapiro, P.R.: arXiv:1209.1835
134. Suárez, A., Robles, V.H., Matos, T.: arXiv:1302.0903
135. Dwornik, M., Keresztes, Z., Gergely L.A.: arXiv:1312.3715
136. Rindler-Daller, T., Shapiro, P.R.: Mod. Phys. Lett. A **29**, 1430002 (2014)
137. Chavanis, P.H.: Int. J. Mod. Phys. B **20**, 3113 (2006)
138. Fabbri, R., Jantzen, R., Ruffini, R.: Astron. Astrophys. **114**, 219 (1982)
139. Ruffini, R., Stella, L.: Astron. Astrophys. **119**, 35 (1983)
140. Gao, J.G., Merafina, M., Ruffini, R.: Astron. Astrophys. **235**, 1 (1990)
141. Bilic, N., Viollier, R.D.: Phys. Lett. B **408**, 75 (1997)
142. Bilic, N., Viollier, R.D.: Eur. Phys. J. C **11**, 173 (1999)
143. Bilic, N., Lindebaum, R.J., Tupper, G.B., Viollier, R.D.: Phys. Lett. B **515**, 105 (2001)
144. Bilic, N., Tupper, G.B., Viollier, R.D.: Lect. Notes Phys. **616**, 24 (2003)
145. Lynden-Bell, D.: Mon. Not. R. Astron. Soc. **136**, 101 (1967)
146. Kull, A., Treumann, R.A., Böhringer, H.: Astrophys. J. **466**, L1 (1996)
147. Chavanis, P.H., Sommeria, J.: Mon. Not. R. Astron. Soc. **296**, 569 (1998)
148. Chavanis, P.H.: Astron. Astrophys. **381**, 340 (2002)

Chapter 7
Quantum Amplitudes in Black–Hole Evaporation with Local Supersymmetry

P.D. D'Eath and A.N.St.J. Farley

Abstract In 1974, Hawking showed that a Schwarzschild black hole (mass M) radiates all dynamical fields out to infinity, at a calculable rate. If one changes the system by including a heat bath at a suitable temperature, $\theta = \hbar c^3/8\pi GMk$, where k is Boltzmann's constant, then the entire system will be in thermal balance. One says that θ is the **temperature of the black hole**. The analogy between the black hole and a thermal body is more than formal: for example, one can assign an **entropy** to the black hole, $Ac^3/4\hbar G$, where $A = 16\pi M^2$ is the area of the black hole, and formulate a generalised second law of thermodynamics. The rate of loss of mass by radiation implies that the black hole will have lost all its mass in a time which scales as M^3. The quasi–classical approximations involved in the above derivation are expected to have broken down well before this time. These difficulties should be reflected in a full quantum treatment. In 1975/1976, Hawking described black–hole evaporation in the language of **density matrices**: one only attempts to calculate **probabilities** for quantum processes, **not quantum amplitudes** with their extra phase information. It will be seen below that in the case that the action functional is invariant under local supersymmetry (that is, for supergravity + supermatter), quantum amplitudes involving black holes **can** be calculated. Indeed, in a certain sense (below), such an amplitude is **semi-classical**. The first three to four pages of this chapter will expand on this background description.

Keywords Black holes · Evaporation · Quantum amplitudes · Probabilities · Density matrices · Local supersymmetry · 'Semi-classical' amplitudes · Particle emission

P.D. D'Eath (✉) · A.N.St.J. Farley
Department of Applied Mathematics and Theoretical Physics,
Centre for Mathematical Sciences, University of Cambridge, Wilberforce Road,
Cambridge, CB3 0WA, UK
e-mail: pdd1000@damtp.cam.ac.uk

X. Calmet (ed.), *Quantum Aspects of Black Holes*,
Fundamental Theories of Physics 178, DOI 10.1007/978-3-319-10852-0_7

7.1 Introduction

Since 1974, it has been known that a Schwarzschild–like black hole (mass M), formed from gravitational collapse, radiates dynamical fields thermally to infinity at **temperature**, $\theta = \hbar c^3/8\pi GMk$, where k is Boltzmann's constant and $\hbar = 1$ [1, 2]. The analogy between a black hole and a thermal body is more than formal: one assigns an **entropy**, $Akc^3/4G$, to the black hole, where $A = 16\pi GM^2/c^3$ is the area of the black hole, with a generalised second law of thermodynamics [3, 4]. The rate of loss of mass by radiation implies that the black hole will have lost all its mass in a time proportional to G^2M^3/c^4. The quasi–classical approximations involved above are expected to have broken down well before this time. These features should be reflected in a full quantum treatment. However, since 1975/1976 [5], black–hole evaporation has been mistakenly described in the language of **density matrices**: assuming that one can only calculate **probabilities** for quantum processes, instead of **quantum amplitudes**, with their extra phase information. Since 2001, it became clear that, provided the action is invariant under local supersymmetry (that is, for supergravity + supermatter [6]), quantum amplitudes involving black holes **can** be calculated [7]. Indeed, in a certain sense (below), such amplitudes are **semi–classical**.

This Chapter is concerned with the quantum–mechanical decay of a four-dimensional Schwarzschild-like black hole, formed by gravitational collapse, into almost–flat space–time and weak radiation at late times, within the framework of quantum field theory. We consider **quantum amplitudes** (not just probabilities) for transitions from initial to final configurations, allowing for possible formation and evaporation of (one or more) black hole(s). Such quantum amplitudes are indeed found when one takes a **locally–supersymmetric** generalisation of Einstein gravity, such as $N = 1$ supergravity, plus possible supermatter [7–10]. We follow Dirac's approach to the quantisation of constrained Hamiltonian systems (systems having local invariances, as in general relativity, supergravity or gauge theory) [11]. Boundary data for a quantum amplitude are set on asymptotically–flat initial and final space–like hypersurfaces, $\Sigma_{I,F}$, separated by a time–interval, T, at spatial infinity. Below, we take T slightly complex, with $\mathrm{Im}(T) < 0$. One can have (for example) in a Hamiltonian treatment, as bosonic 'co–ordinate boundary data' on $\Sigma_{I,F}$, the intrinsic spatial three–metric, $h_{ij}(x)$, and a scalar field, $\phi(x)$. Suitable components of the spin–$\frac{1}{2}$ and spin–$\frac{3}{2}$ potentials give fermionic data on $\Sigma_{I,F}$. One asks for the quantum amplitude to go from initial to final data in time, T. Such amplitudes, in the '**field representation**', are **not, in a simple way, related** to the familiar scattering amplitudes of quantum field theory, defined in a **particle representation**, *via* harmonic–oscillator particle eigenstates for asymptotic in– or out–modes. Following Dirac's approach, one finds, remarkably, that for a field theory with local supersymmetry in four dimensions and boundary data as above, quantum amplitudes have a '**semi–classical' form**, $\delta\delta\,\exp\bigl(-I_{\mathrm{class}}\bigr)$ [8]. I_{class} denotes the Euclidean action of the classical solution joining initial to final data; such a solution is expected to exist, provided $\mathrm{Im}(T) < 0$. The terms, $\delta\delta$, denote a fermionic delta–functional—a

product of the fermionic supersymmetry constraints (the normal components of the gravitino field equation) at the boundaries. For other field–theory Lagrangians containing Einstein gravity plus possible matter (but which are not locally supersymmetric) in four dimensions, quantum amplitudes (and, hence, the model itself) are typically infinite and meaningless.

In the black–hole example, one can take the time–interval, T, sufficiently large that (for preference) Σ_F catches all the quantum radiation. One deforms T into the lower–half complex plane: $T \longrightarrow |T| \exp(-i\theta)(0 < \theta \leq \pi/2)$. This corresponds to Feynman's $+i\epsilon$ prescription [12, 13]. First, for simplicity, consider a 'background' **spherically–symmetric classical bosonic solution**, with gravitational data, $h_{ijI,F}$, on $\Sigma_{I,F}$, and scalar data, $\phi(r)_{I,F}$. Then, take **non–spherical perturbations** of the four–metric, $g_{\mu\nu}$, and ϕ, at linear order, obeying the classical field equations linearised about the spherically–symmetric background, subject to boundary data on $\Sigma_{I,F}$. Calculate the second–variation classical Euclidean action, $I^{(2)}_{\rm class}$, appearing in the amplitude, $\propto \exp(-I_{\rm class})$, above, as a functional of the boundary data. This leads (*inter alia*) to the **quantum amplitude** (real and imaginary parts) for weak final scalar fields [10]. The treatment involves adiabatic solutions of the scalar wave equation. In such locally–supersymmetric examples, no information is lost because of the black hole.

7.2 'Semi–Classical' Amplitudes

7.2.1 Locally–Supersymmetric Quantum Mechanics

Work by Bern et al. [14] indicates that Feynman–diagram amplitudes in $N = 8$ supergravity might be finite. An alternative approach to quantum amplitudes in supergravity, based on **Dirac's canonical quantisation of constrained Hamiltonian systems**, has been pursued since 1981 [15–17]. In this Section, Dirac's approach is outlined (i) for locally–supersymmetric quantum mechanics (QM) [18, 19] and (ii) for $N = 1$ supergravity [8, 15–17]. The main result is that, in both cases, (i) and (ii), with suitable local boundary data on initial and final asymptotically–flat hypersurfaces, Σ_I, Σ_F, the quantum amplitude has a 'semi–classical' form, in a precise sense [Eq. (7.2.20), below]. The amplitude involves the semi–classical exponential, $\exp\left(-I_{\rm class}\right)$, where $I_{\rm class}$ is the **Euclidean action of a classical solution** joining initial and final data, times a product of delta–functionals of the **classical fermionic supersymmetry constraints** at Σ_I, Σ_F (in $N = 1$ supergravity, of the normal components of the gravitino field equation.)

A simple example, showing how such 'semi–classical' amplitudes arise in locally–supersymmetric QM, follows from Witten [18] and Alvarez [19]. Standard non–relativistic QM, with bosonic spatial co–ordinate, q, is extended to a QM model invariant under local supersymmetry [19] by adjoining the odd (anti–commuting) co–ordinates, (ξ, η), with odd gravitino variables, (ψ_1, ψ_2), and a bosonic 'vierbein', e.

The last three variables appear algebraically in the Lagrangian [19], with no time– or space–derivatives—such variables are not dynamical, nor part of the boundary data.

In Alvarez' notation, setting his constant, g, to 1 (without loss of generality), the **Witten model with rigid N = 2 supersymmetry** has Lagrangian,

$$L = \frac{1}{2}\dot{q}^2 + i\Big(\xi\dot{\xi} + \eta\dot{\eta}\Big) - \frac{1}{2}\Big(W'\Big)^2 - 2iW''\xi\eta, \tag{7.2.1}$$

where $W = W(q)$ is a smooth function of q, otherwise unrestricted. A dot $\dot{}$ denotes a t–derivative, and a prime $'$ a q–derivative. The action is **invariant**, *modulo* boundary terms, under rigid $N = 2$ supersymmetry transformations, with constant anti–commuting parameters, ϵ_1, ϵ_2:

$$\delta q = -i\sqrt{2}\Big(\epsilon_1\xi + \epsilon_2\eta\Big), \quad \delta\xi = \frac{\epsilon_1}{\sqrt{2}}\dot{q} + \frac{\epsilon_2}{\sqrt{2}}\Big(W'\Big),$$
$$\delta\eta = -\frac{\epsilon_1}{\sqrt{2}}\Big(W'\Big) + \frac{\epsilon_2}{\sqrt{2}}\dot{q}. \tag{7.2.2}$$

The generators of rigid supersymmetry transformations are

$$Q_1 = -i\sqrt{2}\Big(\xi\dot{q} - \eta W'\Big), \tag{7.2.3a}$$
$$Q_2 = -i\sqrt{2}\Big(\eta\dot{q} + \xi W'\Big). \tag{7.2.3b}$$

Alvarez' model, with local N = 2 supersymmetry, includes $\big(\psi_1(t), \psi_2(t)\big)$ and $e(t)$. This model has a **(bosonic) local invariance under re–parametrisations**:

$$t \longrightarrow \tau(t). \tag{7.2.4}$$

The corresponding generator is the Hamiltonian density,

$$\mathcal{H} = e\Big[\big(Q_1\big)^2 + \big(Q_2\big)^2 + i\psi_1 Q_1 + i\psi_2 Q_2\Big]. \tag{7.2.5}$$

Alvarez' model also has **(fermionic) local supersymmetry invariances**. **Local supersymmetry transformations** are parametrised by independent (odd) fermionic functions, $\epsilon_1(t)$, $\epsilon_2(t)$. The local **(fermionic) classical supersymmetry generators**, related to Eqs. (7.2.2, 7.2.3a, 7.2.3b), vanish at a classical solution:

$$Q_1 = 0, \qquad Q_2 = 0. \tag{7.2.6}$$

These **local supersymmetry constraints** are preserved in classical evolution of the model. The **bosonic constraint**,

$$\mathcal{H} = 0, \tag{7.2.7}$$

corresponds to invariance under local re–parametrisations, Eq. (7.2.4).

In Dirac quantisation, **constraint generators** are promoted to operators, $\hat{Q}_1$, $\hat{Q}_2$ and $\hat{\mathcal{H}}$, which **annihilate any physical wave–functional**, Ψ:

$$\hat{Q}_1\Psi = 0, \tag{7.2.8a}$$

$$\hat{Q}_2\Psi = 0, \tag{7.2.8b}$$

$$\hat{\mathcal{H}}\Psi = 0. \tag{7.2.8c}$$

Since the anti–commutator of $\hat{Q}_1$ and $\hat{Q}_2$ involves $\hat{\mathcal{H}}$ [18, 19], it is sufficient to solve only the **quantum supersymmetry constraints**, $\hat{Q}_1\Psi = 0$, $\hat{Q}_2\Psi = 0$. These are simplified by the fermionic re–definition:

$$\phi = \xi + i\eta, \qquad \overline{\phi} = \xi - i\eta. \tag{7.2.9}$$

In the Dirac procedure, one can take (say) q and ϕ as bosonic and fermionic co–ordinates for (or arguments of) Ψ. In the quantum theory, $\underline{p}$, the **momentum conjugate** to q, corresponds to $-i\partial/\partial q$. By anti–commutation, $\overline{\phi}$ acts as a momentum conjugate to ϕ; more precisely, $\overline{\phi}$ corresponds to the **left fermionic derivative**, $\partial/\partial\phi$ [6]. To calculate a left derivative, $\partial/\partial\phi$, acting on a quantity, α, one moves each appearance of ϕ in α to the left, using anti–commutation, before differentiating [6].

In the simplest gauge [19], $\psi_1 = \psi_2 = 0, e = 1$, the quantum supersymmetry constraints, Eqs. (7.2.8a, 7.2.8b, 7.2.8c), read:

$$\left(\phi + \frac{\partial}{\partial\phi}\right)\frac{\partial\Psi}{\partial q} - W'(q)\left(\phi - \frac{\partial}{\partial\phi}\right)\Psi = 0, \tag{7.2.10}$$

$$\left(\phi - \frac{\partial}{\partial\phi}\right)\frac{\partial\Psi}{\partial q} - W'(q)\left(\phi + \frac{\partial}{\partial\phi}\right)\Psi = 0. \tag{7.2.11}$$

Since $\phi^2 = 0$ (anti–commutation), the quantum constraints, Eqs. (7.2.10, 7.2.11), imply:

$$\Psi(q,\phi) = A(q) + \phi B(q), \tag{7.2.12}$$

for functions, $A(q)$, $B(q)$. The general solution of Eqs. (7.2.10, 7.2.11) is:

$$A(q) = c_1 \exp\Big(W(q)\Big), \tag{7.2.13a}$$

$$B(q) = c_2 \exp\Big(-W(q)\Big), \tag{7.2.13b}$$

where c_1, c_2 are (independent) constants and $W(q)$ appears in Eq. (7.2.1). In Dirac's approach, the arguments of Ψ are '**co–ordinate boundary data**' (below).

For comparison with the four–dimensional case [Sects. (7.2.2–7.2.4)], consider classical bosonic/fermionic solutions in the local QM theory. The classical con-

straints, $Q_1 = 0$, $Q_2 = 0$, imply that ξ and η are proportional. For non–trivial (ξ, η), the determinant,

$$\dot{q}^2 + \Big(W'(q)\Big)^2 = 0, \tag{7.2.14}$$

vanishes. Real classical motion occurs only in the 'Euclidean' régime, $\tau = \pm it$, with τ real, whence,

$$\left(\frac{dq}{d\tau}\right)^2 = \left(\frac{dW}{dq}\right)^2, \tag{7.2.15}$$

with two roots:

$$\left(\frac{dq}{d\tau}\right) = \pm W'(q). \tag{7.2.16}$$

The motion is integrable, with two classical solutions. The exponential terms in the amplitude, Eqs. (7.2.13a, 7.2.13b), correspond to $\exp(-I_{\text{class}})$ for one or other classical solution, where I_{class} is the Euclidean action of the classical solution joining initial to final data.

Subject to the boundary data, this leads to Eqs. (7.2.17a, 7.2.17b), below, for the quantum amplitude to go from initial position, q_a, and initial fermionic data, to analogous final data, in time–interval, T. [In standard QM, following Feynman and Hibbs [12], the amplitude would be denoted by $K(q_b, t_b; q_a, t_a)$, where $T = (t_b - t_a)$.]

A classical solution must have **either**:

(i) $\widetilde{\phi} = 0$ in the interior, with $(dq/d\tau) = e(\tau)W'(q)$, **or**
(ii) $\phi = 0$ in the interior, with $(dq/d\tau) = -e(\tau)W'(q)$.

In **cases (i) and (ii)**, respectively, from the classical and quantum constraints, one finds the boundary data and amplitude:

$$\begin{aligned} &K\big(q_b, \phi_b;\ q_a, \phi_a;\ T = -i\tau_0\big) \\ &\qquad = \text{const.}\delta\big(Q_1 + iQ_2\big)_a \delta\big(Q_1 + iQ_2\big)_b \exp\big(-I_{\text{class}}\big), \end{aligned} \tag{7.2.17a}$$

$$\begin{aligned} &K\big(q_b, \widetilde{\phi}_b;\ q_a, \widetilde{\phi}_a;\ T = -i\tau_0\big) \\ &\qquad = \text{const.}\delta\big(Q_1 - iQ_2\big)_a \delta\big(Q_1 - iQ_2\big)_b \exp\big(-I_{\text{class}}\big). \end{aligned} \tag{7.2.17b}$$

Equations (7.2.17a, 7.2.17b) contain semi–classical exponentials, multiplied by **fermionic delta–functions**. The delta–functions (below) impose the classical supersymmetry constraints, Eq. (7.2.6), at the boundaries. These constraints are part of the classical field equations. The 'vierbein', $e(t)$, must be chosen such that q changes from q_a to q_b along the classical path, during the time–interval, $T = -i\tau_0$, with τ_0 real.

7.2.2 $N = 1$ Supergravity: Dirac Approach

Turn to **N = 1 supergravity** in four space–time dimensions, with 'co–ordinate' data on Σ_I and Σ_F, *via* the Dirac approach. (Hence, ultimately, to questions concerning **black–hole evaporation**.) The quantum amplitude in $N = 1$ supergravity is found (below) to have the 'semi–classical' form, Eq. (7.2.20), analogous to Eqs. (7.2.17a, 7.2.17b) for locally–supersymmetric QM. As in Eqs. (7.2.17a, 7.2.17b), the quantities, δ, in Eq. (7.2.20), are **delta–functionals** of the supersymmetry constraints at the bounding surfaces. In calculating such quantum amplitudes, one is led to study **classical N = 1 supergravity** (generalising **classical general relativity**), as a **boundary–value problem**. This is only **well posed** if the time–interval, T, at spatial infinity, is complex, with $\mathrm{Im}(T) < 0$ [16].

As a simple example of the need for the condition, $\mathrm{Im}(T) < 0$, in a **boundary–value problem**, consider the **scalar wave equation**, $\left(\partial^2\phi/\partial t^2\right) - \left(\partial^2\phi/\partial x^2\right) = 0$, in Minkowski space–time, with co–ordinates, (t, x). The rôles of Σ_I and Σ_F are taken by the lines, $t = 0$ and $t = T$. For simplicity, choose boundary data with $\phi(0, x) = 0$, $\phi(T, x) = \phi_1(x)$, where ϕ_1 is a smooth function of rapid decrease as $|x| \longrightarrow \infty$. Taking the **Fourier transform**, $\widetilde{\phi}(t, k)$, with respect to x, one has the (formal) solution:

$$\phi(t, x) = \text{const.} \int d^3k \frac{\widetilde{\phi}_1(T, k)}{\sin(kT)} e^{ikx} \sin(kt). \tag{7.2.18}$$

For **real** T and **generic data**, $\phi_1(x)$, there is **no classical solution** obeying the boundary conditions. With real T, $\widetilde{\phi}_1(T, k)$ would need to obey the very restrictive conditions, $\widetilde{\phi}_1(T, n\pi) = 0, \forall n \in \mathbb{Z}$, to provide a solution. When $\mathrm{Im}(T) < 0$, however, Eq. (7.2.18) defines a (complex) solution, for any smooth data, $\phi_1(x)$, of rapid decrease.

As in locally–supersymmetric QM, a classical solution to the boundary–value problem in $N = 1$ supergravity exists only when the classical supersymmetry constraints hold at the boundaries [15, 16]. It was recognised in [21] that the term, $\exp\left(-I_{\text{class}}\right)$, in the supergravity amplitude, should be multiplied by an infinite product of fermionic terms. These fermionic factors are, in fact, those in Eq. (7.2.20). Similarly, in locally–supersymmetric QM, the arguments of the delta–functions in Eqs. (7.2.17a, 7.2.17b) are the classical supersymmetry constraints [Eq. (7.2.6)] at the boundaries.

As stated in Sect. 7.1, the boundary conditions taken in Eqs. (7.2.20, 7.2.30), below, for $N = 1$ supergravity, **are not the same as those used in scattering theory** (*via* Feynman diagrams). The relation between the two types of boundary condition or amplitude is quite complicated (below). As with Eq. (7.2.17a, 7.2.17b), the boundary conditions in the Dirac approach involve suitable 'co–ordinate' fields at Σ_I, Σ_F, analogous to those in the amplitude, $K(q_b, t_b; q_a, t_a)$, for non–relativistic QM [12].

In **N = 1 supergravity** or its generalisations, there are necessarily spin–$\frac{3}{2}$ gravitino fields (possibly spin–$\frac{1}{2}$ fields). Spinor fields can only be defined on a

curved space–time admitting a pseudo–orthonormal **tetrad field** [22], denoted by $e^a_\mu(x)(a = 0, 1, 2, 3)$. Here, a is a **tetrad index**, and μ is a **space–time** or **one–form index**.

In the classical or quantum boundary–value problem for supergravity, one natural choice of **bosonic boundary data** ('field co–ordinates') is to specify the **spatial tetrad** (asymptotically–flat), $e^a_i(x)(a = 0, 1, 2, 3)$, on Σ_I and Σ_F [15, 16]. Here, $i = 1, 2, 3$ is a **spatial one–form index**. The **intrinsic spatial three–metric** is:

$$h_{ij}(x) = e^a_i(x)e_{aj}(x). \tag{7.2.19}$$

For **fermionic co–ordinates**, one can take the **primed spatial gravitino field**, $\widetilde{\psi}^{A'}_i(x)$, on Σ_I, and **unprimed field**, $\psi^A_i(x)$, on Σ_F [15, 16]. [Or, the rôles of Σ_I and Σ_F can be reversed.] A, A' are two–component spinor indices, streamlined for four space–time dimensions [23]. For harmony of language, with fermionic data, $\widetilde{\psi}^{A'}_i(x)$ or $\psi^A_i(x)$, describe the spatial geometry *via* the spinor–valued one–form, $e^{AA'}_i(x)$ [16], rather than the equivalent spatial tetrad, $e^a_i(x)$. Specify the time interval, T, at spatial infinity, between Σ_I and Σ_F (with $\mathrm{Im}(T) < 0$, for a **well–posed classical boundary–value problem**).

In the Dirac approach, one has a field representation with 'co–ordinate' boundary data. For scattering theory, with Feynman diagrams, one instead has a particle representation with 'particle' in– and out–data.

(In $N = 1$ supergravity, Feynman diagrams give finite scattering amplitudes at 1–, 2–loop orders [24, 25]. Scattering amplitudes at 3–, 4–, . . .–loop order (if meaningful) are not known. Feynman diagrams in $N = 8$ supergravity give indications of finiteness [14].)

With this choice of data for $N = 1$ supergravity, and $\mathrm{Im}(T) < 0$, the quantum amplitude has the 'semi–classical' form:

$$K = \text{const.}\delta\big(S_A(x_I)\big)\delta\big(\widetilde{S}_{A'}(x_F)\big)\exp\big(-I_{\text{class}}\big), \tag{7.2.20}$$

analogous to Eqs. (7.2.17a, 7.2.17b) for locally–supersymmetric QM [Sect. (7.2.3)].

In Eq. (7.2.20), the 'Euclidean' action, I_{class}, includes fermionic contributions [16]. Here, $\widetilde{S}_{A'}(x_F)$ denotes the **primed classical supersymmetry constraint** [Eq. (7.2.24), below] at Σ_F, and $S_A(x_I)$ the **unprimed constraint** at Σ_I [16].

The **delta–functional** of the odd (anti–commuting) spinor field, $S_A(x)$, in Eq. (7.2.20), is an (infinite) product of $S_A(x_I)$ over all points, x_I, and spinor indices, $A = 0, 1$, on Σ_I. For given x_I, each factor is a **fermionic delta–function**, $\delta(S_A(x_I))$, defined in the **holomorphic representation** for fermions [13, 26, 27]. In this representation, fermionic and bosonic fields are treated on an equal footing. Fermionic quantities anti–commute among themselves. In the finite–dimensional case, one has variables $a_n (n = 1, 2, \ldots, Q)$ (say) and their conjugates, a^*_n. Functions of the form, $f(a_n)$, are **holomorphic functions**, describing **state vectors** of the system. **Berezin integration** [26, 27] defines the integral of a function involving both fermions and

bosons. As in [26, 27], the (fermionic) delta–function of (a_n) can be identified with the product, $\prod_{n=1}^{Q} a_n$.

The explicit form, Eq. (7.2.20), for a quantum amplitude in four–dimensional $N = 1$ supergravity, *via* the Dirac approach, highlights the question of different boundary conditions and amplitudes, relevant to the Dirac and Feynman approaches, respectively. Different, but (*a priori*) equally valid types of boundary condition are natural to one or the other approach. As in a first course on quantum field theory, scattering (Feynman–diagram) boundary conditions are included *via* the LSZ (Lehmann, Symanzik, Zimmermann) description [13]. One studies quantum states which, at early or late times, resemble a product of 1–particle states (one for each particle) and of no–particle states. Each 1–particle state involves a first excited state of a harmonic oscillator, for a given momentum, **k**. A finite product of such 1–particle states multiplies an infinite product of the remaining ground states. Is there a unitary transformation, linking the amplitudes of Eq. (7.2.20) to scattering amplitudes, which refer to an asymptotic particle basis?

Consider the description of in– and out–states, but in language natural to the **Dirac approach**. The transcription, implicit above, between harmonic–oscillator and 'co–ordinate' descriptions, is made at fixed, finite time–separation, T, between Σ_I and Σ_F. Only after the transcription does one take the limit, $|T| \longrightarrow \infty$. One must allow for possible large deviations from flat or trivial 'co–ordinate' data on each boundary. These deviations arise from large excursions allowed (with low probability) in the co–ordinates (or arguments), $x_{kI}, x_{\ell F}$, of harmonic–oscillator wave–functions, corresponding, respectively, to spatial momenta, **k**, **l**. Roughly speaking, the exponential factor of each harmonic oscillator is multiplied by $\exp(-I_{\text{class}})$, where I_{class} is the classical action for the corresponding non–linear boundary–value problem in classical supergravity, with boundary data possibly far from flatness, and T fixed. The result must then be integrated over all excursions. Finally, take $T \longrightarrow \infty$, to obtain a (putative) Feynman diagram, *via* this elaborate construction. Studying the behaviour of I_{class} for the classical boundary–value problem in general relativity or supergravity, as a functional of the boundary data, involves very strong non–linear gravitational (and other) fields. This problem is not understood even qualitatively, although one might attempt some form of 'large–excursion' classical perturbative approach. At present, it is very complicated to compare Feynman–diagram results with results from the Dirac approach, *via* the algorithm just suggested. The main difficulty resides in the **classical boundary–value problem**.

The Dirac approach is intrinsically Hamiltonian, with its one–parameter family of space–like hypersurfaces [11, 28]. Dirac's approach is well adapted to $N = 1$ supergravity and its gauge–invariant version [6, 16]—both theories have a large amount of local symmetry. The continuous invariances comprise:

(i) the co–ordinate transformations of general relativity;
(ii) the gauge symmetries of particle physics (if appropriate) [6];
(iii) local Lorentz transformations, acting on the indices, $a, b, \ldots$, of a pseudo–orthonormal tetrad in curved space–time, $e_{\mu}^{a}(x)$.
(iv) local supersymmetry transformations [6, 15, 16, 24].

These invariances provide a large number of local–symmetry generators in the Hamiltonian approach. The most useful involve one power of momentum, namely,

(i) three generators of spatial co–ordinate transformations,
(ii) generators of gauge symmetries (if appropriate),
(iii) generators of local Lorentz transformations,
(iv) half of the local supersymmetry generators—the relevant splitting (into primed and unprimed spinors) is explicit with two–component spinors [16, 23]. For the above 'co–ordinate' boundary data on Σ_I, Σ_F, the primed quantum supersymmetry operator, $\hat{\bar{S}}_{A'}$, involves a first–order functional derivative at Σ_F [Eq. (7.2.29), below]. The unprimed supersymmetry operator, $\hat{S}_A$, is of second order at Σ_F [16], though of first order at Σ_I.

To summarise: The perpective gained from Dirac's approach to quantum theories with local symmetries, such as $N = 1$ supergravity, may be quite different from a view based only on scattering theory and Feynman diagrams.

7.2.3 The Quantum Constraints

As in [15, 16], a simple choice of canonical variables for $N = 1$ supergravity is:

(i) Bosonic variables: the spinor–valued spatial one–forms, $e_i^{AA'}(x)$, and conjugate momenta, $p^i_{AA'}(x)$. For later use, the **unit (Lorentzian) normal vector**, $n^{AA'}$, at each spatial point, x, is defined (up to a choice between future and past directions) by [15, 16]:

$$n_{AA'}n^{AA'} = 1, \qquad n_{AA'}e_i^{AA'} = 0 \qquad (i = 1, 2, 3). \tag{7.2.21}$$

(ii) Fermionic variables: the odd (anti–commuting) spatial spinor–valued one–forms, $\psi_i^A(x)$, $\widetilde{\psi}_i^{A'}(x)$ (spatial projections of the spinor–valued one–forms, $\psi_\mu^A(x)$, $\widetilde{\psi}_\mu^{A'}(x)$). Here, $\psi_i^A(x)$, $\widetilde{\psi}_i^{A'}(x)$, are liberated from being hermitian conjugates of each other (as holds in Lorentzian $N = 1$ supergravity [6, 16, 24]). This liberation is inevitable in Riemannian (or complexified) supergravity [29]. The (odd) classical momentum, conjugate to $\psi_i^A(x)$,

$$\pi^i_A(x) = -\frac{1}{2}\epsilon^{ijk}\widetilde{\psi}_j^{A'}(x)e_{AA'k}(x), \tag{7.2.22}$$

involves the gravitino variable of opposite chirality, $\widetilde{\psi}_i^{A'}(x)$ [16]. Equation (7.2.22) can be inverted to give $\widetilde{\psi}_j^{A'}(x)$ linearly in terms of $\pi^i_A(x)$ [15, 16]. A complete treatment of this matter involves the use of Dirac brackets [11, 15, 16, 28].

The classical Hamiltonian takes a standard form for a theory with gauge–like invariances—a finite sum over generators, $G_s(x)$, one for each local symmetry, with

Lagrange multiplier, $L_s(x)$ [11, 15, 16, 28]:

$$H = \int d^3x L_s(x) G_s(x), \tag{7.2.23}$$

summed over s. In our case, the generators, G_s, are:

(i) the generator, $\mathcal{H}_{AA'}(x)$, of infinitesimal space–time co–ordinate transformations,
(ii) the independent odd generators, $S_A(x)$ and $\widetilde{S}_{A'}(x)$, of unprimed and primed local supersymmetry transformations,
(iii) the generators, $J^{AB} = J^{(AB)}$, $\widetilde{J}^{A'B'} = \widetilde{J}^{(A'B')}$, of local Lorentz transformations.

Each G_s is a function of the canonical variables, $(e_i^{AA'}(x),\ p^i_{AA'}(x);\ \psi_i^A(x),\ \widetilde{\psi}_i^{A'}(x))$, and of their first or second spatial derivatives.

Remarkably, the classical generators, S_A and $\widetilde{S}_{A'}$, become simple when expressed in terms of the standard (torsion–free) covariant derivative, ${}^{3s}D_j$, on spinors [15, 16, 28]:

$$\widetilde{S}_{A'} = \epsilon^{ijk} e_{AA'i} \left({}^{3s}D_j \psi_k^A \right) + \frac{1}{2} i\kappa^2 p^i_{AA'} \psi_i^A, \tag{7.2.24}$$

with S_A given by the 'conjugate' expression, with ψ_k^A replaced by $\widetilde{\psi}_k^{A'}$ and i by $-i$. Define $\kappa^2 = 8\pi$ in **geometrical units**, where $c = G = 1$. Analogous expressions hold for the other generators [16].

Following the Dirac approach [11], take, say, $(e_i^{AA'}(x),\ \psi_i^A(x))$ as bosonic and fermionic co–ordinates [16]. In the (natural) holomorphic description, the momentum variables, $(p^i_{AA'}(x),\ \pi^i_A(x))$, are represented by first–order derivative operators on the wave–functional, $\Psi[e_i^{AA'}(x),\ \psi_i^A(x)]$, which lives in a **Grassmann algebra** [16, 26, 27]. From the classical (Dirac) brackets between the momentum, $\pi^i_A(x)$ [Eq. (7.2.22)] and co–ordinate, $\psi_i^A(x)$, the quantum version of $\widetilde{\psi}_{A'i}(x)$ is [16]:

$$\hat{\widetilde{\psi}}_{A'i}(x) = -i D^A_{A'ji}(x) \delta / \delta \psi_j^A(x), \tag{7.2.25}$$

$$D^A_{A'ji} = -2ih^{-\frac{1}{2}} e_i^{AB'} e_{BB'j} n^B_{A'}, \tag{7.2.26a}$$

$$h = \det(h_{ij}). \tag{7.2.26b}$$

In Dirac's approach [11, 15, 16, 28], the classical constraint generators become quantum operators: $\hat{\mathcal{H}}_{AA'}$, $\hat{S}_A$, $\hat{\widetilde{S}}_{A'}$, $\hat{J}_{AB}$, $\hat{\widetilde{J}}_{A'B'}$. The wave–functional of a **physically-allowed quantum state**, $\Psi[e_i^{AA'}(x),\ \psi_i^A(x)]$, is (by definition) annihilated by the **quantum constraint operators** (giving the **quantum constraint equations**):

$$\hat{\widetilde{S}}_{A'} \Psi = 0, \tag{7.2.27a}$$

$$\hat{S}_A \Psi = 0, \tag{7.2.27b}$$

$$\hat{J}_{AB}\Psi = 0, \tag{7.2.27c}$$

$$\hat{\bar{J}}_{A'B'}\Psi = 0. \tag{7.2.27d}$$

The (anti–)commutation relations among these operators imply the remaining quantum constraint:

$$\hat{\mathcal{H}}_{AA'}\Psi = 0, \tag{7.2.28}$$

with a suitable definition of $\hat{\mathcal{H}}_{AA'}$ [16].

Equation (7.2.27c, 7.2.27d) describe the invariance of Ψ under local Lorentz transformations, applied to its arguments.

The constraint, Eq. (7.2.27a), involves only first–order functional derivatives, and leads to a simple expression for the transformation of $\Psi[e_i^{AA'}(x), \psi_i^A(x)]$ under an infinitesimal **primed local supersymmetry transformation**, parametrised by an (odd) spinor field, $\widetilde{\epsilon}^{A'}(x)$ [6, 15, 16]. In this representation, the classical generator, $\widetilde{S}_{A'}$, of Eq. (7.2.24), becomes the quantum operator [15, 16]:

$$\hat{\widetilde{S}}_{A'} = \epsilon^{ijk} e_{AA'i} \left({}^{3s}D_j \psi_k^A \right) + \frac{1}{2}\kappa^2 \psi_i^A \frac{\delta}{\delta e_i^{AA'}}. \tag{7.2.29}$$

A corresponding property of the **unprimed quantum constraint**, Eq. (7.2.27b), holds with respect to **infinitesimal unprimed local supersymmetry transformations**. To express this so as to treat primed and unprimed quantities symmetrically, define a 'dual' wave–functional, $\widetilde{\Psi}[e_i^{AA'}(x), \widetilde{\psi}_i^{A'}(x)]$, as in Eqs. (7.2.36–7.2.38), below—the **fermionic Fourier transform** of the original wave–functional, $\Psi[e_i^{AA'}(x), \psi_i^A(x)]$. The first sentence of the paragraph above can be repeated, on interchanging:

(i) 'primed' $\leftrightarrow$ 'unprimed', (ii) $\psi_i^A(x) \leftrightarrow \widetilde{\psi}_i^{A'}(x)$, (iii) $\Psi \leftrightarrow \widetilde{\Psi}$, (iv) $\epsilon^A(x) \leftrightarrow \widetilde{\epsilon}^{A'}(x)$.

In applying the Dirac approach to $N = 1$ supergravity, assume provisionally that there is a classical solution joining asymptotically–flat initial and final data on Σ_I and Σ_F, with $\mathrm{Im}(T) < 0$ (up to gauge). One builds up a **bosonic/fermionic classical solution** of the supergravity field equations, starting from the (complex–valued) **bosonic solution** of the classical Einstein boundary–value problem—the solution which remains (up to gauge) when fermionic fields are set to zero. Given a bosonic solution, one solves the classical supergravity field equations perturbatively in powers of fermionic data, ψ or $\widetilde{\psi}$, about the bosonic solution [16]. The classical fields and action live in appropriate Grassmann algebras. The question of building up non–linear bosonic/fermionic solutions of the $N = 1$ supergravity field equations was addressed rigorously in [30], for the **Cauchy problem** in Lorentzian signature. We follow [30], but for a boundary–value problem (Riemannian or complexified). Since $\mathrm{Im}(T) < 0$, one expects, in general, a complex **strongly elliptic boundary–value problem** [31]. Such problems have many of the good properties of real elliptic

boundary–value problems, with existence and uniqueness. **Riemannian** Einstein boundary–value problems are, in general, expected to be **elliptic**.

This approach, based on rotation of T into the complex (or Feynman's $+i\epsilon$ prescription [12, 13]), has led to the calculation of **quantum amplitudes**, not just **probabilities**, concerning **gravitational collapse to a black hole**, for energetically–possible many–particle outcomes at late times, in the **quantum state** which continues to exist after collapse and during subsequent quantum evaporation [4, 7, 9, 10, 20, 32–38].

For such boundary data, the quantum amplitude is written, after Feynman and Hibbs [12], as:

$$K = K\left(e_i^{AA'}(x_I), \widetilde{\psi}_i^{A'}(x_I); e_i^{AA'}(x_F), \psi_i^{A}(x_F); T\right). \tag{7.2.30}$$

Here, K lives in an infinite–dimensional Grassmann algebra over the complex numbers, $\mathbb{C}$, in the holomorphic representation above.

The classical supersymmetry constraint equations imply that K is proportional to a (fermionic) delta–functional of $\widetilde{S}_{A'}(x)$ at Σ_F, and to a delta–functional of $S_A(x)$ at Σ_I. Further investigation (below) leads to the semi–classical form, Eq. (7.2.20), for K.

7.2.4 *'Semi–Classical' Amplitude in N = 1 Supergravity*

In the locally–supersymmetric Witten/Alvarez QM model [18, 19], one can verify that the wave function, K, of Eqs. (7.2.17a, 7.2.17b), **is the quantum amplitude** for the given boundary data, by checking that:

(i) for each local invariance of the classical model, the corresponding **Dirac quantum constraint** holds;
(ii) the **Schrödinger equation** holds, for all $T > 0$ (or for all $\tau > 0$, with $\tau = it$) [this is automatic, given (i)]; and
(iii) K tends to a delta–function(al) of the boundary data, as (say) $\tau \longrightarrow 0_+$, just as the amplitude in non–relativistic QM [12] tends to $\delta(q_a, q_b)$, as $\tau \longrightarrow 0_+$.

We test in a similar way the proposed expression, Eq. (7.2.20), for the quantum amplitude, K, in $N = 1$ supergravity, given the boundary data of Eq. (7.2.30). Write Eq. (7.2.20) as:

$$K = \left(\prod_{x_I, B} S_B(x_I)\right)\left(\prod_{x_F, B'} \widetilde{S}_{B'}(x_F)\right) \exp\left(-I_{\text{class}}/\hbar\right). \tag{7.2.31}$$

For (i), K must obey the quantum constraints, Eqs. (7.2.27a, 7.2.27b, 7.2.27c, 7.2.27d), at the boundaries, Σ_I, Σ_F. The local–Lorentz constraints, Eqs. (7.2.27c, 7.2.27d), hold automatically, since the right–hand side of Eq. (7.2.20) is invariant under local Lorentz transformations.

One can verify that the **primed constraint operator**, $\hat{\bar{S}}_{A'}(x)$, at Σ_F, annihilates the amplitude, K:

$$\hat{\bar{S}}_{A'}(x_F)K = 0, \tag{7.2.32}$$

as follows: From the first–order expression, Eq. (7.2.29), for $\hat{\bar{S}}_{A'}(x_F)$;

$$\hat{\bar{S}}_{A'}(x_F)\exp\bigl(-I_{\text{class}}/\hbar\bigr) = \widetilde{\bar{S}}_{A'}(x_F)\exp\bigl(-I_{\text{class}}/\hbar\bigr). \tag{7.2.33}$$

Since operators such as $\hat{\bar{S}}_{A'}(x_{1F})$, $\hat{\bar{S}}_{B'}(x_{2F})$ anti–commute [15, 16], K can be written as:

$$K = \Bigl(\prod\nolimits_{x_I,B} S_B(x_I)\Bigr)\Bigl(\prod\nolimits_{x_F,B'}\hat{\bar{S}}_{B'}(x_F)\Bigr)\exp\bigl(-I_{\text{class}}/\hbar\bigr). \tag{7.2.34}$$

Apply $\hat{\bar{S}}_{A'}(x)$ to K. Note the commutation relation, $\bigl[\hat{\bar{S}}_{A'}(x_F),\, K\bigr] = 0$. Hence, for $x \in \Sigma_F$:

$$\begin{aligned}&\hat{\bar{S}}_{A'}(x)\Bigl(\prod\nolimits_{x_I,B} S_B(x_I)\Bigr)\Bigl(\prod\nolimits_{x_F,B'}\hat{\bar{S}}_{B'}(x_F)\Bigr)\exp\bigl(-I_{\text{class}}/\hbar\bigr)\\ &\quad= \Bigl(\prod\nolimits_{x_I,B} S_B(x_I)\Bigr)\hat{\bar{S}}_{A'}(x)\Bigl(\prod\nolimits_{x_F,B'}\hat{\bar{S}}_{B'}(x_F)\Bigr)\exp\bigl(-I_{\text{class}}/\hbar\bigr).\end{aligned} \tag{7.2.35}$$

The right–hand side of Eq. (7.2.35) includes one repeated pair of factors, among the terms, $\hat{\bar{S}}_{A'}(x)\bigl(\prod_{x_F,B'}\hat{\bar{S}}_{B'}(x_F)\bigr)$, for which $x = x_F$ and $A' = B'$. By anti–commutation among operators $\hat{\bar{S}}_{A'}(x)$, $\hat{\bar{S}}_{B'}(y)$, this product of two identical fermionic expressions gives zero. Hence, the primed constraint equation, (7.2.32), holds at Σ_F.

The **unprimed supersymmetry constraint operator**, $\hat{S}_A$, is of second order at Σ_F, involving mixed functional derivatives, $\delta^2/\delta e\delta\psi$, with respect to $(e_i^{AA'}(x_F)$, $\psi_i^A(x_F))$ (Sect. 3.4 of [16]). One might, therefore, expect to need a more difficult argument to establish that $\hat{S}_A K = 0$ at Σ_F. This is simplified *via* symmetry properties of K:

(a) interchange of the boundary surfaces, Σ_I, Σ_F, and
(b) interchange of the rôles of the unprimed and primed fermionic arguments, $\psi_i^A(x)$ and $\widetilde{\psi}_i^{A'}(x)$, on a given hypersurface, Σ ($e_i^{AA'}(x)$ remaining unchanged).

Given the expression, Eq. (7.2.22), for the fermionic momentum, $\pi_A^i(x)$, (b) corresponds to interchanging fermionic co–ordinates and momenta. We proceed (Eqs. (3.2.35), (3.3.5–16) of [16]) by defining the **fermionic Fourier transform,** which maps a wave–functional, schematically, $f(e,\psi)$, to its **transform**, $\widetilde{f}(e,\widetilde{\phi})$. Sequentially:

$$C^{ij}_{AA'}(x) = -i\epsilon^{ijk}e_{AA'k}(x), \tag{7.2.36}$$

$$\exp\Big[-iC\psi\widetilde{\phi}\Big] = \exp\Big[-i\int d^3x' C^{ij}_{AA'}(x')\psi^A_i(x')\widetilde{\phi}^{A'}_j(x')\Big], \tag{7.2.37}$$

$$\widetilde{f}\big(e,\widetilde{\phi}\big) = D^{-1}(e)\int \mathcal{D}\psi f(e,\psi)\exp\Big[-iC\psi\widetilde{\phi}\Big]. \tag{7.2.38}$$

Berezin integration is used [26, 27]. The determinant, $D(e)$, is defined in Eq. (3.3.7) of [16].

The **inverse transform** is defined similarly, the factor, $+i$, replacing $-i$. These Fourier transforms have their finite–dimensional analogues in the holomorphic description of QM [26, 27]; they map between holomorphic and anti–holomorphic representations.

Consider next the **unprimed quantum constraint**, $\hat{S}_A K = 0$, at Σ_F. Since the **classical constraints**, $S_A = 0$, $\widetilde{S}_{A'} = 0$, are conserved in Hamiltonian evolution, Eq. (7.2.20) can equivalently be written:

$$K = \text{const.}\delta\big(S_A(x_F)\big)\delta\big(\widetilde{S}_{A'}(x_I)\big)\exp\big(-I_{\text{class}}\big), \tag{7.2.39}$$

the unprimed constraint now taken at Σ_F, the primed constraint at Σ_I. [The boundary data are still as in Eq. (7.2.30).] Make a functional Fourier transform at Σ_F, as in Eqs. (7.2.36–7.2.38), changing the final fermionic argument from ψ^A_i to a new primed quantity, $\widetilde{\phi}^{A'}_i$, but leaving invariant the final bosonic data. At Σ_I, make a reverse transform, replacing the original, $\widetilde{\psi}^{A'}_i$, with new unprimed data, ϕ^A_i. The new data on Σ_I, Σ_F, should again give a well–posed boundary–value problem, leading to a 'new' classical solution. The action, I_{class}, at a classical solution, reduces to a sum of boundary contributions [16]—a gravitational part and a gravitino part. The sign of a gravitino boundary contribution depends on whether ψ^A_i or $\widetilde{\psi}^{A'}_i$ is held fixed there (see Sects. 3.3–5 of [16]). Correspondingly, the above pair of 'Fourier transforms' change the 'old' classical action with original boundary data into the 'new' classical action for the 'new' data, $(e^{AA'}_i(x_I), \phi^A_i(x_I))$ and $(e^{AA'}_i(x_F), \widetilde{\phi}^{A'}_i(x_F))$. This gives the transformation of the semi–classical factor, $\exp(-I_{\text{class}})$, under the change to 'new' boundary data.

These transforms yield a simple form of $\hat{S}_A(x_F)$, with respect to the 'new' variables on Σ_F; given Eq. (7.2.29) for $\hat{\widetilde{S}}_{A'}(x_I)$, one replaces $\psi^A_k(x)$ by $\widetilde{\psi}^{A'}_k(x)$. Analogously, the 'new' quantum constraint, $\hat{S}_A(x_F)\Psi = 0$, is related to the transformation of the 'new' amplitude under an **unprimed local supersymmetry transformation** at Σ_F. (Similarly, at Σ_I, the primed operator, $\hat{\widetilde{S}}_{A'}(x_I)$, becomes simple with respect to the new variables.) At Σ_F, the interchange (b) of primed and unprimed fermionic data shows that $\hat{S}_A(x_F)K = 0$, following Eqs. (7.2.33–7.2.35) for $\hat{\widetilde{S}}_{A'}(x_F)K = 0$. Thus, K obeys the quantum constraints, Eqs. (7.2.27a, 7.2.27b, 7.2.27c, 7.2.27d).

For (ii) and (iii), consider the Schrödinger equation (Lorentzian) or heat equation (Riemannian), for the evolution of K with T or τ [the remaining data of Eq. (7.2.30) being fixed]. In particular, examine the property that K tends to a delta–function(al)

of the boundary data, analogous to $\delta(q_a, q_b)$, as (say) $\tau \longrightarrow 0_+$. In supergravity, these conditions are most simply analysed in the Riemannian case, $\tau = iT$, real.

Property (ii) holds since K, the right–hand side of Eq. (7.2.30), obeys the equations,

$$(\partial K)/(\partial \tau) + [(\partial I_{\text{class}})/(\partial \tau)]K = 0, \tag{7.2.40a}$$

$$(\partial I_{\text{class}})/(\partial \tau) = M. \tag{7.2.40b}$$

Equation (7.2.40b) is the Riemannian version of the **Hamilton–Jacobi equation** [39]. The **mass**, M, is a functional of the boundary data, including τ. As in [16], this gives the evolution equation of the amplitude.

For (iii), examine in more detail the QM condition [12],

$$K(q_b, q_a; \tau) \longrightarrow \delta(q_b, q_a), \tag{7.2.41}$$

as $\tau \longrightarrow 0_+$. In this limit, further information is available from an asymptotic expansion of K, as $\tau \longrightarrow 0_+$, other variables being fixed. First, note the **exact solution** for K for a **free particle** of mass m [12]:

$$K(q_b, q_a; \tau) = \left(\frac{m}{2\pi\tau}\right)^{1/2} \exp\left(\frac{-m(q_b - q_a)^2}{2\tau}\right). \tag{7.2.42}$$

When a **potential**, $V(q)$, is included in this QM model, Eq. (7.2.42) still gives the **leading term** in an **asymptotic expansion** of $K(q_a, q_b; \tau)$, as $\tau \longrightarrow 0_+$, with q_a, q_b, held fixed (not necessarily equal to each other) [12].

Correspondingly, for quantum amplitudes in $N = 1$ supergravity, with data as in Eq. (7.2.30) and $T = -i\tau(\tau > 0)$, one can study the proposed amplitude, Eq. (7.2.20), defined *modulo* solution of the **classical boundary–value problem**. Given the **non–linearity** of this problem, one cannot expect classical solutions (or amplitude, K) to arise in closed form. Rather, following [40], one can make an asymptotic expansion of K for $N = 1$ supergravity, as $\tau \longrightarrow 0_+$, other data being held fixed, analogous to Eq. (7.2.42). This is discussed for Riemannian signature in Sect. 4.4 of [16]. For the bosonic (Einstein) part of the Lagrangian, one finds:

$$I_{\text{class}}(h_{ijF}, h_{ijI}; \tau) \sim \tau^{-1} \nu(h_{ijF}, h_{ijI}), \tag{7.2.43}$$

where ν is a non–negative functional of the bounding three–geometries, plus smaller corrections, as $\tau \longrightarrow 0_+$.

The limiting behaviour of the **fermionic part** of I_{class} gives the appropriate fermionic behaviour when τ is small. Following Eq. (3.5.5) of [16] and Eqs. (7.2.36–7.2.38), the fermionic contribution to I_{class}, for small τ, is proportional to $\int d^3x C^{ij}_{AA'}(x)\psi_i^A(x)\widetilde{\psi}_j^{A'}(x)$. Integrated against a wave–functional, $f(e, \psi)$, as in Eq. (7.2.38), this gives the transformed wave–functional, $\widetilde{f}(e, \widetilde{\psi})$, at the other surface, whence, the correct fermionic behaviour as $\tau \longrightarrow 0_+$. The two delta–functionals in Eq. (7.2.20),

present for all interior τ, require that the boundary data obey the classical constraints, $S_A(x_I) = 0$, $\widetilde{S}_{A'}(x_F) = 0$.

The asymptotic expansion of K in $N = 1$ supergravity, *via* estimates of $I_{\rm class}$ and $M_{\rm class}$ for the infilling **classical Einstein geometry**, as $\tau \longrightarrow 0_+$ [16, 40], thus agrees (up to a constant factor) with the small–τ expansion of K in Eq. (7.2.20) for fixed boundary data. Hence, as in the asymptotic version of Eq. (7.2.42), Eq. (7.2.20) satisfies the asymptotic version of (iii).

The quantum amplitude, K, with boundary data, Eq. (7.2.30), is given by Eq. (7.2.20). Apart from the fermionic delta–functionals in Eq. (7.2.20), associated with the classical supersymmetry constraints, $S_B(x_I) = 0$, $\widetilde{S}_{B'}(x_F) = 0$, the amplitude, K, is exactly semi–classical, proportional to $\exp(-I_{\rm class}/\hbar)$. Emphasis is thrown back entirely onto the **classical bosonic/fermionic N = 1 supergravity boundary–value problem**.

7.3 Quantum Amplitudes in Black–Hole Evaporation

7.3.1 Introduction

This Section is concerned with the simplest example of quantum radiation following gravitational collapse to a black hole—we take the bosonic part of the Lagrangian to describe Einstein gravity coupled minimally to a massless scalar field, ϕ [7, 9, 37]. The spin–1, spin–2 (graviton) and fermionic spin–$\frac{1}{2}$ cases are treated similarly [7, 33, 36].

Given the results of Sect. 7.2, it will be assumed that the full Lagrangian is locally supersymmetric, describing $N = 1$ supergravity + supermatter. The simplest possibility is the model of [41], with $m = g = 0$. This has a complex massless scalar field coupled to Einstein gravity, with spin–$\frac{1}{2}$ and spin–$\frac{3}{2}$ partners. In the present context, we (consistently) truncate the scalar field to be real.

As in Sects. (7.2.2–7.2.4), pose boundary data on $\Sigma_{I,F}$ and require

$$T = |T| \exp(-i\theta) \quad (0 < \theta \leq \pi/2), \tag{7.3.1}$$

for a well–posed classical boundary–value problem. A small negative imaginary part in T induces an imaginary part in the total Lorentzian action—crucial in calculating the quantum amplitude. Conversely, even for small values of θ, solution of the rotated classical boundary–value problem is expected to smooth variations or oscillations of the boundary data, as one moves from the boundary, Σ_I or Σ_F, into the interior by a few multiples of the relevant wavelength.

To fix physical intuition, imagine that the initial scalar field, ϕ_I, on Σ_I, is nearly spherically symmetric and very diffuse, with most of the mass distributed over radii much greater than the 'Schwarzschild radius', $2M_0$. Here, M_0 is the Arnowitt–Deser–Misner (ADM) mass, defined *via* the r^{-1} fall–off of initial data, at large radii on a spacelike hypersurface [42]. The three–metric, h_{ijI}, on Σ_I, is almost spherically

symmetric, and varies slowly with radius. The value of T at Σ_F is chosen large and positive, to register all the evaporated radiation. The total ADM mass on Σ_F must also equal M_0, since otherwise the classical boundary–value problem with time–interval, T, at spatial infinity, will have no solution [40, 43]. Regarding the classical solution in the interior ($0 < t < T$), the geometry is well approximated at late times by the radiating Schwarzschild–like Vaidya metric [34, 44, 45]. The classical scalar–field solution will depend on the enormous amount of detail which, in general, is present in the prescribed final data, ϕ_F, on Σ_F.

In Sect. 7.3.3, we discuss the 'background' spherically–symmetric four–metric, $\gamma_{\mu\nu}$, and scalar field, Φ, as part of a self–consistent treatment of the classical field equations. The Einstein field equations give, at lowest order, a 'source' for $\gamma_{\mu\nu}$ which includes the energy–momentum tensor of the scalar field, ϕ, and a source quadratic in graviton perturbations (and for other matter fields). In Sect. 7.3.3, we treat the decomposition of scalar perturbations in spherical harmonics. We also describe the classical action functionals, S_{class} (Lorentzian action), or I_{class} (Euclidean or Riemannian action), related by

$$i S_{\text{class}} = -I_{\text{class}}, \tag{7.3.2}$$

for the Einstein/scalar system. Since S_{class} or I_{class} are evaluated at a solution of the classical field equations, they reduce to a sum of boundary terms. Section 7.3.3 also treats adiabatic radial equations for the (linearised) scalar field. For adiabatic perturbations (high frequencies), the time–dependence is approximately harmonic and can be factored out, leading to a second–order radial equation for given frequency, ω, and angular quantum numbers, ℓ, m. Further, 'co–ordinates' are described which are suited to specifying final data, ϕ_F, on Σ_F, and a suitable basis of radial eigenfunctions on Σ_F is discussed. The Lorentzian quantum amplitude is defined as the limit, $\theta \longrightarrow 0_+$, of the amplitude for complex T, following Feynman [12, 13]. By these methods, one can evaluate the real and imaginary parts of the lowest–order perturbative classical action, $S^{(2)}_{\text{class}}$, and, hence, of the semi–classical amplitude, $\exp(i S^{(2)}_{\text{class}})$. Section 7.3.4 contains the Conclusion.

7.3.2 The Quantum Amplitude for Bosonic Boundary Data

From one point of view, this amplitude can be regarded as a Feynman path integral over all Riemannian infilling four–geometries and other fields. Each configuration is weighted by $\exp(-I)$, where I is the Euclidean action. The 'differential' Dirac approach of Sect. 7.2 is dual to the 'integral' Feynman approach. In the present boundary–value context, the Dirac approach appears to give the quantum amplitude more directly and explicitly than does the path–integral approach. Following the Dirac approach, given local supersymmetry, the amplitude has the 'semi–classical' form, Eq. (7.2.20). Related semi–classical behaviour holds for $N = 1$ supergravity with (gauge–invariant) supermatter [8, 17].

We assume, as in Sect. 7.2, the existence of a (complex) classical solution to the Dirichlet boundary–value problem, posed in Sect. 7.2, given Eq. (7.3.1). The solution should vary smoothly with $\theta (\epsilon \leq \theta \leq \pi/2)$, and the expression, Eq. (7.2.20), should continue to give the quantum amplitude as θ varies. In particular, this would occur if strong ellipticity [31] held for the coupled Einstein/bosonic–matter field equations, up to gauge. As above, we consider locally supersymmetric models. For simplicity, take only gravitational and scalar quantities to be present in the data and solution, but no fermions.

Consider the division, above, of $(g_{\mu\nu}, \phi)$ into 'background' and perturbative parts. Classical solutions, $(g_{\mu\nu}, \phi)$, of the coupled Einstein/scalar field equations are taken to have a 'background' time–dependent **spherically–symmetric** part, $(\gamma_{\mu\nu}, \Phi)$, together with a 'small' **perturbative part**, $(\beta_{\mu\nu}, \phi_{\rm pert})$. The fields, $(\beta_{\mu\nu}, \phi_{\rm pert})$, live (mathematically speaking) on the background four–geometry, with metric, $\gamma_{\mu\nu}$. $(\beta_{\mu\nu}, \phi_{\rm pert})$ can be expanded in terms of sums over tensor (spin–2), vector (spin–1) and scalar harmonics [46, 47]. Each harmonic is weighted by a function of time and radius, (t, r).

The Einstein field equations are:

$$G_{\mu\nu} \equiv R_{\mu\nu} - \frac{1}{2} R g_{\mu\nu} = 8\pi T_{\mu\nu}, \tag{7.3.3}$$

$$T_{\mu\nu} = \phi_{,\mu}\, \phi_{,\nu} - \frac{1}{2} g_{\mu\nu} \left(\phi_{,\alpha}\, \phi_{,\beta}\, g^{\alpha\beta} \right). \tag{7.3.4}$$

The scalar field equation is:

$$\partial_\mu \left((-g)^{\frac{1}{2}} g^{\mu\nu} \phi_{,\nu} \right) = 0, \tag{7.3.5}$$

where g denotes $\det(g_{\mu\nu})$, and $g_{\mu\nu}$ has Lorentzian signature, whence, $g < 0$.

The corresponding Lorentzian action is [16]

$$S = \frac{1}{16\pi} \int d^4x \left(-g\right)^{\frac{1}{2}} R - \frac{1}{2} \int d^4x \left(-g\right)^{\frac{1}{2}} \left(\nabla\phi\right)^2 + \text{boundarycontributions}, \tag{7.3.6}$$

in geometrical units. Boundary terms will be discussed in Sect. 7.3.3.

In Lorentzian signature, the spherically–symmetric 'background' four–metric, $\gamma_{\mu\nu}$, and scalar field can be written *via*:

$$ds^2 = -e^b dt^2 + e^a dr^2 + r^2 \left(d\theta^2 + \sin^2\theta d\phi^2 \right),$$

$$b = b(t, r), \quad a = a(t, r), \quad \phi = \Phi(t, r). \tag{7.3.7}$$

The classical field equations, assuming that one had exact spherical symmetry in Lorentzian signature, are given in [48, 49].

In a typical bosonic black–hole evaporation problem, the classical metric and scalar field are not spherically symmetric. Similarly, for non–zero spin–$\frac{1}{2}$ and spin–$\frac{3}{2}$ classical (odd Grassmann–algebra–valued [16]) fermionic solutions in a locally–supersymmetric generalisation [6]. In particle language, rather than the field language of this Chapter, huge numbers of gravitons and scalar particles are continually given off by the black hole (together with any fermions allowed), leading effectively to a stochastic distribution, in which, for given spin, s, the field fluctuates around a spherically–symmetric reference field.

Consider, say, a one–parameter family of gravitational and scalar perturbations about a spherically–symmetric reference four–metric, $\gamma_{\mu\nu}$, and field, Φ:

$$g_{\mu\nu}(x,\epsilon) \sim \gamma_{\mu\nu}(x) + \epsilon\beta^{(1)}_{\mu\nu}(x) + \epsilon^2\beta^{(2)}_{\mu\nu}(x) + \cdots , \tag{7.3.8}$$

$$\phi(x,\epsilon) \sim \Phi(t,r) + \epsilon\phi^{(1)}(x) + \epsilon^2\phi^{(2)}(x) + \cdots . \tag{7.3.9}$$

The background field, Φ, will be non–zero if the scalar data, ϕ, at early and late times, t, contain a non–trivial spherical component. The perturbation fields, $\phi^{(1)}(x), \phi^{(2)}(x), \ldots$ typically contain all non–spherical angular harmonics. These fields must be chosen such that the entire system obeys the classical coupled Einstein/scalar field equations, and agrees with the (prescribed) small non–spherical perturbations in the initial and final data, gravitational and scalar. The effective energy–momentum source for the background part of the metric, $\gamma_{\mu\nu}$, includes contributions quadratic in the non–spherical gravitational and scalar quantities, $\big(\beta^{(1)}_{\mu\nu}, \phi^{(1)}\big)$—see [7, 10] for further detail.

The linearised (ϵ^1) part of the Einstein equations reads (Sect. 35.13 of [42]):

$$\begin{aligned}&\bar\beta^{(1);\sigma}_{\mu\nu;\sigma} - 2\bar\beta^{(1);\sigma}_{\sigma(\mu;\nu)} - 2R^{(0)}_{\sigma\mu\nu\alpha}\bar\beta^{(1)\sigma\alpha} - 2R^{(0)\alpha}_{(\mu}\,\bar\beta^{(1)}_{\nu)\alpha}\\ &\quad + \gamma_{\mu\nu}\Big(\bar\beta^{(1);\alpha\beta}_{\alpha\beta} - \bar\beta^{(1)\alpha\beta}R^{(0)}_{\alpha\beta}\Big) + \bar\beta^{(1)}_{\mu\nu}R^{(0)} = -16\pi T^{(1)}_{\mu\nu}.\end{aligned} \tag{7.3.10}$$

Here, $\bar\beta^{(1)}_{\mu\nu}$ is defined by

$$\bar\beta^{(1)}_{\mu\nu} = \beta^{(1)}_{\mu\nu} - \frac{1}{2}\gamma_{\mu\nu}\beta^{(1)}, \tag{7.3.11a}$$

$$\beta^{(1)} = \beta^{(1)\mu}_{\mu}. \tag{7.3.11b}$$

The Riemann tensor of the background geometry, $\gamma_{\mu\nu}$, is denoted $R^{(0)}_{\sigma\mu\nu\alpha}$. Further, $T^{(1)}_{\mu\nu}$ denotes the linearisation or $O(\epsilon^1)$ part of the energy–momentum tensor, $T_{\mu\nu}(x,\epsilon)$:

$$\begin{aligned}T^{(1)}_{\mu\nu} &= 2\nabla_{(\mu}\phi^{(1)}\nabla_{\nu)}\Phi - \gamma_{\mu\nu}\big(\nabla_\alpha\Phi\big)\big(\nabla^\alpha\phi^{(1)}\big)\\ &\quad + \tfrac{1}{2}\Big(\gamma_{\mu\nu}\beta^{(1)\sigma\rho} - \beta^{(1)}_{\mu\nu}\gamma^{\sigma\rho}\Big)\big(\nabla_\sigma\Phi\big)\big(\nabla_\rho\Phi\big).\end{aligned} \tag{7.3.12}$$

The linearised Einstein equations, (7.3.10–7.3.12), are most easily studied in a 'linearised harmonic gauge' [42, 50], in which, following an infinitesimal co–ordinate transformation,

$$\bar{h}^{(1);\alpha}_{\mu\alpha} = 0. \tag{7.3.13}$$

The Einstein equations, (7.3.10–7.3.12), linearised about spherical symmetry, can be decomposed into three independent sets. These describe, respectively, scalar (spin–0) perturbations associated with matter–density changes, ($T^{(1)}_{\tau\tau}$), vector (spin–1) perturbations for matter–velocity changes, ($T^{(1)}_{\tau i}$), and gravitational radiation (spin–2) for anisotropic stresses, ($T^{(1)}_{ij}$) [51]. The resulting equations and their solutions are described in [36].

The linearised (ϵ^1) part of the scalar–field equation, (7.3.5), reads:

$$\gamma^{\mu\nu}\phi^{(1)}_{;\mu\nu} - \left(\bar{\beta}^{(1)\mu\nu}\Phi_{,\nu}\right)_{;\mu} = 0. \tag{7.3.14}$$

The linearised Einstein and scalar–field equations, (7.3.10–7.3.12, 7.3.14), are coupled. The remaining perturbative field equations, needed to complete this calculation, are in [7, 10].

These field equations arise, for example, in studying the Vaidya metric [44]; as shown in [34], this describes approximately the late–time region of the geometry following gravitational collapse to a black hole, containing a nearly–steady outgoing flux of radiation. The Einstein field equations, averaged over small regions, give the contribution of massless scalar particles, gravitons, etc., to the nearly–isotropic flux.

As above, for perturbed boundary data which contain numerous high harmonics, the interior perturbations can be regarded as effectively stochastic in nature. Averaged over a number of wavelengths, the effective perturbative energy–momentum tensor, $T^{EFF}_{\mu\nu}$, yields a spherically–symmetric smoothed–out quantity, $< T^{EFF}_{\mu\nu} >$ [52, 53].

The averaged form of $T^{EFF}_{\mu\nu}$ accounts for the gradual loss of mass of a black hole by radiation, in a slightly–complexified (nearly–Lorentzian) 'space–time', with $\theta = \delta \ll 1$ in Eq. (7.3.1). Although $< T^{EFF}_{\mu\nu} >$ is small [$O(\epsilon^2)$], its effects on the black–hole geometry, including those on the mass, build up in secular fashion, over a time–scale of order $O(\epsilon^{-2})$. Secular behaviour appears often in perturbation problems [54, 55]—for example, in the perihelion precession of nearly–circular orbits in the Schwarzschild geometry [56]. In our boundary–value problem, classical or quantum, the initial boundary data are spread over a 'background' extent of $O(1)$, measured by the co–ordinate, r, on Σ_I. Corresponding to the $O(\epsilon^{-2})$ time–scale for the black hole to radiate, the data on Σ_F will be spread over a radial–coordinate scale of $O(\epsilon^{-2})$. Thus, even the classical boundary–value problem is an example of singular perturbation theory [54, 55].

High–frequency averaging in general relativity was treated by Brill and Hartle [52], Isaacson [53]. Let $<>$ denote an average over a time, T_0, longer than typical wave periods, and a spatial average over several wavelengths, $\bar{\lambda}$. Rules for

manipulating these averages in the high–frequency aproximation are in [53]. In particular, one finds [7, 10]:

$$< T^{(1)}_{\mu\nu} >= 0, \tag{7.3.15}$$

$$< T^{(2)}_{\mu\nu} >= < \nabla_{(\mu}\phi^{(1)}\nabla_{\nu)}\phi^{(1)} - \frac{1}{2}\gamma_{\mu\nu}\nabla_{\alpha}\phi^{(1)}\nabla^{\alpha}\phi^{(1)} > . \tag{7.3.16}$$

The background field equations can be re–written in a form smoothed by averaging [52, 53].

7.3.3 Classical Action and Amplitude for Weak Perturbations

Consider small bosonic perturbations, $\left(\beta^{(1)}_{\mu\nu}, \phi^{(1)}\right)$, obeying the linearised classical field equations, (7.3.10, 7.3.14), about a spherically–symmetric classical solution, $(\gamma_{\mu\nu}, \Phi)$ [10]. The background data for $\gamma_{\mu\nu}$ and Φ are posed, as in Sects. 7.1 and 7.2, on $\Sigma_{I,F}$, separated at spatial infinity by time, T, with $\mathrm{Im(T)} < 0$. Similarly, the linearised classical perturbations, $\left(\beta^{(1)}_{\mu\nu}, \phi^{(1)}\right)$, are solutions of a (complex) linear strongly–elliptic problem, with prescribed perturbations, $\left(\beta^{(1)}_{ij}, \phi^{(1)}\right)$, on $\Sigma_{I,F}$.

Given the background spherical symmetry, one can expand $\phi^{(1)}$ as:

$$\phi^{(1)}(t, r, \theta, \phi) = \frac{1}{r}\sum_{\ell=0}^{\infty}\sum_{m=-\ell}^{\ell} Y_{\ell m}(\Omega)R_{\ell m}(t, r), \tag{7.3.17}$$

where $Y_{\ell m}(\Omega)$ is the (ℓ, m) scalar spherical harmonic of [57].

Similarly, a metric perturbation, $\beta^{(1)}_{\mu\nu}$, can be expanded as a sum over tensor, vector and scalar (ℓ, m) harmonics, weighted by functions of t and r [46, 47, 58–61]. Because of the coupling in the linearised field equations, (7.3.10, 7.3.14), for $\left(\beta^{(1)}_{\mu\nu}, \phi^{(1)}\right)$, the linear field equations for $R_{\ell m}(t, r)$ in Eq. (7.3.17) and its gravitational analogues are also coupled in the strong–field 'collapse' region of the space–time.

The boundary conditions on $R_{\ell m}(t, r)$, as $r \longrightarrow 0$, follow from regularity of the solution, $\left(g_{\mu\nu}, \phi\right)$, viewed in 'nearly–Cartesian co–ordinates' near $r = 0$. Regularity follows since the coupled field equations are 'strongly–elliptic *modulo* gauge'. The asymptotically–flat boundary data on $\Sigma_{I,F}$, are chosen smooth over $\mathbb{R}^3$. The field equations (up to gauge) should be strongly elliptic [31], giving analytic classical fields in the interior.

Take the final boundary data to describe very weak, diffuse scalar and gravitational fields, viewed as perturbations of nearly–flat space–time. (As in Sect. 7.3.1, the ADM mass of h_{ijF} must equal the ADM mass of Σ_I.) Physically, such final data may be imagined as a possible late–time remnant of gravitational collapse, namely, a snap–shot of a large number of scalar particles and gravitons, as they make their way out to infinity. Near Σ_F, the coupling in Eqs. (7.3.10, 7.3.14) between $\beta^{(1)}_{\mu\nu}$ and $\phi^{(1)}$ will

almost disappear. The perturbed scalar field equation is then:

$$\nabla^{\mu}\nabla_{\mu}\phi^{(1)} = 0, \tag{7.3.18}$$

with respect to the spherically–symmetric geometry, $\gamma_{\mu\nu}$.

From the decomposition, Eq. (7.3.17), of $\phi^{(1)}$, one finds the (ℓ, m) mode equation:

$$\Big(e^{(b-a)/2}\partial_r\Big)^2 R_{\ell m} - \big(\partial_t\big)^2 R_{\ell m} - \frac{1}{2}\Big(\partial_t\big(a-b\big)\Big)\big(\partial_t R_{\ell m}\big) - V_{\ell}\big(t,r\big)R_{\ell m} = 0. \tag{7.3.19}$$

The potential, $V_{\ell}(t,r)$, and function, $m(t,r)$, are defined by:

$$V_{\ell}(t,r) = \frac{e^{b(t,r)}}{r^2}\Big(\ell(\ell+1) + \frac{2\,m(t,r)}{r}\Big), \tag{7.3.20}$$

$$\exp\Big(-a(t,r)\Big) = 1 - \frac{2m(t,r)}{r}. \tag{7.3.21}$$

In an exact Schwarzschild solution with no scalar field, one has $1 - (2M/r) = e^{-a} = e^{b}$, with M the Schwarzschild mass; in that case, $m(t,r)$ is identically M. The potential, $V_{\ell}(t,r)$, generalises the well–known massless–scalar effective potential in the Schwarzschild geometry [42], which vanishes at the event horizon, $\{r = 2M\}$, and at spatial infinity, and has a peak near $\{r = 3M\}$.

The definition, Eq. (7.3.21), of $m(t,r)$, is consistent with the usual description in Lorentzian signature of the Vaidya metric [44, 45]. In terms of a null co–ordinate, u, and intrinsic radial co–ordinate, r, the Vaidya metric reads:

$$ds^2 = -2dudr - \Big(1 - \frac{2m(u)}{r}\Big)du^2 + r^2\big(d\theta^2 + \sin^2\theta d\phi^2\big). \tag{7.3.22}$$

Here, $m(u)$ is a monotonic–decreasing smooth function of u, corresponding to a spherically–symmetric outflow of null particles—for example, from the energy–momentum tensor of a black hole evaporating *via* emission of scalar particles at the speed of light. The Vaidya metric has been used often to give an approximate gravitational background for black–hole evaporation at late times [62–64]. In connection with the present work, see [34].

An analogous decoupled harmonic decomposition is valid near Σ_F, for late–time gravitational–wave perturbations of the spherically–symmetric background—again as in [36]. To simplify the exposition, restrict attention to non–zero weak–field final configurations with spin 0 , and calculate their quantum amplitudes (below). Make the further assumption that the final three–metric, h_{ijF}, is exactly spherically symmetric (in addition to the assumed spherical symmetry of the initial data, (h_{ijI}, ϕ_I)).

Consider an asymptotically–flat classical solution, $(g_{\mu\nu}, \phi)$, of the coupled Einstein/massless–scalar field equations, between Σ_I and Σ_F, with $\mathrm{Im(T)} < 0$. The classical Riemannian and Lorentzian actions, for fixed boundary data, $(h_{ij}, \phi)_I$,

$(h_{ij}, \phi)_F$, are related by Eq. (7.3.2). At a solution [16, 65], the classical action is:

$$S_{\text{class}}\big[(h_{ij}, \phi)_I; (h_{ij}, \phi)_F; T\big] = \tfrac{1}{32\pi}\Big(\int_{\Sigma_F} - \int_{\Sigma_I}\Big) d^3x \pi^{ij} h_{ij} + \tfrac{1}{2}\Big(\int_{\Sigma_F} - \int_{\Sigma_I}\Big) d^3x \pi_\phi \phi - MT. \tag{7.3.23}$$

Here, $\pi^{ij} = \pi^{ji}$ is 16π times the (Lorentzian) momentum conjugate to the 'co–ordinate' variable, h_{ij}, on a space–like hypersurface, in a $3+1$ Hamiltonian decomposition of the Einstein/massless–scalar theory. In terms of the second fundamental form, $K_{ij} = K_{(ij)}$, of the hypersurface [16, 50], π^{ij} is

$$\pi^{ij} = h^{\frac{1}{2}}\big(K^{ij} - K h^{ij}\big), \tag{7.3.24}$$

with $h = \det(h_{ij})$, $K = h^{ij} K_{ij}$. Also, π_ϕ is the momentum conjugate to the 'co–ordinate' variable, ϕ. Explicitly,

$$\pi_\phi = h^{\frac{1}{2}} n^\mu \nabla_\mu \phi. \tag{7.3.25}$$

The quantity, M, in Eq. (7.3.23) is the ADM mass of the space–time. As above, it is essential, for a well–posed asymptotically–flat boundary–value problem, that the intrinsic metrics, h_{ijI} and h_{ijF}, have the same value of M. Otherwise, if $M_I \neq M_F$, a classical infilling space–time will have Σ_I and Σ_F badly embedded near spatial infinity, and the four–metric, $g_{\mu\nu}$, will not fall off to flatness at the standard $1/r$ rate, as $r \longrightarrow \infty$ [43].

Without loss of generality, assume that any spherically–symmetric $\ell = 0$ linear–order perturbation modes have been absorbed into the spherically–symmetric background, $(\gamma_{\mu\nu}, \Phi)$. The Lorentzian classical action, S_{class}, of Eq. (7.3.23), may be split as

$$S_{\text{class}} = S^{(0)}_{\text{class}} + S^{(2)}_{\text{class}} + S^{(3)}_{\text{class}} + \cdots. \tag{7.3.26}$$

(The formal device of including a small parameter, ϵ, has been relaxed; we now set $\epsilon = 1$.)

Here, $S^{(0)}_{\text{class}}$ is the background action, evaluated at the spherically–symmetric solution, $(\gamma_{\mu\nu}, \Phi)$. The mass, M, appearing in $S^{(0)}_{\text{class}}$, is that determined from (either of) γ_{ijI} or γ_{ijF}. The next term, $S^{(2)}_{\text{class}}$, is formed quadratically from the linear–order perturbations. The linear–order term, $S^{(1)}_{\text{class}}$, is zero, since one is perturbing around a classical solution. In an obvious notation:

$$S^{(2)}_{\text{class}} = \frac{1}{32\pi}\Big(\int_{\Sigma_F} - \int_{\Sigma_I}\Big) d^3x \pi^{(1)ij} \beta^{(1)}_{ij} + \frac{1}{2}\Big(\int_{\Sigma_F} - \int_{\Sigma_I}\Big) d^3x \pi^{(1)}_\phi \phi^{(1)}. \tag{7.3.27}$$

Thus, $S^{(2)}_{\rm class}$ is contructed only from first–order quantities on Σ_I and Σ_F. Note that there is no contribution to $S^{(2)}_{\rm class}$ from the $-MT$ term in Eq. (7.3.23), since, from the above definitions, both M and T are known (zeroth–order) quantities.

The expression, Eq. (7.3.23), for $S_{\rm class}[(h_{ij}, \phi)_I; (h_{ij}, \phi)_F; T]$, together with the asymptotic series, Eqs. (7.3.11a, 7.3.11b), for the classical action, and Eq. (7.3.27) for $S^{(2)}_{\rm class}$, are basic to the calculations below, leading to explicit forms for quantum amplitudes.

Return to the evolution of linearised scalar perturbations, $\phi^{(1)}$, *via* the mode sum of Eq. (7.3.17). For quantum amplitudes of interest, one computes expressions of the form,

$$\text{Amplitude} = \text{const.} \times \exp\Big\{ i S_{\rm class}\big[\big(h_{ij}, \phi\big)_I; \big(h_{ij}, \phi\big)_F; T\big]\Big\}, \tag{7.3.28}$$

As above, take T as in Eq. (7.3.1), to give a strongly–elliptic boundary–value problem. The classical action, $S_{\rm class}$, is that of Eq. (7.3.23), subject to the classical field equations.

Consider the perturbative amplitude corresponding to weak–field non–spherical data, $\big(h^{(1)}_{ijF}, \phi^{(1)}\big)_F$, on Σ_F, given at lowest order by $\exp\big(i S^{(2)}_{\rm class}\big)$. For simplicity, take the initial data to be exactly spherically symmetric, $(\gamma_{ij}, \Phi)_I$. Equivalently,

$$\beta^{(1)}_{ijI} = 0, \quad \phi^{(1)}_I = 0. \tag{7.3.29}$$

The amplitude, $\exp\big(i S_{\rm class}\big)$, depends only on the contributions at Σ_F, in Eq. (7.3.27) [which themselves depend on $(\beta^{(1)}_{ijF}, \phi^{(1)}_F; T)$]. As a practical matter, one could put non–zero $(\beta^{(1)}_{ij}, \phi^{(1)})_I$ back into the calculations that follow. Physically, the analogous step of 'turning back on the early–time perturbations' corresponds, in 'particle language' rather than 'field language', to the inclusion of extra particles in the in–states, together with the original spherical collapsing matter, and asking for the late–time consequences. This was first carried out by Wald [66].

At present, study the scalar–field contribution to the quantum amplitude, $\exp(i S_{\rm class})$: consider

$$S^{(2)}_{\rm class,scalar} = \frac{1}{2} \int_{\Sigma_F} d^3x \pi^{(1)}_\phi \phi^{(1)}, \tag{7.3.30}$$

where $(\beta^{(1)}_{\mu\nu}, \phi^{(1)})$ obey the linearised field equations, (7.3.10–7.3.12, 7.3.14), about the spherically–symmetric background, $(\gamma_{\mu\nu}, \Phi)$. Here, $(\beta^{(1)}_{\mu\nu}, \phi^{(1)})$ must agree with the prescribed final data, $(\beta^{(1)}_{ij}, \phi^{(1)})_F$, at Σ_F, and be zero at Σ_I. In the present case, with complex time–interval, T [Eq. (7.3.1)], one expects the linear boundary–value problem to be well–posed. The other, gravitational, contribution,

$$S^{(2)}_{\rm class,grav} = \frac{1}{32\pi} \int_{\Sigma_F} d^3x \pi^{(1)ij} \beta^{(1)}_{ij}, \tag{7.3.31}$$

to $S^{(2)}_{\text{class.}}$ in Eq. (7.3.37), is studied in [36].

Consider late–time high–frequency oscillations of the scalar field in the nearly–Lorentzian case, with $\theta = \delta \ll 1$ in Eq. (7.3.1), and a solution, $R_{\ell m}(t, r)$, of the form

$$R_{\ell m}(t, r) \sim \exp(ikt)\xi_{k\ell m}(t, r), \tag{7.3.32}$$

as $r \longrightarrow \infty$, where k is a 'large' frequency, but $\xi_{k\ell m}(t, r)$ varies 'slowly' with t. In particular, require that, as $r \longrightarrow \infty$, $R_{\ell m}(t, r)$ reduces to a flat space–time separated solution, in which $\xi_{k\ell m}(t, r)$ loses its t–dependence [Eqs. (7.3.34, 7.3.36) below].

Our boundary–value problem is for scalar perturbations, $\phi^{(1)}(t, r, \theta, \phi)$, or, equivalently, functions, $R_{\ell m}(t, r)$, as in Eqs. (7.3.17, 7.3.19), subject to the initial condition, $\phi^{(1)}\big|_{t=0} = 0$, and to prescribed real final data, $\phi^{(1)}\big|_{t=T}$. Were the propagation simply in flat space–time, the solution would be of the form:

$$\phi^{(1)} = \frac{1}{r}\sum_{\ell=0}^{\infty}\sum_{m=-\ell}^{\ell}\int_{-\infty}^{\infty} dk a_{k\ell m}\xi_{k\ell m}(r)\frac{\sin(kt)}{\sin(kT)}Y_{\ell m}(\Omega), \tag{7.3.33}$$

where the $\{a_{k\ell m}\}$ are real coefficients and each function, $\xi_{k\ell m}(r)$, is proportional (up to a factor of r) to a spherical Bessel function, $j_\ell(kr)$ [67]. In our gravitational–collapse case, $\xi_{k\ell m}$ becomes a function of t as well as r, but the pattern remains:

$$\phi^{(1)} = \frac{1}{r}\sum_{\ell=0}^{\infty}\sum_{m=-\ell}^{\ell}\int_{-\infty}^{\infty} dk a_{k\ell m}\xi_{k\ell m}(t, r)\frac{\sin(kt)}{\sin(kT)}Y_{\ell m}(\Omega). \tag{7.3.34}$$

The $\{a_{k\ell m}\}$ characterise the final data: they can be constructed from the given $\phi^{(1)}\big|_{t=T}$ by inverting Eq. (7.3.34). The functions, $\xi_{k\ell m}(t, r)$, are defined in the adiabatic or large–$|k|$ limit, as in the previous paragraph, *via* Eq. (7.3.32), where $R_{\ell m}(t, r)$ obeys the mode equation, (7.3.19).

More precisely, given that k is large, in that the adiabatic approximation,

$$|k| \gg \frac{1}{2}|\dot{a} - \dot{b}|, \tag{7.3.35a}$$

$$|k| \gg \left|\frac{\dot{\xi}_{k\ell m}}{\xi_{k\ell m}}\right|, \tag{7.3.35b}$$

$$k^2 \gg \left|\frac{\ddot{\xi}_{k\ell m}}{\xi_{k\ell m}}\right|, \tag{7.3.35c}$$

holds, the mode equation reduces approximately to

$$e^{(b-a)/2}\frac{\partial}{\partial r}\left(e^{(b-a)/2}\frac{\partial \xi_{k\ell m}}{\partial r}\right) + \left(k^2 - V_\ell\right)\xi_{k\ell m} = 0. \tag{7.3.36}$$

Of course, the functions, $e^{(b-a)/2}$ and V_ℓ, do still vary with the time–coordinate, t, but only adiabatically or 'slowly'.

As described in [7, 22, 44], one expects the geometry in the radiative region of the space–time to be approximated accurately by a spherically–symmetric Vaidya metric [44, 45], with a luminosity in the radiated particles which varies slowly with time. Such a metric can be put in diagonal form:

$$e^{-a} = 1 - \frac{2m(t,r)}{r}, \qquad e^{b} = \left(\frac{\dot{m}}{f(m)}\right)^2 e^{-a}, \tag{7.3.37}$$

where $m(t,r)$ is a slowly–varying function, with $\dot{m} = (\partial m/\partial t)$. The function, $f(m)$, depends on the details of the radiation. The adiabatic condition is then:

$$|k| \gg \left|\frac{\dot{m}}{m}\right|, \tag{7.3.38}$$

provided that $2m(t,r) < r < 4m(t,r)$. Then, the rate of change of the metric with time is slow compared to typical radiation frequencies. Equivalently, the time–scale of variations of the background metric, $\gamma_{\mu\nu}$, is much greater than the period of the waves. With frequencies of magnitude, $|k| \sim m^{-1}$, dominating the radiation, and with $|\dot{m}|$ of order m^{-2} [5], the adiabatic approximation is equivalent to $m^2 \gg 1$, corresponding to the semi–classical approximation.

It is natural to define a generalisation, r^*, of the standard Regge–Wheeler co–ordinate, r_s^*, for the Schwarzschild geometry [42, 58], according to

$$\frac{\partial}{\partial r^*} = e^{(b-a)/2}\frac{\partial}{\partial r}. \tag{7.3.39}$$

Under adiabatic conditions, the time–dependence of $r^*(t,r)$ is negligibly small, and $r^* \sim r_s^*$ for large r. By definition,

$$r_s^* = r + 2M\log\Big(\big(r/2M\big) - 1\Big), \tag{7.3.40}$$

with r the Schwarzschild radial co–ordinate. In terms of r^*, the approximate (adiabatic) mode equation, (7.3.36), reads

$$\frac{\partial^2 \xi_{k\ell m}}{\partial r^{*2}} + \big(k^2 - V_\ell\big)\xi_{k\ell m} = 0. \tag{7.3.41}$$

We consider, in more detail, a set of suitable radial functions, $\{\xi_{k\ell m}(r)\}$, on Σ_F. Since the mode equation, (7.3.19), does not depend on the quantum number, m, we choose $\xi_{k\ell m}(r) = \xi_{k\ell}(r), \forall m$.

We seek a complete set, such that any smooth perturbation field, $\phi^{(1)}(T,r,\theta,\phi)$, of rapid decay near spatial infinity, when restricted to the final surface, $\{t = T\}$,

can be expanded in terms of the $\xi_{k\ell m}(r)$. The 'left' boundary condition on the radial functions, $\{\xi_{k\ell}(r)\}$, is that of regularity at the origin, $r = 0$:

$$\xi_{k\ell}(0) = 0. \tag{7.3.42}$$

The solution to the radial equation, regular near the origin, is:

$$\xi_{k\ell}(r) = r\phi_{k\ell}(r) \sim \Big\{(\text{const.}) \times \big[rj_\ell(kr)\big]\Big\}$$

$$\propto \Big\{\big(\text{const.} \times (kr)^{\ell+1}\big) + O\big((kr)^{\ell+3}\big)\Big\}. \tag{7.3.43}$$

Again, j_ℓ denotes a spherical Bessel function [67]; we have assumed that $m(r) \propto r^3$ for small r, and neglected $O(r^2)$ terms. These radial functions are real, for real k and r. For k real and positive, the radial functions describe standing waves, which, for mode time–dependence, $e^{\pm ikt}$, have equal amounts of 'ingoing' and 'outgoing' radiation.

For the 'right' boundary condition, the potential, $V_\ell(r)$, of Eq. (7.3.20), vanishes rapidly as $r \longrightarrow \infty$, such that a real solution to Eq. (7.3.41) obeys

$$\xi_{k\ell}(r) \sim \Big(z_{k\ell} \exp\big(ikr_s^*\big) + z_{k\ell}^* \exp\big(-ikr_s^*\big)\Big), \tag{7.3.44}$$

as $r \longrightarrow \infty$. The $z_{k\ell}$ are dimensionless complex coefficients, which can be determined *via* the differential equation, using regularity at $r = 0$. Note that the radial functions, $\{\xi_{k\ell}\}$, form a complete set only for $k > 0$, as a result of the boundary conditions [7, 10].

This makes it possible to evaluate the contribution, $S^{(2)}_{\text{class,scalar}}$ [Eq. (7.3.30)], to $S^{(2)}_{\text{class}}$ [Eq. (7.3.27)] in the classical action, $S_{\text{class}} = S^{(0)}_{\text{class}} + S^{(2)}_{\text{class}} + \cdots$, [Eq. (7.3.26)]:

$$S^{(2)}_{\text{class}}\big[\phi^{(1)}; T\big] = \frac{1}{2}\sum_{\ell=0}^{\infty}\sum_{m=-\ell}^{\ell}\int_0^{R_\infty} dr e^{(a-b)/2} R_{\ell m}\big(\partial_t R^*_{\ell m}\big)\,\big|_T. \tag{7.3.45}$$

With the adiabatic approximation above, this gives the frequency–space expression [10]:

$$S^{(2)}_{\text{class}}\big[\{a_{k\ell m}\}; T\big] = \pi\sum_{\ell=0}^{\infty}\sum_{m=-\ell}^{\ell}\int_0^{\infty} dk k\big|z_{k\ell}\big|^2\big|a_{k\ell m} + a_{-k\ell m}\big|^2 \cot(kT), \tag{7.3.46}$$

in terms of the final data, $\{a_{k\ell m}\}$.

Define

$$\psi_{\ell m}(r) = r\int d\Omega Y_{\ell m}(\Omega)\phi^{(1)}(t, r, \Omega)\,\big|_{t=T}. \tag{7.3.47}$$

The inverse of Eq. (7.3.34) can be shown to be [7]:

$$a_{k\ell m} + a_{-k\ell m} = \frac{1}{2\pi \left| z_{k\ell} \right|^2} \int_0^{R_\infty} dr e^{(a-b)/2} \xi_{k\ell}(r) \psi_{\ell m}(r). \tag{7.3.48}$$

The perturbative classical scalar action, $S^{(2)}_{\rm class}$, of Eq. (7.3.46), was derived subject to the adiabatic approximation and to the requirement, Eq. (7.3.1). In this case, the term, $k \cot(kT)$, in the integrand of Eq. (7.3.46) remains bounded near $k = 0$, and one expects to obtain a finite complex–valued action, $S^{(2)}_{\rm class}[\{a_{k\ell m}\}; T]$, given square–integrable data, $\phi^{(1)}$, on Σ_F. The dependence of the complex function, $S^{(2)}_{\rm class}[\{a_{k\ell m}\}; T]$, on the complex variable, T, should be analytic in this domain $(0 < \theta \leq \pi/2)$. Following Feynman [12, 13], Lorentzian–signature quantum amplitudes are the limit of $\exp(i S_{\rm class})$, as $\theta \longrightarrow 0_+$.

If, on the other hand, one takes real Lorentzian geometries ($\theta = 0$), the integral in Eq. (7.3.46) will typically diverge, due to the simple poles on the real–frequency axis at

$$k = k_n = \frac{n\pi}{T} \quad (n = 1, 2, 3, \ldots). \tag{7.3.49}$$

Consider an integral such as Eq. (7.3.46) for $S^{(2)}_{\rm class}[\{a_{k\ell m}\}; T]$, in the form,

$$J = \sum_{\ell m} \int_0^\infty dk f_{\ell m}(k) \cot(kT), \tag{7.3.50}$$

$$f_{\ell m}(k) = \pi k \left| z_{k\ell} \right|^2 \left| a_{k\ell m} + a_{-k\ell m} \right|^2. \tag{7.3.51}$$

There are infinitely many simple poles of the integrand at $k = k_n (n = 1, 2, \ldots)$, just above the positive real k–axis. One deforms the original contour, C, along the positive real k–axis into three parts, C_ϵ, C_R, and C_α, where $0 < \alpha \ll 1$. The contour, C_ϵ, lies in the lower half–plane, half–encircling each of the simple poles near the positive real k–axis, with radius ϵ. The curve, C_R, also in the lower half–plane, is an arc of a circle, $|k| = R$, of large radius. The curve, C_α, is part of the radial line, $\arg(k) = -\alpha$.

In studying these integrals, one needs an estimate of the rate of decay of $f_{\ell m}(k)$, as $|k| \longrightarrow \infty$. On dimensional grounds, one expects:

$$\left| f_{\ell m}(k) \right| \sim \text{const.} \times \left| k \right|^{-3}, \tag{7.3.52}$$

as $|k| \longrightarrow \infty$. To see this, re–write the radial equation, (7.3.41), in terms of the operator,

$$\mathcal{L}_\ell = e^{(b-a)/2} \frac{d}{dr} \left(e^{(b-a)/2} \frac{d}{dr} (\,) \right) - V_\ell(r), \tag{7.3.53}$$

self–adjoint with respect to the relevant inner product [7, 10]. Note that Eq. (7.3.48) can be re–written as:

$$a_{k\ell m} + a_{-k\ell m} = \frac{-1}{2\pi k^2 \left|z_{k\ell}\right|^2} \int_0^{R_\infty} dr e^{(a-b)/2} \xi_{k\ell}(r) \mathcal{L}_\ell \psi_{\ell m}(r). \tag{7.3.54}$$

We have used the boundary condition, Eq. (7.3.42), and assumed that $\psi_{\ell m}(r)$ decays at large r. The form, Eq. (7.3.54), is an expression of self–adjointness of the radial equation. One finds that $\psi_{\ell m}(r)$ has dimensions of length and that $|z_{k\ell}|^2$ is dimensionless [10]. In the limit, $R_\infty \longrightarrow \infty$, and for large k (hence, a WKB approximation for the radial functions), the integral in Eq. (7.3.54) can only involve the dimensionless frequency, $2Mk$, where M is the mass. This gives the desired behaviour, Eq. (7.3.52), at large $|k|$.

One further definition is needed:

$$\sigma_n = \frac{n\pi}{|T|} \quad (n = 1, 2, 3, \ldots). \tag{7.3.55}$$

Note the difference between the definitions, Eq. (7.3.49) of k_n and Eq. (7.3.55) of σ_n.

The classical action for massless scalar–field perturbations, with $\theta = \delta \ll 1$ in Eq. (7.3.1), in terms of boundary data on Σ_F, is:

$$\begin{aligned} S^{(2)}_{\text{class}}\big[\{a_{k\ell m}\}; |T|\big] &= \text{realpart} + \tfrac{2i\pi}{|T|} \sum_{\ell=0}^{\infty} \sum_{m=-\ell}^{\ell} \sum_{n=1}^{\infty} f_{\ell m}(\sigma_n) \\ &= \text{realpart} + \tfrac{2i\pi^2}{|T|} \sum_{\ell m n} \sigma_n \left|z_{n\ell}\right|^2 \left|a_{n\ell m} + a_{-n\ell m}\right|^2. \end{aligned} \tag{7.3.56}$$

The real part of $S^{(2)}_{\text{class}}$ is also calculable.

The main, semi–classical, contribution to the quantum amplitude is $\exp(i S^{(2)}_{\text{class}}[\{a_{k\ell m}\}; |T|])$. The probability distribution for final configurations involves $\text{Im}(S^{(2)}_{\text{class}})$; the more probable configurations have $S^{(2)}_{\text{class}}$ lying only infinitesimally in the upper half–plane. Probable or not, those final configurations, $\{a_{k\ell m}\}$, which contribute to the probability distribution must yield finite expressions in the infinite sums over (n, ℓ) in Eq. (7.3.56). There will be a corresponding restriction when the data are instead described in terms of the spatial configurations, $\{\psi_{\ell m}(r)\}$. Also (see [37]), the complex quantities, $z_{n\ell}(a_{n\ell m} + a_{-n\ell m})$, appearing in Eq. (7.3.56), are related to Bogoliubov transformations between initial and final states, providing a further characterisation of the finiteness of $\text{Im}(S^{(2)}_{\text{class}})$ in Eq. (7.3.56).

With regard to the sum over ℓ in Eq. (7.3.56), one expects that a cut–off, $\ell_{\max}$, can be provided by the radial equation, (7.3.41). In the region, $(V_\ell(r) - k^2) > 0$, one has exponentially–growing radial functions; for $(V_\ell(r) - k^2) < 0$, one has oscillatory radial functions. One defines $\ell_{\max}$ by $(V_{\ell_{\max}}(r) - k^2) = 0$, and restricts attention mainly to oscillatory solutions.

Given initial and final non–zero Dirichlet data labelled by 'co–ordinates', $\{a^{(I)}_{k\ell m}\}$, $\{a^{(F)}_{k\ell m}\}$, the perturbative classical scalar action, $S^{(2)}_{\rm class}$, includes separate terms of the form, Eq. (7.3.56), from Σ_I, Σ_F. But $S^{(2)}_{\rm class}$ also includes a cross–term between $a^{(I)}_{k\ell m}$ and $a^{(F)}_{k\ell m}$, representing the correlation or mixing between initial and final data. The total action is symmetric in $a^{(I)}_{k\ell m}$ and $a^{(F)}_{k\ell m}$, and the coefficients, $z_{n\ell}$, are the same (they are time–independent) up to a phase. For large $|T|$, the cross–term becomes negligible, and one has two independent contributions to the classical action, from $\{a^{(I)}_{k\ell m}\}$ and $\{a^{(F)}_{k\ell m}\}$.

7.3.4 Comments

The work in Sect. 7.3 began as a doctoral dissertation at Cambridge by one of the present authors [7] in 1997–2001. The thesis being approved in summer 2002, the results were published in the joint papers [4, 9, 10, 20, 32–38]. This work used local supersymmetry in an essential way to find quantum amplitudes in explicit form. Unsubstantiated opposition (since 1975) to the idea that one could calculate amplitudes for quantum processes involving gravitational collapse to a black hole continued until our 2004 (and following) publications. In response to our work, the paper [68] appeared in 2005. The author, despite earlier, strongly–held views (1975–2004), finally admitted that, for a particular bosonic field theory in four space–time dimensions, quantum amplitudes did, after all, exist [68]. That argument was based on quantum field theory, though not on local supersymmetry. Further, it applied only to the case of asymptotically–anti–deSitter space–time, but not to asymptotically–flat space–times. Moreover, by working with a Lagrangian that was not locally supersymmetric, it failed to deal with the problem of infinities in field–theoretic quantum gravity.

We have arrived at a quantum amplitude (not just a probability distribution) for such processes, simply by following Feynman's $+i\epsilon$ prescription, applied to the 'semi–classical' expression, Eq. (7.2.20), for the quantum amplitude. This, in turn, was derived *via* Dirac's canonical–quantisation approach for a locally–supersymmetric Lagrangian, outlined in Sect. 7.2. We studied the classical and quantum–mechanical boundary–value problems, before rotating θ [of Eq. (7.3.1)] back towards zero.

These ideas have also been applied to black–hole evaporation for particles of spin 1 and 2 [36], and to the fermionic spin–$\frac{1}{2}$ case [33]. In [33, 36], the form of the complex quantum amplitudes was not derived in the greater detail obtained in [10] for spin–0 amplitudes.

In [20, 37], we described a relation between the present approach and the familiar description in terms of Bogoliubov coefficients [2, 3, 69]. A more general conceptual framework has been provided in the language of coherent and squeezed states [35, 38].

References

1. Hawking, S.W.: Black hole explosions. Nature **248**, 30 (1974)
2. Hawking, S.W.: Particle creation by black holes. Commun. Math. Phys. **43**, 199 (1975)
3. Frolov, V.P., Novikov, I.D.: Black Hole Physics. Kluwer Academic, Dordrecht (1998)
4. Farley, A.N.St.J., D'Eath, P.D.: Relic radiation from an evaporating black hole. Int. J. Mod. Phys. **(D17)**, 1–23 (2008). arXiv:hep-th/0708.2012
5. Hawking, S.W.: Breakdown of predictability in gravitational collapse. Phys. Rev. **D14**, 2460 (1976)
6. Wess, J., Bagger, J.: Supersymmetry and Supergravity, 2nd edn. Princeton University Press, Princeton (1992)
7. Farley, A.N.St.J.: Quantum Amplitudes in Black-Hole Evaporation. Ph.D. dissertation. Cambridge, approved 2002 (unpublished)
8. D'Eath, P.D.: Dirac quantization of $N = 1$ supergravity and gauge-invariant $N = 1$ supergravity (in preparation)
9. Farley, A.N.St.J., D'Eath, P.D.: Scalar-field amplitudes in black-hole evaporation. Phys. Lett. **B601**, 184–191 (2004). arXiv:gr-qc/0407086
10. Farley, A.N.St.J., D'Eath, P.D.: Quantum amplitudes in black-hole evaporation: Complex approach and spin-0 amplitudes. Int. J. Mod. Phys. **D20** 133–159 (2011). arXiv:gr-qc/1002.3979
11. Dirac, P.A.M.: Lectures on Quantum Mechanics. Academic Press, New York (1965)
12. Feynman, R.P., Hibbs, A.R.: Quantum Mechanics and Path Integrals. McGraw-Hill, New York (1965)
13. Itzykson, C., Zuber, J.-B.: Quantum Field Theory. McGraw-Hill, New York (1980)
14. Bern, Z., et al.: Phys. Rev. Lett. **103**, 081301 (2009). arXiv:0902.3765 [hep-th]. arXiv:1103.1848 [hep-th]. arXiv:1309.2498 [hep-th]
15. D'Eath, P.D.: Phys. Rev. D **29**, 2199 (1984)
16. D'Eath, P.D.: Supersymmetric Quantum Cosmology. Cambridge University Press, Cambridge (1996)
17. D'Eath, P.D.: In: Gibbons, G.W., Shellard, E.P.S., Rankin, S.J. (eds.) The Future of Theoretical Physics and Cosmology. Cambridge University Press, Cambridge, pp. 693–722 (2003). arXiv:gr-qc/0511042
18. Witten, E.: Dynamical breaking of supersymmetry. Nucl. Phys. B **185**, 513 (1981)
19. Alvarez, E.: Locally supersymmetric quantum mechanics. Phys. Rev. D **29**, 320 (1984)
20. Farley, A.N.St.J., D'Eath, P.D.: Bogoliubov transformations for amplitudes in black-hole evaporation. Phys. Lett. **B613**, 181–188 (2005). arXiv:gr-qc/0510027
21. Carroll, S.M., et al.: Physical states in canonically quantized supergravity. Nucl. Phys. B **433**, 661 (1994)
22. Geroch, R.P.: Limits of spacetimes. J. Math. Phys. **9**, 1739 (1968)
23. Penrose, R., Rindler, W.: Spinors and Space-Time, vols. 1, 2. Cambridge University Press, Cambridge (1984, 1986)
24. van Nieuwenhuizen, P.: Supergravity. Phys. Rep. **68**, 189 (1981)
25. Duff, M.J.: In: Ferrara, S., Taylor, J.G. (eds.) Supergravity '81. Cambridge University Press, Cambridge, pp. 197–265 (1982)
26. Faddeev, L.D., Slavnov, A.A.: Gauge Fields: Introduction to Quantum Theory. Benjamin Cummings, Reading (1980)
27. DeWitt, B.S.: Supermanifolds, 2nd edn. Cambridge University Press, Cambridge (1992)
28. Hanson, A., Regge, T., Teitelboim, C.: Constrained Hamiltonian Systems. Accademia Nazionale dei Lincei, Rome (1976)
29. Hawking, S.W.: In: Lévy, M., Deser, S. (eds.) Recent Developments in Gravitation. Plenum, New York, pp. 145–173 (1979)
30. Bao, D., et al.: The well-posedness of $N = l$ classical supergravity. J. Math. Phys. **26**, 329 (1985)

31. McLean, W.: Strongly Elliptic Systems and Boundary Integral Equations. Cambridge University Press, Cambridge (2000)
32. Farley, A.N.St.J., D'Eath, P.D.: Spin-1 and spin-2 amplitudes in black-hole evaporation. Class. Quantum Grav. **22**, 2765–2776 (2005)
33. Farley, A.N.St.J., D'Eath, P.D.: Spin-$\frac{1}{2}$ amplitudes in black-hole evaporation. Class. Quantum Grav. **22**, 3001–3014 (2005). arXiv:gr-qc/0510036
34. Farley, A.N.St.J., D'Eath, P.D.: Vaidya space-time in black-hole evaporation. Gen. Relativ. Gravit. **38**, 425–443 (2006). arXiv:gr-qc/0510040
35. Farley, A.N.St.J., D'Eath, P.D.: Coherent and squeezed states in black-hole evaporation. Phys. Lett. **B634**, 419–426 (2006). arXiv:gr-qc/0603092
36. Farley, A.N.St.J., D'Eath, P.D.: Quantum amplitudes in black-hole evaporation: spins 1 and 2. Ann. Phys. (NY) **321**, 1334–1374 (2006). arXiv:gr-qc/0708.2013
37. Farley, A.N.St.J., D'Eath, P.D.: Bogoliubov transformations in black-hole evaporation. Int. J. Mod. Phys. **D16**, 569–590 (2007). arXiv:gr-qc/0510043
38. Farley, A.N.St.J., D'Eath, P.D.: Quantum amplitudes in black-hole evaporation: coherent and squeezed states. Class. Quantum Grav. **24**, 105–127 (2007). arXiv:gr-qc/0708.2018
39. Scheck, F.: Mechanics. Springer, Heidelberg (2007)
40. D'Eath, P.D.: Perturbation methods in quantum gravity. The multiple-scattering expansion. Phys. Rev. **D24**, 811 (1981)
41. Das, A., Fischler, M., Roček, M.: Massive, self-interacting scalar multiplet coupled to supergravity. Phys. Lett. **B69**, 186 (1977)
42. Misner, C.W., Thorne, K.S., Wheeler, J.A.: Gravitation. Freeman, San Francisco (1973)
43. Wheeler, J.A.: In: DeWitt, C.M., Wheeler, J.A. (eds.) Battelle Rencontres. W.A.Benjamin, New York, p. 303 (1968)
44. Vaidya, P.C.: The gravitational field of a radiating star. Proc. Indian Acad. Sci. A **33**, 264 (1951)
45. Lindquist, R.W., Schwartz, R.A., Misner, C.W.: Vaidya's radiating Schwarzschild metric. Phys. Rev. **137**, 1364 (1965)
46. Mathews, J.: Soc. Ind. Appl. Math. **10**, 768 (1962)
47. Goldberg, J.N., MacFarlane, A.J., Newman, E.T., Rohrlich, F., Sudarshan, E.C.G.: Spin–s spherical harmonics and edth. J. Math. Phys. **8**, 2155 (1967)
48. Choptuik, M.W.: In: d'Inverno, R. (eds.) Approaches to Numerical Relativity. Cambridge University Press, Cambridge (1992)
49. Choptuik, M.W.: Universality and scaling in gravitational collapse of a massless scalar field. Phys. Rev. Lett. **70**, 9 (1993)
50. Hawking, S.W., Ellis, G.F.R.: The large scale structure of space-time. Cambridge University Press, Cambridge (1973)
51. Gerlach, U.H., Sengupta, U.K.: Homogeneous collapsing star: Tensor and vector harmonics for matter and field asymmetries. Phys. Rev. **D18**, 1789 (1978)
52. Brill, D., Hartle, J.B.: Method of self-consistent field in general relativity and its application to the gravitational geon. Phys. Rev. **135**, 1327 (1964)
53. Isaacson, R.: Gravitational radiation in the limit of high frequency, I: the linear approximation and geometrical optics, II: Nonlinear terms and the effective stress-tensor. Phys. Rev. **166**, 1263, 1272 (1968)
54. Nayfeh, A.: Perturbation Methods. Wiley-Interscience, New York (1973)
55. Bender, C.M., Orszag, S.A.: Advanced Mathematical Methods for Scientists and Engineers. Springer, New York (1999)
56. d'Inverno, R.: Introducing Einstein's Relativity. Oxford University Press, Oxford (1992)
57. Jackson, J.D.: Classical Electrodynamics. Wiley, New York (1975)
58. Regge, T., Wheeler, J.A.: Stability of a Schwarzschild singularity. Phys. Rev. **108**, 1063 (1957)
59. Vishveshwara, C.V.: Stability of the Schwarzschild metric. Phys. Rev. **D1**, 2870 (1970)
60. Zerilli, F.J.: Gravitational field of a particle falling in Schwarzshield geometry analysed in tensor harmonics. Phys. Rev. **D2**, 2141 (1970)
61. Futterman, J.A.H., Handler, F.A., Matzner, R.A.: Scattering from Black Holes. Cambridge University Press, Cambridge (1988)

62. Hájíček, P., Israel, W.: What, no black hole evaporation?. Phys. Lett. **A80**, 9 (1980)
63. Bardeen, J.: Black holes do evaporate thermally. Phys. Rev. Lett. **46**, 382 (1981)
64. Hiscock, W.A.: Models of evaporating black holes I, II. Effects of the outgoing created radiation. Phys. Rev. **D23**, 2813, 2823 (1981)
65. Gibbons, G.W., Hawking, S.W.: Cosmological event horizons, thermodynamics and particle creation. Phys. Rev. **D15**, 2738 (1977)
66. Wald, R.M.: Stimulated emission effects in particle creation near black holes. Phys. Rev. **D13**, 3176 (1976)
67. Abramowitz, M., Stegun, I.A.: Handbook of Mathematical Functions. Dover, New York (1964)
68. Hawking, S.W.: Information loss in black holes. Phys. Rev. **D72**, 084013 (2005)
69. Birrell, N.D., Davies, P.C.W.: Quantum Fields in Curved Space. Cambridge University Press, Cambridge (1982)

Chapter 8
Hawking Radiation from Higher-Dimensional Black Holes

Panagiota Kanti and Elizabeth Winstanley

Abstract We review the quantum field theory description of Hawking radiation from evaporating black holes and summarize what is known about Hawking radiation from black holes in more than four space-time dimensions. In the context of the Large Extra Dimensions scenario, we present the theoretical formalism for all types of emitted fields and a selection of results on the radiation spectra. A detailed analysis of the Hawking fluxes in this case is essential for modelling the evaporation of higher-dimensional black holes at the LHC, whose creation is predicted by low-energy models of quantum gravity. We discuss the status of the quest for black-hole solutions in the context of the Randall–Sundrum brane-world model and, in the absence of an exact metric, we review what is known about Hawking radiation from such black holes.

Keywords Hawking radiation · Large extra dimensions · Warped extra dimensions

8.1 Introduction

Hawking radiation [1] is one of the most important effects arising from quantum field theory in curved space, a semi-classical approach to quantum gravity. In this framework space-time is described by a classical geometry, governed by the Einstein equations (or an alternative classical theory of gravity). The behaviour and propagation of quantum fields on a fixed (but not necessarily stationary) space-time is then studied. Hawking radiation is thermal in nature, giving non-extremal black holes an intrinsic temperature proportional to the surface gravity of the event horizon. For a

P. Kanti
Division of Theoretical Physics, Department of Physics, University of Ioannina,
451 10 Ioannina, Greece
e-mail: pkanti@cc.uoi.gr

E. Winstanley (✉)
Consortium for Fundamental Physics, School of Mathematics and Statistics,
The University of Sheffield, Hicks Building, Hounsfield Road, Sheffield S3 7RH, UK
e-mail: e.winstanley@sheffield.ac.uk

X. Calmet (ed.), *Quantum Aspects of Black Holes*,
Fundamental Theories of Physics 178, DOI 10.1007/978-3-319-10852-0_8

Schwarzschild black hole in asymptotically flat space, the specific heat is negative, so that the temperature increases as the black hole evaporates, leading to a black hole explosion. The ultimate fate of the black hole depends on unknown details of quantum gravity, but black hole evaporation raises many deep questions about the nature of quantum gravity and the fundamental laws of physics (such as the information loss paradox, see, for example [2, 3]). Here we will not address these important issues, but instead focus on the detailed properties of the Hawking radiation itself.

Hawking radiation from four-dimensional black holes in asymptotically flat space was studied in detail by Page [4–6]. Over the past fifteen or so years, there has been great interest in higher-dimensional black holes. Within the context of classical general relativity, a menagerie of black-hole-like solutions of the Einstein equations has been discovered (see for example [7, 8] for reviews). It is then natural to study the properties of Hawking radiation from higher-dimensional black holes.

This avenue of research gained much impetus from the exciting possibility of producing microscopic higher-dimensional black holes in high-energy collisions either at the LHC or in cosmic rays [9–16]. This is a prediction of higher-dimensional brane-world models [17–21] in which the energy scale of quantum gravity is much lower than the traditional value of 10^{19} GeV, and may be as low as the TeV-scale. If such a microscopic black hole is produced, it will initially be rapidly rotating and rather asymmetric. Its subsequent evolution can be modelled as four stages [11]:

- During the *balding phase* the black hole sheds its asymmetries through the emission of gravitational radiation and also loses any gauge field charges arising from the particles which formed it. At the end of this stage the black hole is axisymmetric and still rapidly rotating.
- The black hole then emits Hawking radiation, and loses both mass and angular momentum. At the end of this *spin-down phase* the black hole is no longer rotating.
- Now with zero angular momentum, the black hole continues to radiate during the *Schwarzschild phase*, shrinking as it loses mass.
- During the final *Planck phase* the semi-classical approximation for the Hawking radiation is no longer valid and the black hole emission depends on the details of quantum gravity.

It is expected that the spin-down and Schwarzschild phases will dominate the lifetime of the black hole. A detailed understanding of the Hawking radiation from higher-dimensional black holes in brane-world models is therefore necessary for simulating microscopic black hole events [22, 23] and experimental searches, as well as being of intrinsic theoretical interest.

In this chapter we focus on the theoretical modelling of Hawking radiation from higher-dimensional black holes. We begin with a discussion of the quantum-field-theoretic derivation of Hawking radiation and its description using the Unruh vacuum state [24]. We then briefly review some key features of black holes in brane world models. We describe the formalism for studying quantum fields on higher-dimensional Myers-Perry black holes [25], which model black holes in an ADD brane-world [17–19]. We also present a selection of results on the properties of the Hawking radiation from these black holes. The literature on this subject is vast and

so we cannot claim to do all aspects justice. The reviews [12, 26–29] contain further discussion of results which space does not permit us to include. In the RS brane-world [20, 21], analysis of the Hawking radiation is more challenging because no exact metric describing a five-dimensional black hole localised on the brane is known in general—for a more detailed discussion of this topic, see the reviews [30–32]. We close the chapter with a discussion of what is known about the Hawking radiation in this case.

8.2 Hawking Radiation

8.2.1 Hawking Radiation from a Black Hole Formed by Gravitational Collapse

Hawking's original derivation [1] considered a quantum scalar field propagating on a fixed, but dynamic, background space-time corresponding to the formation of a four-dimensional Schwarzschild black hole by the gravitational collapse of matter in asymptotically flat space. The Penrose diagram for this process is shown in Fig. 8.1 (cf. the Penrose diagram for an eternal Schwarzschild black hole in Fig. 8.2).

For the moment consider a massless scalar field in a two-dimensional version of the space-time shown in Fig. 8.1, with space-time co-ordinates (t, r). In this case, because

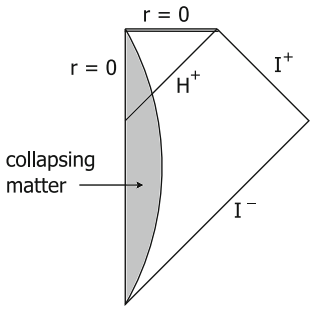

Fig. 8.1 Penrose diagram for a Schwarzschild black hole formed by gravitational collapse

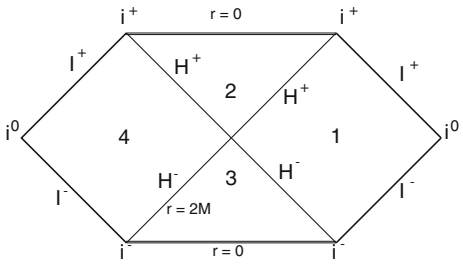

Fig. 8.2 Penrose diagram for an eternal Schwarzschild black hole

two-dimensional space-times are locally conformally flat, a basis of field modes is formed simply from plane waves. These plane waves are not normalizable, but normalizable wave-packets can be constructed from appropriate linear combinations of the plane wave modes. At very early times, long before the collapse starts, a suitable basis of field modes is:

$$\phi_\omega \propto \mathrm{e}^{-i\omega t}\mathrm{e}^{\pm i\omega r}, \tag{8.1}$$

where $\omega > 0$ corresponds to positive frequency. The quantum scalar field $\hat{\Phi}$ is written in terms of these basis modes:

$$\hat{\Phi} = \int_{\omega=0}^{\infty} d\omega \left[\hat{a}_\omega \phi_\omega + \hat{a}_\omega^\dagger \phi_\omega^*\right], \tag{8.2}$$

where the expansion coefficients a_ω have been promoted to operators in the canonical quantization of the scalar field. Working in the Heisenberg picture, the quantum state is defined to be the "in" vacuum at early times near I^-, namely the state $|0\rangle_{\rm in}$ which is annihilated by the $\hat{a}_\omega$ operators:

$$\hat{a}_\omega |0\rangle_{\rm in} = 0 \qquad \forall \omega > 0. \tag{8.3}$$

At late times, long after the black hole has formed, we can form a basis of field modes similar to (8.1), write the quantum scalar field in terms of these modes along the lines of (8.2) but with the expansion coefficients $\hat{a}_\omega$ now replaced by operators $\hat{b}_\omega$, and define an "out" vacuum state $|0\rangle_{\rm out}$ which is annihilated by the $\hat{b}_\omega$ operators.

The crux of Hawking's derivation [1] is that the "in" and "out" vacuum states are not the same: the "in" vacuum $|0\rangle_{\rm in}$ contains a thermal flux of outgoing particles at late times near I^+ (we use units in which $c = \hbar = G = k_B = 1$):

$${}_{\rm in}\left\langle 0 \left| \hat{b}_\omega^\dagger \hat{b}_\omega \right| 0 \right\rangle_{\rm in} = \frac{1}{\mathrm{e}^{\omega/T_H} - 1} \tag{8.4}$$

where

$$T_H = \frac{\kappa}{2\pi} \tag{8.5}$$

is the Hawking temperature and κ is the surface gravity of the black hole. There are many different derivations of this effect (see, for example [33–44]). Hawking's result is very robust, and essentially kinematic: it is independent of the Einstein equations or the theory of gravity under consideration. There are a number of different pictures to understand the origin of the thermal flux, such as quantum tunnelling of classically forbidden trajectories from behind the event horizon [40], or the pair creation of quantum particles close to the event horizon, one of which carries negative energy down the event horizon and the other of which escapes to infinity. In terms of modes,

the thermal factor arises because outgoing modes at I^+ can be traced back to ingoing modes which enter the collapsing body just before the last ingoing mode (which then forms the event horizon of the black hole after reflection from the co-ordinate centre $r = 0$), resulting in a "pile-up" of highly blue-shifted modes near this last ingoing mode.

Using a geometric optics argument, Hawking's result can be extended to black holes in four or more space-time dimensions [1]. The complication is that, even for a massless scalar field, in more than two space-time dimensions the quantum field interacts with a gravitational potential which surrounds the black hole. As a result, a wave which is outgoing near the event horizon of the black hole will partly escape to infinity and partly be reflected back down the event horizon. The part which escapes to I^+ will contribute to the Hawking flux. In four or more space-time dimensions, each mode of a quantum field of spin s will be characterized by its frequency ω, a total angular momentum quantum number ℓ, an azimuthal quantum number m (indexing the angular momentum about the z-axis) and, in more than four space-time dimensions, further angular quantum numbers j. To describe this scattering effect we introduce the grey-body factor $\Gamma_{s\omega\ell mj}$ which is given by the outgoing flux near I^+ for each mode divided by the outgoing flux near the horizon in that mode (that is, the fraction of each outgoing mode near the horizon which is transmitted to I^+). The Hawking flux (8.4) is then modified to be, for each quantum field mode:

$$ {}_{\text{in}}\left\langle 0 \left| \hat{b}^\dagger_\omega \hat{b}_\omega \right| 0 \right\rangle_{\text{in}} = \frac{\Gamma_{s\omega\ell mj}}{\mathrm{e}^{\omega/T_H} \pm 1}, \tag{8.6} $$

where the $+$ sign in the denominator is for fermionic fields and the $-$ sign for bosonic fields. While Hawking's original derivation [1] was for a quantum scalar field, we emphasize that the result carries over to quantum fields of all spins. Furthermore, although in the above we have considered a Schwarzschild black hole, any black hole with a non-extremal event horizon will emit Hawking radiation, including rotating black holes. In this article we will consider only rotating black holes with a single axis of rotation (which we take to be the z-axis). In this case the denominator of the Hawking flux (8.6) is modified by the rotation of the black hole to be

$$ \mathrm{e}^{\tilde{\omega}/T} \pm 1 \tag{8.7} $$

where

$$ \tilde{\omega} = \omega - m\Omega_H, \tag{8.8} $$

with m the azimuthal quantum number and Ω_H is the angular velocity of the event horizon.

8.2.2 The Unruh State

In practice, dealing with quantum fields on the dynamical space-time shown in Fig. 8.1 is technically difficult. In computing Hawking radiation, a different approach is usually employed. Instead of considering the collapse geometry of Fig. 8.1, the eternal black hole space-time (such as that for the Schwarzschild black hole shown in Fig. 8.2) is considered. We restrict our attention to the right-hand-diamond of Fig. 8.2, representing the region exterior to the black hole event horizon. Charged and/or rotating black holes have more complex Penrose diagrams than Fig. 8.2, but the diamond-shaped region exterior to the event horizon is the same for all asymptotically-flat black holes. For black holes in de Sitter space, the relevant region is that between the event and cosmological horizons, which has the same diamond shape.

The Unruh state [24] is the quantum state on the eternal black hole space-time which models the Hawking radiation. The construction of this state proceeds as follows, where for simplicity we consider a free massless scalar field Φ and a four-dimensional Schwarzschild black hole with co-ordinates (t, r, θ, φ). In this case the scalar field modes $\phi_{\omega\ell m}$ are separable:

$$\phi_{\omega\ell m}(t, r, \theta, \varphi) = \mathrm{e}^{-i\omega t}\mathrm{e}^{im\varphi}R_{\omega\ell m}(r)Y_{\ell m}(\theta), \tag{8.9}$$

where ω is the frequency of the mode, m is the azimuthal quantum number, ℓ is the total-angular-momentum quantum number, $R_{\omega\ell m}(r)$ is the radial function and $Y_{\ell m}(\theta)$ is a spherical harmonic. First a basis of quantum field modes is required. We take as a basis the "in" and "up" modes depicted in Fig. 8.3. The "in" modes $\phi^{\mathrm{in}}_{\omega\ell m}$ are incoming from past null infinity I^-. Part of each wave is reflected by the gravitational potential and scatters back to infinity, and part goes down the future event horizon H^+. The "up" modes $\phi^{\mathrm{up}}_{\omega\ell m}$ are outgoing from close to the past event horizon H^-. In this case part of each wave is reflected back down the future event horizon H^+, while part is transmitted to future null infinity I^+.

Having chosen a suitable basis of field modes, we now need to split these modes into positive and negative frequency. For the "in" modes, we choose 'positive frequency' to mean 'positive frequency as seen by a static observer far from the black hole', so that, for a field mode $\phi_{\omega\ell m}$ we have:

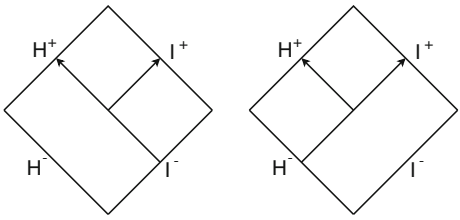

Fig. 8.3 "In" (*left*) and "up" (*right*) modes

$$\frac{\partial}{\partial t}\phi_{\omega\ell m} = -i\omega\phi_{\omega\ell m}, \tag{8.10}$$

where $\omega > 0$. Since the "in" modes originate from near I^-, this is the most natural choice of positive frequency for these modes. For the "up" modes, we choose 'positive frequency' to mean 'positive frequency with respect to Kruskal time near the event horizon'. Since the "up" modes originate from near H^-, this choice of positive frequency, with respect to co-ordinates which are regular across the event horizon, is also very natural. We decompose our quantum field $\hat{\Phi}$ in terms of this basis of positive frequency modes:

$$\hat{\Phi} = \sum_{\text{modes}} \left[\hat{a}^{\text{in}}_{\omega\ell m}\phi^{\text{in}}_{\omega\ell m} + \hat{a}^{\text{in}\dagger}_{\omega\ell m}\phi^{\text{in}*}_{\omega\ell m}\right] + \sum_{\text{modes}} \left[\hat{a}^{\text{up}}_{\omega\ell m}\phi^{\text{up}}_{\omega\ell m} + \hat{a}^{\text{up}\dagger}_{\omega\ell m}\phi^{\text{up}*}_{\omega\ell m}\right] \tag{8.11}$$

where in each case the sum is taken over the positive frequency modes and we have promoted the expansion coefficients for the classical scalar field to operators satisfying the usual commutation relations:

$$\left[\hat{a}^{\text{in/up}}_{\omega\ell m}, \hat{a}^{\text{in/up}\dagger}_{\omega'\ell'm'}\right] = \delta(\omega-\omega')\delta_{\ell,\ell'}\delta_{m,m'}, \left[\hat{a}^{\text{in/up}}_{\omega\ell m}, \hat{a}^{\text{in/up}}_{\omega'\ell'm'}\right] = 0 = \left[\hat{a}^{\text{in/up}\dagger}_{\omega\ell m}, \hat{a}^{\text{in/up}\dagger}_{\omega'\ell'm'}\right]. \tag{8.12}$$

The Unruh state $|U\rangle$ [24] is then defined as that state which is annihilated by the operators $\hat{a}^{\text{in/up}}_{\omega\ell m}$:

$$\hat{a}^{\text{in/up}}_{\omega\ell m}|U\rangle = 0. \tag{8.13}$$

This state has no particles in the "in" modes near I^- as was the case for the "in" vacuum $|0\rangle_{\text{in}}$ describing the state for a black hole formed by gravitational collapse. However, due to the choice of positive frequency for the "up" modes, these modes are thermally populated with temperature T_H (8.5). Therefore, near future null infinity I^+, a static observer will see an outgoing flux of particles in the "up" modes, which is precisely the Hawking radiation. Furthermore, the flux in each mode will be given by (8.6), with the grey-body factor $\Gamma_{\omega\ell m}$ (with spin $s = 0$ and no index j because we are in four space-time dimensions) representing the proportion of each "up" mode which escapes to I^+.

Here we have discussed the construction of the Unruh state for the particular example of a massless scalar field on a four-dimensional Schwarzschild space-time. The extension of this construction to higher-dimensional, spherically-symmetric space-times is straightforward. For higher-spin fields, the field modes are more complicated than (8.9) but the construction works in a similar way (bearing in mind that the Hawking flux (8.6) has a $+$ sign in the denominator for fermion fields and a $-$ sign for bosonic fields). The Unruh state can also be constructed for rotating black holes. In this case the frequency ω in the thermal factor in (8.6) becomes $\tilde{\omega}$ (8.8). This shift arises because $\tilde{\omega}$ rather than ω is the natural frequency of field modes near the

horizon of a rotating black hole, from where the Hawking radiation emanates. For details of this construction on four-dimensional Kerr black holes, see [45] (scalars), [46] (fermions) and [47] (electromagnetism).

In order to compute the fluxes of particles, energy and angular momentum emitted in Hawking radiation we calculate expectation values of the appropriate operators in the Unruh state on an eternal black hole space-time. The flux of particles per unit time is given by summing the individual mode flux (8.6) over all field modes:

$$\frac{dN}{dt} = \sum_{\text{modes}} \frac{\Gamma_{s\omega\ell mj}}{e^{\tilde{\omega}/T_H} \pm 1}, \tag{8.14}$$

where the exact form of the sum over the modes will be made precise in Sect. 8.4, and $\tilde{\omega} = \omega$ if the black hole is non-rotating. The fluxes of energy and (for a rotating black hole) angular momentum per unit time are given by expectation values of the quantum stress-energy tensor for the particular quantum field under consideration:

$$\frac{dE}{dt} = \int r^2 \, d\Omega \left\langle U \left| \hat{T}^r_t \right| U \right\rangle, \qquad \frac{dJ}{dt} = \int r^2 \, d\Omega \left\langle U \left| \hat{T}^{r\varphi} \right| U \right\rangle, \tag{8.15}$$

where the integral is taken over the sphere at infinity and we have given the expressions for four-dimensional black holes.

Expectation values of the stress-energy tensor typically require renormalization, due to their involving products of two operators at the same space-time point. One method of renormalization is covariant geodesic point separation, in which the two operators whose products are taken are evaluated at different space-time points x and x', yielding a finite bitensor stress-energy tensor, whose expectation value is written $T_{\mu\nu}(x, x')$. This expectation value is renormalized by the subtraction of purely geometric, state independent renormalization terms $T^{\text{div}}_{\mu\nu}(x, x')$ (see for example [48, 49] for expressions for these geometric terms for fields of spin 0, 1/2 and 1 in four dimensions, and [50] for a scalar field in higher-dimensional space-time). The points x and x' are then brought together and a finite renormalized expectation value for the stress-energy tensor is yielded.

Fortunately, for the black holes in which we are interested, it can be shown that the two stress-energy tensor components in (8.15) do not require renormalization. For a quantum scalar field on a four-dimensional Kerr black hole, this was shown by Frolov and Thorne [51]. Their argument involved two key properties: (i) the symmetry of the underlying space-time under the reflection $(t, \varphi) \to (-t, -\varphi)$ (simultaneous reversal of time and the azimuthal angle); and (ii) each of the geometric subtraction terms involves an even number of covariant derivatives σ^μ of the biscalar of geodetic interval [52] when an average has been taken over a separation in the σ^μ and $-\sigma^\mu$ directions. Choosing radial point-splitting, these two properties ensure that the geometric subtraction terms $T^{\text{div}}_{tr}(x, x')$ and $T^{\text{div}}_{r\varphi}(x, x')$ both vanish. Since the two properties above are shared by the simply-rotating black holes which we shall consider in Sect. 8.4, the above argument can be readily extended to show that $T^{\text{div}}_{tr}(x, x')$ and $T^{\text{div}}_{r\varphi}(x, x')$ both vanish for these black holes as well [53].

The exact form of the stress-energy tensor components in (8.15) depends on the spin of the quantum field under consideration (see, for example [12, 53–56] for details). However, the resulting fluxes of energy and angular momentum have the following simple forms:

$$\frac{dE}{dt} = \sum_{\text{modes}} \frac{\omega \Gamma_{s\omega\ell mj}}{e^{\tilde{\omega}/T_H} \pm 1}, \qquad \frac{dJ}{dt} = \sum_{\text{modes}} \frac{m \Gamma_{s\omega\ell mj}}{e^{\tilde{\omega}/T_H} \pm 1}, \tag{8.16}$$

where m is the azimuthal quantum number. More precise details of the mode sums can be found in Sect. 8.4.2.

8.3 Brane World Black Holes

8.3.1 Black Holes in ADD Brane-Worlds

In the ADD brane-world scenario [17–19] space-time has $d = 4 + n$ dimensions. Our universe is a four-dimensional brane in this higher-dimensional bulk space-time. The n extra dimensions are flat and compactified (the radius of compactification is typically large compared with the Planck length but sufficiently small to agree with searches for deviations from Newton's Law of Gravitation). To avoid contradictions with precision particle-physics experiments, the forces and particles of the Standard Model are constrained to live on the brane; only gravitational degrees of freedom (gravitons and possibly scalars) can propagate in the bulk.

We model black holes in the ADD scenario in a very simple way, assuming that the brane is tensionless and infinitely thin. We also assume that the black-hole horizon is much smaller than the compactification radius of the extra dimensions. Effectively we are considering black holes in an asymptotically flat, $(4+n)$-dimensional, space-time. Furthermore, we are particularly interested in microscopic black holes formed by the collision of particles on the brane (such a collision will not necessarily be head-on). In this case, by conservation of angular momentum, the resulting black hole will have a single axis of rotation, which will also lie in the brane.

Rotating black-hole solutions of the vacuum Einstein equations in $(4 + n)$-dimensional space-time are described by the Myers-Perry metric [25]. Unlike the situation in four space-time dimensions, the Myers-Perry metric is not unique if $n > 0$ [7, 8], and black holes need not have a spherical event-horizon topology. The general Myers-Perry metric [25] is rather lengthy, and the metrics for more complicated black objects (such as black rings) are very complex. For this reason, we restrict our attention to Myers-Perry black holes with a spherical event-horizon topology and a single axis of rotation. In this case the general Myers-Perry metric simplifies to [25]:

$$ds^2 = -\left(1 - \frac{\mu}{\Sigma r^{n-1}}\right) dt^2 - \frac{2a\mu \sin^2\theta}{\Sigma r^{n-1}}\, dt\, d\varphi + \frac{\Sigma}{\Delta}\, dr^2 + \Sigma\, d\theta^2 + \left(r^2 + a^2 + \frac{a^2 \mu \sin^2\theta}{\Sigma r^{n-1}}\right) \sin^2\theta\, d\varphi^2 + r^2 \cos^2\theta\, d\Omega_n^2, \tag{8.17}$$

where

$$\Delta = r^2 + a^2 - \frac{\mu}{r^{n-1}}, \qquad \Sigma = r^2 + a^2 \cos^2\theta, \tag{8.18}$$

and $d\Omega_n^2$ is the metric on the n-dimensional unit sphere. The mass M and angular momentum J of the black hole are given by:

$$M = \frac{1}{16\pi}\,(n+2)\,\mu\, A_{n+2}, \qquad J = \frac{2}{n+2}\, aM, \tag{8.19}$$

and $A_{n+2} = 2\pi^{(n+3)/2}/\Gamma[(n+3)/2]$ is the area of the $(n+2)$-dimensional unit sphere. The horizon radius r_h of the black hole is determined through the equation $\Delta(r_h) = 0$ and it may be written as $r_h^{n+1} = \mu/(1+a_*^2)$, where $a_* = a/r_h$. When $a = 0$ and the black hole is non-rotating, the metric (8.17) reduces to the Schwarzschild-Tangherlini spherically-symmetric metric [57].

In (8.17), the co-ordinates (t, r, θ, φ) are the co-ordinates on the brane and the $d\Omega_n^2$ is the part of the metric coming from the extra dimensions. To find the metric of the higher-dimensional black hole as seen by an observer on the brane, we simply fix the co-ordinates in the extra dimensions and obtain:

$$ds^2 = -\left(1 - \frac{\mu}{\Sigma r^{n-1}}\right) dt^2 - \frac{2a\mu \sin^2\theta}{\Sigma r^{n-1}}\, dt\, d\varphi + \frac{\Sigma}{\Delta}\, dr^2 + \Sigma\, d\theta^2 + \left(r^2 + a^2 + \frac{a^2 \mu \sin^2\theta}{\Sigma r^{n-1}}\right) \sin^2\theta\, d\varphi^2. \tag{8.20}$$

Note that the brane metric (8.20) still depends on n, the number of extra dimensions. It reduces to the usual Kerr metric when $n = 0$. Although the higher-dimensional Myers-Perry metric (8.17) is a solution of the vacuum Einstein equations in $(4+n)$ dimensions, the brane metric (8.20) is not a solution of the four-dimensional vacuum Einstein equations [58]. Instead, the space-time (8.20) has a non-zero classical stress-energy tensor representing an effective fluid seen by an observer on the brane. This arises from the fact that the black hole is a higher-dimensional object, but a brane observer cannot directly probe the extra dimensions [58].

8.3.2 Black Holes in RS Brane-Worlds

In the RS brane-world, only one extra dimension is assumed to exist transverse to our brane. The bulk is not empty but filled with a negative cosmological constant $\Lambda_B < 0$. The higher-dimensional space-time is therefore an anti-de Sitter (AdS) space-time that contains either two (RS-I model [20]) or one (RS-II model [21]) Minkowski branes. The branes have a non-vanishing tension that, together with the bulk cosmological constant, cause the warping of the metric along the fifth dimension. In the context of the RS-I model, where two flat branes are separated in the extra dimension by a distance a few times the Planck length, this warping is used to address the hierarchy problem. The RS-II model is by far the more interesting one from the gravitational point of view: the second brane is sent to infinity, and the warping causes the localisation of graviton close to the brane and the restoration of four-dimensional gravity despite the presence of an infinitely-extended extra dimension.

Substituting the Minkowski line-element on the brane by the Schwarzschild line-element, the following brane-world solution was found soon after in [59]:

$$ds^2 = e^{-2|y|/\ell_{AdS}} \left[-\left(1 - \frac{2M}{r}\right) dt^2 + \left(1 - \frac{2M}{r}\right)^{-1} dr^2 + r^2 \, d\Omega_2^2 \right] + dy^2 \,, \tag{8.21}$$

where $\ell_{AdS} = \sqrt{-6/\Lambda_B}$ is the AdS curvature length. The projection of the above five-dimensional solution on the brane, located at $y = 0$, has exactly the form of a four-dimensional black hole. However, it was demonstrated that it does not describe a regular black hole localised on the brane but rather an AdS black string that, in the context of the RS-II model, has an infinitely-extended singularity along the bulk. In addition, it suffers from a Gregory-Laflamme instability [60, 61].

Despite the numerous attempts to derive a regular, asymptotically AdS black-hole solution localised on a brane with a non-vanishing tension (for an indicative list of papers, see [62–72]; for a more complete list of references, see [30–32]), up to today no analytical solution has been constructed. Numerical studies [73–75] found black-hole solutions with horizon radius smaller than or of the order of the AdS length ℓ_{AdS} in the context of five- and six-dimensional warped models. The failure to find larger, static black-hole solutions, combined with the results following from lower-dimensional constructions of brane-world black holes [76–78], led to arguments for the non-existence of such black holes in the context of the RS model [79–84].

A central role in this conjecture is played by the AdS/CFT correspondence: when applied in the context of the RS model [85], it dictates that classical gravity in the AdS bulk is equivalent to a strongly-coupled quantum Conformal Field Theory (CFT) living on the brane. If a five-dimensional classical solution exists, describing a regular black hole localised on the brane, then the large number of CFT modes that couple to four-dimensional gravity on the brane will cause the rapid evaporation of the black hole (we will return to this topic in Sect. 8.5). Therefore, the projection of the metric on the brane ought to describe a quantum-corrected, non-static black hole; its classical counterpart in the bulk will then have to be non-static, too.

This argument applies only for large-mass black holes for which the quantum corrections in the AdS bulk are negligible so that the five-dimensional solution can be considered as classical.

There are several results in the literature supporting the validity of the AdS/CFT correspondence in the RS model [30, 32], such as: the agreement in the form of the Newtonian potential on the brane, calculated through the Kaluza-Klein graviton states or the CFT brane modes, and the automatic appearance of a radiation term, that may be associated to the emission of brane CFT modes by the black hole, in the Friedmann equation on the brane. But there are also counter-arguments to the above [86–88] according to which one should not expect important quantum corrections on the brane. In support of the latter view, recent numerical studies [89–91] find solutions that describe both small and large black holes in the context of the RS model (see also [92–96]).

The complexity of the bulk equations and junction conditions that one should solve to find a complete bulk/brane solution, and the non-trivial topology of the AdS space-time background are two decisive factors contributing to the difficulty in finding viable black-hole solutions in the RS model. For large-mass black holes, there might be additional, more subtle, reasons: in [70] it was shown that the brane trajectories in the background of a bulk Schwarzschild-AdS black hole are more finely-tuned for large-mass black holes; also, the recoil effect [97], that may be caused by the asymmetric emission of bulk modes resulting in the black hole leaving the brane, is more effective for large black holes than for small ones [30].

8.4 Hawking Radiation from Black Holes in the ADD Model

In this section we consider Hawking radiation from black holes in the ADD model, both on the brane and in the bulk. The presentation of the formalism will be based on the simply-rotating Myers-Perry black hole discussed in Sect. 8.3.1—when necessary, the spherically-symmetric limit may be recovered by setting $a = 0$. We first bring together all the relevant field equations for the different types of radiation before discussing a selection of results. The formalism for the different types of quantum field is quite involved, and here we are attempting a unified presentation. Some compromises in notation are inevitable in this situation. In particular, we always label our field modes by an index Λ, although the exact form of Λ will vary depending on the spin of the field and whether we are considering brane or bulk emission.

8.4.1 Formalism for Field Perturbations

In this subsection we consider only massless particles. The formalism outlined can be readily extended to include mass and charge. We will briefly discuss some of the effects of mass and charge on the Hawking radiation in Sect. 8.4.6.

8.4.1.1 Teukolsky Formalism on the Brane

We now consider the formalism for massless particles of spin 0, 1/2 and 1 on the brane metric (8.20). Teukolsky [98, 99] developed a unified formalism for describing perturbations of a four-dimensional Kerr black hole with these spins (see also [100]). Teukolsky's original formalism also applies to spin-2 perturbations but we shall consider those separately. Teukolsky's formalism extends easily to perturbations of spin 0, 1/2 and 1 on the brane metric (8.20).

The Newman-Penrose formalism [101] is used to write the perturbation equations for each type of particle as a single master equation for a quantity $\Psi_s = \Psi_s(t, r, \theta, \varphi)$. The form of Ψ_s depends on the spin s of the field under consideration—details can be found in [12]. The resulting Teukolsky equation for the variable Ψ_s takes the form [55]

$$\begin{aligned}\mathcal{J}_s = &\left[\frac{(r^2+a^2)^2}{\Delta} - a^2\sin^2\theta\right]\partial_t\Psi_s + \frac{2a\mu}{\Delta r^{n-1}}\partial_t\partial_\varphi\Psi_s + \left[\frac{a^2}{\Delta} - \frac{1}{\sin^2\theta}\right]\partial_\varphi\Psi_s \\ &- \Delta^{-s}\frac{\partial}{\partial r}\left(\Delta^{s+1}\partial_r\Psi_s\right) - \frac{1}{\sin\theta}\frac{\partial}{\partial\theta}\left(\sin\theta\,\partial_\theta\Psi_s\right) - 2s\left[\frac{a\Delta'}{2\Delta} + \frac{i\cos\theta}{\sin^2\theta}\right]\partial_\varphi\Psi_s \\ &+ 2s\left[r + \bar{\rho} - \frac{(r^2+a^2)\Delta'}{2\Delta}\right]\partial_t\Psi_s + s\left[s\cot^2\theta - 1 + (2-\Delta'')\delta_{s,|s|}\right]\Psi_s\,,\end{aligned} \tag{8.22}$$

where $\bar{\rho} = r + ia\cos\theta$ and $\mathcal{J}_s$ is a source term, whose details for each spin s can be found in [12]. The metric function Δ is given by (8.18). The Teukolsky equation (8.22) is separable. We write

$$\Psi_s = \mathrm{e}^{-i\omega t}\mathrm{e}^{im\varphi}R_\Lambda(r)\,S_\Lambda(\theta), \tag{8.23}$$

where $\Lambda = \{s, \omega, \ell, m\}$, ω is the field mode frequency, $m = -\ell, -\ell+1, \ldots, \ell-1, \ell$ is the azimuthal quantum number and $\ell \geq s$ is the total angular momentum quantum number. Then the following radial and angular equations are obtained [12, 55]:

$$\begin{aligned}0 = &\Delta^{-s}\frac{d}{dr}\left(\Delta^{s+1}\frac{dR_\Lambda}{dr}\right) + \left[\Delta^{-1}\left(K_{\omega m}^2 - isK_{\omega m}\Delta'\right) + 4is\omega r\right. \\ &\left.+ s\delta_{s,|s|}\left(\Delta'' - 2\right) - a^2\omega^2 + 2ma\omega - \lambda_\Lambda\right]R_\Lambda(r),\end{aligned} \tag{8.24}$$

$$\begin{aligned}0 = &\frac{1}{\sin\theta}\frac{d}{d\theta}\left(\sin\theta\frac{dS_\Lambda}{d\theta}\right) + \left[-\frac{2ms\cot\theta}{\sin\theta} - \frac{m^2}{\sin^2\theta} + a^2\omega^2\cos^2\theta - 2as\omega\cos\theta\right. \\ &\left.+ s - s^2\cot^2\theta + \lambda_\Lambda\right]S_\Lambda(\theta),\end{aligned} \tag{8.25}$$

where

$$K_{\omega m} = \left(r^2 + a^2\right)\omega - am. \tag{8.26}$$

The angular functions $S_\Lambda(\theta)$ are spin-weighted spheroidal harmonics [102, 103], and they and the eigenvalues λ_Λ have to be computed numerically when $a\omega \neq 0$. For $a\omega = 0$, the eigenvalues are:

$$\lambda_\Lambda = \ell\left(\ell + 1\right) - s\left(s + 1\right), \tag{8.27}$$

and the angular functions $S_\Lambda(\theta)$ reduce to spin-weighted spherical harmonics [104].

8.4.1.2 Bulk Fields

We now consider the equations satisfied by scalar and graviton perturbations of the higher-dimensional bulk metric (8.17).

Firstly, consider a massless scalar field propagating on the metric (8.17). The massless scalar wave equation is separable. We write the scalar field Ψ_0 as

$$\Psi_0 = \mathrm{e}^{-i\omega t}\mathrm{e}^{im\varphi} R_\Lambda(r)\, S_\Lambda(\theta)\, Y_{jn}(\Omega), \tag{8.28}$$

where the index Λ is now $\{\omega, \ell, m, j, n\}$ and $Y_{jn}(\Omega)$ is a hyper-spherical harmonic [105] depending on the higher-dimensional bulk co-ordinates and indexed by an integer j. The following radial and angular equations are obtained from the scalar field equation [53]:

$$\begin{aligned} 0 =& \frac{1}{r^n}\frac{d}{dr}\left(r^n \Delta \frac{dR_\Lambda}{dr}\right) + \Big[\Delta^{-1}K_{\omega m}^2 - a^2 r^{-2} j\left(j + n - 1\right) \\ & - a^2\omega^2 + 2ma\omega - \lambda_\Lambda\Big] R_\Lambda(r), \end{aligned} \tag{8.29}$$

$$\begin{aligned} 0 =& \frac{1}{\sin\theta\cos^n\theta}\frac{d}{d\theta}\left(\sin\theta\cos^n\theta\frac{dS_\Lambda}{d\theta}\right) + \left[\omega^2 a^2\cos^2\theta - \frac{m^2}{\sin^2\theta} - \frac{j\left(j + n - 1\right)}{\cos^2\theta}\right. \\ & \left. + \lambda_\Lambda\right] S_\Lambda(\theta). \end{aligned} \tag{8.30}$$

Gravitational perturbations are much more difficult to deal with as Teukolsky's four-dimensional formalism does not readily extend to higher dimensions. A complete analysis is currently available only for higher-dimensional spherically-symmetric black holes. For spherically-symmetric black holes, a general gravitational perturbation decomposes into three parts: a symmetric traceless tensor T, a vector V and a scalar part S [106]. The master equation for each type of gravitational perturbation is separable and the relevant field quantity is written in a form similar to (8.28) (see [106] for details). For each type of gravitational perturbation, the radial

functions satisfy the equation [107]

$$0 = \left[1 - \left(\frac{r_h}{r}\right)^{n+1}\right] \frac{d}{dr}\left\{\left[1 - \left(\frac{r_h}{r}\right)^{n+1}\right] \frac{dR_\Lambda}{dr}\right\} + \left[\omega^2 - \mathcal{V}_\Lambda\right] R_\Lambda(r), \quad (8.31)$$

where the form of the potential $\mathcal{V}_\Lambda$ depends on the type of gravitational perturbation. The angular functions are simply spin-weighted hyper-spherical harmonics. The index Λ now takes the form $\{B, \omega, \ell, n\}$ where $B \in \{S, V, T\}$ indicates whether we are considering a scalar (S), vector (V) or tensor (T) type of gravitational perturbation and the other labels are as before. For tensor-like and vector-like perturbations the potential $\mathcal{V}_\Lambda$ is [107]

$$\mathcal{V}_{T/V,\omega,\ell,n} = \frac{1}{r^2}\left[1 - \left(\frac{r_h}{r}\right)^{n+1}\right]\left[\ell\,(\ell + n + 1) + \frac{n\,(n+2)}{4} - \frac{k}{4}\,(n+2)^2\,\frac{r_h^{n+1}}{r^{n+1}}\right], \quad (8.32)$$

where $k = -1$ for tensor-like (T) perturbations and $k = 3$ for vector-like (V) perturbations. For scalar-like (S) graviton perturbations, the potential has the more complicated form [107]:

$$\mathcal{V}_{S,\omega,\ell,n} = \frac{1}{r^2}\left[1 - \left(\frac{r_h}{r}\right)^{n+1}\right] \frac{qx^3 + px^2 + wx + z}{4\,[2u + (n+2)(n+3)x]^2}, \quad (8.33)$$

where

$$x = \frac{r_h^{n+1}}{r^{n+1}}, \qquad u = \ell\,(\ell + n + 1) - n - 2, \quad (8.34)$$

and

$$\begin{aligned} q &= (n+2)^4\,(n+3)^2\,, \\ p &= (n+2)\,(n+3)\left[4u\left(2n^2 + 5n + 6\right) + n\,(n+2)\,(n+3)\,(n-2)\right], \\ w &= -12u\,(n+2)\,[u\,(n-2) + n\,(n+2)\,(n+3)], \\ z &= 16u^3 + 4u^2\,(n+2)\,(n+4). \end{aligned} \quad (8.35)$$

For rotating higher-dimensional black holes, the general gravitational perturbation equations are much more complicated [108–110]. In general they are not separable, which means that a computation of the Hawking radiation for gravitons has to date proved intractable. However, some progress can be made in the case where the higher-dimensional gravitational background is the warped product of an m-dimensional space-time $\mathcal{N}$ and an n-dimensional space $\mathcal{K}$ of constant curvature, a class of backgrounds that includes the simply-rotating Myers-Perry metric

(8.17). In that case, the equations for tensor-type perturbations simplify considerably [111, 112] and are separable. The radial and angular equations take the forms (8.29–8.30) respectively, that is, the equations for the scalar field modes in the bulk—the only difference is that $\ell \geq 0$ for scalars and $\ell \geq 2$ for gravitons [112].

8.4.2 Grey-Body Factors and Fluxes

We are interested in the fluxes of particles N, energy E and angular momentum J for the various different fields. The differential fluxes per unit time and unit frequency ω take the form:

$$\frac{d^2N}{dt\,d\omega} = \frac{1}{2\pi} \sum_j \sum_{\ell=s}^{\infty} \sum_{m=-\ell}^{\ell} \frac{1}{e^{\tilde{\omega}/T_H} \pm 1} \mathcal{N}_\Lambda \Gamma_\Lambda, \tag{8.36}$$

$$\frac{d^2E}{dt\,d\omega} = \frac{1}{2\pi} \sum_j \sum_{\ell=s}^{\infty} \sum_{m=-\ell}^{\ell} \frac{\omega}{e^{\tilde{\omega}/T_H} \pm 1} \mathcal{N}_\Lambda \Gamma_\Lambda, \tag{8.37}$$

$$\frac{d^2J}{dt\,d\omega} = \frac{1}{2\pi} \sum_j \sum_{\ell=s}^{\infty} \sum_{m=-\ell}^{\ell} \frac{m}{e^{\tilde{\omega}/T_H} \pm 1} \mathcal{N}_\Lambda \Gamma_\Lambda. \tag{8.38}$$

Here we have written out precisely the mode sums represented schematically in (8.14, 8.16). As well as the usual sums over the angular momentum quantum numbers ℓ, m, there is an additional sum over j for scalar field emission in the bulk and tensor-type graviton emission from a rotating black hole, where j indexes the hyperspherical harmonics in these cases. There is no sum over j for graviton emission from spherically-symmetric higher-dimensional black holes. In the thermal factor, the $+$ sign is for fermionic fields and the $-$ sign for bosonic fields. In the above, $\tilde{\omega}$ is given by (8.8), while the temperature T_H and angular velocity Ω_H of the simply-rotating Myers-Perry black hole (8.17) are found to be:

$$T_H = \frac{(n+1) + (n-1)a_*^2}{4\pi(1+a_*^2)r_h}, \qquad \Omega_H = \frac{a}{r_h^2 + a^2}. \tag{8.39}$$

For each mode, the fluxes (8.36–8.38) depend on the grey-body factor Γ_Λ, and also a degeneracy factor $\mathcal{N}_\Lambda$ accounting for the multiplicity of modes having the quantum numbers $\{\omega, \ell, m, j\}$. The degeneracy factors are always independent of the mode frequency ω and azimuthal quantum number m, but depend on ℓ, j (where applicable) and the number of extra dimensions n.

On the brane, for fields of spin-1/2 and spin-1, there are field modes with two polarizations, so to take this into account we set the degeneracy factors equal to

$$\mathcal{N}_\Lambda = \begin{cases} 1 \text{ for } s = 0, \\ 2 \text{ for } s = \frac{1}{2}, \\ 2 \text{ for } s = 1. \end{cases} \tag{8.40}$$

For bulk scalar fields, the degeneracy factor is [53]:

$$\mathcal{N}_\Lambda = \frac{(2j+n-1)\,(j+n-2)!}{j!\,(n-1)!}. \tag{8.41}$$

For bulk graviton fields, we need to consider each type of gravitational perturbation separately. If we consider a rotating black hole, we only have separable field equations for tensor-type gravitational perturbations, in which case the degeneracy factor is [113]

$$\mathcal{N}_\Lambda = \frac{(n+1)\,(n-2)\,(n+j)\,(j-1)\,(n+2j-1)\,(n+j-3)!}{2\,(j+1)!\,(n-1)!}. \tag{8.42}$$

If, on the other hand, we consider a non-rotating black hole, all three types of gravitational perturbation (scalar S, vector V and tensor T) can be considered. The degeneracy values are then [114–116]:

$$\begin{aligned} \mathcal{N}_{S,\omega,\ell,n} &= \frac{(2\ell+n+1)\,(\ell+n)!}{(2\ell+1)\,\ell!\,(n+1)!}, \\ \mathcal{N}_{V,\omega,\ell,n} &= \frac{\ell\,(\ell+n+1)\,(2\ell+n+1)\,(\ell+n-1)!}{(2\ell+1)\,(\ell+1)!n!}, \\ \mathcal{N}_{T,\omega,\ell,n} &= \frac{n\,(n+3)\,(\ell+n+2)\,(\ell-1)\,(2\ell+n+1)\,(\ell+n-1)!}{2\,(2\ell+1)\,(\ell+1)!\,(n+1)!}. \end{aligned} \tag{8.43}$$

To compute the Hawking fluxes (8.36–8.38), it remains to find the grey-body factors Γ_Λ. These are computed by numerically integrating the relevant radial equation (8.24, 8.29, 8.31). For an "up" mode, the grey-body factor Γ_Λ is the ratio of the flux in the mode at infinity and the flux in the out-going part of the mode near the event horizon, in other words it is the transmission coefficient for each "up" mode. The exact form of the flux depends on the spin of the field considered (see [12, 100] for details). Here we simply state the results for the grey-body factors in each case.

We first consider scalar and graviton fields, which are each described by a single radial function R_Λ which satisfies the relevant radial equation: (8.24) for scalar fields on the brane; (8.29) for scalar fields in the bulk; (8.31) for all types of graviton emission from a non-rotating black hole; or (8.29) for tensor-type graviton emission from a simply-rotating black hole. The "up" modes then have radial functions of the form:

$$R_\Lambda \sim \begin{cases} (r-r_h)^{i\tilde{\omega}/4\pi T_H} + C_{R,\Lambda}\,(r-r_h)^{-i\tilde{\omega}/4\pi T_H} & r \to r_h \\ C_{T,\Lambda} r^{-y} e^{i\omega r} & r \to \infty, \end{cases} \tag{8.44}$$

where $C_{R,\Lambda}$ and $C_{T,\Lambda}$ are complex constants, and

$$y = \begin{cases} 1 & \text{for brane emission of scalars,} \\ 1 + \frac{n}{2} & \text{for bulk emission of scalars, and tensor-type graviton} \\ & \text{emission from rotating black holes,} \\ 0 & \text{for graviton emission from non-rotating black holes.} \end{cases} \tag{8.45}$$

The grey-body factor is then simply

$$\Gamma_\Lambda = 1 - \left|C_{R,\Lambda}\right|^2 = \frac{\omega}{\tilde{\omega}} \left|C_{T,\Lambda}\right|^2 . \tag{8.46}$$

If the black hole is non-rotating, $\tilde{\omega} = \omega$ and $\Gamma_\Lambda = |C_{T,\Lambda}|^2$. If the black hole is rotating, for modes with $\omega/\tilde{\omega} < 0$, Eq. (8.46) implies that $\Gamma_\Lambda < 0$, so we have super-radiance [100].

We next consider fermion (spin-$\frac{1}{2}$) and gauge boson (spin-1) fields, for which there are two radial functions, corresponding to $s = +|s|$ and $s = -|s|$. The radial functions R_Λ satisfy (8.24) and, for an "up" mode, have the asymptotic forms [12, 55]

$$\begin{aligned} R_\Lambda^{s=+|s|} &\sim \begin{cases} C_{R,\Lambda} \Delta^{-s} (r - r_h)^{-i\tilde{\omega}/4\pi T_H} & r \to r_h \\ 0 & r \to \infty, \end{cases} \\ R_\Lambda^{s=-|s|} &\sim \begin{cases} (r - r_h)^{i\tilde{\omega}/4\pi T_H} & r \to r_h \\ C_{T,\Lambda} r^{-\delta_{s,1}} e^{i\omega r} & r \to \infty, \end{cases} \end{aligned} \tag{8.47}$$

for complex constants $C_{R,\Lambda}$ and $C_{T,\Lambda}$. For gauge bosons with $|s| = 1$, the grey-body factor is given by (8.46), and there is super-radiance for modes with $\tilde{\omega} < 0$. For fermion fields with $|s| = \frac{1}{2}$, the grey-body factor is:

$$\Gamma_\Lambda = 1 - \left|C_{R,\Lambda}\right|^2 = \left|C_{T,\Lambda}\right|^2 . \tag{8.48}$$

For fermions, we therefore have $\Gamma_\Lambda > 0$ for all modes and no super-radiance [100].

8.4.3 Emission of Massless Fields on the Brane

We now present a selection of results on the decay of higher-dimensional black holes through the emission of Hawking radiation. The presentation of the results will be by no means exhaustive, rather we hope that it will reveal some of the main features of the radiation spectra from these black holes. We will start from the emission of particles along the brane, then consider the bulk emission and finish with a discussion of the energy balance between the two decay channels.

For a brane-localised observer, the emission of particles along the brane is the only observable decay channel of a higher-dimensional black hole. Drawing information from black holes in four dimensions, we expect that higher-dimensional black holes will emit Hawking radiation during both their rotating and spherically-symmetric

phase. The rotating phase is the most generic, however, it is also the most technically involved. Therefore, we will start from the spherically-symmetric phase, that, although it is chronologically second, has a significantly simpler treatment.

8.4.3.1 Non-rotating Black Holes

The gravitational background describing the space-time around a non-rotating, higher-dimensional black hole, i.e. the Schwarzschild-Tangerlini line-element [57], and the corresponding field equations follow easily from (8.20) and (8.24–8.25), respectively, by setting $a = 0$. In particular, the angular equation (8.25) now reduces to the one for the spin-weighted spherical harmonics with a well-defined eigenvalue, and offers no new information given the spherically-symmetric emission. Therefore, it is only the radial equation (8.24), significantly simplified after setting $a = 0$, that needs to be integrated. This has been performed both analytically [117–119] and numerically [120]. In the former case, an approximation technique needs to be applied: in this, the radial equation is solved in the two asymptotic regimes, i.e. near the horizon ($r \simeq r_h$) and far away from it ($r \gg r_h$), and the two solutions are matched at an intermediate point. The analytic result derived for the grey-body factor is valid only under the assumption that the energy of the emitted particle satisfies the constraint $\omega r_h \ll 1$. Therefore, for the derivation of the radiation spectra beyond the low-energy regime, one needs to employ numerical methods.

In [120], the complete spectra for all types of brane particles and for arbitrary energy ω were thus numerically derived. In Fig. 8.4a, we depict the differential energy emission rate per unit time and unit frequency for gauge bosons emitted on the brane by a spherically-symmetric black hole, for variable n [12, 120]. We observe that, as the number of extra dimensions that are transverse to the brane increases, the black hole radiates more energy per unit time and over a much wider spectrum of frequencies. This is due to the combined effect of the grey-body factors Γ_Λ and the temperature T_H of the black hole (8.39), with the latter being clearly an increasing

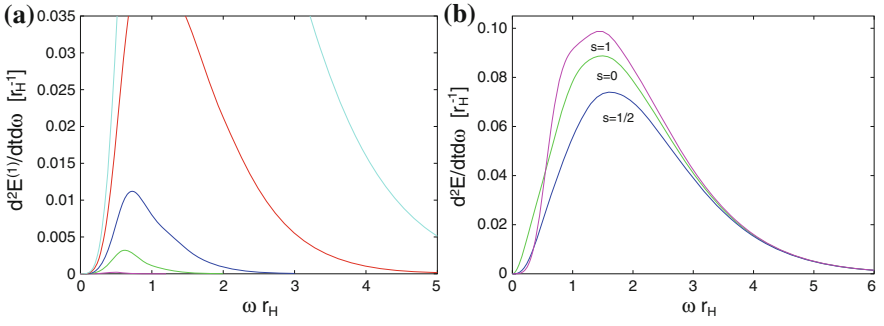

Fig. 8.4 Energy emission rates **a** for gauge bosons, for $n = 0, 1, 2, 4$ and 6 (from *bottom* to *top*) [12], and **b** for all species of brane-localised particles for $n = 6$ [120]

function of n, for a fixed horizon radius r_h. The same behaviour is observed for all types of brane particles, i.e. scalars, fermions and gauge bosons [12, 120]. By integrating the energy spectra over ω, we find that the total emissivities are enhanced by a factor of the order of 10^3–10^4, as n increases from 0 to 7.

The exact value of the enhancement factor, however, depends on the spin s of the particle, and that leads to the question whether the black hole prefers to emit different species of particle for different values of n. In Fig. 8.4b, we depict the power fluxes for particles with spin $s = 0, 1/2$ and 1, for the case $n = 6$ [120]: the gauge bosons clearly dominate over both scalars and fermions. This result is to be compared to the four-dimensional one [4, 121–123] where scalars dominate, and to the case where n takes intermediate values, where the black hole emits almost equal amounts of energy in the three particle channels [120]. One could then propose that the emission by a higher-dimensional, spherically-symmetric black hole on the brane could reveal the number of additional spacelike dimensions [117, 118, 120].

8.4.3.2 Rotating Black Holes

We now turn to the preceding rotating phase that, for black holes created during a non-head-on collision, is the most generic and perhaps the only phase realised due to their short life-time. In this case, the space-time around the black hole is not spherically-symmetric—instead, the axis of rotation provides a preferred direction in space. Therefore, the angular equation, too, contains vital information about the emission process, and it is thus the set of equations (8.24–8.25) that we now need to solve. The radial equation will provide us again with the value of the grey-body factor. For this, we need the eigenvalue λ_Λ whose value may be found by numerically integrating the angular equation. There is, however, an infinite power-series expansion [102, 103, 124], in the limit of small $a\omega$, of the form

$$\lambda_\Lambda = -s(s+1) + \sum_k f_k \, (a\omega)^k = \ell(\ell+1) - s(s+1) - \frac{2ms^2}{\ell(\ell+1)} a\omega + \cdots . \quad (8.49)$$

The use of the above expression for λ_Λ allows for the analytical solution of the radial equation [119, 125, 126] for the rotating phase, too, and the derivation of a formula for the grey-body factor. As before, the validity of the result is limited: it applies only for emission by a slowly-rotating black hole ($a_* < 1$) in the low-energy regime ($\omega r_h \ll 1$); for the sake of comparison, in Fig. 8.5a, b, we present both the analytic [126] and the numerical result [55], respectively, for the grey-body factor of brane-localised fermions for the mode $\ell = -m = 1/2$ in the 10-dimensional case and for various values of a_*. The agreement between the two results is very good in the low-energy part of the spectrum and for small angular-momenta, however, it clearly worsens as either ω or a_* increases.

The complete radiation spectra, under no restrictions on the energy and angular momentum, were derived in [54–56, 127] for brane-localised scalars, fermions and

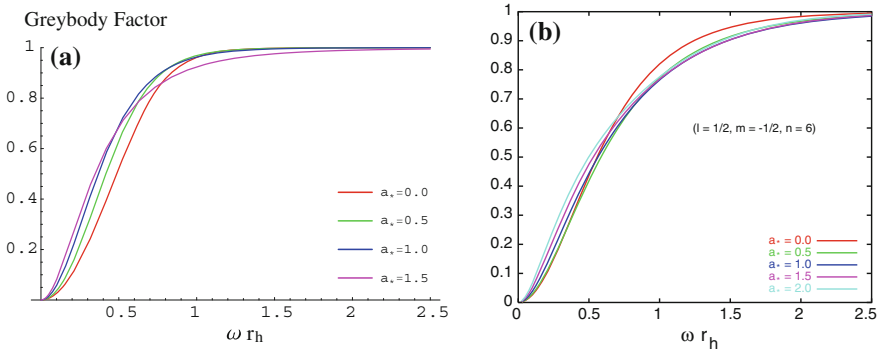

Fig. 8.5 Grey-body factors of brane-localised fermions derived **a** analytically [126] and **b** numerically [55] for $\ell = -m = 1/2$, $n = 6$ and variable a_*

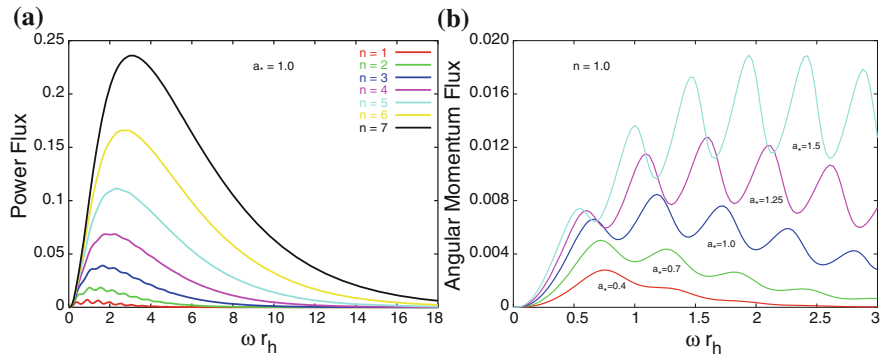

Fig. 8.6 **a** Energy emission rate for fermions in terms of n, for $a_* = 1$ [55], and **b** angular-momentum emission rate for scalars, in terms of a_*, for $n = 1$ [54]

gauge bosons by employing numerical techniques. In each case, the angular equation (8.25) was integrated first to derive the exact values of both the angular eigenvalue λ_Λ and the spin-weighted spheroidal harmonics S_Λ. The radial equation (8.24) was solved next from the horizon to infinity under the appropriate boundary conditions. The numerical integration of the set of radial and angular equations presents different challenges for different species of fields—we address the interested reader to [54–56, 127] for further information on how to overcome these.

For a rotating black hole, the grey-body factor depends both on the number of extra dimensions n and the angular-momentum a_* of the black hole, but also on the part of the energy spectrum and the particular mode considered. An indicative result for the grey-body factor for fermions [55] with $\ell = -m = 1/2$, $n = 6$ and various values of a_* was presented in Fig. 8.5b. Using the values of the numerically-derived grey-body factors, one may proceed to determine the fluxes of particles N, energy E and angular momentum J for a rotating black hole on the brane. The profile of each flux shows an

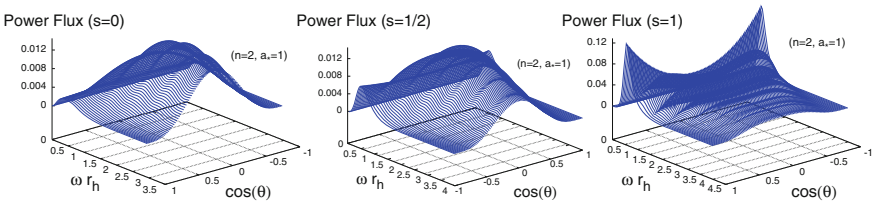

Fig. 8.7 Angular distribution of the power spectra for scalars [54] (*left plot*), fermions [55] (*middle plot*) and gauge bosons [56] (*right plot*) for $n = 2$ and $a_* = 1$

enhancement, in terms of both n and a_*, for all species of brane-localised particles. In Fig. 8.6a, b, we depict indicative cases of the energy emission rate for fermions, for $a_* = 1$ and various values of n [55], and of the angular-momentum emission rate for scalars, for $n = 1$ and various values of a_* [54], respectively. The enhancement factor in the total emissivity of all three fluxes, when n varies from 1 to 7, is typically of $\mathcal{O}(100)$ while the one when a_* changes from 0 to 1 is of $\mathcal{O}(10)$.

The angular equation (8.25) is also a source of valuable information for the emission process: the spin-weighted spheroidal harmonics $S_\Lambda(\theta)$ contain information on the angular distribution of the emitted particles. The differential fluxes (8.36–8.38) are derived by integrating the appropriate operators over a sphere at infinity. If we therefore take a step back, one may derive the differential emission rates per unit time, unit energy and unit of $\cos\theta$, where θ is the angle measured from the rotation axis of the black hole. All fluxes exhibit a non-trivial angular distribution as a result of two factors: (i) the centrifugal force, that forces all types of particles to be emitted on the equatorial plane, particularly for large values of ω or a_*, (ii) the spin-rotation coupling, which tends to align all particles with non-vanishing spin with the rotation axis—this factor has a different effect on different radiative components and is more prominent the larger the value of the spin and the smaller the energy of the particle. In Fig. 8.7, we present three-dimensional graphs depicting the differential energy emission rate in terms of ω_* and $\cos\theta$ for scalars, fermions and gauge bosons, for $n = 2$ and $a_* = 1$ [54–56], that clearly present the above behaviour. Note, that for fermions and gauge bosons, the distribution is symmetric over the two hemispheres since both radiative components, $s = \pm\frac{1}{2}$ and $s = \pm 1$, respectively, have been taken into account in the expression of the energy emission rates in each case.

The aforementioned angular distribution of the emitted particles will be a distinct observable effect, and will last for as long as the angular-momentum of the black hole is non-zero. However, for a rotating black hole, the task of drawing quantitative information from the Hawking radiation spectra, regarding the parameters of spacetime, presents a serious difficulty: both the number of extra spacelike dimensions n and the angular-momentum parameter a_* cause an enhancement of the emission rates (8.36–8.38). One therefore needs to break this degeneracy, by using an observable that would depend rather strongly on the value of only one of these parameters and, at the same time, be almost insensitive to the value of the other.

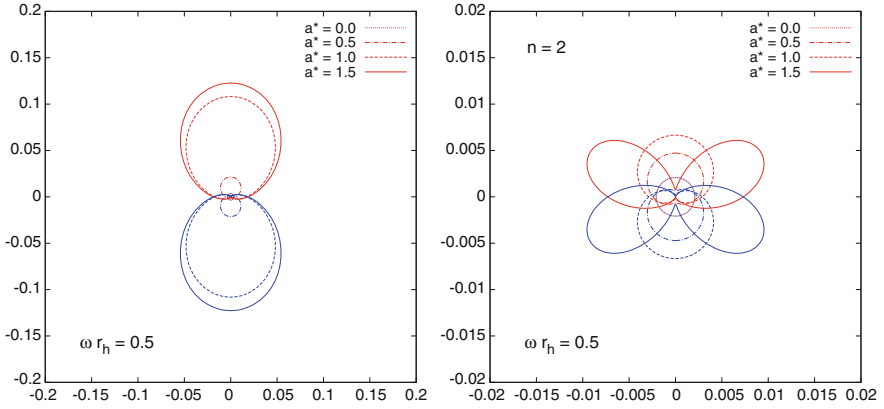

Fig. 8.8 Polar plots with the angular distribution of gauge bosons (*left plot*) and fermions (*right plot*) for $\omega r_h = 0.5$, $n = 6$ and variable a_* [128]. *Red* (*upper*) curves correspond to positive helicity particles and *blue* (*lower*) curves to negative helicity particles

As we mentioned above, one of the two factors that determine the angular distribution of the emitted particles is the spin-rotation coupling that is dominant at the low-energy regime. If we then focus on this part of the energy spectrum, and consider the emission of fermions and gauge bosons, we find the behaviour depicted in Fig. 8.8 [128]: the gauge bosons (left plot) are aligned parallel or anti-parallel to the rotation axis of the black hole [128], while the fermions (right plot) have an angle of emission that depends on the value of the angular momentum of the black hole [128, 129]. The aforementioned pattern is in fact independent of the value n of extra dimensions. Therefore, by observing the angles of emission of gauge bosons and fermions in a low-energy channel, one could in principle determine the orientation of the rotation axis and the angular momentum, respectively, of the black hole. The diferential fluxes (8.36–8.38) could then be used to determine the value of n, too.

The results depicted in Fig. 8.8 were found by numerically integrating both the radial and angular equations for gauge bosons and fermions. However, since the behaviour found above takes place in a low-energy channel, one could attempt to use analytic methods to solve both equations and derive the angular emission pattern. As we have already discussed, the radial equation (8.24) has been solved analytically for all species of brane particles [119, 125, 126]. The angular equation (8.25) also admits an analytic solution in the form of an infinite power-series [130]. In [131], a constraint was thus derived that semi-analytically determines the angle of maximum emission for different types of fields; the angular emission pattern of scalars, gauge bosons and fermions was then found, for a wide range of values of the angular-momentum parameter a_* and energy ω of the emitted particle.

8.4.4 Emission of Massless Fields in the Bulk

Having studied the emission of Hawking radiation on the brane, i.e. the part of the emitted energy that a brane observer could potentially detect, we now turn to the emission of Hawking radiation in the bulk, i.e. the part of the emitted energy that would literally go missing. Brane observers have no access to the bulk, nevertheless, we need to study the different types of emission and estimate the amount of energy that is channeled in the bulk. Since Standard Model particles are constrained to live on the brane, the only degrees of freedom allowed to propagate in the bulk are scalars and gravitons. In what follows, we review the existing results in the literature for the corresponding radiation spectra.

We start with the emission of scalar fields: the set of equations, for the more complex rotating phase, are given in (8.29–8.30), while the ones for the spherically-symmetric phase follow by setting $a = 0$. These equations have been solved, for both phases, by employing either analytical [117, 132, 133] or numerical [53, 120, 134] methods. For the analytical approach, based on the same approximation method as in the case of brane emission, we need the angular eigenvalue λ_Λ in an analytical form: for the spherically-symmetric phase, this is known and given by [105]

$$\lambda_\Lambda = \ell(\ell + n + 1), \tag{8.50}$$

while for the rotating phase there is again a power-series expression [135, 136]. The analytical results thus derived for the grey-body factor may be used to describe the effect of Hawking radiation in the bulk very accurately in the low-energy regime and, at times, even in the intermediate-energy regime.

However, the complete spectra may be derived only through numerical integration. For the spherically-symmetric case, the angular equation (8.30) contains again no new information for the radiation process—it is only the radial equation (8.29), with $a = 0$, that needs to be numerically integrated. For the rotating phase, the angular equation (8.30) is integrated first to provide the eigenvalue λ_Λ—note that, in the absence of an observer in the bulk, there is no motivation for the study of the angular distribution of the emitted particles. The radial equation (8.29) is integrated next to determine the grey-body factors and, subsequently, the emitted fluxes.

We will focus on the presentation of results for the rotating phase, since the dependence on the number of extra dimensions n will become manifest when we fix the value of the angular-momentum parameter a_*. In Fig. 8.9a [53], we present exact numerical results for the grey-body factor for a scalar field emitted in the bulk by a six-dimensional black hole with $a_* = 0.4$: the different curves correspond to various modes characterised by the set of (j, ℓ, m) quantum numbers and show a hierarchical splitting first on ℓ, then on m and finally on j. Figure 8.9b [53] depicts the behaviour of the grey-body factor for a bulk scalar field, in the background of a black hole with $n = 1$ and $a_* = 1.5$, in the super-radiant regime, $\omega < m\,\Omega_H$: as in the case of brane emission, the super-radiance effect is most important for the maximally co-rotating modes $\ell = m$ and $j = 0$, and for low values of n.

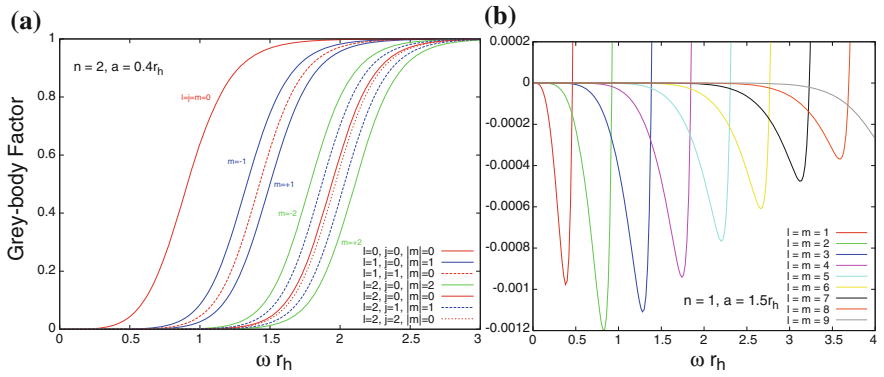

Fig. 8.9 Grey-body factors for a bulk scalar field: **a** complete results for various modes (j, ℓ, m), for $n = 2$ and $a_* = 0.4$, and **b** the super-radiant regime for various co-rotating modes $\ell = m$, for $n = 1$ and $a_* = 1.5$ [53]

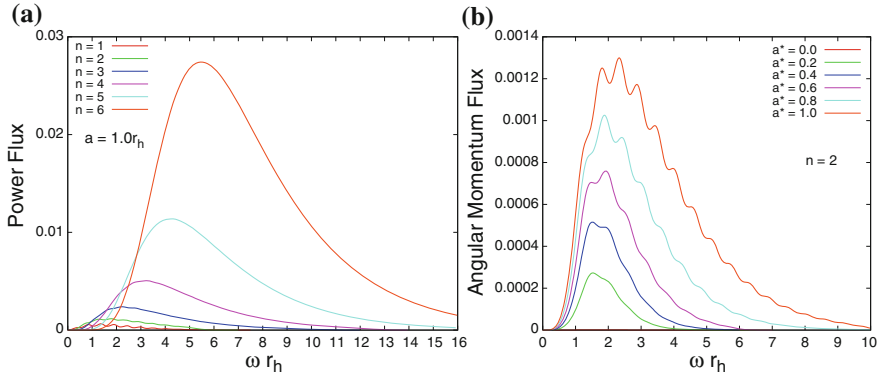

Fig. 8.10 **a** Energy emission rate for bulk scalar fields from a black hole with $a_* = 1$ and variable n, and **b** angular-momentum emission rate for bulk scalar fields from a black hole with $n = 2$ and variable a_* [53]

In Fig. 8.10a, we depict the differential energy emission rate for bulk scalar fields [53], for fixed angular-momentum parameter $a_* = 1$, and variable n. The power flux shows a significant overall enhancement as n increases, with a small suppression at the low-energy regime and a shift of the peak of the curve towards larger energies—this behaviour is also identical to the one observed in the case of a spherically-symmetric black hole emitting scalar particles in the bulk [120]. The particle and angular-momentum fluxes were also found to have the same behaviour. The angular-momentum emission rates, presented in Fig. 8.10b for $n = 2$, show a significant enhancement over the whole energy regime, as a_* increases. The power and particle fluxes, on the other hand, have a more particular profile: for low values of n, the emission curves are also shifted to the high-energy regime, as a_* increases, but their

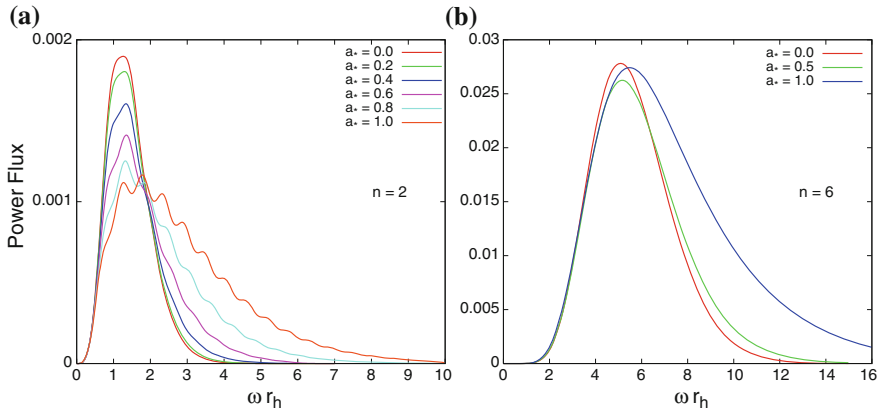

Fig. 8.11 Energy emission rates for scalar fields in the bulk from a black hole with **a** $n = 2$, and **b** $n = 6$, and variable a_* [53]

peak values are significantly suppressed, as shown in Fig. 8.11a; for large values of n, the energy and particle emission curves remain almost unchanged as a_* increases, apart from a small enhancement in the amount of emission at the high-energy regime; see Fig. 8.11b.

We now turn to the emission of gravitons in the bulk by a higher-dimensional black hole. For a spherically-symmetric black hole, the analysis is now complete. The radial equation (8.31), obeyed by all three types of gravitational perturbations—scalar, vector and tensor ones—has been solved analytically both in the low [114] and intermediate-energy regime [137]. The low-energy analysis [114] revealed that the graviton spectra exhibit the same behaviour as bulk scalar fields [120], i.e. a suppression at the low-energy regime and a shift of the emission curve towards higher energies, as n increased. The same analysis showed that, at the lower part of the energy spectrum, the emission of gravitons is negligible compared to that of bulk scalar fields, however that was expected to change at higher energies where higher partial modes would dominate.

That expectation was indeed proved right by the exact numerical analysis performed in [138–140]. It was thus demonstrated that the graviton radiation spectra were strongly enhanced at the higher part of the spectrum and for large values of n. The latter was largely due to the fact that the degeneracy factors of the graviton states (8.43) increase rapidly with both n and ℓ with the higher modes dominating at the upper part of the spectrum. For example, for a moderate value of ℓ, i.e. $\ell = 5$, the number of graviton states, as n varies from 1 to 6, increases by a factor of 10^4 [114]. An interesting twist is that the tensor graviton modes, the most negligible degrees of freedom at the low-energy regime [114], proliferate as n increases. Overall, it is found [138, 139] that, as n reaches the value 7, a spherically-symmetric black hole emits 35 times more energy in the bulk in the form of gravitons than in any other particle on the brane.

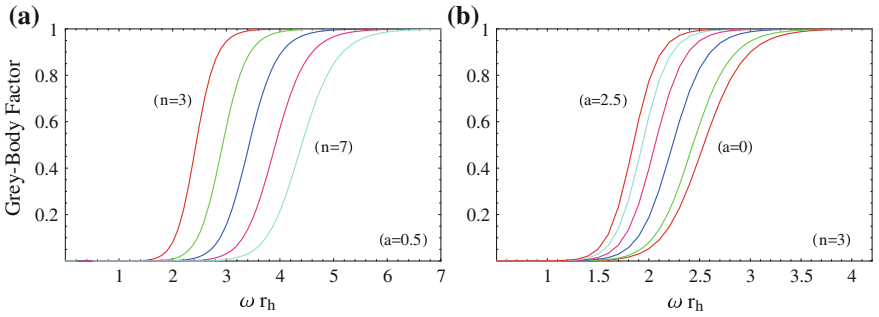

Fig. 8.12 Grey-body factors for tensor-type graviton modes ($\ell = j = 2, m = 0$) for: **a** $a_* = 0.5$ and variable n, and **b** $n = 3$ and variable a_* [113]

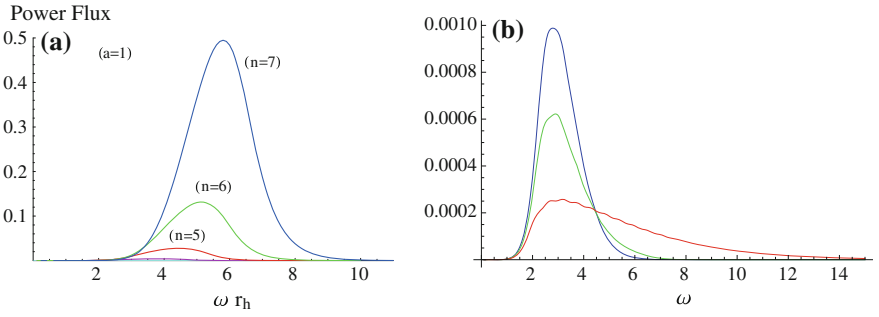

Fig. 8.13 Energy emission rate for tensor-type gravitons **a** for $a_* = 1$ and variable n, and **b** for $n = 3$ and $a_* = 0, 0.5, 1.2$ (from top to bottom) [113]

For the case of the simply-rotating black hole (8.17), only the equations for tensor-type perturbations have been derived, and these are identical to the ones for a bulk scalar field (8.29–8.30) apart from the allowed values of the angular-momentum number ℓ (i.e. $\ell \geq 2$ instead of $\ell \geq 0$). These equations were solved both analytically and numerically in [113], with the two sets shown to agree remarkably well even up to the intermediate-energy regime. In Fig. 8.12a, b, we present exact numerical results for the grey-body factor of the lowest tensor-type mode ($\ell = j = 2, m = 0$), in terms of n and a_*, respectively [113]. We observe that, as the number of extra dimensions n increases, the grey-body factor is suppressed over the whole energy regime—a similar suppression is exhibited also by bulk scalar fields [53, 120, 133]. On the other hand, the grey-body factor is strongly enhanced with the angular momentum of the black hole. Turning to the fluxes, the indicative case of the energy emission rate is presented in Fig. 8.13a, b [113], in terms again of n and a_*. Similarly to the case of bulk scalars, the graviton emission rates are significantly enhanced with n, while the emission is suppressed at the low and intermediate-energy regimes and enhanced at the high-energy regime as a_* increases (for large n, the suppression at the low and intermediate-energy regimes is replaced again by a mild dependence on a_*).

8.4.5 Energy Balance Between the Brane and the Bulk

The question of the energy balance between the brane and bulk emission channels is an important one, not only for its theoretical interest but also for practical purposes: if we determine what fraction of the available energy of the black hole is lost in the bulk, we will know how much remains for emission on the brane, and thus how likely the observation of the Hawking radiation effect will be for the brane observer.

The study of the higher-dimensional spherically-symmetric black hole is, as we saw, now complete with the exact spectra for all types of brane and bulk particles being determined. In [53, 120], exact numerical analyses were performed in order to compare the scalar emissivity of the black hole in the brane and bulk channels. In the first row of Table 8.1 we display some indicative values of the proportion of the total power emitted in the bulk by a non-rotating black hole [53, 120]: we see that the bulk scalar channel is always subdominant to the brane one, but not necessarily negligible. Although bulk and brane scalar fields "see" the same black-hole temperature, their grey-body factors behave differently with n, leading to the emission of more energetic, but significantly fewer bulk scalar fields compared to the brane ones.

For the brane-localised fermions and gauge bosons and the bulk gravitons, it is again the relative behaviour of their grey-body factors, but also of their degeneracy factors, that will determine the result. Regarding the latter, we have already discussed the rapid proliferation, with n, of the gravitons in the bulk, however, the large number of Standard Model degrees of freedom living on the brane must also be taken into account. When all the above are implemented in the analysis, it is found [138, 139] that the brane channel is the most dominant during the spherically-symmetric phase of the black hole, a result that agrees with an early analytical argument [141].

The same question of the bulk-to-brane energy balance needs to be posed also for the rotating phase. The relative scalar emissivity can again be derived since the radiation spectra for bulk and brane emission are known [53, 54, 127]. The entries of Table 8.1 reveal that, not only is the bulk scalar channel the subdominant one also during the rotating phase, but the proportion of the energy emitted in the bulk reduces with the angular-momentum of the black hole. This is due to the fact that the enhancement of the grey-body factor with a_* is not as large for bulk scalar emission as it is for the brane one.

Since we still lack the complete emission spectra for all types of gravitational perturbations in the bulk, the question of the energy balance between the brane and bulk channels for the rotating phase remains open. In [113], the total emissivity of

Table 8.1 Total proportion of scalar power emitted in the bulk by a black-hole [53]

n	1 (%)	2 (%)	3 (%)	4 (%)	5 (%)	6 (%)
$a_* = 0.0$	28.3	19.9	17.9	19.6	24.8	34.0
$a_* = 0.5$	20.9	13.5	11.8	13.0	16.7	24.0
$a_* = 1.0$	12.5	7.1	6.2	6.8	9.1	14.7

tensor-type gravitons was compared to the one for scalar bulk emission. It was found that the energy emitted in the bulk, for small values of n, in the form of tensor modes is less than 1 % of the scalar emissivity but it becomes of the order of 25 %, for $n = 5$ and for the indicative value of $a_* = 1$. Recalling that the tensor modes were the dominant gravitational ones in the bulk in the case of the spherically-symmetric phase, we may conclude that, for low values of n, the brane channel wins the energy-balance contest in the rotating phase, too. Whether the same situation holds for large values of n (or larger values of a_*) will be decided only when the exact emission spectra for vector and scalar-type graviton modes are found.

8.4.6 Additional Effects in Hawking Radiation

We now discuss some further aspects of the Hawking radiation emission process. In all the studies mentioned so far, the different types of particles emitted by the black hole were assumed for simplicity to be massless. The presence of the mass, however, is expected to cause a suppression of the grey-body factors since the emission of a massive field demands more energy, and thus it is less likely to happen. The effect of the mass on the radiation spectra was studied in [58, 142, 143], for scalar fields emitted by a higher-dimensional rotating black hole, and in [144, 145], for vector fields, both transverse and longitudinal modes, on a D-dimensional Schwarzschild background. It was demonstrated that the suppression is indeed more prominent the larger the mass of the emitted field, as depicted in Fig. 8.14a [142]. Although the brane channel remains the dominant one, in [142], it was shown that the presence of the mass enhances the bulk-over-brane energy ratio up to a factor of 34 %.

The effect of the charge of the emitted particles was studied in [143, 145, 146]. In [146], a spherically-symmetric Reissner-Nordström black hole was considered,

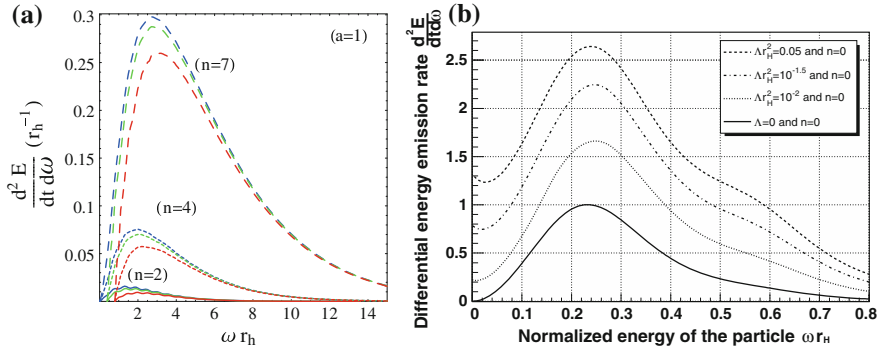

Fig. 8.14 Energy emission rates for scalar fields on the brane: **a** with $a_* = 1$, and a mass $m_\Phi = 0, 0.4, 0.8$ (from *top* to *bottom* in each set of curves) [142], and **b** from a Schwarzschild-de Sitter black hole with various values of Λ [147]

and it was shown that the charge of a scalar particle, similarly to its mass, causes a suppression in the bulk and brane emission spectra and enhances the bulk-to-brane emissivity. In [145], the case of a charged vector field was studied, and an inverted charge splitting effect as well as the analogue of a superradiance effect were observed in the radiation spectra. The case of a higher-dimensional rotating black hole with a brane-localised Maxwell field was considered in [143]. Although only brane emission of scalars and fermions was studied, an interesting effect was found: the radiation process exhibits a charging-up phase at the low-energy regime (where the black hole emits particles with an opposite charge compared to its own) while a phase of discharging dominates at higher energies.

In addition to particle properties, parameters that characterize the black-hole space-time background may also affect the radiation spectra and subsequently the bulk-to-brane energy balance. The cosmological constant Λ, that may be present in the part of the space-time where the black hole is formed, is one of these parameters. In [147], the radiation spectra for scalar fields emitted by a higher-dimensional Schwarzschild-de Sitter black hole were studied. It was found that both bulk and brane emission rates are enhanced as the value of Λ increases, with the spectrum exhibiting a novel feature, i.e. a non-vanishing emission rate at the lowest part of the energy regime (see Fig. 8.14b). The presence of the cosmological constant was shown to increase the bulk-to-brane relative emissivity. In the case of a Kerr-de Sitter black hole [148], a similar enhancement is found when the Bousso-Hawking definition of the black hole temperature is used, whereas the use of the Hawking definition leads instead to a small decrease.

Higher-order curvature terms, such as the Gauss-Bonnet term, may be also taken into account during the decay of the black hole. Their effect on the emission spectra strongly depends on the mass of the black hole, the value of the coupling constant, and the type and energy of the emitted particle: for scalar fields, they can tilt the bulk-to-brane energy ratio in favour of the bulk [149], while, for gravitons, they can cause the suppression of their emission by many orders of magnitude leading to an increased life-time of the black hole [150]. Another counter-example of the claim that black holes radiate mainly on the brane appeared in [151] where it was shown that, in the context of a supersymmetric split-fermion model, the bulk fermion emission dominates over the brane one for $n > 1$. On the other hand, including non-commutative geometry-inspired corrections to the black hole metric significantly lowers the black hole temperature, and the bulk emission is greatly suppressed [152].

8.5 Hawking Radiation from Black Holes in the RS Model

Given the absence of an analytical solution describing a five-dimensional asymptotically AdS black hole localised on the brane, no exact results may be presented for the Hawking radiation process from such a black hole. Nevertheless, a number of partial or approximate results have appeared in the literature that may shed light on some aspects of this process.

In the RS-II model, the AdS length scale ℓ_{AdS} plays the role of the effective size of the fifth dimension. On the other hand, the size of the black hole is given by the horizon radius r_h. If $r_h \ll \ell_{AdS}$, the black hole is insensitive to the warping along the fifth dimension, and it resembles a black hole in a five-dimensional flat space-time whose line-element is described by either the Myers-Perry (8.17) or the Tangherlini solution. In this limit, it shares all the properties of black holes in a higher-dimensional flat space-time. For example, if we assume for simplicity that the black hole is non-rotating, its horizon radius-mass relation and temperature will be given by

$$r_h = \sqrt{\frac{8}{3\pi}}\,\frac{1}{M_5}\left(\frac{M}{M_5}\right)^{1/2}, \qquad T_{BH} = \frac{1}{2\pi r_h}, \tag{8.51}$$

where M and M_5 are the black-hole mass and the fundamental Planck scale, respectively. The above expressions follow readily from the corresponding $(4+n)$-dimensional ones [153] after setting $n = 1$. Compared to a four-dimensional black hole of the same mass, for which $r_h = 2M/M_P^2$ and $T_{BH} = 1/4\pi r_h$, a small brane-world black hole has a larger horizon radius and, thus, a smaller temperature. Therefore, its evaporation rate will be significantly suppressed leading to a longer lifetime [154]

$$\frac{t_{\rm evap}(5D)}{t_{\rm evap}(4D)} \sim \left(\frac{\ell_{AdS}}{r_h(5D)}\right)^2, \tag{8.52}$$

the smaller the horizon radius of the five-dimensional black hole is compared to ℓ_{AdS}. The above, combined with an increased accretion rate for a brane-world black hole being formed in the early universe, radically change the mass spectrum of the primordial black holes that are expected to decay today [154–156].

As the horizon radius increases, the black hole starts to perceive the warping of the fifth dimension and its properties are correspondingly modified. Unfortunately, only numerical solutions are available in the literature in this regime. In [157], the thermodynamic properties of such a five-dimensional black-hole solution localised on the brane were studied. It was demonstrated that, for a small value of the horizon radius, the properties of the black hole match those of a five-dimensional Schwarzschild-AdS black hole. For a large value of the horizon radius, they tend to the ones of a four-dimensional Schwarzschild black hole, while in the intermediate regime they remain quite distinct from these two limits.

For $r_h \gg \ell_{AdS}$, we expect the brane-world black hole to obtain a peculiar shape: while there is no limit on its size along the brane directions, in the bulk it cannot extend at distances larger than ℓ_{AdS} due to the localisation of gravity. Thus, a large brane-world black hole has a "pancake" shape. Although it is genuinely a higher-dimensional object, it extends so little along the extra dimension and so much along the usual three that we expect it to be effectively four-dimensional and thus to

resemble the Schwarzschild solution. That is, if it is allowed by the theory to exist. Even then, it is not exactly Schwarzschild.

As it was briefly mentioned in Sect. 8.3.1, in reality, the projected line-element on the brane is not a vacuum solution. A four-dimensional observer would independently write the effective Einstein's equations on the brane as $G_{\mu\nu} = 8\pi G_N T_{\mu\nu}$. According to the AdS/CFT correspondence [85], this $T_{\mu\nu}$ is the expectation value of the stress-energy tensor operator for the CFT modes for a suitably chosen vacuum state. The correspondence dictates that the number of CFT modes living on the brane is given by $N \sim (\ell_{AdS}/\ell_P)^2$ (where ℓ_P is the Planck length) and thus, for $\ell_{AdS} \gg \ell_P$, this number is expected to be very large. In [82], it was then argued that the presence of such a large number of fields in the vicinity of the black hole will greatly enhance its evaporation rate resulting in a large-mass black hole having a life-time given by [84]

$$t_{\rm evap} = 116 \times \left(\frac{1\,{\rm mm}}{\ell_{AdS}}\right)^2 \left(\frac{M}{M_\odot}\right)^3 \text{ years}\,. \tag{8.53}$$

For such a rapidly evaporating black hole, no static solution can be found to describe it even approximately. Since the line-element on the brane is merely the projection of the five-dimensional one, the bulk solution could not be static either, but rather must describe an evaporating black hole on the brane while remaining classical. In [82], a "classical evaporation" process was proposed: instabilities of the solution along the bulk cause the deformation of the horizon radius and its elongation towards the AdS boundary; for its total horizon area to remain constant, the area of the intersection of the black hole with the brane will have to decrease, and that will be viewed by a four-dimensional observer as an evaporation process.

The authors of [86] counter-argued that the above scenario assumes the involvement of all CFT brane modes in the evaporation process. But if the CFT on the brane is strongly-coupled, as the AdS/CFT correspondence dictates, would all modes be available to interact with the four-dimensional black hole? Most likely not, therefore one should not expect important quantum corrections to the four-dimensional line-element. In support of this, in [87] a Schwarzschild-AdS$_4$ black string, proven to be stable, was considered and the question was asked: why is this five-dimensional classical solution quantum-corrected on the brane (the same question for the black string of [59] loses part of its validity due to its instability)? The stress-energy tensor for the boundary field theory was computed and shown to lead to a mere renormalization of the effective cosmological constant, and not to a radiation term. In addition, in [88] it was recently suggested that a low-energy theory, such as the CFT theory on the brane, needs to be carefully UV-completed before predictions for the IR behaviour of the theory are made. When this is properly done, it follows that the emission of CFT modes in the RS-II model is significantly suppressed—in fact, it was argued that, at distances $L \leq N\,\ell_P$, low-energy CFT does not even exist.

The numerical nature of the solutions found in [89–91], describing both small and large black holes in the RS-II model, does not allow us to analytically study the effect that the brane tension or the bulk cosmological constant have on the evaporation

process. In the context of a six-dimensional model, a solution was found [158] that described a black hole localised on a codimension-two brane with tension. The solution was asymptotically flat, and not AdS as in the RS-II model, and it had a peculiar horizon radius-mass relation: the closer the brane tension to the fundamental scale M_6, the larger the horizon radius is. It was shown [159] that an increase in the brane tension simultaneously decreases the black-hole temperature and increases the potential barrier, thus causing the suppression of both bulk and brane emission rates.

8.6 Conclusions

In this chapter we have reviewed some key aspects of our understanding of Hawking radiation from higher-dimensional black holes. One motivation for this study, apart from its intrinsic theoretical interest, is the exciting possibility of observing Hawking radiation from microscopic higher-dimensional black holes produced in high-energy collisions at either the LHC or in cosmic rays.

We began with a discussion of the quantum-field-theoretic foundations of Hawking radiation, from its original derivation for a quantum field on a dynamical spacetime representing a black hole formed by gravitational collapse, to its modelling using the Unruh state on an eternal black hole geometry. After a brief review of classical black hole geometries in both the ADD and RS brane-worlds, most of this chapter has been devoted to the Hawking emission from these black holes.

For black holes in the ADD brane-world, for which we have an exact spacetime metric, we gave an overview of the formalism used to describe the emission of massless particles both on the brane and in the bulk. We then reviewed a selection of results on the nature of the emission, including the important question of how much Hawking radiation escapes into the bulk and is therefore inaccessible to a brane-localised observer. Except for the emission of scalar- and vector-like graviton modes from a rotating black hole, our understanding of the emission of massless particles is essentially complete. We also briefly summarized some features of the Hawking radiation when other effects, such as the mass and charge of the emitted particles or a cosmological constant, are included.

In the RS brane-world, the lack of an exact classical metric for a black hole localized on the brane implies a scarcity of precise results on the nature of the Hawking emission from such black holes. We have therefore just briefly outlined some of the work in the literature in this case.

Our review has revealed that Hawking radiation from higher-dimensional black holes is more complicated than from four-dimensional black holes, with many features depending on the number of extra dimensions and the angular momentum of the black hole. Many of the results we have outlined in this chapter have been incorporated into simulations of black hole events at the LHC [22, 23]. Hawking radiation from black holes at the LHC characteristically involves large numbers of energetic particles, the details of the distribution and nature of the particles depending on the number of extra dimensions, the mass of the black hole and its angular momentum.

Searches for these types of events have been made at the LHC, with no evidence to date for black holes [160–165]. This non-observation of black hole events sets lower bounds on the energy scale of quantum gravity. With the LHC planned to run at higher energies and searches for high-energy black hole events in cosmic rays, accurate modelling of Hawking radiation from higher-dimensional black holes continues to be essential for experimental probes of quantum gravity.

Acknowledgments The work of E.W. is supported by the Lancaster-Manchester-Sheffield Consortium for Fundamental Physics under STFC Grant ST/J000418/1. The work of P.K. has been co-financed by the European Union (European Social Fund—ESF) and Greek national funds through the Operational Program "Education and Lifelong Learning" of the National Strategic Reference Framework (NSRF)—Research Funding Program: "ARISTEIA. Investing in the society of knowledge through the European Social Fund". Part of this work was supported by the COST Actions MP0905 "Black Holes in a Violent Universe" and MP1210 "The String Theory Universe".

References

1. Hawking, S.W.: Commun. Math. Phys. **43**, 199–220 (1975)
2. Hossenfelder, S., Smolin, L.: Phys. Rev. D **81**, 064009 (2010)
3. Mathur, S.D.: Class. Quantum Gravity **26**, 224001 (2009)
4. Page, D.N.: Phys. Rev. D **13**, 198–206 (1976)
5. Page, D.N.: Phys. Rev. D **14**, 3260–3273 (1976)
6. Page, D.N.: Phys. Rev. D **16**, 2402–2411 (1977)
7. Emparan, R., Reall, H.S.: Living Rev. Relativ. **11**, 6 (2008)
8. Tomizawa, S., Ishihara, H.: Progress Theoret. Phys. Suppl. **189**, 7–51 (2011)
9. Banks, T., Fischler, W.: hep-th/9906038 (1999)
10. Dimopoulos, S., Landsberg, G.L.: Phys. Rev. Lett. **87**, 161602 (2001)
11. Giddings, S.B., Thomas, S.D.: Phys. Rev. D **65**, 056010 (2002)
12. Kanti, P.: Int. J. Mod. Phys. A **19**, 4899–4951 (2004)
13. Landsberg, G.L.: Eur. Phys. J. C **33**, S927–S931 (2004)
14. Majumdar, A.S., Mukherjee, N.: Int. J. Mod. Phys. D **14**, 1095–1129 (2005)
15. Park, S.C.: Prog. Part. Nucl. Phys. **67**, 617–650 (2012)
16. Webber, B.: hep-ph/0511128 (2005)
17. Arkani-Hamed, N., Dimopoulos, S., Dvali, G.R.: Phys. Lett. B **429**, 263–272 (1998)
18. Antoniadis, I., Arkani-Hamed, N., Dimopoulos, S., Dvali, G.R.: Phys. Lett. B **436**, 257–263 (1998)
19. Arkani-Hamed, N., Dimopoulos, S., Dvali, G.R.: Phys. Rev. D **59**, 086004 (1999)
20. Randall, L., Sundrum, R.: Phys. Rev. Lett. **83**, 3370–3373 (1999)
21. Randall, L., Sundrum, R.: Phys. Rev. Lett. **83**, 4690–4693 (1999)
22. Dai, D.-C., Starkman, G., Stojkovic, D., Issever, C., Rizvi, E., Tseng, J.: Phys. Rev. D **77**, 076007 (2008)
23. Frost, J.A., Gaunt, J.R., Sampaio, M.O.P., Casals, M., Dolan, S.R., Parker, M.A., Webber, B.R.: JHEP **0910**, 014 (2009)
24. Unruh, W.G.: Phys. Rev. D **14**, 870–892 (1976)
25. Myers, R.C., Perry, M.J.: Ann. Phys. **172**, 304–347 (1986)
26. Casanova, A., Spallucci, E.: Class. Quantum Gravity **23**, R45–R62 (2006)
27. Kanti, P.: Lect. Notes Phys. **769**, 387–423 (2009)
28. Kanti, P.: Rom. J. Phys. **57**, 879–893 (2012)
29. Winstanley, E.: arXiv:0708.2656 [hep-th] (2007)
30. Gregory, R.: Lect. Notes Phys. **769**, 259–298 (2009)

31. Kanti, P.: J. Phys.: Conf. Ser. **189**, 012020 (2009)
32. Tanahashi, N., Tanaka, T.: Progress Theoret. Phys. Suppl. **189**, 227–268 (2011)
33. Hartle, J.B., Hawking, S.W.: Phys. Rev. D **13**, 2188–2203 (1976)
34. Damour, T., Ruffini, R.: Phys. Rev. D **14**, 332–334 (1976)
35. Gerlach, U.H.: Phys. Rev. D **14**, 1479–1508 (1976)
36. Parentani, R., Brout, R.: Int. J. Mod. Phys. D **1**, 169–191 (1992)
37. Brout, R., Massar, S., Parentani, R., Spindel, P.: Phys. Rep. **260**, 329–454 (1995)
38. Hu, B.L., Raval, A.: Mod. Phys. Lett. A **11**, 2625–2638 (1996)
39. Massar, S., Parentani, R.: Nucl. Phys. B **575**, 333–356 (2000)
40. Parikh, M.K., Wilczek, F.: Phys. Rev. Lett. **85**, 5042–5045 (2000)
41. Schutzhold, R.: Phys. Rev. D **64**, 024029 (2001)
42. Shankaranarayanan, S., Padmanabhan, T., Srinivasan, K.: Class. Quantum Gravity **19**, 2671–2688 (2002)
43. Visser, M.: Int. J. Mod. Phys. D **12**, 649–661 (2003)
44. Peltola, A.: Class. Quantum Gravity **26**, 035014 (2009)
45. Ottewill, A.C., Winstanley, E.: Phys. Rev. D **62**, 084018 (2000)
46. Casals, M., Dolan, S.R., Nolan, B.C., Ottewill, A.C., Winstanley, E.: Phys. Rev. D **87**, 064027 (2013)
47. Casals, M., Ottewill, A.C.: Phys. Rev. D **71**, 124016 (2005)
48. Christensen, S.M.: Phys. Rev. D **14**, 2490–2501 (1976)
49. Christensen, S.M.: Phys. Rev. D **17**, 946–963 (1978)
50. Decanini, Y., Folacci, A.: Phys. Rev. D **78**, 044025 (2008)
51. Frolov, V.P., Thorne, K.S.: Phys. Rev. D **39**, 2125–2154 (1989)
52. Synge, J.L.: Relativity: The General Theory. North-Holland, Amsterdam (1960)
53. Casals, M., Dolan, S.R., Kanti, P., Winstanley, E.: JHEP **0806**, 071 (2008)
54. Duffy, G., Harris, C., Kanti, P., Winstanley, E.: JHEP **0509**, 049 (2005)
55. Casals, M., Dolan, S.R., Kanti, P., Winstanley, E.: JHEP **0703**, 019 (2007)
56. Casals, M., Kanti, P., Winstanley, E.: JHEP **0602**, 051 (2006)
57. Tangherlini, F.R.: Nuovo Cimento **27**, 636–651 (1963)
58. Sampaio, M.O.P.: JHEP **0910**, 008 (2009)
59. Chamblin, A., Hawking, S.W., Reall, H.S.: Phys. Rev. D **61**, 065007 (2000)
60. Gregory, R., Laflamme, R.: Phys. Rev. Lett. **70**, 2837–2840 (1993)
61. Gregory, R.: Class. Quantum Gravity **17**, L125–L132 (2000)
62. Dadhich, N., Maartens, R., Papadopoulos, P., Rezania, V.: Phys. Lett. B **487**, 1–6 (2000)
63. Kofinas, G., Papantonopoulos, E., Zamarias, V.: Phys. Rev. D **66**, 104028 (2000)
64. Kanti, P., Tamvakis, K.: Phys. Rev. D **65**, 084010 (2002)
65. Kanti, P., Olasagasti, I., Tamvakis, K.: Phys. Rev. D **68**, 124001 (2003)
66. Casadio, R., Fabbri, A., Mazzacurati, L.: Phys. Rev. D **65**, 084040 (2002)
67. Frolov, V.P., Snajdr, M., Stojkovic, D.: Phys. Rev. D **68**, 044002 (2003)
68. Karasik, D., Sahabandu, C., Suranyi, P., Wijewardhana, L.C.R.: Phys. Rev. D **70**, 064007 (2004)
69. Galfard, C., Germani, C., Ishibashi, A.: Phys. Rev. D **73**, 064014 (2006)
70. Creek, S., Gregory, R., Kanti, P., Mistry, B.: Class. Quantum Gravity **23**, 6633–6658 (2006)
71. Casadio, R., Ovalle, J.: Phys. Lett. B **715**, 251–255 (2012)
72. Kanti, P., Pappas, N., Zuleta, K.: Class. Quantum Gravity **30**, 235017 (2013)
73. Kudoh, H., Tanaka, T., Nakamura, T.: Phys. Rev. D **68**, 024035 (2002)
74. Kudoh, H.: Phys. Rev. D **69**, 104019 (2004) [Erratum-ibid. D **70**, 029901 (2004)]
75. Tanahashi, N., Tanaka, T.: JHEP **0803**, 041 (2008)
76. Emparan, R., Horowitz, G.T., Myers, R.C.: JHEP **0001**, 007 (2000)
77. Emparan, R., Horowitz, G.T., Myers, R.C.: JHEP **0001**, 021 (2000)
78. Anber, M., Sorbo, L.: JHEP **0807**, 098 (2008)
79. Bruni, M., Germani, C., Maartens, R.: Phys. Rev. Lett. **87**, 231302 (2001)
80. Govender, M., Dadhich, N.: Phys. Lett. B **538**, 233–238 (2002)
81. Kofinas, G., Papantonopoulos, E.: JCAP **0412**, 011 (2004)

82. Tanaka, T.: Progress Theoret. Phys. Suppl. **148**, 307–316 (2003)
83. Emparan, R., Fabbri, A., Kaloper, N.: JHEP **0208**, 043 (2002)
84. Emparan, R., Garcia-Bellido, J., Kaloper, N.: JHEP **0301**, 079 (2003)
85. Hawking, S.W., Hertog, T., Reall, H.S.: Phys. Rev. D **62**, 043501 (2000)
86. Fitzpatrick, A.L., Randall, L., Wiseman, T.: JHEP **0611**, 033 (2006)
87. Gregory, R., Ross, S.F., Zegers, R.: JHEP **0809**, 029 (2008)
88. Kaloper, N.: Phys. Rev. D **86**, 104052 (2012)
89. Figueras, P., Wiseman, T.: Phys. Rev. Lett. **107**, 081101 (2011)
90. Abdolrahimi, S., Cattoen, C., Page, D.N., Yaghoobpour-Tari, S.: Phys. Lett. B **720**, 405–409 (2013)
91. Abdolrahimi, S., Cattoen, C., Page, D.N., Yaghoobpour-Tari, S.: JCAP **1306**, 039 (2013)
92. Heydari-Fard, M., Sepangi, H.R.: JCAP **0902**, 029 (2009)
93. Dai, D.-C., Stojkovic, D.: Phys. Lett. B **704**, 354–359 (2011)
94. Yoshino, H.: JHEP **0901**, 068 (2009)
95. Kleihaus, B., Kunz, J., Radu, E., Senkbeil, D.: Phys. Rev. D **83**, 104050 (2011)
96. Cuadros-Melgar, B., Papantonopoulos, E., Tsoukalas, M., Zamarias, V.: Phys. Rev. Lett. **100**, 221601 (2008)
97. Frolov, V.P., Stojkovic, D.: Phys. Rev. D **66**, 084002 (2002)
98. Teukolsky, S.A.: Phys. Rev. Lett. **29**, 1114–1118 (1972)
99. Teukolsky, S.A.: Astrophys. J. **185**, 635–647 (1973)
100. Chandrasekhar, S.: The Mathematical Theory of Black Holes. Oxford University Press, Oxford (1998)
101. Newman, E., Penrose, R.: J. Math. Phys. **3**, 566–578 (1962)
102. Fackerell, E.D., Crossman, R.G.: J. Math. Phys. **18**, 1849–1854 (1977)
103. Seidel, E.: Class. Quantum Gravity **6**, 1057–1062 (1989)
104. Goldberg, J.N., MacFarlane, A.J., Newman, E.T., Rohrlich, F., Sudarshan, E.C.G.: J. Math. Phys. **8**, 2155–2161 (1967)
105. Muller, C.: Spherical Harmonics. Springer, New York (1966)
106. Kodama, H., Ishibashi, A.: Progress Theoret. Phys. **110**, 701–722 (2003)
107. Ishibashi, A., Kodama, H.: Progress Theoret. Phys. **110**, 901–919 (2003)
108. Durkee, M., Reall, H.S.: Phys. Rev. D **83**, 104044 (2011)
109. Reall, H.S.: Int. J. Mod. Phys. D **21**, 1230001 (2012)
110. Murata, K.: Progress Theoret. Phys. Suppl. **189**, 210–226 (2011)
111. Kodama, H.: Progress Theoret. Phys. Suppl. **172**, 11–20 (2008)
112. Kodama, H.: Lect. Notes Phys. **769**, 427–470 (2009)
113. Kanti, P., Kodama, H., Konoplya, R.A., Pappas, N., Zhidenko, A.: Phys. Rev. D **80**, 084016 (2009)
114. Creek, S., Efthimiou, O., Kanti, P., Tamvakis, K.: Phys. Lett. B **635**, 39–49 (2006)
115. Rubin, M.A., Ordonez, C.R.: J. Math. Phys. **25**, 2888–2894 (1984)
116. Rubin, M.A., Ordonez, C.R.: J. Math. Phys. **26**, 65–67 (1985)
117. Kanti, P., March-Russell, J.: Phys. Rev. D **66**, 024023 (2002)
118. Kanti, P., March-Russell, J.: Phys. Rev. D **67**, 104019 (2003)
119. Ida, D., Oda, K.Y., Park, S.C.: Phys. Rev. D **67**, 064025 (2003) [Erratum-ibid. D **69**, 049901 (2004)]
120. Harris, C.M., Kanti, P.: JHEP **0310**, 014 (2003)
121. Sanchez, N.: Phys. Rev. D **16**, 937–945 (1977)
122. Sanchez, N.: Phys. Rev. D **18**, 1030–1036 (1978)
123. Sanchez, N.: Phys. Rev. D **18**, 1798–1804 (1978)
124. Starobinskii, A.A., Churilov, S.M.: Sov. Phys. JETP **38**, 1–5 (1974)
125. Creek, S., Efthimiou, O., Kanti, P., Tamvakis, K.: Phys. Rev. D **75**, 084043 (2007)
126. Creek, S., Efthimiou, O., Kanti, P., Tamvakis, K.: Phys. Rev. D **76**, 104013 (2007)
127. Harris, C.M., Kanti, P.: Phys. Lett. B **633**, 106–110 (2006)
128. Casals, M., Dolan, S.R., Kanti, P., Winstanley, E.: Phys. Lett. B **680**, 365–370 (2009)
129. Flachi, A., Sasaki, M., Tanaka, T.: JHEP **0905**, 031 (2009)

130. Leaver, E.W.: Proc. R. Soc. Lond. A **402**, 285–298 (1985)
131. Kanti, P., Pappas, N.: JHEP **1212**, 019 (2012)
132. Frolov, V., Stojkovic, D.: Phys. Rev. D **67**, 084004 (2003)
133. Creek, S., Efthimiou, O., Kanti, P., Tamvakis, K.: Phys. Lett. B **656**, 102–111 (2007)
134. Jung, E., Park, D.K.: Nucl. Phys. B **731**, 171–187 (2005)
135. Berti, E., Cardoso, V., Casals, M.: Phys. Rev. D **73** 024013 (2006) [Erratum-ibid. D **73** 109902 (2006)]
136. Cardoso, V., Siopsis, G., Yoshida, S.: Phys. Rev. D **71**, 024019 (2005)
137. Cornell, A.S., Naylor, W., Sasaki, M.: JHEP **0602**, 012 (2006)
138. Cardoso, V., Cavaglia, M., Gualtieri, L.: Phys. Rev. Lett. **96**, 071301 (2006) [Erratum-ibid. **96**, 219902 (2006)]
139. Cardoso, V., Cavaglia, M., Gualtieri, L.: JHEP **0602**, 021 (2006)
140. Park, D.K.: Phys. Lett. B **638**, 246–252 (2006)
141. Emparan, R., Horowitz, G.T., Myers, R.C.: Phys. Rev. Lett. **85**, 499–502 (2000)
142. Kanti, P., Pappas, N.: Phys. Rev. D **82**, 024039 (2010)
143. Sampaio, M.O.P.: JHEP **1002**, 042 (2010)
144. Herdeiro, C., Sampaio, M.O.P., Wang, M.: Phys. Rev. D **85**, 024005 (2012)
145. Wang, M., Sampaio, M.O.P., Herdeiro, C.: Phys. Rev. D **87**, 044011 (2013)
146. Jung, E., Park, D.K.: Nucl. Phys. B **717**, 272–303 (2005)
147. Kanti, P., Grain, J., Barrau, A.: Phys. Rev. D **71**, 104002 (2005)
148. Doukas, J., Cho, H.T., Cornell, A.S., Naylor, W.: Phys. Rev. D **80**, 045021 (2009)
149. Grain, J., Barrau, A., Kanti, P.: Phys. Rev. D **72**, 104016 (2005)
150. Konoplya, R.A., Zhidenko, A.: Phys. Rev. D **82**, 084003 (2010)
151. Cho, H.T., Cornell, A.S., Doukas, J., Naylor, W.: Phys. Rev. D **77**, 016004 (2008)
152. Nicolini, P., Winstanley, E.: JHEP **1111**, 075 (2011)
153. Argyres, P.C., Dimopoulos, S., March-Russell, J.: Phys. Lett. B **441**, 96–104 (1998)
154. Guedens, R., Clancy, D., Liddle, A.R.: Phys. Rev. D **66**, 043513 (2002)
155. Majumdar, A.S.: Phys. Rev. Lett. **90**, 031303 (2003)
156. Sendouda, Y., Nagataki, S., Sato, K.: Phys. Rev. D **68**, 103510 (2003)
157. Kudoh, H.: Progress Theoret. Phys. **110**, 1059–1069 (2004)
158. Kaloper, N., Kiley, D.: JHEP **0603**, 077 (2006)
159. Dai, D.C., Kaloper, N., Starkman, G.D., Stojkovic, D.: Phys. Rev. D **75**, 024043 (2007)
160. Aad, G., et al.: ATLAS collaboration. Phys. Lett. B **709**, 322–340 (2012)
161. Aad, G., et al.: ATLAS collaboration. Phys. Lett. B **716**, 122–141 (2012)
162. Aad, G., et al.: ATLAS collaboration. Phys. Rev. D **88**, 072001 (2013)
163. Khachatryan, V., et al.: CMS collaboration. Phys. Lett. B **697**, 434–453 (2011)
164. Chatrchyan, S., et al.: CMS collaboration. JHEP **1204**, 061 (2012)
165. Chatrchyan, S., et al.: CMS collaboration. JHEP **1307**, 178 (2013)

Chapter 9
Black Holes at the Large Hadron Collider

Greg Landsberg

Abstract The very successful 2010–2012 operation of the Large Hadron Collider (LHC) has changed the landscape of particle physics. The long-awaited Higgs boson has been discovered, and—yet—there are no signs of new physics beyond the standard model. The LHC set stringent limits on the existence of TeV-scale new physics phenomena, including models with low-scale quantum gravity, which predict—among other phenomena—copious production of black holes at the LHC. This chapter reviews the current state of these searches and the limits on the possibility to produce black holes at the LHC, as well as future directions, which will be made possible by a significant increase in the LHC energy in 2015 and beyond.

Keywords Randall–Sundrum · Large extra dimensions · Warped extra dimensions · Quantum black holes · String balls · Microscopic black holes · LHC · ATLAS · CMS · Quantum gravity · Searches for new physics · Hawking radiation

9.1 Introduction

Since the Large Hadron Collider (LHC) started its first successful high-energy operations in 2010, the expectations that new physics beyond the standard model (SM) would appear at any moment were quite high. With the large accumulated amount of proton-proton data at center-of-mass energies $\sqrt{s} = 7$ and 8 TeV, more and more sophisticated searches for new physics came along. Among the theoretical paradigms tested to a great extent are the recent models with extra spatial dimensions, either flat or curved, that had appeared about a decade ago and quickly gained a lot of attention of both the theoretical and experimental communities. These models offer a different solution to the infamous "hierarchy problem" that plagues the SM, and promise an exciting possibility of studying quantum gravity at the LHC, including the most mysterious of its consequences: the existence of black holes.

G. Landsberg (✉)
Department of Physics, Brown University, 182 Hope St, Providence, RI 02912, USA
e-mail: landsberg@hep.brown.edu

X. Calmet (ed.), *Quantum Aspects of Black Holes*,
Fundamental Theories of Physics 178, DOI 10.1007/978-3-319-10852-0_9

While so far all the searches for new physics came empty-handed, several new experimental methods and techniques have been developed. Among these techniques is an empirical method to predict QCD background in high-multiplicity events from low-multiplicity samples, which has been developed for the purpose of searches for black holes.

The negative results of the LHC searches changed the very way we think about the "naturalness" (i.e. non-fine-tuned solutions to the hierarchy problem) and paved the way to the ultimate attack on the standard model, which will become possible once the design LHC energy is reached in the next few years.

9.2 Low-Scale Gravity Models

Several models with extra dimensions have appeared in recent years following the original, nearly century-old proposal by Kaluza [1] and Klein [2, 3] to achieve a unification of electromagnetism and gravity by introducing a compact additional dimension in space. While the Kaluza–Klein model did not quite work, huge progress in string theory of the past two decades helped to revive the concept of extra dimensions and resulted in modern attempts to utilize them to solve the hierarchy problem of the standard model, namely the very large ratio between the electroweak symmetry breaking (EWSB) and Planck energy scales.

Among several modern models with extra dimensions, which result in a rich LHC phenomenology, in this chapter we focus on the following two:

- Model with large extra dimensions by Arkani-Hamed et al. [4–6] (ADD). In this model, only gravity propagates in n flat dimensions assumed to be compactified with a radius R either on a sphere or on a torus. All the SM particles are confined to a 3D membrane ("brane") in the $(4 + n)$-dimensional space-time. The apparent weakness of gravity (i.e., the large value of the Planck mass, M_{Pl}) can be attributed to the volume suppression of the fundamentally strong gravity in $3 + n$ spatial dimensions (fundamental Planck scale being $M_D \sim 1$ TeV), from the point of view of a three-dimensional observer. Typical values of n being considered are between 2 and 6, with the $n = 2$ case already being significantly constrained by direct gravity measurements at short distances and by astrophysical and cosmological observations [7–9]. The radius of extra dimensions depends on their number, and the relationship between M_D and M_{Pl} can be established via Gauss's law [4]: $M_{\mathrm{Pl}}^2 = 8\pi M_D^{n+2} R^n$ (for extra dimensions compactified on a torus). Setting $M_D = 1$ TeV gives $R \sim 1$ mm ($n = 2$) to 1 fm ($n = 6$). These values are *large* compared to the characteristic scales of particle physics interactions, hence the name: *large extra dimensions*.
- Randall–Sundrum (RS) model [10, 11] with a single, "warped" extra dimension, which is realized in five-dimensional anti-deSitter space-time (AdS_5). The metric of the AdS_5 space is given by $ds^2 = \exp(-2kR|\varphi|)\eta_{\mu\nu}dx^\mu dx^\nu - R^2 d\varphi^2$, where $0 \le |\varphi| \le \pi$ is the coordinate along the compact dimension of radius R, k is

the curvature of the AdS_5 space, often referred to as the "warp factor", x^μ are the conventional $(3+1)$-space-time coordinates, and $\eta^{\mu\nu}$ is the metric tensor of Minkowski space-time. Two 3-dimensional branes with equal and opposite tensions are positioned at the fixed points of the S_1/Z_2 orbifold in the AdS_5 space, at $\phi = 0$ (SM brane) and at $\phi = \pi$ (Planck brane). In this model, gravity is generated on the Planck brane, whereas at least some of the SM particles are confined to the SM brane, separated from the Planck brane in the extra dimension. Due to the warped metric in the direction of the extra dimension, operators with a characteristic size of $M_{\rm Pl}$ on the Planck brane give rise to exponentially suppressed energy scales on the SM brane: $M_D = \overline{M}_{\rm Pl} \exp(-\pi k R)$, where $\overline{M}_{\rm Pl} \equiv M_{\rm Pl}/\sqrt{8\pi}$ is the reduced Planck scale.[1] Thus the EWSB scale can be connected to the Planck scale with a relatively low degree of fine tuning by requiring the product of the warp factor and the compactification radius of the extra dimension to be $kR \sim 10$. In this model, R could have a "natural" value of $\sim 1/M_{\rm Pl}$, thus offering a rigorous solution to the hierarchy problem. One can also introduce a five-dimensional (5D) Planck scale M, which is related to the four-dimensional (4D) as follows [10]:

$$\overline{M}_{\rm Pl}^2 = \frac{M^3}{k}(1 - e^{-2\pi k R}) \approx M^3/k.$$

The 5D Planck scale reduced by the warp factor, $\hat{M} \equiv M e^{-\pi k R}$, plays similar role to M_D in the RS model. In certain variations of the RS model, some of the SM particles could be displaced w.r.t. the SM brane; therefore gravitational coupling may not be universal as it does depend on the geometrical overlap of the graviton and SM particle wave functions in the extra dimension.

The phenomenology from the point of view of $(3+1)$-dimensional space-time in all these models can be represented by a tower of Kaluza–Klein (KK) excitations of particles propagating in extra dimensions. For compactified extra dimensions, such particle could only have quantized values of the momentum projection on the compact dimensions (cf. classical "particle in a box" problem in quantum mechanics). From the point of view of a 3D observer, this quantized momentum in the direction orthogonal to the 3D brane appears as a "tower" of massive states, with the n-th excitation having a mass of $m_n^2 = m_0^2 + (n/R)^2$, where m_0 is the mass of the zeroth KK mode, representing the ground state, or the particle confined to a 3D brane.

9.2.1 Probing the ADD Model at the LHC

There are three different classes of signatures that can be used to test the predictions of the ADD model:

[1] In the literature the scale M_D is often referred to as Λ_π.

- *Virtual graviton effects.* In the ADD model, the KK modes of the graviton are very finely spaced in energy, as the size of extra dimensions is large by particle physics standards. Hence, it is experimentally impossible to distinguish between the individual KK states of the graviton, and their spectrum appears to be continuous. Each KK mode couples to the SM particles with the gravitational coupling, $\sqrt{4\pi G_N}$, where G_N is the Newton's constant; since there are many KK modes that can be excited when the momentum transfer is large, the effective gravitational coupling becomes strong and the processes normally transmitted by other gauge bosons, e.g., Drell–Yan fermion pair production, can now be also carried via virtual gravitons. Generally, the graviton-mediated diagrams interfere with their SM counterparts, resulting in a modification of the DY spectrum, particularly at large difermion masses, for which the amplification of the gravitational interaction due to the a large number of the accessible KK excitations becomes significant. This modification can be described via an effective field theory (EFT) approximation, similar to the compositeness operators [12–14], where the "compositeness scale" (i.e., the EFT cutoff) M_S, is expected to be of order M_D. The dependence on the number of extra dimensions is predicted to be weak [13].
- *Direct graviton emission.* Since gravity couples to the energy-momentum tensor, any SM Feynman diagram vertex can be modified by attaching an extra graviton (G) line to it. Thus, one can take any three-point s-channel production vertex, e.g., $q\bar{q}g$ or ggg, and transform it into a four-point vertex, resulting in a $q\bar{q} \to gG$ or $gg \to gG$ process, where a gluon jet is recoiling against the graviton, which escapes in extra dimensions. Just as in the virtual graviton case, when the momentum transfer is large, the corresponding effective coupling increases and the cross section for this reaction could become sizable. The signature for such a process in a collider detector is a single jet, countered by a significant missing momentum in the direction transverse to the beam, i.e. a *monojet*. This is a spectacular signature, quite different from usual SM jet pair production. Similarly, other objects can recoil against the graviton, giving rise to, e.g., monophoton signature. The probability of such a process is $\sim 1/M_D^{n+2}$ (see Ref. [15]), and thus strongly depends both on the fundamental Planck scale and on the number of extra dimensions.
- *Black hole production.* One of the most spectacular signatures predicted [16–20] in the ADD model is a possibility to produce microscopic black holes (BH) when the collision energy exceeds the value of the fundamental Planck scale M_D. These BH may act either as their semiclassical counterparts in general relativity and evaporate via thermal Hawking radiation of various particle species; or they may have more complicated properties of their quantum precursors. Lacking the full picture of quantum gravity, it is impossible to have exact predictions on how these black holes evaporate, so many different possibilities should be considered. Since the Hawking temperature is inversely proportional to the Schwarzschild radius of such a BH [19, 20], and since the BH are tiny, the temperature is very hot and therefore the BH is expected to evaporate very fast either thermally (i.e., with an emission of a dozen or so particles, each carrying hundreds of GeV of energy), or via a decay, as a quantum state, into a pair of even more energetic particles.

In either case, the signature is quite spectacular and can be also used to probe more general models with low-scale quantum gravity. The terminal stage of BH evaporation is not known. Some models predict that either a stable or unstable remnant with the mass of order of the fundamental Planck scale is formed as the evaporating BH mass approaches the Planck scale. In other models it is assumed that thermal evaporation continuous to the very end.

Most stringent limits on the ADD model come from recent LHC searches for virtual graviton effects and direct emission. While there is some model dependence in interpreting the results of these searches, generally the lower limit on the fundamental Planck scale in the ADD model is about 4 TeV at a 95 % confidence level (CL) has been established to date.

For a more comprehensive review of the current limits, see Ref. [21].

9.2.2 Probing the RS Model at the LHC

The LHC phenomenology of the RS model involves high-mass KK excitations of the graviton and, possibly, other bosons of the SM. There are many "flavors" of the RS model, with various particles allowed to propagate in the bulk, so depending on a particular realization, the graviton may not couple to all the particle species in the same way, as was the case in the ADD model. Consequently, it's important to explore various decay channels of KK graviton and also look for KK excitations of other bosons.

Another possible experimental probe for RS model is production of microscopic BH [22–24]. In general these black holes are expected to act similar to the ADD black holes for the $n = 1$ case [23], however, it has been argued [24] that because of their higher temperature and shorter lifetime, RS black holes don't have time to thermalize and decay as quantum black holes in a small number of final-state particles.

While the RS model can be described using the following two parameters: the curvature of the anti-deSitter metric k and the radius of the compact dimension R, phenomenologically it's more convenient to use a different equivalent set of parameters, namely the mass of the first graviton KK excitation $M_1 \sim 1$ TeV and the dimensionless coupling $\tilde{k} \equiv k/\overline{M}_{\rm Pl}$, where $\overline{M}_{\rm Pl} \equiv M_{\rm Pl}/\sqrt{8\pi}$ is the reduced Planck mass. The spacing between the KK modes of the graviton is given by the subsequent zeroes x_i of the Bessel function J_1 ($J_1(x_i) = 0$): $M_i = kx_i e^{-\pi kR} = \tilde{k} x_i M_D$. The coupling $\tilde{k}$ determines the strength of coupling of the graviton to the SM particles and the width of the KK excitations. Generally, it's expected that $\tilde{k} = O(10^{-2}) - O(10^{-1})$. Larger values of $\tilde{k}$ correspond to stronger coupling and broader KK resonances.

Since at the LHC limits are typically set on the mass of the first KK excitation of the graviton, $M_1 = \tilde{k} x_1 M_D \approx 3.83\,\tilde{k} M_D$, a lower limit on M_D can be inferred from a lower limit on the M_1 for any given $\tilde{k}$ as:

Table 9.1 Lower limits on the parameters M_1, M_D, and $\hat{M}$ at a 95 % CL (in TeV) in the Randall–Sundrum model for different values of the coupling parameter $\tilde{k}$

$\tilde{k}$	0.01	0.03	0.05	0.10	0.20
95 % CL limit on M_1 [26]	1.25	1.96	2.28	2.68	3.05
95 % CL limit on M_D	33	17	12	7.0	4.0
95 % CL limit on $\hat{M}$	7.0	5.3	4.4	3.2	2.3
95 % CL limit on M_1 [25]			2.03	2.39	
95 % CL limit on M_D			11	6.2	
95 % CL limit on $\hat{M}$			3.9	2.9	

$$M_D \approx \frac{M_1}{3.83\,\tilde{k}}.$$

Finally, one could also translate limits on M_1 versus $\tilde{k}$ into limits on the 5D Planck scale reduced by the warp factor $\hat{M}$ as [24]:

$$\hat{M} \approx \frac{M_1}{3.83\,\tilde{k}^{2/3}}.$$

The most stringent limits on the RS model come from searches for narrow resonances in the dillepton invariant mass spectrum in CMS [25] and ATLAS [26] experiments. These limits are shown in Table 9.1, together with the corresponding lower limits on M_D and $\hat{M}$. As can be seen from the Table, the LHC started to exclude RS model parameters beyond "natural" values of $M_D \lesssim 10$ TeV for small values of the coupling parameter $\tilde{k}$. Nevertheless, as also seen from the Table, the warped 5D Planck scale $\hat{M}$ limits largely remain within the LHC energy reach.

9.3 Black Hole Phenomenology

In general relativity, black holes are well understood if their mass M_{BH} far exceeds the Planck scale. Consequently, in the models of low-scale gravity, general relativity would give accurate description of BH properties when its mass is much greater than the fundamental Planck scale $M_D \sim 1$ TeV. As its mass decreases and approaches M_D, the BH becomes a quantum gravity object with unknown and presumably complex properties. Production of black holes at the LHC is also possible in other beyond the standard model extensions, e.g., in models with unparticles [27, 28]. For more detailed reviews of modern BH phenomenology in models with low-scale gravity, see Refs. [23, 29, 30].

In this chapter, following Refs. [19, 20], we will ignore this obstacle[2] and estimate the properties of light black holes by simple semiclassical arguments, strictly valid only for $M_{\rm BH} \gg M_D$. We expect this to be an adequate approximation, since the important experimental signatures rely on two simple qualitative properties: the absence of small couplings and the "democratic" nature of BH decays, both of which may survive as average properties of the light precursors of semiclassical black holes.

In the literature, one finds several conventions for the Planck scale M_D. In this chapter we use the definition of Ref. [20] ($M_D^{\rm GT}$), which has been also adapted by the Particle Data Group [32] and used by the LHC experiments. The other possible choice is the definition of Ref. [19] ($M_D^{\rm DL}$). There is a trivial relationship between the two conventions (see Appendix A of Ref. [20]):

$$M_D^{\rm GT} = M_D^{\rm DL} \frac{2\pi}{(16\pi^3)^{\frac{1}{n+2}}}.$$

Thus, for $n = 2$, $M_D^{\rm GT} \approx 1.3 M_D^{\rm DL}$, while for $n = 6$, $M_D^{\rm GT} \approx 2.9 M_D^{\rm DL}$.

As we expect unknown quantum gravity effects to play an increasingly important role for the BH mass approaching the fundamental Planck scale, following the prescription of Ref. [19], we do not consider BH masses below the Planck scale. It is expected that the BH production rapidly turns on, once the relevant energy threshold $\sim M_D$ is crossed. At lower energies, we expect BH production to be exponentially suppressed due to string excitations or other quantum effects.

We will first focus on the production in particle collisions and subsequent decay of small Schwarzschild black holes with the size much less than the compactification radius of extra dimensions. In this case, standard Schwarzschild solution found for a flat $(3 + n)$-dimensional metric fully applies. The expression for the Schwarzschild radius R_S of such a BH in $(3 + n)$ spacial dimensions is well known [33]:

$$R_S(M_{\rm BH}) = \frac{1}{M_D}\left[\frac{M_{\rm BH}}{M_D}\Gamma\left(\frac{n+3}{2}\right)\frac{2^n\pi^{\frac{n-3}{2}}}{n+2}\right]^{\frac{1}{n+1}}. \qquad (9.1)$$

Given $M_D \sim 1$ TeV and taking into account the fact that BH masses accessible at the current generation of particle colliders and in ultrahigh-energy cosmic ray collisions are at most a few TeV, we note that the Schwarzschild radius of such black holes is $\sim 1/M_D$, i.e. indeed much smaller than the size of large extra dimensions even when their number approaches six or seven (the preferred number of extra dimensions expected in string theory). We also note that for $M_{\rm BH} \sim M_D$ the Schwarzschild radius does not depend significantly on the number of extra dimensions n.

Given the current lower constraints on the fundamental Planck scale in the model with large extra dimensions of several TeV, the black holes that we may be able to study at colliders and in cosmic rays will be barely transplanckian. Hence, the unknown quantum corrections to their classical properties are expected to be large, and therefore it is reasonable to focus only on the most robust properties of these

[2] Some of the properties of the "stringy" subplanckian "precursors" of black holes are discussed in Ref. [31] and later in this chapter.

mini black holes that are expected to be affected the least by unknown quantum gravity corrections. Consequently, when discussing production and decay of black holes, we do not consider the effects of spin and other BH quantum numbers, as well as grey-body factors. Further in this chapter, we discuss some of the subsequent attempts to take these effects into account using semiclassical approximation.

9.3.1 Black Hole Production in Particle Collisions

Consider two partons with the center-of-mass energy $\sqrt{\hat{s}} = M_{\rm BH}$ colliding head-on. Semiclassical reasoning suggests that if the impact parameter of the collision is less than the Schwarzschild radius R_S, corresponding to this energy, a BH with the mass $M_{\rm BH}$ is formed. Therefore the total cross section of BH production in particle collisions can be estimated from pure geometrical arguments and is of order πR_S^2.

Soon after the original calculations [19, 20] have appeared, it has been suggested [34, 35] that the geometrical cross section is in fact exponentially suppressed, based on the Gibbons–Hawking action [36] argument. Detailed subsequent studies performed in simple string theory models [31], using full general relativity calculations [37–39], or a path integral approach [40–42] did not confirm this finding and proved that the geometrical cross section is modified only by a numeric factor of order one. A flaw in the Gibbons–Hawking action argument of [34] was further found in [43]: the use of this action implies that the BH has been already formed, so describing the evolution of the two colliding particles before they cross the event horizon and form the BH via Gibbons–Hawking action is not justified. By now there is a broad agreement that the production cross section is not significantly suppressed compared to a simple geometrical approximation, which we will consequently use through this review.

Using the expression (9.1) for the Schwarzschild radius [33], we derive the following parton level BH production cross section [19]:

$$\sigma(M_{\rm BH}) \approx \pi R_S^2 = \frac{\pi}{M_D^2}\left[\frac{M_{\rm BH}}{M_D}\Gamma\left(\frac{n+3}{2}\right)\left(\frac{2^n\pi^{\frac{n-3}{2}}}{n+2}\right)\right]^{\frac{2}{n+1}}. \qquad (9.2)$$

In order to obtain the production cross section in pp collisions at the LHC, we use the parton luminosity approach [19, 20, 44]:

$$\frac{d\sigma(pp \to {\rm BH} + X)}{dM_{\rm BH}} = \frac{dL}{dM_{\rm BH}}\hat{\sigma}(ab \to {\rm BH})\Big|_{\hat{s}=M_{\rm BH}^2},$$

where the parton luminosity $dL/dM_{\rm BH}$ is defined as the sum over all the types of initial partons:

$$\frac{dL}{dM_{\rm BH}} = \frac{2M_{\rm BH}}{s} \sum_{a,b} \int_{M_{\rm BH}^2/s}^{1} \frac{dx_a}{x_a} f_a(x_a) f_b(\frac{M_{\rm BH}^2}{s x_a}),$$

and $f_i(x_i)$ are the parton distribution functions.

Nevertheless, the above formulas may be modified due to inelasticity (energy/momentum loss) in the collision that creates a BH. The losses can happen due to the fact that not the entire energy of the colliding partons is trapped behind the event horizon [45].

9.3.2 Black Hole Evaporation

In general relativity, BH evaporation is expected to occur in three distinct stages: "balding," spin-down, and Hawking evaporation. During the first stage, the BH loses its multipole momenta and quantum numbers via emission of gauge bosons until it reaches the Kerr solution for a spinning BH; at the second stage it gets rid of the residual angular momentum and becomes a Schwarzschild BH; and at the last stage it decays via emission of black-body radiation [46] with a characteristic Hawking temperature [19, 20]:

$$T_H = \frac{n+1}{4\pi R_S} \tag{9.3}$$

of $\sim$1 TeV.

Note that if a certain quantum number (e.g., $B-L$) is gauged, it will be conserved in the process of BH evaporation. Since the majority of black holes at the LHC are produced in quark-quark collisions, one would expect many of them to have the baryon number and fractional electric charge. Consequently, the details of BH evaporation process will allow to determine if these quantum numbers are truly conserved.

In quantum gravity, it is expected that there is a fourth, Planckian stage of BH evaporation, which is reached when the mass of the evaporating BH approaches the Planck scale. The details of the Planckian stage are completely unknown, as they are governed by the effects of quantum gravity, which should be dominant at such low BH masses. Some authors speculate that the Planckian stage terminates with a formation of a stable or semistable BH remnant with the mass $\sim M_{\rm Pl}$. Others argue that the evaporation proceeds until the entire mass of the BH is radiated. The truth is that no predictions about the Planckian regime are possible, given our lack of knowledge of quantum gravity.

The average multiplicity of particles produced in the process of BH evaporation is given by: $\langle N \rangle = \left\langle \frac{M_{\rm BH}}{E} \right\rangle$, where E is the energy spectrum of the decay products. In

order to find $\langle N \rangle$, we note that evaporation is a black-body radiation process, with the energy flux per unit of time given by Planck's formula:

$$\frac{df}{dx} \sim \frac{x^3}{e^x + c}, \tag{9.4}$$

where $x \equiv E/T_H$, and c is a constant, which depends on the quantum statistics of the decay products ($c = -1$ for bosons, $+1$ for fermions, and 0 for Boltzmann statistics).

The spectrum of the decay products in the massless particle approximation is given by: $\frac{dN}{dE} \sim \frac{1}{E}\frac{df}{dE} \sim \frac{x^2}{e^x+c}$. For averaging the multiplicity, we use the average of the distribution in the inverse particle energy:

$$\left\langle \frac{1}{E} \right\rangle = \frac{1}{T_H} \frac{\int_0^\infty dx \frac{1}{x}\frac{x^2}{e^x+c}}{\int_0^\infty dx \frac{x^2}{e^x+c}} = \frac{a}{T_H}, \tag{9.5}$$

where a is a dimensionless constant that depends on the type of produced particles and numerically equals 0.68 for bosons, 0.46 for fermions, and $\frac{1}{2}$ for Boltzmann statistics. Since a mixture of fermions and bosons is produced in the BH decay, we can approximate the average by using Boltzmann statistics, which gives the following formula for the average multiplicity: $\langle N \rangle \approx \frac{M_{\rm BH}}{2T_H}$. Using expression (9.3) for Hawking temperature, we obtain:

$$\langle N \rangle = \frac{2\pi}{n+1} \left(\frac{M_{\rm BH}}{M_D} \right)^{\frac{n+2}{n+1}} \left(\Gamma\left(\frac{n+3}{2} \right) \frac{2^n \pi^{\frac{n-3}{2}}}{n+2} \right)^{\frac{1}{n+1}}, \tag{9.6}$$

which corresponds to about half-a-dozen for typical BH masses accessible at the LHC. Note that the above formula is only applicable to semiclassical black holes; a recent work suggests that for black holes with the mass close to the Planck scale Hawking radiation occurs at a lower temperature and results in a higher number of softer particles emitted [47].

Naïvely, one would expect that a large fraction of Hawking radiation is emitted in the form of gravitons, escaping in the bulk space. However, as was shown in Ref. [18], this is not the case, since the wavelength $\lambda = \frac{2\pi}{T_H}$ corresponding to the Hawking temperature is larger than the size of the BH. Therefore, the BH acts as a point-radiator and consequently emits mostly s-waves. Since the s-wave emission is sensitive only to the radial coordinate, bulk radiation per graviton degree of freedom is the same as radiation of any standard model degree of freedom on the brane. While many angular degrees of freedom are available in the bulk space, the s-wave emission cannot take advantage of them, thus suppressing bulk graviton component. Since there are many more particles on the brane than in the bulk space, this has the crucial consequence that the BH mainly decays to visible standard model particles.

Since the gravitational coupling is flavor-blind, a BH emits all the $\approx$120 standard model particle and antiparticle degrees of freedom with roughly equal probability. Accounting for the colour and spin and ignoring the graviton emission, we expect

≈75 % of particles produced in BH decays to be quarks and gluons, ≈10 % charged leptons, ≈5 % neutrinos, and ≈5 % photons or W/Z bosons, each carrying hundreds of GeV of energy. Similarly, if there exist new particles with masses $\lesssim$100 GeV, they would be produced in the decays of black holes with the probability similar to that for the standard model species. For example, a sufficiently light Higgs boson is expected to be emitted with ∼1 % probability. This has exciting consequences for searches for new physics at the LHC and beyond, as the production cross section for any new particle via this mechanism is large and depends only weakly on the particle mass, in contrast with an exponential dependence characteristic of direct production.

A relatively large fraction of prompt and energetic photons, electrons, and muons expected in the high-multiplicity BH decays would make it possible to select pure samples of black holes, which are also easy to trigger on [19, 20]. At the same time, only a small fraction of particles produced in the BH decays are undetectable gravitons and neutrinos, so most of the BH mass is radiated in the form of visible energy, making it easy to detect.

It has been argued [48] that the fragmentation of quarks and jets emitted in the BH evaporation might be significantly altered by the presence of a dense and hot QCD plasma ("chromosphere") around the event horizon. If this argument is correct, one would expect much softer hadronic component in the BH events. However, we would like to point out that one would still have a significant number of energetic jets due to the decay of weakly interacting W/Z and Higgs bosons, as well as tau leptons, emitted in the process of BH evaporation and penetrating the chromosphere before decaying into jetty final states. In any case, tagging of the BH events by the presence of an energetic lepton or a photon and large total energy deposited in the detector is a fairly model-independent approach.

The lifetime of a BH can be estimated using Stefan's law of thermal radiation. Since BH evaporation occurs primarily in three spatial dimensions, the canonical three-dimensional (3D) Stefan's law applies, and therefore the power dissipated by the Hawking radiation per unit area of the event horizon is $p = \sigma T_H^4$, where σ is the Stefan-Boltzmann constant and T_H is the Hawking temperature. Since the effective evaporation area of a BH is the area of a 3D-sphere with radius R_S and Stefan's constant in natural units is $\sigma = \pi^2/60 \sim 1$, dropping numeric factors of order unity we obtain the following expression for the total power dissipated by a BH: $P \sim R_S^2 T_H^4 \sim R_S^{-2}$.

The BH lifetime τ then can be estimated as: $\tau \sim M_{\rm BH}/P \sim M_{\rm BH} R_S^2$, and using (9.1) we find:

$$\tau \sim \frac{1}{M_D} \left(\frac{M_{\rm BH}}{\rm M_D} \right)^{\frac{n+3}{n+1}} . \tag{9.7}$$

Therefore, a typical lifetime of a mini BH is $\sim 10^{-27} - 10^{-26}$ s. A multi-TeV BH would have a relatively narrow width ∼100 GeV, i.e. similar to, e.g., a W' or Z' resonance of a similar mass. This is not surprising, as the strength of gravity governing the BH evaporation rate is similar in the model with large extra dimensions to that of electroweak force responsible for the W' or Z' decay rates.

9.3.3 Accounting for the Black Hole Angular Momentum and Grey-Body Factors

In the above discussion we used a number of approximations in deriving production cross section and decay properties of mini black holes. While reliable accounting for more complicated effects related to quantum properties of black holes (spin, quantum numbers, etc.) is not possible without intimate knowledge of the underlying theory of quantum gravity, a number of authors attempted to estimate some of the above effects using simple semiclassical approach. While we don't believe that these estimates are any more reliable than the ones obtained in the above simple approximation, we discuss these refinements here in some detail.

The most studied properties of mini black holes beyond our simple picture are the effects of its angular momentum and grey-body factors, which have to do with the emissivity of particles of various types in the process of BH evaporation.

An emissivity of a certain type of particle depends, in general, on its spin, S. Indeed, for a small BH the Schwarzschild radius is comparable with the Compton wavelength of the emitted particles. Thus the wave function of a spin-0 particle would have more overlap with the BH event horizon than that for a spin-1/2 or spin-1 particle. Consequently, one would expect that scalar particles are emitted by a BH more efficiently than spin-1/2 or higher-spin particles. This qualitative feature can be parameterized as a grey-body factor, $g(S, x)$, where $x = E/T_H$ is a dimensionless variable proportional to the energy of the particle. Thus, the modified expression (9.4) for the emitted flux is:

$$\frac{df}{dx} \sim \frac{g(S, x)x^3}{e^x + c}. \tag{9.8}$$

The grey-body factors can be calculated classically in general relativity. This calculation has been extended recently to the case of multidimensional black holes in the model with large extra dimensions by a number of authors [49–61].

In special cases, the grey-body factors can be calculated analytically, but most general calculations that exist to date are performed numerically. The grey-body factor for the emissivity of spin-1/2 particles as a function of their energy is given in Fig. 9.1 from Ref. [53]. As seen from the figure, the effect of grey-body factors is small for characteristic black-body radiation energies and $n \geq 2$.

Not so long ago, grey-body factors for the brane and bulk emission of gravitons have been calculated as well [54–60]. While complete calculations applicable to all graviton energies are not available yet, it appears that the fraction of Hawking radiation of bulk and brane gravitons is relatively small, except for the cases of very high BH angular momentum or very large number of extra dimensions ($n = 7$).

Since black holes in particle collisions are produced by particles with non-vanishing impact parameter, they may carry non-zero angular momentum and thus produce a spinning BH. Given that the characteristic impact parameter is R_S, while the relative momentum of the colliding particles is M_{BH}, one expects a BH produced in such a grazing collision to carry angular momentum

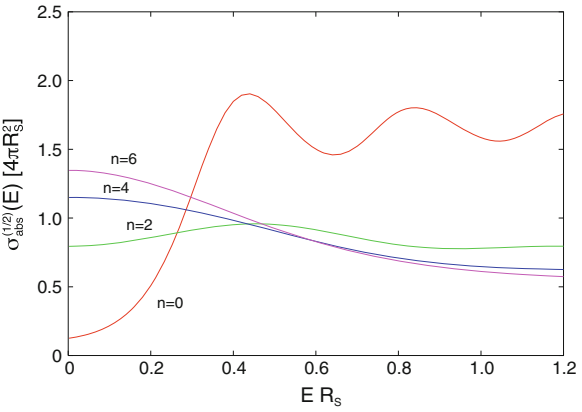

Fig. 9.1 Grey-body factors for the emissivity of spin-1/2 particles on the brane as a function of their energy, E. *Vertical axis* shows the effective area of the black hole horizon for the emission of a spin-1/2 particle expressed in the units of the geometrical surface of the event horizon of a three-dimensional black hole, $4\pi R_S^2$. From Ref. [53]

$$L \sim R_S M_{\rm BH} \sim \left(\frac{M_{\rm BH}}{M_D}\right)^{\frac{n+2}{n+1}}.$$

For black holes with masses close to the fundamental Planck scale, typical angular momentum is of the order of one. Note that although numerically this is rather small angular momentum, it is close to the maximum angular momentum that a BH of such a small mass could have.

For a rotating BH, the solution of Einstein's equation is given by Kerr's, rather than Schwarzschild's formula and contains explicit dependence on the angular momentum of the BH. A number of authors have studied properties of Kerr black holes in theories with extra dimensions [62–75]. Both the spin-down effects and modification of the grey-body factors due to the angular momentum of the BH have been looked at. In general, for a large number of extra dimensions and for a large initial angular momentum of the BH it is expected that modification of the classical black-body radiation picture becomes non-trivial and will have to be taken into account for an accurate description of BH evaporation.

Several authors looked at other details of Hawking evaporation process. The effects of using the microcanonical ensemble approach, which takes into account that the energy of the emitted particles is comparable to the BH mass, have been discussed in Refs. [76, 77] and generally result in the increased BH lifetime. The recoil effect in the evaporation has been studied [78] as well.

To summarize, while the recent angular momentum and grey-body factor studies are important and encouraging, for the black holes with the masses close to the fundamental Planck scale they are likely to be modified in a profound way via

unknown quantum corrections. Thus, detailed studies of the particle content in BH evaporation probably won't be possible until either their discovery at the LHC or a formulation of a complete theory.

An interesting possibility studied in Ref. [31] is production of a precursor of a BH, i.e. a long and jagged highly exited string state, dubbed as a "string ball" due to its folding in a ball-like object via a random walk. As shown in Ref. [31], there are three characteristic string ball production regimes, which depend on the mass of the string ball M, the string scale $M_S < M_D$, and the string coupling $g_s < 1$. For $M_S < M < M_S/g_s$, the production cross section increases $\propto M^2$, until it reaches saturation at $M \sim M_S/g_s$ and stays the same up to the string ball mass $\sim M_S/g_s^2$, at which point a BH is formed and the production cross section agrees with that from Refs. [19, 20].

A string ball has properties similar to those of a BH, except that its evaporation temperature, known as Hagedorn temperature [79], is constant: $T_S = M_S/(2\sqrt{2}\pi)$. Thus, the correlation between the temperature of the characteristic spectrum and the string ball mass may reveal the transition from the Hagedorn to Hawking regime, which can be used to estimate M_S and g_s. Another possibility is a production of higher-dimensional objects, e.g. black p-branes, rather than spherically symmetric black holes ($p = 0$) [80]. For a detailed review see, e.g. Ref. [83].

Finally, for a BH mass close to M_D, the formation and decay of BH may not allow for thermalization. In this case, the BH would decay not thermally, but as a quantum object, typically in a pair of particles. Most often such a quantum black hole would decay into pair of jets, but if baryon and/or lepton number(s) are violated in the decay, other decays, e.g. into a quark and a lepton, or a pair of leptons is possible. For more details on the properties of quantum black holes see Refs. [84–86].

9.3.4 Simulation of Black Hole Production and Decay

In order to study properties of black holes at colliders, it's important to have tools capable of simulating their production and decay. Currently, there are three modern Monte Carlo generators capable of describing semiclassical BH production and decay: BlackMax [87, 88], Charybdis [89, 90], and CatFish [86, 91]. They are capable of simulating both rotating and non-rotating black holes, with stable or unstable remnant, with variety of models of energy/momentum loss in collision and evaporation models. For quantum black holes, the main simulation package is QBH [86].

All these generators have been successfully interfaced with the LHC detector simulation packages. For the experimental results covered in this chapter, Charybdis (v1 and v2), BlackMax, and QBH event generators have been used.

9.3.5 Randall–Sundrum Black Holes

Mini black holes can be also produced in TeV particle collisions in the RS model [22–24, 92–95]. In this case, the warp-factor-suppressed Planck scale, $\hat{M} \sim M_D \sim 1$ TeV, plays the role of the fundamental Planck scale in the model with large extra dimensions.

The event horizon of RS black holes has a pancake shape with the radius in the fifth dimension suppressed compared to the radius R_S on the standard model brane by the warp factor $e^{-\pi kR}$. Thus, for $R_S e^{-\pi kR} \ll \pi R$, the BH can be considered "small" and has properties similar to that in the $n = 1$ (5D) large extra dimensions scenario, if the effects of the curvature of the AdS space at the standard model brane are ignored.

In order to derive properties of RS black holes, it is convenient to introduce the fundamental 5D Planck scale M, which enters the Lagrangian of the RS model. The relationship between the reduced 4-dimensional Planck scale $\overline{M}_{\rm Pl}$ and M is as follows: $\overline{M}_{\rm Pl}^2 = \frac{\hat{M}^3}{k}(1 - e^{-2\pi kR}) \approx \hat{M}^3/k$. Since k is 0.01–0.1 $\times$ $\overline{M}_{\rm Pl}$, $\hat{M} =$ 0.2–0.5 $\times$ $\overline{M}_{\rm Pl}$, i.e. both the 5D and 4D Planck scales are of the same order. Since the curvature of the slice of the AdS space is given by $k^2/M^2 \sim \tilde{k}^2 \ll 1$ [92–95], one can indeed ignore higher-order curvature effects and consider RS black holes as if they were black holes in flat Minkowski space.

The Schwarzschild radius of a BH of mass $M_{\rm BH}$ is given by [16, 33, 92–94][3]:

$$R_S = \frac{1}{\pi M e^{-\pi kR}} \sqrt{\frac{M_{\rm BH}}{3 M e^{-\pi kR}}}.$$

Taking into account $M^3 \approx k\overline{M}_{\rm Pl}^2 = M_D^2 k e^{2\pi kR}$, we get:

$$R_S \approx \frac{1}{\sqrt{3}\pi M_D} \sqrt{\frac{M_{\rm BH}}{\tilde{k} M_D}}. \tag{9.9}$$

Since the expression under the square root is ~10 for a typical range of $M_{\rm BH}/M_D = O(1)$ and $k/\overline{M}_{\rm Pl} = O(0.01)$, we find that a typical Schwarzschild radius of the Randall–Sundrum BH is $R_S \sim 1/M_D \sim 1$ TeV^{-1}, similar to that for black holes in models with large extra dimensions. Indeed, using (9.1) for the ADD model with $n = 1$, we get:

$$R_S(\text{ADD}, 5D) = \frac{1}{M_D} \sqrt{\frac{2M_{\rm BH}}{3\pi M_D}},$$

which turns into (9.9) for $\tilde{k} = \frac{1}{2\pi} \approx 0.16$.

[3] Note that this expression differs from the analogous expression (9) in Ref. [22] by a $\sqrt{2}$ factor; the difference stems from the fact that the mass parameter M used in Ref. [22] is different from the true 5D Planck scale, that enters in the Lagrangian of the model, which we refer to as M in this chapter.

Moreover, it is easy to see that such a BH is still small from the point of view of the 5th dimension, as the condition of the BH "smallness" mentioned above can be expressed as:

$$R_S \ll \frac{\pi R}{\exp(-\pi k R)} = \frac{k\pi R}{\frac{k}{\overline{M}_{\rm Pl}}\overline{M}_{\rm Pl}\exp(-\pi k R)} = \frac{k\pi R}{M_D \tilde{k}} \sim \frac{36}{M_D \tilde{k}}.$$

Given that $\tilde{k}$ is between 0.01 and 0.1, the inequality becomes:

$$R_S \ll \frac{360 - 3{,}600}{M_D},$$

which is clearly satisfied for $R_S \sim 1/M_D$. In fact, one would need to produce a BH with the mass $\sim 10^6$ TeV to exceed this limit. Such energy is achievable neither at any foreseen collider nor in fixed-target collisions of ultra-high-energy particles from cosmic accelerators.

Hawking temperature of a Randall–Sundrum BH can be found from expression (9.3) for a BH in models with large extra dimensions by requiring $n = 1$, i.e.

$$T_H = \frac{1}{2\pi R_S}, \tag{9.10}$$

which, given $R_S \sim 1/M_D$, makes it very similar to that for the case of large extra dimensions. Consequently, for the preferred range of model parameters both the production cross section and the decay properties of a Randall–Sundrum BH are very similar to those of a ADD one. In fact, both the BLACKMAX and CHARYBDIS generators can be used to simulate RS black holes by setting $n = 1$ and using an appropriate choice for M_D. Nevertheless, given the arguments of Ref. [24] of potential non-thermality and inelasticity in RS black hole formation, experimental searches so far only focused on quantum RS black holes decaying non-thermally in a pair of particles.

There has been a suggestion [96] that black holes in the RS and ADD models can nevertheless be distinguished by the different dynamics of an early stage of BH evaporation due to the fact that the angular momentum of a Randall–Sundrum BH, unlike that for a BH in large extra dimensions, cannot have any bulk component (due to the existence of a discrete Z_2 orbifold symmetry). Thus, bulk evaporation for a Randall–Sundrum BH is suppressed compared to that for a BH of a similar mass in models with large extra dimensions. Since it is argued that the bulk component of Hawking radiation of gravitons for a BH in large extra dimensions may be significant during the early stages of its evaporation, it is suggested that the BH evaporation may result in less missing energy in the RS scenario.

There also have been studies of modification of BH properties due to Gauss–Bonnet or Lovelock terms added to the Einstein–Hilbert action. These modifications affect properties of black holes in models with either large or warped extra dimensions. Additional terms could naturally introduce a minimum threshold on the

BH mass. For detailed studies of modifications related to these higher-order terms, see [92–95].

9.3.6 Limits on Semiclassical Black Holes

The CMS experiment has pioneered searches for microscopic black holes with the very first LHC data at $\sqrt{s} = 7$ TeV [97]. Already with this small amount of data, corresponding to an integrated luminosity of just 0.034 fb^{-1}, stringent limits on semiclassical BH production were set, using a novel method of predicting the dominant background coming from QCD multijet production. The analysis since then has evolved considerably and its later reincarnations [98, 99] probed many more additional BH models, including quantum black holes and string balls. Here we summarize the most recent analysis [99] based on a $\sqrt{s} = 8$ TeV data sample with an integrated luminosity of 12.1 fb^{-1}.

This analysis was performed in inclusive final states, thus maximizing the sensitivity to BH production and decay. Semiclassical black holes are expected to evaporate in a large ($\sim$10) number of energetic particles, emitted nearly isotropically, with the major fraction of the emitted particles being quarks and gluons [19], resulting in a multijet final state. Quantum effects and grey-body factors may change the relative fraction of emitted quarks and gluons, but generally it is expected that these particles appear most often even in the decays of quantum black holes or their precursors, due to a large number of color degrees of freedom that quarks and gluons possess, compared to other SM particles.

The discriminating variable between the signal and the dominant QCD multijet background used in the search is the scalar sum of transverse momenta of all particles in the event, for which the p_T value exceeds 50 GeV. This variable, S_T, was further corrected for any significant missing transverse momentum $\not{E}_T$ in the event by adding the $\not{E}_T$ value to the S_T variable, if the former exceeds 50 GeV. The choice of S_T as the discriminating variable is very robust and rather insensitive to the exact particle content in the process of BH evaporation, as well to the details of the final, sub-Planckian evaporation phase. The addition of $\not{E}_T$ to the definition of S_T further ensures high sensitivity of the search for the case of stable non-interacting remnant with the mass of order of the fundamental Planck scale, which may be produced in the terminal stage of the BH evaporation process.

The main challenge of the search is to describe the inclusive multijet background in a robust way, as the BH signal corresponds to a broad enhancement in the S_T distribution at high end, rather than a narrow peak. Since the BH signal is expected to correspond to high multiplicity of final-state particles, one has to reliably describe the background for large jet multiplicities, which is quite challenging theoretically, as higher-order calculations that fully describe multijet production simply do not exist. Thus, one can not rely on the Monte Carlo simulations to reproduce the S_T spectrum correctly.

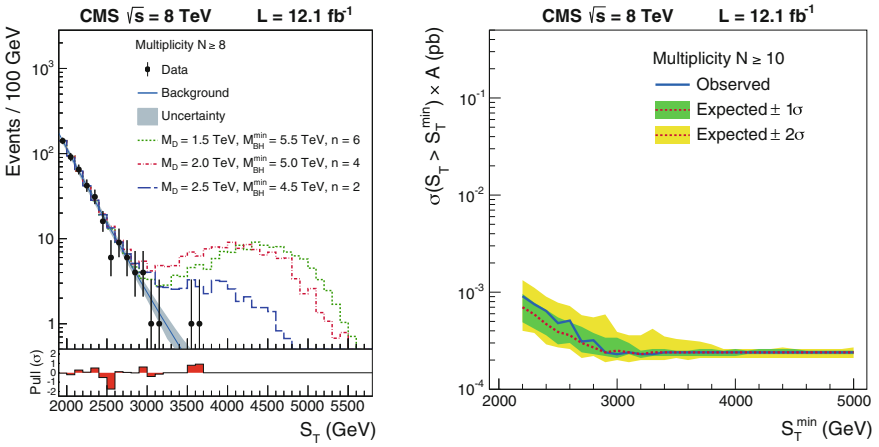

Fig. 9.2 *Left* predicted QCD multijet background with its uncertainties (the *shaded band*), data, and several reference BH signal benchmarks, as a function of S_T, in the final state with the multiplicity of eight or more particles. *Right* model-independent upper limits at a 95 % CL on the cross section of a new physics signal decaying in the final state with 10 or more particles, as a function of the minimum S_T requirement. From Ref. [99]

To overcome this problem, the CMS Collaboration developed and utilized a novel method of predicting the QCD background directly from collision data. It has been found empirically, first via simulation-based studies, and then from the analysis of data at low jet multiplicities that the shape of the S_T distribution for the dominant QCD multijet background does not depend on the multiplicity of the final state, above a certain turn-on threshold. This observation, motivated by the way parton shower is developed via nearly collinear emission, which conserves S_T, allows one to predict S_T spectrum of a multijet final state using low-multiplicity QCD events, e.g. dijets or three-jet events. This provides a powerful method of predicting the dominant background for BH production by taking the S_T shape from dijet events, for which the signal contamination is expected to be negligible, and normalizing it to the observed spectrum at high multiplicities at the low end of the S_T distribution, where signal contamination is negligible even for large multiplicities of the final-state objects. The results are shown in Fig. 9.2 (left).

The CMS data with high final-state multiplicities is well fit by the background shape obtained from the dijet events, No excess characteristic of a BH production is observed even for highest multiplicities. This lack of an apparent signal can be interpreted in a model-independent way by providing a limit on the cross section for any new physics signal for S_T values above a certain cutoff, for any given inclusive final-state multiplicity. An example of such a limit is shown in Fig. 9.2 (right), for the final-state multiplicity $N \geq 10$. For signals corresponding to large values of S_T (above 2 TeV or so) the cross section limit reaches ∼0.3 fb. These limits can be compared with the production cross section for black holes in a variety of models and used to set limits on the minimum BH mass ($M_{\mathrm{BH}}^{\mathrm{min}}$) that can be produced in

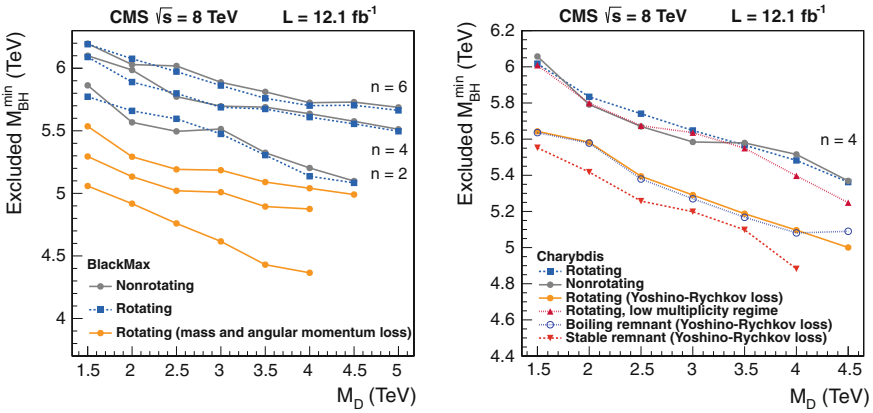

Fig. 9.3 Limits on the minimum BH mass as a function of the fundamental Planck scale for a few semiclassical benchmark models with and without BH rotation and with or without a remnant. Note that the semiclassical approximation used in setting these limits is not expected to hold for BH masses close to the Planck scale. From Ref. [99]

these models. They are also applicable to other final states, e.g., from cascade decays of massive supersymmetric particles, thus making the search even more general. In fact, this very limit has been recently reinterpreted in terms of constraints on supersymmetry in Ref. [100].

For several specific models of semiclassical black holes limits have been set explicitly via optimization of the analysis for these particular scenarios. These limits, although not very reliable for the BH masses approaching the fundamental Planck scale, are shown in Fig. 9.3.

The ATLAS Collaboration performed a number of searches for semiclassical black holes in specific final states, including those with possible lepton or baryon number violation. While more model-dependent than generic CMS searches, they are complementary to the multiobject search approach used in CMS and have an advantage of lower (and different) backgrounds. The combination of the two approaches allows to cover rather large landscape of possible signatures and scenarios.

The first search from ATLAS explored like-sign dimuon final state [101], which has very low standard model background. The analysis was based of a data sample of pp collisions with an integrated luminosity of 1.3 fb^{-1} at the center-of-mass energy $\sqrt{s} = 7$ TeV. The track multiplicity in the event was used as a discriminating variable between the SM background (relatively low track multiplicity) and a BH signal (large track multiplicity). Most recent version of this analysis is based on an integrated luminosity of 20 fb^{-1} at the center-of-mass energy $\sqrt{s} = 8$ TeV [102] and set limits on non-rotating and rotating black holes in the ADD model for $n = 2, 4$, and 6 between 4 and 6 TeV, for the range of M_D between 1 and 3 TeV, see Fig. 9.4 (left). Note that the limits set in this search are very model-dependent, as in calculation of the (small) like-sign dimuon branching fraction, they assume conservation of all the quantum numbers and fixed classical grey-body factors; none of these assumptions

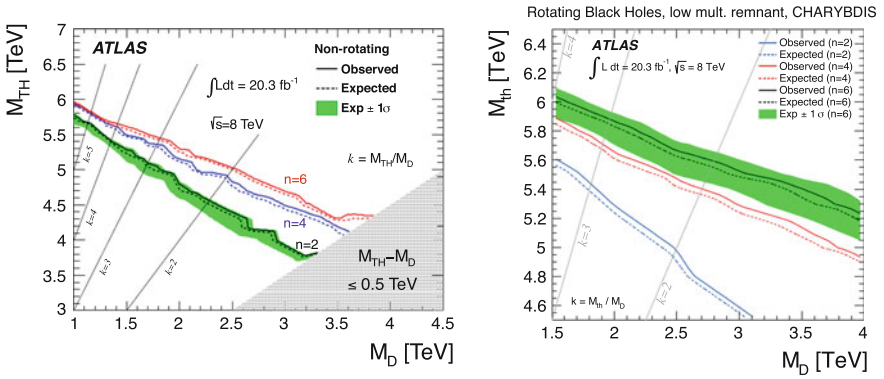

Fig. 9.4 *Left* limits on the minimum BH mass as a function of the fundamental Planck scale for non-rotating ADD black holes for $n = 2$, 4, and 6 from the like-sign dimuon analysis. From Ref. [102]. *Right* limits on the minimum BH mass as a function of the fundamental Planck scale for rotating ADD black holes with low-multiplicity remnant decay for $n = 2$, 4, and 6. From Ref. [104]. The *thin dotted lines* $k = 2$–5 indicate the minimum black hole mass equal to $k\ M_D$

may hold for black holes close to the production threshold, thus potentially changing the branching fraction dramatically.

Another class of searches conducted by ATLAS includes lepton+jets channel. Similar to the previous search, it was first conducted based on a data sample with an integrated luminosity of 1.6 fb^{-1} at $\sqrt{s} = 7$ TeV [103] and recently was superseded by a similar search based on an integrated luminosity of 20.3 fb^{-1} at $\sqrt{s} = 8$ TeV [104]. The discriminating variable in this search is the total scalar transverse momentum sum of the lepton and energetic jets, similar to the S_T variable employed in the CMS search. The lepton+jets analysis explored a variety of models with rotating and non-rotating black holes, high- and low-multiplicity decaying remnant, lepton number violation, as well as with production energy/momentum loss. Limits on the minimum BH mass set in these models range from 4.5 to 6.0 TeV for the range of M_D between 1.5 and 4 TeV, see Fig. 9.4 (right). While a similar caveat about the assumed branching fractions also applies to this search, given relatively high probability of lepton or jet emission in the BH decay, the results are less model-dependent as in the like-sign dimuon case.

As can be seen from the CMS and ATLAS results, the excluded minimum BH masses reach 5–6 TeV, which is close to the energy limit of the LHC machine at $\sqrt{s} = 8$ TeV. Therefore, the present searches are completely energy limited and will gain a significant boost once the LHC is restarted at $\sqrt{s} = 13$ TeV in 2015. Even with early high-energy data, significantly higher BH masses and fundamental Planck scale values could be probed. Nevertheless, it is clear that if an excess is found in these searches, we would be dealing with fundamentally quantum objects, given that the fundamental Planck scale limits from other searches already reached ∼5 TeV. Thus it is very important to also look for quantum black holes, which are expected to decay before they thermalize, resulting in just a few particles in the final state.

9.3.7 Limits on Quantum Black Holes and String Balls

The ATLAS Collaboration has pioneered searches for quantum black holes with early 2010 data, corresponding to an integrated luminosity of 0.036 fb^{-1} at $\sqrt{s} = 7$ TeV, using the dijet invariant mass spectrum in an inclusive dijet final state [105]. While quantum black holes are not resonances, their production is expected to turn on sharply at a threshold close to M_D, while steeply falling parton distribution functions result in the cross section dropping fast above the threshold. This behavior results in a rather narrow peak-like invariant mass distribution, resembling a resonant shape. Thus standard searches for resonances in two-body final states can be interpreted as searches for quantum black holes by replacing a Gaussian or Breit–Wigner resonant shape with a template typical of a BH. Given that quantum black holes are expected to decay in two colored partons in most of the cases [84, 85], there is little model dependence for searches in the dijet final states. The original dijet analysis was later repeated with an integrated luminosity of 4.8 fb^{-1} at the same energy [106], and is based on the invariant mass spectrum and coarse angular information for the dijet system. It sets a lower limit on the M_D of around 4 TeV, assuming that quantum black holes are produced with the minimum mass equal to M_D, see Fig. 9.5.

Searches for quantum black holes have also been conducted by ATLAS in the dilepton [26], lepton+jet [107], and photon+jet [108] final states. The second final state is also used to look for semiclassical black holes, except that the semiclassical BH search is based on an inclusive S_T spectrum rather than on the two-body invariant mass spectrum. The branching fractions in these final states are significantly more model dependent than in the dijet final state. These searches are complementary to the dijet search as they can explicitly probe lepton or baryon number violation in quantum BH decays. All three searches have been conducted at $\sqrt{s} = 8$ TeV

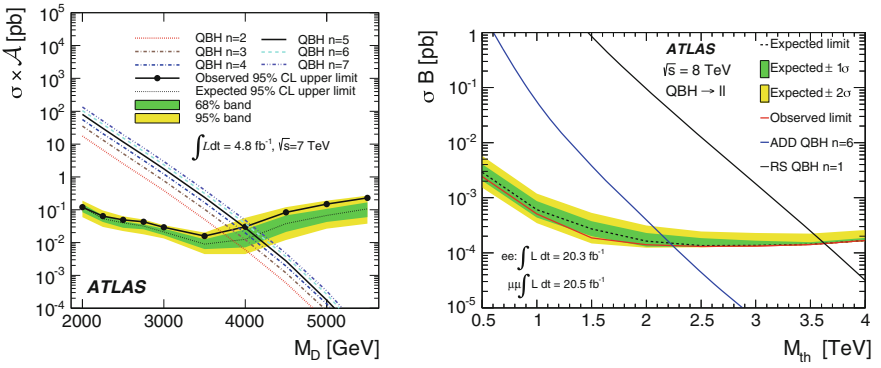

Fig. 9.5 *Left* limits on the fundamental Planck scale M_D in the ADD model for quantum black holes using dijet data. From Ref. [106]. *Right* limits on the minimum quantum black hole mass in the ADD and RS models using dilepton data. From Ref. [26]

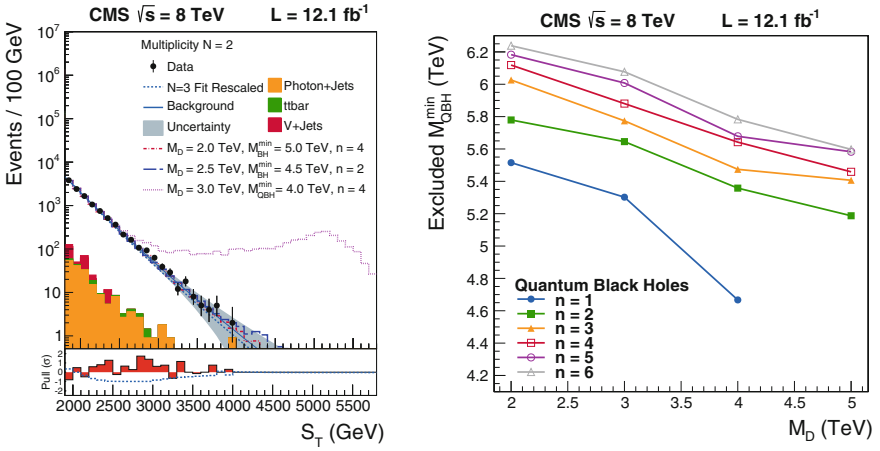

Fig. 9.6 *Left* the $N = 2$ S_T spectrum with the background extrapolated from the low-S_T region. The *dashed blue line* shows an alternative background prediction based on $N = 3$ S_T spectrum. A benchmark quantum BH signal is shown with a *dotted magenta line*. *Right* limits on the minimum quantum BH mass for various numbers of extra dimensions. The $n = 1$ case corresponds to limits in the Randall–Sundrum model. From Ref. [99]

with an integrated luminosity of 20.3 fb^{-1}. The limits set by these analyses are expressed in terms of minimum BH mass and reach 3.65, 4.6, and 5.3 TeV at a 95 % confidence level for ADD quantum black holes for $n = 6$ in the dilepton, lepton+jet, and photon+jet analyses, respectively. The dilepton analysis also set a limit on RS black holes, excluding their production with the masses below 2.24 TeV (see Fig. 9.5 (right)). In the case of RS black holes the threshold BH mass is expected to be close to the five-dimensional Planck scale $\hat{M}$.

The inclusive S_T-based CMS analysis [99] that was used to set limits on semiclassical black holes, can be also used to set limits on quantum black holes. In this case, the result is based on the S_T spectrum at low final-state object multiplicity ($N = 2$). Given that for $N = 2$ one would expect a contamination of the S_T spectrum from signal, the QCD background at large S_T is predicted by simply extrapolating the fit function from the low-S_T range, which has negligible signal contamination and thus can be used to determine the parameters of a smooth background template (see Fig. 9.6). The background prediction obtained in this way is also checked by comparing it with the prediction based on the template obtained from the $N = 3$ spectrum (dashed blue line), which falls well within the uncertainties of the extrapolated background estimate. In this case, CMS also sets limits on RS quantum black holes (shown in the plot as $n = 1$).

Another search for quantum black holes in CMS was done using the dijet invariant mass spectrum [109] obtained in the $\sqrt{s} = 7$ TeV dataset with an integrated luminosity of 5 fb^{-1}. In this case, the spectrum is fit with a sum of a smooth background template and a signal mass template obtained for these black holes in simulation [see Fig. 9.7 (left)]. The analysis is a part of a general program of dijet resonance searches

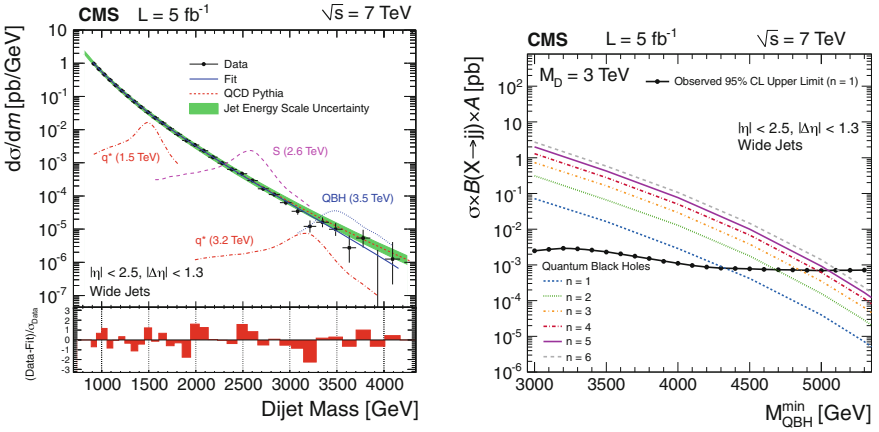

Fig. 9.7 *Left* the dijet invariant mass spectrum fitted with a smooth parametric background. The *dashed blue line* shows a signal from a quantum BH with the mass of 3.5 TeV. *Right* lower limits on the quantum BH mass for various numbers of extra dimensions. The $n = 1$ case corresponds to quantum black hole limits in the Randall–Sundrum model. The M_D value of 3 TeV is assumed. From Ref. [109]

and set similar limits on quantum BH [see Fig. 9.6 (right)] as an earlier, $\sqrt{s} = 7$ TeV S_T-based analysis [98].

While the properties of quantum black holes remain an enigma, one could address a question of a light BH formation in simple string theory models, which may correctly describe the effects of quantum gravity. One of the suggestions is that a precursor of a BH is a highly excited excited string state, randomly folded in a "string ball" [31]. The properties of such a string ball are expected to be similar to those

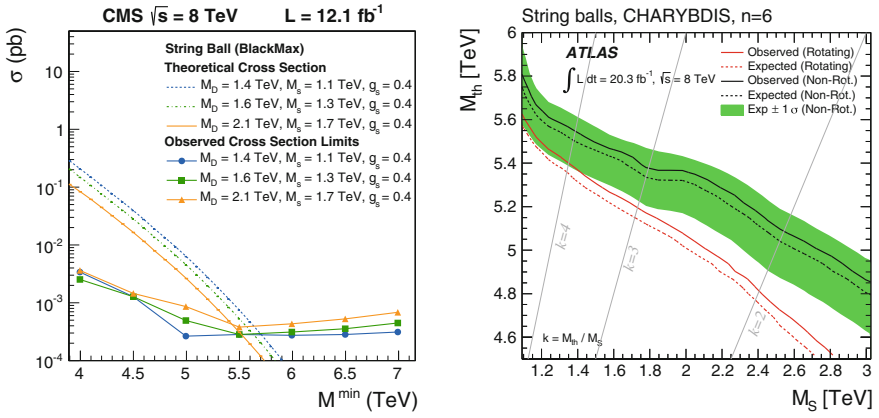

Fig. 9.8 Lower limits on the minimum string ball mass for a range of values of the fundamental Planck scale M_D, string scale M_s, and string coupling constant g_s. *Left* from CMS multi-object analysis [99]. *Right* from ATLAS lepton+jets analysis [104]

of a semiclassical BH, with the exception that its evaporation takes place at a fixed, Hagedorn temperature [79], which does not depend on the string ball mass, but only on the string scale M_s. Thus, the semiclassical BH analyses can be also used to set limits on string balls [110]. The first limit on string balls was set by the CMS BH analysis [98]. The ATLAS experiment set limits on string balls from the lepton+jets [103, 104] and like-sign dimuon [102] analyses. The latest results from the ATLAS and CMS collaborations [99, 102, 104] set limits on the minimum string ball mass in the range of 5.0–5.5 TeV for a range of string ball model parameters. These limits are shown in Fig. 9.8.

9.4 Conclusions

A large variety of ATLAS and CMS analyses based on 2010–2012 LHC data resulted in stringent limits on the existence of extra dimensions and low-scale quantum gravity, in a number of models. While the possibility to see these effects at the LHC is diminishing, the current searches are completely limited by the maximum machine energy of 8 TeV reached so far. There is still a lot of uncovered model parameter space left, which will be explored as early as 2015 by exploiting the LHC potential close to its design energy of 14 TeV.

Acknowledgments I'm indebted to my many ATLAS and CMS colleagues, who built, commissioned, and ran the state-of-the-art detectors, and produced beautiful results included in this review. This work is partially supported by the DOE Award No. DE-SC0010010-003376.

References

1. Kaluza, Th.: Sitzungsber. Preuss. Akad. Wiss. Phys. Math. Klasse, 996 (1921)
2. Klein, O.: Z. F. Physik **37**, 895 (1926)
3. Klein, O.: Nature **118**, 516 (1926)
4. Arkani-Hamed, N., Dimopoulos, S., Dvali, G.: Phys. Lett. B **429**, 263 (1998)
5. Antoniadis, I., et al.: Phys. Lett. B **436**, 257 (1998)
6. Arkani-Hamed, N., Dimopoulos, S., Dvali, G.: Phys. Rev. D **59**, 086004 (1999)
7. Landsberg, G. arXiv:0808.1867
8. Hewett, J.L., Spiropulu, M.: Ann. Rev. Nucl. Part. Sci. **52**, 397 (2002)
9. Barger, V.D., et al.: Phys. Lett. B **461**, 34 (1999)
10. Randall, L., Sundrum, R.: Phys. Rev. Lett. **83**, 3370 (1999)
11. Randall, L., Sundrum, R.: Phys. Rev. Lett. **83**, 4690 (1999)
12. Giudice, G., Rattazzi, R., Wells, J.: Nucl. Phys. B **544**, 3 (1999), revised version hep-ph/9811291v2
13. Han, T., Lykken, J., Zhang, R.: Phys. Rev. D **59**, 105006 (1999), revised version hep-ph/9811350v4
14. Hewett, J.: Phys. Rev. Lett. **82**, 4765 (1999)
15. Mirabelli, E.A., Perelstein, M., Peskin, M.E.: Phys. Rev. Lett. **82**, 2236 (1999)
16. Argyres, P.C., Dimopoulos, S., March-Russell, J.: Phys. Lett. B **441**, 96 (1998)
17. Banks, T., Fischler, W. hep-th/9906038

18. Emparan, R., Horowitz, G.T., Myers, R.C.: Phys. Rev. Lett. **85**, 499 (2000)
19. Dimopoulos, S., Landsberg, G.: Phys. Rev. Lett. **87**, 161602 (2001)
20. Giddings, S.B., Thomas, S.: Phys. Rev. D **65**, 056010 (2002)
21. Antoniadis, I., Benakli, K. (eds.): Extra dimensions vs collider physics. Special IJMPA issue (2014)
22. Anchordoqui, L.A., Goldberg, H., Shapere, A.D.: Phys. Rev. D **66**, 024033 (2002)
23. Landsberg, G.: J. Phys. G **32**, R337 (2006)
24. Meade, P., Randall, L.: JHEP **05**, 003 (2008)
25. CMS Collaboration: Phys. Lett. B **720**, 63 (2013)
26. ATLAS Collaboration: Phys. Rev. D **90**, 052005 (2014)
27. Georgi, H.: Phys. Rev. Lett. **98**, 221601 (2007)
28. Mureika, J.R.: Phys. Lett. B **660**, 561 (2008)
29. Kanti, P.: Int. J. Mod. Phys. A **19**, 4899 (2004)
30. Park, S.C.: Prog. Part. Nucl. Phys. **67**, 617 (2012)
31. Dimopoulos, S., Emparan, R.: Phys. Lett. B **526**, 393 (2000)
32. Particle Data Group Collaboration: Chin. Phys. C **38**, 090001 (2014)
33. Myers, R.C., Perry, M.J.: Ann. Phys. **172**, 304 (1986)
34. Voloshin, M.B.: Phys. Lett. B **518**, 137 (2001)
35. Voloshin, M.B.: Phys. Lett. B **524**, 376 (2002)
36. Gibbons, G.W., Hawking, S.W.: Phys. Rev. D **15**, 2752 (1977)
37. Eardley, D.M., Giddings, S.B.: Phys. Rev. D **66**, 044011 (2002)
38. Yoshino, H., Nambu, Y.: Phys. Rev. D **66**, 065004 (2002)
39. Yoshino, H., Nambu, Y.: Phys. Rev. D **67**, 024009 (2003)
40. Hsu, S.D.H.: Phys. Lett. B **555**, 92 (2003)
41. Solodukhin, S.N.: Phys. Lett. B **533**, 153 (2002)
42. Bilke, S., Lipartia, E., Maul, M. hep-ph/0204040
43. Jevicki, A., Thaler, J.: Phys. Rev. D **66**, 024041 (2002)
44. Eichten, E., et al.: Rev. Mod. Phys. **56**, 579 (1984)
45. Yoshino, H., Rychkov, V.S.: Phys. Rev. D **71**, 104028 (2005). Erratum-ibid. D **77**, 089905 (2008)
46. Hawking, S.W.: Commun. Math. Phys. **43**, 199 (1975)
47. Nicolini, P., Winstanley, E.: JHEP **11**, 075 (2011)
48. Anchordoqui, L., Goldberg, H.: Phys. Rev. D **67**, 064010 (2003)
49. Kanti, P., March-Russell, J.: Phys. Rev. D **66**, 024023 (2002)
50. Kanti, P., March-Russell, J.: Phys. Rev. D **67**, 104019 (2003)
51. Kanti, P., Grain, J., Barrau, A.: Phys. Rev. D **71**, 104002 (2005)
52. Harris, C.M.: Physics beyond the standard model: exotic leptons and black holes at future colliders. Ph.D. thesis, University of Cambridge (2005). hep-ph/0502005
53. Harris, C.M., Kanti, P.: JHEP **10**, 014 (2003)
54. Cornell, A.S., Naylor, W., Sasaki, M.: JHEP **02**, 012 (2006)
55. Cardoso, V., Cavaglia, M., Gualtieri, L.: Phys. Rev. Lett. **96**, 071301 (2006)
56. Cardoso, V., Cavaglia, M., Gualtieri, L.: JHEP **02**, 021 (2006)
57. Park, D.K. hep-th/0512021
58. Creek, S., Efthimiou, O., Kanti, P., Tamvakis, K.: Phys. Lett. B **635**, 39 (2006)
59. Park, D.K.: Phys. Lett. B **638**, 246 (2006)
60. Kanti, P., et al.: Phys. Rev. D **80**, 084016 (2009)
61. Kanti, P., Pappas, N.: Phys. Rev. D **82**, 024039 (2010)
62. Kotwal, A.V., Hays, C.: Phys. Rev. D **66**, 091901 (2002)
63. Ida, D., Oda, K.Y., Park, S.C., Phys. Rev. D **67**, 064025 (2003). Erratum-ibid. D **69**, 049901 (2004)
64. Ida, D., Oda, K.Y., Park, S.C.: Phys. Rev. D **71**, 124039 (2005)
65. Park, S.C., Song, H.S.: J. Korean Phys. Soc. **43**, 300 (2003)
66. Frolov, V.P., Stojkovic, D.: Phys. Rev. D **67**, 084004 (2003)
67. Frolov, V.P., Fursaev, D.V., Stojkovic, D.: JHEP **06**, 057 (2004)

68. Jung, E., Kim, S., Park, D.K.: Phys. Lett. B **615**, 273 (2005)
69. Jung, E., Kim, S., Park, D.K.: Phys. Lett. B **619**, 347 (2005)
70. Nomura, H., et al.: Progress Theoret. Phys. **114**, 707 (2005)
71. Jung, E., Park, D.K.: Nucl. Phys. B **731**, 171 (2005)
72. Duffy, G., et al.: JHEP **09**, 049 (2005)
73. Harris, C.M., Kanti, P.: Phys. Lett. B **633**, 106 (2006)
74. Casais, M., Kanti, P., Winstanley, E.: JHEP **02**, 051 (2006)
75. Ida, D., Oda, K.Y., Park, S.C.: Phys. Rev. D **73**, 124022 (2006)
76. Casadio, R., Harms, B.: Int. J. Mod. Phys. A **17**, 4635 (2002)
77. Kotwal, A.V., Hays, C.: Phys. Rev. D **66**, 116005 (2002)
78. Frolov, V.P., Stojkovic, D.: Phys. Rev. D **66**, 084002 (2002)
79. Hagedorn, R.: Nuovo Cimento Suppl. **3**, 147 (1965)
80. Ahn, E.-J., Cavaglia, M., Olinto, A.V.: Phys. Lett. B **551**, 1 (2003)
81. Jain, P., et al.: Int. J. Mod. Phys. D **12**, 1593 (2003)
82. Anchordoqui, L.A., Feng, J.L., Goldberg, H.: Phys. Lett. B **535**, 302 (2002)
83. Cheung, K.: Phys. Rev. D **66**, 036007 (2002)
84. Calmet, X., Gong, W., Hsu, S.D.H.: Phys. Lett. B **668**, 20 (2008)
85. Gingrich, D.M.: J. Phys. G **37**, 105108 (2010)
86. Gingrich, D.M.: Comput. Phys. Commun. **181**, 1917 (2010)
87. Dai, D.C., et al.: Phys. Rev. D **77**, 076007 (2008)
88. Dai, D.-C., et al. arXiv:0902.3577
89. Harris, C.M., Richardson, P., Webber, B.R.: JHEP **08**, 033 (2003)
90. Frost, J.A., et al.: JHEP **10**, 14 (2009)
91. Cavaglia, M., et al.: Comput. Phys. Commun. **177**, 506 (2007)
92. Rizzo, T.G.: JHEP **01**, 028 (2005)
93. Rizzo, T.G. hep-ph/0510420
94. Rizzo, T.G. hep-ph/0603242
95. Rizzo, T.G.: JHEP **06**, 079 (2005)
96. Stojkovic, D.: Phys. Rev. Lett. **94**, 011603 (2005)
97. CMS Collaboration: Phys. Lett. B **697**, 434 (2011)
98. CMS Collaboration: JHEP **04**, 061 (2012)
99. CMS Collaboration: JHEP **07**, 178 (2013)
100. Evans, J.A., Kats, Y., Shih D., Strassler, M.J.: JHEP **07**, 101 (2014)
101. ATLAS Collaboration: Phys. Lett. B **709**, 322 (2012)
102. ATLAS Collaboration: Phys. Rev. D **88**, 072001 (2013)
103. ATLAS Collaboration: Phys. Lett. B **716**, 122 (2012)
104. ATLAS Collaboration. JHEP **08**, 103 (2014)
105. ATLAS Collaboration. New J. Phys. **13**, 053044 (2011)
106. ATLAS Collaboration: JHEP **01**, 029 (2013)
107. ATLAS Collaboration: Phys. Rev. Lett. **112**, 091804 (2014)
108. ATLAS Collaboration: Phys. Lett. B **728**, 562 (2014)
109. CMS Collaboration: JHEP **01**, 013 (2013)
110. Gingrich, D.M., Martell, K.: Phys. Rev. D **78**, 115009 (2008)

Chapter 10
Minimum Length Effects in Black Hole Physics

Roberto Casadio, Octavian Micu and Piero Nicolini

Abstract We review the main consequences of the possible existence of a minimum measurable length, of the order of the Planck scale, on quantum effects occurring in black hole physics. In particular, we focus on the ensuing minimum mass for black holes and how modified dispersion relations affect the Hawking decay, both in four space-time dimensions and in models with extra spatial dimensions. In the latter case, we briefly discuss possible phenomenological signatures.

Keywords Minimum length · Black holes · Planck scale · Hawking effect · Extra spatial-dimensions

10.1 Gravity and Minimum Length

Physics is characterized by a variety of research fields and diversified tools of investigation that strongly depend on the length scales under consideration. As a result, one finds an array of sub-disciplines, spanning from cosmology, to astrophysics, geophysics, molecular and atomic physics, nuclear and particle physics. In a nutshell, we can say that Physics concerns events occurring at scales between the radius of the Universe and the typical size of observed elementary particles. It is not hard to

R. Casadio (✉)
Dipartimento di Fisica e Astronomia, Università di Bologna, Sezione di Bologna,
via Irnerio 46, 40126 Bologna, Italy
e-mail: casadio@bo.infn.it

R. Casadio
I.N.F.N., Sezione di Bologna, via Irnerio 46, 40126 Bologna, Italy

O. Micu
Institute of Space Science, P.O. Box MG-23, 077125 Bucharest-Magurele, Bucharest, Romania
e-mail: octavian.micu@spacescience.ro

P. Nicolini
Frankfurt Institute for Advanced Studies (FIAS), Science Campus Riedberg,
Ruth-Moufang-Strasse 1, 60438 Frankfurt am Main, Germany
e-mail: nicolini@fias.uni-frankfurt.de

X. Calmet (ed.), *Quantum Aspects of Black Holes*,
Fundamental Theories of Physics 178, DOI 10.1007/978-3-319-10852-0_10

understand that such a rich array of physical phenomena requires specific formalisms. For instance, at macroscopic scales, models of the Universe are obtained in terms of general relativity, while at microscopic scales quantum physics has been proven to be the adequate theory for the miniaturised world.

Despite the generality of such a scheme, it cannot be considered as complete. One may be tempted to conclude that at microscopic scales, we can, at least in principle, figure out arbitrarily small lengths. In quantum mechanics, or more precisely in quantum field theory, particle sizes are described by the Compton wavelength, which accounts for the Heisenberg uncertainty in localising a microscopic object at a given energy. From this, it descends a "rule of thumb" according to which the higher the energy, the smaller is the size one can probe in a particle physics experiment. Apparently there is no minimal length scale. The limitations to the accuracy in measuring a length seems to be only a technological problem related to the possibility of reaching higher and higher energy scales.

In the reasoning above, however, we give for granted that quantum physics can be considered unmodified at any energy scale. On the contrary, we should better say that the standard quantum formalism is valid for studying particles and fundamental interactions, provided one of these interactions, gravity, does not produce relevant effects at the energy under consideration. The weakness of gravity allows quantum mechanics and quantum field theory to be efficient tools in a vast variety of physical situations. On the other hand, already for the Heisenberg microscope, namely a thought experiment concerning a particle illuminated by light, one should take into account the gravitational interaction between the particle and the effective mass associated with the energy of the photon. In doing so, one can discover an additional position uncertainty due to the acceleration the particle is subject to [1]. Accordingly, one has to conclude that there exists a *minimal length* limiting the accuracy in localising the particle itself [2]. Not surprisingly, such a minimal length depends on the gravitational coupling G and it is defined as the Planck length through the relation $\ell_{\rm P} \equiv \sqrt{\hbar G/c^3} \sim 10^{-35}\,{\rm m}$.

The Planck scale discloses other important features. Matter compression (e.g. by smashing particles in colliders) is limited by the gravitational collapse to a black hole, whose size turns out to be the Planck length [3]. A further increase of energy in the collision would not lead to a smaller particle but rather to a bigger black hole, its radius being proportional to the mass. As a result, the Planck length is not only the smallest scale in particle physics, but also the smallest admissible size of a black hole. From this viewpoint, black holes can be reinterpreted as a new "phase" of matter [4–6] occurring at energies exceeding the Planck mass, i.e., $M_{\rm P} \equiv \hbar\, c^{-1}\, \ell_{\rm P}^{-1} = \sqrt{\hbar\, c/G}$. This general idea is what lies behind the generalised uncertainty principle (GUP), which we shall derive in a rather new fashion in Sect. 10.2.1 (see Ref. [7] for a fairly comprehensive account of other derivations).

Despite the simplifications, the idea of a minimal length is supported by all major formulations of quantum gravity, i.e., an ongoing attempt to formulate a consistent quantum theory of the gravitational interaction. Specifically, the existence of a minimum length was evident since the early contribution to quantum gravity [8]. It was clear that space-time has to change its nature when probed at energies of the order

of the Planck scale: rather than a smooth differential manifold, the space-time, in its quantum regime, is expected to be a fluctuating, foamy structure plagued by loss of local resolution. This scenario is confirmed by Planckian scattering of strings [9], whose theory can be interpreted as a "field theory" of extended objects encoding a quantum of length $\lambda = \sqrt{\hbar\alpha'}$ [10–14]. In the context of loop quantum gravity, a minimum resolution length emerges from the discreteness of the spectra of area and volume operators [15]. The idea of implementing a gravitational ultraviolet cutoff has followed several routes like string inspired non-commutative geometry [16] or asymptotically safe gravity [17]. According to the latter proposal, the gravitational interaction becomes weaker and weaker as the energy increases: in the ultraviolet regime there is a non-trivial fixed point at which the theory is safe from divergences [18]. Further analyses of the emergence of a minimal length in quantum gravity can be found in Refs. [19, 20] (for recent reviews see [7, 21]).

In the following sections we present the relationship between black holes and a minimum resolution length. Such a relationship is dual: we have already mentioned that the size of Planck scale black holes provides a natural ultraviolet cutoff; on the other hand, it is instructive to explore the complementary possibility, namely the study of modifications of classical black hole metrics that we expect by assuming that the space-time is endowed with a quantum gravity induced minimal length.

10.2 Minimum Black Hole Mass

Before we tackle the issue of the existence of a minimum black hole mass, let us briefly review the key ingredient that suggests it is sensible to put together Heisenberg's fundamental uncertainty principle and a gravitational source of error, thus yielding a GUP and a minimum measurable length [7].

Quantum mechanics is built upon uncertainty relations between pairs of canonical variables, of which the position and momentum of a particle represent the prototype. For example, in the ideal Heisenberg microscope, in which a photon of energy $\hbar\omega$ is used to locate an electron, one finds the wavelength of the photon sets a limit to the precision in, say, the position of the electron along the x coordinate given by[1]

$$\Delta x \gtrsim \frac{1}{\omega \, \sin\theta} \, , \tag{10.1}$$

where θ represents the angular aperture of the microscope within which the photon must travel in order to be seen. At the same time, the electron will suffer a recoil

$$\Delta p \gtrsim \hbar\omega \, \sin\theta . \tag{10.2}$$

[1] Factors of order one are neglected for simplicity.

Putting the two bounds together one obtains the standard quantum mechanical uncertainty

$$\Delta x \Delta p \gtrsim \hbar \,, \tag{10.3}$$

which suggests that infinite precision can be achieved in determining x at the price of giving up precision in p (and *vice versa*). Clearly, this requires photons scattering against the electron at higher and higher energy.

Now, a groundbreaking feature of gravity, which has not been proven rigorously but shown to hold in great generality, is encoded by Thorne's *hoop conjecture* [23]: a black hole forms whenever the amount of energy m is compacted inside a region that in no directions extends outside a circle of circumference (roughly) equal to $2\pi R_{\rm H}$, where

$$R_{\rm H} = \frac{2\,G m}{c^2} = 2\,\ell_{\rm P}\,\frac{m}{M_{\rm P}} \,, \tag{10.4}$$

is the gravitational Schwarzschild radius. This result implies that once the energy $\hbar\,\omega$ has reached the above threshold, instead of scattering off the electron and reach the microscope, the photon (along with the electron) will be trapped inside a black hole and no measurement will occur. Several arguments [7] thus suggest the size of the black hole contributes to the total uncertainty according to

$$\Delta x \gtrsim \frac{\hbar}{\Delta p} + G\,\Delta p \simeq \ell_{\rm P}\left(\frac{M_{\rm P}}{\Delta p} + \frac{\Delta p}{M_{\rm P}}\right) \,, \tag{10.5}$$

where we estimated $m \sim \omega \sim \Delta p$. It is then easy to see that Eq. (10.5) leads to a minimum uncertainty $\Delta x_{\rm min} \simeq \ell_{\rm P}$ obtained for $\Delta p \simeq M_{\rm P}$.

Let us also mention in passing that this kind of GUP can be formally derived from modified canonical commutators and that it can be extended to the models with extra spatial dimensions (see, e.g., Ref. [22]) of the type we shall consider in Sect. 10.3.

10.2.1 GUP, Horizon Wave-Function and Particle Collisions

It is believed that black holes can form by the gravitational collapse of astrophysical objects, such as the imploding cores of supernovae, or by coalescing binary systems, which are the cases that originally inspired the hoop conjecture. Another possible mechanism is given by colliding particles, provided the particles involved in the process have a sufficiently high energy and small impact parameter to meet the requirements of the hoop conjecture. Note that no minimum value of m (or $R_{\rm H}$) is however implied by this classical conjecture.

Once quantum physics is considered, black holes are expected to exist only above a minimum mass of the order of the fundamental scale of gravity [24–30]. In fact, if we

neglect the spin and charge for the sake of simplicity, general relativity associates to a point-like source of mass m the gravitational Schwarzschild radius (10.4), whereas quantum mechanics introduces an uncertainty in the particle's spatial localisation, typically of the order of the Compton length,

$$\lambda_m \simeq \ell_{\rm P}\,\frac{M_{\rm P}}{m}. \tag{10.6}$$

Assuming quantum physics is a more refined description of classical physics, the clash of the two lengths, $R_{\rm H}$ and λ_m, implies that the former only makes sense if it is larger than the latter, $R_{\rm H} \gtrsim \lambda_m$. In terms of the particle's mass, this means

$$m \gtrsim M_{\rm P}, \tag{10.7}$$

or the size of the black hole $R_{\rm H} \gtrsim 2\,\ell_{\rm P}$. Note that this bound is obtained from the flat space Compton length (10.6), but it is still reasonable to assume the condition (10.7) yields an order of magnitude estimate of the minimum possible black hole mass. Moreover, we have seen above that a minimum uncertainty of the same order follows from GUPs (and modified commutators) precisely formulated in order to account for black hole formation that should occur according to the hoop conjecture.

Instead of employing a GUP, we shall here show that the above argument leading to Eq. (10.7) can be actually given a probabilistic implementation, without modifying the commutators of quantum mechanics, by associating to the particles an auxiliary "horizon wave-function" [24–26]. In order to introduce this tool, let us consider a state $\psi_{\rm S}$ representing a massive particle localised in space and at rest in the chosen reference frame. Having defined suitable Hamiltonian eigenmodes,

$$\hat{H}\,|\,\psi_E\,\rangle = E\,|\,\psi_E\,\rangle, \tag{10.8}$$

where H can be specified depending on the model we wish to consider, the state $\psi_{\rm S}$ can be decomposed as

$$|\,\psi_{\rm S}\,\rangle = \sum_E C(E)\,|\,\psi_E\,\rangle. \tag{10.9}$$

If we further assume the particle is spherically symmetric, we can invert the expression of the Schwarzschild radius (10.4) to obtain E as a function of $R_{\rm H}$. We then define the *horizon wave-function* as

$$\psi_{\rm H}(R_{\rm H}) \propto C\left(M_{\rm P}\,R_{\rm H}/2\,\ell_{\rm P}\right), \tag{10.10}$$

whose normalisation can finally be fixed in a suitable inner product. We interpret the normalised wave-function $\psi_{\rm H}$ as yielding the probability that we would detect a horizon of areal radius $r = R_{\rm H}$ associated with the particle in the quantum state $\psi_{\rm S}$. Such a horizon is necessarily "fuzzy", like the position of the particle itself, and

unlike its purely classical counterpart. The probability density that the particle lies inside its own horizon of radius $r = R_{\rm H}$ will next be given by

$$P_<(r < R_{\rm H}) = P_{\rm S}(r < R_{\rm H})\, P_{\rm H}(R_{\rm H}), \tag{10.11}$$

where

$$P_{\rm S}(r < R_{\rm H}) = 4\,\pi \int_0^{R_{\rm H}} |\psi_{\rm S}(r)|^2\, r^2\, {\rm d}r \tag{10.12}$$

is the probability that the particle is found inside a sphere of radius $r = R_{\rm H}$, and

$$P_{\rm H}(R_{\rm H}) = 4\,\pi\, R_{\rm H}^2\, |\psi_{\rm H}(R_{\rm H})|^2 \tag{10.13}$$

is the probability that the horizon is located on the sphere of radius $r = R_{\rm H}$. Finally, the probability that the particle described by the wave-function $\psi_{\rm S}$ is a black hole will be obtained by integrating (10.11) over all possible values of the radius,

$$P_{\rm BH} = \int_0^\infty P_<(r < R_{\rm H})\, {\rm d}R_{\rm H}. \tag{10.14}$$

As a check that this formalism leads to sensible results in agreement with the bound (10.7), one can easily apply it to a particle described by a spherically symmetric Gaussian wave-function of width $\ell \simeq \hbar/m$,

$$\psi_{\rm S}(r) = \frac{e^{-\frac{r^2}{2\,\ell^2}}}{\ell^{3/2}\,\pi^{3/4}}, \tag{10.15}$$

for which one obtains a vanishing probability that the particle is a black hole when its mass is smaller than about $M_{\rm P}/4$ [24–26] (see Fig. 10.1). Moreover, by adding to the uncertainty in position Δr determined by the wave-function $\psi_{\rm S}$ the uncertainty in the size of the horizon $\Delta R_{\rm H}$ obtained from the corresponding horizon wave-function $\psi_{\rm H}$, one is able to recover a GUP [26]. In particular,

$$\langle\, \Delta r^2\, \rangle = 4\,\pi \int_0^\infty |\psi_{\rm S}(r)|^2\, r^4\, {\rm d}r \simeq \ell^2, \tag{10.16}$$

and

$$\langle\, \Delta R_{\rm H}^2\, \rangle = 4\,\pi \int_0^\infty |\psi_{\rm H}(R_{\rm H})|^2\, R_{\rm H}^4\, {\rm d}R_{\rm H} \simeq \frac{\ell_{\rm P}^4}{\ell^2}. \tag{10.17}$$

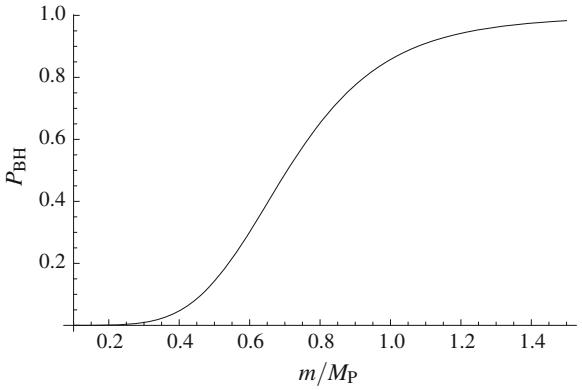

Fig. 10.1 Probability $P_{\rm BH}$ that particle of mass m is a black hole

Since

$$\langle\, \Delta p^2 \,\rangle = 4\,\pi \int_0^\infty |\psi_{\rm S}(p)|^2\, p^4\, {\rm d}p \simeq M_{\rm P}^2\, \frac{\ell_{\rm P}^2}{\ell^2} \equiv \Delta p^2, \tag{10.18}$$

we can also write

$$\ell^2 \simeq \ell_{\rm P}^2\, \frac{M_{\rm P}^2}{\Delta p^2}. \tag{10.19}$$

Finally, by combining the uncertainty (10.16) with (10.17) linearly, we find

$$\Delta r \equiv \sqrt{\langle\, \Delta r^2 \,\rangle} + \gamma\, \sqrt{\langle\, \Delta R_{\rm H}^2 \,\rangle} \simeq \ell_{\rm P}\, \frac{M_{\rm P}}{\Delta p} + \gamma^2\, \ell_{\rm P}\, \frac{\Delta p}{M_{\rm P}}, \tag{10.20}$$

where γ is a coefficient of order one, and the result is plotted in Fig. 10.2 (for $\gamma = 1$). This is precisely the kind of GUP leading to a minimum measurable length

$$\Delta r \gtrsim \gamma\, \ell_{\rm P}, \tag{10.21}$$

obtained for $\Delta p \simeq M_{\rm P}$.

Of course, the physically interesting problem of particles colliding at very high energy, and forming a black hole, is clearly going to require significantly more work and overcoming much harder technical difficulties. A flavour of what is going on can however be obtained by extending the above construction to a state containing two free particles in one-dimensional flat space [27]. We represent each particle at a given time and position X_i ($i = 1$ or 2) by means of Gaussian

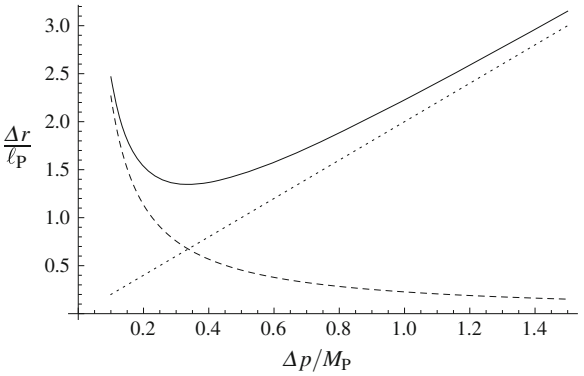

Fig. 10.2 Uncertainty relation (10.20) (*solid line*) as a combination of the quantum mechanical uncertainty (*dashed line*) and the uncertainty in horizon radius (*dotted line*)

wave-functions,

$$\langle\, x_i \mid \psi_{\rm S}^{(i)} \,\rangle \equiv \psi_{\rm S}(x_i) = e^{-i\,\frac{P_i\,x_i}{\hbar}}\,\frac{e^{-\frac{(x_i-X_i)^2}{2\,\ell_i}}}{\sqrt{\pi^{1/2}\,\ell_i}}, \tag{10.22}$$

where ℓ_i is the width and P_i the linear momentum (which remain constant). The total wave-function is then just the product of the two one-particle states,

$$\langle\, x_1, x_2 \mid \psi_{\rm S}^{(1,2)} \,\rangle \equiv \psi_{\rm S}(x_1, x_2) = \psi_{\rm S}(x_1)\,\psi_{\rm S}(x_2). \tag{10.23}$$

It is convenient to go through momentum space in order to compute the spectral decomposition. We find

$$\langle\, p_i \mid \psi_{\rm S}^{(i)} \,\rangle \equiv \psi_{\rm S}(p_i) = e^{-i\,\frac{p_i\,X_i}{\hbar}}\,\frac{e^{-\frac{(p_i-P_i)^2}{2\,\Delta_i}}}{\sqrt{\pi^{1/2}\,\Delta_i}}, \tag{10.24}$$

where $\Delta_i = \hbar/\ell_i$, and we shall use the relativistic dispersion relation

$$E_i = \sqrt{p_i^2 + m_i^2}. \tag{10.25}$$

If the particles were at rest ($P_i = 0$), we could assume $\ell_i = \lambda_{m_i}$ (and $\Delta_i = m_i$). For realistic elementary particles $m_1 \simeq m_2 \ll M_{\rm P}$, and, from Eq. (10.7) one expects the probability of forming a black hole will become significant only for $|P_i| \sim E_i \sim M_{\rm P}$. From $P_i = \frac{m_i\,{\rm v}_i}{\sqrt{1-{\rm v}_i^2}}$, we obtain

$$\ell_i = \frac{\hbar}{\sqrt{P_i^2 + m_i^2}} \simeq \frac{\ell_{\rm P}\,M_{\rm P}}{|P_i|}, \qquad \text{and} \qquad \Delta_i \simeq |P_i|. \tag{10.26}$$

The two-particle state can now be written as

$$| \psi_{\rm S}^{(1,2)} \rangle = \prod_{i=1}^{2} \left[\int_{-\infty}^{+\infty} {\rm d}p_i \, \psi_{\rm S}(p_i) \, | \, p_i \rangle \right], \tag{10.27}$$

and the relevant coefficients in the spectral decomposition (10.9) are given by the sum of all the components of the product wave-function (10.27) corresponding to the same total energy E,

$$C(E) = \int_{-\infty}^{+\infty} \int_{-\infty}^{+\infty} \psi_{\rm S}(p_1) \, \psi_{\rm S}(p_2) \, \delta(E - E_1 - E_2) \, {\rm d}p_1 \, {\rm d}p_2 . \tag{10.28}$$

For this two-particle collision, the horizon wave-function must be computed in the centre-of-mass frame of the two-particle system, so that

$$P_1 = -P_2 \equiv P > 0 . \tag{10.29}$$

From $P \sim M_{\rm P} \gg m_1 \simeq m_2$, we can also set

$$X_1 \simeq -X_2 \equiv X > 0 . \tag{10.30}$$

After replacing the expression of the Schwarzschild radius (10.4) into Eq. (10.28), and (numerically) normalising the result in the inner product

$$\langle \, \psi_{\rm H} \, | \, \phi_{\rm H} \, \rangle \equiv \int_{0}^{\infty} \psi_{\rm H}^{*}(R_{\rm H}) \, \phi_{\rm H}^{*}(R_{\rm H}) \, {\rm d}R_{\rm H} , \tag{10.31}$$

we finally obtain the wave-function $\psi_{\rm H} = \psi_{\rm H}(R_{\rm H}; X, P)$. One then finds that $P_{\rm H} = |\psi_{\rm H}(R_{\rm H})|^2$ shows a mild dependence on X and a strong dependence on P, in agreement with the fact that the energy of the system only depends on P, and not on the spatial separation between the two particles. It is also worth noting that $P_{\rm H} = P_{\rm H}(R_{\rm H})$ always peaks around $R_{\rm H} \simeq 2 \, \ell_{\rm P} \, (2P/M_{\rm P})$, in very good agreement with the hoop conjecture (10.4).

The probability (10.14) that the system of two particles is a black hole can next be computed numerically as a function of the distance from the centre of mass X of each particle, and the total energy $2P$. Figure 10.3 shows the result for a suitable range of X and P. Note that a first estimate of what happens as the two particles evolve in time can be obtained by considering the probability $P_{\rm BH} = P_{\rm BH}(X, 2P)$ along lines of constant P and decreasing X: $P_{\rm BH}$ clearly increases up to the maximum reached for $X = 0$, when the two (non-interacting) particles exactly superpose. There is therefore a significant probability that the collision produces a black hole, say $P_{\rm BH}(X, 2P \gtrsim 2M_{\rm P}) \gtrsim 80 \, \%$, if the distance from the centre of mass and linear

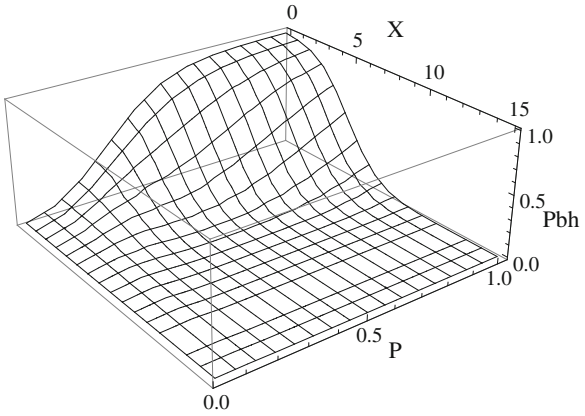

Fig. 10.3 Probability the two-particle system is a black hole as a function of X and P (in units of Planck length and mass respectively)

momentum satisfy

$$X \lesssim 2\,\ell_{\rm P}\,(2P/M_{\rm P}) - \ell_{\rm P} = R_{\rm H}(2P) - \ell_{\rm P}, \tag{10.32}$$

where the term $-\ell_{\rm P}$ on the right is the "quantum mechanical correction" to the hoop formula (10.4) for $E \simeq 2P \gtrsim 2\,M_{\rm P}$. This correction is indeed arbitrary (as is the choice of $P_{\rm BH} \gtrsim 80\,\%$) and applies to the formation of large (semi)classical black holes, for which it is practically negligible. For lower values of P, one instead finds $P_{\rm BH}(X, 2P \lesssim 2M_{\rm P}) \gtrsim 80\,\%$ if

$$2P - M_{\rm P} \gtrsim M_{\rm P}\,X^2/9\,\ell_{\rm P}^2, \tag{10.33}$$

which yields the minimum energy $2P \simeq M_{\rm P}$ [instead of $2P \simeq M_{\rm P}/2$, as it would follow from the linear relation (10.32)]. Equation (10.33) represents a significant quantum mechanical correction to the hoop conjecture (10.4) for quantum black hole production, that fully entails the existence of a minimum black hole mass (albeit a "fuzzy" one).

Notably, the above result is obtained without assuming any specific microscopic structure for the (quantum) black holes, and should therefore represent a quite generic expectation. Similarly to the bound (10.7), it implies that black holes fall well outside the realm of experimental physics on earth. There is however a catch, as we shall discuss in Sect. 10.3.

10.2.2 Regular Black Holes

We have just shown that (quantum) black holes cannot have arbitrarily small mass. In this section we shall see that a similar conclusion also follows from considering the

possibility of improving the short distance behaviour of classical black hole metrics. This is one of the key points for the validity of any candidate theory to quantum gravity. However, despite the progress and the formulation of several approaches to quantum gravity, the mechanism of regularisation of black hole space-times still evades a complete understanding (for instance, see Ref. [31] for the case of string theory, and [32] for the case of loop quantum gravity).

Given this background, one can address the problem of curvature singularities by following alternative routes. The earliest attempts of singularity avoidance were based on the assumption of a de Sitter core placed at the space-time origin. Actually de Sitter cores offer regular space-time regions where gravity becomes locally repulsive and prevents a complete gravitational collapse into a singular configuration. Despite the effective nature of the approach, de Sitter cores can be interpreted as the effect of the graviton quantum vacuum energy. This fact is confirmed by a local violation of energy conditions, which certify the non-classical nature of the resulting space-time geometry.

The first black hole with a regular de Sitter core is maybe the Bardeen space-time [33]. This model has inspired a variety of additional improved black hole metrics, based on different regularising mechanisms, such as: matching an outer Schwarzschild geometry and an inner de Sitter geometry along time-like [34–36] and space-like [37] matter shells; coupling of gravity with non-linear electrodynamics [38]; prescribing a stress tensor for the quantum vacuum energy density at the origin [39–42]; implementing quantum gravity effects in classical backgrounds [43–50] (for a review see Ref. [51]). Despite the progress and virtues of such proposals, one finds that the resulting metrics are affected by either one or a combination of the following factors: (1) lack of a stress tensor; (2) lack of a natural transition between inner and asymptotic geometries; (3) lack of a neutral solution; (4) need of additional hypotheses to achieve the regularity; (5) lack of equations describing the space-time geometry at all distances; (6) lack of a clear connection with some quantum gravity formulation.

A simple way to overcome the above limitations is offered by the so-called non-commutative geometry inspired black hole solutions [52]. Here, we briefly summarise the procedure to derive such a family of regular black holes. One can start by considering the action $S_{\rm tot}$ describing the space-time generated by a static massive source

$$S_{\rm tot} = S_{\rm grav} + S_{\rm matt}\,, \tag{10.34}$$

where $S_{\rm grav}$ is the usual Einstein-Hilbert action, while the matter action $S_{\rm matt}$ reads

$$S_{\rm matt} = -\int \mathrm{d}^4x\,\sqrt{-g}\,\rho(x), \quad \rho(x) = \frac{M}{\sqrt{-g}}\int \mathrm{d}\tau\;\delta\left(x - x(\tau)\right), \tag{10.35}$$

with $\rho(x)$ being the energy density describing a massive, point-like particle. By varying (10.34) with respect to the metric $g_{\mu\nu}$, one finds the Einstein's equations with a pressure-less source term

$$T^0{}_0 = -\frac{M}{4\pi\, r^2}\delta(r). \tag{10.36}$$

Customarily, one ignores the distributional profile of the source, i.e., $\delta(r)$, accounting for the singular behaviour of the resulting space-time geometry. Rather one prefers to solve the Einstein equations outside the source, i.e., in an open domain $\mathscr{D} = \mathbb{R}^4 \setminus \mathbf{0}$. The Schwarzschild solution is then obtained by integrating Einstein's equations *à la* Laplace, namely by exploiting boundary conditions. Although mathematically acceptable, this procedure has several drawbacks from a physical viewpoint: for instance, the mass term emerges as an integration constant and it is placed at the point that one has excluded by hypothesis. Not surprisingly black hole solutions are often labeled as *vacuum solutions*, a definition that might sound in contradiction to the basic tenet of general relativity according to which gravity, expressed in terms of curvature, is the result of the presence of mass and energy in the space-time (for additional details see Refs. [53, 54]).

More importantly, Eq. (10.36) is instrumental for the present discussion: we expect any candidate theory of quantum gravity to improve the source term, by providing a new, ultraviolet finite profile for the energy density. This is the case of non-commutative geometry, which is based on the idea of implementing a fundamental length by allowing a non-trivial commutation relation for coordinate operators

$$\left[X^\mu, X^\nu\right] = i\,\Theta^{\mu\nu}, \tag{10.37}$$

where $\Theta^{\mu\nu}$ is a constant anti-symmetric tensor with determinant $|\Theta^{\mu\nu}| = \theta$, having units of a length squared. The parameter $\sqrt{\theta}$ will act as a quantum of length and it is natural to assume $\sqrt{\theta} = \ell_{\rm P}$. However $\sqrt{\theta}$ is not fixed *a priori* and can be treated as a parameter adjustable to those scales at which non-commutative effects set in. By averaging coordinate operators X^μ on suitable coherent states, it has been shown, in a series of papers [55–61], that the integration measures in momentum space, are exponentially suppressed in the ultraviolet sector by a factor $\exp(-\theta k^2)$, where k is the magnitude of the Euclidean momentum. As a result, by adopting free falling Cartesian-like coordinates, we have that the usual representation of the source term (10.36) switches to a new, regular profile

$$\delta^{(3)}(\boldsymbol{x}) = \frac{1}{(2\pi)^3}\int \mathrm{d}^3k\, e^{i\boldsymbol{k}\cdot\boldsymbol{x}} \to \rho_\theta(\boldsymbol{x}) = \frac{1}{(2\pi)^3}\int \mathrm{d}^3k\, e^{-\theta k^2 + i\boldsymbol{k}\cdot\boldsymbol{x}} = \frac{e^{-x^2/4\theta}}{(4\pi\theta)^{3/2}}, \tag{10.38}$$

namely a Gaussian distribution whose width is the minimal resolution length $\sqrt{\theta}$ [62, 63]. This result consistently reproduces the classical limit (10.36) for $\sqrt{\theta} \to 0$. More importantly the Gaussian approaches a finite, constant value at the origin as expected for a de Sitter core. The latter requires negative pressure terms to sustain the Gaussian profile and prevent the collapse into a Dirac delta distribution. By the conservation of the energy-momentum tensor $\nabla_\mu T^{\mu\nu} = 0$, one can determine

all pressure terms, namely the radial pressure $p_{\rm rad}(r) = -M\rho_\theta(r)$ and the angular pressure $p_\perp(r) = -M\rho_\theta(r) - \frac{r}{2} M\partial_r\rho_\theta(r)$, where

$$T_\nu^{\ \mu} = \text{diag}\left(-M\rho_\theta(r), p_{\rm rad}(r), p_\perp(r), p_\perp(r)\right). \tag{10.39}$$

As a result the energy momentum tensor describes an anisotropic fluid, that violates energy conditions in the vicinity of the origin, as expected.

By solving the Einstein equations with the above source term one finds

$$\begin{aligned} ds^2 = &-\left(1 - \frac{2MG}{r}\frac{\gamma(3/2; r^2/4\theta)}{\Gamma(3/2)}\right) dt^2 + \left(1 - \frac{2MG}{r}\frac{\gamma(3/2; r^2/4\theta)}{\Gamma(3/2)}\right)^{-1} dr^2 \\ &+ r^2 d\Omega^2 \end{aligned} \tag{10.40}$$

known as the non-commutative geometry inspired Schwarzschild solution [64]. Here $\gamma(a/b, x) = \int_0^x \frac{dt}{t} t^{a/b} e^{-t}$ is the incomplete Euler gamma function and $\Gamma(3/2) = \frac{1}{2}\sqrt{\pi}$. Before presenting the properties of the line element (10.40), we recall that the above results has been confirmed by two alternative derivations: the Gaussian profile (10.38) can be obtained by means of a Voros product approach to non-commutative geometry [65], as well as by solving the gravitational field equations derived by non-local deformations of Einstein gravity [66]. In the latter case, the non-local character of gravity is an alternative way to accounting for the presence of a minimal resolution length at extreme energy scales (see [67–71] for recent non-local gravity proposals). Interestingly the space-time (10.40) has been interpreted as a condensate of gravitons [72], according to a recently proposed conjecture about the nature of black holes [73–76].

The line element (10.40) consistently matches the Schwarzschild geometry in the large distance limit $r \gg \sqrt{\theta}$. Conversely at small distance, $r \sim \sqrt{\theta}$, the incomplete Euler gamma function goes like $\gamma(3/2, r^2/4\theta) \sim r^3$ and therefore a deSitter core develops at the origin. The curvature is easily obtained: the Ricci scalar is finite, constant and positive at the origin and reads

$$R(0) = \frac{4M}{\sqrt{\pi}\theta^{3/2}}. \tag{10.41}$$

The analysis of the horizon equation requires a preliminary comment. Here the parameter M is defined as the integrated flux of energy

$$M \equiv \int_\Sigma d\sigma^\mu\, T^0_\mu \tag{10.42}$$

where Σ is an asymptotic closed space-like surface. Equivalently M results as the limit $r \to \infty$ of the cumulative mass distribution

$$m(r) = -4\pi \int_0^r dt\, t^2\, T^0{}_0. \tag{10.43}$$

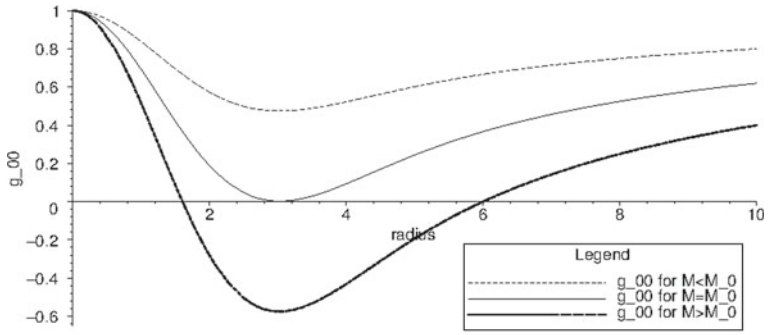

Fig. 10.4 The metric element $g_{00} = 1 - \frac{2MG}{r}\frac{\gamma(3/2;r^2/4\theta)}{\Gamma(3/2)}$ as a function of r for different values of the parameter M

Depending on the values of M, the horizon equation $1 - \frac{2MG}{r}\frac{\gamma(3/2;r^2/4\theta)}{\Gamma(3/2)} = 0$ has two, one or no solutions. Specifically there exists a value $M_0 \simeq 1.90\sqrt{\theta}/G$ for the mass parameter such that (see Fig. 10.4)

- for $M < M_0$ there is no solution, corresponding to the case of a regular manifold without horizons;
- for $M > M_0$ there are two solutions, corresponding to an inner horizon r_- and an outer horizon r_+:
- for $M = M_0$ there is just one solution, corresponding to a single degenerate horizon $r_0 \simeq 3.02\sqrt{\theta}$.

The global structure of the solution resembles that of the Reissner-Norström geometry, with a never ending chain of space-time quadrants. However, contrary to the latter case, there is no singularity. The global structure of the solution differs also from that of the Kerr geometry because the space-time is geodesically complete. As a result the negative r geometry does not represent an analytical continuation of Eq. (10.40), but rather an additional, horizonless, regular space-time. Horizons have the conventional meaning, i.e., r_+ is an event horizon and r_- is a Cauchy horizon. Analyses of possible blue shift instability at r_- are controversial [77, 78]: it is not yet clear how quantum gravity effects might tame the occurrence of a possible mass inflation. Finally r_0 is the radius of the extremal black hole, we expect it to be a zero temperature configuration.

The thermodynamics of the non-commutative geometry inspired black hole [79] can be studied as follows. The periodicity of the imaginary time of the metric (10.40) gives the temperature of the black hole (see Fig. 10.5)

$$T = \frac{1}{4\pi r_+}\left(1 - \frac{r_+^3}{4\theta^{3/2}}\frac{e^{-r_+^2/4\theta}}{\gamma(3/2;\, r_+^2/4\theta)}\right). \tag{10.44}$$

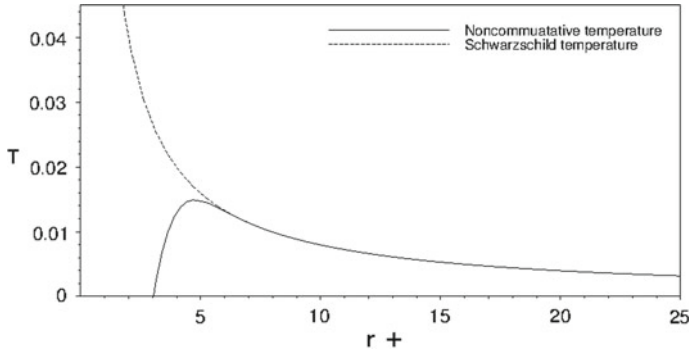

Fig. 10.5 The metric element $g_{00} = 1 - \frac{2MG}{r}\frac{\gamma(3/2;r^2/4\theta)}{\Gamma(3/2)}$ as a function of r for different values of the parameter M

We see that at large distances $r_+ \gg \sqrt{\theta}$ the non-commutative corrections are exponentially vanishing and the temperature matches the Hawking result $\sim 1/r_+$. On the other hand, at shorter distances, i.e., at $r_+ \simeq 4.76\sqrt{\theta}$ the temperature admits a maximum $T_{\max} \simeq 0.015\,\sqrt{\theta}/G$, signalling the presence of a transition from a negative heat capacity phase to a positive heat capacity phase. The final stage of the evaporation is completely new: instead of the runaway divergent behaviour of the temperature, the black hole slowly cools down towards the zero temperature extremal configuration at r_0. Such a new terminal phase of the evaporation, often called "SCRAM phase"[2] downplays any concerns about the quantum back reaction. One can check that the emitted energy is always negligible with respect to black hole mass, i.e., $T/M < T_{\max}/M_0 \simeq 7.89 \times 10^{-3}$. This is equivalent to saying that the metric correctly describes the gravity/matter system during all the evaporation process.

The presence of a phase transition from an unstable phase to a locally stable SCRAM can be seen by analysing the heat capacity of the hole. As a preliminary step one calculates the black hole entropy by integrating $\mathrm{d}S \equiv \mathrm{d}M/T$, which yields

$$S = \frac{1}{4}\left(\frac{A_+\,\Gamma(3/2)}{\gamma(3/2;\,r_+^2/4\theta)} - \frac{A_0\,\Gamma(3/2)}{\gamma(3/2;\,r_0^2/4\theta)}\right) + \frac{\pi}{2\theta^{3/2}}\int_{r_0}^{r_+}\frac{t^2 e^{-t^2/4\theta}\,dt}{\gamma^2(3/2;\,t^2/4\theta)}, \tag{10.45}$$

where $A_+ = 4\pi r_+^2$ and $A_0 = 4\pi r_0^2$. We see that, for large holes, i.e., $A_+ \gg A_0$, Eq. (10.45) reproduces the usual area law. On the other hand for smaller holes, the presence of the extremal configuration becomes important and leads to a vanishing entropy for $r_+ = r_0$. This fact implies that the extremal configuration is a stable remnant of the evaporation. The stability of the remnant can also been seen through

[2] One borrows the terminology of critical shutdowns of thermonuclear reactors.

the black hole heat capacity

$$C(r_+) = T_H \left(\frac{dS_H}{dr_+}\right)\left(\frac{dT_H}{dr_+}\right)^{-1} . \tag{10.46}$$

which vanishes at r_0. As a result remnants are extremal black hole configurations with $T = S = C = 0$. More importantly, C admits an asymptote $\frac{dT_H}{dr_+} = 0$, i.e., at $T_{\rm max}$ which corresponds to a transition from a un-stable to a stable phase preceding the remnant formation. Such properties greatly improve the scenario based on the GUP [3, 80, 81], which suffers from the following weak points: huge back reaction due to Planckian values of remnant temperature; instability due a negative heat capacity in the phase preceding the remnant formation; sign ambiguity in the expression of the temperature; absence of any metric whose surface gravity reproduces the black hole temperature.

For the above attracting feature, the metric (10.40) has been studied in several contexts. For instance it has been shown that zero temperature remnants might have copiously been produces during the early ages of the Universe, as a consequence of the de Sitter space quantum instability [82]. On the other hand, the novel thermodynamic properties have been displayed by considering an anti-de Sitter background for (10.40): the intriguing new feature is the possibility of improving the conventional Hawking-Page phase transition in terms of a real gas phase diagram. In the isomorphism of variables, the black hole remnant size actually plays the role of the constant b' representing the molecule size in the van der Waals theory [83–85].

The metric (10.40) has companion geometries like traversable wormholes [86], whose throat is sustained by negative pressure terms, dirty black holes [87] and collapsing matter shells [88]. More importantly, the non-commutative geometry inspired Schwarzschild black hole has been studied in the presence of large extra dimensions [89]. As a special result, higher-dimensional non-commutative black holes tend to emit softer particles mainly on the brane, in marked contrast with the emission spectra of conventional Schwarzschild-Tangherlini black holes [90–92]. This peculiar emission spectrum might be a distinctive signature for detecting black holes resulting from particle collisions. However, the energy required for black hole formation might exceed current accelerator capabilities, as explained in Refs. [93, 94]. Lower dimensional versions of the metric (10.40) have also been studied in the context of dilatonic gravity: surprisingly, the regularity of the manifold gives rise to a richer topology, admitting up to six horizons [95].

Finally non-commutativity inspired black holes have been extended by including all possible black hole parameters. Charged [96, 97], rotating [98], and charged rotating [99] black holes have been derived in order to improve the Reissner-Nordström, Kerr and Kerr-Newman geometries. Specifically in the case of rotating black holes, the cure of the ring singularity is accompanied by the absence of conventional pathologies of the Kerr metric, such as an "anti-gravity" universe with causality violating time-like closed world-lines and a "super-luminal" matter disk.

10.3 Extra Dimensions

Models of the Universe with large additional dimensions were proposed around the year 2000 to bypass the constraints of not having observable Kaluza-Klein modes. In these scenarios the Standard Model particles and interactions are confined on a thin "brane" embedded in a higher-dimensional space-time, while gravity leaks into the extra dimensions [100–104]. Because gravity propagates in the entire "bulk" space-time, its fundamental scale $M_{\rm G}$ is related to the observed Planck mass $M_{\rm P} \simeq 10^{16}$ TeV by a coefficient determined by the volume of the (large or warped) extra dimensions. Therefore in these models there appear several length scales, namely the spatial extension(s) L of the extra dimensions in the ADD scenario [100–102], or the anti-de Sitter scale in the RS scenario ℓ [103, 104], and possibly the finite thickness Δ of the brane in either. The size L of the extra dimensions or the scale ℓ, determines the value of the effective Planck mass $M_{\rm P}$ from the fundamental gravitational mass $M_{\rm G}$. At the same time all of them determine the scale below which one should measure significant departures from the Newton law.

For suitable choices of L or ℓ, and the number d of extra dimensions, the mass $M_{\rm G}$ in these scenarios can be anywhere below $M_{\rm P} \simeq 10^{16}$ TeV, even as low as the electro-weak scale, that is $M_{\rm G} \simeq 1$ TeV. This means that the scale of gravity may be within the experimental reach of our high-energy laboratories or at least in the range of energies of ultra-high energy cosmic rays.

10.3.1 Black Holes in Extra Dimensions

We showed how we expect black holes can exist only above a minimum mass of the order of the fundamental scale of gravity. In four dimensions, this value is about 10^{16} TeV, and it would therefore be impossible to produce black holes at particle colliders or via the interactions between ultra-high cosmic rays with nucleons in the atmosphere. However, if we live in a universe with more than three spatial dimensions, microscopic black holes with masses of the order of $M_{\rm G} \simeq 1$ TeV may be produced by colliding particles in present accelerators or by ultra-high cosmic rays or neutrinos (see, e.g., Refs. [105–111]).

Our understanding of these scattering processes in models with extra spatial dimensions now goes beyond the naive hoop conjecture [23] used in the first papers on the topic. After the black hole is formed, all of its "hair" will be released in the subsequent balding phase. If the mass is still sufficiently large, the Hawking radiation [112] will set off. The standard description of this famous effect is based on the canonical Planckian distribution for the emitted particles, which implies the lifetime of microscopic black holes is very short, of the order of 10^{-26} s [113–115]. This picture (mostly restricted to the ADD scenario [100–102]) has been implemented in several numerical codes [116–124], mainly designed to help us identify black hole events at the Large Hadron Collider (LHC).

We should emphasise that the end-stage of the black hole evaporation remains an open problem to date [125–127], because we do not yet have a confirmed theory of quantum gravity. The semiclassical Hawking temperature grows without bound, as the black hole mass approaches the Planck mass. This is a sign of the lack of predictability of perturbative approaches, in which the effect of the Hawking radiation on the evaporating black hole is assumed to proceed adiabatically (very slowly). Alternatively one can use the more consistent microcanonical description of black hole evaporation, in which energy conservation is granted by construction [128–131]. This would seem an important issue also on the experimental side, since the microcanonical description predicts deviations from the Hawking law for small black hole masses (near the fundamental scale $M_{\rm G}$) and could lead to detectable signatures. However, energy conservation is always enforced in the numerical codes, and the deviations from the standard Hawking formulation are thus masked when the black hole mass approaches $M_{\rm G}$ [120, 121]. The default option for the end-point of microscopic black holes in most codes is that they are set to decay into a few standard model particles when a low mass (of choice) is reached. Another possibility, with qualitatively different phenomenology, is for the evaporation to end by leaving a stable remnant of mass $M \simeq M_{\rm G}$ [132–134].

Given the recent lower bounds on the value of the Planck mass, it has been pointed out that semiclassical black holes seem to be difficult to produce at colliders, as they might indeed require energies 5–20 times larger than the Planck scale $M_{\rm G}$. Similar objects, that generically go under the name of "quantum black holes", could be copiously produced instead [109, 135–137]. Their precise definition is not settled, but one usually assumes their production cross section is the same as that of larger black holes, and they are non-thermal objects, which do not decay according to the Hawking formula. Their masses are close to the scale $M_{\rm G}$ and their decay might resemble strong gravitational rescattering events [138]. It is also typically assumed that non-thermal quantum black holes decay into only a couple of particles. However, depending on the details of quantum gravity, the smallest quantum black holes could also be stable and not decay at all. The existence of remnants, i.e. the smallest stable black holes, have been considered in the literature [132, 133], and most of the results presented here can be found in Refs. [139, 140].

10.3.1.1 Black Hole Production

In the absence of a quantum theory of gravity, the production cross section of quantum black holes is usually extrapolated from the semiclassical regime. Therefore, both semiclassical and quantum black holes are produced according to the geometrical cross section formula extrapolated from the (classical) hoop conjecture [23],

$$\sigma_{\rm BH}(M) \approx \pi\, R_{\rm H}^2, \tag{10.47}$$

and is thus proportional to the horizon area. The specific coefficient of proportionality depends on the details of the models, which is assumed of order one.

In higher-dimensional theories, the horizon radius depends on the number d of extra-dimensions,

$$R_{\rm H} = \frac{\ell_{\rm G}}{\sqrt{\pi}} \left(\frac{M}{M_{\rm G}}\right)^{\frac{1}{d+1}} \left(\frac{8\,\Gamma\left(\frac{d+3}{2}\right)}{d+2}\right)^{\frac{1}{d+1}}, \tag{10.48}$$

where $\ell_{\rm G} = \hbar/M_{\rm G}$ is the fundamental gravitational length associated with $M_{\rm G}$, M the black hole mass, Γ the Gamma function, and the four-dimensional Schwarzschild radius (10.4) is recovered for $d = 0$. The Hawking temperature associated with the horizon is thus

$$T_{\rm H} = \frac{d+1}{4\,\pi\,R_{\rm H}}. \tag{10.49}$$

In a hadron collider like the LHC, a black hole could form in the collision of two partons, i.e. the quarks, anti-quarks and gluons of the colliding protons p. The total cross section for a process leaving a black hole and other products (collectively denoted by X) is thus given by

$$\left.\frac{d\sigma}{dM}\right|_{pp\to {\rm BH}+X} = \frac{dL}{dM}\,\sigma_{\rm BH}(ab \to BH;\, \hat{s} = M^2), \tag{10.50}$$

where

$$\frac{dL}{dM} = \frac{2\,M}{s} \sum_{a,b} \int_{M^2/s}^{1} \frac{dx_a}{x_a} f_a(x_a) f_b\left(\frac{M^2}{s\,x_a}\right), \tag{10.51}$$

a and b represent the partons which form the black hole, $\sqrt{\hat{s}}$ is their centre-mass energy, $f_i(x_i)$ are parton distribution functions (PDF), and $\sqrt{s}$ is the centre-mass collision energy. We recall that the LHC data is currently available at $\sqrt{s} = 8$ TeV, with a planned maximum of 14 TeV.

10.3.1.2 Charged Black Holes

It is important to note that, since black holes could be produced via the interaction of electrically charged partons (the quarks), they could carry a non vanishing electric charge, although the charge might be preferably emitted in a very short time. In four dimensions, where the fundamental scale of gravity is the Planck mass $M_{\rm P}$, the electron charge e is sufficient to turn such small objects into naked singularities. This can also be shown to hold in models with extra-spatial dimensions for black holes with mass $M \sim M_{\rm G}$ and charge $Q \sim e$. However, since the brane self-gravity is not neglected in brane-world models of the RS scenario [103, 104], a matter source

located on the brane will give rise to a modified energy momentum tensor in the Einstein equations projected on the three-brane [141]. By solving the latter, one finds that this backreaction can be described in the form of a tidal "charge" q which can take both positive and negative values [142]. The interesting range of values for q are the positive ones. Provided the tidal charge is large enough, microscopic black holes can now carry an electric charge of the order of e [143]. In this particular case, the horizon radius is given by

$$R_{\rm H} = \ell_{\rm P}\,\frac{M}{M_{\rm P}}\left(1+\sqrt{1-\tilde{Q}^2\,\frac{M_{\rm P}^2}{M^2}+\frac{q\,M_{\rm P}^2}{\ell_{\rm G}^2\,M^2}}\right), \tag{10.52}$$

where $\tilde{Q}$ is the electric charge in dimensionless units,

$$\tilde{Q} \simeq 10^8\left(\frac{M}{M_{\rm P}}\right)\frac{Q}{e}. \tag{10.53}$$

Reality of Eq. (10.52) for a remnant of charge $Q = \pm e$ and mass $M \simeq M_{\rm G}$ then requires

$$q \gtrsim 10^{16}\,\ell_{\rm G}^2\left(\frac{M_{\rm G}}{M_{\rm P}}\right)^2 \sim 10^{-16}\,\ell_{\rm G}^2. \tag{10.54}$$

Configurations satisfying the above bound were indeed found recently [144, 145].

10.3.1.3 Black Hole Evolution

In the standard picture, the evolution and decay process of semiclassical black holes can be divided into three characteristic stages:

1. **Balding phase**. Since no collision is perfectly axially symmetric, the initial state will not be described by a Kerr-Newman metric. Because of the no-hair theorems, the black hole will therefore radiate away the multipole moments inherited from the initial configuration, and reach a hairless state. A fraction of the initial mass will also be radiated as gravitational radiation, on the brane and into the bulk.
2. **Evaporation phase**. The black hole loses mass via the Hawking effect. It first spins down by emitting the initial angular momentum, after which it proceeds with the emission of thermally distributed quanta. The radiation spectrum contains all the standard model particles, (emitted on our brane), as well as gravitons (also emitted into the extra dimensions). For this stage, it is crucial to have a good estimate of the grey-body factors [146–153].
3. **Planck phase**. The black hole has reached a mass close to the effective Planck scale $M_{\rm G}$ and falls into the regime of quantum gravity. It is generally assumed that the black hole will either completely decay into standard model particles [113–115] or a (meta-)stable remnant is left, which carries away the remaining energy [132].

Admittedly, we have limited theoretical knowledge of the nature of quantum black holes, since these objects should be produced already at stage 3. We should therefore keep our analysis open to all possible qualitative behaviours. In particular, we shall focus on the case in which the initial semiclassical or quantum black hole emits at most a fraction of its mass in a few particles and lives long enough to exit the detector. In other words, we will here focus on the possibility that the third phase ends by leaving a (sufficiently) stable remnant.

10.3.2 Minimum Mass and Remnant Phenomenology

It was shown in a series of articles [154, 155] that it is possible for Planck scale black holes to result in stable remnants. Given the present lower bounds on the value of the fundamental scale $M_{\rm G}$, the centre of mass energy of the LHC is only large enough to produce quantum black holes. (We remind the mass of the lightest semiclassical black holes is expected to be between 5 and 20 times $M_{\rm G}$, depending on the model.) In this case, the remnant black holes could not be the end-point of the Hawking evaporation, but should be produced directly.

At the LHC, black holes could be produced by quarks, anti-quarks and gluons, and would thus typically carry a $\mathrm{SU}(3)_c$ charge (as well as a QED charge, as we pointed out before). Quantum black holes could in fact be classified according to representations of $\mathrm{SU}(3)_c$, and their masses are also expected to be quantised [137]. Since we are considering the case that black holes do not decay completely, we expect that they will hadronize, i.e. absorbe a particle charged under $SU(3)_c$ after traveling over a distance of some 200^{-1} MeV and become an $SU(3)_c$ singlet. They could also loose colour charge by emitting a fraction of their energy before becoming stable. Finally, the hadronization process could possibly lead to remnants with a (fractional) QED charge. To summarise, black hole remnants could be neutral or have the following QED charges: $\pm 4/3$, ± 1, $\pm 2/3$, and $\pm 1/3$. Depending on its momentum, a fast moving black hole is likely to hadronize in the detector, whereas for a black hole which is moving slowly, this is likely to happen before it reaches the detector.

Monte Carlo simulations of black hole production processes which result in stable remnants have been performed using the code CHARYBDIS2. They have shown that approximately 10% of the remnants will carry an electric charge $Q = \pm e$ [139]. This code was not specifically designed to simulate the phenomenology of quantum black holes, but it could be employed since they are produced according to the same geometrical cross section as semiclassical black holes, and the details of their possible partial decay are not phenomenologically relevant when searching for a signature of the existence of remnants. In fact, the initial black hole mass cannot be much larger than a few times $M_{\rm G}$, even for $\sqrt{s} = 14\,\mathrm{TeV}$. So in the simulations the black holes emit at most a fraction of their energy in a small number of standard model particles before becoming stable. Such a discrete emission process in a relatively narrow range of masses is constrained by the conservation of energy and standard

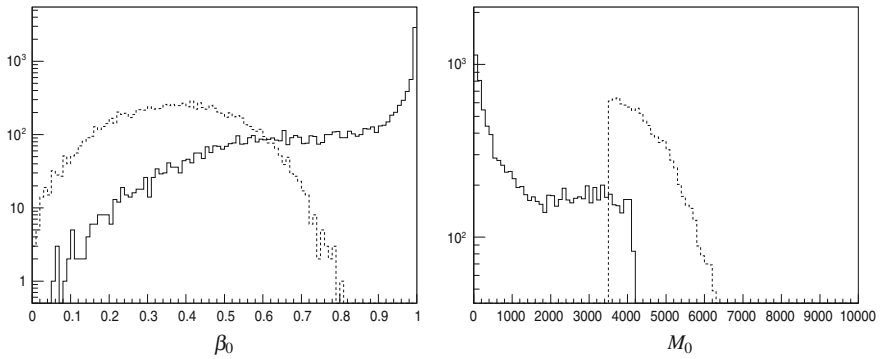

Fig. 10.6 Distribution of speed β_0 (*left panel*) and mass M_0 (in GeV; *right panel*) of the remnant black holes for KINCUT = TRUE (*dashed line*) and KINCUT = FALSE (*solid line*). Both plots are for $\sqrt{s} = 14\,\text{TeV}$ with $M_\text{G} = 3.5\,\text{TeV}$ and initial $M_\text{BH} \geq 2\,M_\text{G}$ in $D = 6$ total dimensions and 10^4 total black hole events

model charges, and cannot differ significantly for different couplings of the quantum black holes to standard model particles. In Monte Carlo generators the decays are assumed to be instantaneous. The following analysis does therefore not include the possibility that the black holes partially decay off the production vertex, nor the effects of hadronization by absorption of coloured particles.

The numerical simulations show that the remnant black holes are expected to have a typical speed $\beta_0 = v_0/c$ with the distribution shown in the left panel of Fig. 10.6, for a sample of 10^4 black holes, where two different scenarios for the end-point of the decay were assumed. The dashed line represents the case when the decay is prevented from producing a remnant with proper mass M_0 below M_G (but could stop at $M_0 > M_\text{G}$), whereas the solid line represents black hole remnants produced when the last emission is only required to keep $M_0 > 0$. The mass M_0 for the remnants in the two cases is distributed according to the plots in the right panel of Fig. 10.6. In the former case, with the remnant mass $M_0 \gtrsim M_\text{G}$, a smaller amount of energy is emitted before the hole becomes a remnant, whereas in the latter much lighter remnants are allowed. The first scenario provides a better description for black hole remnants resulting from the partial decay of quantum black holes, and the second scenario is mostly presented for the sake of completeness.

The same quantities, speed β_0 and mass M_0, but only for the charged remnants, are displayed in Fig. 10.7, again for a sample of 10^4 black hole events. The left panel shows that, including both scenarios, one can expect the charged remnant velocity is quite evenly distributed on the entire allowed range, but β_0 is generally smaller when the remnant mass is larger than M_G. As it was shown earlier, black hole remnants are likely to have masses of the order of M_G or larger, therefore from now on we will focus on this case only.

For phenomenological reasons, it is very instructive to consider the distribution of the speed β_0 with respect to transverse momenta P_T for remnant black holes.

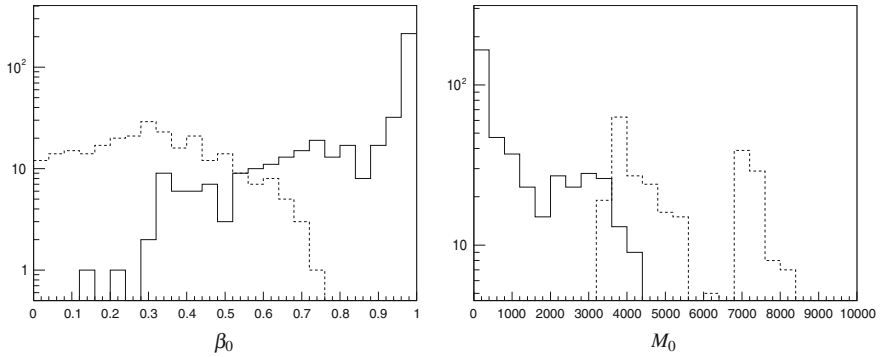

Fig. 10.7 Distribution of speed β_0 (*left panel*) and mass M_0 (in GeV; *right panel*) of the charged remnant black holes for $M_0 > M_{\rm G}$ (*dashed line*) and $M_0 > 0$ (*solid line*). Both plots are for $\sqrt{s} = 14\,\text{TeV}$ with $M_{\rm G} = 3.5\,\text{TeV}$ in $D = 6$ total dimensions and 10^4 total events

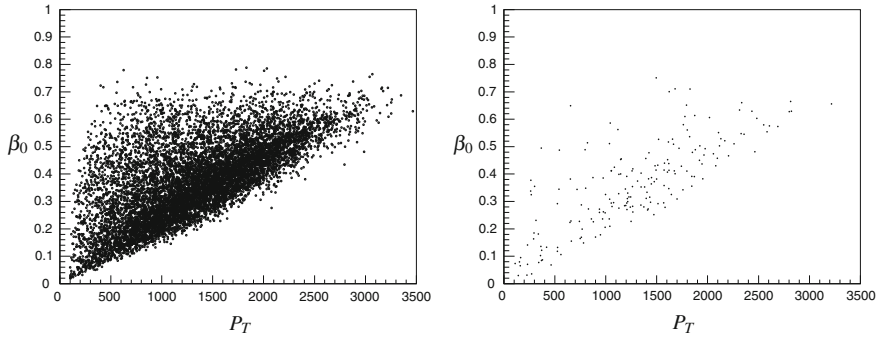

Fig. 10.8 Distribution of β_0 vs P_T (in GeV) with $M_0 > M_{\rm G}$ for neutral remnants (*left panel*) and charged remnants (*right panel*) for $P_T > 100\,\text{GeV}$. Both plots are for $\sqrt{s} = 14\,\text{TeV}$ with $M_{\rm G} = 3.5\,\text{TeV}$ in $D = 6$ total dimensions and 10^4 total events.

A cut-off is set for particles with transverse momentum of $P_T > 100\,\text{GeV}$. Figure 10.8 shows separately the distributions of β_0 for neutral and charged remnants. We first recall that the remnant velocities are lower because the masses of remnant black holes in this case are typically larger. Figure 10.9 shows the similar plot β_0 versus P_T for the background particles. When comparing the two plots, remnants appear clearly distinguished since there is hardly any black hole with $\beta_0 \gtrsim 0.7$, whereas all the background particles have $\beta \simeq 1$. The speeds β_0 of the remnants can also be compared with the distributions of β for the $t\bar{t}$ process (which can be considered as one of the main backgrounds) shown in Fig. 10.10. Taking into account the production cross section $\sigma_{t\bar{t}}(14\,\text{TeV}) \simeq 880\,\text{pb}$, and the branching ratio for single-lepton decays (final states with significant missing transverse energy), for a luminosity of $L = 10\,\text{fb}^{-1}$ a number of 3.9×10^6 such events are expected. This must be compared

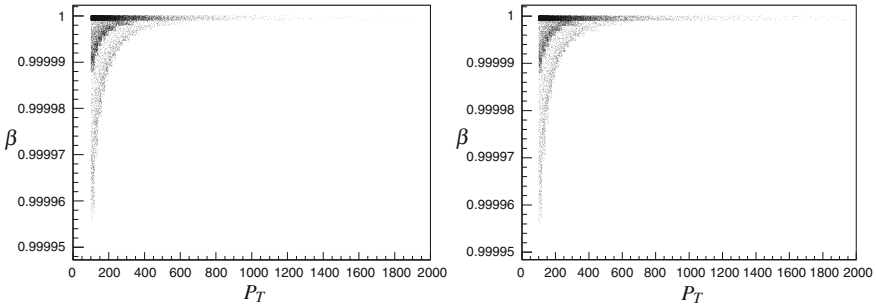

Fig. 10.9 Distribution of β versus P_T (in GeV) for background particles with $P_T > 100\,\text{GeV}$, in events with remnant black holes and $M_0 > M_\text{G}$ (*left panel*) or $M_0 > 0$ (*right panel*). Both plots are for $\sqrt{s} = 14\,\text{TeV}$ with $M_\text{G} = 3.5\,\text{TeV}$ in $D = 6$ total dimensions and 10^4 total events

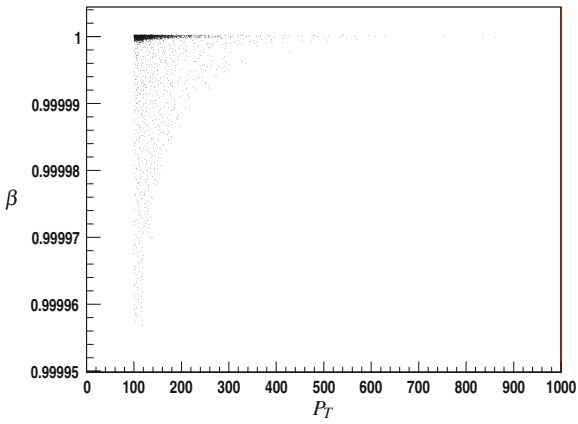

Fig. 10.10 Distribution of β versus P_T (in GeV) for particles with $P_T > 100\,\text{GeV}$, in events with $t\,\bar{t}$ for $\sqrt{s} = 14\,\text{TeV}$.

with the expected number of 400 black hole events that could be produced for the same luminosity.

Charged particles also release energy when traveling through a medium. The energy released by a particle of mass M and charge $Q = z\,e$ can be estimated using the well-known Bethe-Bloch equation. For particles moving at relativistic speeds, one has an energy loss per distance travelled given by

$$\frac{dE}{dx} = -4\,\pi\,N_A\,r_e^2\,m_e\,c^2\,\frac{Z\,\rho}{A\,\beta^2}\left[\ln\left(\frac{2\,m_e\,c^2\,\beta^2}{I}\right) - \beta^2 - \frac{\delta}{2}\right], \qquad (10.55)$$

where N_A is Avogadro's number, m_e and r_e the electron mass and classical radius, Z, A and ρ the atomic number, atomic weight and density of the medium, $I \simeq 16\,Z^{0.9}\,\text{eV}$ its mean excitation potential, and δ a constant that describes the screening of the electric field due to medium polarisation. For the LHC, one can use the values for

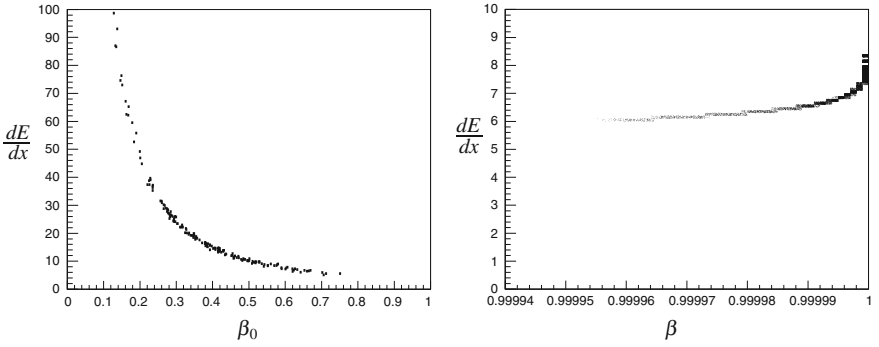

Fig. 10.11 Typical energy loss per unit distance (in MeV/cm) from charged remnant black holes vs β_0, for $M_0 > M_G$ (*left panel*) and analogous quantity for background particles (*right panel*). Both plots are for $\sqrt{s} = 14\,\text{TeV}$ with $M_G = 3.5\,\text{TeV}$ in $D = 6$ total dimensions and 10^4 total events

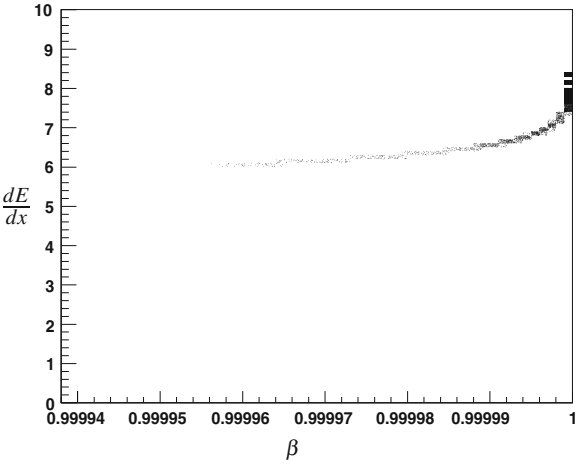

Fig. 10.12 Typical energy loss per unit distance (in MeV/cm) from charged particles versus β in 10^4 total events with $t\bar{t}$ at $\sqrt{s} = 14\,\text{TeV}$

Si, as the dE/dX can be effectively measured in the ATLAS Inner Detector, namely $\rho = 2.33\,\text{g/cm}^3$, $Z = 14$, $A = 28$, $I = 172\,\text{eV}$ and $\delta = 0.19$. On using the β_0 for charged remnant black holes from the right panel of Fig. 10.8, one then obtains the typical distributions displayed in Fig. 10.11, where the energy loss from remnant black holes is compared with analogous quantities for ordinary particles coming from black hole evaporation. One can then also compare with the energy loss in $t\bar{t}$ events displayed in Fig. 10.12. It can be seen that a cut around $10\,\text{MeV/cm}$ would clearly isolate remnants black holes, since they would mostly loose more energy.

The charged stable remnants behave as massive muons, travelling long distances through the detector and releasing only a negligible fraction of their total energy.

The main problem in detecting such states at the LHC is the trigger time width of 25 ns (1 bunch crossing time). Due to their low speed, most of them will reach the muon system out of time and could not be accepted by the trigger. A study performed at ATLAS set a threshold cut of $\beta > 0.62$ in order to have a muon trigger in the event (slower particles end up out of the trigger time window). In order to access the low β range, one can imagine to trigger on the missing transverse energy ($E_T^{\rm miss}$), copiously produced by the charged remnants, or on other standard particles produced in the black hole evaporation (typically electrons or muons). Another possibility is to trigger on ordinary particles, typically electrons or muons with high transverse momentum P_T, in order to reduce the high potential background coming from QCD multi-jet events. Once the events have been accepted by the trigger the signal has to be isolated from the background by means of the dE/dX measurement.

10.4 Concluding Remarks

We have seen that the very existence of black holes in gravity is at the heart of GUPs for quantum mechanics, which imply the existence of a minimum measurable length. These modifications of quantum mechanics, in turn, imply that black holes can only exist above a minimum mass threshold. Minimum mass black holes could be stable, or metastable remnants with zero Hawking temperature. In any case, they would belong to the realm of quantum objects, for which we still have limited theoretical understanding.

In four-dimensional gravity, this minimum mass is usually predicted to be of the order of the Planck mass, $M_{\rm P} \simeq 10^{16}$ TeV, well above the energies that can be reached in our laboratories. However, if the universe really contains extra spatial dimensions hidden to our direct investigation, the fundamental gravitational mass could be much lower and potentially within the reach of our experiments. Black holes might therefore be produced in future colliders, and deviations from the standard uncertainty relations of quantum mechanics might be testable at length scales much larger than the Planck length, $\ell_{\rm P} \simeq 10^{-35}$ m.

All of the above considered, black holes and a minimum measurable length scale are at the very frontiers of contemporary fundamental physics.

References

1. Adler, R.J.: Am. J. Phys. **78**, 925 (2010)
2. Kempf, A., Mangano, G., Mann, R.B.: Phys. Rev. D **52**, 1108 (1995)
3. Adler, R.J., Chen, P., Santiago, D.I.: Gen. Rel. Grav. **33**, 2101 (2001)
4. Amati, D., Ciafaloni, M., Veneziano, G.: JHEP **02**, 049 (2008)
5. Dvali, G., Giudice, G.F., Gomez, C., Kehagias, A.: JHEP **08**, 108 (2011)
6. A. Aurilia and E. Spallucci, "Planck's uncertainty principle and the saturation of Lorentz boosts by Planckian black holes", arXiv:1309.7186 [gr-qc]

7. Hossenfelder, S.: Living Rev. Rel. **16**, 2 (2013)
8. DeWitt, B.S.: The quantization of geometry. In: Witten, Louis (ed.) Gravitation: An Introduction to Current Research, pp. 266–381. J. Wiley and Sons, New York (1962)
9. Amati, D., Ciafaloni, M., Veneziano, G.: Phys. Lett. B **197**, 81 (1987)
10. Veneziano, G.: Europhys. Lett. **2**, 199 (1986)
11. Amati, D., Ciafaloni, M., Veneziano, G.: Phys. Lett. B **216**, 41 (1989)
12. Yoneya, T.: Mod. Phys. Lett. A **4**, 1587 (1989)
13. Konishi, K., Paffuti, G., Provero, P.: Phys. Lett. B **234**, 276 (1990)
14. Aurilia, A., Spallucci, E.: Adv. High Energy Phys. **2013**, 531696 (2013)
15. C. Rovelli and L. Smolin, Nucl. Phys. B 442, 593 (1995) [Erratum-ibid. B 456, 753 (1995)]
16. Seiberg, N., Witten, E.: JHEP **09**, 032 (1999)
17. S. Weinberg, "Ultraviolet divergences in quantum theories of gravitation", in General Relativity: an Einstein centenary survey, ed. S. W. Hawking and W. Israel. Cambridge University Press. pp. 790–831
18. Reuter, M.: Phys. Rev. D **57**, 971 (1998)
19. Amelino-Camelia, G.: Mod. Phys. Lett. A **9**, 3415 (1994)
20. Garay, L.J.: Int. J. Mod. Phys. A **10**, 145 (1995)
21. Sprenger, M., Nicolini, P., Bleicher, M.: Eur. J. Phys. **33**, 853 (2012)
22. Scardigli, F., Casadio, R.: Int. J. Mod. Phys. D **18**, 319 (2009)
23. K.S. Thorne, Nonspherical gravitational collapse: A short review, in J.R. Klauder, Magic Without Magic, San Francisco (1972), 231
24. R. Casadio, "Localised particles and fuzzy horizons: A tool for probing Quantum Black Holes", arXiv:1305.3195 [gr-qc]
25. R. Casadio, "What is the Schwarzschild radius of a quantum mechanical particle?", arXiv:1310.5452 [gr-qc]
26. Casadio, R., Scardigli, F.: Eur. Phys. J. C **74**, 2685 (2014)
27. Casadio, R., Micu, O., Scardigli, F.: Phys. Lett. B **732**, 105 (2014)
28. Casadio, R., Ovalle, J.: Gen. Rel. Grav. **46**, 1669 (2014)
29. Casadio, R., Ovalle, J.: Phys. Lett. B **715**, 251 (2012)
30. Alberghi, G.L., Casadio, R., Micu, O., Orlandi, A.: JHEP **09**, 023 (2011)
31. Berkooz, M., Reichmann, D.: Nucl. Phys. Proc. Suppl. **171**, 69 (2007)
32. C. Rovelli, Living Rev. Rel. 1, 1 (1998); Living Rev. Rel. 11, 5 (2008), Chapt. 8, pp 42
33. J. M. Bardeen, "Non-singular general-relativistic gravitational collapse," in Proceedings of International Conference GR5, p. 174, USSR, Tbilisi, Georgia, 1968
34. Aurilia, A., Denardo, G., Legovini, F., Spallucci, E.: Phys. Lett. B **147**, 258 (1984)
35. Aurilia, A., Denardo, G., Legovini, F., Spallucci, E.: Nucl. Phys. B **252**, 523 (1985)
36. Aurilia, A., Kissack, R.S., Mann, R.B., Spallucci, E.: Phys. Rev. D **35**, 2961 (1987)
37. Frolov, V.P., Markov, M.A., Mukhanov, V.F.: Phys. Rev. D **41**, 383 (1990)
38. Ayon-Beato, E., Garcia, A.: Phys. Rev. Lett. **80**, 5056 (1998)
39. Dymnikova, I.G.: Int. J. Mod. Phys. **D5**, 529 (1996)
40. Dymnikova, I.G.: Int. J. Mod. Phys. **D12**, 1015 (2003)
41. Mbonye, M.R., Kazanas, D.: Phys. Rev. D **72**, 024016 (2005)
42. Mbonye, M.R., Kazanas, D.: Int. J. Mod. Phys. D **17**, 165 (2008)
43. Hayward, S.A.: Phys. Rev. Lett. **96**, 031103 (2006)
44. Spallucci, E., Smailagic, A.: Phys. Lett. B **709**, 266 (2012)
45. Nicolini, P., Spallucci, E.: Adv. High Energy Phys. **2014**, 805684 (2014)
46. Modesto, L.: Class. Quant. Grav. **23**, 5587 (2006)
47. Modesto, L., Premont-Schwarz, I.: Phys. Rev. D **80**, 064041 (2009)
48. Bonanno, A., Reuter, M.: Phys. Rev. D **62**, 043008 (2000)
49. Carr, B.J.: Mod. Phys. Lett. A **28**, 1340011 (2013)
50. B. Carr, L. Modesto and I. Premont-Schwarz, "Generalized Uncertainty Principle and Self-dual Black Holes", arXiv:1107.0708 [gr-qc]
51. S. Ansoldi, "Spherical black holes with regular center: a review of existing models including a recent realization with Gaussian sources", in Proceedings of Conference on Black Holes and Naked Singularities, 10–12 May 2007, Milan, Italy, arXiv:0802.0330 [gr-qc]

52. Nicolini, P.: Int. J. Mod. Phys. A **24**, 1229 (2009)
53. Balasin, H., Nachbagauer, H.: Class. Quant. Grav. **10**, 2271 (1993)
54. Balasin, H., Nachbagauer, H.: Class. Quant. Grav. **11**, 1453 (1994)
55. Smailagic, A., Spallucci, E.: J. Phys. A **36**, L467 (2003)
56. Smailagic, A., Spallucci, E.: J. Phys. A **36**, L517 (2003)
57. A. Smailagic and E. Spallucci, J. Phys. A 37, 1 (2004) [Erratum-ibid. A 37, 7169 (2004)]
58. Spallucci, E., Smailagic, A., Nicolini, P.: Phys. Rev. D **73**, 084004 (2006)
59. Kober, M., Nicolini, P.: Class. Quant. Grav. **27**, 245024 (2010)
60. Casadio, R., Cox, P.H., Harms, B., Micu, O.: Phys. Rev. D **73**, 044019 (2006)
61. Casadio, R., Gruppuso, A., Harms, B., Micu, O.: Phys. Rev. D **76**, 025016 (2007)
62. P. Nicolini, A. Smailagic and E. Spallucci, ESA Spec. Publ. 637, 11.1 (2006).
63. Nicolini, P.: J. Phys. A **38**, L631 (2005)
64. Nicolini, P., Smailagic, A., Spallucci, E.: Phys. Lett. B **632**, 547 (2006)
65. Banerjee, R., Gangopadhyay, S., Modak, S.K.: Phys. Lett. B **686**, 181 (2010)
66. Modesto, L., Moffat, J.W., Nicolini, P.: Phys. Lett. B **695**, 397 (2011)
67. Moffat, J.W.: Eur. Phys. J. Plus **126**, 43 (2011)
68. P. Nicolini, "Nonlocal and generalized uncertainty principle black holes", arXiv:1202.2102 [hep-th]
69. Isi, M., Mureika, J., Nicolini, P.: JHEP **1311**, 139 (2013)
70. Modesto, L.: Phys. Rev. D **86**, 044005 (2012)
71. Biswas, T., Gerwick, E., Koivisto, T., Mazumdar, A.: Phys. Rev. Lett. **108**, 031101 (2012)
72. Casadio, R., Orlandi, A.: JHEP **08**, 025 (2013)
73. Dvali, G., Gomez, C.: Fortsch. Phys. **59**, 579 (2011)
74. Dvali, G., Gomez, C.: Fortsch. Phys. **61**, 742 (2013)
75. Dvali, G., Gomez, C.: Phys. Lett. B **719**, 419 (2013)
76. Dvali, G., Flassig, D., Gomez, C., Pritzel, A., Wintergerst, N.: Phys. Rev. D **88**, 124041 (2013)
77. Batic, D., Nicolini, P.: Phys. Lett. B **692**, 32 (2010)
78. Brown, E., Mann, R.B.: Phys. Lett. B **694**, 440 (2011)
79. Banerjee, R., Majhi, B.R., Samanta, S.: Phys. Rev. D **77**, 124035 (2008)
80. Scardigli, F.: Phys. Lett. B **452**, 39 (1999)
81. Chen, P., Adler, R.J.: Nucl. Phys. Proc. Suppl. **124**, 103 (2003)
82. Mann, R.B., Nicolini, P.: Phys. Rev. D **84**, 064014 (2011)
83. Nicolini, P., Torrieri, G.: JHEP **1108**, 097 (2011)
84. Smailagic, A., Spallucci, E.: Int. J. Mod. Phys. D **22**, 1350010 (2013)
85. Spallucci, E., Smailagic, A.: J. Grav. **2013**, 525696 (2013)
86. Garattini, R., Lobo, F.S.N.: Phys. Lett. B **671**, 146 (2009)
87. Nicolini, P., Spallucci, E.: Class. Quant. Grav. **27**, 015010 (2010)
88. Nicolini, P., Orlandi, A., Spallucci, E.: Adv. High Energy Phys. **2013**, 812084 (2013)
89. Rizzo, T.G.: JHEP **09**, 021 (2006)
90. Casadio, R., Nicolini, P.: JHEP **11**, 072 (2008)
91. Gingrich, D.M.: JHEP **05**, 022 (2010)
92. Nicolini, P., Winstanley, E.: JHEP **11**, 075 (2011)
93. Mureika, J., Nicolini, P., Spallucci, E.: Phys. Rev. D **85**, 106007 (2012)
94. M. Bleicher and P. Nicolini, "Mini-review on mini-black holes from the mini-Big Bang", arXiv:1403.0944 [hep-th]
95. Mureika, J.R., Nicolini, P.: Phys. Rev. D **84**, 044020 (2011)
96. Ansoldi, S., Nicolini, P., Smailagic, A., Spallucci, E.: Phys. Lett. B **645**, 261 (2007)
97. Spallucci, E., Smailagic, A., Nicolini, P.: Phys. Lett. B **670**, 449 (2009)
98. Smailagic, A., Spallucci, E.: Phys. Lett. B **688**, 82 (2010)
99. Modesto, L., Nicolini, P.: Phys. Rev. D **82**, 104035 (2010)
100. Arkani-Hamed, N., Dimopoulos, S., Dvali, G.R.: Phys. Lett. B **429**, 263 (1998)
101. Arkani-Hamed, N., Dimopoulos, S., Dvali, G.R.: Phys. Rev. D **59**, 086004 (1999)
102. Antoniadis, I., Arkani-Hamed, N., Dimopoulos, S., Dvali, G.R.: Phys. Lett. B **436**, 257 (1998)
103. Randall, L., Sundrum, R.: Phys. Rev. Lett. **83**, 4690 (1999)

104. Randall, L., Sundrum, R.: Phys. Rev. Lett. **83**, 3370 (1999)
105. Cavaglia, M.: Int. J. Mod. Phys. A **18**, 1843 (2003)
106. Kanti, P.: Int. J. Mod. Phys. A **19**, 4899 (2004)
107. Cardoso, V., Gualtieri, L., Herdeiro, C., Sperhake, U., Chesler, P.M., Lehner, L., Park, S.C., Reall, H.S., et al.: Class. Quant. Grav. **29**, 244001 (2012)
108. Park, S.C.: Prog. Part. Nucl. Phys. **67**, 617 (2012)
109. Calmet, X., Caramete, L.I., Micu, O.: JHEP **11**, 104 (2012)
110. Arsene, N., Calmet, X., Caramete, L.I., Micu, O.: Astropart. Phys. **54**, 132 (2014)
111. N. Arsene, L. I. Caramete, P. B. Denton and O. Micu, "Quantum Black Holes Effects on the Shape of Extensive Air Showers", arXiv:1310.2205 [hep-ph]
112. Hawking, S.W.: Nature 248, 30 (1974); Comm. Math. Phys. **43**, 199 (1975)
113. Dimopoulos, S., Landsberg, G.: Phys. Rev. Lett. **87**, 161602 (2001)
114. T. Banks and W. Fischler, "A model for high energy scattering in quantum gravity", arXiv:hep-th/9906038
115. Giddings, S.B., Thomas, S.D.: Phys. Rev. D **65**, 056010 (2002)
116. Harris, C.M., Richardson, P., Webber, B.R.: JHEP **08**, 033 (2003)
117. S. Dimopoulos and G. Landsberg, Black hole production at future colliders, in Proc. of the APS/DPF/DPB Summer Study on the Future of Particle Physics (Snowmass 2001), edited by N. Graf, eConf C010630, P321 (2001)
118. Ahn, E.J., Cavaglia, M.: Phys. Rev. D **73**, 042002 (2006)
119. Cavaglia, M., Godang, R., Cremaldi, L., Summers, D.: Comput. Phys. Commun. **177**, 506 (2007)
120. Alberghi, G.L., Casadio, R., Tronconi, A.: J. Phys. G **34**, 767 (2007)
121. G. L. Alberghi, R. Casadio, D. Galli, D. Gregori, A. Tronconi and V. Vagnoni, "Probing quantum gravity effects in black holes at LHC", hep-ph/0601243
122. Dai, D.-C., Starkman, G., Stojkovic, D., Issever, C., Rizvi, E., Tseng, J.: Phys. Rev. D **77**, 076007 (2008)
123. Frost, J.A., Gaunt, J.R., Sampaio, M.O.P., Casals, M., Dolan, S.R., Parker, M.A., Webber, B.R.: JHEP **10**, 014 (2009)
124. M.O.P. Sampaio, "Production and evaporation of higher dimensional black holes", Ph.D. thesis, http://www.dspace.cam.ac.uk/handle/1810/226741
125. Landsberg, G.: J. Phys. G **32**, R337 (2006)
126. Harris, C.M., Palmer, M.J., Parker, M.A., Richardson, P., Sabetfakhri, A., Webber, B.R.: JHEP **05**, 053 (2005)
127. Casanova, A., Spallucci, E.: Class. Quant. Grav. **23**, R45 (2006)
128. Casadio, R., Harms, B., Leblanc, Y.: Phys. Rev. D **57**, 1309 (1998)
129. Casadio, R., Harms, B.: Phys. Rev. D **58**, 044014 (1998)
130. Casadio, R., Harms, B.: Mod. Phys. Lett. **A14**, 1089 (1999)
131. Casadio, R., Harms, B.: Entropy **13**, 502 (2011)
132. Koch, B., Bleicher, M., Hossenfelder, S.: JHEP **10**, 053 (2005)
133. Hossenfelder, S.: Nucl. Phys. A **774**, 865 (2006)
134. Gingrich, D.M.: JHEP **05**, 022 (2010)
135. Calmet, X., Gong, W., Hsu, S.D.H.: Phys. Lett. B **668**, 20 (2008)
136. Calmet, X., Fragkakis, D., Gausmann, N.: Eur. Phys. J. C **71**, 1781 (2011)
137. X. Calmet, D. Fragkakis and N. Gausmann, "Non Thermal Small Black Holes", in Black Holes: Evolution, Theory and Thermodynamics, A.J. Bauer and D.G. Eiffel editors, Nova Publishers, New York, 2012 arXiv:1201.4463
138. Meade, P., Randall, L.: JHEP **05**, 003 (2008)
139. Bellagamba, L., Casadio, R., Di Sipio, R., Viventi, V.: Eur. Phys. J. C **72**, 1957 (2012)
140. Alberghi, G.L., Bellagamba, L., Calmet, X., Casadio, R., Micu, O.: Eur. Phys. J. C **73**, 2448 (2013)
141. Shiromizu, T., Maeda, K., Sasaki, M.: Phys. Rev. D **62**, 043523 (2000)
142. Dadhich, N., Maartens, R., Papadopoulos, P., Rezania, V.: Phys. Lett. **B487**, 1 (2000)
143. Casadio, R., Harms, B.: Int. J. Mod. Phys. A **17**, 4635 (2002)

144. Casadio, R., Ovalle, J.: Phys. Lett. B **715**, 251 (2012)
145. R. Casadio and J. Ovalle, "Brane-world stars from minimal geometric deformation, and black holes", arXiv:1212.0409
146. D. Ida, K. -y. Oda and S. C. Park, Phys. Rev. D 67, 064025 (2003) [Erratum-ibid. D 69 (2004) 049901]
147. Ida, D.: K. -y. Oda and S. C. Park. Phys. Rev. D **71**, 124039 (2005)
148. Ida, D.: K. -y. Oda and S. C. Park. Phys. Rev. D **73**, 124022 (2006)
149. Creek, S., Efthimiou, O., Kanti, P., Tamvakis, K.: Phys. Rev. D **75**, 084043 (2007)
150. Creek, S., Efthimiou, O., Kanti, P., Tamvakis, K.: Phys. Rev. D **76**, 104013 (2007)
151. Duffy, G., Harris, C., Kanti, P., Winstanley, E.: JHEP **09**, 049 (2005)
152. Casals, M., Kanti, P., Winstanley, E.: JHEP **02**, 051 (2006)
153. Casals, M., Dolan, S.R., Kanti, P., Winstanley, E.: JHEP **03**, 019 (2007)
154. Casadio, R., Fabi, S., Harms, B., Micu, O.: JHEP **02**, 079 (2010)
155. Casadio, R., Harms, B., Micu, O.: Phys. Rev. D **82**, 044026 (2010)